frontiers | Research Topics

Innovation in tackling the global challenge of eradicating antibiotic-resistant microorganisms

Edited by
Israel Nissan, Fernando Reyes and Avi Peretz

Published in
Frontiers in Microbiology

ISSN 1664-8714
ISBN 978-2-8325-7418-8
DOI 10.3389/978-2-8325-7418-8

Generative AI statement
Any alternative text (Alt text) provided alongside figures in the articles in this ebook has been generated by Frontiers with the support of artificial intelligence and reasonable efforts have been made to ensure accuracy, including review by the authors wherever possible. If you identify any issues, please contact us.

About Frontiers

Frontiers is more than just an open access publisher of scholarly articles: it is a pioneering approach to the world of academia, radically improving the way scholarly research is managed. The grand vision of Frontiers is a world where all people have an equal opportunity to seek, share and generate knowledge. Frontiers provides immediate and permanent online open access to all its publications, but this alone is not enough to realize our grand goals.

Frontiers journal series

The Frontiers journal series is a multi-tier and interdisciplinary set of open-access, online journals, promising a paradigm shift from the current review, selection and dissemination processes in academic publishing. All Frontiers journals are driven by researchers for researchers; therefore, they constitute a service to the scholarly community. At the same time, the *Frontiers journal series* operates on a revolutionary invention, the tiered publishing system, initially addressing specific communities of scholars, and gradually climbing up to broader public understanding, thus serving the interests of the lay society, too.

Dedication to quality

Each Frontiers article is a landmark of the highest quality, thanks to genuinely collaborative interactions between authors and review editors, who include some of the world's best academicians. Research must be certified by peers before entering a stream of knowledge that may eventually reach the public - and shape society; therefore, Frontiers only applies the most rigorous and unbiased reviews. Frontiers revolutionizes research publishing by freely delivering the most outstanding research, evaluated with no bias from both the academic and social point of view. By applying the most advanced information technologies, Frontiers is catapulting scholarly publishing into a new generation.

What are Frontiers Research Topics?

Frontiers Research Topics are very popular trademarks of the *Frontiers journals series*: they are collections of at least ten articles, all centered on a particular subject. With their unique mix of varied contributions from Original Research to Review Articles, Frontiers Research Topics unify the most influential researchers, the latest key findings and historical advances in a hot research area.

Find out more on how to host your own Frontiers Research Topic or contribute to one as an author by contacting the Frontiers editorial office: frontiersin.org/about/contact

Innovation in tackling the global challenge of eradicating antibiotic-resistant microorganisms

Topic editors

Israel Nissan — Kimron Veterinary Institute, Ministry of Agriculture and Rural Development, Israel

Fernando Reyes — Fundación MEDINA, Spain

Avi Peretz — The Baruch Padeh Medical Center, Poriya, Israel

Citation

Nissan, I., Reyes, F., Peretz, A., eds. (2026). *Innovation in tackling the global challenge of eradicating antibiotic-resistant microorganisms*.

Lausanne: Frontiers Media SA. doi: 10.3389/978-2-8325-7418-8

Table of contents

frontiers | Frontiers in Microbiology

TYPE Editorial
PUBLISHED 12 January 2026
DOI 10.3389/fmicb.2025.1774105

OPEN ACCESS

EDITED AND REVIEWED BY
Rustam Aminov,
University of Aberdeen, United Kingdom

*CORRESPONDENCE
Israel Nissan
✉ israel.nissan@gmail.com

RECEIVED 23 December 2025
ACCEPTED 26 December 2025
PUBLISHED 12 January 2026

CITATION
Nissan I and Peretz A (2026) Editorial: Innovation in tackling the global challenge of eradicating antibiotic-resistant microorganisms.
Front. Microbiol. 16:1774105.
doi: 10.3389/fmicb.2025.1774105

Editorial: Innovation in tackling the global challenge of eradicating antibiotic-resistant microorganisms

Israel Nissan[1]* and Avi Peretz[2]

[1]Department of Avian Diseases, Kimron Veterinary Institute, Beit Dagan, Israel, [2]Clinical Microbiology Laboratory, Tzafon Medical Center, Poriya, Tiberias, Affiliated with Azrieli Faculty of Medicine, Bar Ilan University, Safed, Israel

KEYWORDS

AMR, bacteriophage, genomic epidemiology, metagenomics, NGS, One Health, repurposed therapeutics, stewardship

Editorial on the Research Topic
Innovation in tackling the global challenge of eradicating antibiotic-resistant microorganisms

Antimicrobial resistance (AMR) is no longer a distant risk; it is a daily constraint on routine clinical care, animal and plant health and the safety of food systems. The World Health Organization ranked AMR among the top global public health and development threats, with an estimated 1.27 million deaths directly attributable to bacterial AMR and 4.95 million AMR-associated deaths in 2019. These threats do not distribute evenly due to gaps in prevention infrastructure, diagnostics and access to effective therapy, resulting in heaviest burden on low-resource settings. In contrast, resistant pathogens and mobile resistance elements ignore borders and travel with patients, animals, food, water and trade.

In parallel, antibiotic innovation has been slow, with only 12 new antibacterial drugs approved between 2017 and 2021, most belonging to existing classes where resistance mechanisms are already established. This tension between rising resistance and limited therapeutic novelty, is pushing the field toward a dual mandate, namely, improving stewardship, prevention and diagnostics, while expanding the therapeutic and surveillance toolbox with alternatives to classic small-molecule antibiotics, new targets and One Health approaches that address reservoirs beyond the hospital.

This Research Topic, "*Innovation in tackling the global challenge of eradicating antibiotic-resistant microorganisms*," presents 15 papers that reflect that broadened demands of innovation. The contributions span bacterial and fungal pathogens, hospitals, communities, soils and crops, with methods ranging from bacteriophage therapeutics and phage-derived enzymes to hybrid genome assembly, metagenomics, microbiome analytics and implementation of focused stewardship research. Together, they show that progress against AMR will require a combination of complementary tools, validated under real-world biological and operational constraints.

Bacteriophages and phage-derived antibacterials: precision that faces biofilm reality

Bacteriophages are often framed as "precision antibacterials," with performance depending on host range, bacterial physiology, clinical workflow and biofilm architecture. Using isothermal microcalorimetry, Lafranca et al. quantify the efficacy of a commercial phage cocktail against skin pathogens in planktonic culture and both thin and thick biofilms, and found that biofilm thickness and maturity can limit phage impact. They also noted that chronic wound settings may require biofilm disruption (e.g., mechanical debridement) to create conditions conducive to phage activity.

Two additional phage studies focus on the hypervirulent and multidrug-resistant *Klebsiella pneumoniae*. Peng et al. report the isolation, characterization and genomic analysis of a novel lytic phage (vB_Kp_XP4) targeting *K. pneumoniae*, and demonstrate that genomic inspection can support safer and more rational phage selection for therapeutic development. At the population level, Tellez-Carrasquilla et al. combine lytic phages with high activity against high-risk, globally disseminated *K. pneumoniae* clones (CG258 and ST307), and emphasize the essentiality of cocktail design and performance testing when lineages co-circulate and diversify.

In a plant-health context, Liu L. et al. investigate bacteriophage LDT325 as a biocontrol strategy against *Pseudomonas syringae*-associated bud blight in tea (*Camellia sinensis*). Their work links phage treatment to improved antioxidant defenses and enhanced disease tolerance, which can indirectly reduce antimicrobial use, selection and dissemination across agricultural and environmental interfaces.

Finally, the Topic includes a forward-looking perspective on "enzybiotics"—phage-derived lytic enzymes that may offer controllable, protein-based antibacterials. Bałdysz et al. argue that enzybiotic bioinformatics must mature to include better annotation standards, curated datasets and benchmarking that connects *in silico* predictions to measurable antimicrobial activity.

Genomic epidemiology and resistome intelligence: tracking genes, plasmids, and transmission

Several papers in this Research Topic sharpen surveillance scope and capacities by addressing elements that traverse wards, institutions and bacterial lineages. Piispa et al. use hybrid genome assembly to resolve plasmids carrying carbapenemase genes across Enterobacterales isolated from patients and from multiple Finnish healthcare environments. Two complementary clinical datasets illustrate implications of local epidemiology on day-to-day decision-making. Liu Z. et al. analyze the distribution and resistance profiles of bacteria isolated from ICU blood cultures over several years, and provide evidence that can refine empiric therapy and stewardship in high-risk settings. Qiu et al. characterize carbapenem resistance mechanisms in clinical *K. pneumoniae* isolates and examine genotypic-phenotypic correlations and transmission patterns. Together, these studies reinforce the need for strict surveillance of "units of spread," which can be a clone, lineage, plasmid, or even an ecological reservoir.

One Health perspectives: plants, soils, and livestock as AMR arenas

Using metagenomics, Yu et al. profile soil microbial communities, antibiotic resistance genes and virulence factors in tea plantation soils after two decades of conventional vs. organic management. Their work shows how agricultural practice and environmental conditions can shape the background resistome, i.e., the genetic "starting point" from which resistance determinants may persist or spread.

Wagner et al. address reliance on relative abundances in standard 16S rRNA amplicon sequencing, which can be misleading when total microbial loads shift and is biased due to variable 16S copy numbers. By incorporating absolute abundance calculations, they show a substantially different inferred impact, both in magnitude and statistical significance, of antibiotic treatment on the fecal microbiota of young pigs. This methodological advance can reshape how we interpret intervention in human and veterinary medicine and, consequently, how we assess selection pressure and downstream AMR risk.

Stewardship and implementation: making innovation durable

Using an interrupted time-series approach, Abdelsalam-Elshenawy et al. examine how seasonal variation and the COVID-19 pandemic influenced antimicrobial stewardship activities and antibiotic prescribing for respiratory tract infections in a UK secondary care setting. Their results demonstrate that external shocks and seasonal pressures can rapidly shift prescribing behavior and therefore, stewardship programs must be designed to remain effective when routines are disrupted.

Novel or repurposed therapeutics and targets

Aloriby et al. evaluate the efficacy of *Olea europaea* and *Ficus carica* leaf extracts against multidrug-resistant pathogens through an integrated pipeline combining *in vitro* testing, *in vivo* toxicity assessment and *in silico* modeling. Their workflow illustrates a disciplined path for prioritizing plant-derived antimicrobial candidates.

Shaalan et al. examine three urease inhibitors (acetohydroxamic acid, ebselen and baicalin) and their effects on *Helicobacter pylori* viability, urease activity and urease gene expression.

Their insights can be applied to weaken colonization-critical functions which could complement antibiotic regimens and counteract the rising resistance-driven *H. pylori* treatment failure.

Wang et al. combine virtual screening targeting the transcriptional regulator AbaA, with experimental validation and transcriptomic analysis to identify small-molecule candidates active against *Sporothrix globosa* and to illuminate underlying response pathways. In *Candida glabrata*, Zheng et al. uncover a connection between tunicamycin-induced respiratory deficiency and reduced fluconazole tolerance, emphasizing that tolerance phenotypes can be governed by cellular physiology and may represent actionable vulnerabilities.

Outlook: integration is the strategy

These 15 papers do not claim a single solution for AMR. Instead, they offer a portfolio of approaches that resolve the vehicles of resistance, provide metagenomic views of environmental reservoirs, improve microbiome analytics, develop novel or repurpose molecules in both bacteriology and mycology and research system-level behavior.

The unifying message is both sobering and hopeful. No "silver bullet" will eradicate antibiotic-resistant microorganisms. Durable progress will arise from integration of new therapeutics with improved diagnostics, faster genomic surveillance and stewardship programs resilient to real-world pressures. By building bridges between bench and bedside, farm and clinic, genome and guidelines, the innovations showcased here can transition from promising studies to agents with sustained impact on the fight against antibiotic-resistant microorganisms.

Author contributions

IN: Project administration, Supervision, Writing – original draft, Writing – review & editing. AP: Project administration, Supervision, Writing – review & editing.

Conflict of interest

The author(s) declared that this work was conducted in the absence of any commercial or financial relationships that could be construed as a potential conflict of interest.

Generative AI statement

The author(s) declared that generative AI was used in the creation of this manuscript. AI was used to test and improve the text as well as for proofreading purposes.

Any alternative text (alt text) provided alongside figures in this article has been generated by Frontiers with the support of artificial intelligence and reasonable efforts have been made to ensure accuracy, including review by the authors wherever possible. If you identify any issues, please contact us.

Publisher's note

frontiers | Frontiers in Microbiology

TYPE Opinion
PUBLISHED 05 September 2024
DOI 10.3389/fmicb.2024.1474633

OPEN ACCESS

EDITED BY
Avi Peretz,
The Baruch Padeh Medical Center,
Poria, Israel

REVIEWED BY
Bozena Nejman-Falenczyk,
University of Gdansk, Poland

*CORRESPONDENCE
Sophia Bałdysz
✉ sopbal@amu.edu.pl;
✉ sophiabaldysz@gmail.com

RECEIVED 02 August 2024
ACCEPTED 26 August 2024
PUBLISHED 05 September 2024

CITATION
Bałdysz S, Dąbrowska K and Barylski J (2024) What do we need to move enzybiotic bioinformatics forward?
Front. Microbiol. 15:1474633.
doi: 10.3389/fmicb.2024.1474633

What do we need to move enzybiotic bioinformatics forward?

Sophia Bałdysz[1]*, Krystyna Dąbrowska[2] and Jakub Barylski[1]

[1]Department of Molecular Virology, Institute of Experimental Biology, Adam Mickiewicz University, Poznań, Poland, [2]Faculty of Medicine, Wroclaw Institute of Science and Technology, Wrocław, Poland

KEYWORDS

enzybiotic, bioinformatics, forward, consortium, lysins

Highlights

- Lytic enzymes are a promising alternative to treating antibiotic-resistant bacteria.
- Many tools and databases developed to study lysins are no longer maintained or outdated.
- This paper reviews the current state of endolysin computational methods.
- There is an opportunity for the scientific community to develop a tailored database for these proteins with coherent ontology.

In the age of increasing numbers of infections caused by antibiotic-resistant bacteria alternative strategies for combating these superbugs are in high demand. One of the most promising approaches involves the use of lytic enzymes, or simply enzybiotics such as autolysins, bacteriocins, endolysins, and virion-associated lysins, as well as biofilm degrading depolymerases. The effectiveness of such proteins has been proven in numerous *in vitro* studies, animal models, and several clinical trials (Murray et al., 2021; Schmelcher and Loessner, 2021; Liu et al., 2023). Unfortunately, enzybiotics targeting many important pathogens are still unavailable and identification of novel therapeutic proteins through traditional wet-lab methods is time-consuming and expensive. Publicly available databases provide access to millions of metagenomic sequences that could serve as a virtually inexhaustible source of novel lytic enzymes. However, identification of enzybiotic-coding sequences and matching them with susceptible bacteria still remains the major problem.

In previous years several bioinformatic tools have been developed for searching for bacteriolytic proteins. These included machine-learning based classifiers, designed to distinguish between lytic and non-lytic proteins based on the frequencies of amino acids within the proteins, as well as their order in the sequence (Lypred, CWLy-SVM, CWLy-pred and CWLy-RF) (Chen et al., 2016; Meng et al., 2020a,b; Jiao et al., 2021). Unfortunately, all of the tools used a very similar small, unbalanced, and barely curated collection of sequences to construct training and testing datasets. Additionally, one may wonder if authors of some of these tools (Chen et al., 2016) had enzymological knowledge required to critically evaluate bioinformatic results since they referred to lytic proteins as "lyases". Importantly, Lypred has not been updated since its release and the other tools are not available.

Currently, the only accessible tool is phiBiScan, which uses 16 models (profile hidden Markov models) representing conserved lysin-related domains to search for lytic proteins. Although versions of these models are regularly updated (the current version of this tool uses profiles from Pfam 35.0), the list of lysin-related domains has not been revised since its release in 2013 (Hojckova et al., 2013). It seems unlikely that just 16 domains reflect the entire diversity of lytic proteins observed in nature (Fernández-Ruiz et al., 2018; Bałdysz et al., 2024).

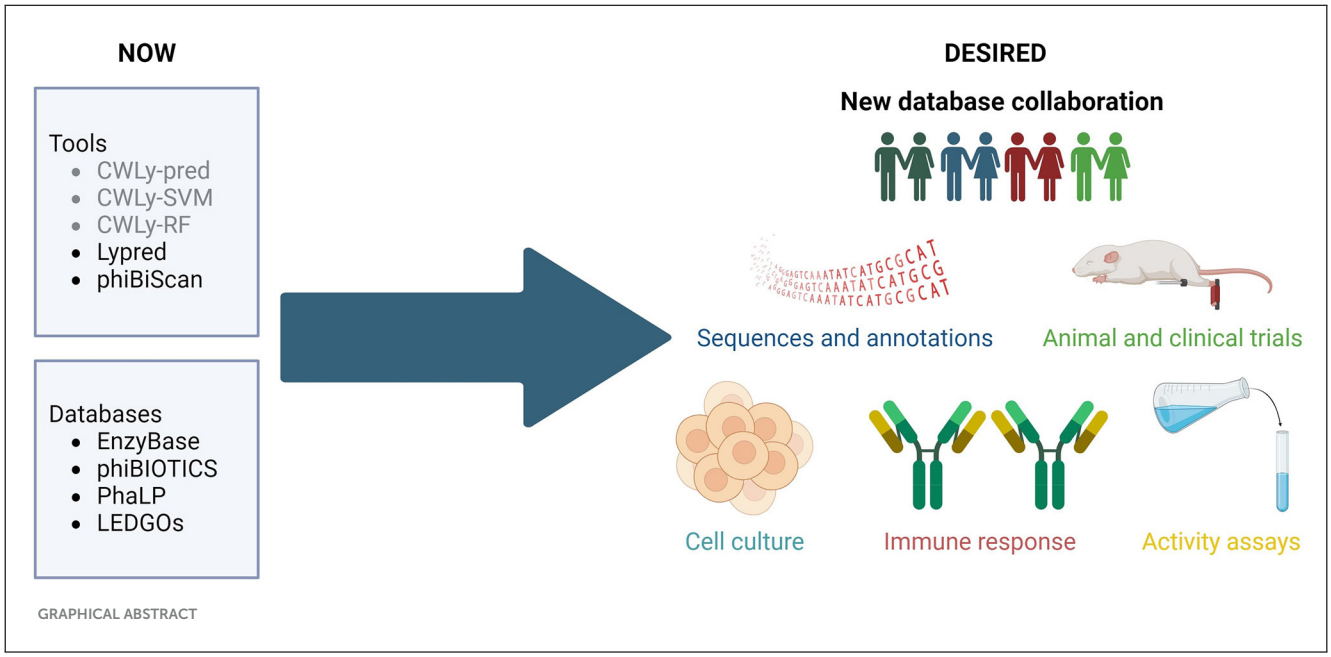

All of these examples demonstrate that although bioinformatic lytic protein detection tools have been developed, their use is restricted mainly to homologs of known proteins, and the repertoire of well characterized enzybiotics is rather limited. More importantly, it is difficult to assess the effectiveness of programs developed to identify enzybiotics because we simply do not have a representative test set of validated enzybiotic sequences.

The databases published up to date (EnzyBase, phiBIOTICS, PhaLP, and LEDGOs) (Wu et al., 2012; Hojckova et al., 2013; Criel et al., 2021; Mitchell et al., 2021) are either too small (e.g., hold <1,000 enzymes) and/or rely heavily on *in silico* annotation instead of experimental information. They are also taxonomically biased—only a handful of protein groups (e.g., against staphylococci) are well represented in these databases. What's more discouraging, the majority of the included sequences have been selected based merely on similarity but the real range of their activity has not been validated by wet-lab methods. Additionally, most lysin databases have not been updated in many years and some are no longer available. Obviously, the lack of large, well annotated, enzybiotic databases is particularly detrimental to the development of machine-learning tools, because these require comprehensive well-balanced training and test sets. The same can be concluded about the inconsistent, and poorly standardized metadata, which does not follow any formal ontology and often fails to track current taxonomy. Hence, although such lysin identification tools are desperately needed in the scientific market, they do not reach broader researchers' audiences and do not gain recognition.

The research community needs a representative and consistent database containing enzybiotic sequences, along with accurate, detailed annotations, wet-lab confirmation of the activity of the protein, and, if available, results from animal tests or clinical trials, along with other relevant information, like safety for human cells or immunogenicity.

We firmly believe that such a database shouldn't result from the work of one specialized group, to avoid bias from this group's specific scientific background. Instead, it should be a collective work of the larger community. Such an approach will ensure that the structure of the new database and the information stored within will cater for the needs of diverse groups, including enzymologists, bioinformaticians, machine-learning specialists, medical professionals or biotechnology and pharmaceutical companies. We firmly believe that collaboration between different laboratories, regular maintenance of tools and databases, as well as exploration of novel *in silico* methods may prompt flourishing of enzybiotics studies leading to numerous new breakthroughs. Therefore, we call for the creation of a consortium that will prepare a tailored database, guarantee its coherent, formalized ontology and sequence nomenclature, gather scattered sequences and integrate biochemical, molecular and evolutionary information, like domains and families. Current boom in language processing tools may also be a unique opportunity to include literature information in a consistent manner, while under careful supervision of human curators.

Author contributions

SB: Conceptualization, Formal analysis, Investigation, Writing – original draft, Writing – review & editing. KD: Conceptualization, Writing – original draft, Writing – review & editing. JB: Conceptualization, Writing – original draft, Writing – review & editing.

Funding

The author(s) declare that no financial support was received for the research, authorship, and/or publication of this article.

Conflict of interest

The authors declare that the research was conducted in the absence of any commercial or financial relationships that could be construed as a potential conflict of interest.

Publisher's note

References

Bałdysz, S., Nawrot, R., and Barylski, J. (2024). 'Tear down that wall'—a critical evaluation of bioinformatic resources available for lysin researchers. *Appl. Environm. Microbiol*. 90:7. doi: 10.1128/aem.02361-23

Chen, X. X., Tang, H., Li, W. C., Wu, H., Chen, W., Ding, H., et al. (2016). Identification of bacterial cell wall lyases via pseudo amino acid composition. *BioMed Res. Int*. 2016:1654623. doi: 10.1155/2016/1654623

Criel, B., Taelman, S., Van Criekinge, W., Stock, M., and Briers, Y. (2021). PhaLP: a database for the study of phage lytic proteins and their evolution. *Viruses* 13:1240. doi: 10.3390/v13071240

Fernández-Ruiz, I., Coutinho, F. H., and Rodriguez-Valera, F. (2018). Thousands of novel endolysins discovered in uncultured phage genomes. *Front. Microbiol.* 9:1033. doi: 10.3389/fmicb.2018.01033

Hojckova, K., Stano, M., and Klucar, L. (2013). phiBIOTICS: catalogue of therapeutic enzybiotics, relevant research studies and practical applications. *BMC Microbiol.* 13:53. doi: 10.1186/1471-2180-13-53

Jiao, S., Xu, L., and Ju, Y. (2021). CWLy-RF: a novel approach for identifying cell wall lyases based on random forest classifier. *Genomics* 113:2919–2924. doi: 10.1016/j.ygeno.2021.06.038

Liu, H., Hu, Z., Li, M., Yang, Y., Lu, S., and Rao, S. (2023). Therapeutic potential of bacteriophage endolysins for infections caused by gram-positive bacteria. *J. Biomed. Sci.*30:29. doi: 10.1186/s12929-023-00919-1

Meng, C., Guo, F., and Zou, Q. (2020a). CWLy-SVM: a support vector machine-based tool for identifying cell wall lytic enzymes. *Computat. Biol. Chem.* 87:107304. doi: 10.1016/j.compbiolchem.2020.107304

Meng, C., Wu, J., Guo, F., Dong, B., and Xu, L. (2020b). CWLy-Pred: a novel cell wall lytic enzyme identifier based on an improved MRMD feature selection method. *Genomics* 112, 4715–4721. doi: 10.1016/j.ygeno.2020.08.015

Mitchell, S. J., Verma, D., Griswold, K. E., and Bailey-Kellogg, C. (2021). Building blocks and blueprints for bacterial autolysins. *PLoS Comput. Biol.* 17:e1008889. doi: 10.1371/journal.pcbi.1008889

Murray, E., Draper, L. A., Ross, R. P., and Hill, C. (2021). The advantages and challenges of using endolysins in a clinical setting. *Viruses* 13:680. doi: 10.3390/v13040680

Schmelcher, M., and Loessner, M. J. (2021). Bacteriophage endolysins - extending their application to tissues and the bloodstream. *Curr. Opin. Biotechnol.* 68, 51–59. doi: 10.1016/j.copbio.2020.09.012

Wu, H., Lu, H., Huang, J., Li, G., and Huang, Q. (2012). EnzyBase: a novel database for enzybiotic studies. *BMC Microbiol.* 12:54. doi: 10.1186/1471-2180-12-54

frontiers | Frontiers in Microbiology

TYPE Original Research
PUBLISHED 15 November 2024
DOI 10.3389/fmicb.2024.1464484

OPEN ACCESS

EDITED BY
Gabriel Trueba,
Universidad San Francisco de Quito, Ecuador

REVIEWED BY
Silvia Di Lodovico,
"G. d'Annunzio" University of Chieti, Italy
Mikaeel Young,
Baylor University, United States

*CORRESPONDENCE
Avi Peretz
✉ aperetz@tzmc.gov.il

RECEIVED 14 July 2024
ACCEPTED 28 October 2024
PUBLISHED 15 November 2024

CITATION
Shaalan H, Azrad M and Peretz A (2024) The effect of three urease inhibitors on *H. pylori* viability, urease activity and urease gene expression. *Front. Microbiol.* 15:1464484. doi: 10.3389/fmicb.2024.1464484

The effect of three urease inhibitors on *H. pylori* viability, urease activity and urease gene expression

Hanaa Shaalan[1], Maya Azrad[2] and Avi Peretz[1,2]*

[1]The Azrieli Faculty of Medicine, Bar-Ilan University, Safed, Israel, [2]Clinical Microbiology Laboratory, Tzafon Medical Center, Poriya, Israel, Affiliated with Azrieli Faculty of Medicine, Bar Ilan University, Safed, Israel

Background: Treatment of *Helicobacter pylori* (*H. pylori*) infections is challenged by antibiotic resistance. The urease enzyme contributes to *H. pylori* colonization in the gastric acidic environment by producing a neutral microenvironment. We hypothesized that urease inhibition could affect *H. pylori* viability. This work aimed to assess the effects of acetohydroxamic acid (AHA), ebselen and baicalin on urease activity, bacterial viability and urease genes expression in *H. pylori* isolates.

Methods: Forty-nine *H. pylori* clinical isolates were collected. Urease activity was assessed using the phenol red method. The urease inhibition assay assessed inhibitors' effects on urease activity. Flow cytometry assessed the effect of inhibitors on bacterial viability. Real time PCR was used to compare urease genes expression levels following urease inhibition.

Results: Urease activity levels differed between isolates. Acetohydroxamic acid inhibited urease activity at a concentration of 2.5 mM. Although baicalin inhibited urease activity at lower concentrations, major effects were seen at 8 mM. Ebselen's major inhibition was demonstrated at 0.06 mM. Baicalin (8 mM) significantly reduced ATP production compared to untreated isolates. Baicalin, ebselen and acetohydroxamic acid significantly reduced *H. pylori* viability. Increased urease genes expression was detected after exposure to all urease inhibitors.

Discussion: In conclusion, higher concentrations of baicalin were needed to inhibit urease activity, compared to acetohydroxamic acid and ebselen. Baicalin, ebselen and acetohydroxamic acid reduced *H. pylori* viability. Therefore, these inhibitors should be further investigated as alternative treatments for *H. pylori* infection.

KEYWORDS

***Helicobacter pylori*, urease inhibitors, urease activity, bacterial viability, urease genes**

1 Introduction

Helicobacter pylori (*H. pylori*) is a Gram-negative, microaerophilic, spiral-shaped bacterium, which colonizes the human gastric mucosa (Malfertheiner et al., 2023) and is present in the gut of over 50% of the world population (García et al., 2014). While the infection is often asymptomatic, chronic infection can cause gastritis, gastric ulcer, mucosa-associated lymphoid tissue (MALT) lymphoma and gastric adenocarcinoma (Diaconu et al., 2017; Kusters et al., 2006). Currently accepted treatment for *H. pylori* infections is mostly a combination of proton pump inhibitor (PPI) with two antibiotics (clarithromycin, metronidazole or levofloxacin) (Lee et al., 2022; Azrad et al., 2022). Yet, many epidemiological studies have shown increased rates of *H. pylori* antibiotic resistance in recent years, which interferes with treatment efficacy (Azrad et al., 2022; Kuo et al., 2017).

H. pylori produces large quantities of urease (6–10% of the total protein) which converts urea into ammonia and carbamate, enabling the bacterium to survive in the acidic gastric environment by generation of a neutral microenvironment (Ansari and Yamaoka, 2017). In addition to its role in colonization, urease mediates inflammatory responses by activating monocytes and neutrophils, which elicit damage to the gastric epithelial cells (Lee and Buck, 1996).

Urease is a heterodimer composed of the UreA and UreB subunits, with two-nickel ions bound to the active site of each dimer (Ansari and Yamaoka, 2017; Woo et al., 2021). In addition to these two structural genes, the urease gene cluster contains seven accessory genes important for enzyme activation and insertion of the nickel ions (Collins and D'Orazio, 1993).

Due to its role in pathogenesis, urease has become an important target in the search for new antimicrobial agents to treat *H. pylori* infection. Several studies have demonstrated the inhibitory effects of many compounds, including natural products and synthetic drugs, against purified *H. pylori* urease (Follmer, 2010; Hassan and Šudomová, 2017). However, little is known about their performance in clinical *H. pylori* isolates. Urease inhibitors can be a substrate structure analog, which competes with urea over the active site, or a compound that interferes with the enzymatic reaction (Upadhyay, 2012).

Taking into consideration the importance of urease enzyme and the large number of studies that aimed to investigate the inhibitory effect of different compounds on purified *H. pylori* urease, our study aimed to elucidate the knowledge in this field by measuring urease activity of different clinical *H. pylori* isolates and investigating its association with infection severity. Additionally, three known *H. pylori* urease inhibitors, including natural and synthetic compounds, which differ in their inhibition mechanism, were chosen to assess their effect on 49 *H. pylori* clinical isolates, and investigated their effect on microbial cell viability. Acetohydroxamic acid (AHA) competitively inhibits urease by forming a complex with the enzyme's nickel ions (Suenaga et al., 2023; Kafarski, 2018). It is also a drug used to treat chronic urea-splitting urinary infections. It was approved by the Food and Drug Administration (FDA) as an orphan drug for the prevention of struvite stones (Marwick, 1983). Baicalin is a component of the root and aerial part of a medical plant known as *Scutellaria baicalensis*. It is considered a non-competitive inhibitor of *H. pylori* urease that interacts with Cys321 on the mobile flap of the enzyme (Yu et al., 2015). It was also reported to reduce gastric inflammation caused by *H. pylori* infection (Shih et al., 2007). Moreover, it has anti-inflammatory, anti-allergic, anti-oxidant and neuroprotective properties (Yu et al., 2015). Ebselen is a selenoorganic compound with anti-inflammatory, antioxidant, and cytoprotective activities (Macegoniuk et al., 2023). It acts as a competitive urease inhibitor that reacts with the nickel ions and cysteine 322 in the enzyme active site (Macegoniuk et al., 2016). In addition to its anti-urease activity, its antiulcer properties were demonstrated in a rat model (Tabuchi and Kurebayashi, 1993).

2 Materials and methods

2.1 Urease inhibitors

AHA, baicalin and ebselen were purchased from Acros Organics (Geel, Belgium). AHA was dissolved in double distilled water (DDW) to create a stock solution of 20 mM. Baicalin and ebselen were dissolved in 1% dimethyl sulfoxide (DMSO) (Sigma-Aldrich, Louis, USA) to create stock solutions of 16 mM for baicalin, and 0 0.25 mM for ebselen. The prepared solutions (Table 1) were stored at −20°C until further use. The concentrations were chosen based on previous reports (Yu et al., 2015; Macegoniuk et al., 2016; Goldie et al., 1991).

2.2 Bacterial isolates

Forty-nine clinical *H. pylori* isolates were randomly chosen from the isolates bank of the clinical microbiology laboratory at the Tzafon Medical Center. The isolates had been previously isolated from gastric specimens of patients undergoing gastroscopy between January 2018 and December 2021, due to symptomatic gastroduodenal pathologies. Histological data regarding infection severity was collected from patient records. The study was approved by the Medical Center Helsinki Committee, Approval no. POR 0007-20. ATCC strain 43504 (American Type Culture Collection, USA) served as a positive control.

2.3 Bacterial culture

H. pylori isolates were grown from frozen bead stocks on modified BD Helicobacter agar (Becton Dickinson, Heidelberg, Germany), and incubated under microaerophilic conditions, at 37°C, for 7 days. Then, colonies were harvested and suspended in brain-heart infusion broth supplemented with yeast extract and 0.1% L-cysteine (BHIS) (Hy Laboratories Ltd., Rehovot, Israel) or with phosphate buffered saline (PBS) (Biological Industries, Beit-Haemek, Israel).

2.4 Urease activity assay

Urease activity was determined using the phenol red method (Chang et al., 2020). In brief, *H. pylori* isolates were grown on modified BD Helicobacter agar for 7 days under microaerophilic conditions at 37°C, and then diluted in PBS (Biological Industries) to achieve 1 McFarland turbidity. The assay was carried out in 96-well plates, wherein a *H. pylori* suspension (50 μl/well) was mixed with 50 μl/well urease test broth (Novamed, Jerusalem, Israel) which contained a pH indicator (phenol red) and the urease substrate (urea). In case of urease activity, the pH rises, and the solution color changes from yellow to pink. Optical density (OD) at 570 nm was measured every minute, for 20 min, using a Multiskan FC microplate reader (Thermo

TABLE 1 Tested urease inhibitor concentrations.

Urease inhibitor	Concentration I (mM)	Concentration II (mM)	Concentration III (mM)
Acetohydroxamic acid	2.5	5	10
Baicalin	2	4	8
Ebselen	0.03125	0.0625	0.125

Scientific, Waltham, USA). Urease activity was calculated using the following equation:

$$Urease\ activity = OD_{570\text{nm}}\ (max) - OD_{570\text{nm}}\ (min)$$
$$OD_{\max} = OD_{t=20};\ OD_{\min} = OD_{t=0}$$

2.5 Urease inhibition assay

A bacterial suspension of one McFarland turbidity was prepared as described above. *H. pylori* isolates (50 μl) were incubated with 50 μl of each inhibitor (50 μM-20 mM) for 15 min in 96-well plates, under microaerophilic conditions, at 37°C. Urease activity was measured as described above. Control wells contained bacterial suspension and DDW (without inhibitor). Blank wells contained inhibitor and PBS.

2.6 Microbial cell viability assay

The BacTiter-Glo™ Microbial Cell Viability Kit (Promega, Madison, USA) was used to determine the number of viable microbial cells based on ATP quantification. *H. pylori* colonies, grown as described above, were suspended in BHIS to McFarland 1 turbidity. The bacterial suspension (50 μl) was then incubated with 50 μl of the inhibitor or 50 μl DDW (control), in triplicates, in a 96-well plate, for 24 h, under microaerophilic conditions. BacTiter-Glo™ Reagent (100 μl) was placed in each well, and luminescence was recorded using the Fluoroskan™ FL Microplate Fluorimeter and Illuminometer (Thermo Fisher Scientific, *Waltham,* USA).

2.7 Flow cytometry

Flow cytometry was performed to determine bacterial viability following exposure to urease inhibitors compared to untreated isolates, in representative isolates ($n = 10$). *H. pylori* suspension (100 μl) at 0.6 McFarland turbidity was incubated in a tube with 100-μl urease inhibitor for 24 h, under microaerophilic conditions. Then, tubes were centrifuged and the pellet was resuspended in 200-μl NaCl 0.9% and then diluted 10-μl suspension in 477 μl NaCl 0.9%. A mixture of 1.5 μl SYTO®9 green fluorescent nucleic acid stain (for live bacteria) and 1.5 μl red-fluorescent nucleic acid stain, propidium iodide (PI) (for dead bacteria) (Thermo Fisher Scientific, Waltham, Massachusetts, United States) was then mixed with the suspension, to stain the bacteria. Flow cytometry was performed using a Gallios Flow Cytometer (Beckman Coulter, Indianapolis, USA), with excitation/emission wavelengths of 488/520 nm for SYTO®9 and 488/>630 nm for PI.

TABLE 2 Primers used for real-time qPCR reactions.

Gene	Forward primer (5′-3′)	Reverse primer (5′-3′)
ureA	CGTGGCAAGCATGATCCAT	GGGT ATGCACGGTTACGAGTTT
ureB	TCTATCCCTACCCCACAACC	CCATCCACGAACACATGGTA
16s	TATGACGGGTATCCGGC	ATTCCACTTACCTCTCCCA

2.8 Quantitative real-time PCR

Urease gene (*ureA*, *ureB*) expression levels in representative isolates were quantified using RT PCR. Briefly, *H. pylori* isolate suspensions in BHIS were incubated with each urease inhibitor, for 24 h, as described above. Then, total RNA was extracted from suspensions using the RNeasy Mini Kit (QIAGEN, Hilden, Germany) and then reverse-transcribed using the qPCRBIO cDNA Synthesis Kit (PCR Biosystems Inc, Pennsylvania, USA). Each real-time qPCR reaction included 10 μl PowerUp™ SYBR™ Green Master Mix (Thermo Fisher Scientific, Baltics, UAB), 0.5 μl primers (forward, and reverse, at final concentration of 500 nm each; Table 2) (Hy Laboratories), 4 ng cDNA and water to a final volume of 20 μl. The 16s rRNA gene served as a housekeeping gene. The PCR was performed using the CFX96 Real-Time PCR System (Bio Rad, California, USA), under the following conditions: for *16s* and *ureB* −95°C for 15 s, 58°C for 15 s and 72°C for 1 min, 40 cycles and for *urea* −95°C for 15 s, and 60°C for 1 min, 40 cycles. Results were analyzed using the ΔΔCt method.

2.9 Statistical analysis

The analysis of variance (ANOVA) test was applied to identify differences in urease activity between the different isolates and between urease inhibitor-treated and untreated isolates. The ANOVA test was also applied to assess differences in ATP production and bacterial cell viability between urease inhibitor-treated vs. untreated isolates. *T*-test was applied to compare gene expression levels of urease inhibitor-treated vs. control isolates, for each inhibitor. All tests applied were two-tailed, and a *p*-value of 5% or less was consider statistically significant. The data were analyzed using the Graphpad Prism software, version 9.5.1.733 (GraphPad Software, Florida, Boston, MA).

3 Results

3.1 Urease activity of the clinical isolates and association with infection severity

The clinical isolates exhibited urease activity in the range of 0.04–0.09 (arbitrary units) (Figure 1A). No significant association was found between urease activity and infection severity (Figure 1B).

3.2 Inhibition of urease activity in clinical isolates by the different inhibitors

3.2.1 Acetohydroxamic acid

Urease activity of isolates was significantly lower in AHA-treated isolates compared to untreated bacteria. Almost full inhibition (84% reduction) was already achieved at an inhibitor concentration of 2.5 mM ($p < 0.001$) (Figure 2A). There was no significant difference in the effect of the three tested concentrations on urease activity (Figure 2B).

3.2.2 Baicalin

During the first 15 min of the assay, urease activity in isolates treated with 2 mM or 4 mM baicalin was lower than urease activity of controls. However, at 20 min, they reached the same levels of activity as those of controls (Figure 3A). From a concentration of 2 mM, baicalin significantly inhibited urease activity, with a 50% reduction in activity measured upon treatment with 8 mM baicalin ($p < 0.001$) (Figure 3B).

3.2.3 Ebselen

Significantly reduced urease activity was measured throughout the entire assay, in all isolates treated with any of the three tested concentrations of ebselen (Figure 3C). Even at the low concentration of 0.03 mM, a 71% reduction from control was measured in urease activity ($p < 0.001$) (Figure 3D).

3.3 Effect of urease inhibitors on ATP production in clinical isolates

To determine whether the urease inhibitors affect bacterial cell viability, ATP production was measured is an indicator of cell metabolism. ATP levels in isolates following incubation baicalin 8 mM were significantly lower compared to their levels in untreated control cells. In contrast, AHA 2.5 mM and ebselen 0.06 mM had no effect on bacterial cell activity (Figure 4).

3.4 Effect of urease inhibitors on clinical isolate cell viability

Exposure to urease inhibitors significantly decreased the percentage of live bacteria compared to untreated bacteria (Figure 5A; Table 3). For example, exposure to AHA resulted in 21.9% live cells, as compared to the control untreated strains, in which 74.4% of the cells were viable. The greatest decrease (61.82% decrease and 60.97% decrease, respectively) in the percentage of viable bacteria was observed following baicalin and ebselen treatment ($p < 0.001$) (Figure 5B).

3.5 Urease gene expression following exposure of clinical isolates to urease inhibitors

ureA and *ureB* gene expression was upregulated in cells exposed to urease inhibitors. However, this increase was only statistically significant in baicalin-treated isolates, where 3-fold increase compared to control were measured for both genes ($p < 0.05$) (Figure 6).

4 Discussion

Antibiotic resistance poses an increasing challenge to the effectiveness of *H. pylori* treatment. The search for alternative treatments has become crucial and many researchers have focused on urease inhibition (Woo et al., 2021; Kafarski, 2018; Svane et al., 2020). In contrast to previous studies that investigated urease inhibitors on enzymes, mostly purified from a limited number of strains, the present study assessed the effects of three inhibitors on urease enzymes of 49 clinical isolates.

4.1 Urease activity and infection severity

While the different isolates exhibited different levels of urease activity, no association was found between urease activity and infection severity. In contrast, previous studies showed a correlation between urease activity and disease severity (Ito et al., 1995; Ghalehnoei et al., 2016; Igarashi et al., 2001). For example, one study found higher urease activity in *H. pylori* strains isolated from patients with intestinal metaplasia, compared to isolates from patients with peptic ulcer disease (Ghalehnoei et al., 2016). Another study measured higher urease activity in *H. pylori* isolates from oncology patients compared to than isolates from duodenal ulcer patients (Ito et al., 1995). Although no such association was found here, a correlation may exist between the disease severity and other virulence factors, such as Cag A and Vac A as presented in other studies (Ghalehnoei et al., 2016; Roshrosh et al., 2023).

4.2 Inhibition of urease activity by AHA, ASA, baicalin and ebselen

This study focused on three urease inhibitors. AHA is a competitive inhibitor that forms a complex with nickel ions in the metallo-center of the enzyme (Suenaga et al., 2023; Kafarski, 2018) and is used to treat chronic urea-splitting urinary infections. Zhou et al. (2017) ound that a concentration of 0.07 mM AHA was needed

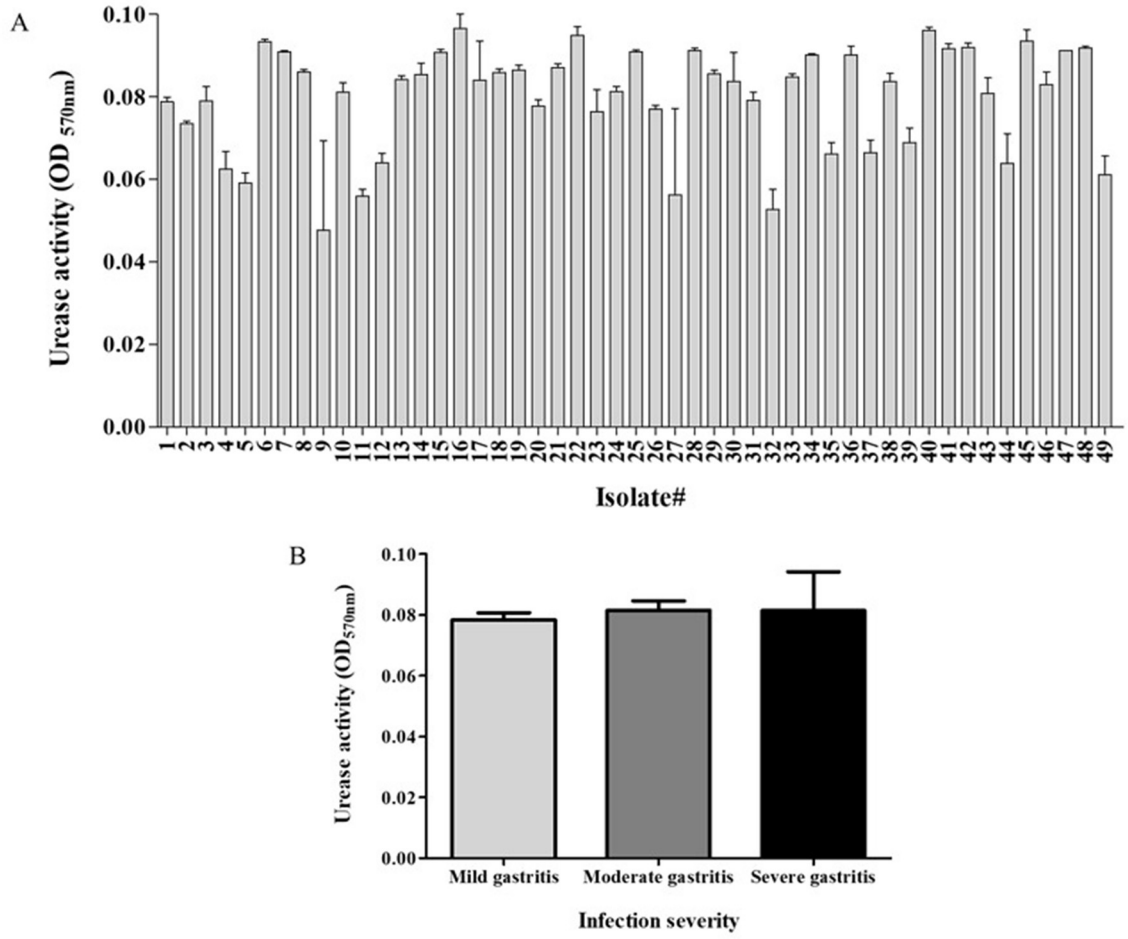

FIGURE 1
Urease activity of study's isolates and relation to disease severity. Activity of *H. pylori* urease was measured as the difference between the optical density measured in 570 nm- OD_{570} ($t = 20$ min) and initial OD_{570} ($t = 0$). **(A)** The urease activity of the different isolates. **(B)** Urease activity in relation to infection severity. Each experiment was conducted in triplicates, $n = 49$.

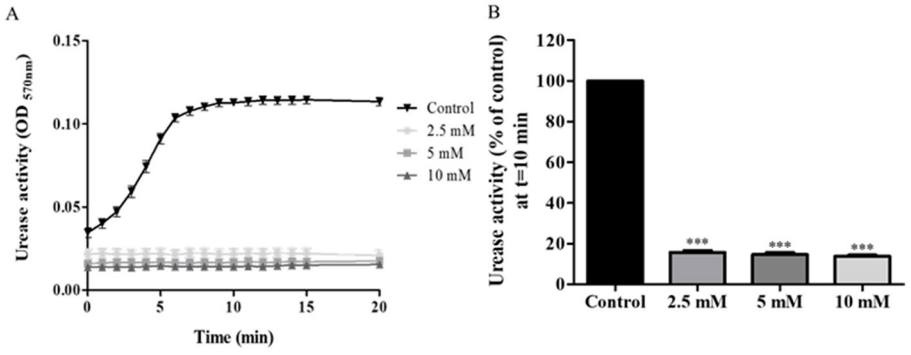

FIGURE 2
Urease activity of acetohydroxamic acid (AHA)-treated. *H. pylori* isolates were treated with different concentration of AHA for 15 min, then urease activity was assessed over 20 min by measuring OD_{570nm}. **(A)** A representative graph of urease activity of one isolate, which was treated, with three different concentrations of AHA or untreated (Control). **(B)** Urease activity of 49 isolates treated for 10 min, with three different concentrations of AHA for 15 min was detected at $t = 10$ min and compared to the control (untreated). ***$p < 0.001$, $n = 49$. Each experiment was conducted in triplicates. AHA, acetohydroxamic acid.

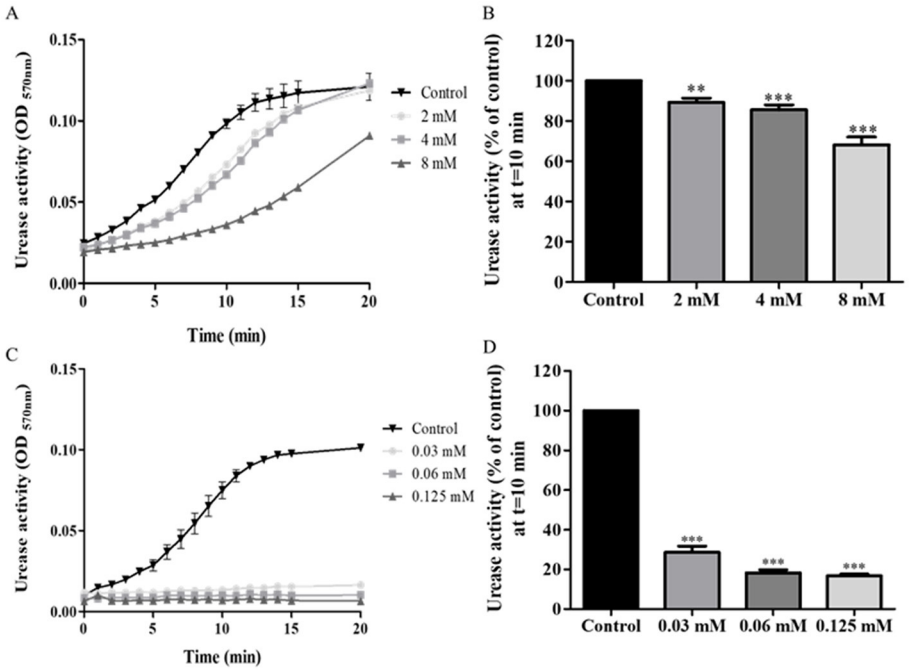

FIGURE 3
Urease activity of isolates treated with baicalin and ebselen. *H. pylori* isolates were treated with different concentration of baicalin or ebselen for 15 min, and then urease activity was detected by measuring OD at 570 nm, during 20 min. **(A)** A representative graph of urease activity of one isolate, which was treated with baicalin at three different concentrations or untreated (Control). **(B)** Urease activity of the isolates treated with three different concentrations of baicalin for 15 min was detected at $t = 10$ min and compared to the control (untreated). **(C)** A representative graph of urease activity of one isolate which was treated with ebselen at three different concentrations for 15 min or untreated (Control). **(D)** Urease activity of the isolates treated with three different concentrations of ebselen for 15 min was detected at $t = 10$ min and compared to the control (untreated), $^{***}p < 0.001$, $n = 49$. Each experiment was conducted in triplicates. $^{**}p < 0.01$.

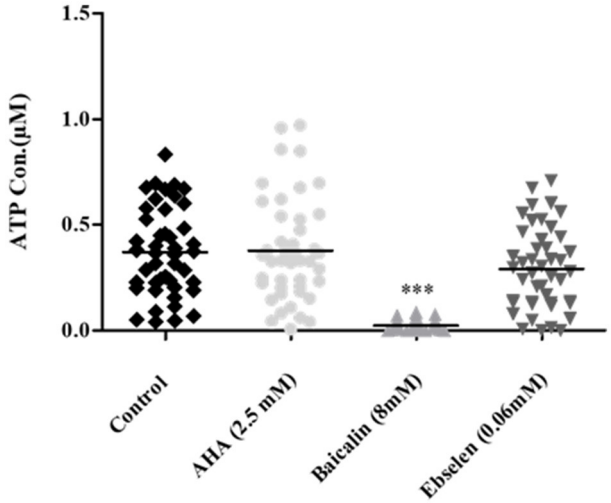

FIGURE 4
ATP production in *H. pylori* isolates treated with urease inhibitors. Isolates were treated with the minimal urease inhibitory concentration of each inhibitor (AHA = 2.5 mM, baicalin = 8 mM and ebselen = 0.06 mM) for 24 h. ATP concentration was determined by luminescence. Untreated isolates served as control. $^{***}p < 0.001$, $n = 47$. AHA, Acetohydroxamic acid.

to achieve 50% urease inhibition. Another study reported that the ideal AHA inhibition concentration was 2.6 mM (Goldie et al., 1991), almost the same as the concentration found most effective in the current study.

Baicalin has anti-inflammatory, anti-allergic and anti-oxidant properties. The compound is a non-competitive inhibitor which interacts with Cys321 on the mobile flap of urease (Yu et al., 2015). A previous work measured 0.82 mM as the IC_{50} of baicalin toward purified *H. pylori* urease, a concentration much lower than the present results (Yu et al., 2015).

Ebselen is a competitive inhibitor, reacting with the nickel ions and cysteine322 (Macegoniuk et al., 2016), and induces anti-inflammatory, antioxidant and cytoprotective effects. Biernat et al. found reported that the IC_{50} of ebselen toward *H. pylori* urease at time zero was 45 and 3.69 µM if the cells were preincubated with ebselen for 2 h (Macegoniuk et al., 2016). The authors concluded that the difference in the concentrations needed for inhibition was due to the time needed for diffusion of the inhibitor through the bacterial membrane. This finding underscores the importance of the present analysis of clinical isolates, as most previous studies tested the effects of inhibitors on purified urease.

The inhibition mode of each compound was reflected in the results. AHA and ebselen, both competitive inhibitors, achieved almost full inhibition of urease, even at very low

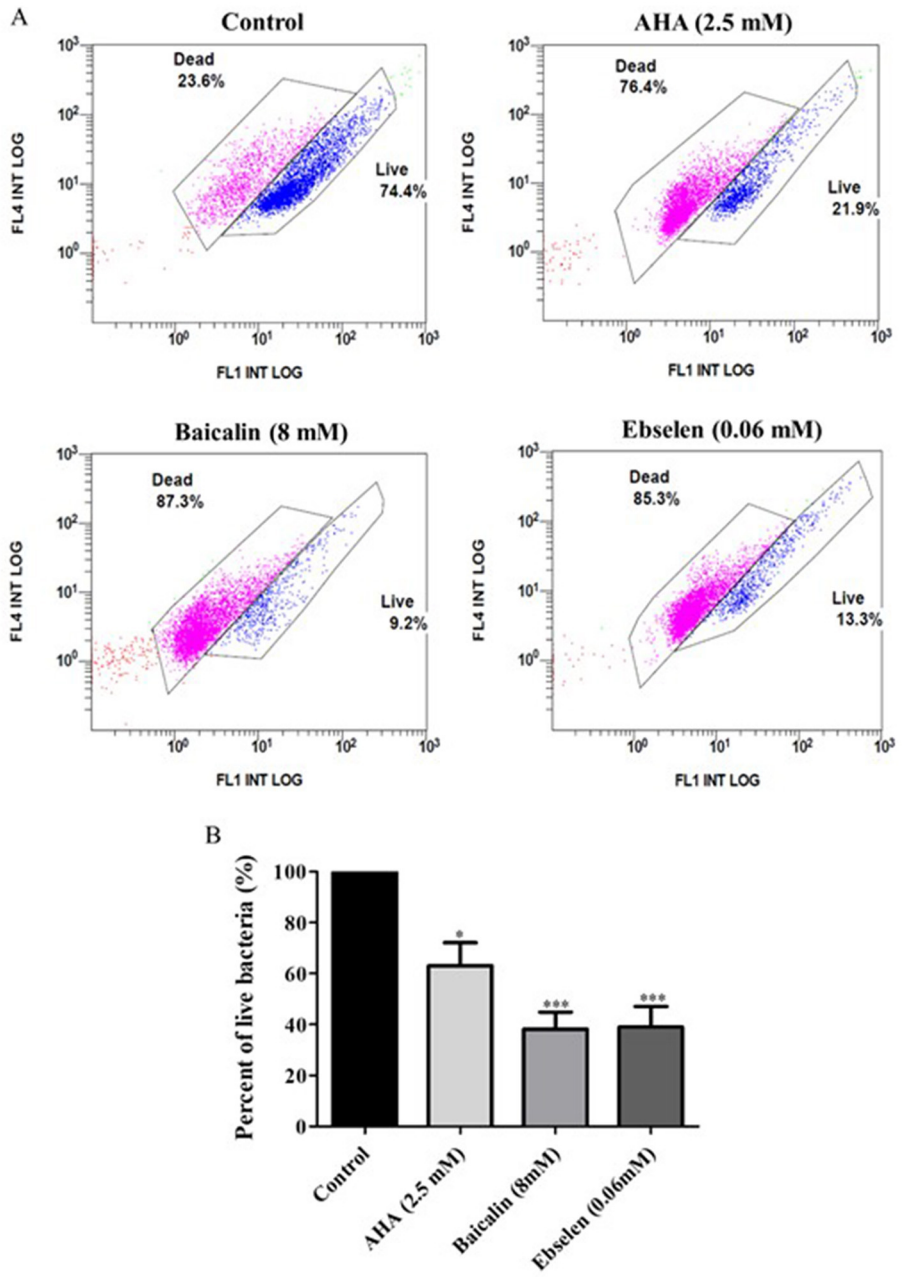

FIGURE 5
Viability of bacterial isolates treated with different urease inhibitors. Viability of bacterial isolates treated with different urease inhibitors. *H. pylori* representative isolates were incubated with urease inhibitors for 24 h (AHA = 2.5 mM, baicalin = 8 mM or ebselen = 0.06 mM) and then bacterial viability was measured by flow cytometry. The graphs in **(A)** present viable (blue) and dead (pink) cells of Control (untreated isolates), 2.5 mM AHA-treated isolates, 8 mM baicalin-treated isolates, and 0.06 mM-ebselen treated isolates. Propidium iodide, which stains dead bacteria, was detected by the FL4 channel, and SYTO9, which stains live bacteria, was detected by the FL1 channel. The graph in **(B)** present the percent of live bacteria in isolates treated with urease inhibitors, compared to control. *$p < 0.05$, ***$p < 0.001$, $n = 10$. AHA, acetohydroxamic acid.

concentrations, with no significant differences measured between the different tested inhibitor concentrations. In comparison, the urease inhibition capacity of baicalin, a non-competitive inhibitor, differed at the three tested concentrations, with significant urease inhibition achieved only at high concentrations. Interestingly, the effect of the inhibitors was not uniform across all the 49 isolates; in some cases, the treatment had a noticeable inhibitory effect on some isolates but no effect on other isolates. For example, after treatment with 2.5 mM AHA, <80% urease inhibition was measured in 10 isolates, 80–90% inhibition in 29 isolates and above 90% inhibition in 10 isolates. These differences may be associated with the expression and activities of other virulence factors of the bacterium, which protect against urease inhibition.

TABLE 3 Effect of urease inhibitors on bacterial cell viability.

Control	AHA (2.5 mM)	Baicalin (8 mM)	Ebselen (0.06 mM)
100%	63.5%	26.68%	38.6%
100%	67%	47.62%	25.21%
100%	63.36%	28%	79.13%
100%	7.811%	5.6%	19.76%
100%	74.42%	38.24%	67.33%
100%	87.47%	54.92%	74.29%
100%	15.02%	31.68%	8.64%
100%	87.03%	44.76%	35.02%
100%	80.03%	21.05%	27.78%
100%	84.52%	83.25%	14.55%

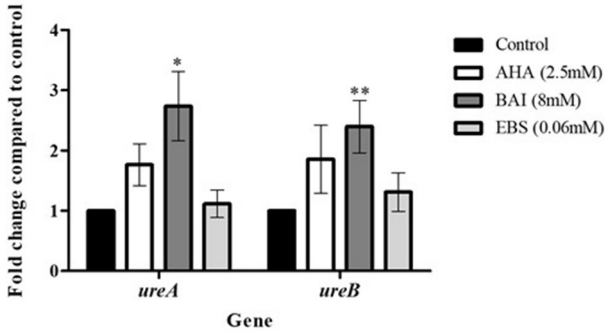

FIGURE 6
Urease genes expression following exposure to urease inhibitors. Urease genes expression following exposure to urease inhibitors. *H. pylori* isolates were treated with urease inhibitors for 24 h, then RNA was extracted and real-time PCR was performed to detect the expression levels of *ureA*, *ureB* and the housekeeping gene *16s*. *$p < 0.05$, ** $p < 0.01$, $n = 13$. AHA, acetohydroxamic acid; BAI, Baiclain; EBS, Ebselen.

4.3 Effect of urease inhibitors on bacterial cell viability

Several studies assessed the effect of urease inhibitors on *H. pylori* growth (Woo et al., 2021), morphology (Tran Trung et al., 2020), viability (Goldie et al., 1991), and adhesion to gastric epithelial cells (Chang et al., 2020). In the present study, the lowest inhibitor concentration that showed a significant inhibitory effect on enzyme activity, was applied to test its effect on *H. pylori* viability. Ebselen and AHA, which had a notable inhibitory effect at very low concentrations, did not reduce ATP production, but did reduced bacterial cells viability. In contrast, baicalin, which only inhibited urease activity at high concentrations, significantly reduced ATP production. From these results, it can be concluded that ATP production is not necessarily an indicator of cell viability and that urease inhibition does not necessarily correlate with *H. pylori* eradication. Exposure to stressful conditions may have different effects on bacterial community; on one hand, it can reduce bacterial viability, however on the one hand it may alter a survival mechanism to produce a large amount of ATP. Thus, in order to choose an effective urease inhibitor for *H. pylori* infection treatment, its effect on bacterial cell viability should be taken into consideration.

4.4 Effect of urease inhibition on urease gene expression levels

H. pylori urease consists of six copies of two structural subunits (*Ure*A and *Ure*B), with two nickel ions in the UreB subunit, in addition to six accessory subunits (*Ure*E, *Ure*F, *Ure*G, *Ure*I, *Ure*D) (Mobley et al., 1995). Examination of the effect of urease inhibition on *ureA* and *ureB* gene expression found that only baicalin significantly increased gene expression. Such upregulation may be a bacterial mechanism to compensate for inhibited urease activity.

5 Conclusions

In this study, we showed that the three compounds, AHA, baicalin and ebselen have an inhibitory effect on *H. pylori* urease. AHA and ebselen were more potent compared to baicalin. Baicalin, AHA, and ebselen significantly reduced *H. pylori* viability, and further study should investigate their usefulness for eradication of *H. pylori* infection. Additional studies are still needed to assess the effect of these inhibitors on human host cells.

6 Limitations of the study

One limitation of this study is the narrow spectrum of inhibitors concentrations; it is important to check more concentrations to assess the maximum and minimum inhibitory concentration of each inhibitor. Moreover, no additional pathogenic factors were taken into account in this study, for example, we didn't check correlations of our results with CagA and flagella. Future studies are needed to check these correlations.

Data availability statement

The original contributions presented in the study are included in the article/supplementary material, further inquiries can be directed to the corresponding author.

Ethics statement

The studies involving humans were approved by the Tzafon Medical Center Helsinki Committee, Approval No. POR 0007-20. The studies were conducted in accordance with the local legislation and institutional requirements. The ethics committee/institutional review board waived the requirement of written informed consent for participation from the participants or the participants' legal guardians/next of kin because the study investigated bacterial isolates without patients' data.

Author contributions

HS: Conceptualization, Data curation, Formal analysis, Investigation, Methodology, Project administration, Supervision, Validation, Visualization, Writing – original draft, Writing – review & editing. MA: Conceptualization, Data curation, Formal analysis, Investigation, Methodology, Project administration, Supervision, Validation, Visualization, Writing – original draft, Writing – review & editing. AP: Conceptualization, Data curation, Formal analysis, Investigation, Methodology, Project administration, Supervision, Validation, Visualization, Writing – original draft, Writing – review & editing.

Funding

The author(s) declare that no financial support was received for the research, authorship, and/or publication of this article.

Conflict of interest

The authors declare that the research was conducted in the absence of any commercial or financial relationships that could be construed as a potential conflict of interest.

Publisher's note

All claims expressed in this article are solely those of the authors and do not necessarily represent those of their affiliated organizations, or those of the publisher, the editors and the reviewers. Any product that may be evaluated in this article, or claim that may be made by its manufacturer, is not guaranteed or endorsed by the publisher.

References

Ansari, S., and Yamaoka, Y. (2017). Survival of *Helicobacter pylori* in gastric acidic territory. *Helicobacter* 22:12386. doi: 10.1111/hel.12386

Azrad, M., Vazana, D., On, A., Paritski, M., Rohana, H., Roshrosh, H., et al. (2022). Antibiotic resistance patterns of *Helicobacter pylori* in North Israel – A six-year study. *Helicobacter* 27, 1–8. doi: 10.1111/hel.12932

Chang, S. H., Hsieh, P. L., and Tsai, G. J. (2020). Chitosan inhibits *Helicobacter pylori* growth and urease production and prevents its infection of human gastric carcinoma cells. *Mar. Drugs* 18:542. doi: 10.3390/md18110542

Collins, C. M., and D'Orazio, S. E. (1993). Bacterial ureases: structure, regulation of expression and role in pathogenesis. *Mol. Microbiol.* 9, 907–913. doi: 10.1111/j.1365-2958.1993.tb01220.x

Diaconu, S., Predescu, A., Moldoveanu, A., Pop, C. S., and Fierbinţeanu-Braticevici, C. (2017). *Helicobacter pylori* infection: old and new. *J. Med. Life* 10, 112–117.

Follmer, C. (2010). Ureases as a target for the treatment of gastric and urinary infections. *J. Clin. Pathol.* 63, 424–430. doi: 10.1136/jcp.2009.072595

García, A., Salas-jara, M. J., Herrera, C., and González, C. (2014). Biofilm and *Helicobacter pylori* : from environment to human host. *World J. Gastroenterol.* 20, 5632–5638. doi: 10.3748/wjg.v20.i19.5632

Ghalehnoei, H., Ahmadzadeh, A., Farzi, N., Alebouyeh, M., Aghdaei, H. A., Azimzadeh, P., et al. (2016). Relationship between ure B sequence diversity, urease activity and genotypic variations of different *Helicobacter pylori* strains in patients with gastric disorders. *Pol. J. Microbiol.* 65, 153–159. doi: 10.5604/17331331.1204761

Goldie, J., Veldhuyzen van Zanten, S. J., Jalali, S., Richardson, H., and Hunt, R. H. (1991). Inhibition of urease activity but not growth of *Helicobacter pylori* by acetohydroxamic acid. *J. Clin. Pathol.* 44, 695–697. doi: 10.1136/jcp.44.8.695

Hassan, S. T., and Šudomová, M. (2017). The development of urease inhibitors: What opportunities exist for better treatment of *Helicobacter pylori* infection in children? *Children* 4:2. doi: 10.3390/children4010002

Igarashi, M., Kitada, Y., Yoshiyama, H., Takagi, A., Miwa, T., Koga, Y., et al. (2001). Ammonia as an accelerator of tumor necrosis factor alpha-induced apoptosis of gastric epithelial cells in *Helicobacter pylori* infection. *Infect. Immun.* 69, 816–821. doi: 10.1128/IAI.69.2.816-821.2001

Ito, S., Kohli, Y., Kato, T., Murakita, H., Ohotaki, Y., Hirai, M., et al. (1995). Differences in urease activity in live *Helicobacter pylori* cultured from patients with gastroduodenal diseases. *Eur. J. Gastroenterol. Hepatol.* 7(Suppl. 1), S83–S88.

Kafarski, P. M. (2018). Recent advances in design of new urease inhibitors : a review. *J. Adv. Res.* 13, 101–112. doi: 10.1016/j.jare.2018.01.007

Kuo, Y. T., Liou, J. M., El-Omar, E. M., Wu, J. Y., Leow, A. H. R., Goh, K. L., et al. (2017). Primary antibiotic resistance in *Helicobacter pylori* in the Asia-Pacific region: a systematic review and meta-analysis. *Lancet Gastroenterol. Hepatol.* 2, 707–715. doi: 10.1016/S2468-1253(17)30219-4

Kusters, J. G., van Vliet, A. H., and Kuipers, E. J. (2006). Pathogenesis of *Helicobacter pylori* infection. *Clin. Microbiol. Rev.* 19, 449–490. doi: 10.1128/CMR.00054-05

Lee, A., and Buck, F. (1996). Vaccination and mucosal responses to *Helicobacter pylori* infection. *Aliment. Pharmacol. Ther.* 10 (Suppl.), 129–138. doi: 10.1046/j.1365-2036.1996.22164013.x

Lee, Y. C., Dore, M. P., and Graham, D. Y. (2022). Diagnosis and treatment of *Helicobacter pylori* infection. *Annu. Rev. Med.* 73, 183–195. doi: 10.1146/annurev-med-042220-020814

Macegoniuk, K., Grela, E., Palus, J., Rudzińska-Szostak, E., Grabowiecka, A., Biernat, M., et al. (2016). 1,2-benzisoselenazol-3(2 H) - one derivatives as a new class of bacterial urease inhibitors. *J. Med. Chem.* 3, 2–10. doi: 10.1021/acs.jmedchem.6b00986

Macegoniuk, K., Tabor, W., Mazzei, L., Cianci, M., Giurg, M., Olech, K., et al. (2023). optimized ebselen-based inhibitors of bacterial ureases with nontypical mode of action. *J. Med. Chem.* (2023) 66, 2054–2063. doi: 10.1021/acs.jmedchem.2c01799

Malfertheiner, P., Camargo, M. C., El-Omar, E., Liou, J. M., Peek, R., et al. (2023). *Helicobacter pylori* infection. *Nat. Rev. Dis. Prim.* 9:19. doi: 10.1038/s41572-023-00431-8

Marwick, C. (1983). New drugs selectively inhibit kidney stone formation. *JAMA J. Am. Med. Assoc.* 250:321. doi: 10.1001/jama.1983.03340030003001

Mobley, H. L., Island, M. D., and Hausinger, R. P. (1995). Molecular biology of microbial ureases. *Microbiol. Rev.* 59, 451–480. doi: 10.1128/mr.59.3.451-480.1995

Roshrosh, H., Rohana, H., Azrad, M., Leshem, T., Masaphy, S., Peretz, A., et al. (2023). Impact of *Helicobacter pylori* virulence markers on clinical outcomes in adult populations. *World J. Gastroenterol.* 29, 190–199. doi: 10.3748/wjg.v29.i1.190

Shih, Y. T., Wu, D. C., Liu, C. M., Yang, Y. C., Chen, I. J., and Lo, Y. C. (2007). San-Huang-Xie-Xin-Tang inhibits Helicobacter pylori-induced inflammation in human gastric epithelial AGS cells. *J. Ethnopharmacol.* 112, 537–544. doi: 10.1016/j.jep.2007.04.015

Suenaga, S., Takano, Y., and Saito, T. (2023). Unraveling binding mechanism and stability of urease inhibitors: a QM/MM MD study. *Molecules* 28:2697. doi: 10.3390/molecules28062697

Svane, S., Sigurdarson, J. J., Finkenwirth, F., Eitinger, T., and Karring, H. (2020). Inhibition of urease activity by different compounds provides insight into the modulation and association of bacterial nickel import and ureolysis. *Sci. Rep.* 10:18503. doi: 10.1038/s41598-020-65107-9

Tabuchi, Y., and Kurebayashi, Y. (1993). Antisecretory and antiulcer effects of ebselen, a seleno-organic compound, in rats. *Jpn. J. Pharmacol.* 61, 255–257. doi: 10.1254/jjp.61.255

Tran Trung, H., Truong Thi Huynh, H., Nguyen Thi Thuy, L., Nguyen Van Minh, H., Thi Nguyen, M. N., Luong Thi, M. N., et al. (2020). Growth-inhibiting, bactericidal, antibio fi lm, and urease inhibitory activities of *Hibiscus rosa* sinensis L. flower constituents toward antibiotic sensitive- and resistant-strains of *Helicobacter pylori*. *ACS Omega* 5, 20080–20089. doi: 10.1021/acsomega.0c01640

Upadhyay, L. S. B. (2012). Urease inhibitors : a review. *Indian J. Biotechnol.* 11, 381–388.

Woo, H. J., Yang, J. Y., Lee, P., Kim, J. B., and Kim, S. H. (2021). Zerumbone inhibits *Helicobacter pylori* urease activity. *Molecules* 26, 1–8. doi: 10.3390/molecules26092663

Yu, X. D., Zheng, R. B., Xie, J. H., Su, J. Y., and Huang, X. Q. (2015). Biological evaluation and molecular docking of baicalin and scutellarin as *Helicobacter pylori* urease inhibitors. *J. Ethnopharmacol.* 162, 69–78. doi: 10.1016/j.jep.2014.12.041

Zhou, J. T., Li, C. L., Tan, L. H., Xu, Y. F., Liu, Y. H., Mo, Z. Z., et al. (2017). Inhibition of *Helicobacter pylori* and its associated urease by palmatine : investigation on the potential mechanism. *PLoS ONE* 12:e0168944. doi: 10.1371/journal.pone.0168944

frontiers | Frontiers in Microbiology

TYPE Original Research
PUBLISHED 09 December 2024
DOI 10.3389/fmicb.2024.1502593

OPEN ACCESS

EDITED BY
Avi Peretz,
The Baruch Padeh Medical Center, Poriya, Israel

REVIEWED BY
Damir Gavric,
University of Novi Sad, Serbia
Ricardo Calderón González,
Queen's University Belfast, United Kingdom

*CORRESPONDENCE
J. Natalia Jiménez
✉ jntalia.jimenez@udea.edu.co

†These authors have contributed equally to this work and share first authorship

RECEIVED 27 September 2024
ACCEPTED 25 November 2024
PUBLISHED 09 December 2024

CITATION
Tellez-Carrasquilla S, Salazar-Ospina L and Jiménez JN (2024) High activity and specificity of bacteriophage cocktails against carbapenem-resistant *Klebsiella pneumoniae* belonging to the high-risk clones CG258 and ST307.
Front. Microbiol. 15:1502593.
doi: 10.3389/fmicb.2024.1502593

High activity and specificity of bacteriophage cocktails against carbapenem-resistant *Klebsiella pneumoniae* belonging to the high-risk clones CG258 and ST307

Sara Tellez-Carrasquilla†, Lorena Salazar-Ospina† and J. Natalia Jiménez*

Grupo de Investigación en Microbiología Básica y Aplicada (MICROBA), Escuela de Microbiología, Universidad de Antioquia, Medellín, Colombia

Introduction: The widespread clinical and environmental dissemination of successful clones of carbapenem-resistant *Klebsiella pneumoniae* (CRKP) represents a serious global public health threat. In this context, lytic bacteriophages have emerged as a promising alternative for controlling these pathogens. This study describes the biological, structural, and genomic characteristics of lytic bacteriophages against the high-risk CRKP clones CG258 and ST307 and describes their performance in combination.

Methods: An experimental study was carried out. Bacteriophages were isolated from hospital wastewater and from wastewater treatment plants (WWTP). Bacteriophages were isolated using the double layer agar technique and their characterization included host range (individual and cocktail), plating efficiency (EOP), infection or bacterial killing curve, one-step curve, bacteriophage stability at pH and temperature conditions, transmission electron microscopy (TEM) and whole genome sequencing.

Results: After purification, five active bacteriophages against CRKP were obtained, three bacteriophages (FKP3, FKP4 and FKP14) had targeted activities against CG258 CRKP and two (FKP10 and FKP12) against ST307 isolates. Seven cocktails were prepared, of which Cocktail 2, made up of the bacteriophages FKP3, FKP10, and FKP14, showed the best activity against 85.7% (n = 36/42) of CRKP isolates belonging to both clones, CG258 (80.8%; n = 21/26) and ST307 (93.8%, n = 15/16). The efficiency of the plating (EOP), infection curve, and one-step growth curve showed that the cocktail phages efficiently infected other CRKP isolates (EOP ≥ 0.5), controlled bacterial growth up to 73.5%, and had short latency periods, respectively, (5–10 min). In addition, they were stable at temperatures between 4°C and 50°C and pH between 4 and 10. All bacteriophages belonged to the *Caudoviricetes* class, and no genes associated with virulence factors or antibiotic resistance were detected.

Conclusion: These findings showed bacteriophages and phage cocktails with high specificity against CRKP belonging to the successful clones CG258 and ST307 with promising characteristics, making them an alternative for controlling these clones in different environmental or health settings, biocontrol agents, or disinfectants in industry and in the field of diagnosis.

KEYWORDS

carbapenem-resistant, *Klebsiella pneumoniae*, bacteriophage, CG258, ST307, cocktails, high-risk clones

1 Introduction

Carbapenem-resistant *Klebsiella pneumoniae* (CRKP) infections have a major clinical impact globally, given their high levels of multidrug resistance (MDR), increased mortality (33–50%), length of hospital stays, and high healthcare costs (Xu et al., 2017). Currently, this microorganism is considered an urgent priority by the Centers for Disease Control and Prevention (CDC) (2024) and the World Health Organization (2024).

Several CRKP clones have been described around the world, which differ according to geographical location. Among the most important clones, ST14, ST15, ST147, and ST101 have been reported with the highest frequency; however, the global spread of CRKP has been mainly linked to an expansion of successful clones belonging to CG258 (including ST258, ST512 and ST11) harboring principally KPC-type carbapenemase (*K. pneumoniae* carbapenemase) (Wyres et al., 2020; Lee et al., 2016). These clones account for 70–90% of all CRKP strains and are responsible for 68% of outbreaks in hospital settings. In addition, they have been reported to cause outbreaks in the United States, Canada, European, Asian, and Latin American countries (Wyres et al., 2020; Yang et al., 2021; Munoz-Price et al., 2013; Kitchel et al., 2009; Schwaber et al., 2011). In recent years, CRKP clones belonging to ST307 have successfully emerged in the United States, Italy, and Colombia owing to their virulence factors, which provide them with adaptive advantages in various scenarios (Villa et al., 2017; Bonnin et al., 2020; Peirano et al., 2020).

On the other hand, CRKP has spread worryingly to other settings, such as the community and the environment, because it harbors successful mobile genetic elements that confer resistance and easy dissemination and inappropriate use of antibiotics in diverse anthropogenic activities (Kahn, 2017). Several studies have described the presence of this microorganism in effluents from hospital wastewater and domestic wastewater treatment plants (WWTPs) (Surleac et al., 2020; Moges et al., 2014). In addition, these bacteria have been classified as emerging pollutants that persist in effluents because WWTPs are not designed to remove them, increasing the risk of dissemination and infection due to the use of these waters (Li et al., 2022).

Considering that therapeutic options are becoming scarce and that environmental biocontrol alternatives are necessary to contain this problem, strategies based on the use of lytic bacteriophages have been reconsidered in recent years (Hobson et al., 2022; Dancer, 2014). These viruses have a great potential to infect bacteria in a specific way; they do not affect other bacterial communities or eukaryotic cells, making them safe alternatives for humans and friendly to the environment (Sharma et al., 2017). Bacteriophages have a wide field of application, and there are currently a variety of studies evaluating their activity in different scenarios like compassionate therapy in humans, disinfectants in hospital settings, the removal of biofilms, and as an alternative biocontrol agent for the treatment of wastewater (McCallin and Zheng, 2019; Dedrick et al., 2023; Accolti et al., 2018; Ho et al., 2016; Łusiak-Szelachowska et al., 2020; Fu et al., 2010; Jassim et al., 2016). However, bacteriophage characterization processes based on biological, structural, and genomic analyses form the basis of application studies.

Numerous studies have been conducted to characterize bacteriophages that are active against antibiotic-resistant pathogens, specifically bacteria belonging to the ESKAPE group (*Enterococcus faecium*, *Staphylococcus aureus*, *K. pneumoniae*, *Acinetobacter baumannii*, *Pseudomonas aeruginosa* y *Enterobacter* spp.) (Yoon et al., 2013; Chen et al., 2021; Peng et al., 2014; Adnan et al., 2019; Zhao et al., 2019). However, studies of bacteriophages against specific *K. pneumoniae* clones have been limited and have focused on the isolation of active bacteriophages against other clones, such as ST11, ST16, and ST15 (Martins et al., 2022a; Horváth et al., 2023; Fang and Zong, 2022). Only a few of them are described in the characterization of bacteriophages active against ST258 (Tisalema-Guanopatín et al., 2023; Thiry et al., 2019; D'Andrea et al., 2017). In this context, this study describes the biological and structural characteristics of bacteriophages with high specificity against CRKP belonging to CG258 and ST307. In addition, their activity in combination was evaluated to obtain an effective alternative for controlling endemic clones disseminated worldwide.

2 Materials and methods

2.1 Specimen collection

Wastewater samples were collected from the effluents of a tertiary-care hospital (these effluents comprising wastewater from emergency rooms, hospitalization, intensive care unit, special care unit, internal medicine and food service) and from the affluents and effluents of a wastewater treatment plant (WWTP) in the city of Medellín (Colombia), between September 2021 and November 2022. Five hundred milliliters of each wastewater sample were collected and processed within the first 2–24 h to avoid alterations in the microbial communities (Van Charante et al., 2021).

2.2 Selection of host bacteria

Three carbapenem-resistant *K. pneumoniae* isolates harboring *bla*-$_{KPC}$ belonging to two successful clones were used as host bacteria for the search for bacteriophages. These included isolates from CG258 (ST512 $n = 1$ and ST258 $n = 1$) and ST307 ($n = 1$) (Supplementary Table S1). The bacterial isolates had clinical origins and were obtained from the Microbiological strain collection of the Grupo de Investigación en Microbiología Básica y Aplicada (MICROBA) (Ocampo et al., 2016; Cienfuegos-Gallet et al., 2017). The bacterial isolates were previously characterized, and identification and susceptibility tests were performed using a semi-automated method VITEK® 2 Compact system (bioMérieux, Inc. Hazelwood, MO). In addition, genes encoding carbapenemases were identified by PCR and sequenced to determine gene-variants; further, molecular typing was performed using Multilocus sequence typing (MLST)

(Ocampo et al., 2016; Poirel et al., 2011; Ellington et al., 2007; Diancourt et al., 2005).

2.3 Bacteriophages isolation

2.3.1 Samples processing

Wastewater samples were processed with chloroform (Merck, KGaA, Darmstadt, Germany) to release the bacteriophages from organic matter (relation 1:10). Subsequently, the aqueous phase was recovered, centrifuged (4500 rpm for 10 min at 4°C), and filtered through 0.22 µm syringe filters (Minisart® Sartorius AG, Germany) according to a modification to the protocol by Kropinski and Clokie (2009). To selectively increase the number of bacteriophages in the processed samples, enrichment was performed. The processed sample was placed in contact with each host bacterium in LB broth (Miller, Becton Dickinson Difco™) with $CaCl_2$ (2 mM, Biobasic). Subsequently, samples were incubated at 35 ± 2°C for 24 h in a shaking humidified bath, centrifuged (4500 rpm for 10 min at 4°C), and filtered (0.22 µm syringe Filter, Minisart® Sartorius AG, Germany) (Kropinski and Clokie, 2009).

2.3.2 Bacteriophage detection and plaque purification

To detect bacteriophages in the enriched samples, the spot test method described by Clokie et al. was performed (Kropinski and Clokie, 2009). Subsequently, to obtain isolated plaques, positive samples were serially diluted (1:10) and seeded using the double-layer agar method (Adams, 1959). The plaques were selected based on size and translucency, and only one plaque was collected and deposited in Eppendorf tubes with 500 µL of SM buffer (100 mM, NaCl Merck Millipore; 50 mM Tris–HCl [pH 7.5]; 8 mM, $MgSO_4$ Scharlau; 0.01% gelatin Oxoid). Subsequently, the plaques were mixed in SM buffer until homogeneous, and serial dilutions were made (1:10) and seeded using the double layer agar method (Adams, 1959). Each bacteriophage plaque was purified three times with repeated isolation to obtain a single bacteriophage.

2.3.3 Concentration and quantification of bacteriophages

Bacteriophages were concentrated using the double-layer agar method (Swanstrom and Adams, 1951). Briefly, plaques in SM buffer obtained after purification were mixed and serially diluted (1:10). Subsequently, dilutions of higher phage concentrations (less diluted) were plated using the double-layer agar method. This procedure was repeated nine times until 10 replicates were completed. After incubation, the entire top-agar layer of the ten replicas was collected and added to 15 mL of SM buffer; it was then mixed, centrifuged (4500 rpm for 10 min at 4°C), and the supernatant was filtered (0.22 µm Minisart® Syringe Filter) (Swanstrom and Adams, 1951). Finally, bacteriophage solutions were quantified twice on different days and each dilution was plated in duplicate using the double-layer agar method and stored in SM buffer at 4°C and at-80°C with 50% glycerol (Amresco, Inc., Solon Ohio, United States) (Kropinski and Clokie, 2009; Adams, 1959). The stability of the bacteriophages under these storage conditions is monitored over time.

2.4 Characterization of bacteriophages

2.4.1 Host range evaluation

A host range was performed using 131 bacterial isolates to determine the specificity of bacteriophage infection. The evaluation was performed in triplicate using the spot test method, and plaque formation was verified by performing serial dilutions of the phages and plating in the quantitative spot test to confirm productive infection in the bacteriophage-susceptible isolates (Kropinski and Clokie, 2009). An inter-species and inter-genus assessment was performed on 31 isolates other than *K. pneumoniae*: *Klebsiella oxytoca* ($n = 3$), *Citrobacter freundii* ($n = 3$), *Enterobacter cloacae* ($n = 3$), *Escherichia coli* ($n = 5$), *Serratia* spp. ($n = 4$), *Pseudomonas aeruginosa* ($n = 3$), *Acinetobacter baumannii* ($n = 3$), *Aeromonas* SPP ($n = 2$), *Ralstonia paucula* ($n = 2$), and *Staphylococcus aureus* ($n = 3$). Additionally, the intra-species host range was determined in 100 isolates of *K. pneumoniae*: 25 carbapenem-susceptible and 75 carbapenem-resistant KPC (bla_{KPC-2} $n = 45$ and bla_{KPC-3} $n = 30$), belonging to CG258 ($n = 25$), ST307 ($n = 15$), ST14 ($n = 10$), and other STs ($n = 25$) (Supplementary Table S2). The CRKP isolates were also resistant to other antibiotic families (Supplementary Table S3), such as aminoglycosides (57.9%, $n = 44/76$), quinolones (82.14%, $n = 23/28$), fluoroquinolones (72.7%, $n = 56/77$), glycylcycline (67.2%, $n = 39/58$), and nitrofurans (100%, $n = 10/10$). The bacterial isolates were obtained from the strain collection of the Grupo de Investigación en Microbiología Básica y Aplicada (MICROBA).

2.4.2 Efficiency of plating

Efficiency of plating was assessed for bacteriophage-susceptible *K. pneumoniae* isolates identified in the host range. This assessment was conducted using the quantitative spot test to determine the efficiency of phage infection against different *K. pneumoniae* isolates by comparing plaque production (Kropinski and Clokie, 2009). The EOP was calculated by dividing the number of plaques produced by the evaluated bacteria by the number of plaques produced by the host bacterium. Efficiency of plating values ≥0.5 were considered an efficient infection, values between 0.1 and less than 0.5 were considered a moderately efficient infection, values between 0.001 and less than 0.1 an infection with low efficiency, and values <0.001 were an inefficient infection (Khan Mirzaei and Nilsson, 2015). Each experiment was conducted in triplicate.

2.4.3 Preparation and evaluation of bacteriophage cocktails

Different bacteriophage cocktails were prepared using combinations of 2 until 4 phages, each at a final concentration of 3×10^7 UFP/ml, according to previous studies to prevent aggregation among bacteriophages (Zurabov et al., 2023; Asghar et al., 2022). The selection of the combination of bacteriophages for each cocktail was based on host range and EOP results. Cocktail assessments were performed using the same strains used in the intraspecies host range. First, the activity of the cocktails was determined using a spot-test. Then, serial dilutions of the cocktails were performed and seeded using the quantitative drop test to confirm productive infection in cocktail-susceptible isolates (Kropinski and Clokie, 2009). Finally, the best performing cocktail was selected, and individual characterization (biological, structural, and genomic) of the cocktail phages was performed. All experiments were performed in triplicate.

2.4.4 Infection or killing curve

To evaluate the control of bacteriophage on bacterial growth, the host bacteria in exponential phase (approximate concentration of 1.5–5×10^8 CFU/ml) were placed in contact with different concentrations of the phage (MOI 1, 0.1, and 0.01). The experiment was conducted on 96-well plates, and absorbance readings were taken every hour for 23 h at 600 nm using a Multiskan GO Microplate Spectrophotometer, using SkanIt™ Software (Thermo Scientific, v6.1.1) (Martins et al., 2022b). Additionally, the effects of the cocktail at different concentrations (MOI 1, 0.1, 0.01) on the inhibition of bacterial growth were evaluated. Each experiment was conducted in triplicate.

2.4.5 Adsorption time and one-step growth curve

To define the adsorption time, the host bacterium in the exponential phase (1×10^8 CFU/ml) was placed in contact with the bacteriophage at an MOI of 0.01 (1×10^6 PFU/ml), followed by incubation at 37°C in a shaking humidified bath. Subsequently, samples were collected every 5 min for 20 min. Each sample was filtered, and serial dilutions (1:10) were performed to quantify the number of phages each time using the double-layer agar technique (Adams, 1959). To obtain the one-step curve, adsorption was first performed. The phages (1×10^6 UFP/ml) were placed in contact with host bacteria in the exponential phase (1×10^8 CFU/ml) at an MOI of 0.01 and incubated for 10 min at 37°C. After this time, it was centrifuged (4500 rpm for 10 min at 4°C), and the supernatant was discarded; the pellet was re-suspended in the same volume of broth and incubated at 37°C. Two samples were taken every 5 min for 45 min; one of them was treated with chloroform (1:10 ratio) to determine the eclipse time, and the other sample was used to determine the latency time (Zhao et al., 2019). Both samples were filtered and serially diluted to quantify the number of bacteriophages each time using the double-layer agar method (Adams, 1959). The burst size was determined by dividing the average number of viral particles produced by the number of infected cells (D'Andrea et al., 2017). The experiments were conducted in triplicate.

2.4.6 Susceptibility to different pH and temperature conditions

Each bacteriophage at a concentration of 1×10^6 PFU/ml was exposed to temperatures of 4°C, 25°C, 37°C, 50°C, 60°C, and 70°C to determine temperature susceptibility. After 1 h of exposure, serial dilutions (1:10) were prepared and plated using the quantitative spot test (Kropinski and Clokie, 2009). To assess pH sensitivity, the bacteriophages were diluted in SM buffer adjusted to different pH (CDC, 2024; Wyres et al., 2020; Yang et al., 2021; Munoz-Price et al., 2013; Kitchel et al., 2009; Villa et al., 2017; Peirano et al., 2020) to reach a final concentration of 1×10^6 PFU/ml. After 1 h of exposure, serial dilutions (1:10) were prepared and plated using the quantitative spot test (Kropinski and Clokie, 2009). The experiments were conducted in triplicate.

2.4.7 Transmission electron microscopy

The bacteriophages (1 × 10^{10} UFP/ml) were purified by ultracentrifugation and washed with ammonium acetate (Merck KGaA, Darmstadt, Garmany) according to Kropinski and Clokie (2009). To obtain transmission electron micrographs of the phages, a drop of each high-titer phage was deposited on a carbon-coated Formvar layer held by a copper grid. The samples were allowed to dry for 30 min, and excess liquid was removed. Finally, the phages were negatively stained with 2% phosphotungstic acid and examined under a transmission electron microscope (Domingo-Calap et al., 2020). All measurements were performed using Image J program v1.51 2018. Three different particles of which phage were measured.

2.4.8 Genetic material extraction and sequencing

A solution of bacteriophages at a concentration of 10^{10} PFU/ml was used, which was enzymatically digested with RNAse (Sigma-Aldrich, St. Louis, United States) and DNAse I (Thermo Scientific, Massachusetts, United States) overnight at 37°C. After incubation, the enzymes were inactivated at 80°C for 15 min. Subsequently, a proteolysis buffer was added [final concentration: Proteinase K (50 µg/mL) (Thermo Scientific, Vilnius, Lithuania), EDTA pH8 (20 nM) (Honeywell, Wunstorfer, Germany), and SDS (0.5%) (Merck KGaA, Darmstadt, Garmany)], followed by incubation at 56°C for 1 h, and extraction was continued using the phenol-chloroform protocol with some modifications (Payaslian et al., 2021). The genetic material was quantified by fluorometry using Qubit (Life Technologies, Singapore) and Picogreen (Quant-iT™ PicoGreen™ Life Technologies, Oregon, United States). Genome quality and integrity were assessed using NanoDrop (Thermo Scientific, United States) and Agilent genomic DNA screen tape (DIN, DNA integrity number). Phage genomic DNA libraries and sequencing were performed by Psomagen Inc. (Rockville, Maryland, United States). Briefly, DNA libraries were prepared using an Illumina Truseq DNA PCR-free (350 bp insert) Library Prep Kit (Illumina, California, United States). The libraries were sequenced on the Illumina NovaSeq 6000 S4 platform with 151 bp paired end reads (2×151), with an approximate yield of 24 million reads per sample.

2.4.9 Genome assembly and annotation

Quality control of the raw sequences was performed using FastQC v0.12.1. Low-quality bases (Phred <30), adapters, and duplicate sequences were removed using FastP v0.23.4, and Trimmomatic v0.39 (Chen et al., 2018; Bolger et al., 2014). Subsequently, contaminated sequences were removed from the Illumina sequencing vector phage PhiX174 (NC_001422.1), and from the phage host *K. pneumoniae* F17KP0040 (GCA_012971225.1) using BBDuk v39.01 from the BBMap suite tools[1] (Mukherjee et al., 2015). The filtered readings were assembled using SPAdes v3.15.5 (Prjibelski et al., 2020). The resulting contigs were lined with *K. pneumoniae* phages previously reported using BLASTn,[2] and the readings that were mapped to these counts using BBDuk were retrieved and assembled *de novo* using SPAdes. Phageterm v3.0.1 was used for the prediction of physical endings and the rearrangement of phage genomes (Garneau et al., 2017). Complete, high-quality genomes were obtained using Pilon v1.24, and genome quality and integrity were assessed using QUAST v5.2.0 and CheckV v.1.0.1 (Walker et al., 2014; Gurevich et al., 2013; Nayfach et al., 2021). Genome annotation was performed using Pharokka v1.7.1 (Bouras et al., 2023). Briefly, coding sequences (CDS) were predicted using PHANOTATE v1.5.1, tRNAs were predicted using tRNAscan-SE v2.0.12, mRNAs were predicted using Aragorn, and CRISPR sequences were predicted using CRT. Functional annotation was

1 https://sourceforge.net/projects/bbmap/

2 https://blast.ncbi.nlm.nih.gov/Blast.cgi

performed by searching the PHROGS database for CDS using MMseqs2 and PyHMMER (Terzian et al., 2021; Steinegger and Söding, 2017; Larralde and Zeller, 2023). Virulence factors and resistance genes were predicted using the VFDB databases and CARD (Chen et al., 2005; Alcock et al., 2020). Contigs were matched to their closest hit in the INPHARED database using mash (Cook et al., 2021; Ondov et al., 2016). The annotation was improved using Phold v0.1.3,[3] a bacteriophage genome annotation tool based on protein structural homology. Finally, the annotation of the phage replicative cycle was predicted *in silico* using BACPHLIP, PhageAI v.1.0.0, and phaTYP (Hockenberry, 2021; Tynecki et al., 2020; Shang et al., 2023). The bacteriophage genomes were submitted to the National Center for Biotechnology Information (NCBI) database. The genome figures were created in PATRIC (Davis et al., 2019).

2.4.10 Comparative genomics and phylogenetic analysis

First, the genomic similarity of the phages was compared using ProgressiveMauve (Darling et al., 2010). Closely related phages were identified using BLASTn on the GenBank NCBI virus database. Then, the average nucleotide identity (ANI) was calculated based on BLAST + (ANIb) by comparing the three phage genomes to those with highest score and identify (> = 90%) using JSpeciesWS (Richter et al., 2016). Based on this comparison, closely related phages with the highest ANIb values and other dsDNA phages were used to classify the phages to family levels using a proteome-based clustering strategy on the ViPTree server (Nishimura et al., 2017). Phages with the highest VipTree tBLASTx scores (S_G) and outgroups from the *Autographiviridae* and *Drexleviridae* families were selected to perform a genome-genome distance phylogenetic analysis of phages using the Virus Classification and Tree Building Online Resource (VICTOR) (Meier-Kolthoff and Göker, 2017).

2.4.11 Statistical analysis

The host range and cocktail evaluation results were described using absolute and relative frequencies. Quantitative variables were described using mean and standard deviation, and the assumption of normality was evaluated using Shapiro–Wilk. The analysis of quantitative variables was performed according to the assumption of normality; parametric tests included analysis of variance (ANOVA) or Student's *t*-test, and nonparametric tests included the Kruskal–Wallis test or Wilcoxon test. The efficiency of plating results were classified according to the M. Khan Mirzaei et al. criteria (Khan Mirzaei and Nilsson, 2015). Values of $p < 0.05$ were considered statistically significant. The obtained information was analyzed using R studio v 2023.09.1 + 494.

3 Results

3.1 Bacteriophage isolation

Fourteen wastewater samples were collected, including 10 from hospital effluents and 4 from WWTPs (affluent $n = 1$, effluent $n = 3$). In total, 22 plaques of different morphologies were collected using the double-layer agar technique. After plaque purification process, 5 bacteriophages with large, sharp-edged, and translucent plaques were selected. Of the five isolated bacteriophages, three had the host bacterium CRKP belonging to CG258 (ST512, $n = 2$ and ST258, $n = 1$) and were named FKP3, FKP4, and FKP14. On the other hand, the remaining two bacteriophages had CRKP of ST307 as host bacteria and were designated FKP10 and FKP12. Bacteriophages produced plaques between 1 and 2 mm in diameter; in addition, the plaques produced by the bacteriophages FKP10 and FKP12 formed a double halo of inhibition (Figure 1).

3.2 Characterization of bacteriophages

3.2.1 Host range evaluation

The evaluation of the inter-species and inter-genus host range showed that the isolated bacteriophages were not active against any of the bacterial strains of other genus and species evaluated ($n = 0/31$). Regarding the evaluation of intra-species strains (*K. pneumoniae*), bacteriophages showed lytic activity between 16 and 21%; the bacteriophage FKP12 had the highest activity by lysing 21 of the 100 *K. pneumoniae* isolates evaluated (Figure 2A). Bacteriophages were mainly active against *K. pneumoniae* isolates belonging to the same clonal group as their host bacterium. Bacteriophages FKP3, FKP4, and FKP14 obtained from CG258 host bacteria were active against 56% (14/25) and 60% (15/25) of CRKP of the same clonal group (CG258). Likewise, the FKP10 and FKP12 bacteriophages isolated from *K. pneumoniae* from ST307 were active against 66.7% (10/15) and 93.3% (14/15) of isolates belonging to the same ST of the host bacteria, respectively. Regarding the activity of phages in carbapenem-susceptible strains, FKP10 and FKP12 exhibited activity against 20% ($n = 5/25$) of the strains compared with FKP3, FKP4, and FKP14 phages, which exhibited activity against 4% ($n = 1/25$). In general, bacteriophages showed no activity against the CRKP strains of other STs, except for FKP10 and FKP12, which exhibited activity against ST231.

3.2.2 Efficiency of plating

The efficiency of the plating results is shown in Figure 3. In general, bacteriophages efficiently infected other *K. pneumoniae* isolates, when compared to infection against their host bacteria (EOP $\geq$ 0.5) (Figure 3A). FKP3, FKP4, and FKP14 phages efficiently infected 93.75% ($n = 15$), 93.75% ($n = 15$), and 94.1% ($n = 16$) of the isolates evaluated (Figure 3B), with EOP averages of 1.06 ± 0.27, 1.19 ± 0.31, and 1.00 ± 0.31, respectively. These three bacteriophages did not differ in the production of plaques ($p = 0.204$) (Figure 3A). On the other hand, the FKP10 and FKP12 bacteriophages efficiently infected 100% ($n = 17$) and 95.2% ($n = 20$) of the evaluated strains, respectively (EOP $\geq$ 0.5) (Figure 3B). In addition, they had EOP averages of 1.31 ± 0.40 and 1.45 ± 0.66, which did not differ significantly ($p = 0.15$) (Figure 3A). Finally, moderately efficient infection (0.1 $\leq$ EOP < 0.5) was observed in 6.25% ($n = 1$), 6.25% ($n = 1$), 5.9% ($n = 1$), and 4.8% ($n = 1$) of the isolates with the bacteriophages FKP3, FKP4, FKP14, and FKP12, respectively; further, low infection efficiency (0.001 $\leq$ EOP < 0.1) and inefficient infection (< 0.001) were not observed (Figure 3B).

3 https://github.com/gbouras13/phold

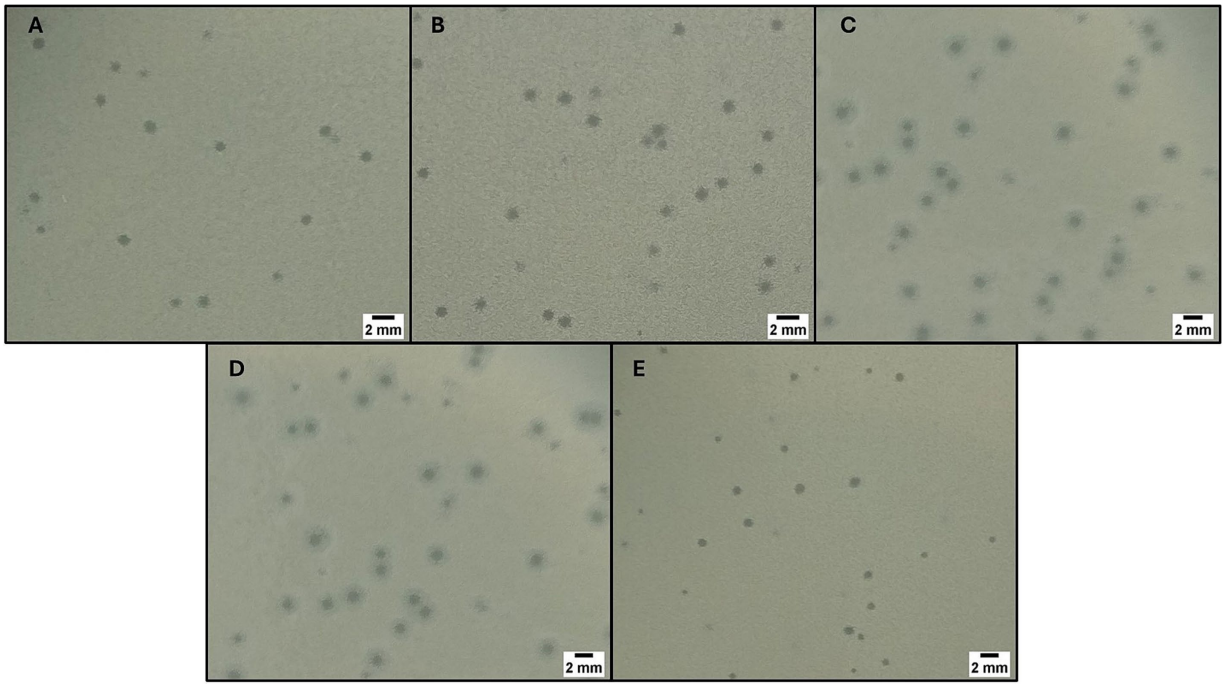

FIGURE 1
Bacteriophage plaque morphology. The figure shows the morphology of the plaques obtained using double-layer agar for the phages FKP3 **(A)**, FKP4 **(B)**, FKP10 **(C)**, FKP12 **(D)** and FKP14 **(E)**. The size of the plaques was between 1 and 2 mm, and FKP10 and FKP12 phages had a double halo.

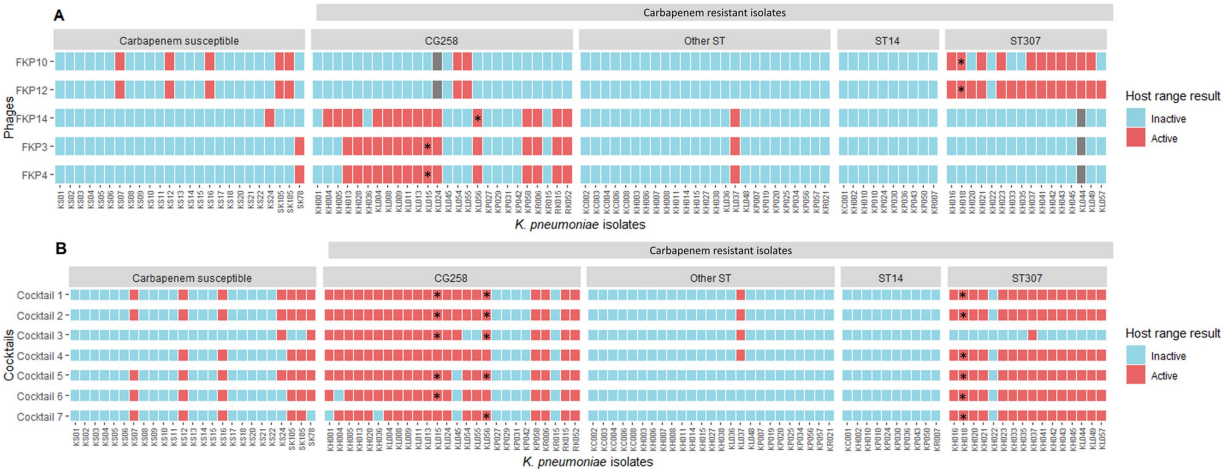

FIGURE 2
Intraspecies host range using individual bacteriophages and cocktails. **(A)** Shows the intraspecies host range of individual bacteriophages. * Host bacteria from which the bacteriophages were isolated: FKP3, FKP4, and FKP14 were obtained from CG258 isolates, whereas FKP10 and FKP12 were obtained from ST307 isolates. Gray squares correspond to strains against which the bacteriophages were not evaluated. **(B)** Presents the results of the intra-species host range of the evaluated cocktails. Considering that the individual host range showed high specificity for bacteriophages against some clones, bacteriophage combinations were performed to evaluate their performance in combination. Because the bacteriophages FKP3 and FKP4 had the same host range, one of them was selected to perform the combinations, except for Cocktail 3.

3.2.3 Preparation and evaluation of bacteriophage cocktails

In total, seven cocktails were prepared, five aimed at increasing the host range against clones belonging to CG258 and ST307 (Cocktails 1, 2, 5, 6, and 7), one aimed at isolates of ST307 (Cocktail 4), and another aimed at isolates of CG258 (Cocktail 3). The conformation of the cocktails is described in Table 1.

The evaluation of the intra-species host range of the cocktails showed a broadening of the host range up to 43.1% ($n = 44/102$) compared with the values of the individual host range, which reached

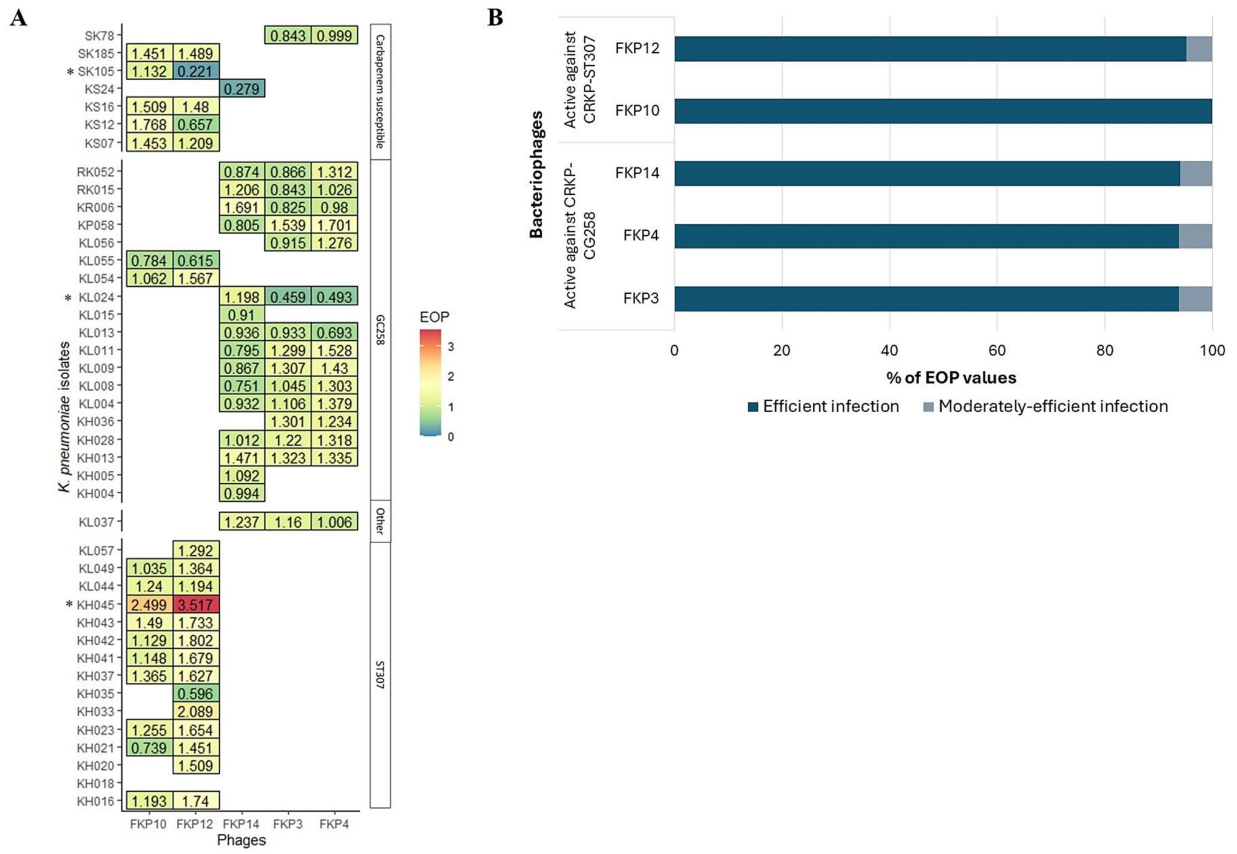

FIGURE 3
Efficiency of plating (EOP) of CRKP bacteriophages. **(A)** Shows the efficiency of plating evaluated in susceptible isolates in the host range. EOP values ≥ 0.5 indicate efficient infection; 0.1 ≤ EOP < 0.5, moderately efficient infection; and 0.001 ≤ EOP < 0.1, infection with low efficiency. * Bacteriophage FKP3 exhibited reduced infection efficiency with the KL024 isolate (EOP = 0.459; $p < 0.05$). The same result was observed for the FKP12 bacteriophage with isolate SK105 (EOP = 0.221; $p < 0.05$). On the other hand, the bacteriophages FKP10 (EOP = 2.499; $p < 0.001$) and FKP12 (EOP = 3.517; $p < 0.001$) exhibited statistically significant high infection efficiency with the KH045 isolate. **(B)** Presents the percentage of efficient and moderate infection values observed in bacteriophages.

TABLE 1 Conformation of bacteriophages cocktails against *K. pneumoniae*.

Cocktails	Bacteriophages				
	Against CRKP of CG258			Against CRKP of ST307	
	FKP3	FKP4	FKP14	FKP10	FKP12
Cocktail 1	X		X		X
Cocktail 2	X		X	X	
Cocktail 3	X	X	X		
Cocktail 4				X	X
Cocktail 5	X		X	X	X
Cocktail 6	X			X	X
Cocktail 7			X	X	X

CRKP, carbapenem resistant *Klebsiella pneumoniae*.

21%. Furthermore, all seven cocktails showed an increase in activity for both CRKP isolates belonging to CG258 and ST307 (Figure 2B). Cocktails 1, 2, and 4 were active against 85.7% ($n = 36/42$; CG258 80.7%, $n = 21/26$; ST307, 93.75%, $n = 15/16$) of the isolates belonging to both clones. Cocktail 4, prepared to increase activity only against ST307 isolates, expanded the host range against CG258 isolates (85.7%; $n = 36/42$; CG258 $n = 21$; ST307 $n = 15$); while Cocktail 3, targeting CG258 strains, maintained its specificity against this same clonal group (47.6%; $n = 20/42$; CG258 $n = 19$; ST307 $n = 1$). Finally, Cocktails 1, 2, and 5 were active against 28% ($n = 7$) carbapenem-susceptible isolates, followed by cocktails 6 and 7 with 24% ($n = 6$) and cocktails 3 and 4 active against 8% ($n = 2$) and 20% ($n = 5$), respectively.

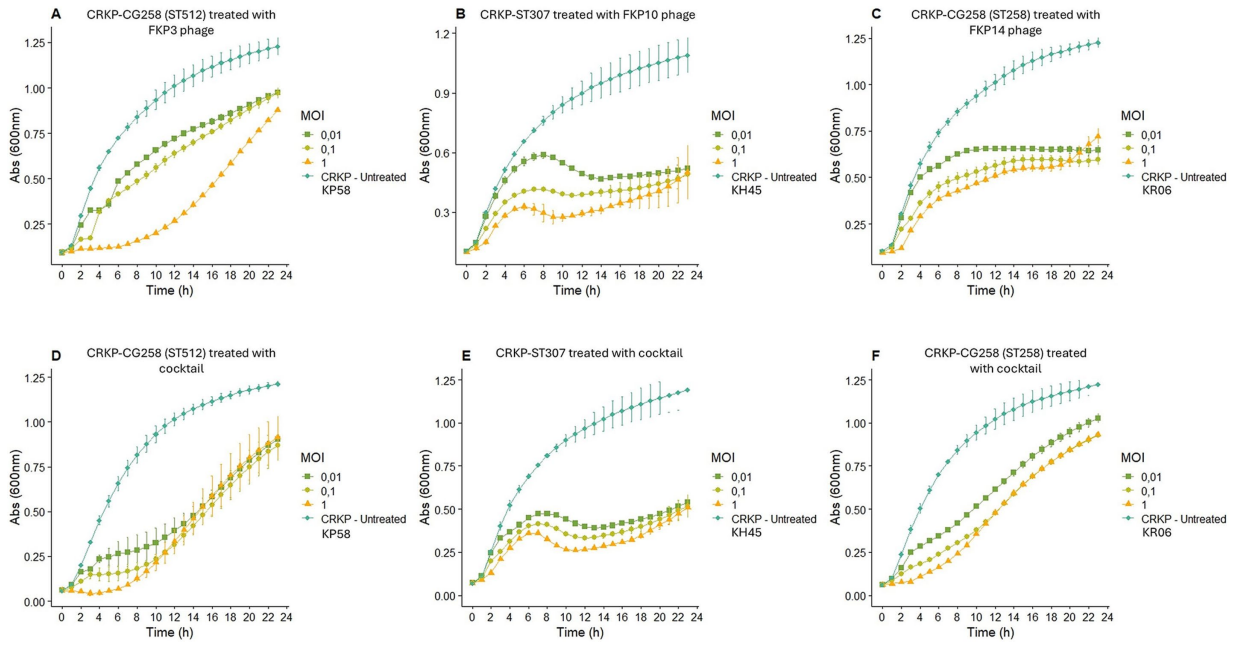

FIGURE 4
Bacterial infection or elimination curve. **(A–C)** Show the elimination curve of bacteriophage FKP3, FKP10 and FKP14, respectively. **(D–F)** Show the elimination curve of cocktail 2 (conformed for the bacteriophages FKP3, FKP10 and FKP14) with the host bacteria of each bacteriophage that composed that cocktail. MOI: multiplicity of infection.

The results of the intra-species host range using cocktails (using the spot test) were confirmed using the plaque count to identify productive infection. These results allowed us to determine low plaque production of Cocktail 4, compared to Cocktails 1 and 2. Finally, of the seven cocktails prepared, cocktail 2, composed of the bacteriophages FKP3, FKP10, and FKP14, showed the best performance considering its high specificity for both CG258 and ST307 isolates (80.8 and 93.75%, respectively). Furthermore, the bacteriophages in this cocktail had higher EOP results. Phages from Cocktail 2 were then selected for individual characterization (biological, structural, and genomic).

3.2.4 Infection or killing curves of individual phages and cocktail

Bacteriophage FKP3 showed a greater reduction in bacterial growth (82.70%) after 6 h of treatment at an MOI of 1, whereas lower MOIs (0.1 and 0.01) showed reduced effectiveness (Figure 4A). Overall, significant control of bacterial growth of the FKP3 phage was observed at 6, 12, and 23 h; however, the MOI of 1 remained superior throughout treatment (Figure 4A). On the other hand, when the selected cocktail 2 was used in the host strain of the FKP3 phage [CRKP-ST 512 isolate (KP58)], the MOI of 1 showed a similar behavior to that observed with the individual phage (MOI 1), but the cocktail 2 at lower MOIs performed better between hours 6 and 12 (MOI 0.1 69.02 to 77.63%; MOI 0.01 59.91 to 65.25%), showing a greater reduction than the individual phage (MOI 0.1 36.98 and 42.88%; MOI 0.0128.6 to 32.69%) (Figures 4A,D).

When the performance of phage FKP10 was evaluated against the CRKP-ST307 isolate (KH45), it was observed that the phage exerted maximum control of bacterial growth at 12 (67.55%), 18 (58, 65%), and 20 (52.73%) hours at MOIs of 1, 0, 1, and 0.01, respectively (Figure 4B). No differences were observed in the control of bacterial growth at the different MOIs, and a constant growth control was observed with the MOI of 1 (between 8 to 20 h; 61.3 to 67.5%), 0.1 (between 10 to 23 h, 53.32 to 58.65%), and 0.01 (between 14 to 23 h, 50.84 to 52.73%) (Figure 4B). In general, the use of the cocktail showed no difference in the control of bacterial growth at MOI of 1 and 0.1 compared with that observed for the individual phage; however, the cocktail at an MOI of 0.01 improved performance between hours 4 and 11 (Figure 4E).

Finally, the bacteriophage FKP14 evaluated against the CG258 isolate (KR06), maintained its highest peak activity at 2 (61.43%), 22 (51.6%) and 23 (47.28%) hours after treatment, for MOI of 1, 0.1, and 0.01, respectively, (Figure 4C). Likewise, a significant growth control was observed with the 3 MOI at 6, 12, and 23 h, and no differences were observed between phage activity at each MOI. On the other hand, the activity of the phage at different MOIs was constant over time (MOI 1; reduction from 47.46 to 53.14%; MOI 0.1 reduction from 40.40 to 51.6%; MOI 0.01, reduction from 40.87 and 47.28%) (Figure 4C). In contrast, the cocktail did not show a better performance than that observed with the individual bacteriophage; however, the cocktail exhibited a significant reduction in bacterial growth at 6, 12, and 23 h (Figure 4F).

3.2.5 Adsorption time and one-step growth curve

The adsorption time of the three bacteriophages was 5 min, during which 95–99% of the viral particles were adsorbed (Figure 5A). The one-step curve showed that the bacteriophage replication times were between 30 and 45 min (Figures 5B–D); in addition, we found eclipse times of 5 min for the three bacteriophages and latency periods of 5, 5, and 10 min for FKP3, FKP10, and FKP14, respectively. Finally,

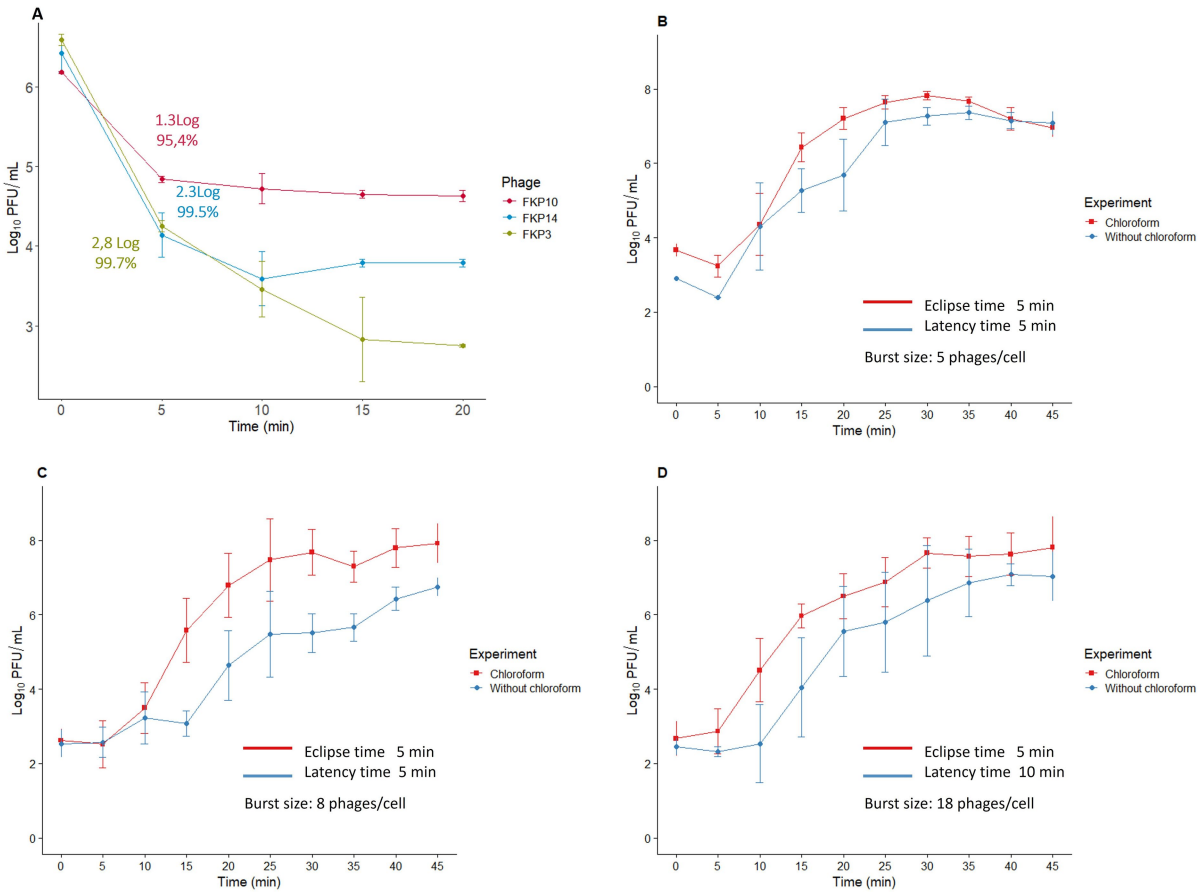

FIGURE 5
Characterization of bacteriophage replication cycle. This figure shows the results of the adsorption time **(A)**, and the one-step curve for the bacteriophages FKP3 **(B)**, FKP10 **(C)**, and FKP14 **(D)**.

a burst size of 5 PFU/cell was observed for phage FKP3, 8 PFU/cell for phage FKP10, and 18 PFU/cell for phage FKP14 (Figures 5B–D).

3.2.6 Susceptibility to different pH and temperature conditions

All three bacteriophages were stable at temperatures between 4°C and 50°C. The bacteriophage FKP3 reduced 3.9 Log when exposed to a temperature of 70°C ($p = 4.22 \times 10^{-11}$***), and FKP10 decreased 2.8 Log at 60°C ($p = 1.0$) and 6.6 Log at 70°C ($p = 0.258$) (Figure 6A). Regarding pH stability, similar behavior was observed in the three bacteriophages, which maintained stability at a pH between 4 and 10 (FKP3, $p = 0.849$; FKP10, $p = 0.700$; FKP14, $p = 0.957$); however, they were susceptible to extreme pH levels of 2 and 12, so a complete reduction in bacteriophage titers was observed for both pHs (Figure 6B).

3.2.7 Transmission electron microscopy

Phages FKP3, FKP10, and FKP14 had approximate lengths of 206.2 ± 3.6, 165.6 ± 1.2 and 208.1 ± 1.1 nanometers, respectively, and all of them had tail, so they belong to the *Caudoviricetes* class. All three phages had icosahedral isometric capsids with sizes of 89.05 ± 2.6 nm (FKP3), 73.8 ± 3 nm (FKP10) and 92.2 ± 1.9 nm (FKP14). The tails were straight and short with approximate sizes of 116.7 ± 0,5 nm (FKP3), 89.09 ± 1,6 nm (FKP10) and 114.2 ± 2.4 nm (FKP14) (Figure 7).

3.2.8 Genome characteristics and annotation

The genome features are described in Table 2. Bacteriophages had double-stranded DNA (dsDNA), and the three presented high-quality genomes with integrity >99%. The genomes had a length between ~142 and ~ 159 kbp; further, the FKP3 (GenBank: PP895363.1) genome was linear, whereas FKP10 (GenBank: PP974338.1) and FKP14 (GenBank: PP974339.1) had circularly permuted genomes. More than 230 open reading frames (ORFs) and coding sequences (CDS) were annotated; but, most corresponded to genes encoding hypothetical proteins (~60%) and about 33% corresponded to genes encoding proteins with known functions. These genes were classified into functional categories, such as structural and packaging proteins, associated with lysis, moron, integration and excision, auxiliary metabolic genes and host takeover, and DNA, RNA, and metabolism genes (Figure 6). All three phages had CDS associated with lytic lifestyles such as Rz-like spanins, endolysin, lysis inhibitors, and endolysins; however, FKP3 also had a CDS (0063) that was identified as a site-specific recombination directionality factor (RDF) and assigned to the integration and excision module. The presence of this recombination factor decreased the probability to 46.25% that this bacteriophage was virulent when implementing the BACHLIP tool;

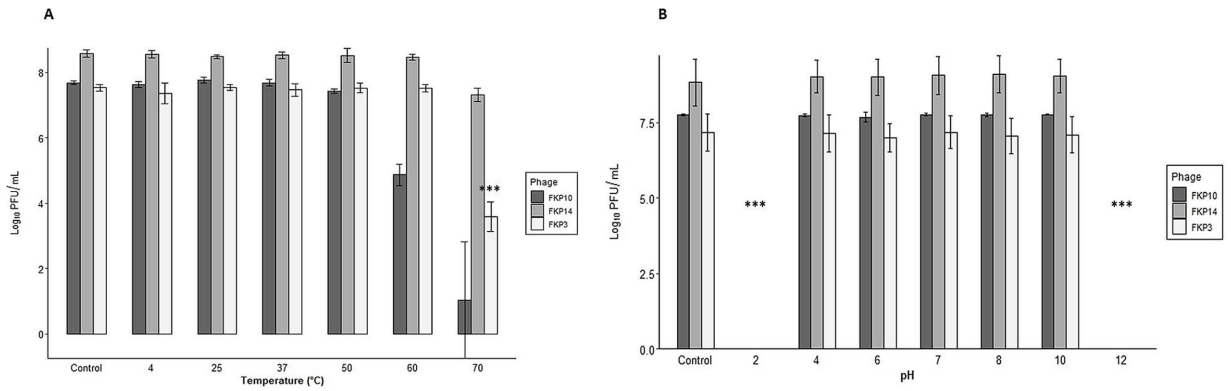

FIGURE 6
Characterization of bacteriophage susceptibility to pH and temperature conditions. **(A,B)** Show the results of phage stability at different temperatures and pH conditions, respectively. In general, all three bacteriophages were stable at temperatures between 4°C and 50°C. A decrease of 3.9 Log was observed in the FKP3 bacteriophage at a temperature of 70°C (ANOVA, $p = 4.22 \times 10^{-11}$ ***). A decrease of 2.8 Log at 60°C was observed in phage FKP10 (Kruskal-Wallis, Dunnet test adjusted with the Bonferroni method; $p = 1.0$) and 6.6 Log at 70°C (Kruskal-Wallis, Dunnet test adjusted with Bonferroni method; $p = 0.258$). All three bacteriophages were stable at pH 4–10 (FKP3, Kruskal-Wallis $p = 0.849$; FKP10, ANOVA $p = 0.700$ and FKP14, Kruskal-Wallis $p = 0.957$), whereas they lost their stability at pH 2 and 12.

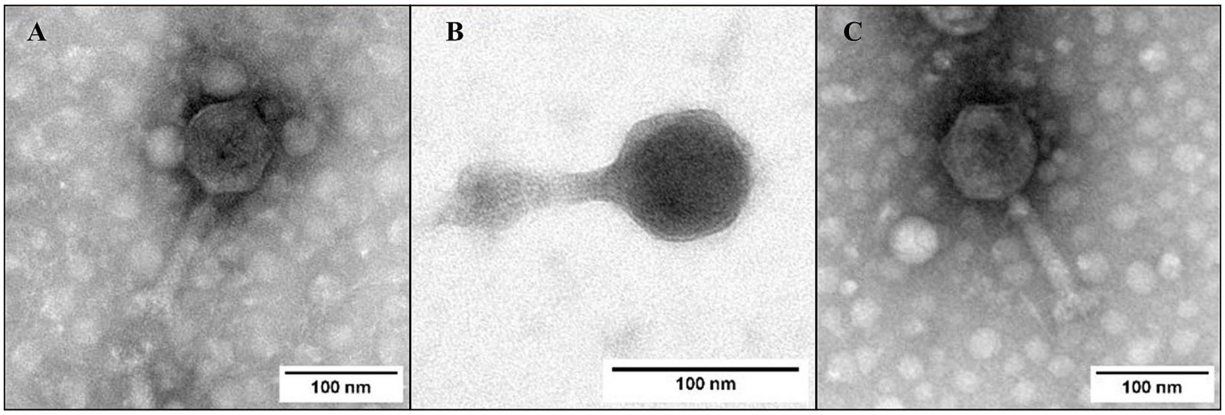

FIGURE 7
Bacteriophage morphology. **(A–C)** Show photographs taken by transmission electron microscopy (TEM) of FKP3, FKP10, and FKP14, respectively. The three bacteriophages had tails sized 165.6 nm ±1.2 and 208.1 nm ±1.1. The scale bar represents 100 nm.

however, both the Phage AI and phaTYP tools predicted with high probabilities (> 90%) that all three bacteriophages were virulent (Table 2). No virulence-associated or antimicrobial resistance genes were detected in the bacteriophages.

3.2.9 Comparative genomics and phylogenetic analysis

Figure 8A shows multiple alignments of *Klebsiella* phage genomes containing two syntenic colinear blocks (homologous regions). This alignment was consistent with high ANIb values between FKP10 and FKP14 (ANIb% between 95.83 to 96.04%), indicating greater genomic similarity, and lower ANIb values for FKP3 (ANIb% with FKP10 between 62.08 to 62.26%; ANIb% with FKP14 between 67.11 to 70.08%). Based on these results, FKP10 and FKP14 phages were more closely related to each other than to FKP3. Figure 8B presents a comparative circular map of the protein-coding genes of the three annotated genomes. Furthermore, a genome-to-genome distance-based phylogenetic tree was constructed using closely related phages based on ANIb values and Viptree Sg scores, with distant members set as outgroups from the *Drexlerviridae* and *Autographiviridae* families. This phylogenetic tree was composed of 4 families, 4 genera and 43 species clusters; and the phages FKP10 and FKP14 belonged to the *Ackermannviridae* family and *Taipeivirus* genus, whereas FKP3 belonged to the *Stephanstirmvirinae* and *Justusliebigvirus* families (Figure 9).

4 Discussion

Although bacteriophages were discovered more than 100 years ago, during the last two decades, the use of these viruses to combat antibiotic-resistant bacteria has increased, making them attractive alternatives for the control of carbapenem-resistant clones of *K. pneumoniae* (CRKP), which have successfully spread in clinical and

TABLE 2 Genomic profile of FKP3, FKP10, and FKP14 bacteriophages active against *K. pneumoniae*.

Genomic profile	*Klebsiella* phage FKP3	*Klebsiella* phage FKP10	*Klebsiella* phage FKP14
Size (bp)	142277	159358	157205
Genome organization	Linear	Circularly permuted	Circularly permuted
Depth	125X	111X	139X
GC content (%)	39.56	46.57	46.3
Completeness	100	100	99.94
ORF	305	246	233
CDS	303	244	231
Hypothetical proteins	212	140	129
Functional proteins	91	104	102
tRNA*	21	8	7
Termini	Short direct terminal repeats (DTRs) of 317 bp length	Headful packaging (PAC)	Non identified**
Taxonomy			
Family	*Stephanstirmvirinae*	*Ackermannviridae*	*Ackermannviridae*
Genus	*Justusliebigvirus*	*Taipeivirus*	*Taipeivirus*
In silico replicative cycle			
PhageAI (virulent)	91.74%	92.49%	92.80%
BACHLIP (virulent)	46.25%	98.39%	94.50%
PhaTYP (virulent)	1.0	1.0	1.0

GC, guanine-cytokine content; ORF, Open Reading Framework; CDS, coding sequences; tRNA, transfer RNA. * Four transfer RNAs were identified in all phages (tRNAMet, tRNATyr, tRNAAsn, tRNAGln). ** Owing to the lack of identified termini in FKP14 genome, the genome was re-arranged it using the large terminase subunit as the start base through the Pharokka pipeline, and as recommended in Shen and Millard 2021.

environmental settings. This study allowed the isolation of highly specific bacteriophages against the CRKP strains CG258 and ST307 with promising biological, structural, and genomic traits.

Although it is important to isolate specific bacteriophages against the strains of interest, it is necessary to perform an individual characterization of bacteriophages to determine their safety and predict their performance in various applications, whether in biocontrol or phage therapy. At present, there are no standardized guidelines that determine which characteristics should be evaluated for the subsequent implementation of bacteriophages; however, some entities, such as the Food and Drug Administration (FDA) and the European Medicines Agency (EMA), have made recommendations to ensure the use of bacteriophages in various applications. These recommendations include confirmation of activity against the strains of interest, origin of the phage, effective concentration of the phage, absence of antibiotic resistance genes, virulence genes, and genes associated with integration or lysogeny (Yang et al., 2023; Furfaro et al., 2018). However, other important characteristics could help predict the performance of bacteriophages against different isolates, including host range, plating efficiency, and infection or killing curves. Considering that these methodologies can be diverse, the selection of criteria for characterization must be aligned with the objective of the research and the type of application.

In recent years, it has become more common to find publications that focus on identifying bacteriophages against high-risk clones; some studies have described the isolation of active phages against clones such as ST11, ST101, ST16, ST13, and ST15, among others (Martins et al., 2022a; Fang and Zong, 2022; Tan et al., 2019; Ciacci et al., 2018; Laforêt et al., 2022; Horváth et al., 2020). Likewise, the isolation of active bacteriophages against CRKP-ST258 has been reported, whereas publications of active phages against emerging clones such as ST307 are limited (Tisalema-Guanopatín et al., 2023; Thiry et al., 2019; D'Andrea et al., 2017; Venturini et al., 2020; Hesse et al., 2020; Ponsecchi et al., 2024).

The FKP3, FKP4, and FKP14 phages exhibited a broad host range with high specificity against CG258 isolates (56 to 60%). This finding aligns with a study by D'Andrea et al., where *K. pneumoniae* bacteriophages displayed a host range covering 52.4% of strains from CG258 (clade II) (D'Andrea et al., 2017). On the contrary, a study published in 2020 by Venturini C et al. reported the isolation of bacteriophages from ST258 (CG258) strains, which only had activity against their host bacteria and not against other strains tested (Venturini et al., 2020).

The high specificity of infection observed in the selected bacteriophages could be associated with the presence of common bacterial receptors in these clones, which are specifically recognized by the receptor binding proteins (RBP) of the phage (De Jonge et al., 2018). In *K. pneumoniae* phages have been described important receptors involved in the specificity of infection, such as capsular type, in these sense Venturini et al. isolated specific bacteriophages against *K. pneumoniae* from CG258, finding a correlation between the host range of the bacteriophages and the capsular type, as well as with the clade to which these clones belonged (Venturini et al., 2020).

On the other hand, phages FKP10 and FKP12 show a wide host range of 66.7–93.3% against CRKP from ST307; which is in line with previous studies conducted at Lyon University Hospital in France (2021), where it was described the isolation and characterization of one *K. pneumoniae* jumbo phage with activity against 80% (24/30) ST307 clones (unpublished data). Recent studies reported the isolation of two phages active against CRKP-ST307 with a host range of up to 85.8% (10/12) of isolates (Ponsecchi et al., 2024).

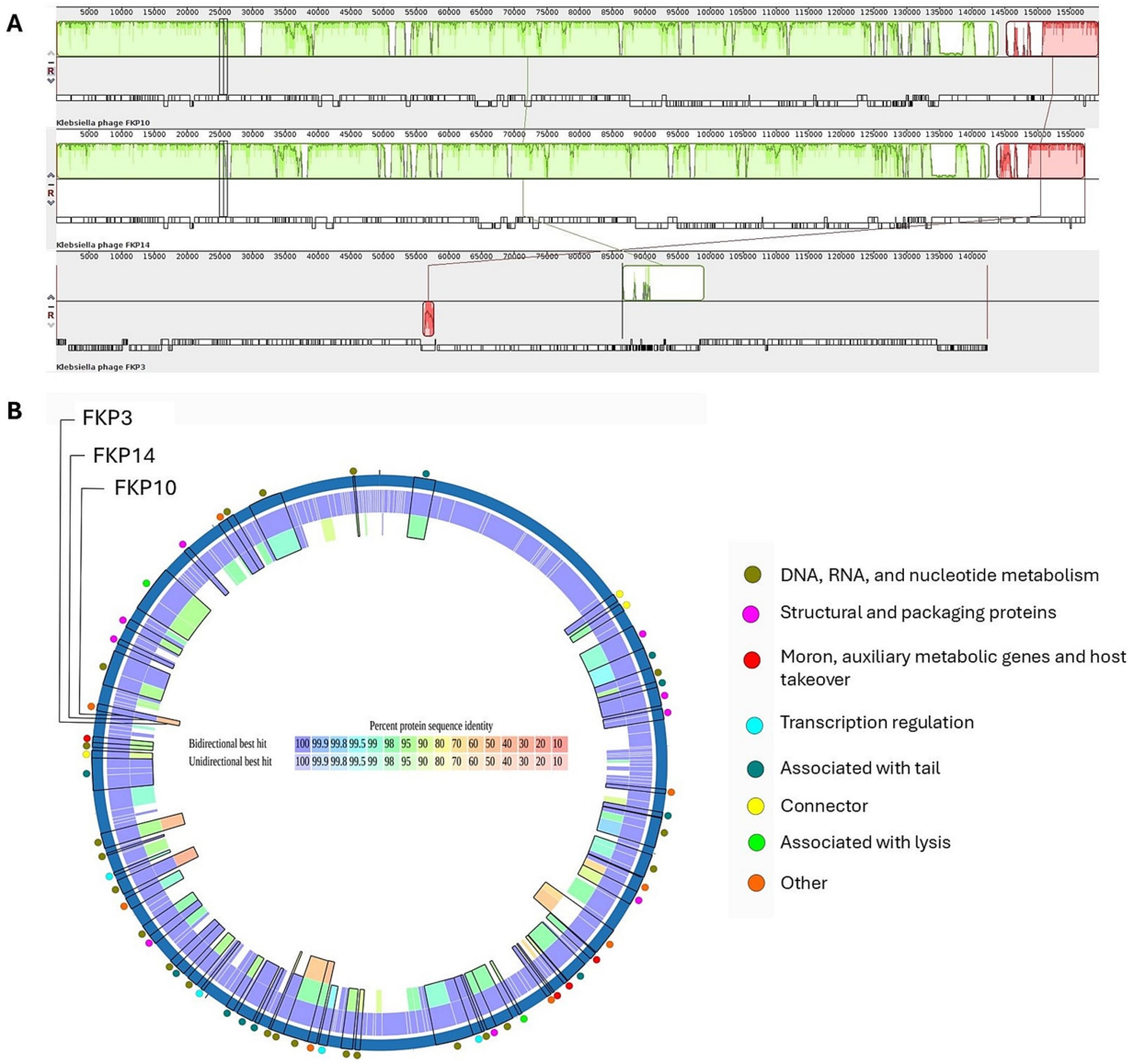

FIGURE 8
Comparative genomics of *K. pneumoniae* bacteriophages. **(A)** Presents a comparison of the genomes of FKP10, FKP14, and FKP3 phages generated using Progressive MAUVE. These phage genomes are arranged horizontally with homologous genomic regions (locally collinear blocks) delineated in the same color. **(B)** Presents a comparative circular map of the protein-coding genes of FKP3, FKP10, and FKP14 phages using PATRIC. The outer colored circles indicate the putative functions of the protein-coding genes. Proteomic analysis revealed the orthology of protein-coding genes between FKP10 and FKP14 phages with >90% sequence identity **(B)**. These protein-coding genes were linked to head and packaging, moron, auxiliary metabolic functions, host interaction, transcription regulation, tail, and lysis. Notably, three lysis-associated genes: endolysin (FKP10 ORF 3, FKP14 ORF 61), RIIB (FKP10 ORF 199, FKP14 ORF 172), and RIIA lysis inhibitors (FKP10 ORF 200, FKP14 ORF 173), had >90% protein sequence identity and were shared exclusively by FKP10 and FKP14. Phage FKP3 exhibited lower protein sequence identity (up to 50%) than FKP10 and FKP14 phages. The shared protein-coding genes among the three phages were involved in DNA, RNA, and nucleotide metabolism.

Finally, phage studies against CRKP from CG258 and ST307 have not only focused on characterization but also evaluated other aspects of the phage's activity related to the mechanisms of resistance to bacteriophages and the effects of bacterial fitness during this process (Thiry et al., 2019; Hesse et al., 2020; Hesse et al., 2021; De Angelis et al., 2021).

The findings of this study are of great interest considering that few publications have reported the isolation and characterization of CRKP phages belonging to CG258 and ST307. Moreover, not all studies that report the isolation of phages against these clones perform host range using a large number of isolates, and in some cases, authors did not evaluate the host range (Tisalema-Guanopatín et al., 2023; D'Andrea et al., 2017; Venturini et al., 2020). Furthermore, many of these studies only assessed host range using the spot test and did not confirm productive phage infection by determining plaque formation in susceptible strains, which may have overestimated phage activity and host range results (D'Andrea et al., 2017; Venturini et al., 2020). Unlike the limitations of these studies, in this work, the productive infection of bacteriophage was determined, and we confirmed that the results of the spot test effectively overestimated the host range from 2.4 to 29.4%, in comparison with the host range assessed by the

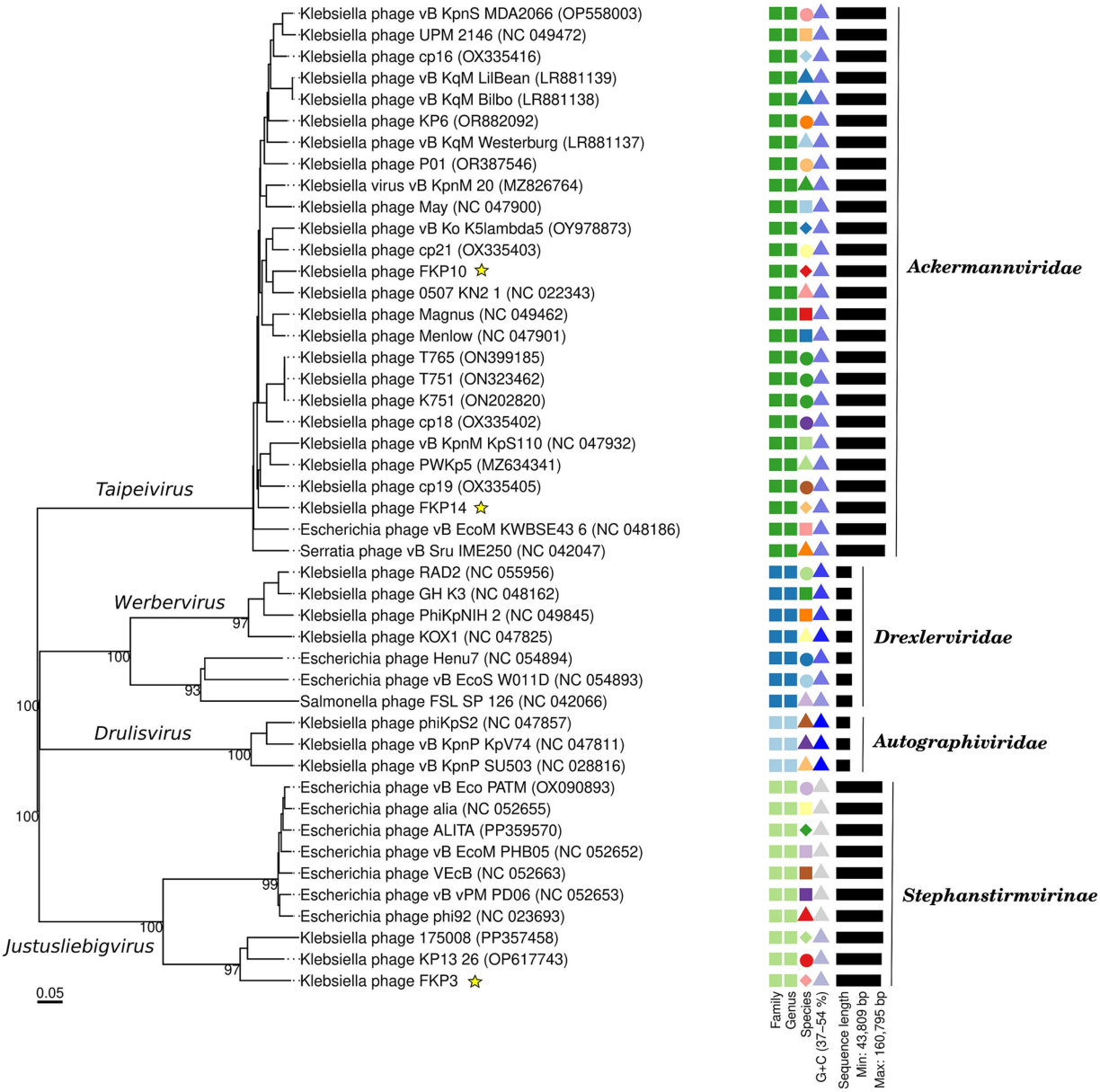

FIGURE 9
Genome-based phylogenetic tree of bacteriophages FKP3, FKP10 and FKP14. The phylogenetic tree was generated by VICTOR nucleotide pairwise comparisons. Yellow stars indicate the phages of interest in this study. The colors and shapes on the right indicate similarities of bacteriophages according to characteristics such as family, genus, species, guanine-cytosine content, and genome size.

determination of plaque formation, highlighting the importance of this confirmation. Finally, our findings showed that bacteriophages efficiently infected 94% of the susceptible strains in the host range (EOP values ≥0.5); which again underlines the importance of this study in comparison to others reported, where the infection efficiency of phages against these important clones is not evaluated (Tisalema-Guanopatín et al., 2023; D'Andrea et al., 2017). Overall, the EOP results for non-CG258 and non-ST307 CRKP phages are diverse and depend on each bacteriophage. Some studies have reported high infection efficiency in the 54.5% of the strains (Kim et al., 2023; Balcão et al., 2022).

Evaluation of the host range in many strains and determination of EOP are important procedures for characterizing bacteriophages because they allow estimation of the probability of success of a bacteriophage against specific groups of bacteria during its application. The host range allows us to identify which bacteria are susceptible to the action of a phage by recognizing common receptors between them. Further, EOP shows how bacteria are permissive for phage replication, which allows us to determine how well phages replicate in infected bacteria compared to their host bacteria by identifying productive infection (Khan Mirzaei and Nilsson, 2015; Kutter, 2009). Permissiveness is also related to the presence of resistance mechanisms to bacteriophages; therefore, our EOP results with values equal to or greater than 1 probably indicate that the strains do not share phage resistance mechanisms; thus, they replicate efficiently in most strains (Hyman and Abedon, 2010).

Although individual bacteriophages showed high species specificity (100%) and specific activity against CRKP from CG258 and ST307, the use of bacteriophage cocktails increased the intra-species host range up to 85.7% ($n = 36/42$) of isolates belonging to both clones, which makes it a very interesting alternative for its implementation in places where both clones circulate frequently, such as hospital settings. The activity of the phages of this study against both clones (85.7%) could indicate additive activity of the phages FKP3, FKP14 (CG258), and FKP10 (ST307); however, it was observed that the cocktail increased the host range up to 80.8% of the CG258 strains and 93.8% of the ST307 strains vs. 56 and 66.7% of the activity obtained with the individual phages, respectively. Furthermore, some bacteria that were not susceptible to either phage individually were susceptible to the cocktail, indicating the possible synergistic activity of the phages in these strains. This work also allowed us to determine whether the cocktail's bacteriophages were replicating during infection by confirming the formation of plaques in susceptible strains, an aspect that has been rarely evaluated in other studies. These findings are of great relevance because they reject the effect of "lysis from without" and confirm that a productive infection of the cocktail phages is taking place; besides, demonstrate that antagonism phenomena during co-infection probably do not occur in most strains (Molina et al., 2022; Kerr et al., 2008).

Several studies have described the use of bacteriophage cocktails to control *K. pneumoniae*; however, a specific cocktail has not been described to control high-risk clones such as CG258 and ST07. Other publications have focused on the evaluation of phage cocktails in biofilm-producing *K. pneumoniae* or animal infection models to determine the activity of the cocktails against specific strains (Zurabov et al., 2023; Kelly and Jameson, 2024; Liang et al., 2023; Singh et al., 2022). Furthermore, most studies that evaluate the activity of cocktails only determine their effectiveness through a killing curve with some strains, and there are few publications that re-evaluate the performance of cocktails with various isolates as is usual with the host range (Jokar et al., 2023). According to a study published in 2023, the use of a cocktail of 4 bacteriophages increased the host range from 52 to 75% of the isolates, preventing bacterial regrowth (Jokar et al., 2023). Another study published in Kenya determined the performance of a cocktail in 8 strains and reported no differences between the administration of individual or combination bacteriophages (Michodigni et al., 2022). These studies contrast with the present work, in which various cocktails were evaluated against several isolates and productive infection was confirmed. Furthermore, the use of cocktails significantly increased the host range against CG258 and ST307, with higher percentages observed than those reported in previous studies, indicating a greater probability of cocktail success.

Additionally, the performance of the cocktails was determined using the infection curve obtained after 23 h, which differs from some studies on *K. pneumoniae* phages in which evaluation is shorter, making it more difficult to identify phage-resistant subpopulations over time (Fayez et al., 2023). In general, our phages showed significant control of bacterial growth but did not exhibit complete elimination. Furthermore, the cocktails presented mixed results, and in some cases, an improvement in the performance of the cocktail was observed at low MOIs compared to the performance of the individual phage. The use of the cocktail at MOIs of 0.1 and 0.01 on the host bacteria of phages FKP3 (CRKP-ST 512, strain KP58) and FKP10 (CRKP-ST307, strain KH45) delayed the appearance of phage-resistant bacteria; compared to the individual phage results at the same MOIs. Therefore, the cocktail achieved a performance like the individual phage FKP3 and FKP10 at an MOI of 1 (FKP3, 82.70% control first 6 h; FKP10, 67.55% control first 12 h), whose concentration was the best in all cases. These findings coincide with those of other studies in which the use of the cocktail delayed the appearance of subpopulations resistant to phages (Kondo et al., 2023). However, other publications have reported that the use of cocktails did not perform significantly better than that of phage alone (Concha-Eloko et al., 2023); which was also evidenced in our results with the host bacteria of phage FKP14 (CRKP-ST258, strain KR06). These findings demonstrate the importance of evaluating cocktails using infection curves with different strains, considering that the behavior may vary and could be related to the resistance mechanisms of bacteria to phages.

It is well known that the use of cocktails offers advantages compared to the administration of individual phages because they expand the host range, and their use decreases the probability of selecting phage-resistant bacteria. In this sense, it is ideal to use combinations of phages with affinity for different receptors, considering that the use of bacteriophages that recognize the same receptor could be ineffective due to the development of bacterial resistance mechanisms related to mutations that cause cross resistance (Abedon et al., 2021; Yoo et al., 2024). The use of phages that recognize different receptors can delay or prevent the emergence of resistance; which was observed in this study; However, in our case, it could be necessary to use an additional phage to control the remaining resistant subpopulations, administer the phages from the cocktail sequentially over time, or use combinations of bacteriophages with other compounds. Some studies have documented a greater reduction in bacterial growth when *K. pneumoniae* phage cocktails are combined with antibiotics such as meropenem and tigecycline (Martins et al., 2022b; Michodigni et al., 2022). Furthermore, it has been reported that the use of bacteriophages and chemical disinfectants is more effective in eliminating biofilms and bacteria on surfaces (Chen et al., 2024).

On the other hand, the results of the one-step curve indicated rapid replication of the bacteriophages and rapid release of viral particles (latency time 10 min). Some studies have shown that phages with short latency periods lyse more bacteria at each time, demonstrating their potential for rapid control of bacterial populations (Fang et al., 2023). The burst size results were obtained when the infection was carried out at an MOI of 0.01 and under these conditions there was a low production of viral progeny (5–18 per infected cell). In this sense, the burst size results coincide with those observed in the elimination curve at an MOI of 0.01, where there was no evident control of bacterial growth, which is related to the low production of bacteriophages that infect adjacent bacteria. Although it is considered that the bacteriophages with the greatest potential are those with a large burst size, it has been reported that bacteriophages with small burst sizes are associated with short lysis cycles, as observed in this study. This can also be considered an advantage by favoring the development of several replication cycles in shorter timeframes and faster viral particle production (Shao and Wang, 2008). Other authors have described small burst sizes (6 to 63 bacteriophages per infected cell) in *K. pneumoniae* phages, however, the possible limitations caused by burst size could be solved with the use of higher MOI or the combined use of other bacteriophages, antibiotics, or compounds

(Tisalema-Guanopatín et al., 2023; Peng et al., 2023; Gordillo Altamirano and Barr, 2019).

Finally, the bacteriophages that made up the best cocktail belonged to the class of *Caudoviricetes* and to the families *Stephanstirmvirinae* (FKP3) and *Ackermannviridae* (FKP10 and FKP14), with the latter being one of the most frequently reported phages against *Klebsiella* (Tisalema-Guanopatín et al., 2023; Assafiri et al., 2021). All bacteriophages were virulent; however, in phage FKP3, a gene was identified that encodes an RDF (recombination directionality factor) protein. This gene is involved in the directionality of site-specific recombination mediated by integrases (Lewis and Hatfull, 2001). However, FKP3 did not possess other genes related to the lysogenic cycle, and tools *in silico* indicated a high probability (91.74%) of being virulent. Some authors have reported that RDF proteins can accomplish functions related to the process of DNA replication; therefore, the acquisition of the RDF gene may be due to evolutionary processes and requires further studies of its transcription and functionality (Payaslian et al., 2021). In addition, no genes encoding virulence or antibiotic resistance factors were found in the three genomes, which supports the safety of these bacteriophages for their implementation in future applications. Other results showed that bacteriophages harbor several tRNAs in their genomes, which are associated with lytic replication cycles (Bailly-Bechet et al., 2007; Nepal et al., 2022). Likewise, the presence of tRNA enables viral proteins to be translated more efficiently, reducing latency times, which could be evidenced in the three bacteriophages evaluated, whose eclipse and latency periods were short (Bailly-Bechet et al., 2007). Finally, genes associated with lysis proteins, such as endolysins and Rz-type spins, were identified in the genomes of the three bacteriophages, and these genes are related to Gram-negative lysis processes (Kongari et al., 2018; Briers et al., 2014).

The evaluation of the biological and structural characteristics of the bacteriophages isolated in this study supports the development of new applications, particularly in critical scenarios with high CRKP levels in CG258 and ST307. These bacteriophages could be used at higher MOIs in scenarios where the target bacterial population is not very high and under conditions where the bacteria have slower replication rates that allow control of the bacterial population. In this context, bacteriophages could be used as part of a surface disinfection strategy in hospital settings given that CRKPs CG258 and ST307 are frequently found in these settings and spread easily, causing healthcare-associated infections (Centeleghe et al., 2023). In addition, its use could be explored in hospitals and community wastewater where these pathogens have been frequently reported (Jassim et al., 2016). Finally, considering the specificity of infection against these high-risk clones, the bacteriophages isolated in this study could be implemented as diagnostic and epidemiological surveillance tools, considering that CRKP of CG258 and ST307 are the main circulating clones at the local and global levels (Fu et al., 2015).

The limitations and perspectives of this study are related with the evaluation of the mechanism of action of the bacteriophages and receptors involved. Furthermore, the evaluation of phage-resistant populations, resistance mechanisms, and phenomena such as trade-off (resensitization to antibiotics, altered metabolism, decreased virulence) (Burmeister et al., 2020; Gordillo Altamirano et al., 2021; Chan et al., 2016; Fujiki et al., 2023). Finally, additional combinations with antibiotics or other compounds and the study of the functionality of some genes of biotechnological interest, such as endolysins, are expected.

5 Conclusion

In this study, cocktails of bacteriophages with high activity against CRKP isolates belonging to the successful clones CG258 and ST307 were obtained. Through the individual characterization of each of these bacteriophages, promising biological, structural, and genomic traits were identified, infection specificity against *K. pneumonie* of CG258 and ST307, high lytic activity, short latency periods, rapid replication cycles, stability at varying pH and temperature conditions, and the absence of genes associated with antibiotic resistance and virulence. Together, these results show the potential of these bacteriophage combinations for the control of carbapenem-resistant *K. pneumoniae* of the CG258 and ST307 and, in turn, constitute a starting point for future *in vitro* and *in vivo* studies where these bacteriophages are implemented in clinical and environmental scenarios. The characterization results obtained in this work allow the prediction of the performance of bacteriophages during applications.

Data availability statement

The datasets presented in this study can be found in online repositories. The names of the repository/repositories and accession number(s) can be found below: https://www.ncbi.nlm.nih.gov/ (PP895363.1, PP974338.1, and PP974339.1).

Author contributions

ST-C: Conceptualization, Data curation, Investigation, Methodology, Validation, Visualization, Writing – original draft, Writing – review & editing. LS-O: Conceptualization, Data curation, Formal analysis, Investigation, Methodology, Supervision, Visualization, Writing – original draft, Writing – review & editing. JNJ: Conceptualization, Investigation, Methodology, Project administration, Supervision, Writing – original draft, Writing – review & editing.

Funding

The author(s) declare that financial support was received for the research, authorship, and/or publication of this article. This research was supported by the Ministerio de Ciencia y Tecnología (Minciencias, project: 111589785393), Colombia and Escuela de Microbiología, Universidad de Antioquia, Colombia (CODI project: 2021-39930).

Conflict of interest

The authors declare that the research was conducted in the absence of any commercial or financial relationships that could be construed as a potential conflict of interest.

Generative AI statement

The authors declare that no Generative AI was used in the creation of this manuscript.

Publisher's note

All claims expressed in this article are solely those of the authors and do not necessarily represent those of their affiliated organizations, or those of the publisher, the editors and the reviewers. Any product that may be evaluated in this article, or claim that may be made by its manufacturer, is not guaranteed or endorsed by the publisher.

Supplementary material

The Supplementary material for this article can be found online at: https://www.frontiersin.org/articles/10.3389/fmicb.2024.1502593/full#supplementary-material

References

Abedon, S. T., Danis-Wlodarczyk, K. M., and Wozniak, D. J. (2021). Phage cocktail development for bacteriophage therapy: toward improving spectrum of activity breadth and depth. *Pharmaceuticals* 14:1019. doi: 10.3390/ph14101019

Accolti, M. D., Soffritti, I., Piffanell, M., Bisi, M., Mazzacane, S., and Caselli, E. (2018). Efficient removal of hospital pathogens from hard surfaces by a combined use of bacteriophages and probiotics: potential as sanitizing agents. *Infect. Drug Resist.* 11, 1015–1026. doi: 10.2147/IDR.S170071

Adams, M. H. (1959). Bacteriophages. New York: Intersci Publ.

Adnan, M., Ali Shah, M. R., Jamal, M., Jalil, F., Andleeb, S., Nawaz, M. A., et al. (2019). Isolation and characterization of bacteriophage to control multidrug-resistant *Pseudomonas aeruginosa* planktonic cells and biofilm. *Biologicals* 63, 89–96. doi: 10.1016/j.biologicals.2019.10.003

Alcock, B. P., Raphenya, A. R., Lau, T. T. Y., Tsang, K. K., Bouchard, M., Edalatmand, A., et al. (2020). CARD 2020: antibiotic resistome surveillance with the comprehensive antibiotic resistance database. *Nucleic Acids Res.* 48, D517–D525. doi: 10.1093/nar/gkz935

Asghar, S., Ahmed, A., Khan, S., Lail, A., and Shakeel, M. (2022). Genomic characterization of lytic bacteriophages a¥L and a¥M infecting ESBL *K. Pneumoniae* and its therapeutic potential on biofilm dispersal and in-vivo bacterial clearance. *Microbiol. Res.* 262:127104. doi: 10.1016/j.micres.2022.127104

Assafiri, O., Song, A. A.-L., Tan, G. H., Hanish, I., Hashim, A. M., and Yusoff, K. (2021). Klebsiella virus UPM2146 lyses multiple drug-resistant *Klebsiella pneumoniae* in vitro and in vivo. *PLoS One* 16:e0245354. doi: 10.1371/journal.pone.0245354

Bailly-Bechet, M., Vergassola, M., and Rocha, E. (2007). Causes for the intriguing presence of tRNAs in phages. *Genome Res.* 17, 1486–1495. doi: 10.1101/gr.6649807

Balcão, V. M., Moreli, F. C., Silva, E. C., Belline, B. G., Martins, L. F., Rossi, F. P. N., et al. (2022). Isolation and molecular characterization of a novel lytic bacteriophage that inactivates MDR *Klebsiella Pneumoniae* strains. *Pharmaceutics* 14:1421. doi: 10.3390/pharmaceutics14071421

Bolger, A. M., Lohse, M., and Usadel, B. (2014). Trimmomatic: a flexible trimmer for Illumina sequence data. *Bioinformatics* 30, 2114–2120. doi: 10.1093/bioinformatics/btu170

Bonnin, R. A., Jousset, A. B., Chiarelli, A., Emeraud, C., Glaser, P., Naas, T., et al. (2020). Emergence of new non-clonal group 258 high-risk clones among *Klebsiella pneumoniae* Carbapenemase-Producing *K. pneumoniae* isolates, France. *Emerg. Infect. Dis.* 26, 1212–1220. doi: 10.3201/eid2606.191517

Bouras, G., Nepal, R., Houtak, G., Psaltis, A. J., Wormald, P. J., and Vreugde, S. (2023). Pharokka: a fast scalable bacteriophage annotation tool. *Bioinformatics* 39, 1–4. doi: 10.1093/bioinformatics/btac776

Briers, Y., Walmagh, M., Van Puyenbroeck, V., Cornelissen, A., Cenens, W., Aertsen, A., et al. (2014). Engineered Endolysin-based "Artilysins" to combat multidrug-resistant gram-negative pathogens. *MBio* 5, e01379–e01314. doi: 10.1128/mBio.01379-14

Burmeister, A. R., Fortier, A., Roush, C., Lessing, A. J., Bender, R. G., Barahman, R., et al. (2020). Pleiotropy complicates a trade-off between phage resistance and antibiotic resistance. *Proc. Natl. Acad. Sci.* 117, 11207–11216. doi: 10.1073/pnas.1919888117

CDC (2024). AR threats report 2024, 1–2. Available at: https://www.cdc.gov/antimicrobial-resistance/data-research/threats/update-2022.html (Accessed September, 2 2024).

Centeleghe, I., Norville, P., Hughes, L., and Maillard, J.-Y. (2023). *Klebsiella pneumoniae* survives on surfaces as a dry biofilm. *Am. J. Infect. Control* 51, 1157–1162. doi: 10.1016/j.ajic.2023.02.009

Chan, B. K., Sistrom, M., Wertz, J. E., Kortright, K. E., Narayan, D., and Turner, P. E. (2016). Phage selection restores antibiotic sensitivity in MDR *Pseudomonas aeruginosa*. *Sci. Rep.* 6, 1–8. doi: 10.1038/srep26717

Chen, X., Tang, Q., Li, X., Zheng, X., Li, P., Li, M., et al. (2021). Isolation, characterization, and genome analysis of bacteriophage P929 that could specifically lyase the KL19 capsular type of *Klebsiella pneumoniae*. *Virus Res.* 314:198750. doi: 10.1016/j.virusres.2022.198750

Chen, Z., Yang, Y., Li, G., Huang, Y., Luo, Y., and Le, S. (2024). Effective elimination of bacteria on hard surfaces by the combined use of bacteriophages and chemical disinfectants. *Microbiol. Spectr.* 12, 1–14. doi: 10.1128/spectrum.03797-23

Chen, L., Yang, J., Yu, J., Yao, Z., Sun, L., Shen, Y., et al. (2005). VFDB: a reference database for bacterial virulence factors. *Nucleic Acids Res.* 33, D325–D328. doi: 10.1093/nar/gki008

Chen, S., Zhou, Y., Chen, Y., and Gu, J. (2018). Fastp: an ultra-fast all-in-one FASTQ preprocessor. *Bioinformatics* 34, i884–i890. doi: 10.1093/bioinformatics/bty560

Ciacci, N., D'andrea, M. M., Marmo, P., Demattè, E., Amisano, F., Di Pilato, V., et al. (2018). Characterization of vB_Kpn_F48, a newly discovered lytic bacteriophage for *Klebsiella pneumoniae* of sequence type 101. *Viruses* 10, 1–16. doi: 10.3390/v10090482

Cienfuegos-Gallet, A. V., Chen, L., Kreiswirth, B. N., and Jiménez, J. N. (2017). Colistin resistance in Carbapenem-resistant *Klebsiella pneumoniae* mediated by chromosomal integration of plasmid DNA. *Antimicrob. Agents Chemother.* 61:e00404-17. doi: 10.1128/AAC.00404-17

Concha-Eloko, R., Barberán-Martínez, P., Sanjuán, R., and Domingo-Calap, P. (2023). Broad-range capsule-dependent lytic Sugarlandvirus against Klebsiella sp. *Microbiol. Spectr.* 11:e0429822. doi: 10.1128/spectrum.04298-22

Cook, R., Brown, N., Redgwell, T., Rihtman, B., Barnes, M., Clokie, M., et al. (2021). INfrastructure for a PHAge REference database: identification of large-scale biases in the current collection of cultured phage genomes. *Phage* 2, 214–223. doi: 10.1089/phage.2021.0007

D'Andrea, M. M., Marmo, P., Henrici De Angelis, L., Palmieri, M., Ciacci, N., Di Lallo, G., et al. (2017). φbO1E, a newly discovered lytic bacteriophage targeting carbapenemase-producing *Klebsiella pneumoniae* of the pandemic clonal group 258 clade II lineage. *Sci. Rep.* 7, 1–8. doi: 10.1038/s41598-017-02788-9

Dancer, S. J. (2014). Controlling hospital-acquired infection: focus on the role of the environment and new technologies for decontamination. *Clin. Microbiol. Rev.* 27, 665–690. doi: 10.1128/CMR.00020-14

Darling, A. E., Mau, B., and Perna, N. T. (2010). progressiveMauve: multiple genome alignment with gene gain, loss and rearrangement. *PLoS One* 5:e11147. doi: 10.1371/journal.pone.0011147

Davis, J. J., Wattam, A. R., Aziz, R. K., Brettin, T., Butler, R., Butler, R. M., et al. (2019). The PATRIC bioinformatics resource center: expanding data and analysis capabilities. *Nucleic Acids Res.* 48, D606–D612. doi: 10.1093/nar/gkz943

De Angelis, L. H., Poerio, N., Di Pilato, V., De Santis, F., Antonelli, A., Thaller, M. C., et al. (2021). Phage resistance is associated with decreased virulence in kpc-producing *klebsiella pneumoniae* of the clonal group 258 clade II lineage. *Microorganisms* 9:762. doi: 10.3390/microorganisms9040762

De Jonge, P. A., Nobrega, F. L., Brouns, S. J. J., and Dutilh, B. E. (2018). Molecular and evolutionary determinants of bacteriophage host range. *Trends Microbiol.* 27, 51–63. doi: 10.1016/j.tim.2018.08.006

Dedrick, R. M., Smith, B. E., Cristinziano, M., Freeman, K. G., Jacobs-Sera, D., Belessis, Y., et al. (2023). Phage therapy of Mycobacterium infections: compassionate use of phages in 20 patients with drug-resistant mycobacterial disease. *Clin. Infect. Dis.* 76, 103–112. doi: 10.1093/cid/ciac453

Diancourt, L., Passet, V., Verhoef, J., Grimont, P. A. D., and Brisse, S. (2005). Multilocus sequence typing of *Klebsiella pneumoniae* nosocomial isolates. *J. Clin. Microbiol.* 43, 4178–4182. doi: 10.1128/JCM.43.8.4178-4182.2005

Domingo-Calap, P., Beamud, B., Mora-Quilis, L., González-Candelas, F., and Sanjuán, R. (2020). Isolation and characterization of two *Klebsiella pneumoniae* phages

encoding divergent Depolymerases. *Int. J. Mol. Sci.* 21:3160. doi: 10.3390/ijms21093160

Ellington, M. J., Kistler, J., Livermore, D. M., and Woodford, N. (2007). Multiplex PCR for rapid detection of genes encoding acquired metallo-β-lactamases. *J. Antimicrob. Chemother.* 59, 321–322. doi: 10.1093/jac/dkl481

Fang, C., Dai, X., Xiang, L., Qiu, Y., Yin, M., Fu, Y., et al. (2023). Isolation and characterization of three novel lytic phages against K54 serotype carbapenem-resistant hypervirulent *Klebsiella pneumoniae*. *Front. Cell. Infect. Microbiol.* 13, 1–13. doi: 10.3389/fcimb.2023.1265011

Fang, Q., and Zong, Z. (2022). Lytic phages against ST11 K47 Carbapenem-resistant Klebsiella pneumoniae and the corresponding phage resistance mechanisms. *mSphere* 7, 1–11. doi: 10.1128/msphere.00080-22

Fayez, M. S., Hakim, T. A., Zaki, B. M., Makky, S., Abdelmoteleb, M., Essam, K., et al. (2023). Morphological, biological, and genomic characterization of *Klebsiella pneumoniae* phage vB_Kpn_ZC2. *Virol. J.* 20:113. doi: 10.1186/s12985-023-02034-x

Fu, X., Ding, M., Zhang, N., and Li, J. (2015). Mycobacteriophages: an important tool for the diagnosis of *Mycobacterium tuberculosis* (review). *Mol. Med. Rep.* 12, 13–19. doi: 10.3892/mmr.2015.3440

Fu, W., Forster, T., Mayer, O., Curtin, J. J., Lehman, S. M., and Donlan, R. M. (2010). Bacteriophage cocktail for the prevention of biofilm formation by *Pseudomonas aeruginosa* on catheters in an in vitro model system. *Antimicrob. Agents Chemother.* 54, 397–404. doi: 10.1128/AAC.00669-09

Fujiki, J., Nakamura, K., Nakamura, T., and Iwano, H. (2023). Fitness trade-offs between phage and antibiotic sensitivity in phage-resistant variants: molecular action and insights into clinical applications for phage therapy. *Int. J. Mol. Sci.* 24:15628. doi: 10.3390/ijms242115628

Furfaro, L. L., Payne, M. S., and Chang, B. J. (2018). Bacteriophage therapy: clinical trials and regulatory hurdles. *Front. Cell. Infect. Microbiol.* 8, 1–7. doi: 10.3389/fcimb.2018.00376

Garneau, J. R., Depardieu, F., Fortier, L. C., Bikard, D., and Monot, M. (2017). PhageTerm: a tool for fast and accurate determination of phage termini and packaging mechanism using next-generation sequencing data. *Sci. Rep.* 7, 1–10. doi: 10.1038/s41598-017-07910-5

Gordillo Altamirano, F. L., and Barr, J. J. (2019). Phage therapy in the postantibiotic era. *Clin. Microbiol. Rev.* 32:e00066-18. doi: 10.1128/CMR.00066-18

Gordillo Altamirano, F., Forsyth, J. H., Patwa, R., Kostoulias, X., Trim, M., Subedi, D., et al. (2021). Bacteriophage-resistant *Acinetobacter baumannii* are resensitized to antimicrobials. *Nat. Microbiol.* 6, 157–161. doi: 10.1038/s41564-020-00830-7

Gurevich, A., Saveliev, V., Vyahhi, N., and Tesler, G. (2013). QUAST: quality assessment tool for genome assemblies. *Bioinformatics* 29, 1072–1075. doi: 10.1093/bioinformatics/btt086

Hesse, S., Malachowa, N., Porter, A. R., Freedman, B., Kobayashi, S. D., Gardner, D. J., et al. (2021). Bacteriophage treatment rescues mice infected with multidrug-resistant *klebsiella pneumoniae* st258. *MBio* 12, 1–11. doi: 10.1128/mBio.00034-21

Hesse, S., Rajaure, M., Wall, E., Johnson, J., Bliskovsky, V., Gottesman, S., et al. (2020). Phage resistance in multidrug-resistant *klebsiella pneumoniae* st258 evolves via diverse mutations that culminate in impaired adsorption. *MBio* 11, 1–14. doi: 10.1128/mBio.02530-19

Ho, Y. H., Tseng, C. C., Wang, L. Y. L. S., Chen, Y. T., Ho, G. J., Lin, T. Y., et al. (2016). Application of bacteriophage-containing aerosol against nosocomial transmission of carbapenem-resistant *acinetobacter baumannii* in an intensive care unit. *PLoS One* 11, 1–11. doi: 10.1371/journal.pone.0168380

Hobson, C. A., Pierrat, G., Tenaillon, O., Bonacorsi, S., Bercot, B., Jaouen, E., et al. (2022). *Klebsiella pneumoniae* Carbapenemase variants resistant to ceftazidime-avibactam: an evolutionary overview. *Antimicrob. Agents Chemother.* 66, 1–18. doi: 10.1128/aac.00447-22

Hockenberry, A. J. (2021). BACPHLIP: Predicting bacteriophage lifestyle from conserved protein domains. *PeerJ* 9:e11396. doi: 10.7717/peerj.11396

Horváth, M., Kovács, T., Koderivalappil, S., Ábrahám, H., Rákhely, G., and Schneider, G. (2020). Identification of a newly isolated lytic bacteriophage against K24 capsular type, carbapenem resistant *Klebsiella pneumoniae* isolates. *Sci. Rep.* 10:5891. doi: 10.1038/s41598-020-62691-8

Horváth, M., Kovács, T., Kun, J., Gyenesei, A., Damjanova, I., Tigyi, Z., et al. (2023). Virulence characteristics and molecular typing of Carbapenem-resistant ST15 *Klebsiella pneumoniae* clinical isolates, possessing the K24 capsular type. *Antibiotics* 12:479. doi: 10.3390/antibiotics12030479

Hyman, P., and Abedon, S. T. (eds.) (2010). "Bacteriophage host range and bacterial resistance" in Advances in applied microbiology. *1st* ed (Elsevier Inc.), 217–248.

Jassim, S. A. A., Limoges, R. G., and El-Cheikh, H. (2016). Bacteriophage biocontrol in wastewater treatment. *World J. Microbiol. Biotechnol.* 32:70. doi: 10.1007/s11274-016-2028-1

Jokar, J., Saleh, R. O., Rahimian, N., Ghasemian, A., Ghaznavi, G., Radfar, A., et al. (2023). Antibacterial effects of single phage and phage cocktail against multidrug-resistant *Klebsiella pneumoniae* isolated from diabetic foot ulcer. *Virus Genes* 59, 635–642. doi: 10.1007/s11262-023-02004-z

Kahn, L. H. (2017). Antimicrobial resistance: a one health perspective. *Trans. R. Soc. Trop. Med. Hyg.* 111, 255–260. doi: 10.1093/trstmh/trx050

Kelly, L., and Jameson, E. (2024). Bacteriophage cocktail shows no toxicity and improves survival of galleria mellonella infected with Klebsiella spp. *J. Virol.* 98:e0027224:6. doi: 10.1128/jvi.00272-24

Kerr, B., West, J., and Bohannan, B. J. M (2008). Bacteriophages: models for exploring basic principles of ecology. ed. S. T. Abedon. Bacteriophage Ecology: Population Growth, Evolution, and Impact of Bacterial Viruses. Cambridge: Cambridge University Press. 31–63.

Khan Mirzaei, M., and Nilsson, A. S. (2015). Isolation of phages for phage therapy: a comparison of spot tests and efficiency of plating analyses for determination of host range and efficacy. *PLoS One* 10:e0118557. doi: 10.1371/journal.pone.0118557

Kim, Y., Lee, S.-M., Nong, L. K., Kim, J., Kim, S. B., and Kim, D. (2023). Characterization of *Klebsiella pneumoniae* bacteriophages, KP1 and KP12, with deep learning-based structure prediction. *Front. Microbiol.* 13, 1–17. doi: 10.3389/fmicb.2022.990910

Kitchel, B., Rasheed, J. K., Patel, J. B., Srinivasan, A., Navon-Venezia, S., Carmeli, Y., et al. (2009). Molecular epidemiology of KPC-producing *Klebsiella pneumoniae* isolates in the United States: clonal expansion of multilocus sequence type 258. *Antimicrob. Agents Chemother.* 53, 3365–3370. doi: 10.1128/AAC.00126-09

Kondo, K., Nakano, S., Hisatsune, J., Sugawara, Y., Kataoka, M., Kayama, S., et al. (2023). Characterization of 29 newly isolated bacteriophages as a potential therapeutic agent against IMP-6-producing *Klebsiella pneumoniae* from clinical specimens. *Microbiol. Spectr.* 11:e0476122. doi: 10.1128/spectrum.04761-22

Kongari, R., Rajaure, M., Cahill, J., Rasche, E., Mijalis, E., Berry, J., et al. (2018). Phage spanins: diversity, topological dynamics and gene convergence. *BMC Bioinformatics* 19, 1–26. doi: 10.1186/s12859-018-2342-8

Kropinski, A. M., and Clokie, M. R. J. (2009). "Bacteriophages. Methods and protocols, volume 1: isolation, characterization, and interactions" in Methods in molecular biology. eds. C. MRJ and A. M. Kropinski (Totowa, NJ: Humana Press), 588.

Kutter, E. (2009). "Phage host range and efficiency of plating" in Methods in molecular biology. eds. M. R. J. Clokie and A. M. Kropinski, vol. *501* ((Clifton, NJ). Totowa, NJ: Humana Press), 141–149.

Laforêt, F., Antoine, C., Reuter, B. B., Detilleux, J., Pirnay, J. P., Brisse, S., et al. (2022). Vitro and in vivo assessments of two newly isolated bacteriophages against an ST13 urinary tract infection *Klebsiella pneumoniae*. *Viruses* 14:1079. doi: 10.3390/v14051079

Larralde, M., and Zeller, G. (2023). PyHMMER: a Python library binding to HMMER for efficient sequence analysis. *Bioinformatics* 39, 4–6. doi: 10.1093/bioinformatics/btad214

Lee, C.-R., Lee, J. H., Park, K. S., Kim, Y. B., Jeong, B. C., and Lee, S. H. (2016). Global dissemination of Carbapenemase-producing *Klebsiella pneumoniae*: epidemiology, genetic context, treatment options, and detection methods. *Front. Microbiol.* 7:895. doi: 10.3389/fmicb.2016.00895

Lewis, J. A., and Hatfull, G. (2001). Control of directionality in integrase-mediated recombination: examination of recombination directionality factors (RDFs) including Xis and cox proteins. *Nucleic Acids Res.* 29, 2205–2216. doi: 10.1093/nar/29.11.2205

Li, S., Ondon, B. S., Ho, S. H., Jiang, J., and Li, F. (2022). Antibiotic resistant bacteria and genes in wastewater treatment plants: from occurrence to treatment strategies. *Sci. Total Environ.* 838:156544. doi: 10.1016/j.scitotenv.2022.156544

Liang, B., Han, B., Shi, Y., Li, X., Zhao, W., Kastelic, J., et al. (2023). Effective of phage cocktail against *Klebsiella pneumoniae* infection of murine mammary glands. *Microb. Pathog.* 182:106218. doi: 10.1016/j.micpath.2023.106218

Łusiak-Szelachowska, M., Weber-Dąbrowska, B., and Górski, A. (2020). Bacteriophages and Lysins in biofilm control. *Virol. Sin.* 35, 125–133. doi: 10.1007/s12250-019-00192-3

Martins, W. M. B. S., Cino, J., Lenzi, M. H., Sands, K., Portal, E., Hassan, B., et al. (2022a). Diversity of lytic bacteriophages against XDR *Klebsiella pneumoniae* sequence type 16 recovered from sewage samples in different parts of the world. *Sci. Total Environ.* 839:156074. doi: 10.1016/j.scitotenv.2022.156074

Martins, W. M. B. S., Li, M., Sands, K., Lenzi, M. H., Portal, E., Mathias, J., et al. (2022b). Effective phage cocktail to combat the rising incidence of extensively drug-resistant *Klebsiella pneumoniae* sequence type 16. *Emerg. Microbes Infect.* 11, 1015–1023. doi: 10.1080/22221751.2022.2051752

McCallin, S., and Zheng, C. (2019). Current state of compassionate phage therapy. *Viruses* 11:343. doi: 10.3390/v11040343

Meier-Kolthoff, J. P., and Göker, M. (2017). VICTOR: genome-based phylogeny and classification of prokaryotic viruses. *Bioinformatics* 33, 3396–3404. doi: 10.1093/bioinformatics/btx440

Michodigni, N. F., Nyachieo, A., Akhwale, J. K., Magoma, G., Ouédraogo, A.-S., and Kimang'a, A. N. (2022). Formulation of phage cocktails and evaluation of their interaction with antibiotics in inhibiting carbapenemase-producing *Klebsiella pneumoniae* in vitro in Kenya. *Afr. J. Lab. Med.* 11, 1–8. doi: 10.4102/ajlm.v11i1.1803

Moges, F., Endris, M., Belyhun, Y., and Worku, W. (2014). Isolation and characterization of multiple drug resistance bacterial pathogens from waste water in hospital and non-hospital environments, Northwest Ethiopia. *BMC. Res. Notes* 7:215. doi: 10.1186/1756-0500-7-215

Molina, F., Menor-Flores, M., Fernández, L., Vega-Rodríguez, M. A., and García, P. (2022). Systematic analysis of putative phage-phage interactions on minimum-sized phage cocktails. *Sci. Rep.* 12, 1–12. doi: 10.1038/s41598-022-06422-1

Mukherjee, S., Huntemann, M., Ivanova, N., Kyrpides, N. C., and Pati, A. (2015). Large-scale contamination of microbial isolate genomes by illumina Phix control. *Stand. Genomic Sci.* 10, 1–4. doi: 10.1186/1944-3277-10-18

Munoz-Price, L. S., Poirel, L., Bonomo, R. A., Schwaber, M. J., Daikos, G. L., Cormican, M., et al. (2013). Clinical epidemiology of the global expansion of *Klebsiella pneumoniae* carbapenemases. *Lancet Infect. Dis.* 13, 785–796. doi: 10.1016/S1473-3099(13)70190-7

Nayfach, S., Camargo, A. P., Schulz, F., Eloe-Fadrosh, E., Roux, S., and Kyrpides, N. C. (2021). CheckV assesses the quality and completeness of metagenome-assembled viral genomes. *Nat. Biotechnol.* 39, 578–585. doi: 10.1038/s41587-020-00774-7

Nepal, R., Houtak, G., Karki, S., Dhungana, G., Vreugde, S., and Malla, R. (2022). Genomic characterization of three bacteriophages targeting multidrug resistant clinical isolates of Escherichia, Klebsiella and Salmonella. *Arch. Microbiol.* 204:334. doi: 10.1007/s00203-022-02948-0

Nishimura, Y., Yoshida, T., Kuronishi, M., Uehara, H., Ogata, H., and Goto, S. (2017). ViPTree: the viral proteomic tree server. Valencia a, editor. *Bioinformatics* 33, 2379–2380. doi: 10.1093/bioinformatics/btx157

Ocampo, A. M., Chen, L., Cienfuegos, A. V., Roncancio, G., Chavda, K. D., Kreiswirth, B. N., et al. (2016). A two-year surveillance in five Colombian tertiary care hospitals reveals high frequency of non-CG258 clones of carbapenem-resistant *Klebsiella pneumoniae* with distinct clinical characteristics. *Antimicrob. Agents Chemother.* 60, 332–342. doi: 10.1128/AAC.01775-15

Ondov, B. D., Treangen, T. J., Melsted, P., Mallonee, A. B., Bergman, N. H., Koren, S., et al. (2016). Mash: fast genome and metagenome distance estimation using MinHash. *Genome Biol.* 17:132. doi: 10.1186/s13059-016-0997-x

Payaslian, F., Gradaschi, V., Rondón Salazar, L., Dieterle, M. E., Urdániz, E., Di Paola, M., et al. (2021). Isolation and characterization of vB_MsmS_Celfi: a new *Mycobacterium tuberculosis* bacteriophage. *Phage* 2, 43–49. doi: 10.1089/phage.2020.0030

Peirano, G., Chen, L., Kreiswirth, B. N., and Pitout, J. D. D. (2020). Emerging antimicrobial-resistant high-risk *Klebsiella pneumoniae* clones ST307 and ST147. *Antimicrob. Agents Chemother.* 64, 1–14. doi: 10.1128/AAC.01148-20

Peng, Q., Ma, Z., Han, Q., Xiang, F., Wang, L., Zhang, Y., et al. (2023). Characterization of bacteriophage vB_KleM_KB2 possessing high control ability to pathogenic *Klebsiella pneumoniae*. *Sci. Rep.* 13:9815. doi: 10.1038/s41598-023-37065-5

Peng, F., Mi, Z., Huang, Y., Yuan, X., Niu, W., Wang, Y., et al. (2014). Characterization, sequencing and comparative genomic analysis of vB-AbaM-IME-AB2, a novel lytic bacteriophage that infects multidrug-resistant *Acinetobacter baumannii* clinical isolates. *BMC Microbiol.* 14, 1–14. doi: 10.1186/1471-2180-14-181

Poirel, L., Walsh, T. R., Cuvillier, V., and Nordmann, P. (2011). Multiplex PCR for detection of acquired carbapenemase genes. *Diagn. Microbiol. Infect. Dis.* 70, 119–123. doi: 10.1016/j.diagmicrobio.2010.12.002

Ponsecchi, G., Olimpieri, T., Poerio, N., Antonelli, A., Coppi, M., Di Lallo, G., et al. (2024). Characterization of four novel bacteriophages targeting multi-drug resistant *Klebsiella pneumoniae* strains of sequence type 147 and 307. *Front. Cell. Infect. Microbiol.* 14:14. doi: 10.3389/fcimb.2024.1473668

Prjibelski, A., Antipov, D., Meleshko, D., Lapidus, A., and Korobeynikov, A. (2020). Using SPAdes De Novo Assembler. *Curr. Protoc. Bioinformatics* 70, 1–29. doi: 10.1002/cpbi.102

Richter, M., Rosselló-Móra, R., Oliver Glöckner, F., and Peplies, J. (2016). JSpeciesWS: a web server for prokaryotic species circumscription based on pairwise genome comparison. *Bioinformatics* 32, 929–931. doi: 10.1093/bioinformatics/btv681

Schwaber, M. J., Lev, B., Israeli, A., Solter, E., Smollan, G., Rubinovitch, B., et al. (2011). Containment of a country-wide outbreak of Carbapenem-resistant *Klebsiella pneumoniae* in Israeli hospitals via a nationally implemented intervention. *Clin. Infect. Dis.* 52, 848–855. doi: 10.1093/cid/cir025

Shang, J., Tang, X., and Sun, Y. (2023). PhaTYP: predicting the lifestyle for bacteriophages using BERT. *Brief. Bioinform.* 24, 1–11. doi: 10.1093/bib/bbac487

Shao, Y., and Wang, I.-N. (2008). Bacteriophage adsorption rate and optimal lysis time. *Genetics* 180, 471–482. doi: 10.1534/genetics.108.090100

Sharma, S., Chatterjee, S., Datta, S., Prasad, R., Dubey, D., Prasad, R. K., et al. (2017). Bacteriophages and its applications: an overview. *Folia Microbiol. (Praha)* 62, 17–55. doi: 10.1007/s12223-016-0471-x

Singh, A., Singh, A. N., Rathor, N., Chaudhry, R., Singh, S. K., and Nath, G. (2022). Evaluation of bacteriophage cocktail on septicemia caused by Colistin-resistant *Klebsiella pneumoniae* in mice model. *Front. Pharmacol.* 13, 1–11. doi: 10.3389/fphar.2022.778676

Steinegger, M., and Söding, J. (2017). MMseqs2 enables sensitive protein sequence searching for the analysis of massive data sets. *Nat. Biotechnol.* 35, 1026–1028. doi: 10.1038/nbt.3988

Surleac, M., Barbu, I. C., Paraschiv, S., Popa, L. I., Gheorghe, I., Marutescu, L., et al. (2020). Whole genome sequencing snapshot of multidrug resistant *Klebsiella pneumoniae* strains from hospitals and receiving wastewater treatment plants in southern Romania. *PLoS One* 15, 1–17. doi: 10.1371/journal.pone.0228079

Swanstrom, M., and Adams, M. H. (1951). Agar layer method for production of high titer phage stocks. *Exp. Biol. Med.* 78, 372–375. doi: 10.3181/00379727-78-19076

Tan, D., Zhang, Y., Cheng, M., Le, S., Gu, J., Bao, J., et al. (2019). Characterization of *klebsiella pneumoniae* ST11 isolates and their interactions with lytic phages. *Viruses* 11, 1–18. doi: 10.3390/v11111080

Terzian, P., Olo Ndela, E., Galiez, C., Lossouarn, J., Pérez Bucio, R. E., Mom, R., et al. (2021). PHROG: families of prokaryotic virus proteins clustered using remote homology. *NAR Genom. Bioinformatics* 3, 1–12. doi: 10.1093/nargab/lqab067

Thiry, D., Passet, V., Danis-Wlodarczyk, K., Lood, C., Wagemans, J., De Sordi, L., et al. (2019). New bacteriophages against emerging lineages ST23 and ST258 of klebsiella pneumoniae and efficacy assessment in galleria mellonella larvae. *Viruses* 11:411. doi: 10.3390/v11050411

Tisalema-Guanopatín, E., Cabezas-Mera, F., Nolivos-Rodríguez, K., Fierro, I., Pazmiño, L., Garzon-Chavez, D., et al. (2023). New bacteriophages members of the Ackermannviridae family specific for *Klebsiella pneumoniae* ST258. *Phage* 4, 99–107. doi: 10.1089/phage.2022.0039

Tynecki, P., Guziński, A., Kazimierczak, J., Jadczuk, M., Dastych, J., and Onisko, A. (2020). PhageAI-bacteriophage life cycle recognition with machine learning and natural language processing. *BioRxiv*, 1–24. doi: 10.1101/2020.07.11.198606

Van Charante, F., Holtappels, D., Blasdel, B., and Burrowes, B. H. (2021). "Isolation of bacteriophages" in Bacteriophages: biology, technology, therapy, Eds. D. R. Harper, S. T. Abedon, B. H. Burrowes, M. L. McConville. vol. 2, 433–464.

Venturini, C., Ben Zakour, N. L., Bowring, B., Morales, S., Cole, R., Kovach, Z., et al. (2020). Fine capsule variation affects bacteriophage susceptibility in *Klebsiella pneumoniae* ST258. *FASEB J.* 34, 10801–10817. doi: 10.1096/fj.201902735R

Villa, L., Feudi, C., Fortini, D., Brisse, S., Passet, V., Bonura, C., et al. (2017). Diversity, virulence, and antimicrobial resistance of the KPCproducing *klebsiella pneumoniae* ST307 clone. *Microb. Genom.* 3:e000110. doi: 10.1099/mgen.0.000110

Walker, B. J., Abeel, T., Shea, T., Priest, M., Abouelliel, A., Sakthikumar, S., et al. (2014). Pilon: an integrated tool for comprehensive microbial variant detection and genome assembly improvement. *PLoS One* 9:e112963. doi: 10.1371/journal.pone.0112963

World Health Organization (2024). WHO bacterial priority pathogens list, 2024, 1–72.

Wyres, K. L., Lam, M. M. C., and Holt, K. E. (2020). Population genomics of *Klebsiella pneumoniae*. *Nat. Rev. Microbiol.* 18, 344–359. doi: 10.1038/s41579-019-0315-1

Xu, L., Sun, X., and Ma, X. (2017). Systematic review and meta-analysis of mortality of patients infected with carbapenem-resistant *Klebsiella pneumoniae*. *Ann. Clin. Microbiol. Antimicrob.* 16:18. doi: 10.1186/s12941-017-0191-3

Yang, X., Dong, N., Chan, E. W. C., Zhang, R., and Chen, S. (2021). Carbapenem resistance-encoding and virulence-encoding conjugative plasmids in *Klebsiella pneumoniae*. *Trends Microbiol.* 29, 65–83. doi: 10.1016/j.tim.2020.04.012

Yang, Q., Le, S., Zhu, T., and Wu, N. (2023). Regulations of phage therapy across the world. *Front. Microbiol.* 14, 1–8. doi: 10.3389/fmicb.2023.1250848

Yoo, S., Lee, K.-M., Kim, N., Vu, T. N., Abadie, R., and Yong, D. (2024). Designing phage cocktails to combat the emergence of bacteriophage-resistant mutants in multidrug-resistant *Klebsiella pneumoniae*. *Microbiol. Spectr.* 12:e0125823. doi: 10.1128/spectrum.01258-23

Yoon, H., Yun, J., Lim, J. A., Roh, E., Jung, K. S., Chang, Y., et al. (2013). Characterization and genomic analysis of two *Staphylococcus aureus* bacteriophages isolated from poultry/livestock farms. *J. Gen. Virol.* 94, 2569–2576. doi: 10.1099/vir.0.053991-0

Zhao, J., Zhang, Z., Tian, C., Chen, X., Hu, L., Wei, X., et al. (2019). Characterizing the biology of lytic bacteriophage vB_EaeM_φEap-3 infecting multidrug-resistant *Enterobacter aerogenes*. *Front. Microbiol.* 10, 1–9. doi: 10.3389/fmicb.2019.00420

Zurabov, F., Glazunov, E., Kochetova, T., Uskevich, V., and Popova, V. (2023). Bacteriophages with depolymerase activity in the control of antibiotic resistant *Klebsiella pneumoniae* biofilms. *Sci. Rep.* 13:15188. doi: 10.1038/s41598-023-42505-3

frontiers | Frontiers in Microbiology

TYPE Original Research
PUBLISHED 07 January 2025
DOI 10.3389/fmicb.2024.1525040

OPEN ACCESS

EDITED BY
Avi Peretz,
The Baruch Padeh Medical Center,
Poriya, Israel

REVIEWED BY
Domenico Franco,
University of Messina, Italy
Tea Glonti,
Queen Astrid Military Hospital, Belgium

*CORRESPONDENCE
Lei Wang
✉ freshair928@163.com;
✉ Wanglei1@lcu.edu.cn

RECEIVED 08 November 2024
ACCEPTED 16 December 2024
PUBLISHED 07 January 2025

CITATION
Liu L, Huang A, Zhang H, Li Y and Wang L (2025) Bacteriophage LDT325 enhances *Pseudomonas syringae* tolerance by improving antioxidant defense in tea plant [*Camellia sinensis* (L.) O. Kuntze]. *Front. Microbiol.* 15:1525040. doi: 10.3389/fmicb.2024.1525040

Bacteriophage LDT325 enhances *Pseudomonas syringae* tolerance by improving antioxidant defense in tea plant [*Camellia sinensis* (L.) O. Kuntze]

Li Liu[1], Anqi Huang[1], Hua Zhang[2], Yubao Li[2] and Lei Wang[2,3]*

[1]College of Agriculture and Biology, Liaocheng University, Liaocheng, China, [2]School of Pharmaceutical Sciences and Food Engineering, Liaocheng University, Liaocheng, China, [3]National Key Laboratory of Macromolecular Drug Development and Manufacturing, Liaocheng University, Liaocheng, China

Bud blight caused by *Pseudomonas syringae* is a serious disease affecting tea plants and causing severe damage to production output and quality. Phages play an important role in controlling the development of bacterial diseases in plants. Previous studies have shown that the tolerance of phage-treated tea plants to bud blight was notably greater compared with that of the control group. In the present study, we determined the effect of bacteriophage therapy on physiological and biochemical parameters of tea leaves. Transmission electron microscopy (TEM) was used to analyze the cellular structure of tea leaves, and bioinformatics was used to analyze the phage. Results revealed that bacteriophage treatment can enhance the expression of antioxidant enzyme genes (*CsSOD*, *CsCAT*, and *CsPOD*). The levels of osmotic adjustment compounds, including proline and soluble sugars, were also elevated, suggesting that bacteriophage enhances the osmotic adjustment capacity in tea plants. TEM analysis revealed that the integrity of the cell structure of the tea leaves treated with phage was notably better compared with that of the control group. Interestingly, we also observed that the phage lysed the animal pathogen *Salmonella* as well as the plant pathogen *P. syringae*. Using NCBI BLASTn to compare the entire genome with other nucleotide sequences, we found that the phage LDT325 exhibited cross-species characteristics that had not been previously reported. In summary, our findings demonstrate that bacteriophages can protect tea plants from damage caused by bacterial diseases by regulating antioxidant systems.

KEYWORDS

***Camellia sinensis*, *Pseudomonas syringae*, bacteriophage, physiological characters, antioxidant enzyme**

1 Introduction

The tea plant is a notable perennial evergreen crop that thrives in tropical and temperate regions (Hao et al., 2018). However, the warm and humid climate promotes the growth and transmission of pathogens that cause numerous plant diseases. Recently, there has been a significant increase in the occurrence of bacterial bud blight in tea plants throughout China. Diseases caused by *Pseudomonas syringae* are widespread and have affected the United States, Australia, and Korea (Tsuji and Takikawa, 2018). Tea bud blight

primarily impacts the young buds and leaves. Tea plantations suffering from bud blight can experience a decline in productivity and quality (Khandan et al., 2013; Bartoli et al., 2015).

P. syringae causes a wide-range of bacterial diseases in plants worldwide. The emergence and spread of *P. syringae* in many tea-producing areas around the world have negatively impacted the sustainability of tea plants (Xin et al., 2018; Yang et al., 2023). *P. syringae* is highly aggressive and spreads rapidly among different plant varieties (Khandan et al., 2013; Bartoli et al., 2015). At present, the management of bud blight disease primarily depends on copper-based treatments and antibiotics; however, studies have shown that the protective effect of copper preparations significantly decreases after plants become infected with bacterial pathogens and improper use can lead to serious harm to the plants (Zhang et al., 2021). Although antibiotics can effectively reduce bacterial diseases, their overuse can promote bacterial resistance and residue accumulation in tea leaves (Batuman et al., 2024). Thus, the growing public consciousness of food safety has resulted in extensive recognition of the necessity of secure and efficient biological control methods for plant diseases.

Bacteriophage is a kind of virus that can specifically infect and destroy bacteria, and has the ability of self-replication. Unlike most antibiotics, phages generally demonstrate strong specificity for particular bacterial species or strains (Nawaz et al., 2023). Their ability to self-replicate enables them to be used as potent antimicrobial agents. Phages have been used not only for treating and preventing bacterial diseases in humans but also for managing plant diseases, detecting pathogens, and assessing food safety (Davidson et al., 2012; Lahlali et al., 2022). In addition, phages are also used to treat and prevent animal diseases, showing good application prospects in animal medicine and aquaculture. Bacteriophages significantly reduce their impact on the environment and non-target microorganisms. Thus, phages are considered more sustainable and safer compared with antibiotics (Buttimer et al., 2017).

Although significant advancements have been made in examining the role of phage in responses to plant bacterial diseases, little information regarding the effect of phage on bacterial disease tolerance in tea plants is available. In this study, we examined the regulatory mechanisms governing phage-mediated bacterial disease resistance in tea plants and evaluated the effect of phage on bacterial disease in tea plants. We determined the effect of phage treatment on various tea seedling factors during tea bud blight, including chlorophyll content, soluble sugar content, free proline (Pro) content, antioxidant enzyme activity, and the expression of the antioxidant defense system.

2 Materials and methods

2.1 Plant material and treatments

The tea variety used in this experiment was Longjing No. 43 (*Camellia sinensis*), which was grown in plastic boxes and cultured in acidic soil. The surface of the leaves was washed with sterile water and disinfected with 75% ethanol for 1 min. After the surface of the leaves was dried, four holes of equal distance were pierced in the middle of the leaves with sterile needles. The 40 μL of *P. syringae* (2×10^7 CFU/mL) was applied to the surface of the leaves and distributed at four needle puncture sites for air drying. The 40 μL of phage suspension (2×10^7 PFU/mL) was similarly applied to the upper surface of the leaves and spread across the same puncture sites. The treated leaves were covered with sterile cotton to protect the injured areas. For comparison, the control group was only infected with the pathogens (Aftab et al., 2022). The negative control was the sterile water group, in which 40 μL of sterile water was applied to the surface of the leaves and distributed at 4 needle puncture points for air drying. The treated leaves were cultured in a climate box at 25°C and 90% humidity for 3 days.

2.2 Sample collection and enzyme extraction

Leaf samples were collected to evaluate the activity of the antioxidant enzymes. The method of extracting the antioxidant enzymes was modified. Leaf samples (1 g) were ground using 5 mL of 50 mM phosphate buffer (pH 7.8). The resulting homogenate was centrifuged at 10,000 $\times g$ for 30 min at 4°C. The supernatants were immediately used to measure enzyme activity (Wang et al., 2024).

2.3 Superoxide dismutase (SOD) activity

A reaction mixture containing 130 mM methionine, 0.75 mM nitroblue tetrazolium, 0.1 mM ethylenediamine tetraacetic acid, and 0.05 M phosphate buffer (pH 7.8) was used to assess SOD activity. Briefly, 0.1 mL of the leaf extract supernatant was added to 3 mL of the reaction mixture. Then, 0.2 mL of a 0.02 mM riboflavin solution was added and the mixture was exposed to fluorescent light (4,000 lux) for 20 min to start the reaction. The complete reaction mixture without the enzyme extract was used as a control. The absorbance at 560 nm was used to calculate SOD activity.

2.4 Catalase (CAT) activity

CAT activity was determined using an ultraviolet spectrophotometer. The reaction solution was prepared with 30% hydrogen peroxide and 50 mM phosphate buffer (pH 7). Then, 0.1 mL of enzyme extract were added to the reaction mixture to start the reaction. The complete reaction mixture without the enzyme extract was used as a control. The absorbance at 240 nm was recorded every 30 s for 3 min.

2.5 Peroxidase (POD) activity

Peroxidase activity was determined by the guaiacol method. First, 50 mM phosphate buffer (pH 7) was added into a beaker followed by 1 mL of guaiacol; the mixture was heated and stirred. The resulting solution was cooled and mixed with 30% H_2O_2, and the leaf extract supernatant was mixed with the reaction solution. The control group was added to the same volume of 50 mM phosphate buffer (pH 7) solution without the enzyme solution. The absorbance was measured at 470 nm.

2.6 RNA extraction and quantitative real-time PCR

The leaf-damaged part was ground into a fine powder in the presence of liquid nitrogen with a high-pressure sterilized mortar and pestle and stored at −80°C (Aftab et al., 2022). The RNA Isolator Total RNA Extraction Reagent (Vazyme, Nanjing, China) was used to extract total RNA from the tea tree tissues, which was reverse-transcribed into cDNA using a reverse transcriptase (ReverTraAce-α, Toyobo Co.). The internal reference gene was Csβ-actin. Real-time qPCR was done using an Applied Biosystems 7500 Real-Time PCR system (Thermo Fisher Scientific, USA). The amplification program was as follows: 95°C for 30 s; 40 cycles at 95°C for 5 s, and annealing at 60°C for 30 s; 95°C for 15 s, 60°C for 1 min, and 95°C for 15 s. The relative expression was calculated using the $2^{-\Delta\Delta Ct}$ method (Wang et al., 2023). The primer sequences are listed in Figure 1. The expression levels were assessed using three replicates.

2.7 Determination of proline (pro) content in tea leaves

The proline content was measured using a slightly altered method. Leaf samples (1 g) were ground in 10 mL of 3% sulfosalicylic acid and the mixture was centrifuged at 10,000 g for 10 min. Next, 2 mL of supernatant was mixed with 2 mL of glacial acetic acid and 2 mL of ninhydrin reagent, then heated in a water bath for 40 min. After cooling to room temperature, 5 mL of toluene was added and the mixture was shaken (Freitas et al., 2019). After the solution formed a layer, the upper solution was removed and the absorbance at 520 nm was measured.

2.8 Determination of soluble sugar content and chlorophyll content in tea leaves

The anthrone method was used to determine the soluble sugar content. A small amount of distilled water and 1.0 g of leaves were added to grind and homogenize. After heating the mixture in a water bath for 30 min, it was cooled and filtered into a 100 mL volumetric flask. After adding 5 mL of distilled water, the residue was extracted with boiling water and filtered into a volumetric flask to a constant volume. The extract (0.5 mL) was transferred to a 25 mL test tube and 5.0 mL of concentrated sulfuric acid and 0.5 mL of anthrone-ethyl acetate reagent were added. After thorough mixing, the mixture was boiled for 1 min (Luo and Huang, 2011). After cooling, the absorbance value was measured at 630 nm.

The chlorophyll content was measured using a spectrophotometer. The leaves (1 g) were mixed with 2.5 mL of 80% acetone solution and a small amount of quartz sand and ground. Next, 10 mL of acetone solution was added and grinding was continued until the sample appeared white. The sample was filtered into a volumetric flask and 80% acetone solution was added to a constant volume. The absorbance was measured at 652 nm (Pérez-Patricio et al., 2018).

2.9 Transmission electron microscopy (TEM)

The tea leaves were immersed in 2.5% glutaraldehyde for 12 h, then removed and rinsed with 0.1 M phosphate buffer (pH 7.0) 3–5 times. Each rinse lasted 15 min. Then, 1% osmotic acid solution was added and incubated for 1–2 h. To remove the excess osmotic acid solution, the sample was rinsed with the same concentration of phosphate buffer solution (pH 7.0) 3 times for 15 min each. The samples were dehydrated in a series of ethanol washes, with the concentration increasing at each step (50%, 70%, 80%, 90%, and 95%) for 15 min per step. Then, they were rinsed in 100% ethanol for 20 min and 100% acetone for another 20 min. The specimens were immersed in a 3:1 embedding agent and acetone solution for 180 min. The samples were embedded and ultra-thin sections (70–90 nm) were cut using a Leica ecaEMUC7 ultra-thin sectioning machine. The sections were mounted onto grids and stained with saturated aqueous uranyl acetate and leaf citrate for TEM (Hitachi, H-7500) (Li et al., 2014). The sterile water group, the treatment group and the control group were treated in the same way.

2.10 Genome sequencing and analysis of vB_PsS_LDT325

A virus extraction kit was used to extract vB_PsS_LDT325 phage nucleic acid. The phage genome samples were submitted to the BIOZERON company for sequencing and the host bacterial sequences were filtered out to obtain a valid phage sequence. The sequencing results were subjected to quality control using FastQC on the raw data. Genome assembly was done using Unicycle, prediction of the genome ORFs using GeneMarkS, and alignment and annotation of functional proteins using GenBank. BLAST searches against the NCBI database were conducted for sequence similarity analyses. Putative virulence factors were screened using the Virulence Factor Database (http://www.mgc.ac.cn/cgi-bin/VFs/v5/main.cgi) and antibiotic resistance genes were screened by the Comprehensive Antibiotic Resistance Database (https://card.mcmaster.ca/analyze/rgi) (Jia et al., 2016; Liu et al., 2019). For genome visualization, the Proksee Server (https://proksee.ca/) and Easyfig_2.2.5_win were selected. Evolutionary trees were constructed using the ClustalW program in MEGA (Kumar et al., 2018).

2.11 Double-layer plate method was used to verify whether phage LDT325 lyses Salmonella

The double-layer plate method was used to determine whether the phage lyses Salmonella. The 200 μL Salmonella solution (2×10^7 CFU/mL) was poured into 5 mL LB semi-solid agar medium [LB containing 0.4% (w/v) agar] at 55°C, and then immediately poured into the plate of LB solid agar medium [LB containing 1.5% (w/v) agar] to prepare a double-layer plate. Approximately 10 μL of phage filtrate was added to the solidified semi-solid LB plate and cultured at 37°C for 12 h to observe whether there were transparent

Name	Forward primer(5'-3')	Reverse primer(5'-3')
CsSOD	GATGACGGAACTGCTTGCTT	ATCAGGGTCTGCATGGACAA
CsCAT	CCTGAACGTGTTGTCCATGC	AACCTCGAGGATCCCTCAG
CsPOD	GCCACACTTCGCTTATTCTT	AGCCAGGACTACAACATCTC
Csβ-actin	GATTCCGTTGCCCTGAAGTCCT	CCTTGCTCATACGGTCTGCGATA

FIGURE 1
Primers used for gene expression analysis.

areas or plaques at the inoculation site. Purification: A single plaque was taken with a sterile gunhead, placed in SM buffer for 12 h, and filtered with 0.22 μm filter membrane. After filtration, the filtrate and Salmonella were taken to prepare a double-layer plate again, and a single plaque was taken for purification for 4 times to obtain a purified phage (Cao et al., 2022).

2.12 Statistical analysis

Data were analyzed using GraphPad Prism 8.0.2, specifically employing one-way analysis of variance. At least three independent replicates were performed under identical conditions, and data were presented as the mean ± standard deviation. Statistical significance was assessed based on *P*-value, and *P*-values of <0.05 were considered to indicate statistical significance.

3 Results

3.1 Effect of phage on antioxidant enzyme activity in tea plant leaves

Antioxidant enzyme activity in the phage-treated leaves exhibited an upward trend. Inoculation of sterile water did not affect the antioxidant enzyme activity of tea leaves. The antioxidant enzyme activities of SOD, CAT, and POD in the leaves of the control- and phage-treated plants did not change significantly at the initial stage (Figures 2A–C). At 24–72 h, the antioxidant enzyme activity of phage-treated leaves was higher compared with that of the control group. At 24 and 72 h, SOD activity in the phage-treated group was significantly higher compared with that in the control group (13.11% and 11.11% higher, respectively). At 48 and 72 h, CAT activity in the phage-treated group was higher compared with that in the control group (24.35% and 24.03% higher, respectively). At 24 and 72 h, POD activity in the phage-treated group was significantly higher compared with that in the control group (8.33% and 9.38% higher, respectively). The results indicate that phage can enhance the activity of antioxidant enzymes.

3.2 Effect of phage treatment on the expression of antioxidant enzymes in tea plants

As shown in Figures 2D–F, inoculation with sterile water did not affect the relative expression of CsSOD, CsCAT, and CsPOD in tea leaves. The relative expression of *CsSOD*, *CsCAT*, and *CsPOD* in the leaves of the control and phage-treated plants did not change significantly at the initial stage; however, the relative expression of *CsSOD* in phage-treated leaves was significantly higher compared with that in the control at 24–72 h. At 48–72 h, the relative expression of CsCAT in the leaves of the phage-treated group was higher compared with that of the control. The relative expression of CsPOD in the control and phage-treated leaves exhibited a trend of increasing first and then decreasing; however, the relative expression of CsPOD in the phage-treated leaves was significantly higher compared with that in control throughout the experiment, reaching a peak at 24 h. These results indicate that phage treatment significantly increases the expression of antioxidant enzyme-related genes in tea leaves.

3.3 Effects of phage on the pro content, soluble sugar, and chlorophyll content in tea plants

Inoculation of sterile water did not affect the proline content, soluble sugar content, and chlorophyll content in tea leaves. At 48 h, compared with the control group, the proline content in the phage-treated tea increased by 20.83% (Figure 3A). At 72 h, soluble sugar levels in tea leaves treated with phage increased by 45.11%, compared with that in the control group (Figure 3B). Furthermore, during the whole experiment, the soluble sugar and proline content in phage-treated tea leaves remained higher than that in the control group. Chlorophyll in the tea plants was reduced with an increase period of bacterial disease stress and phage treatment slowed the decline of chlorophyll in the leaves. The chlorophyll content in the tea leaves treated with phage consistently exceeded that of the control group (Figure 3C). At 72 h, the chlorophyll content of the phage group was

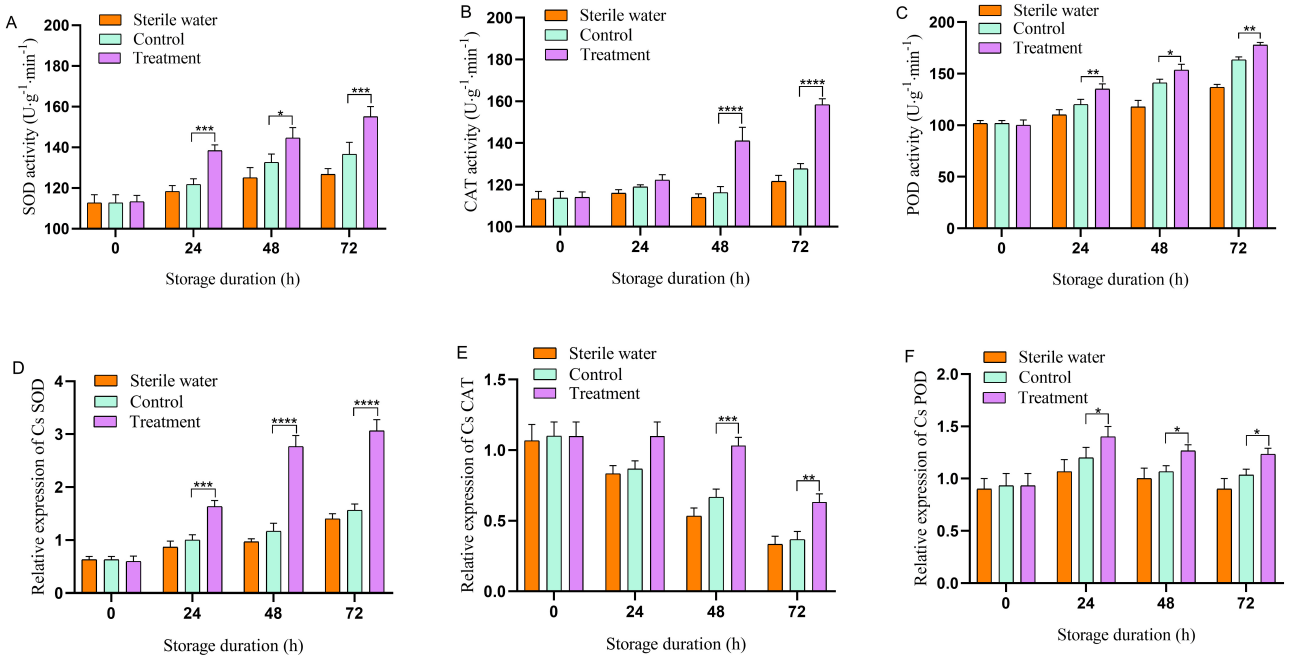

FIGURE 2
Effects of phage on antioxidant enzyme activity and gene expression in tea at designated time. **(A)** Superoxide dismutase (SOD), **(B)** catalase (CAT), **(C)** peroxidase (POD), **(D)** CsSOD, **(E)** CsCAT, **(F)** CsPOD. Vertical bars indicate the standard error of the mean values. Asterisks imply statistically significant differences ($p < 0.05$) between the control and phage treated group in the same day.

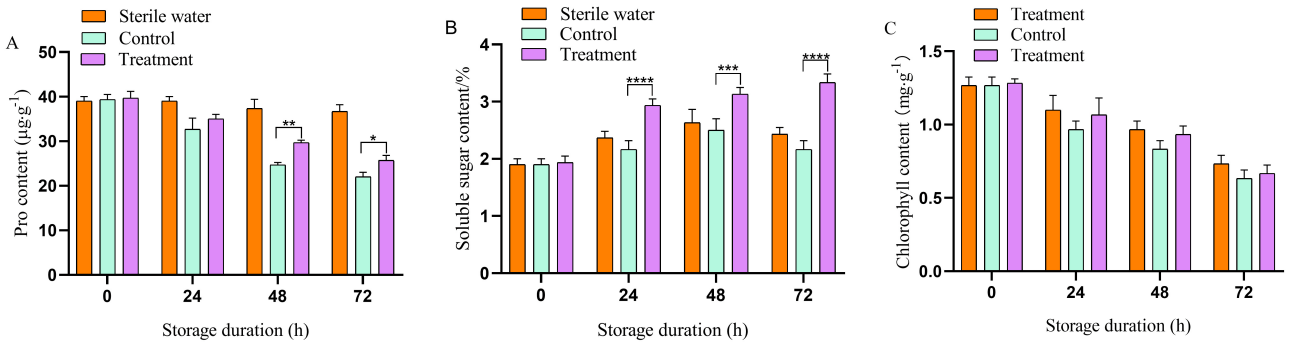

FIGURE 3
Phage affecting on physiological parameters of tea leaves. **(A)** Proline content, **(B)** soluble sugar content, **(C)** chlorophyll content. Vertical bars indicate the standard error of the mean values. Asterisks imply statistically significant differences ($p < 0.05$) between the control and phage treated group in the same day.

significantly higher compared with that of the pathogen-treated group (16.67% higher).

3.4 Transmission electron microscope of tea leaves

Cell morphology was observed by TEM. Image analysis of the sterile water group showed that the cell wall and cell membrane were clear, and there were complete cell structures, such as mitochondria and thylakoids (Figures 4A, B). These characteristics were the same as the internal morphological structure of healthy leaves. In contrast, the images of the control group infected with *Ps* exhibited cell lysis and a lack of cell structure, indicating necrosis (Figures 4C, D). The images of the phage-treated group showed clear cell structures, including a cell wall, mitochondria, thylakoid, and cell membrane (Figures 4E, F). This indicates that phage LDT325 effectively inhibits *P. syringae*.

3.5 Whole genomic and phylogenetic analysis of vB_PsS_LDT325

The sequencing results indicate that vB_PsS_LDT325 is a long-tailed bacteriophage, which is in consistent with the findings from previous electron microscopy studies. Phage LDT325 has a

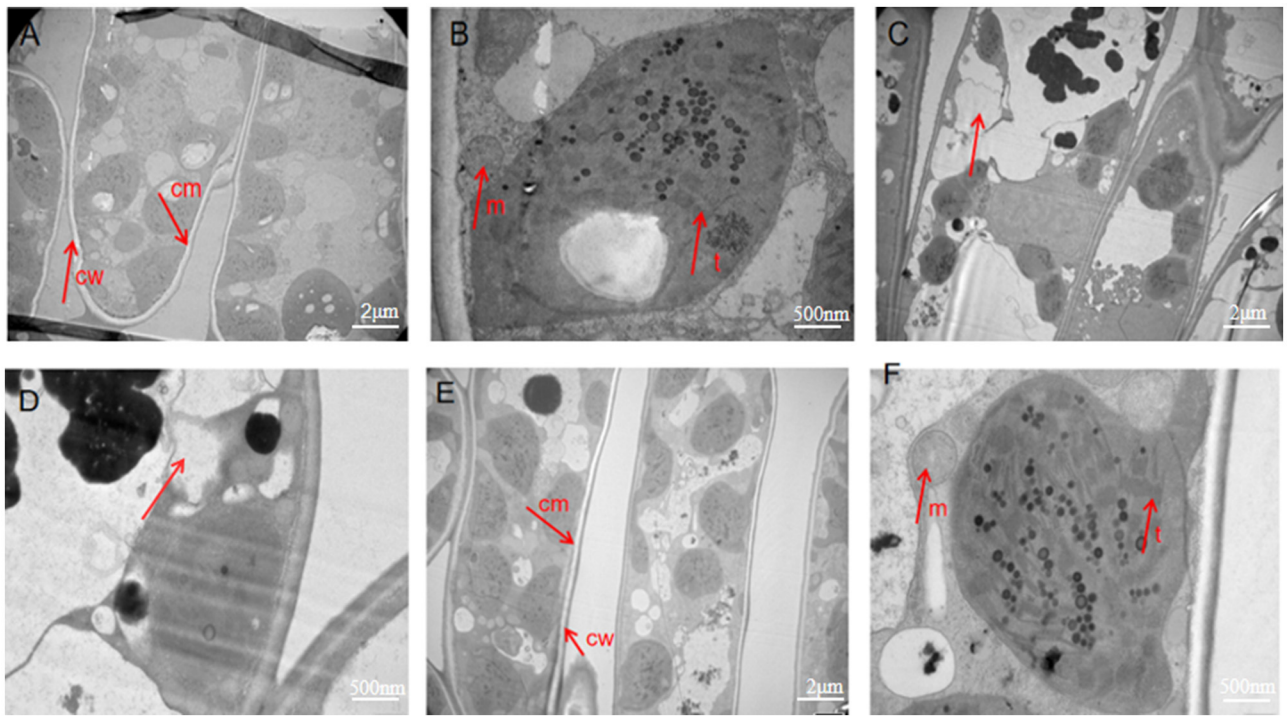

FIGURE 4
Transmission electron microscopy images of ultrathin sections of tea leaves. **(A, B)** Transmission electron microscopy images of ultrathin sections of tea leaves in sterile water group. **(A)** Observed at 1,000×. **(B)** Observed at 5,000×. **(C, D)**Transmission electron microscopy images of ultrathin sections of tea leaves in the control group. **(C)** Observed at 1,000×. **(D)** Observed at 5,000×. **(E, F)** Transmission electron microscopy images of ultrathin sections of tea leaves in phage treatment group. **(E)** Observed at 1,000×. **(F)** Observed at 5,000×. cw, cell wall; cm, cell membrane; m, mitochondria; t, thylakoid.

length of 43,781 bp with a G+C% content of 48.82% (Figure 5A). The entire genomic sequence was subjected to an NCBI BLASTn analysis and the results indicated that it had high similarity with the *Salmonella* phage GRNsp6 (ON526838.1, query coverage 92%, nucleotide homology 94.98%). The complete genomic sequence and annotation information of the phage were submitted to GenBank under accession number PP389045. In addition, a phylogenetic tree was created using the amino acid sequence of the major capsid protein of the vB_PsS_LDT325 bacteriophage. The evolutionary status of the phage LDT325 was also evaluated by phylogenetic analysis to select the 11 existing phages from the database, including 9 *Salmonella* strains, 1 *Escherichia*, and 1 Jersey virus phage. Phylogenetic tree analysis revealed that the LDT325 phage was clustered on a distinct branch and its closest relative was phage GRNsp6 (Figure 5B). Phage LDT325 contains 61 CDS, including 4 DNA replication/repair functional proteins (DNA ligase, DNA polymerase, DNA primer enzyme, DNA helicase, DNA polymerase, RNA polymerase, integrated host factor), and 4 nucleotide metabolism proteins (ribonuclease, recombinant endonuclease, recombinant exonuclease), 15 phage structural proteins (main tail fiber protein, bottom plate protein, tail tube protein, tail sheath protein, main capsid protein, major termination enzyme subunit, gate protein), 1 host lysis/interaction protein (bacteriolysin, hole protein), and 11 other function proteins. The remainder are annotated as hypothetical proteins (Supplementary Table S1). The entire genome was uploaded to the Virulence Factor Database and the Comprehensive Antibiotic Resistance Database; no bacterial toxin genes or antibiotic resistance genes were detected. Additionally, lysogenic-related genes, such as integrase, recombinase, cleavage enzyme, and inhibitory enzyme, were not found.

3.6 Comparative genomics of phage vB_PsS_LDT325

Phage vB_PsS_LDT325 was subjected to a multiple genomic comparison with the phage of the genus "*Salmonella* phage GRNsp6." The results indicated that phage vB_PsS_LDT325 exhibited an extremely high protein homology (>78%). The homologous protein modules primarily included DNA replication/repair, nucleotide metabolism, and phage structure, particularly in terms of phage structure and DNA replication/repair (Figure 6).

3.7 Phage vB_PsS_LDT325 lyses Salmonella

The results showed that there were clear and bright plaques on the double-layer agar plate. After 4 times of purification, plaque with uniform size and

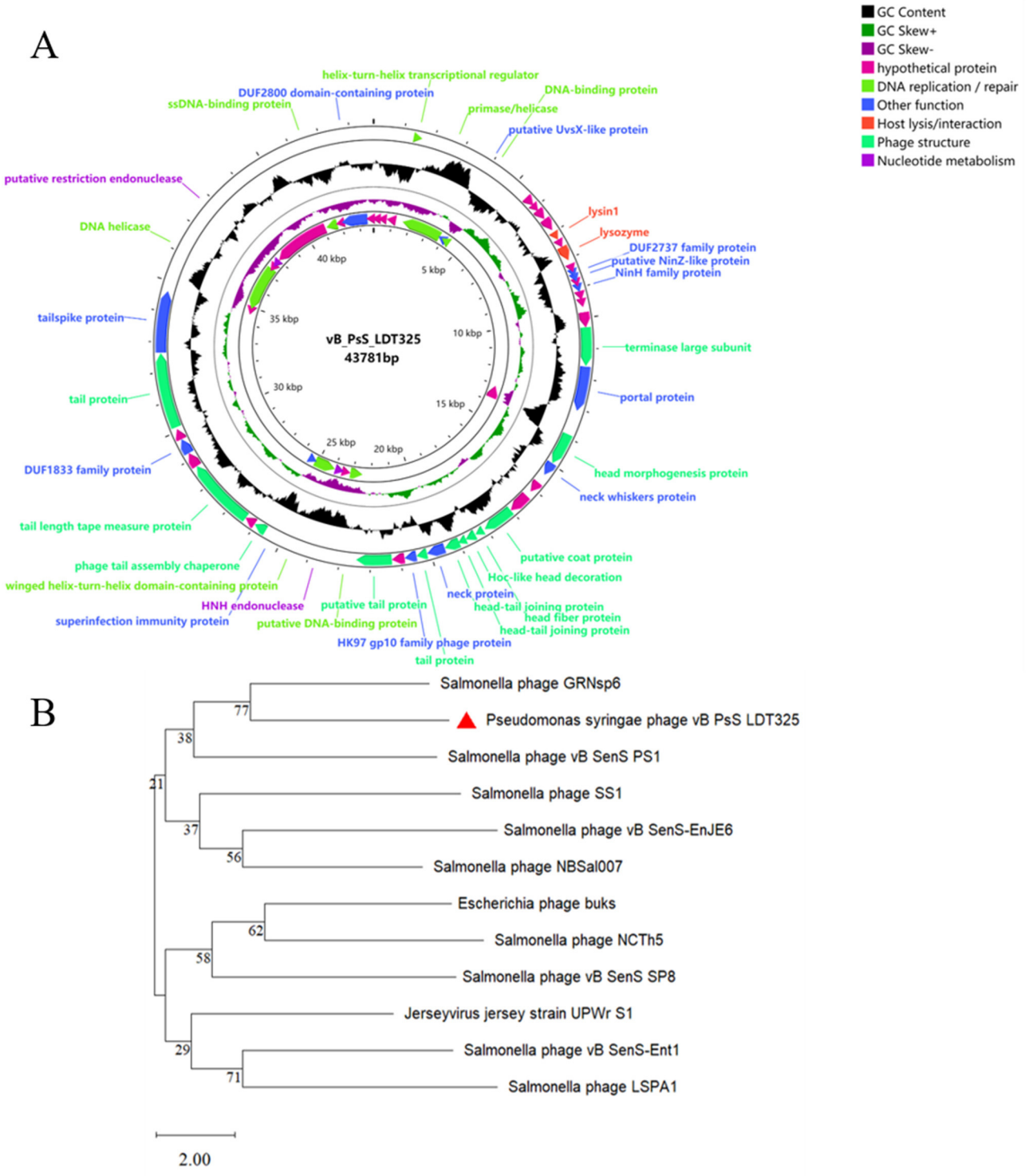

FIGURE 5
Genomic analysis. **(A)** Genome map of phage vB_PsS_LDT325, the genome of phage vB_PsS_LDT325 depicted in the circular. These arrows represent 61 CDS. In addition, the map shows GC skew and content about the genome. **(B)** An expanded view of the region of the tree containing the most closely related phages. The location of phage LDT325 is indicated in the red triangle.

morphology could be observed on the double-layer plate (Figure 7). Therefore, we isolated a phage that can lyse both plant pathogen *Pseudomonas syringae* and animal pathogen Salmonella.

4 Discussion

P. syringae can infect many economically important plants, causing the spread of plant diseases and serious economic

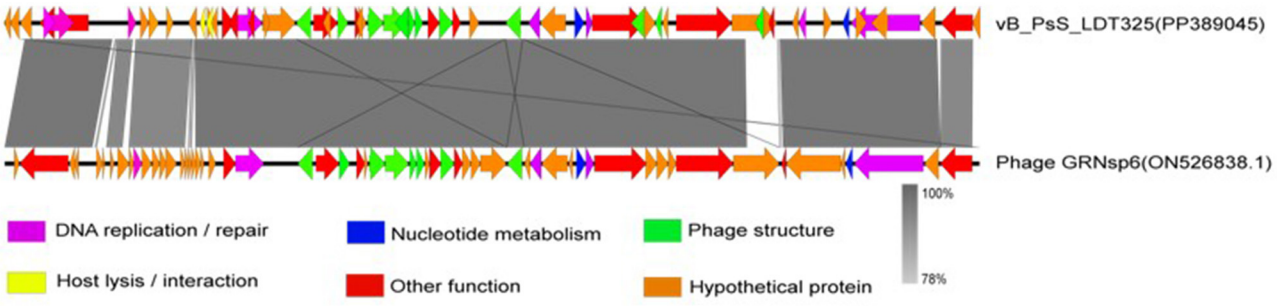

FIGURE 6
Genome structure. Arrows indicate the direction of transcription for predicted ORFs. ORFs with different functions are shown in different colors.

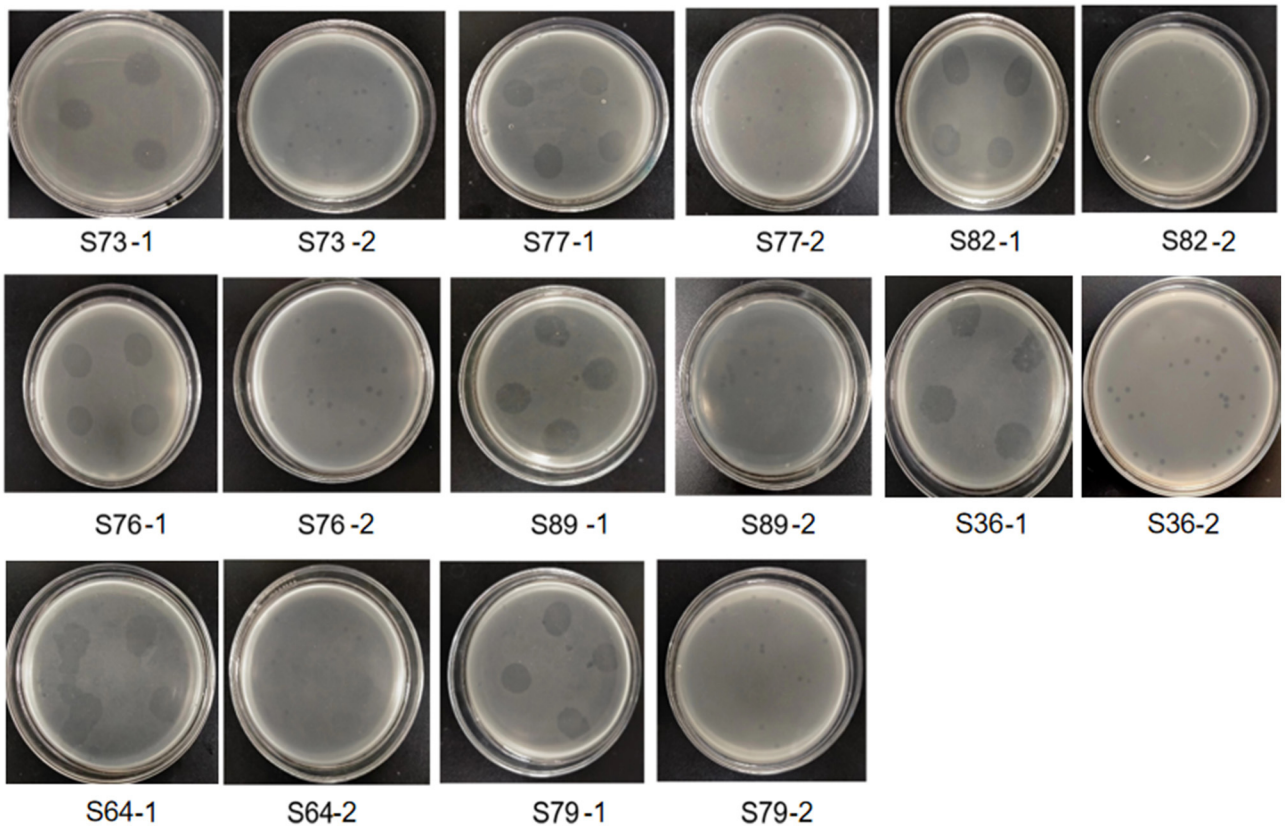

FIGURE 7
Several animal pathogenic Salmonella strains lysed by phage LDT325. The number below the picture is the number of Salmonella. Image S73-1 showed that after 12 h of culture, the phage suspension showed a clear cleavage area on the double-layer plate covered with Salmonella suspension numbered S73, showing the lysing bacteria. Picture S73-2 was further purified from the clear cleavage region of phage in picture S73-1. The same below.

losses. Because of the increased resistance of plant pathogens to widely used copper-based fungicides and antibiotics, phages have become an alternative method of biological control owing to their strong specificity and self-replication (Nachimuthu et al., 2021). Bacteriophages are capable of specifically infecting bacteria and can more effectively remove pathogens without affecting normal bacterial populations. Phage infection can activate the host immune response, thereby enhancing the host tolerance to bacterial infection. The interaction between phages, pathogens and beneficial bacteria is a complex and important ecosystem. Bacteriophages specifically infect specific bacterial hosts, and the enzymes released by phages during the lysis phase can directly dissolve the bacterial cell wall, leading to the death of pathogens. Bacteriophages also help maintain the balance of beneficial bacteria. Beneficial bacteria inhibit the growth of pathogens by competing for nutrients, producing antimicrobial substances and changing the microenvironment (Fernández et al., 2019). There are few reports to date on biological control methods related to the

prevention and treatment of tea bud blight (Gu et al., 2021; Kim et al., 2019; Wang et al., 2020). Moreover, there are only a limited number of studies showing the effectiveness of phage inhibition on *P. syringae* infection by analyzing the expression of antioxidant enzymes and related genes or through TEM of tea leaves.

The accumulation of reactive oxygen species causes oxidative damage to plants; therefore, they have evolved a set of antioxidant systems, including antioxidant enzymes (SOD, POD, CAT) (Hasanuzzaman et al., 2020). Antioxidant enzymes can maintain the balance between the production and scavenging of reactive oxygen species and free radicals to maintain homeostasis. During pathogen infection, plant cells often experience oxidative stress, resulting in damage to cell membranes, proteins, and DNA. Increasing the activity of antioxidant enzymes can reduce these damages and help plants maintain normal physiological functions and growth. Plants may establish a long-term effective defense mechanism by increasing the activity of phage-induced antioxidant enzymes. The phage itself can directly infect and lyse *Pseudomonas syringae*, reducing the number of pathogens, thereby reducing the risk of plant infection. At the same time, phage infection may stimulate the immune response of plant cells and improve disease resistance (Alkadi, 2020). The increase of antioxidant enzyme activity induced by phage and the enhancement of plant immune response promote each other, and jointly improve the resistance to *Pseudomonas syringae*. Peroxidase (POD) is a key enzyme in the enzymatic defense system of plants under stress conditions. For example, balancing zinc nutrition can improve the antioxidant activity of lily flowers to extend storage time (Shaheen et al., 2015). We analyzed the effects of phages on the expression of antioxidant (*CsSOD*, *CsCAT*, and *CsPOD*). The results indicated that phage significantly increased the transcription levels of these genes. Another study demonstrated that treatment with spermidine increased the expression of antioxidant genes and the activity of antioxidant enzymes, while decreasing reactive oxygen species production in alfalfa exposed to salt stress (Lou et al., 2018). Consistent with these findings, we demonstrated that phage treatment enhances the activities of key antioxidant enzymes under abiotic stress by increasing the expression levels of their associated genes, thus improving disease resistance in tea plants. The sterile water group had no effect on antioxidase activity and related gene expression, proline content, soluble sugar content and chlorophyll content.

Proline and soluble sugar are important osmotic adjustment substances in plants. They are one of the indicators that reflect the level of plant stress resistance. Furthermore, the application of phage upregulated chlorophyll and soluble sugar levels in tea leaves, which was consistent with studies showing that COS in wheat enhanced the accumulation of these components (Naz et al., 2021). Chlorophyll is the main substance required for photosynthesis of plants (Baltazar et al., 2021). Soluble sugar is used for plant metabolism and is an important energy source for plant growth and development (Afzal et al., 2021). During stress, proline levels in plants increases significantly (Qamar et al., 2015). Proline also activates the expression of plant defense genes, enhances the function of the immune system, and improves the resistance of plants to pathogens. During abiotic stress, proline levels increase as a result of significant protein degradation. In the present study, the notable rise in proline levels in tea leaves is indicative of disease resistance. The use of phages in tea cultivation enhances the growth of tea plants and boosts production yields. Therefore, phages positively influence the physiological responses of tea plants by promoting their growth and development.

The cell membrane has various physiological functions, including the role of a barrier to maintain a stable intracellular environment (Stewart et al., 2018). It controls the exchange of internal and external substances of cells and regulates the life activities of cells. We showed that the integrity of cells in the control group was compromised, which was confirmed by TEM. Specifically, the cell membrane in the control group was completely ruptured, which resulted in the collapse of intracellular structures. This indicates that pathogens destroy the cell membrane structure, interfere with cell membrane permeability, and induce apoptosis. The images of the phage treatment group showed clear cell structures, including a cell wall, mitochondria, thylakoid, and a cell membrane. Thus, phage may severely impede the growth of *Ps*, which has a marked impact on its propagation. This indicates that phage LDT325 effectively inhibits *P. syringae*. Whole genome analysis of vB_PsS_LDT325 phage provides a theoretical basis for its effect on *P. syringae*. The phage genome obtained in this study was 43,781 bp in length with a GC content of 48.82% and 61 ORFs. The GC content of phage LDT325 was higher compared with that of *P. syringae* phages, such as KIL1 and KIL2, with an average GC content of 44.8% (Rombouts et al., 2016). The host specificity of bacteriophages comes from the specific recognition of the host surface receptors. The tail filament proteins of most bacteriophages are responsible for the specific recognition of host receptors. Phage LDT325 has four ORFs encoding the family proteins, ORF16, ORF19, ORF37, and ORF49. A group or several groups of proteins with similar amino acid sequences are known as protein families and evidence of the evolution of multiple species can be obtained by analyzing protein family members. Phage LDT325 contains a gene that encodes the portal protein ORF24. The function of the portal protein is similar to that of a DNA sensor, which can couple genome packaging with icosahedral capsid maturation (Lokareddy et al., 2017). The tail proteins, ORF36, ORF51, and ORF47, comprise the tail phage, which indicates that the phage LDT325 belongs to the tail phage (Chibani et al., 2019). Phage LDT325 expresses two genes encoding endolysin, ORF12 and ORF14. Compared with traditional broad-spectrum antibiotics, the main advantage of endolysin is its high specificity; moreover, it does not kill beneficial bacteria (Gontijo et al., 2021; Rahman et al., 2021). Therefore, as a medicinal bacteriostatic agent, phages have obvious advantages compared with traditional antibiotics. Interestingly, we found that the phage LDT325 lysed the animal pathogen *Salmonella* as well as the plant pathogen *P. syringae*. This phenomenon has not been reported to date. In addition, bacterial toxin genes, antibiotic resistance genes, integrase, recombinase, cleavage enzymes, and inhibitory enzymes related to lysogenic genes were not found in the genome of vB_PsS_LDT325, and indicates its safety as an antibacterial agent for potential clinical application. Whole genome

phylogenetic tree construction, linear analysis of amino acid sequences, and the development of a tree based on the major capsid protein indicate that vB_PsS_LDT325 has a close relationship with other bacteriophages and demonstrates the genetic diversity among bacteriophages.

In conclusion, we demonstrated that phages have multiple roles in preventing *P. syringae* from infecting tea plants, such as inducing antioxidant enzyme activity, enhancing plant resistance to pathogenic bacteria, destroying the cellular structure of *P. syringae*, and inhibiting the expansion of *P. syringae*. Our findings demonstrate that the phage LDT325 has numerous beneficial effects on tea plants, thus indicating the potential for application in the prevention and control of tea leaf blight.

Data availability statement

The datasets presented in this study can be found in online repositories. The names of the repository/repositories and accession number(s) can be found below: NCBI.

Author contributions

LL: Writing – original draft, Methodology, Investigation. AH: Investigation, Writing – review & editing. HZ: Investigation, Writing – review & editing. YL: Software, Writing – review & editing. LW: Methodology, Writing – review & editing.

Funding

The author(s) declare financial support was received for the research, authorship, and/or publication of this article. This study was supported by the regular science and technology assistance project of the Ministry of Science and Technology (No. KY202204002) and the Natural Science Foundation of Shandong Shandong Province (No. ZR2021MC185).

Acknowledgments

Thanks AH, HZ, and YL performed the experiments. Thank you LW designed the experiments and revised the manuscript. Thanks for the regular science and technology assistance project of the Ministry of Science and Technology (No. KY202204002) and the Natural Science Foundation of Shandong Province (No. ZR2021MC185) support.

Conflict of interest

The authors declare that the research was conducted in the absence of any commercial or financial relationships that could be construed as a potential conflict of interest.

Generative AI statement

The author(s) declare that no Gen AI was used in the creation of this manuscript.

Publisher's note

Supplementary material

The Supplementary Material for this article can be found online at: https://www.frontiersin.org/articles/10.3389/fmicb.2024.1525040/full#supplementary-material

SUPPLEMENTARY TABLE S1
Genomic annotation of *Pseudomonas syringae* phage *vB_PsS_LDT325*.

References

Aftab, Z.-H., Aslam, W., Aftab, A., Shah, A. N., Akhter, A., Fakhar, U., et al. (2022). Incorporation of engineered nanoparticles of biochar and fly ash against bacterial leaf spot of pepper. *Sci. Rep.* 12:8561. doi: 10.1038/s41598-022-10795-8

Afzal, S., Chaudhary, N., and Singh, N. K. (2021). "Role of soluble sugars in metabolism and sensing under abiotic stress," in *Plant Growth Regulators*, eds. T. Aftab and K. R. Hakeem (Cham: Springer), 305–334. doi: 10.1007/978-3-030-61153-8_14

Alkadi, H. (2020). A review on free radicals and antioxidants. *Infect. Disord. Drug Targets* 20, 16–26. doi: 10.2174/1871526518666180628124323

Baltazar, M., Correia, S., Guinan, K. J., Sujeeth, N., Bragança, R., Gonçalves, B., et al. (2021). Recent advances in the molecular effects of biostimulants in plants: an overview. *Biomolecules* 11:1096. doi: 10.3390/biom11081096

Bartoli, C., Lamichane, J. R., Berge, O., Guilbaud, C., Varvaro, L., Balestra, G. M., et al. (2015). A framework to gauge the epidemic potential of plant pathogens in environmental reservoirs: the example of kiwifruit canker. *Mol. Plant Pathol.* 16, 137–149. doi: 10.1111/mpp.12167

Batuman, O., Britt-Ugartemendia, K., Kunwar, S., Yilmaz, S., Fessler, L., Redondo, A., et al. (2024). The use and impact of antibiotics in plant agriculture: a review. *Phytopathology* 114, 885–909. doi: 10.1094/PHYTO-10-23-0357-IA

Buttimer, C., McAuliffe, O., Ross, R. P., Hill, C., O'Mahony, J., Coffey, A., et al. (2017). Bacteriophages and bacterial plant diseases. *Front. Microbiol.* 8:34. doi: 10.3389/fmicb.2017.00034

Cao, S., Yang, W., Zhu, X., Liu, C., Lu, J., Si, Z., et al. (2022). Isolation and identification of the broad-spectrum high-efficiency phage vB_SalP_LDW16 and its therapeutic application in chickens. *BMC Vet. Res.* 18:386. doi: 10.1186/s12917-022-03490-3

Chibani, C. M., Farr, A., Klama, S., Dietrich, S., and Liesegang, H. (2019). Classifying the unclassified: a phage classification method. *Viruses* 11:195. doi: 10.3390/v11020195

Davidson, A. R., Cardarelli, L., Pell, L. G., Radford, D. R., and Maxwell, K. L. (2012). Long noncontractile tail machines of bacteriophages. *Adv. Exp. Med. Biol.* 115:142. doi: 10.1007/978-1-4614-0980-9_6

Fernández, L., Gutiérrez, D., García, P., and Rodríguez, A. (2019). The perfect bacteriophage for therapeutic applications—a quick guide. *Antibiotics* 8:126. doi: 10.3390/antibiotics8030126

Freitas, P. A. F., Carvalho, H. H., Costa, J. H., Miranda, R. D. S., Saraiva, K. D. D. C., Oliveira, F. D. B., et al. (2019). Salt acclimation in sorghum plants by exogenous proline: physiological and biochemical changes and regulation of proline metabolism. *Plant Cell Rep.* 38, 403–416. doi: 10.1007/s00299-019-02382-5

Gontijo, M. T. P., Jorge, G. P., and Brocchi, M. (2021). Current status of endolysin-based treatments against gram-negative bacteria. *Antibiotics* 10:1143. doi: 10.3390/antibiotics10101143

Gu, G., Yang, S., Yin, X., Long, Y., Ma, Y., Li, R., et al. (2021). Sulfur induces resistance against canker caused by *Pseudomonas syringae* pv. actinidae via phenolic components increase and morphological structure modification in the kiwifruit stems. *Int. J. Mol. Sci.* 22:12185. doi: 10.3390/ijms222212185

Hao, X., Wang, B., Wang, L., Zeng, J., Yang, Y., Wang, X., et al. (2018). Comprehensive transcriptome analysis reveals common and specific genes and pathways involved in cold acclimation and cold stress in tea plant leaves. *Scientia Horticulturae* 240, 354–368. doi: 10.1016/j.scienta.2018.06.008

Hasanuzzaman, M., Bhuyan, M. B., Zulfiqar, F., Raza, A., Mohsin, S. M., Mahmud, J. A., et al. (2020). Reactive oxygen species and antioxidant defense in plants under abiotic stress: revisiting the crucial role of a universal defense regulator. *Antioxidants* 9:681. doi: 10.3390/antiox9080681

Jia, B., Raphenya, A. R., Alcock, B., Waglechner, N., Guo, P., Tsang, K. K., et al. (2016). CARD 2017: expansion and model-centric curation of the comprehensive antibiotic resistance database. *Nucleic Acids Res.* 45, 566–573. doi: 10.1093/nar/gkw1004

Khandan, H. N., Worner, S. P., Jones, E. E., Villjanen-Rollinson, S. L. H., Gallipoli, L., Mazzaglia, A., et al. (2013). Predicting the potential global distribution of *Pseudomonas syringae* pv actinidiae (Psa). *New Zealand Plant Protect.* 66, 184–193. doi: 10.30843/nzpp.2013.66.5601

Kim, M. J., Chae, D. H., Cho, G., Kim, D. R., and Kwak, Y. S. (2019). Characterization of antibacterial strains against kiwifruit bacterial canker pathogen. *Plant Pathol. J.* 35:473. doi: 10.5423/PPJ.OA.05.2019.0154

Kumar, S., Stecher, G., Li, M., Knyaz, C., and Tamura, K. (2018). MEGA X: molecular evolutionary genetics analysis across computing platforms. *Mol. Biol. Evol.* 35, 1547–1549. doi: 10.1093/molbev/msy096

Lahlali, R., Ezrari, S., Radouane, N., Kenfaoui, J., Esmaeel, Q., El Hamss, H., et al. (2022). Biological control of plant pathogens: a global perspective. *Microorganisms* 10:596. doi: 10.3390/microorganisms10030596

Li, X., Luo, L., Hu, X., Lou, B., and He, Y. (2014). Revealing the chemical changes of tea cell wall induced by anthracnose with confocal Raman microscopy. *Spectrosc. Spec. Anal.* 34, 1571–1576. doi: 10.3964/j.issn.1000-0593(2014)06-1571-06

Liu, B., Zheng, D., Chen, L., and Yang, J. (2019). VFDB 2019: a comparative pathogenomic platform with an interactive web interface. *Nucleic Acids Res.* 47, 687–692. doi: 10.1093/nar/gky1080

Lokareddy, R. K., Sankhala, R. S., Roy, A., Afonine, P. V., Motwani, T., Teschke, C. M., et al. (2017). Portal protein functions akin to a DNA-sensor that couples genome-packaging to icosahedral capsid maturation. *Nat. Commun.* 8:14310. doi: 10.1038/ncomms14310

Lou, Y., Guan, R., Sun, M., Han, F., He, W., Wang, H., et al. (2018). Spermidine application alleviates salinity damage to antioxidant enzyme activity and gene expression in alfalfa. *Ecotoxicology* 27, 1323–1330. doi: 10.1007/s10646-018-1984-7

Luo, X., and Huang, Q. (2011). Relationships between leaf and stem soluble sugar content and tuberous root starch accumulation in cassava. *J. Agric. Sci.* 3:64. doi: 10.5539/jas.v3n2p64

Nachimuthu, R., Royam, M. M., Manohar, P., and Leptihn, S. (2021). Application of bacteriophages and endolysins in aquaculture as a biocontrol measure. *Biol. Control* 160:104678. doi: 10.1016/j.biocontrol.2021.104678

Nawaz, A., Zafar, S., Shahzadi, M., Bukhari, S. M. A. U. S., Khan, N., Shah, A. A., et al. (2023). Bacteriophages: an overview of the control strategies against phytopathogens. *Egypt. J. Biol. Pest Control* 33:108. doi: 10.1186/s41938-023-00751-7

Naz, R., Batool, S., Shahid, M., Keyani, R., Yasmin, H., Nosheen, A., et al. (2021). Exogenous silicon and hydrogen sulfide alleviates the simultaneously occurring drought stress and leaf rust infection in wheat. *Plant Physiol. Biochem.* 166, 558–571. doi: 10.1016/j.plaphy.2021.06.034

Pérez-Patricio, M., Camas-Anzueto, J. L., Sanchez-Alegría, A., Aguilar-González, A., Gutiérrez-Miceli, F., Escobar-Gómez, E., et al. (2018). Optical method for estimating the chlorophyll contents in plant leaves. *Sensors* 18:650. doi: 10.3390/s18020650

Qamar, A., Mysore, K. S., and Senthil-Kumar, M. (2015). Role of proline and pyrroline-5-carboxylate metabolism in plant defense against invading pathogens. *Front. Plant Sci.* 6:503. doi: 10.3389/fpls.2015.00503

Rahman, M. U., Wang, W., Sun, Q., Shah, J. A., Li, C., Sun, Y., et al. (2021). Endolysin, a promising solution against antimicrobial resistance. *Antibiotics* 10:1277. doi: 10.3390/antibiotics10111277

Rombouts, S., Volckaert, A., Venneman, S., Declercq, B., Vandenheuvel, D., Allonsius, C. N., et al. (2016). Characterization of novel bacteriophages for biocontrol of bacterial blight in leek caused by *Pseudomonas syringae* pv. porri. *Front. Microbiol.* 7:279. doi: 10.3389/fmicb.2016.00279

Shaheen, R., Hassan, I., Hafiz, I. A., Jilani, G., and Abbasi, N. A. (2015). Balanced zinc nutrition enhances the antioxidative activities in oriental lily cut-flower leading to improved growth and vase quality. *Scientia Horticulturae* 197, 644–649. doi: 10.1016/j.scienta.2015.10.030

Stewart, M. P., Langer, R., and Jensen, K. F. (2018). Intracellular delivery by membrane disruption: mechanisms, strategies, and concepts. *Chem. Rev.* 118, 7409–7531. doi: 10.1021/acs.chemrev.7b00678

Tsuji, M., and Takikawa, Y. (2018). *Pseudomonas syringae* pv. alliifistulosi pv. nov., the causal agent of bacterial leaf spot of onions. *J. Gener. Plant Pathol.* 84, 343–358. doi: 10.1007/s10327-018-0791-6

Wang, F. M., Mo, Q. H., Ye, K. Y., Gong, H. J., Qi, B. B., Liu, P. P., et al. (2020). Evaluation of the wild Actinidia germplasm for resistance to *Pseudomonas syringae* pv. actinidiae. *Plant Pathol.* 69, 979–989. doi: 10.1111/ppa.13184

Wang, Z., Yi, J., Yu, Q., Liu, Y., Zhang, R., Zhang, D., et al. (2023). Performance evaluation of QuantStudio 1 plus real-time PCR instrument for clinical laboratory analysis: a proof-of-concept study. *Pract. Lab. Med.* 36:e00330. doi: 10.1016/j.plabm.2023.e00330

Wang, B., Huang, A., Liu, L., Li, Y., Zhang, H., Wang, L., et al. (2024). Effects of an exogenous melatonin treatment on the physiological indexes and storage duration of cut chrysanthemum flowers. *Horticult. Sci. Technol.* 42, 533–548. doi: 10.7235/HORT.20240038

Xin, X. F., Kvitko, B., and He, S. Y. (2018). *Pseudomonas syringae*: what it takes to be a pathogen. *Nat. Rev. Microbiol.* 16, 316–328. doi: 10.1038/nrmicro.2018.17

Yang, P., Zhao, L., Gao, Y. G., and Xia, Y. (2023). Detection, diagnosis, and preventive management of the bacterial plant pathogen *pseudomonas syringae*. *Plants* 12:1765. doi: 10.3390/plants12091765

Zhang, X., Zhang, Z., Shu, Q., Xu, C., Zheng, Q., Guo, Z., et al. (2021). Copper clusters: an effective antibacterial for eradicating multidrug-resistant bacterial infection *in vitro* and *in vivo*. *Adv. Funct. Mat.* 31:2008720. doi: 10.1002/adfm.202008720

frontiers | Frontiers in Microbiology

TYPE Original Research
PUBLISHED 07 March 2025
DOI 10.3389/fmicb.2025.1491961

OPEN ACCESS

EDITED BY
Israel Nissan,
Ministry of Agriculture and Rural Development (Israel), Israel

REVIEWED BY
Ronen Nissan Hazan,
Hebrew University of Jerusalem, Israel
Mzia Kutateladze,
George Eliava Institute of Bacteriophage, Microbiology and Virology, Georgia

*CORRESPONDENCE
Zhihua Zhang
✉ zzh19641229@163.com
Wei Zhang
✉ 15369318318@163.com
Bu Wang
✉ 289974726@qq.com

†These authors have contributed equally to this work

RECEIVED 05 September 2024
ACCEPTED 12 February 2025
PUBLISHED 07 March 2025

CITATION
Peng X, Chang J, Zhang H, Li X, Zhang C, Jiao S, Lv C, Wang N, Zhao J, Wang B, Zhang W and Zhang Z (2025) Isolation, characterization, and genomic analysis of a novel bacteriophage vB_Kp_XP4 targeting hypervirulent and multidrug-resistant *Klebsiella pneumoniae*. *Front. Microbiol.* 16:1491961. doi: 10.3389/fmicb.2025.1491961

Isolation, characterization, and genomic analysis of a novel bacteriophage vB_Kp_XP4 targeting hypervirulent and multidrug-resistant *Klebsiella pneumoniae*

Xiaocui Peng[1,2†], Jianliang Chang[1,2†], Hongxia Zhang[2], Xiaoyu Li[1,2], Changhong Zhang[2], Shiyan Jiao[1], Chengxiu Lv[3], Na Wang[4], Jun Zhao[1,2], Bu Wang[2*], Wei Zhang[4*] and Zhihua Zhang[2*]

[1]Department of Postgraduate, Hebei North University, Zhangjiakou, China, [2]Respiratory and Critical Care Medicine Department, The First Affiliated Hospital of Hebei North University, Zhangjiakou, China, [3]Department of Clinical Laboratory, Zibo First Hospital, Zibo, China, [4]Central Laboratory, The First Affiliated Hospital of Hebei North University, Zhangjiakou, China

Introduction: Hypervirulent and multidrug-resistant *Klebsiella pneumoniae* (hvKP and MDR-KP) are significant public health threats. This study aimed to isolate a lytic bacteriophage targeting these high-risk strains, systematically characterize its biological properties, genomic features, and therapeutic efficacy, and establish a foundation for clinical phage therapy and novel antimicrobial development.

Methods: The phage vB_Kp_XP4 was isolated from river water using the double-layer agar plate method with the clinically isolated strain P4 as the host. Morphology was analyzed via transmission electron microscopy (TEM). Host range, pH, and thermal stability were assessed using spot assays and OD_{630} measurements. One-step growth curves determined the latent period and burst size. Whole-genome sequencing and phylogenetic analysis were performed. Therapeutic efficacy and safety were evaluated in a *Galleria mellonella* infection model.

Results: TEM revealed Phage vB_Kp_XP4 as a tailed phage with an icosahedral head and a long, flexible tail. It lysed an hvKP strain (carrying *rmp*, *peg*, *iuc*, *iro* genes) and an MDR-KP strain (resistant to carbapenems, fluoroquinolones, etc.), with an optimal MOI of 0.1 and latent period <10 minutes. Stability was maintained at pH 4–11 and ≤70°C. Whole-genome sequencing revealed a linear double-stranded DNA genome of 44,344 bp with a G+C content of 53.80%. The genome comprised 54 coding sequences and lacked lysogenic, virulence, or antibiotic resistance genes. Phylogenetic analysis positioned phage vB_Kp_XP4 as a novel species within the genus *Drulisvirus*, family *Autographiviridae*. In the *Galleria mellonella* model, vB_Kp_XP4 prolonged survival of P4-infected larvae ($P < 0.001$)

Conclusion: Phage vB_Kp_XP4 exhibits high stability, specificity, potent lytic activity, and no undesirable genes, demonstrating effective in vivo therapeutic efficacy, suggest its potential for clinical applications against *Klebsiella pneumoniae* infections. The presence of multiple halos during plaque formation further enhances its research value. The complete genome sequence has been submitted to GenBank under accession number PP663283.

KEYWORDS

phage therapy, biological characteristics, whole-genome sequencing, *Klebsiella pneumoniae*, multidrug resistance, hypervirulence

1 Introduction

Klebsiella pneumoniae is a ubiquitous opportunistic Gram-negative enterobacterium (Beamud et al., 2023). Recent national and international surveys have identified it as one of the predominant clinical isolates, particularly among immunocompromised individuals. It is associated with community-acquired and hospital-acquired infections, including pneumonia, meningitis, urinary tract infections, bacteremia, and liver abscesses (Lee et al., 2017; Lan et al., 2021; Pu et al., 2023). The incidence and mortality rates have shown a steady increase in recent years. According to the 2023 CHINET (China Antimicrobial Surveillance Network) report, *K. pneumoniae* ranks as the second most common clinical isolate after *Escherichia coli*, with a rising prevalence and multiple drug resistance trend. Globally, without effective measures to curb the spread of resistance, the annual death toll is projected to reach 10 million by 2050 (Antimicrobial Resistance Collaborators, 2022; Programme TUE, 2023; Antimicrobial Resistance Collaborators, 2024). On May 17, 2024, the World Health Organization (WHO) updated its list of critical bacterial pathogens, categorizing carbapenem-resistant Enterobacteriaceae within the Critical group (World Health Organization, 2024a). A global alert was issued on July 31 concerning a highly virulent, multidrug-resistant *K. pneumoniae* strain, highlighting its rapid transmission and broad infection range, which poses a global health crisis (World Health Organization, 2024b). In the search for new effective strategies to combat this growing threat, phage therapy has regained global attention (Wang et al., 2021). Advances in genomic sequencing have enhanced the understanding and utilization of bacteriophages. Bacteriophages can specifically infect, lyse bacteria, and co-evolve with them, demonstrating significant potential in treating bacterial infections (Castledine et al., 2022). Increasingly explored as an alternative to antibiotics, phage therapy has shown success in numerous reported case (Brives and Pourraz, 2020). The demand for phages is rising, leading to the establishment of several phage banks worldwide, such as the G. Eliava Institute of Bacteriophages, Microbiology, and Virology in Tbilisi, Georgia (Kutateladze, 2015); the Ludwik Hirszfeld Institute of Immnology and Experimental Therapy, Wrocław, Poland (Międzybrodzki et al., 2012); The Center for Innovative Phage Applications and Therapeutics (IPATH) (UCSD, 2019); The Félix d'Hérelle Reference Center for Bacterial Viruses (Université Laval, 2024); The Leibniz Institute DSMZ-German Collection of Microorganisms and Cell Cultures (DSMZ, 2024); Queen Astrid Military Hospital in Brussels (Pirnay et al., 2024); The IPTC in Israel (Yerushalmy et al., 2023); Phage Australia (Sacher et al., 2022) and Phage Canada (Hufsky et al., 2023), etc. The aim is to achieve effective treatment outcomes for bacterial infections through phage therapy and phage-antibiotic combination therapies. However, given the biological activity of phages, a comprehensive understanding of their biological properties and genomic characteristics is essential to optimize their role as clinical therapeutic agents against infectious diseases.

This study successfully isolated a novel bacteriophage, vB_Kp_XP4, from a natural water source. This phage demonstrates lytic activity against highly virulent and multidrug-resistant strains. Basic experiments were conducted to analyze its biological characteristics. Whole-genome sequencing and analysis techniques were employed to perform comparative genomic analysis, gene annotation, and functional prediction of the phage's complete genome sequence. These findings provide a material foundation and theoretical basis for the application of bacteriophages in treating *K. pneumoniae* infections.

2 Materials and methods

2.1 Origin and identification of *Klebsiella pneumoniae* strains

The *Klebsiella pneumoniae* strains used in this experiment were identified using a fully automated microbial identification and susceptibility testing system (BD, phoenix100). The host bacterium P4, verified in preliminary experiments, possesses several virulence genes, including *rmp*, *peg*, *iuc*, and *iro*. The antibiotic resistance of the remaining *K. pneumoniae* strains was assessed using the disk diffusion method and PCR, with PCR amplification specifically targeting the *KPC* gene. The string test was employed to measure the viscosity of *K. pneumoniae* strains (Shon et al., 2013). Bacteria were inoculated on LB agar plates and incubated at 37°C for 16 h. A single colony was then picked to observe the string formation. A positive result, indicating a hypermucoviscous phenotype, was defined by the formation of a viscous string greater than 5 mm in length. A negative result indicated a non-hypermucoviscous phenotype.

2.2 Phage isolation, purification, and amplification

Following the method described by Mohammadi et al. (2023), flowing river water samples were collected from the Han River in Xiangyang, Hubei Province, a tributary of the Yangtze River. The samples were centrifuged at 10,000 rpm for 15 min, and the supernatant was collected. The supernatant was then filtered through a 0.22 μm syringe filter and stored in 50 mL centrifuge tubes at 4°C. The culture was grown to the logarithmic phase using *K. pneumoniae* P4 as the host bacterium. Then, mix 1 mL of filtered solution with the host bacteria and incubate overnight in a shaker at 37°C and 160 rpm. After incubation, the mixture was centrifuged at 10,000 rpm for 15 min, followed by filtration to collect the supernatant. A further step involved mixing 100 μL of this supernatant with 100 μL of the host bacterial culture in the logarithmic phase, incubating at 37°C in a shaker at 220 rpm for 15 min. Subsequently, 5 mL of 50°C 0.7–0.8% LB semi-solid medium was added, mixed thoroughly, and quickly poured onto the surface of an LB solid medium. After solidification, the plates were inverted and incubated overnight at 37°C. The double-layer agar plate method (Hyman and Abedon, 2009) was employed to observe the presence of bacteriophage plaques. Upon verification, individual plaques were picked and subjected to multiple rounds of purification to obtain a pure phage. For amplification, 5 mL

of purified phage solution was mixed with 5 mL of the host bacterial culture in the logarithmic phase, and a liquid LB medium was added to reach a total volume of 50 mL. This mixture was incubated at 37°C with shaking for 6–8 h. The suspension was then centrifuged at 10,000 rpm for 15 min, followed by filtration through a 0.22 μm pore-size membrane to obtain the supernatant, resulting in an amplified phage solution. The amplified phage solution was aliquoted and stored at −80°C in glycerol for future use.

2.3 Examination of phage by transmission electron microscopy

To examine the phage morphology, 20 μL of the amplified phage suspension was pipetted onto a 200-mesh copper grid and allowed to adsorb naturally for 5–10 min. Excess liquid was removed using a filter paper strip, and the grid was air-dried briefly. A 2% phosphotungstic acid solution (20 μL) was then applied to the grid for negative staining and left for 3–5 min. Afterward, the excess stain was removed with a filter paper strip, and the grid was air-dried under an incandescent lamp. The morphology of the phages was then observed using transmission electron microscopy (HITACHI, HT7700, Japan).

2.4 Phage host range and efficiency of plating

Host range analysis was performed using a panel of 21 *K. pneumoniae* strains by spot tests as previously described with slight modifications. Briefly, the purified phage stocks were gradient diluted with LB liquid medium and 2 μL of gradient diluted phage concentrate (10^2–10^9 PFU/mL) was added to the tested bacterial lawn and incubated at 37°C for 12 h. The presence of clear plaque on the bacterial lawn indicated that the tested strains were susceptible to the phage (Han et al., 2023). All *K. pneumoniae* isolates that were sensitive to phage vB_Kp_XP4 in the spot test assay ($n = 2$) were selected for the determination of the Efficiency of Plating (EOP), following the method described by Khan Mirzaei and Nilsson (2015). The EOP was calculated as the ratio of plaque-forming units (PFU/mL) on a sensitive strain to PFU/mL on the indicator strain. Each combination of bacterial strain and phage dilution was tested in triplicate, and the results are presented as the mean of three observations.

2.5 Optimal multiplicity of infection determination

The bactericidal activity of phage vB_Kp_XP4 was assessed by determining its time-killing curves. Phage solutions (500 μL) were mixed with 500 μL of host bacterial culture in the logarithmic phase at varying multiplicities of infection (MOIs) of 10, 1, 0.1, 0.01, 0.001, and 0.0001. The mixtures were incubated at 37°C with shaking at 220 rpm for 1 h. After incubation, the cultures were centrifuged at 10,000 rpm for 8 min, and the supernatant was filtered. The supernatant was then serially diluted, and the phage titer was determined using the double-layer agar plate method. The MOI with the highest phage titer was considered the optimal MOI for this phage. The experiment was repeated three times to ensure accuracy.

2.6 Monitoring changes in phage load and the effect of bacteriophages on bacterial morphology

Following the method described by Mohammadi et al. with slight modifications (Feng et al., 2023), the phage suspension was mixed with the host bacterial culture at the optimal multiplicity of infection (MOI) and incubated at 37°C for 15 min. Following incubation, the mixture was subjected to immediate centrifugation at 10,000 rpm, and the supernatant was discarded. The pellet was washed multiple times with LB liquid medium and then resuspended in LB medium. The suspension was incubated in a shaker at 37°C and 180 rpm. Samples (300–400 μL) were collected at 0, 10, 20, 30, 40, 50, 60, 70, 80, 90, 100, 110, and 120 min. Each sample was immediately centrifuged at 10,000 rpm, and the supernatant was filtered through a 0.22 μm pore-size membrane. The filtrate was serially diluted in an LB liquid medium, and 100 μL of each dilution was mixed with 100 μL of host bacterial culture. The mixtures were incubated for 15 min and then plated using the double-layer agar plate method. The plates were inverted and incubated overnight at 37°C to observe plaque formation and calculate the phage titer. Three parallel experiments were conducted for each time point. Burst size was calculated using the following formula: (titer after burst—titer at T0)/ (added phage—titer at T0). The curve of phage titer changes was constructed based on the phage titer at each time point. Perform Gram staining on the P4 strain both before and after bacteriophage treatment within a 12-h period. Bacterial morphology was observed using an optical microscope at 1,000× magnification.

2.7 Phage temperature and pH stability

Phage stability under different temperatures was assessed by placing the phage suspension in metal baths at 4°C, 10°C, 20°C, 30°C, 37°C, 40°C, 50°C, 60°C, 70°C, and 80°C for 60 min. For pH stability, the pH of the solutions was adjusted from 2 to 11 using HCl and NaOH. Four mL of phage solution (approximately 10^8 PFU/mL) was incubated at each pH level for 60 min. Phage solutions were then added to host bacteria cultures at an MOI of 0.1, while control groups received LB medium. These were placed in a shaker at 220 rpm and 37°C. Bacterial OD630 was measured at 30-min intervals to monitor changes in bacterial growth. Measurements were taken continuously for 3 to 12 h, with each group tested in triplicate.

2.8 Phage genome sequencing and characterization

2.8.1 Whole genome sequencing and annotation of phage

The DNBSEQ-T7 platform was used for sequencing. To ensure the reliability of subsequent analyses, the raw sequencing data were filtered and quality-controlled using fastp (Chen et al., 2018). This step included adapter trimming and the removal of low-quality reads and reads with a high proportion of 'N', resulting in clean reads. The metaSPAdes (Nurk et al., 2017) software was employed for the *de novo* assembly of the clean reads, testing different kmer lengths to achieve optimal assembly results. The clean reads were then aligned

to the assembled genome using BWA software (Li and Durbin, 2009). Open reading frames (ORFs) were identified using the NCBI ORFfinder server, with methionine and alternative start codons as initiation codons. The protein sequences were compared to the NR database using Blastp to identify sequences with high similarity. Functional annotation of the genes was performed using eggNOG-mapper (Cantalapiedra et al., 2021), which provided annotations from databases such as COG, GO, KEGG, CAZy, BiGG, and PFAM. Additionally, the predicted ORFs and coding sequences were cross-validated with the ORFs and coding sequences predicted by PHASTER (Seemann, 2014). An additional round of ORF prediction and functional annotation was conducted using RASTtk (Aziz et al., 2008; Overbeek et al., 2014; Brettin et al., 2015) and BV-BRC (Olson et al., 2023) to enhance confidence in the predicted coding genes. The presence of antibiotic-resistance genes within the phage genome was assessed using the resfinder database (Bortolaia et al., 2020). Homology searches against the VFDB (Liu et al., 2022) database were conducted to evaluate the presence of virulence genes. The presence of tRNA in the phage genome was determined using the tRNAscan-SE SearchServer online database.[1] The DeepTMHMM online tool[2] was utilized to screen for proteins with transmembrane domains (Hallgren et al., 2022).

Linear genome comparison and visualization of coding regions were performed utilizing Easyfig (Sullivan et al., 2011) and Mauve software (Darling et al., 2004). The lifestyle of the phage was predicted using the PHACTS program (McNair et al., 2012). Sequence similarity for further bioinformatic studies was determined using BLASTp searches in the NCBI database.[3]

2.8.2 Phylogenetic analysis of phage

The phylogenetic analysis of the phage's core proteins, such as terminase large subunit and tail fiber protein, was conducted using the BLASTp tool in the NCBI database to check for sequence similarity of the amino acid sequences. Phages with homologous amino acid sequences to these phage proteins were selected. A phylogenetic tree was then generated using MAGE11 software (Tamura et al., 2021). The phylogeny was constructed using the Maximum Likelihood method (Rokas and Charlesworth, 2001) and the JTT matrix-based model (Jones et al., 1992), with 1,000 bootstrap replicates to ensure the robustness of the analysis. Meanwhile, we predicted its protein structure using AlphaFold3 (Chen et al., 2024).

2.9 Therapeutic effect of phage vB_Kp_XP4 in the *Galleria mellonella* larvae

Galleria mellonella larvae model was used to assess the potential *in vivo* efficacy of phage against *K. pneumoniae*. The methods for larval injection and incubation were carried out with reference (Han et al., 2023; Li et al., 2023). The experimental procedures are as follows: the larvae selected were 25 ± 5 mm in length, 300 ± 50 mg in weight, with high activity and no visible black spots on the surface. All injections were performed using a Hamilton syringe into the left or right hind leg. Larvae were considered dead when they did not respond to touch. *In vivo* experiment, the larvae were divided into 12 groups, with 10 larvae randomly selected per group: (i)10 μL PBS injection, (ii) 10 μL of 10^7 CFU/mL strain P4, (iii) 10 μL of 10^8 CFU/mL strain P4 injection, (iv) 10 μL of 10^8 CFU/mL bacteriophage, (v) injection of 10 μL of PBS in the right leg (symmetrical position) at 0 h, (vi) injection of 10 μL of PBS in the right leg after 1 h; (vii-ix) MOI = 0.1 (P4 = 10^8 CFU/mL), 1 (P4 = 10^7 CFU/mL), 10 (P4 = 10^7 CFU/mL), with 10 μL of the corresponding concentration of strain P4 injected into the left hind leg, while 10 μL of bacteriophage with titers of 10^8, 10^7, or 10^8 PFU/mL was injected into the right hind leg, respectively; for MOI = 0.1, 10 μL of 10^8 CFU/mL strain P4 was injected into the left hind leg in three groups of larvae, followed by 10 μL of 10^7 PFU/mL bacteriophage in the right hind leg at 1 h, 2 h, and 4 h intervals. After completing the above procedures, all larvae were incubated at 37°C and monitored for mortality every 2 h for a total of 60 h. Survival curves were generated using GraphPad Prism v.10.1 and the survival rates were analyzed using Kaplan–Meier and log-rank test. Differences with $p < 0.05$ were considered statistically significant.

2.10 Statistical methods

Statistical analysis and plotting were performed using GraphPad Prism version 10.1 software. Student's t-test was used for both intra-group and inter-group comparisons, with the significance level set at $p \leq 0.05$.

3 Results

3.1 Origin and identification of *Klebsiella pneumoniae* strains

Phage-sensitive strains were tested for antibiotic susceptibility using the disk diffusion method, including imipenem, meropenem, ertapenem, levofloxacin, ceftazidime, ciprofloxacin, and amikacin. Strains resistant to more than three classes of antibiotics were defined as multi-drug resistant (Table 1). The results of capsule typing for the

TABLE 1 Drug sensitivity and virulence genes of phage target strains.

Antibiotic	Strains[#]		Virulence gene	Strains	
	P4	10		P4	10
IPM	24/S	10/R	*iucA 1*	+	-
MEM	25/S	7/R	*iucA 2*	+	ND
EPM	24/S	6/R	*iroB 1*	+	-
LEV	12/R	13/R	*iroB 2*	+	ND
CAZ	16/S	6/R	*prmpA*	+	-
CIP	9/R	8/R	*prmpA2*	+	-
AMK	18/S	18/S	*peg-344*	+	-

IPM: imipenem, MEM: meropenem, EPM: ertapenem, LEV: levofloxacin, CAZ: ceftazidime, CIP: ciprofloxacin, AMK: amikacin, [#]: Antibacterial circle diameter (mm); ND: No detection, "+": positive, "-": negative; R: Drug resistance, S: sensitive.

1 http://lowelab.ucsc.edu/tRNAscan-SE/
2 https://services.healthtech.dtu.dk/services/DeepTMHMM-1.0/
3 http://www.ncbi.nlm.nih.gov/BLAST

10.3389/fmicb.2025.1491961

TABLE 2 Detail information of bacteria of host range test.

Strains	Deduced K-Type	Resistant gene		Wire drawing experiment	Sensitivity	[a]EOP (%)
		KPC	*NDM*			
P4	K1	–	–	+	+	100
1	K64	+	–	–	–	0
2	K64	+	–	–	–	0
3	K64	+	–	–	–	0
4	K64	+	–	–	–	0
5	K64	+	–	+	–	0
6	K19	+	–	–	–	0
7	K64	+	–	–	–	0
8	K64	+	–	–	–	0
9	K64	+	–	–	–	0
10	K19	+	–	–	+	51 ± 8
11	K64	+	–	+	–	0
12	K149	+	–	–	–	0
13	K19	+	–	–	–	0
14	K64	+	–	–	–	0
15	K19	–	–	–	–	0
16	K57	–	–	+	–	0
17	K125	–	–	–	–	0
18	K64	+	–	–	–	0
19	K102	–	+	–	–	0
20	K64	+	–	–	–	0

In this Table "+" represents positive; "-" represents negative. [a]EOP (efficiency of plating) is calculated in percent as the PFU/mL of the phages on the test strain divided by the PFU/mL obtained on strain P4 multiplied by 100.

Klebsiella pneumoniae strains, along with the amplification of *KPC* and *NDM* genes and the outcomes of the string test, are presented in Table 2.

Using the hypervirulent *K. pneumoniae* strain P4 as the host, a bacteriophage was isolated and purified from Han River water and named *Klebsiella* phage vB_Kp_XP4. Serial dilutions of the phage stock solution (≈10^9 PFU/mL) were prepared, and within 12 h of incubation at 36°C on double-layer agar plates, plaques with a diameter of approximately 2 mm formed. These plaques exhibited a halo with multiple semi-transparent layers around them. The plaque morphology at different dilutions (10^{-3}, 10^{-6}, 10^{-7}, 10^{-8}) is shown in Figures 1A,a–d. Over time, the halo gradually expanded, with the plaque and halo diameters reaching up to 15 mm at 24 h under ambient conditions (Figures 1A,e) and 28 mm at 36 h (Figures 1A,f).

3.2 Examination of phage by transmission electron microscopy

Transmission electron microscopy (TEM) revealed the morphological characteristics of phage vB_Kp_XP4. The phage displayed a typical icosahedral head structure with a diameter of approximately 55 ± 2 nm and a non-contractile tail measuring about 168 ± 10 nm in length (Figure 1B). Based on these morphological features, phage vB_Kp_XP4 was classified as a tailed phage with a flexible, non-contractile tail.

3.3 Phage host range and efficiency of plating

The lytic spectrum and efficiency of phage vB_Kp_XP4 were evaluated across 21 *K. pneumoniae* strains. The phage exhibited a lytic rate of 9.5% (2 out of 21 strains). Virulence genes *iucA1*, *iucA2*, *iroB1*, *iroB2*, *prmpA*, *prmpA2*, and *peg-344* were amplified in phage-sensitive strains using PCR. Strains positive for all these genes were defined as 'high-virulence strains' (Table 1). These results suggest that phage vB_Kp_XP4 has therapeutic potential against infections caused by hypervirulent or multidrug-resistant *K. pneumoniae*. The EOP analysis showed that when the bacteriophage-to-bacteria ratio is approximately 0.1, phage vB_Kp_XP4 demonstrates extremely high efficiency in lysing the P4 strain, with fewer than 10 colonies growing (EOP ≈ 1). In contrast, the lysis rate for strain 10 is only 0.51 ± 0.08. Detailed information is presented in Table 2.

3.4 Optimal multiplicity of infection determination

Klebsiella phage vB_Kp_XP4 was tested for its bactericidal activity against its host, *K. pneumoniae* P4, at various MOIs. At an MOI of 0.1, the phage titer reached approximately 10^8 PFU/mL, significantly higher than in other groups (Figure 2A).

10.3389/fmicb.2025.1491961

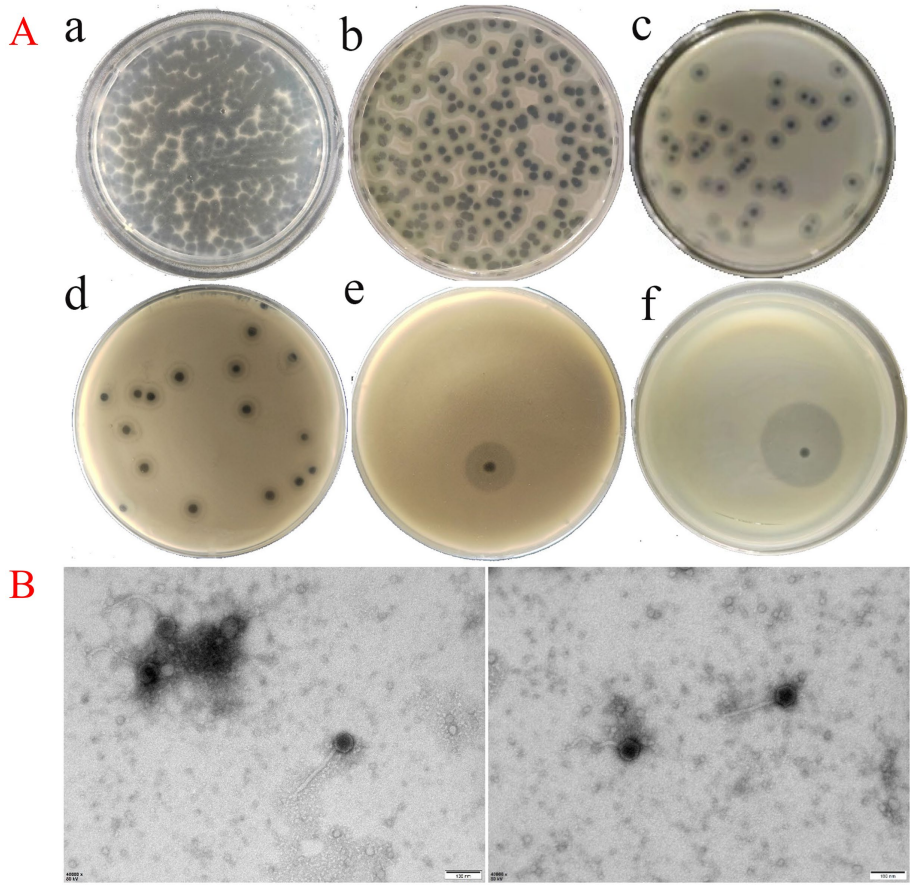

FIGURE 1
(A, a–d) Plaque morphology of phage vB_Kp_XP4 stock solution (≈ 10^9) at various dilution gradients (10^{-3}, 10^{-6}, 10^{-7}, and 10^{-8}), with plaques approximately 2 mm in diameter and surrounded by a halo comprising a multi-layered translucent zone; e: Plaque and halo morphology observed at 24 h post-inoculation; f: Plaque and halo morphology observed at 36 h post-inoculation. **(B)** TEM image of phage vB_Kp_XP4 (scale bar = 100 nm).

3.5 Monitoring changes in phage load and the effect of bacteriophages on bacterial morphology

The parameters of phage reproduction, including but not limited to the latent period and changes in phage quantity during the growth cycle, are valuable for the practical application of phages. Monitoring changes in phage load (Figure 2B) indicated that phage vB_Kp_XP4 has a relatively short latent period of approximately 10 min. When co-cultured with the host bacteria for 10 to 50 min, the phage titer increased rapidly, and the bacterial suspension transitioned from turbid to clear. After 50 min of co-culture, the phage concentration peaked at 10^{14}PFU/mL, entering a plateau phase where the suspension remained relatively clear. The average burst size of this phage was about 387 phages/cell. However, after 100 min, a noticeable decline in phage concentration was observed, and the bacterial suspension gradually became turbid. Under an optical microscope at 1,000× magnification, the morphology of the P4 strain changed after treatment with bacteriophage vB_Kp_XP4. Macroscopically, we observed that the staining intensity in image "a" is higher compared to image "b." Microscopically, individual bacterial cells appeared smaller after phage treatment than before. This suggests that phages may have disrupted the capsule structure of *Klebsiella pneumoniae*. (Figure 2C). However, this morphological change was not observed in strain 10.

3.6 Phage temperature and pH stability

Pathogenic *K. pneumoniae* is distributed across various environmental conditions. Therefore, the ability of phages to control these pathogens under different conditions is crucial for their practical application. The tolerance of phage vB_Kp_XP4 at different titers (10^8 and 10^{12}PFU/mL) was tested across a range of temperatures (4°C, 37°C, 40°C, 50°C, 60°C, 70°C, and 80°C). The results showed that phage vB_Kp_XP4 reached its highest titer at 50°C after 1 h. At 70°C for 1 h, phages with a titer of 10^8 PFU/mL were completely inactivated, while phages with a titer of 10^{12}PFU/mL partially survived, and even at 80°C for 1 h, a small amount of phages with this titer still survived (Figure 3).

The impact of different pH levels on the phage's ability to inhibit its host bacteria was analyzed, as shown in Figure 4. The results indicated that at pH ≤ 3, the growth of host bacteria in both the experimental and control groups was significantly inhibited, suggesting that both phage and bacterial growth are restricted by highly acidic conditions. Within a pH range of 4 to 11, the growth of

10.3389/fmicb.2025.1491961

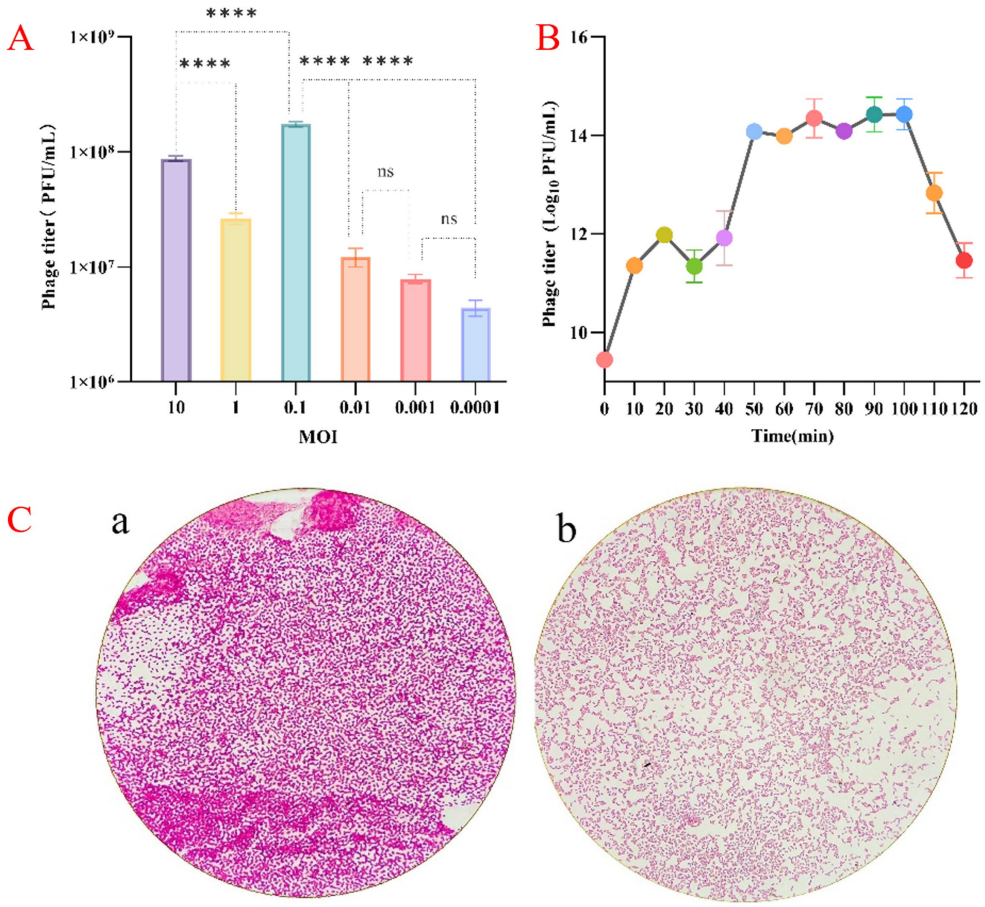

FIGURE 2
(A) Results of the optimal MOI assays for phage vB_Kp_XP4. **(B)** Monitoring changes in phage vB_Kp_XP4 load. **(C, a)** Morphology of the P4 bacterial strain in the absence of phage treatment; **(b)** Morphology of the P4 bacterial strain following exposure to phage vB_Kp_XP4.

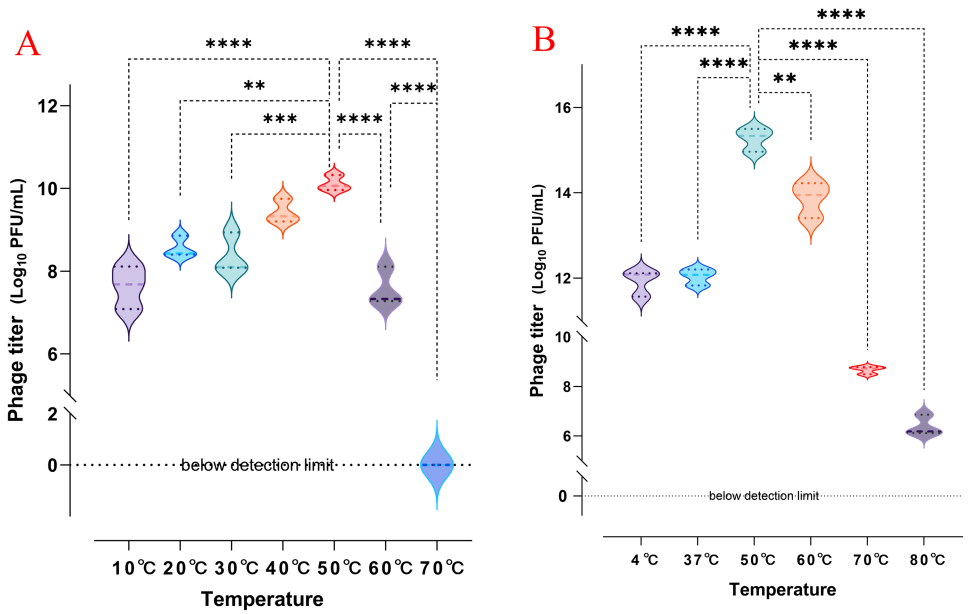

FIGURE 3
(A,B) Changes in phage titer after 1 h of exposure to different temperatures, with initial titers of approximately 10^8 and 10^{12} PFU/mL, respectively.

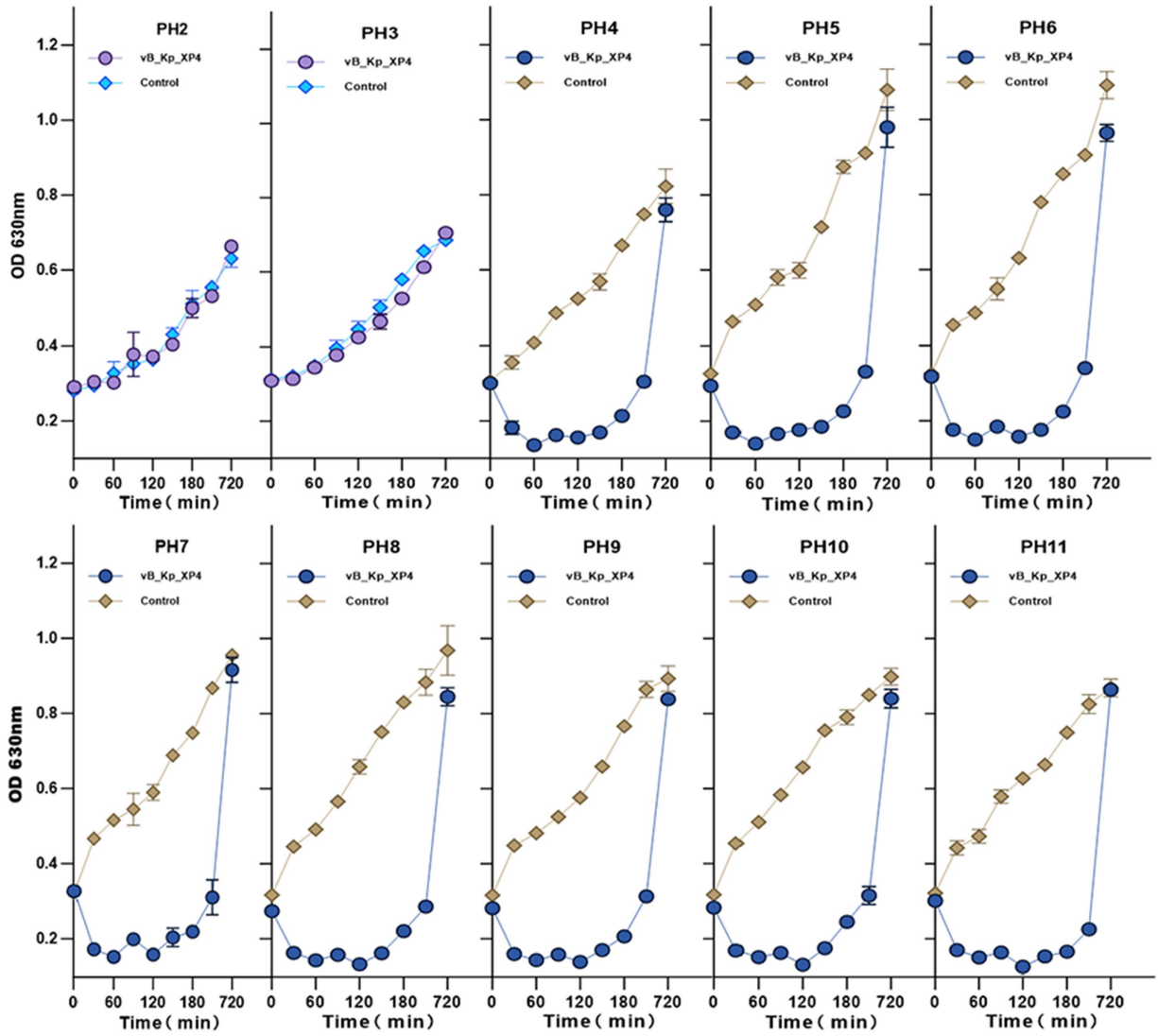

FIGURE 4
Effect of pH on the ability of phage vB_Kp_XP4 to inhibit the growth of host bacteria. Changes in OD at 630 nm were measured for phage-treated bacterial cultures under different pH conditions, with bacterial cultures without phage treatment used as controls. The experiment was carried out in three technical replicates.

host bacteria in the experimental group (MOI of 0.1) was significantly inhibited, indicating that the phage exhibits antibacterial activity across this broad pH spectrum. Additionally, it was observed that after 12 h, the concentration of host bacteria increased markedly, and the difference between the experimental and control groups diminished. This suggests that the phage was unable to completely eradicate the host bacteria, leading to a relative equilibrium between the two over time.

3.7 Phage genome sequencing and characterization

3.7.1 Whole genome basic characteristics

The sequencing results revealed that the genome of phage vB_Kp_XP4 is a linear double-stranded DNA with a genome size of 44,344 bp and a G + C content of 53.80%. A total of 54 coding sequences (CDS) were predicted, all oriented forward (see Supplementary File 1). The online tool tRNAscan-SE predicted that phage vB_Kp_XP4 contains no tRNA genes. Homology analysis using BLAST against the VFDB database found no known virulence genes in phage vB_Kp_XP4. Similarly, analysis with the resfinder database predicted the absence of antibiotic-resistance genes in the genome. The complete nucleotide sequence of phage vB_Kp_XP4 has been submitted to GenBank with the accession number PP663283.

3.7.2 Comparative genomic analysis of phage vB_Kp_XP4

A whole-genome comparison of phage vB_Kp_XP4 was performed using the BLASTn program on the NCBI website. The results showed a high similarity between phage vB_Kp_XP4 and

10.3389/fmicb.2025.1491961

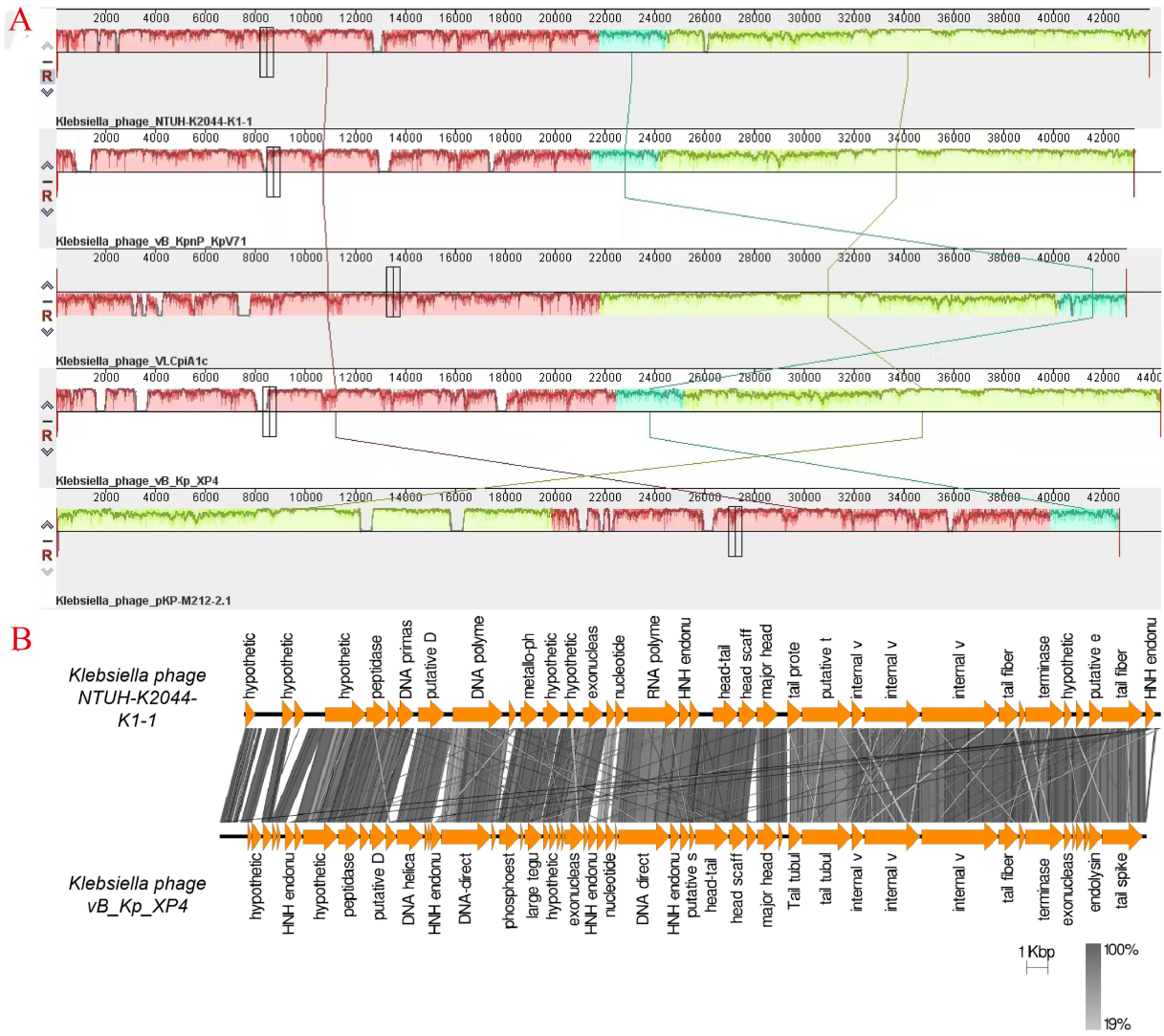

FIGURE 5
(A) Genome comparison of phage vB_Kp_XP4 with phages NTUH-K2044-K1-1, VLCpiA1c, KpV71 and pKP-M212-2.1. Colored blocks indicate regions of similarity between phage genomes, with the height of the panels within the blocks representing the strength of nucleotide similarity; **(B)** Comparison of the phage vB_Kp_XP4 genome with NTUH-K2044-K1-1 using EasyFig software. Arrows indicate predicted CDS based on their genomic functions, while the gray chromatogram reflects genetic similarity percentages.

TABLE 3 Whole genome-based databank homologies of *Klebsiella* phage vB_Kp_XP4 according to NCBI.

Strains	Coverage (%)	Identity (%)	Accession number	E
Klebsiella phage NTUH-K2044-K1-1	88	90.92	ON602748.1	0
Klebsiella phage VLCpiA1c	88	96.39	MK380015.1	0
Klebsiella phage KpV71	88	94.97	NC_031246.1	0
Klebsiella phage pKP-M212-2.1	89	96.93	OQ734493.1	0

phages from the genera *Autographiviridae*, *Slopekvirinae*, and *Drulisvirus*. Based on the BLASTn results, the phages with the highest scores, *Klebsiella* phage NTUH-K2044-K1-1, *Klebsiella* phage VLCpiA1c, *Klebsiella* phage KpV71, and *Klebsiella* phage pKP-M212-2.1, were selected for further comparison, as shown in Table 3. Previous studies have shown that (Lin et al., 2014; Solovieva et al., 2018) *Klebsiella* phage NTUH-K2044-K1-1 and KpV71 exhibit lytic activity against the K1 capsular serotype of *K. pneumoniae*. Collinearity analysis using Mauve software (Darling et al., 2004) revealed that certain regions of the *Klebsiella* phage vB_Kp_XP4 genome are similar to those of other *Klebsiella* phage genomes, indicated by the same colors in Figure 5A. The sequences of *Klebsiella*

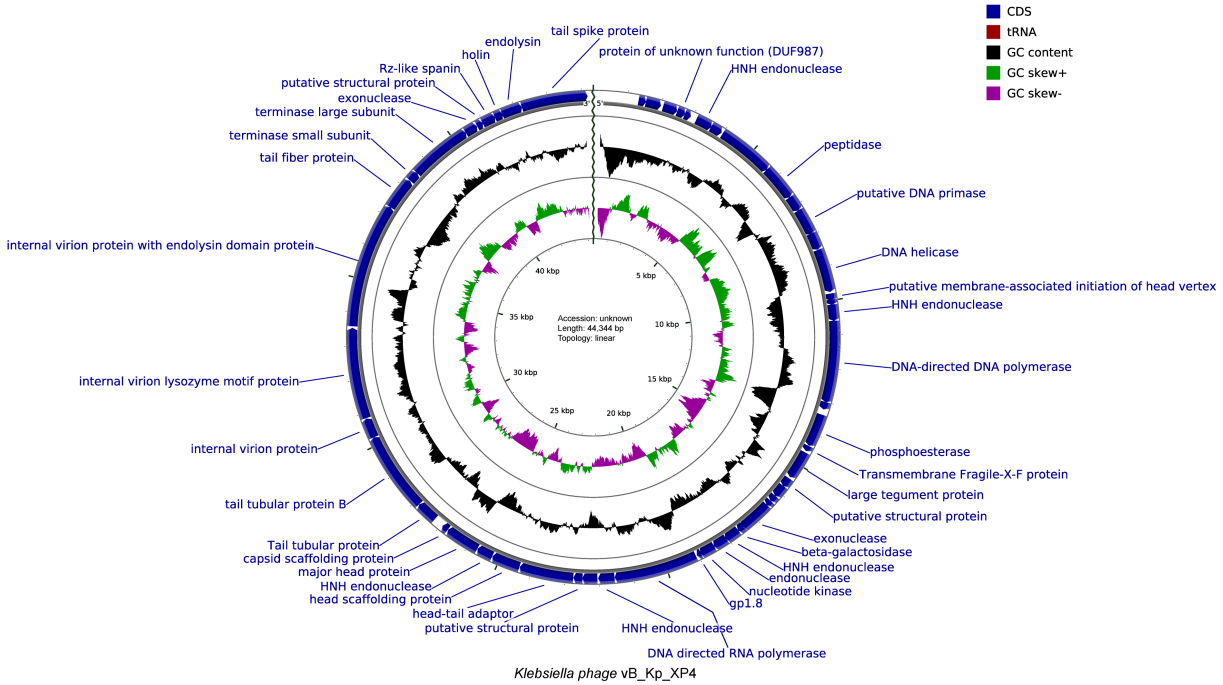

FIGURE 6
Genomic map of *Klebsiella* phage vB_Kp_XP4 with functional annotation.

phage vB_Kp_XP4, KpV71, and pKP-M212-2.1 were found to be highly conserved, with no rearrangements, insertions, or inversions, indicating a strong collinearity and similar conserved framework. Additionally, the genome sequence of *Klebsiella* phage vB_Kp_XP4 was compared with that of *Klebsiella* phage NTUH-K2044-K1-1 using EasyFig software (Sullivan et al., 2011) (Figure 5B).

3.7.3 Gene function prediction and annotation

The functions of the phage genome were predicted and annotated using Prokka, blastp, and eggNOG-mapper, as shown in Figure 6. Among the 54 analyzed coding sequences (CDS), 49 (90.7%) use ATG as the start codon, three (5.6%)—CDS2, CDS13, and CDS16—use GTG, and two (3.7%)—CDS19 and CDS36—use TTG. Fourteen CDSs were annotated as hypothetical proteins or proteins with unknown functions, while the remaining 40 CDSs have clearly defined functions. These include proteins involved in phage morphology and structure, DNA replication, transcription, packaging, and lysis. Thirteen CDSs are related to capsid and tail structural proteins, while 17 CDSs are associated with replication, transcription, and packaging. Proteins related to phage-mediated lysis of the host include glycosidases, transmembrane proteins, lysozymes, holins, and endolysins. None of the predicted CDSs encode lysogenic phage-associated proteins, such as transposases or integrases. Additionally, a screening of the phage genome with Phage Leads (Yukgehnaish et al., 2022) detected no genes indicative of a temperate lifecycle, antibiotic resistance, or virulence factors. These findings suggest that phage vB_Kp_XP4 has a certain level of safety and applicability for clinical therapeutic use. Various proteins and pathways have been identified as participants in phage-mediated bacterial lysis (Kongari et al., 2018). The holin-endolysin pathway is the most well-known mechanism, with additional involvement from transmembrane proteins. Biochemical and genetic studies indicate that Spanins are essential for disrupting the outer membrane (OM) of Gram-negative hosts. Rz-like proteins, which form two-component transmembrane proteins, are capable of degrading and lysing the OM (Summer et al., 2007). Using DeepTMHMM, the transmembrane domains (TMDs) of predicted proteins were analyzed, revealing three potential proteins (CDS: 20, 51, and 52) with TMDs. CDS51 encodes an Rz-like spanin and was found to have one TMD topology (Figure 7B); CDS20 encodes a transmembrane protein, and CDS52 encodes a holin. Two TMD topologies were detected in the predicted proteins of CDS20 and CDS52 (Figures 7A,C).

3.7.4 Evolutionary analysis of phage vB_Kp_XP4

To further investigate the evolutionary relationships of phage vB_Kp_XP4, a phylogenetic tree was constructed based on the conserved terminase large subunit (CDS48) using blastp for protein comparison in the NCBI database. The phylogenetic tree (Figure 8A) showed that phage vB_Kp_XP4 is closely related to phage BUCT86 and other phages. To understand the relationship between host specificity and phage tail fiber protein gene sequences, a phylogenetic tree was also constructed using the tail fiber protein (CDS46) (Figure 8B). This analysis revealed that the tail fiber protein sequence had the highest homology with *Klebsiella* phage KpV71, vB_Kpn_K1PH164C1, and NTUH-K2044-K1-1. Overall, phages with high sequence homology belong to the genus *Drulisvirus*, further confirming the close evolutionary relationship of *Klebsiella* phage vB_Kp_XP4 with the *Drulisvirus* genus. Using AlphaFold3, the protein structures of the terminase large subunit and the tail fiber protein of the *Klebsiella* phage vB_Kp_XP4 were predicted (Figures 8C,D).

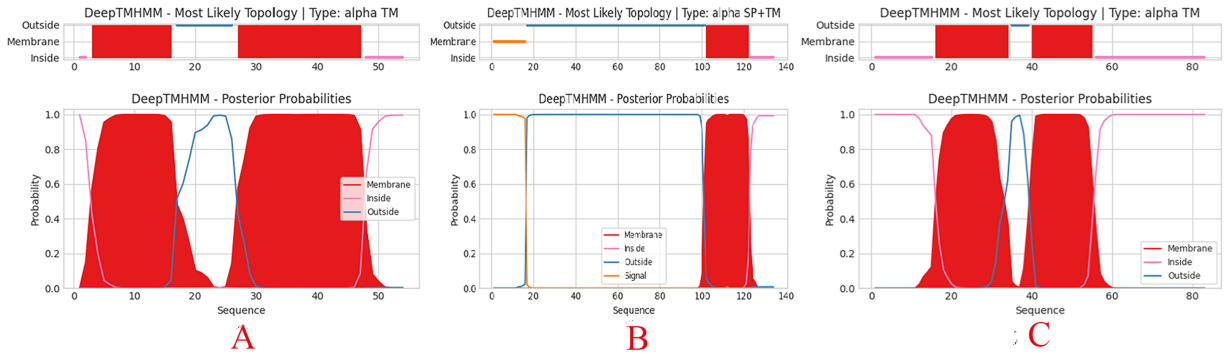

FIGURE 7
Predicted transmembrane topology of hypothetical holin (CDS20 **(A)**, CDS51 **(B)**, and CDS52 **(C)**) using the DeepTMHMM tool. Red squares represent predicted transmembrane domains, while pink and blue lines represent intra-and extra-membrane domains, respectively. The y-axis represents predicted probability, and the x-axis represents amino acid sequence positions.

3.8 Assessment of the efficacy of phage vB_Kp_XP4 against strain P4 *in vivo*

Galleria mellonella larvae model was used to assess the efficacy of phage vB_Kp_XP4 against strain P4 *in vivo*. At 60 h, the survival rate of larvae injected with only PBS and phage was both 90%, while the survival rate of larvae injected with strain P4 (10^8) was 0%, and those injected with strain P4 (10^7) had a survival rate of 10%. The P4 + PBS group had a survival rate of 20%, while the groups injected with P4 + phage at MOI = 0.1, 1, and 10 had survival rates of 40, 80, and 50%, respectively. Notably, at MOI = 0.1, the lower survival rate was related to the higher concentration of P4 in this group (Figure 9A). It can be observed that the phage treatment groups performed significantly better than the untreated group. Larvae injected with strain P4 (10^8) all died within 20 h, and those injected with PBS at 1 h post-injection died within 36 h; when MOI = 0.1, larvae injected with phage at 1 h had a survival rate of 20% at 60 h; larvae injected with phage at 2 h all died by 45 h; larvae injected with phage at 4 h all died within 22 h (Figure 9B). It is evident that under the same infection conditions, the earlier phage treatment is administered, the longer the survival time of *Galleria mellonella* larvae, and the more pronounced the therapeutic effect. Additionally, larvae injected with phage alone still had a high survival rate, demonstrating the safety of phage therapy in this model. The morphology of the *Galleria mellonella* larvae after treatment with phage vB_Kp_XP4 is shown in Figure 9C.

4 Discussion

It is well known that the phenomenon of "mutual inhibition" among organisms is common. At the end of the 19th century, an outbreak of cholera in the Ganges River mysteriously disappeared, suggesting the presence of a natural antagonist to bacteria in the environment, which was later identified as bacteriophages (d'Herelle, 1931; Duckworth, 1976). In the early 20th century, bacteriophages were widely used to treat various bacterial infections, including cholera, dysentery, plague, Staphylococcus, *Escherichia coli*, and Streptococcus (McCallin et al., 2019; Summers, 1993; Myelnikov, 2020). However, with the advent of antibiotics in the mid-20th century, which marked a "golden era" lasting over 40 years, research on bacteriophages nearly halt (Gordillo Altamirano and Barr, 2019). By the end of the 20th century, the development of new antibiotics had slowed significantly, entering what is often referred to as a "dry pipeline," while antimicrobial resistance continued to escalate as a global threat (Gordillo Altamirano and Barr, 2019; Hitchcock et al., 2023). With rapid advancements in biology, medicine, and other fields, our understanding and research on bacteriophages have deepened, and phage therapy has re-emerged as a promising solution to mitigate the antibiotic resistance crisis.

In this study, a lytic environmental phage was isolated from a natural water source using the hypervirulent *K. pneumoniae* strain P4 as the host. At 36°C, within 12 h, the phage formed plaques approximately 2 mm in diameter with surrounding halos consisting of multiple semi-transparent layers. As time progressed, the halos expanded, and by 36 h, the plaques and halos reached a diameter of up to 28 mm, consistent with the findings of Zaki et al. (2023). According to morphological observations and the latest classification data from the International Committee on Taxonomy of Viruses (ICTV),[4] most phages isolated from *K. pneumoniae* are double-stranded DNA phages belonging to the order Caudovirales (Zerbini et al., 2023).

The lysis efficiency of phage vB_Kp_XP4 is positively correlated with temperature between 4°C and 50°C. However, when the temperature exceeds 60°C, this relationship reverses, regardless of whether the titer is high (10^{12} PFU/ml) or low (10^8 PFU/ml). It is similar to the behavior observed in phage vB_KpnP_IME337 (Gao et al., 2020). Increasing the initial dose of the phage allows some activity to be retained, suggesting that adjusting the phage dosage could effectively target heat-resistant bacterial strains in high-temperature environments. The phage also demonstrated strong lytic activity across a pH range of 4 to 11, indicating high stability under various conditions. This stability suggests that Phage vB_Kp_XP4 could be useful not only under standard conditions but also in special environments, such as in the disinfection and cleaning of hospital settings contaminated with multidrug-resistant bacteria (Otter et al.,

4 http://ictv.global/taxonomy

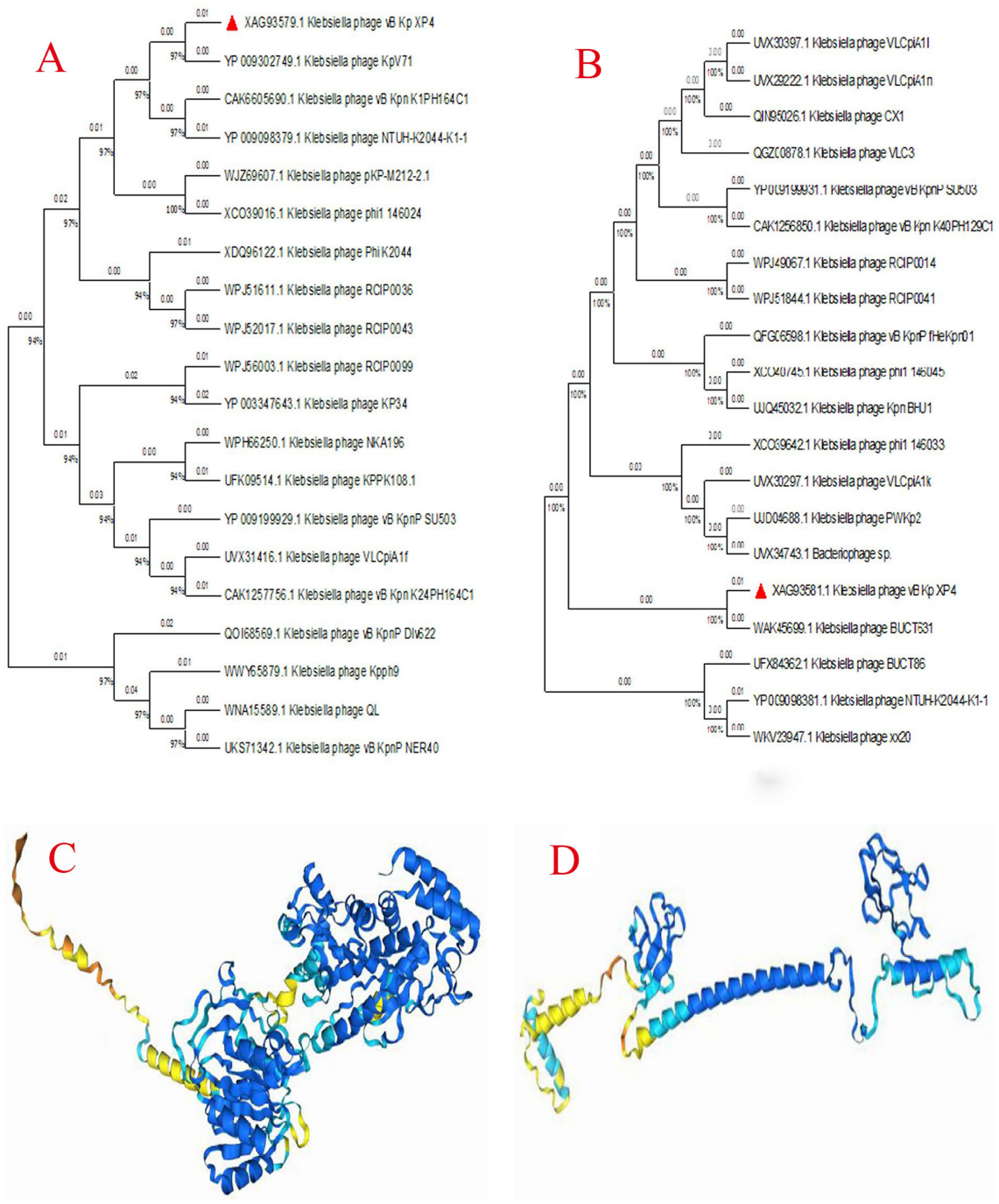

FIGURE 8
(A,B) Phylogenetic tree of the aligned amino acid sequences of key signature proteins, including the terminase large subunit **(A)** and tail fiber protein **(B)**, constructed using the Maximum likelihood method with the JTT matrix-based model and 1,000 replicates in MEGA11; **(C,D)** The predicted protein structures of the terminase large subunit **(C)** and tail fiber protein **(D)**. Deep blue represents "Very high confidence (plDDT>90)," light blue represents "Confidence (90 > plDDT>70)," yellow represents "Low confidence (70 > plDDT>50)," and orange represents "Very low confidence (plDDT<50)".

2015) or in applications within high-temperature, acidic, or alkaline environments (Suja and Gummadi, 2023). These properties confer broad practicality and application value to the phage. The study found that phage vB_Kp_XP4 has a latent period of approximately 10 min, shorter than most phages (Li et al., 2020), allowing for quicker control of pathogenic bacterial infections. The phage titer peaked around 50 min, entering a plateau phase. Due to the strong viscosity of the host bacteria, some free phages were not fully eluted during the experiment, slightly affecting the measurement of the burst size. However, the rapid and efficient lytic capability of the phage remains evident. Lytic phages with short incubation times, meaning they have a rapid replication cycle within the host bacterium, and high productivity, indicating they produce a large number of new phage particles per infected host cell, such as vB_Kp_XP4, are suitable for use during the acute phase of infections (Meile et al., 2022), effectively reducing the number of pathogens and

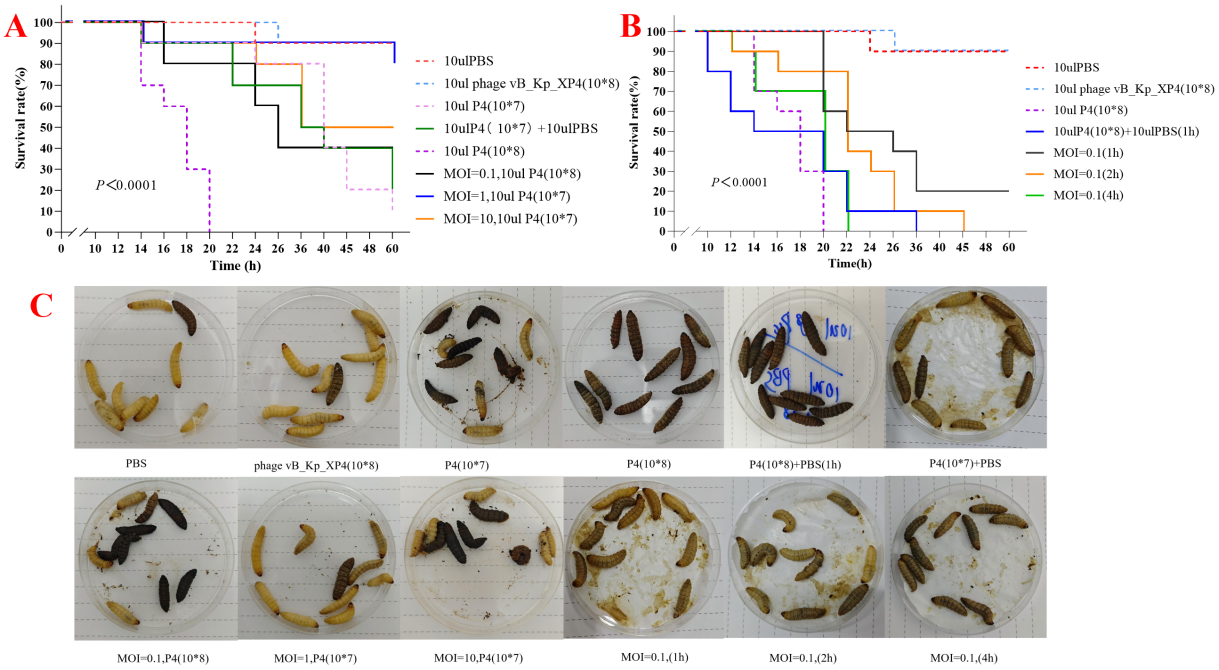

FIGURE 9
(A,B) Survival rates of large wax moth *larvae* treated with varying MOI, time, PBS, and bacteriophages; **(C)** Therapeutic effects of *Klebsiella* phage vB_Kp_XP4 on *larvae* infected with *Klebsiella pneumoniae* P4.

providing more time for the host immune response and clinical treatments, thereby improving patient outcomes. After 100 min, a marked decline in phage titer and an increase in bacterial count were observed, which aligns with the growth pattern of phage ST11 K47 (Fang and Zong, 2022). Continued observation in liquid culture showed that the numbers of phages and bacteria tended to stabilize, indicating that in liquid media, phages cannot eliminate bacteria, as the death of bacteria would also disrupt the phage's limited food chain. On solid plates, when the phage titer reaches a sufficient level, bacterial growth can be completely inhibited, demonstrating that the growth and mutation rates of bacteria and phages are significantly influenced by the culture environment (Chevallereau et al., 2022). On this basis, we adopted *Galleria mellonella* larvae as the infection model. The natural immune system of *Galleria mellonella* has similarities with the human immune system and is easy to obtain and breed (Feng et al., 2023). In this study, a new phage vB_Kp_XP4 was used to prolong the survival time of *Galleria mellonella* larvae after infection. The survival time of the phage treatment group was significantly longer than that of the non-intervention group, and the earlier the phage intervention was carried out, the more obvious the treatment effect was, which was consistent with the conclusion of a certain study (Lin et al., 2014). Further *in vivo* studies are needed to explore the interaction mechanisms between phages and bacteria. Regarding the emergence of phage-resistant bacterial strains, many studies have shown that the acquisition of phage resistance often results in a significant decrease in virulence and antibiotic resistance (Chen et al., 2024). Combining antibiotics (Ziller et al., 2024) and phage cocktails (Yoo et al., 2024) can suppress the emergence of resistant strains. A substantial body of animal studies has demonstrated that the combination of phages, antibiotics, and the host immune system can effectively control bacterial infections (Tang et al., 2024; Pal et al., 2024; Nang et al., 2024). However, clinical cases are relatively limited, and more clinical trials are necessary to optimize, validate, and refine the therapeutic use of phages. *Klebsiella* phage vB_Kp_XP4 shows a narrow lytic spectrum and high specificity, typical of natural phages (Dion et al., 2020). Phages rely primarily on the specificity of their tail structures to recognize host bacteria. Modifying phages through induced culture, co-culture, and genetic engineering strategies can help broaden their lytic spectra (Parker and Nugen, 2024; Ulrich et al., 2024; Hesse et al., 2020).

Based on whole-genome sequencing data, a comparison using Blastn in the NCBI database revealed that *Klebsiella* phage vB_Kp_XP4 is most similar to *Klebsiella* phage NTUH-K2044-K1-1 (ON602748.1), with 88% coverage, 90.92% identity, and an E-value of 0. The nucleotide sequence of *Klebsiella* phage vB_Kp_XP4 differs by more than 5% from that of known phages, indicating it represents a new species (Grigson et al., 2023). Further phylogenetic analysis using conserved proteins confirmed that *Klebsiella* phage vB_Kp_XP4 is closely related to phages in the genus Drulisvirus. Therefore, it is suggested that *Klebsiella* phage vB_Kp_XP4 is a new member of the genus Drulisvirus within the subfamily Slopekvirinae. *Klebsiella* phage vB_Kp_XP4 has relatively small nucleic acid molecular weights, making them easier to edit. This characteristic makes them ideal model phages for genetic engineering and synthetic biology applications, offering significant potential for more in-depth research (Lenneman et al., 2021).

The formation of halos around plaques is likely related to the synthesis of phage protein products, including lytic enzymes, endolysins, and spanins (holin, endolysin, and spanin). Numerous studies have demonstrated that phage depolymerases possess biofilm-degrading properties (Tagliaferri et al., 2019; Gliźniewicz et al., 2023; Drulis-Kawa et al., 2015). According to the National Institutes of Health, more than 80% of bacterial diseases are associated with biofilms (Evans et al., 2023). The significant morphological changes

observed in the P4 strain after treatment with phage vB_Kp_XP4 suggest its ability to remove the capsule of serotype K1 *Klebsiella pneumoniae*. Phage vB_Kp_XP4 encodes endolysin (CDS53), a cell wall hydrolase synthesized in the late stage of phage infection that hydrolyzes peptidoglycan to release progeny phages (Cahill and Young, 2019; Marques et al., 2021). Euler et al. (2023) demonstrated in mouse experiments that phage endolysins have bactericidal effects against multiple Gram-negative ESKAPE pathogens. Chen et al. (2024) ngineered endolysins with different protein peptides, showing significant bactericidal activity against ESKAPEE pathogens. Endolysins in *Klebsiella* phages exhibit diversity and conservation within the genus, providing substantial potential for further exploration (Chang et al., 2022). Future research will focus on phage protein products, such as depolymerases and endolysins, to develop formulations targeting bacterial biofilms and novel antibacterial agents. Such developments could provide a material basis for combining phages and antibiotics, offering more options for treating bacterial infections. In this study, we observed the morphological differences of the strains before and after phage treatment using only light microscopy. Utilizing electron microscopy may provide more detailed insights. As a biological therapy, phage treatment must prioritize safety considerations. Comparisons with existing databases indicate that *Klebsiella* phage vB_Kp_XP4 does not contain tRNA, lysogenic genes, antibiotic resistance genes, or virulence genes, thereby posing no risk of transmitting resistance or virulence genes, which ensures its safety for clinical applications.

5 Conclusion

In conclusion, bacteriophages and their protein products have garnered significant interest globally as potential therapies to reduce or replace antibiotic use. This study successfully isolated a novel *Klebsiella* phage vB_Kp_XP4, and characterized its biological properties and genomic features. *In vivo* experiments demonstrated its therapeutic effect on a *Galleria mellonella* infection model, with high safety and efficacy, making it a promising candidate for phage therapy and a potential synergist in combination with antibiotics, offering additional options for antimicrobial treatment. Furthermore, phage protein products, such as lytic enzymes and endolysins, possess properties that assist in bacterial lysis. Future *in vitro* and *in vivo* experiments could explore the antibacterial effects of phage suspensions, protein synthesis products, and various combinations with antibiotics.

Data availability statement

The datasets presented in this study can be found in online repositories. The names of the repository/repositories and accession number(s) can be found in the article/Supplementary material.

Author contributions

XP: Conceptualization, Formal analysis, Investigation, Methodology, Software, Validation, Visualization, Writing – original draft, Writing – review & editing. JC: Conceptualization, Formal analysis, Investigation, Validation, Visualization, Writing – original draft, Writing – review & editing. HZ: Conceptualization, Funding acquisition, Supervision, Writing – review & editing. XL: Conceptualization, Funding acquisition, Supervision, Writing – review & editing. CZ: Funding acquisition, Methodology, Software, Writing – review & editing. SJ: Methodology, Validation, Software, Writing – review & editing. CL: Resources, Validation, Writing – review & editing. NW: Methodology, Formal analysis, Writing – review & editing. JZ: Formal analysis, Writing – review & editing. BW: Conceptualization, Data curation, Formal analysis, Funding acquisition, Resources, Supervision, Writing – review & editing. WZ: Conceptualization, Formal analysis, Funding acquisition, Resources, Supervision, Writing – review & editing. ZZ: Conceptualization, Data curation, Funding acquisition, Investigation, Methodology, Writing – original draft, Writing – review & editing.

Funding

The author(s) declare that financial support was received for the research, authorship, and/or publication of this article. Funded by 2024 Hebei Province Master's Students Innovation Ability Training Program (CXZZSS2024126) and the Government Funded Clinical Medicine Excellent Talent Training Project (ZF2024224 and ZF2025274).

Acknowledgments

We thank the laboratory research staff in the Central research lab of The First Affiliated Hospital of Hebei North University. We need to thank Shiyan Jiao, Xue Wang, and Jiangming Wei from The Department of postgraduate of Hebei North University for their experimental assistance.

Conflict of interest

The authors declare that the research was conducted in the absence of any commercial or financial relationships that could be construed as a potential conflict of interest.

Publisher's note

Supplementary material

The Supplementary material for this article can be found online at: https://www.frontiersin.org/articles/10.3389/fmicb.2025.1491961/full#supplementary-material

References

Antimicrobial Resistance Collaborators (2022). Global burden of bacterial antimicrobial resistance in 2019: A systematic analysis. *Lancet* 399, 629–655. doi: 10.1016/S0140-6736(21)02724-0

Aziz, R. K., Bartels, D., Best, A. A., DeJongh, M., Disz, T., Edwards, R. A., et al. (2008). The RAST server: rapid annotations using subsystems technology. *BMC Genomics* 9:75. doi: 10.1186/1471-2164-9-75

Beamud, B., García-González, N., Gómez-Ortega, M., González-Candelas, F., Domingo-Calap, P., and Sanjuan, R. (2023). Genetic determinants of host tropism in *Klebsiella* phages. *Cell Rep.* 42:112048. doi: 10.1016/j.celrep.2023.112048

Bortolaia, V., Kaas, R. S., Ruppe, E., Roberts, M. C., Schwarz, S., Cattoir, V., et al. (2020). Res finder 4.0 for predictions of phenotypes from genotypes. *J. Antimicrob. Chemother.* 75, 3491–3500. doi: Res Finder 4.0 for predictions of phenotypes from genotypes. doi: 10.1093/jac/dkaa345

Brettin, T., Davis, J. J., Disz, T., Edwards, R. A., Gerdes, S., Olsen, G. J., et al. (2015). RASTtk: a modular and extensible implementation of the RAST algorithm for building custom annotation pipelines and annotating batches of genomes. *Sci. Rep.* 5:8365. doi: 10.1038/srep08365

Brives, C., and Pourraz, J. (2020). Phage therapy as a potential solution in the fight against AMR: obstacles and possible futures. *Palgrave Commun.* 6:478. doi: 10.1057/s41599-020-0478-4

Cahill, J., and Young, R. (2019). Phage lysis: multiple genes for multiple barriers. *Adv. Virus Res.* 103, 33–70. doi: 10.1016/bs.aivir.2018.09.003

Cantalapiedra, C. P., Hernández-Plaza, A., Letunic, I., Bork, P., and Huerta-Cepas, J. (2021). Egg NOG-mapper v2: functional annotation, Orthology assignments, and domain prediction at the metagenomic scale. *Mol. Biol. Evol.* 38, 5825–5829. doi: 10.1093/molbev/msab293

Castledine, M., Padfield, D., Sierocinski, P., Soria Pascual, J., Hughes, A., Mäkinen, L., et al. (2022). Parallel evolution of *Pseudomonas aeruginosa* phage resistance and virulence loss in response to phage treatment in vivo and in vitro. *eLife* 11:73679. doi: 10.7554/eLife.73679

Chang, R. Y. K., Nang, S. C., Chan, H. K., and Li, J. (2022). Novel antimicrobial agents for combating antibiotic-resistant bacteria. *Adv. Drug Deliv. Rev.* 187:114378. doi: 10.1016/j.addr.2022.114378

Chen, W., Han, L. M., Chen, X. Z., Yi, P. C., Li, H., Ren, Y. Y., et al. (2024). Engineered endolysin of *Klebsiella pneumoniae* phage is a potent and broad-spectrum bactericidal agent against "ESKAPEE" pathogens. *Front. Microbiol.* 15:1397830. doi: 10.3389/fmicb.2024.1397830

Chen, L., Li, Q., Nasif, K. F. A., Xie, Y., Deng, B., Niu, S., et al. (2024). AI-driven deep learning techniques in protein structure prediction. *Int. J. Mol. Sci.* 25:25 (15). doi: 10.3390/ijms25158426

Chen, Q., Zhang, F., Bai, J., Che, Q., Xiang, L., Zhang, Z., et al. (2024). Bacteriophage-resistant carbapenem-resistant *Klebsiella pneumoniae* shows reduced antibiotic resistance and virulence. *Int. J. Antimicrob. Agents* 64:107221. doi: 10.1016/j.ijantimicag.2024.107221

Chen, S., Zhou, Y., Chen, Y., and Gu, J. (2018). Fastp: an ultra-fast all-in-one FASTQ preprocessor. *Bioinformatics* 34, i884–i890. doi: 10.1093/bioinformatics/bty560

Chevallereau, A., Pons, B. J., van Houte, S., and Westra, E. R. (2022). Interactions between bacterial and phage communities in natural environments. *Nat. Rev. Microbiol.* 20, 49–62. doi: 10.1038/s41579-021-00602-y

Darling, A. C., Mau, B., Blattner, F. R., and Perna, N. T. (2004). Mauve: multiple alignment of conserved genomic sequence with rearrangements. *Genome Res.* 14, 1394–1403. doi: 10.1101/gr.2289704

d'Herelle, F. (1931). Bacteriophage as a treatment in acute medical and surgical infections. *Bull. N. Y. Acad. Med.* 7, 329–348

Dion, M. B., Oechslin, F., and Moineau, S. (2020). Phage diversity, genomics and phylogeny. *Nat. Rev. Microbiol.* 18, 125–138. doi: 10.1038/s41579-019-0311-5

Drulis-Kawa, Z., Majkowska-Skrobek, G., and Maciejewska, B. (2015). Bacteriophages and phage-derived proteins--application approaches. *Curr. Med. Chem.* 22, 1757–1773. doi: 10.2174/0929867322666150209152851

DSMZ. (2024). *The Leibniz Institute DSMZ*. Available at: https://www.dsmz.de/ (Accessed January 5, 2019).

Duckworth, D. H. (1976). Who discovered bacteriophage? *Bacteriol. Rev.* 40, 793–802. doi: 10.1128/br.40.4.793-802.1976

Euler, C. W., Raz, A., Hernandez, A., Serrano, A., Xu, S., Andersson, M., et al. (2023). Ply Kp104, a novel phage Lysin for the treatment of *Klebsiella pneumoniae*, Pseudomonas aeruginosa, and other gram-negative ESKAPE pathogens. *Antimicrob. Agents Chemother.* 67:e0151922. doi: 10.1128/aac.01519-22

Evans, S. R., Patel, R., Hamasaki, T., Howard-Anderson, J., Kinamon, T., King, H. A., et al. (2023). The future Ain't what it used to be… out with the old… in with the better: antibacterial resistance leadership group innovations. *Clin. Infect. Dis.* 77, S321–S330. doi: 10.1093/cid/ciad538

Fang, Q., and Zong, Z. (2022). Lytic phages against ST11 K47 Carbapenem-resistant *Klebsiella pneumoniae* and the corresponding phage resistance mechanisms. *mSphere* 7:e0008022. doi: 10.1128/msphere.00080-22

Feng, J., Li, F., Sun, L., Dong, L., Gao, L., Wang, H., et al. (2023). Characterization and genome analysis of phage vB_KpnS_SXFY507 against *Klebsiella pneumoniae* and efficacy assessment in galleria mellonella larvae. *Front. Microbiol.* 14:14 (null): 1081715. doi: 10.3389/fmicb.2023.1081715

Gao, M., Wang, C., Qiang, X., Liu, H., Li, P., Pei, G., et al. (2020). Isolation and characterization of a novel bacteriophage infecting Carbapenem-resistant *Klebsiella pneumoniae*. *Curr. Microbiol.* 77, 722–729. doi: 10.1007/s00284-019-01849-8

Gliźniewicz, M., Miłek, D., Olszewska, P., Czajkowski, A., Serwin, N., Cecerska-Heryć, E., et al. (2023). Advances in bacteriophage-mediated strategies for combating polymicrobial biofilms. *Front. Inmicrobiol.* 14:1320345. doi: 10.3389/fmicb.2023.1320345

Gordillo Altamirano, F. L., and Barr, J. J. (2019). Phage therapy in the Postantibiotic era. *Clin. Microbiol. Rev.* 32:18. doi: 10.1128/CMR.00066-18

Grigson, S. R., Giles, S. K., Edwards, R. A., and Papudeshi, B. (2023). Knowing and naming: phage annotation and nomenclature for phage therapy. *Clin. Infect. Dis.* 77, S352–S359. doi: 10.1093/cid/ciad539

Hallgren, J., Tsirigos, K., Pedersen, M. D., Armenteros, J. J., Marcatili, P., Nielsen, H., et al. (2022). Deep TMHMM predicts alpha and beta transmembrane proteins using deep neural networks. *bioRxiv* 2022:609. doi: 10.1101/2022.04.08.487609

Han, P., Pu, M., Li, Y., Fan, H., and Tong, Y. (2023). Characterization of bacteriophage BUCT631 lytic for K1 *Klebsiella pneumoniae* and its therapeutic efficacy in galleria mellonella larvae. *Virol. Sin.* 38, 801–812. doi: 10.1016/j.virs.2023.07.002

Hesse, S., Rajaure, M., Wall, E., Johnson, J., Bliskovsky, V., Gottesman, S., et al. (2020). Phage resistance in multidrug-resistant *Klebsiella pneumoniae* ST258 evolves via diverse mutations that culminate in impaired adsorption. *MBio* 11:530. doi: 10.1128/mBio.02530-19

Hitchcock, N. M., Devequi Gomes Nunes, D., Shiach, J., Valeria Saraiva Hodel, K., Dantas Viana Barbosa, J., Alencar Pereira Rodrigues, L., et al. (2023). Current clinical landscape and global potential of bacteriophage therapy. *Viruses* 15:1020. doi: 10.3390/v15041020

Hufsky, F., Abecasis, A. B., Babaian, A., Beck, S., Brierley, L., Dellicour, S., et al. (2023). The international virus bioinformatics meeting 2023. *Viruses* 15:2031. doi: 10.3390/v15102031

Hyman, P., and Abedon, S. T. (2009). Practical methods for determining phage growth parameters. *Methods Mol. Biol. (Clifton, NJ)* 501, 175–202. doi: 10.1007/978-1-60327-164-6_18

Jones, D. T., Taylor, W. R., and Thornton, J. M. (1992). The rapid generation of mutation data matrices from protein sequences. *Bioinformatics* 8, 275–282. doi: 10.1093/bioinformatics/8.3.275

Khan Mirzaei, M., and Nilsson, A. S. (2015). Isolation of phages for phage therapy: a comparison of spot tests and efficiency of plating analyses for determination of host range and efficacy. *PLoS One* 10:e0118557. doi: 10.1371/journal.pone.0118557

Kongari, R., Rajaure, M., Cahill, J., Rasche, E., Mijalis, E., Berry, J., et al. (2018). Phage spanins: diversity, topological dynamics and gene convergence. *BMC Bioinformatics* 19:326. doi: 10.1186/s12859-018-2342-8

Kutateladze, M. (2015). Experience of the Eliava institute in bacteriophage therapy. *Virol. Sin.* 30, 80–81. doi: 10.1007/s12250-014-3557-0

Lan, P., Jiang, Y., Zhou, J., and Yu, Y. (2021). A global perspective on the convergence of hypervirulence and carbapenem resistance in *Klebsiella pneumoniae*. *J. Glob. Antimicrob. Resist.* 25, 26–34. doi: 10.1016/j.jgar.2021.02.020

Antimicrobial Resistance Collaborators (2024). The burden of bacterial antimicrobial resistance in the WHO African region in 2019: a cross-country systematic analysis. *Lancet Glob. Health* 12, e201–e216. doi: 10.1016/S2214-109X(23)00539-9

Lee, C. R., Lee, J. H., Park, K. S., Jeon, J. H., Kim, Y. B., Cha, C. J., et al. (2017). Antimicrobial resistance of Hypervirulent *Klebsiella pneumoniae*: epidemiology, Hypervirulence-associated determinants, and resistance mechanisms. *Front. Cell. Infect. Microbiol.* 7:483. doi: 10.3389/fcimb.2017.00483

Lenneman, B. R., Fernbach, J., Loessner, M. J., Lu, T. K., and Kilcher, S. (2021). Enhancing phage therapy through synthetic biology and genome engineering. *Curr. Opin. Biotechnol.* 68, 151–159. doi: 10.1016/j.copbio.2020.11.003

Li, H., and Durbin, R. (2009). Fast and accurate short read alignment with burrows-wheeler transform. *Bioinformatics* 25, 1754–1760. doi: 10.1093/bioinformatics/btp324

Li, Y., Pu, M., Han, P., Li, M., An, X., Song, L., et al. (2023). Efficacy in galleria mellonella larvae and application potential assessment of a new bacteriophage BUCT700 extensively lyse *Stenotrophomonas maltophilia*. *Microbiol. Spectr.* 11:e0403022. doi: 10.1128/spectrum.04030-22

Li, M., Xiao, Y., Li, P., Wang, Z., Qi, W., Qi, Z., et al. (2020). Characterization and genome analysis of *Klebsiella* phage P 509, with lytic activity against clinical carbapenem-resistant *Klebsiella pneumoniae* of the KL64 capsular type. *Arch. Virol.* 165, 2799–2806. doi: 10.1007/s00705-020-04822-0

Lin, T. L., Hsieh, P. F., Huang, Y. T., Lee, W. C., Tsai, Y. T., Su, P. A., et al. (2014). Isolation of a bacteriophage and its depolymerase specific for K1 capsule of *Klebsiella pneumoniae*: implication in typing and treatment. *J. Infect. Dis.* 210, 1734–1744. doi: 10.1093/infdis/jiu332

Liu, B., Zheng, D., Zhou, S., Chen, L., and Yang, J. (2022). VFDB 2022: a general classification scheme for bacterial virulence factors. *Nucleic Acids Res.* 50, D912–D917. doi: 10.1093/nar/gkab1107

Marques, A. T., Tanoeiro, L., Duarte, A., Gonçalves, L., Vítor, J. M. B., and Vale, F. F. (2021). Genomic analysis of prophages from *Klebsiella pneumoniae* clinical isolates. *Microorganisms* 9:null. doi: 10.3390/microorganisms9112252

McCallin, S., Sacher, J. C., Zheng, J., and Chan, B. K. (2019). Current state of compassionate phage therapy. *Viruses* 11:null. doi: 10.3390/v11040343

McNair, K., Bailey, B. A., and Edwards, R. A. (2012). PHACTS, a computational approach to classifying the lifestyle of phages. *Bioinformatics* 28, 614–618. doi: 10.1093/bioinformatics/bts014

Meile, S., Du, J., Dunne, M., Kilcher, S., and Loessner, M. J. (2022). Engineering therapeutic phages for enhanced antibacterial efficacy. *Curr. Opin. Virol.* 52, 182–191. doi: 10.1016/j.coviro.2021.12.003

Międzybrodzki, R., Borysowski, J., Weber-Dąbrowska, B., Fortuna, W., Letkiewicz, S., Szufnarowski, K., et al. (2012). Clinical aspects of phage therapy. *Adv. Virus Res.* 83, 73–121. doi: 10.1016/B978-0-12-394438-2.00003-7

Mohammadi, M., Saffari, M., Siadat, S. D., Hejazi, S. H., Shayestehpour, M., Motallebi, M., et al. (2023). Isolation, characterization, therapeutic potency, and genomic analysis of a novel bacteriophage vB_KshKPC-M against carbapenemase-producing *Klebsiella pneumoniae* strains (CRKP) isolated from ventilator-associated pneumoniae (VAP) infection of COVID-19 patients. *Ann. Clin. Microbiol. Antimicrob.* 22:18. doi: 10.1186/s12941-023-00567-1

Myelnikov, D. (2020). Creature features: the lively narratives of bacteriophages in soviet biology and medicine. *Notes Rec. R. Soc. Lond.* 74, 579–597. doi: 10.1098/rsnr.2019.0035

Nang, S. C., Lu, J., Yu, H. H., Wickremasinghe, H., Azad, M. A. K., Han, M., et al. (2024). Phage resistance in *Klebsiella pneumoniae* and bidirectional effects impacting antibiotic susceptibility. *Clin. Microbiol. Infect.* 30, 787–794. doi: 10.1016/j.cmi.2024.03.015

Nurk, S., Meleshko, D., Korobeynikov, A., and Pevzner, P. A. (2017). meta SPAdes: a new versatile metagenomic assembler. *Genome Res.* 27, 824–834. doi: 10.1101/gr.213959.116

Olson, R. D., Assaf, R., Brettin, T., Conrad, N., Cucinell, C., Davis, J. J., et al. (2023). Introducing the bacterial and viral bioinformatics resource center (BV-BRC): a resource combining PATRIC, IRD and ViPR. *Nucleic Acids Res.* 51, D678–D689. doi: 10.1093/nar/gkac1003

Otter, J. A., Vickery, K., Walker, J. T., de Lancey, P. E., Stoodley, P., Goldenberg, S. D., et al. (2015). Surface-attached cells, biofilms and biocide susceptibility: implications for hospital cleaning and disinfection. *J. Hosp. Infect.* 89, 16–27. doi: 10.1016/j.jhin.2014.09.008

Overbeek, R., Olson, R., Pusch, G. D., Olsen, G. J., Davis, J. J., Disz, T., et al. (2014). The SEED and the rapid annotation of microbial genomes using subsystems technology (RAST). *Nucleic Acids Res.* 42, D206–D214. doi: 10.1093/nar/gkt1226

Pal, N., Sharma, P., Kumawat, M., Singh, S., Verma, V., Tiwari, R. R., et al. (2024). Phage therapy: an alternative treatment modality for MDR bacterial infections. *Infect. Dis.* 56, 785–817. doi: 10.1080/23744235.2024.2379492

Parker, D. R., and Nugen, S. R. (2024). Bacteriophage-based bioanalysis. *Annu. Rev. Anal. Chem.* 17, 393–410. doi: 10.1146/annurev-anchem-071323-084224

Pirnay, J. P., Djebara, S., Steurs, G., Griselain, J., Cochez, C., De Soir, S., et al. (2024). Personalized bacteriophage therapy outcomes for 100 consecutive cases: a multicentre, multinational, retrospective observational study. *Nat. Microbiol.* 9, 1434–1453. doi: 10.1038/s41564-024-01705-x

Programme TUE. (2023). *Bracing for superbugs: Strengthening environmental action in the one health response to antimicrobial resistance*, no. 02.07.

Pu, D., Zhao, J., Chang, K., Zhuo, X., and Cao, B. (2023). "Superbugs" with hypervirulence and carbapenem resistance in *Klebsiella pneumoniae*: the rise of such emerging nosocomial pathogens in China. *Sci. Bul.* 68, 2658–2670. doi: 10.1016/j.scib.2023.09.040

Rokas, A., and Charlesworth, D. (2001). "Molecular evolution and phylogenetics" in Genetics Research. ed. M. Nei, vol. *77* (Oxford, UK: Oxford University Press), 117–120.

Sacher, J. C., Zheng, J., and Lin, R. C. Y. (2022). Data to power precision phage therapy: a look at the phage directory-phage Australia partnership. *Phage (New Rochelle, NY)* 3, 112–115. doi: 10.1089/phage.2022.29030.jcs

Seemann, T. (2014). Prokka: rapid prokaryotic genome annotation. *Bioinformatics* 30, 2068–2069. doi: 10.1093/bioinformatics/btu153

Shon, A. S., Bajwa, R. P., and Russo, T. A. (2013). Hypervirulent (hypermucoviscous) *Klebsiella pneumoniae*: a new and dangerous breed. *Virulence* 4, 107–118. doi: 10.4161/viru.22718

Solovieva, E. V., Myakinina, V. P., Kislichkina, A. A., Krasilnikova, V. M., Verevkin, V. V., Mochalov, V. V., et al. (2018). Comparative genome analysis of novel Podoviruses lytic for hypermucoviscous *Klebsiella pneumoniae* of K1, K2, and K57 capsular types. *Virus Res.* 243:10. doi: 10.1016/j.virusres.2017.09.026

Suja, E., and Gummadi, S. N. (2023). Advances in the applications of bacteriophages and phage products against food-contaminating bacteria. *Crit. Rev. Microbiol.* 50, 702–727. doi: 10.1080/1040841X.2023.2271098

Sullivan, M. J., Petty, N. K., and Beatson, S. A. (2011). Easyfig: a genome comparison visualizer. *Bioinformatics* 27, 1009–1010. doi: 10.1093/bioinformatics/btr039

Summer, E. J., Berry, J., Tran, T. A., Niu, L., Struck, D. K., and Young, R. (2007). Rz/Rz1 lysis gene equivalents in phages of gram-negative hosts. *J. Mol. Biol.* 373, 1098–1112. doi: 10.1016/j.jmb.2007.08.045

Summers, W. C. (1993). Cholera and plague in India: the bacteriophage inquiry of 1927-1936. *J. Hist. Med. Allied Sci.* 48, 275–301. doi: 10.1093/jhmas/48.3.275

Tagliaferri, T. L., Jansen, M., and Horz, H. P. (2019). Fighting pathogenic Bacteria on two fronts: phages and antibiotics as combined strategy. *Front. Cell. Infect. Microbiol.* 9:22. doi: 10.3389/fcimb.2019.00022

Tamura, K., Stecher, G., and Kumar, S. (2021). MEGA11: molecular evolutionary genetics analysis version 11. *Mol. Biol. Evol.* 38, 3022–3027. doi: 10.1093/molbev/msab120

Tang, M., Yao, Z., Liu, Y., Ma, Z., Zhao, D., Mao, Z., et al. (2024). Host immunity involvement in the outcome of phage therapy against hypervirulent *Klebsiella pneumoniae* infections. *Antimicrob. Agents Chemother.*:e0142923. doi: 10.1128/aac.01429-23

UCSD. (2019). *Center for Innovative Phage Applications and Therapeutics*. Available at: http://ipath.ucsd.edu/ (Accessed July 25, 2024).

Ulrich, L., Steiner, L. X., Giez, C., and Lachnit, T. (2024). Optimizing bacteriophage treatment of resistant Pseudomonas. *mSphere* 9:e0070723. doi: 10.1128/msphere.00707-23

Université Laval. (2024). *Félix d'Hérelle Reference Center for Bacterial Viruses*. Available at: https://www.phage.ulaval.ca/en/home/ (Accessed July 25, 2024).

Wang, X., Xie, Z., Zhao, J., Zhu, Z., Yang, C., and Liu, Y. (2021). Prospects of inhaled phage therapy for combatting pulmonary infections. *Front. Cell. Infect. Microbiol.* 11:758392. doi: 10.3389/fcimb.2021.758392

World Health Organization (2024a). WHO updates list of drug-resistant bacteria posing the greatest threat to human health. Geneva: World Health Organization.

World Health Organization (2024b). Antimicrobial Resistance, Hypervirulent *Klebsiella pneumoniae*-Global situation. Geneva: World Health Organization.

Yerushalmy, O., Braunstein, R., Alkalay-Oren, S., Rimon, A., Coppenhagn-Glazer, S., Onallah, H., et al. (2023). Towards standardization of phage susceptibility testing: the Israeli phage therapy center "clinical phage microbiology"-a pipeline proposal. *Clin. Infect. Dis.* 77, S337–S351. doi: 10.1093/cid/ciad514

Yoo, S., Lee, K. M., Kim, N., Vu, T. N., Abadie, R., and Yong, D. (2024). Designing phage cocktails to combat the emergence of bacteriophage-resistant mutants in multidrug-resistant *Klebsiella pneumoniae*. *Microbiol. Spectr.* 12:e0125823. doi: 10.1128/spectrum.01258-23

Yukgehnaish, K., Rajandas, H., Parimannan, S., Manickam, R., Marimuthu, K., Petersen, B., et al. (2022). Phage leads: rapid assessment of phage therapeutic suitability using an ensemble machine learning approach. *Viruses* 14:null. doi: 10.3390/v14020342

Zaki, B. M., Fahmy, N. A., Aziz, R. K., Samir, R., and El-Shibiny, A. (2023). Characterization and comprehensive genome analysis of novel bacteriophage, vB_Kpn_ZCKp20p, with lytic and anti-biofilm potential against clinical multidrug-resistant *Klebsiella pneumoniae*. *Front. Cell. Infect. Microbiol.* 13:1077995. doi: 10.3389/fcimb.2023.1077995

Zerbini, F. M., Siddell, S. G., Lefkowitz, E. J., Mushegian, A. R., Adriaenssens, E. M., Alfenas-Zerbini, P., et al. (2023). Changes to virus taxonomy and the ICTV statutes ratified by the international committee on taxonomy of viruses (2023). *Arch. Virol.* 168:175. doi: 10.1007/s00705-023-05797-4

Ziller, L., Blum, P. C., Buhl, E. M., Krüttgen, A., Horz, H. P., and Tagliaferri, T. L. (2024). Newly isolated Drexlerviridae phage LAPAZ is physically robust and fosters eradication of *Klebsiella pneumoniae* in combination with meropenem. *Virus Res.* 347:199417. doi: 10.1016/j.virusres.2024.199417

frontiers | Frontiers in Microbiology

TYPE Original Research
PUBLISHED 24 March 2025
DOI 10.3389/fmicb.2025.1481197

OPEN ACCESS

EDITED BY
Israel Nissan,
Kimron Veterinary Institute, Ministry of Agriculture and Rural Development (Israel), Israel

REVIEWED BY
Florentin Constancias,
ETH Zürich, Switzerland
Padhmanand Sudhakar,
Kumaraguru College of Technology, India
Shuheng Gan,
University of Texas Southwestern Medical Center, United States

*CORRESPONDENCE
Thilo M. Fuchs
✉ thilom.fuchs@fli.de

RECEIVED 16 August 2024
ACCEPTED 14 February 2025
PUBLISHED 24 March 2025

CITATION
Wagner S, Weber M, Paul L-S, Grümpel-Schlüter A, Kluess J, Neuhaus K and Fuchs TM (2025) Absolute abundance calculation enhances the significance of microbiome data in antibiotic treatment studies.
Front. Microbiol. 16:1481197.
doi: 10.3389/fmicb.2025.1481197

Absolute abundance calculation enhances the significance of microbiome data in antibiotic treatment studies

Stefanie Wagner[1], Michael Weber[1], Lena-Sophie Paul[1], Angelika Grümpel-Schlüter[2], Jeannette Kluess[2], Klaus Neuhaus[3] and Thilo M. Fuchs[1]*

[1]Institute of Molecular Pathogenesis, Friedrich-Loeffler-Institut, Jena, Germany, [2]Institute of Animal Nutrition, Friedrich-Loeffler-Institut, Braunschweig, Germany, [3]Core Facility Microbiome, ZIEL Institute for Food & Health, Technical University of Munich, Freising, Germany

Background: The intestinal microbiota contributes to the colonization resistance of the gut towards bacterial pathogens. Antibiotic treatment often negatively affects the microbiome composition, rendering the host more susceptible for infections. However, a correct interpretation of such a perturbation requires quantitative microbiome profiling to reflect accurately the direction and magnitude of compositional changes within a microbiota. Standard 16S rRNA gene amplicon sequencing of microbiota samples offers compositional data in relative, but not absolute abundancies, and the presence of multiple copies of 16S rRNA genes in bacterial genomes introduces bias into compositional data. We explored whether improved sequencing data analysis influences the significance of the effect exerted by antibiotics on the faecal microbiota of young pigs using two veterinary antibiotics. Calculation of absolute abundances, either by flow cytometry-based bacterial cell counts or by spike-in of synthetic 16S rRNA genes, was employed and 16S rRNA gene copy numbers (GCN) were corrected.

Results: Cell number determination exhibited large interindividual variability in two pig studies, using either tylosin or tulathromycin. Following tylosin application, flow cytometry-based cell counting revealed decreased absolute abundances of five families and ten genera. These results were not detectable by standard 16S analysis based on relative abundances. Here, GCN correction additionally uncovered significant decreases of *Lactobacillus* and *Faecalibacterium*. In another experimental setting with tulathromycin treatment, bacterial abundance quantification by flow cytometry and by a spike-in method yielded similar results only on the phylum level. Even though the spike-in method identified the decrease of four genera, analysis by fluorescence-activated cell sorting (FACS) uncovered eight significantly reduced genera, such as *Prevotella* and *Paraprevotella* upon antibiotic treatment. In contrast, analysis of relative abundances only showed a decrease of *Faecalibacterium* and *Rikenellaceae* RC9 gut group and, thus, a much less detailed antibiotic effect.

Conclusion: Flow cytometry is a laborious method, but identified a higher number of significant microbiome changes in comparison to common compositional data analysis and even revealed to be superior to a spike-in method. Calculation of absolute abundances and GCN correction are valuable methods that should be standards in microbiome analyses in veterinary as well as human medicine.

KEYWORDS

antibiotic, one health, gut microbiome, piglet, flow cytometry, spike-in, 16S rRNA gene sequencing

Introduction

Antibiotic treatment often has a detrimental impact on the gut microbiome integrity, resulting in an increased risk for infection (Stecher et al., 2013; Prax et al., 2021), and an improved functional understanding of this dysbiosis requires a proper analysis of the intestinal microbiota composition. However, 16S sequencing data is generally not fully representative of community composition, due to sampling, DNA isolation, primer choice, 16S rRNA gene copies, and data analysis (Abellan-Schneyder et al., 2021). Concerning data analysis, filtering of spurious taxa and primer trimming seems to have a major impact (Reitmeier et al., 2021; Haider et al., 2024). Another major limitation is that high-throughput 16S rRNA gene sequencing of microbiota samples provides compositional data that appear as relative instead of absolute abundancies. Relative abundancies quantify the different microbial taxa as fractions within a sample irrespective of its total cell numbers. Such relative microbiome profiling (RMP) often results in artefacts with respect to comparative taxon counts. In particular, a comparative analysis does not yield data about extent or directionality of compositional changes of a microbiota upon perturbation. For example, antibiotic treatment that decreases cells belonging to a specific microbial family necessarily results in an apparent increase of the relative abundance of a resistant family when RMP is applied. This hampers the identification of microbial taxa that are significantly affected upon intervention (Jian et al., 2020). Further drawbacks of describing relative abundances were stated in numerous publications (Vandeputte et al., 2021; Vandeputte et al., 2017; Galazzo et al., 2020; Lambrecht et al., 2017; Rao et al., 2021), but they have rarely been assessed in next generation sequencing (NGS) studies on microbiomes (Boshuizen and Te Beest, 2023).

To address this issue, microbial cell numbers of a sample need to be quantified by internal standards. For example, known amounts of DNA can be spiked into microbial samples before DNA extraction (Tkacz et al., 2018; Lin et al., 2019), an approach termed internal standard normalization (ISN) that has been established for quantitative and metagenome analysis (Satinsky et al., 2013). Using a set of environmental samples, Lin *et al*. demonstrated that community profiles and taxon co-occurrence patterns obtained by ISN substantially differed from RMP (Lin and Peddada, 2020). Another option is to spike a sample with a known number of exogeneous bacteria to adjust the microbiome composition (Stämmler et al., 2016). As an alternative, quantitative microbiome profiling (QMP) by qPCR, which targets 16S rRNA genes, is cost-effective, feasible and directly comparable to NGS (Jian et al., 2020). Challenges encountered here are the choice of a reference organism required to construct a standard curve, DNA extraction efficiencies, and the variance of strain-specific16S rRNA operon copy numbers per genome (Bonk et al., 2018). Flow cytometry of cells stained with a fluorescent dye is another feasible method to enumerate bacterial cells. Vandeputte and colleagues (Vandeputte et al., 2017) established a workflow for QMP of 40 faecal samples of a study cohort by flow cytometry and thus demonstrated that the association between Crohn's disease and a low-cell-count Bacteroides enterotype is an artefact due to RMP. However, when DNA-binding stains are used, the fluorescence intensity is directly related to the nucleic acid content of the sample, possibly resulting in a bias due to distinct genome lengths, physiological states of a cell, or a lack of reproducibility in staining and storage conditions that cause DNA to deteriorate (Prest et al., 2013; Kamiya et al., 2007). Following a comparison of qPCR and flow cytometry, Galazzo et al. (2020) concluded that qPCR-based QMP is too imprecise to be an alternative to flow cytometry. In contrast, Jian and colleagues pointed out that microbiota sequenced by 16S rRNA amplicon sequencing differs from microbiota quantified by flow cytometry, because the DNA extracted from a faecal sample does not necessarily correlate with intact bacterial cells (Jian et al., 2020).

A further bias in microbiome analysis is introduced by up to 15 copies of 16S rRNA genes in a single genome (Angly et al., 2014; Vetrovsky and Baldrian, 2013). Bacteria with more than one copy of the 16S rRNA gene appear overrepresented as multiple sequences are attributed to single cells. Variations in 16S rRNA gene copy numbers (GCN) are particularly common in the phylum Bacillota and the class Gammaproteobacteria, which belongs to the phylum Pseudomonadota (Vetrovsky and Baldrian, 2013; Göker and Oren, 2024; Williams and Kelly, 2013). Although the exact number of the 16S rRNA gene is usually taxon-specific, variations among strains of the same species were also observed (Acinas et al., 2004).

In this study, we examined whether an optimized microbiota analysis of faeces samples from animals treated with antibiotics reveals significant effects that were not detected by RMP. The veterinary antibiotics tylosin and tulathromycin were administered to piglets in two independent animal trials. A correction of relative frequencies of bacterial taxa determined via NGS was performed by considering the 16S rRNA GCN. Absolute taxon abundancies were calculated for each taxon by measuring total bacterial cell numbers via by flow cytometry. For method comparison, cell numbers of samples from animals treated with tulathromycin were additionally determined using a spike-in method according to Tourlousse et al. (2017, 2018).

Methods

Piglet feeding trial A with tylosin application

Four weeks old female pigs obtained from the Mörsdorfer Agrar GmbH (Mörsdorf, Thuringia, Germany) were maintained in the animal facility of the Friedrich-Loeffler-Institute (Jena, Germany) in separate pens. After 2 weeks of acclimatization, piglets ($n = 2$ per group in pre-trial, $n = 4$ per group in main trial, 12 animals in total,

Abbreviations: ASV, amplicon sequence variant; OTU, operational taxonomic unit; FC, fold change; GCN, gene copy number; IMNGS2, Integrated Microbial Next Generation Sequencing version 2; SINA, SILVA Incremental Aligner; RDP, ribosomal database project; RMP, relative microbiome profiling; QMP, quantitative microbiome profiling.

10.77 ± 1.39 kg live weight) were fed about 5 g of either pure peanut butter (Netto American Style, Netto Marken-Discount Stiftung & Co. KG, Maxhütte-Haidhof, Germany) or peanut butter supplemented with tylosin tartrate (Sigma-Aldrich Chemie GmbH, Taufkirchen, Germany) at a concentration of 10 mg/kg bodyweight per piglet. Each feeding was done twice in an interval of 24 h. Individual faecal samples were collected before (d0) and 30 h (d1), 48 h (d2), 72 h (d3), and 96 h (d4) after antibiotic treatment. Samples were homogenized, and aliquots were stored either at room temperature (RT) in 600 µL DNA stabilization solution (INVITEK Molecular, Berlin, Germany) for sequencing, or at −20°C without additives.

Piglet feeding trial B with tulathromycin application

Eighty weaned barrows (6.39 ± 1.1 kg live weight) were group-housed (four piglets/pen) and equally assigned to one of four diets with graded copper levels (five pens/diet) during 5 weeks of rearing. At the end of the fourth experimental week, piglets of each dietary group were subdivided into half and were subjected to intramuscular injection of the antibiotic (DRAXXIN® Zoetis, 2.5 mg tulathromycin/kg BW) or a placebo (0.9% NaCl). Individual faecal samples obtained via manual rectal stimulation were collected directly before and 24 h after the respective injection. Faecal material was snap-frozen in liquid nitrogen immediately after collection and stored at −80°C until further processing. Six piglets (antibiotic-treated individuals) of the dietary groups with 150 mg Cu/kg feed were chosen for further analysis in this study for total bacterial counts and sequencing.

Sequencing and raw read processing

Isolation of total DNA and sequencing of 16S rRNA gene amplicons was carried out at the Core Facility Microbiome of the Technical University of Munich (Freising, Germany) as described previously (Reitmeier et al., 2020) with slight modifications. Briefly, DNA was isolated using a MaxWell (Promega, Walldorf, Germany) after bead-beating and used in a 2-step PCR to generate sequencing libraries. The first PCR used primers specific for the V3 and V4 regions (i.e., 341F, CCT ACG GGN GGC WGC AG; 785R, GAC TAC HVG GGT ATC TAA TCC) that contain an overhang for the subsequent PCR for sample barcoding. Cleaned libraries were sequenced PE300 on a MiSeq (Illumina). Spike-in of synthetic full-length 16S rRNA genes was done as described by Tourlousse et al. (2018, 2017). Here, 6 ng of spike DNA, consisting of an equimolar mixture of 13 linearized plasmids, each of which contains an artificial 16S rRNA gene, was added to 600 µL of the faeces-stabilizer mix. In each artificial "gene", the invariant regions of the 16S rRNA were left untouched, while the variable regions were swapped with artificial sequences. Thus, spike reads are clearly distinguishable from true bacterial reads in analysis. Sample weight (i.e., gram of faecal material) was recorded in order to obtain 16S rRNA GCN per gram sample.

Raw reads were processed with pipeline DADA2 (Callahan et al., 2016). Sequences were demultiplexed and filtered, and amplicons with an expected error > 2 were excluded. To limit the analysis of regions with higher error values, reads were trimmed to sequence lengths of 250 bp and 200 bp, respectively, for forward and reverse reads. Remaining reads were merged to paired end reads. Amplicon sequence variants (ASVs) were clustered at 97% sequence identity, and their sample-wise abundances were calculated after removing substitution and chimera errors. Taxonomies were assigned at 80% confidence level by considering results from both the Ribosomal Database Project (RDP) classifier (Wang et al., 2007) and the SILVA Incremental Aligner (SINA; v1.2.11) (Pruesse et al., 2012). Taxon names were verified manually in accordance to the nomenclature defined by the List of Prokaryotic names with Standing in Nomenclature (LPSN) (Parte, 2013; Parte, 2018; Parte et al., 2020; Euzéby, 1997).

16S rRNA GCN correction and synthetic spike-in

ASVs were analysed using parts of the PICRUSt2 pipeline (Douglas et al., 2020) as follows. HMMER version v3.3.2[1] places ASVs, EPA-ng (Barbera et al., 2018) determined the optimal position of these ASVs in a reference phylogeny, and GAPPA (Czech and Stamatakis, 2019) outputs a new tree incorporating ASV placements. This adjusted reference phylogeny allowed for the prediction of 16S rRNA GCN. The IMNGS output ASVs tables were corrected within the PICRUSt2 pipeline by dividing the original read counts by the predicted GCN.

To obtain a more intuitive comparability of both methods, we harmonized absolute abundances obtained by a flow cytometry method, FACS, and the spike-in approach as follows. Since the spike-in method gives only relative numbers of 16S rRNA gene copies between samples, cell counts of piglet 7 determined by FACS on day 0 were used as a reference. Subsequently, read counts for the spikes of this sample were scaled to the cell numbers within this sample using an arbitrary factor. The factor was chosen such that the relative amount of spike in this sample could be converted into the cell number found by FACS. The other samples gave relative numbers of gene copies that were multiplied by this factor in order to calculate cell number equivalents.

Flow cytometry measurements

Frozen faecal samples were split into 0.1-g aliquots in triplicate and slowly thawed on ice. Aliquots were diluted in 10 mL 0.85% (w/v) NaCl and homogenized for 3 min with a Vortex-Genie 2 mixer (Scientific Industries, New York, United States). To remove faecal debris, the solutions were filtered using a sterile syringe filter with 5 µm pore size (Macherey-Nagel, Düren, Germany). Next, 500 µL of the filtered cell suspension were mixed with three volumes of fixation buffer (4% paraformaldehyde, 200 nM Na_2HPO, pH 7.2) for at least 3 hours at RT. Subsequently, the samples were centrifuged at 12,000 × g for 10 min, and the supernatant was discarded. The remaining pellets were dissolved in 500 µL sterile filtered PBS (Sigma-Aldrich, Steinheim, Germany) and stained using the LIVE/DEAD™ *Bac*Light™ kit (Invitrogen, Karlsruhe, Germany).

Quantification of microbial cells in the faecal suspensions was performed using a FACS Canto II flow cytometer (BD Biosciences, NJ, United States). Fluorescence events were monitored using 530 nm and

1 http://www.hmmer.org

660 nm optical detectors. Forward-and sideward-scattered light was also collected. The BD FACSDiva™ Software and FlowJo (both BD Biosciences) were used to gate and separate the microbial fluorescence events on the FITC-PE density plot from the faecal sample background. The gated fluorescence events were evaluated on the forward-sideways density plot to exclude remaining background events and to obtain an accurate microbial cell count. Instrument and gating settings were identical for all samples. Measurements were conducted in triplicates.

Integration of cell counts into relative abundances

To calculate absolute frequencies of individual taxa, flow cytometry-measured bacterial cell counts were integrated into the ASV table created with DADA2 (Callahan et al., 2016). For this purpose, the read counts of each taxon in a sample were divided by the total read count of that sample. Subsequently, these numbers were multiplied by the bacterial cell count of the sample. The sum of all taxa in a sample yielded the total bacterial cell counts.

Statistical analysis

All further analyses were performed in the R programming environment using Rhea (Lagkouvardos et al., 2017), following scripts and instructions available online.[2] A PERMANOVA test (vegan::adonis) was performed in each case to determine if the separation of sample groups was significant, as a whole and in pairs. For the analysis of relative abundances, counts were standard normalized using total sum scaling. To analyse absolute abundances, no normalization was applied after integration of bacterial cell counts. The filtered and, in case of relative abundances, normalized ASVs table used as basis for all analyses is provided in Supplementary Tables 1, 2. α-diversity was computed based on generalized UniFrac distances (Chen et al., 2012). β-diversity was assessed on the basis of species richness and Shannon effective diversity (Jost, 2007) as explained in detail in Rhea. p values were corrected for multiple comparisons according to the Benjamini-Hochberg method. Only taxa with a prevalence ≥30% (proportion of samples positive for the given taxa) in one given group and relative abundance ≥0.25% (Reitmeier et al., 2021) in at least one sample were considered for statistical testing. Statistical analyses were performed as described for each experiment and p values ≤0.05 were considered as significant.

Results and discussion

Relative and absolute bacterial abundances upon tylosin treatment of piglets

In the first experimental setting, 10 mg of tylosin per kg bodyweight was applied twice in a 24 h-interval orally to six animals. Faecal samples were collected immediately before (sample d0) and at day 1 to 4 (samples d1–d4) after application. To investigate effects of tylosin on the composition of the piglet microbiota, we performed 16S rRNA gene amplicon sequencing of faecal samples. Statistical analysis revealed no significant changes in the faecal microbiota compositions of control group piglets, whereas tylosin treatment caused various effects. In more detail, the α-diversity of faecal microbiota compositions on day 1 to 4 of each tylosin treated animal in comparison with day 0 was calculated for each animal (Supplementary Figure 1). Throughout the whole group, the number of species and the Shannon effective number significantly decreased after tylosin application, as previously described for other macrolide antibiotics such as azithromycin (McDonnell et al., 2021). Despite an overall reduction in species richness following tylosin treatment, a significant increase in the relative abundance of Pseudomonadota was observed post-application (Figure 1A; Supplementary Table 3; Supplementary Figure 2). The abundance of this phylum increased in the microbiota of all animals tested here, but only in one piglet to a considerable extent. In sample d3, we observed a marked increase in the abundance of Bacillota, indicating a microbiota rebalancing post-tylosin disturbance, while the abundance of Pseudomonadota decreased. Four days after application, the microbiota composition closely resembled that of sample d0, with a minor increase in the abundance of Bacillota.

The values gained by RMP, however, do not necessarily mirror absolute cell numbers of a taxon present in a sample. For example, the true reduction of a taxon can result in an apparent decrease of the total cell count without affecting absolute frequencies of the other taxa. To overcome this limitation of RMP, we applied flow cytometry to all samples analysed above. Total cell numbers determined at day 0 ranged from 7.20×10^7 cells per gram faeces (c/gf) to 2.49×10^8 c/gf, with the group median of 9.15×10^7 c/gf (Figure 1B; Supplementary Table 4). Along the experimental course, the median number remained nearly constant. Total cell counts not only varied among the animals but also within an individual over time due to cell densities in faeces depending on water content and other physiological factors (Vandeputte et al., 2021; Wang et al., 2007). Nevertheless, results from individual samples of the present study are comparable to each other upon careful sample processing, even if they deviate from the results of other studies (Vandeputte et al., 2021; Vandeputte et al., 2017; Wang et al., 2007). The method used in this study differs from other protocols by an additional fixation and washing step, possibly resulting in a reduced number of bacteria.

Integration of bacterial cell counts into faecal microbiome composition analysis improves the explanatory power of a porcine faecal microbiome analysis

Total cell counts obtained by flow cytometry were integrated into the relative abundances of bacterial taxa as determined by 16S rRNA gene amplicon sequencing. The resulting absolute abundances revealed that the increase of Pseudomonadota, detected by RMP, was not an artefact due to limitations of this method (Figure 1C; Supplementary Table 3; Supplementary Figure 2), but indicated an actual bloom of this phylum. This observation can be explained by the inhibition of other phyla by tylosin, thus creating ecological niches that favour the spread of Pseudomonadota (Morton et al., 2019), in turn contributing to dysbiosis, intestinal diseases, and increased susceptibility towards infections (Shin et al., 2015; Sun et al., 2019; Bonardi, 2017; Bin et al., 2018).

2 https://lagkouvardos.github.io/Rhea/

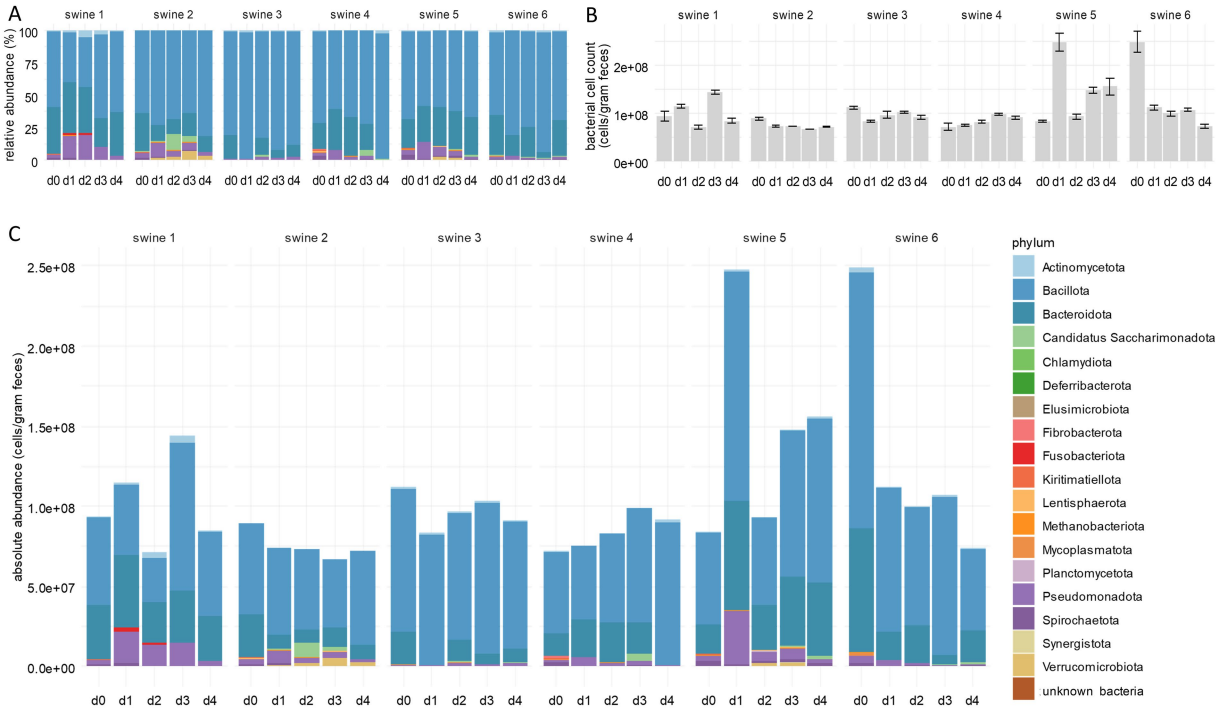

FIGURE 1
Integration of bacterial cells counts into faecal microbiome composition. **(A)** Relative abundances of bacterial phyla deduced from standard microbiome 16S rRNA gene amplicon sequencing. **(B)** Bacterial cell counts per gram faeces measured by flow cytometry. **(C)** Absolute abundances of bacterial phyla following integration of bacterial cell counts into 16S rRNA gene sequencing data. Per phylum, cumulative abundances were calculated from all single ASV classified within one phylum using both RDP and SILVA. The numbers above the bars indicate individual piglets. Samples d0–d4 were taken immediately before and at the 4 days following tylosin treatment. Bar plots for individual piglets are shown (n = 6).

Correction of 16S rRNA GCN increases the accurateness of family-and genus-level analysis

To reduce bias due to 16S rRNA gene copies present in a bacterial genome, we determined the GCN for each molecular species using PICRUSt2 (Douglas et al., 2020) and corrected relative frequencies accordingly. This pipeline has the advantage that it predicts GCN of unknown genera based on similarities to already known sequences.

Of a total of 234 genera, 63 genera (26.9%) were identified in our samples to harbour more than one copy of the 16S rRNA gene in the genome, and most of them carried up to five copies (Supplementary Table 5). Genus *Pseudescherichia* exhibited six copies, genus *Clostridium* sensu stricto 6 eight copies, and genus *Paenibacillus* even nine copies, indicating that the significance of these individual taxa for the overall microbiota composition is overestimated. Following GCN correction of relative abundances, the decrease observed for the families *Rikenellaceae* and Oscillospirales UCG-10 was confirmed (Figures 2A,B top; Supplementary Table 6). On genera level, GCN correction decreased the proportion of taxa with more than one copy of the 16S rRNA gene and thus influenced results of the statistical analysis (Figures 2A,B, bottom). The decrease in unknown *Bacteroidales* RF16 group was not confirmed by GCN correction, which is consistent with the observations already made at the family level. The relative abundance of some genera (i.e., *Lachnospiraceae* ND3007 group, *Lactobacillus*, the *Rikenellaceae* RC9 gut group, and an unknown Bacteroidales RF16 group) showed a decrease on day 1 compared to day 0 only after GCN correction. The *Lachnospiraceae ND3007* group is known to be positively correlated with a health supporting diet, which is rich in fibre and plant-based foods (Ericson et al., 2020; Ma et al., 2021). A restriction of fibre-degrading bacteria by antibiotics may have a negative effect on the energy production and thus on the growth performance of animals. *Lactobacillus* has been identified as one of the core genera in the gastrointestinal tract of pigs (Valeriano et al., 2017), contributing to overall health and growth performance and increasing the productivity of swine husbandry (Kenny et al., 2011; Yang et al., 2015). The *Rikenellaceae* RC9 gut group typically experiences an increase after weaning, coinciding with the transition of swine to solid food digestion (Saladrigas-García et al., 2022). In addition, significant decreases in the abundances of *Faecalibacterium*, *Neglectibacter*, and *Solobacterium* were overlooked due to missing GCN correction (Figures 2A,B, bottom). *Faecalibacterium* is a short chain fatty acids (SCFAs) producing genus with potential benefits for human health (Martin et al., 2023), thus underlining the relevance of GCN correction in microbiome analysis.

Combination of absolute cell numbers and GCN reveals further hidden significant changes of bacterial abundances in tylosin-treated piglets

Integration of total cell counts into GCN-corrected relative abundances revealed several significant changes in different taxa, which were insignificant before. The decrease noted for *Rikenellaceae*

10.3389/fmicb.2025.1481197

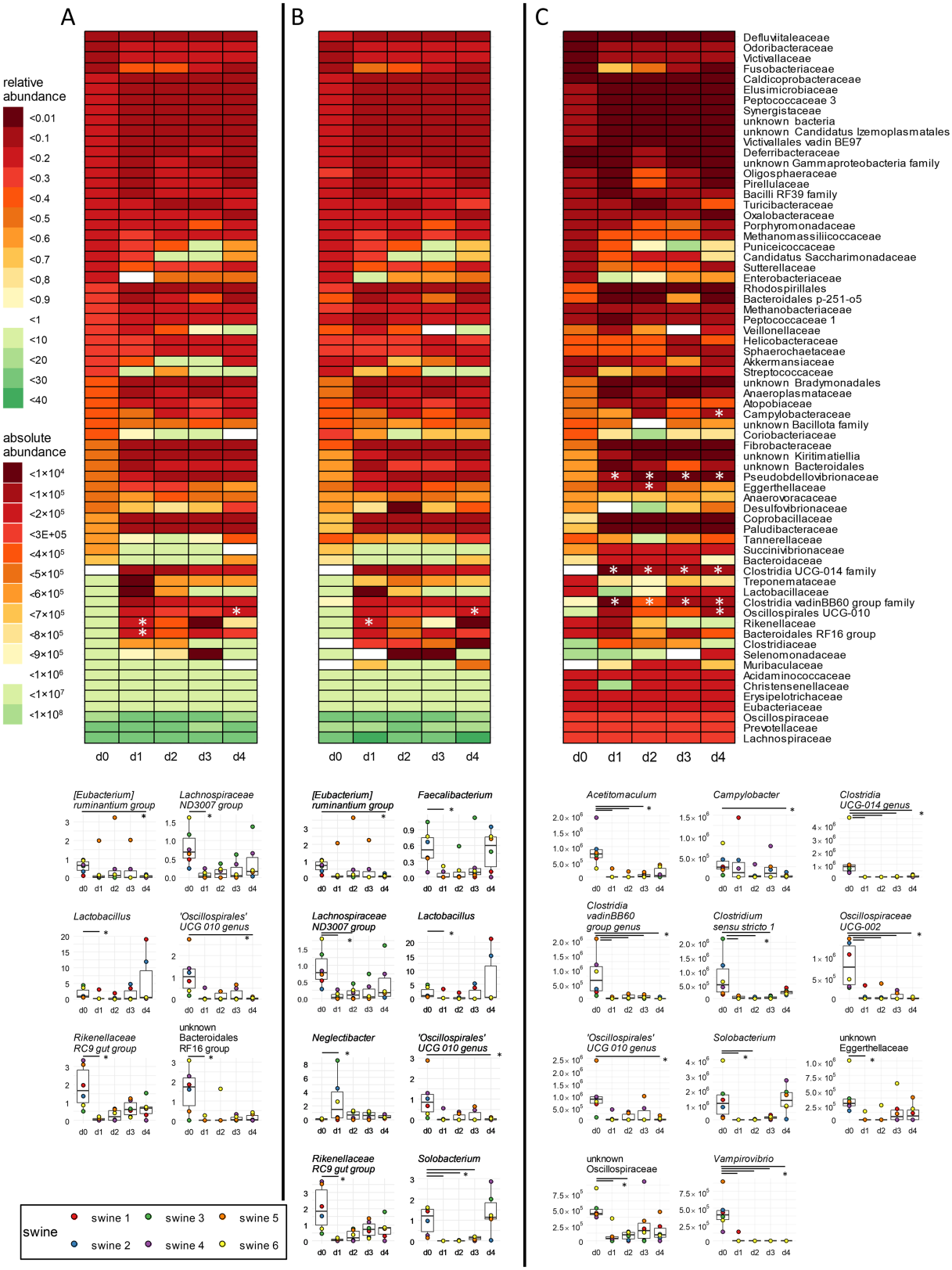

FIGURE 2
Correction of 16S rRNA GCN and integration of bacterial cell counts in family-and genus-level analyses. **(A)** Relative abundances were obtained by standard analysis of 16S rRNA gene sequencing data. **(B)** Same data set as **(A)**, but corrected for GCN of the 16S rRNA genes. **(C)** Same data as in **(B)**, but absolute abundances were obtained by integration of bacterial cells counts via flow cytometry. Heat maps for the occurrence of families over time points are shown as mean values over all six animals. Below each heat map, significantly changed relative and absolute abundances of single genera are shown in boxplots. Cumulative abundances were calculated from all single ASVs classified within one family or genus as per the best possible taxonomy using both RDP and SILVA. * $p < 0.05$ pairwise Fisher's Exact Test, $n = 6$.

by RMP was not confirmed by QMP upon data integration (Figure 2C top; Supplementary Table 6), in contrast to the decrease of the Oscillosporales UCG-10 family on day 4. Significant reductions were noted in the Clostridia UCG-014 family, in the Clostridia vadin BB60 group, and in *Pseudobdellovibrionaceae* from day 1 to day 4 post-treatment. Additionally, a significant decrease was recorded for the abundance of *Eggerthellaceae* on day 2 and of *Campylobacteraceae* on day 4. To summarize, relative abundances corrected with GCN only revealed significant decrease of two different families, while absolute abundance analysis of such data showed a significant change of six different bacterial families over time.

On the genus level, eleven different genera were found to have a significant decrease when absolute abundances together with GCN were considered (Figure 2C, bottom). The decrease of *Solobacterium*, an opportunistic pathogen, and the genus Oscillospirales UCG-010, as already observed upon RMP, was confirmed. In contrast, six different genera showed statistically significant changes in relative abundances, but did not exhibit significant changes in absolute analysis (Figures 2B,C, bottom). Additionally, *Campylobacter* displayed a decreased abundance on day 4 and an unknown genus from *Oscillospiraceae* on day 1 and day 2. *Acetitomaculum* and *Clostridium* sensu stricto 1 showed decreased abundance on days 1 to 3, and Clostridia UCG-014, Clostridia vadin BB60 group, *Oscillospiraceae* UCG-002, and *Vampirovibrio* exhibited decreasing abundances consistently over 4 days. *Oscillospiraceae* UCG-002 support breakdown of aspartate and glycine, and the unknown Clostridia UCG-014 facilitates degradation of tryptophan in the intestine (Atzeni et al., 2022; Yang et al., 2021). Both genera are important for the normal intestinal function of animals. The inhibition of SCFA-producing genera such as Clostridiales vadin BB60, the genus Oscillospirales UCG-010, and *Acetitomaculum*, may reverse the positive effects described above (Sawicka-Smiarowska et al., 2021; Sebastià et al., 2024; Greening and Leedle, 1989). The opportunistic pathogen *Clostridium* sensu stricto 1 was shown to be associated with inflammatory bowel disease and a reduced concentration of SCFA in the intestine (Yang et al., 2019; Hu et al., 2021). Inhibition of these bacteria can have positive effects on the health of animals by preventing relapsing infection (Bublitz et al., 2023).

To summarize the tylosin treatment data, correcting for 16S rRNA gene copies and the integration of bacterial cell counts increased the explanatory power of the data regarding such a perturbation (Kim et al., 2016; Candon et al., 2015; De La Cochetiere et al., 2005; Dethlefsen and Relman, 2011). Until now, any such correction has hardly been applied in microbiome studies. GCN combined with QMP not only revealed tylosin activity against opportunistic pathogens, but also stronger effects of the antibiotic on beneficial commensal bacteria otherwise not detectable by RMP. This result may explain a stronger impairment of functions of the gut microbiota such as the maintenance of colonization resistance and, thus, an increased probability of subsequent infections as compared to previous data (Collington et al., 1972; Kim et al., 2012).

FACS and spike-in counting for QMP are equivalent methods on the phylum level

To compare two methods for calculating abundances, namely flow cytometry-based cell counting and spike-in of synthetic full-length 16S rRNA genes, we analysed the microbiota of samples from tulathromycin-treated piglets of a second experimental setting (see Supplementary Table 7 for an overview of the workflow). For comparability of both methods, we applied an arbitrary factor based on the sample from piglet 7 on day 0 as the reference (see method for details) that revealed cell number equivalents. Since FACS analyses yielded about 6.0×10^7 c/gf, cell number equivalents for swine 7 using spike-in DNA were set to the same level.

RMP of the samples from piglets treated with tulathromycin identified 15 different phyla (Figure 3A; Supplementary Table 8) and a decrease of Bacteroidota across most piglets that correlated with a relative increase of Bacillota. Piglets 9, 10, and 11 exhibited only minor changes at the phylum level, indicating a stable composition of their microbiomes. Incorporating total cell counts obtained by flow cytometry into RMP revealed a consistent decrease in total bacterial cell numbers across all piglets, ranging from 27% for piglet 9 to 68% for piglet 12 (Figure 3B; Supplementary Table 8). These differences, as well as the variation of initial total bacterial cell numbers, which range from 2.3×10^7 to 9.2×10^7 c/gf, underline the high variability of individual faecal microbiomes. In contrast to RMP, Bacillota exhibited a decrease from 4.8×10^7 c/gf on day 0 to 1.9×10^7 c/gf on day 1, which is a fold change [FC] of 0.40 after integration of bacterial cell counts. Similarly, a decrease in Bacteroidota was observed in all piglets, which contrasted with relative increases noted in the microbiome of piglet 11 due to RMP (FC = 1.15).

Next, we compared the results of FACS with those of the spike-in results. The changes of absolute abundancies on the phylum level as revealed by the spike-in method were mostly similar compared to results calculated with total cell counts (Figure 3C; Supplementary Table 8). An exception was observed in piglet 10, where an increase in total absolute abundances of Actinomycetota (1.5-fold), Bacillota (1.8-fold), and Spirochaetota (1.7-fold) was noted. Integration of spike-in sequencing data into GCN-corrected RMP revealed a decreased total cell count for most of the samples in line with flow cytometry-based analysis.

Taken together, the phyla reductions upon tulathromycin treatment observed in absolute abundances were more prominent than those observed for relative abundances.

QMP by FACS is superior to spike-in on the family and genus level

The application of tulathromycin caused dynamic shifts of the abundance of families and genera. Among the 59 families detected by RMP, a relative decrease was observed in 33 families (Figure 4A; Supplementary Table 9; Supplementary Figure 3). For instance, *Rikenellaceae* experienced a significant relative decrease from 2.0 to 1.3%. This decline was associated with a relative increase in 26 other families, including *Tannerellaceae* and *Acidaminococcaceae*.

Integration of flow cytometry data revealed a decrease in mean cell counts from 6.32×10^7 c/gf to 3.3×10^7 c/gf after treatment (Figure 4B; Supplementary Table 9). In contrast to RMP, significant reductions in *Lachnospiraceae*, *Lactobacillaceae*, *Oscillospiraceae*, and *Prevotellaceae* across all piglets during the same time were observed. In contrast, when applying a data analysis using the spike-in method, we also found a decrease for 42 families, but none became significant (Figure 4C; Supplementary Table 9; Supplementary Figure 4). Sample analysis at the genus level revealed distinct trends in relative and absolute abundances. Upon RMP, *Faecalibacterium* decreased relatively from 2.10 to 0.84%, and

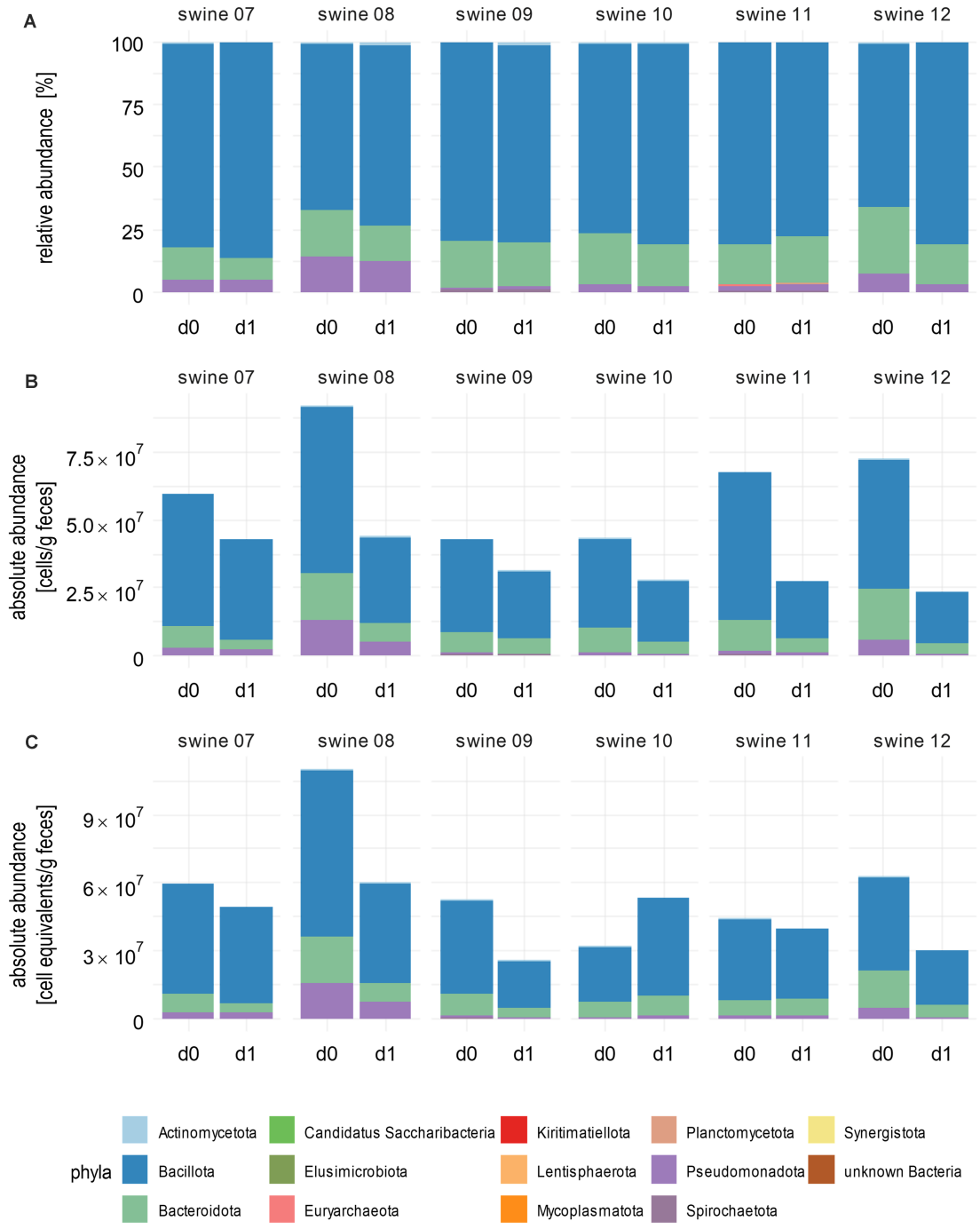

FIGURE 3
Absolute abundances of bacterial phyla after integrating total cells or spike-in counts. **(A)** Stacked bar plots show phyla abundances after correction for GCN of 16S rRNA genes. **(B)** Absolute abundancies as measured by flow cytometry and **(C)** as calculated after using spike-in DNA. Bacterial cell counts per gram faeces are shown. Cumulative abundances were calculated from all single ASVs classified within one phylum as per the best possible taxonomy using both RDP and SILVA. Numbers above the bars indicate individual piglets. Samples were taken before (d0) and 1 day after (d1) tulathromycin treatment (n = 6).

the *Rikenellaceae* RC9 gut group from 1.81 to 1.25% (Figure 4A; Supplementary Figure 3). Integration of FACS data revealed eight genera significantly decreased with respect to absolute abundances, namely *Catenibacterium*, *Duncaniella*, *Lactobacillus*, *Paraprevotella*, *Prevotella*, *Prevotella 9*, *Roseburia*, and an unknown genus of *Oscillospiraceae* (Figure 4B; Supplementary Figure 3). For instance, there was a decrease in the key gut genera and SCFA-producer *Lactobacillus* and *Prevotella*, which contribute to the maintenance of the intestinal barrier, from 3.6×10^6 to 1.1×10^6 and from 2.2×10^6 c/gf to 9.6×10^5 c/gf, respectively (Supplementary Figure 4). While *Faecalibacterium* and *Rikenellaceae* RC9 gut group still decreased from day 0 to day 1, this decrease was no longer significant in pairwise tests.

10.3389/fmicb.2025.1481197

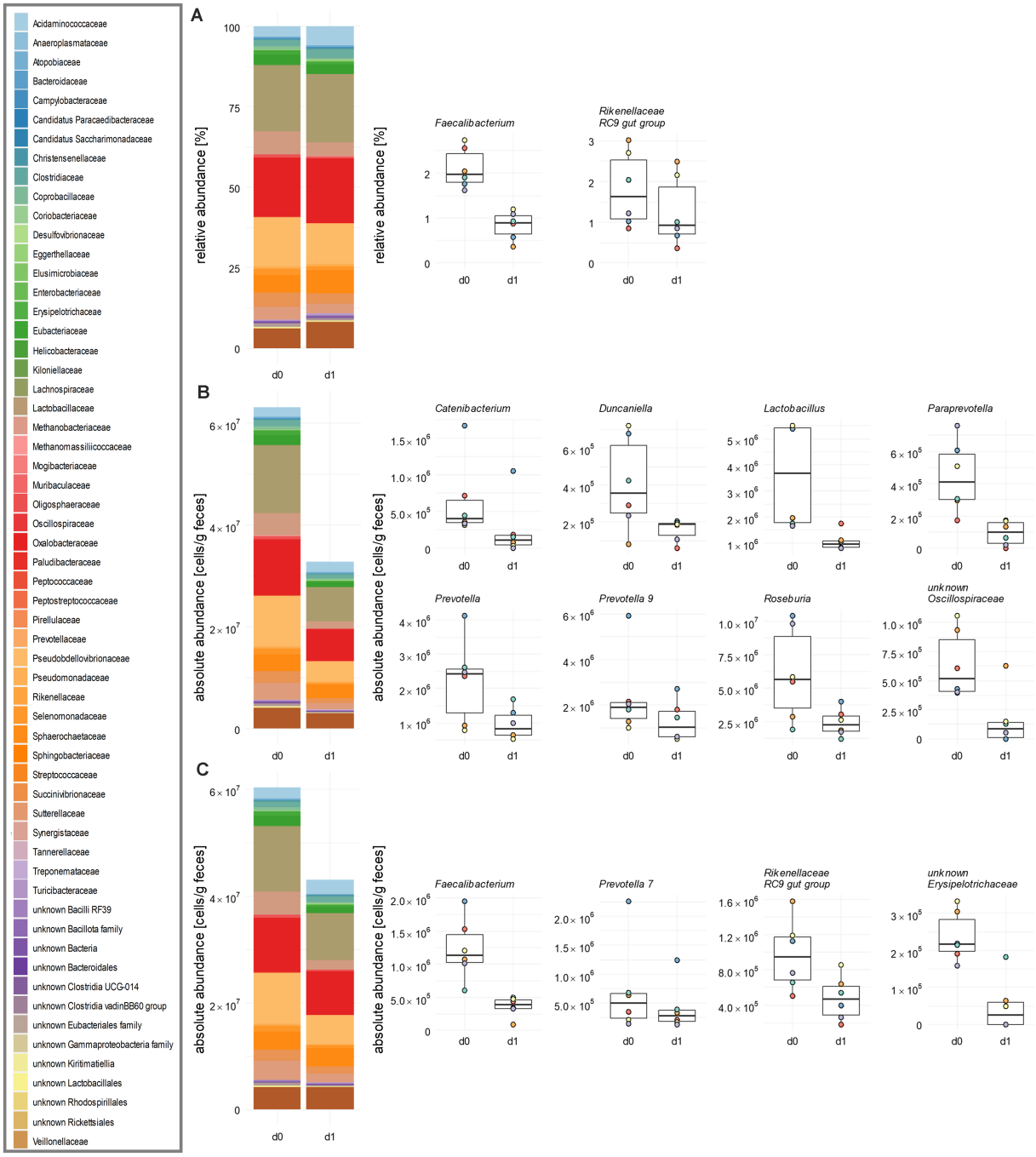

FIGURE 4
Influence of tulathromycin on the family and genus level of porcine faecal microbiota. **(A)** Relative abundances of bacterial families obtained by standard analysis of 16S rRNA gene sequencing data including GCN correction. **(B)** Same data as in **(A)** after integrating total cell counts obtained from flow cytometry and **(C)** after calculating absolute abundances of bacterial families from spike-in DNA after sequencing. In each panel, an overview is given by stacked bar plots for family abundances. Significantly changed relative and absolute abundances of single genera are shown in boxplots. Mean values over all six animals are indicated. Cumulative abundances were calculated from all single ASVs classified within one family as per the best possible taxonomy using both RDP and SILVA. All significant changes were indicated with the Paired Wilcoxon Signed Rank Sum Test with $p \leq 0.05$ ($n = 6$).

Following analysis of spiked-in samples, *Faecalibacterium* and *Rikenellaceae* RC9 gut group were again found to be statistically significantly reduced, with *Faecalibacterium* decreasing by a FC of 0.29 and *Rikenellaceae* RC9 gut group by a FC of 0.05 (Figure 4C; Supplementary Figure 4). Additionally, the number of *Prevotella 7* was reduced by a FC of 0.6, and an unknown genus from *Erysipelotrichaceae* by a FC of 0.2. To summarize, the spike-in method yielded a higher number of significant changes of the microbiota on the family and genus level compared to RMP, but fewer effects than total cell counting by FACS.

Conclusion

Integrating absolute cell counts into relative sequence data is one step further for accurately assessing gut microbiota states (Lin and Peddada, 2020), especially since changes in bacterial density may indicate various health conditions (Morjaria et al., 2019; Contijoch et al., 2019). Our study supports the significance of a precise determination of absolute cell numbers, either by flow cytometry analysis or spike-in of DNA, to avoid misinterpretation of microbiome data. The FACS approach, however, requires a greater effort in preparation than the spike-in method based only on adding appropriate amounts of synthetic DNA to the sample ahead of DNA isolation. We observed a high degree of comparability between the two methods to calculate absolute abundancies. Integration of total cell counts by FACS detected a larger number of significant changes in the compositional data of the microbiomes on the level of families and genera. Although there is potential for errors, for example due to high interindividual variance, the need of standards in cell quantitation, and the lack of comparability between samples to be sequenced on the one hand and the quantified microbiota on the other hand (Jian et al., 2020), the presented benefits of improved data analysis outweigh their drawbacks.

Data availability statement

The data presented in the study are provided by the Supplementary material and deposited in the SRA repository, accession numbers PRJNA1229264 and PRJNA800240, respectively.

Ethics statement

The tylosin study protocol (feeding trial A) was approved by the Thüringer Landesamt für Verbraucherschutz, Bad Langensalza, Germany (approval number 22-2684-04-BFI-17-001). The animal experiment of feeding trial B was conducted according to the European Community regulations concerning the protection of experimental animals and the guidelines of the German Animal Welfare Act and was approved by the Lower Saxony State Office for Consumer Protection and Food Safety, Oldenburg, Germany (file number 33.19-42502-04-19/3237).

Author contributions

SW: Conceptualization, Data curation, Formal analysis, Investigation, Methodology, Software, Validation, Visualization, Writing – original draft, Writing – review & editing. MW: Data curation, Formal analysis, Methodology, Software, Validation, Visualization, Writing – review & editing. L-SP: Data curation, Formal analysis, Software, Validation, Visualization, Writing – review & editing, Investigation. AG-S: Investigation, Validation, Writing – review & editing, Methodology. JK: Investigation, Methodology, Validation, Writing – review & editing. KN: Investigation, Methodology, Validation, Writing – review & editing, Conceptualization. TF: Conceptualization, Investigation, Methodology, Validation, Writing – review & editing, Data curation, Formal analysis, Funding acquisition, Project administration, Resources, Software, Supervision, Visualization, Writing – original draft.

Funding

The author(s) declare that financial support was received for the research and/or publication of this article. This study was supported by a grant from the BMBF (Federal Ministry of Education and Research of Germany) within the frame of InfectControl 2020 (FKZ 03ZZ0823A) to TF.

Acknowledgments

We appreciate the valuable support by Petra Reinhold and the staff of the experimental animal facility of the Friedrich-Loeffler-Institut in Jena.

Conflict of interest

The authors declare that the research was conducted in the absence of any commercial or financial relationships that could be construed as a potential conflict of interest.

Publisher's note

Supplementary material

The Supplementary material for this article can be found online at: https://www.frontiersin.org/articles/10.3389/fmicb.2025.1481197/full#supplementary-material

SUPPLEMENTARY FIGURE 1
α-diversity of faecal microbiota upon tylosin treatment. **(A)** Normalized number of species and **(B)** Shannon effective numbers of faecal microbiota obtained by standard analysis of 16S rRNA gene sequencing data is shown a line plot. Individual piglets are indicated by the corresponding colours. Cumulative abundances were calculated from all single ASVs classified within one family as per the best possible taxonomy using both RDP and SILVA (# $p < 0.05$ after Paired Wilcoxon Signed Rank Sum Test, $n = 6$).

SUPPLEMENTARY FIGURE 2
Correction of 16S rRNA GCN and integration of bacterial cell counts into relative abundance analyses of the phylum Pseudomonadota. **(A)** Relative abundances of Pseudomonadota were obtained by standard analysis of 16S rRNA gene sequencing data. **(B)** Same data set as panel A, but corrected for GCN of the 16S rRNA genes. **(C)** Same data as in panel B, but absolute abundances of Pseudomonadota were obtained by integration of bacterial cells counts via flow cytometry. Relative and absolute abundances in the faecal microbiota of each animal are shown in boxplots. Cumulative abundances were calculated from all single ASVs classified within one phylum as per the best possible taxonomy using both RDP and SILVA (# $p < 0.05$ after Paired Wilcoxon Signed Rank Sum Test, $n = 6$).

SUPPLEMENTARY FIGURE 3
Influence of tulathromycin on the family level of porcine faecal microbiota after integrating total cells or spike-in counts. Relative abundances of bacterial families were obtained by standard analysis of 16S rRNA gene sequencing data including GCN correction (A columns). The same data set as in A columns is shown after integrating total cell

counts obtained from flow cytometry (B columns) and after calculating absolute abundances of bacterial genera from spike-in DNA after sequencing (C columns). Heat maps for the abundance fold change of families following tulathromycin treatment are shown as mean values over all six animals. Cumulative abundances were calculated from all single ASVs classified within one family as per the best possible taxonomy using both RDP and SILVA.

SUPPLEMENTARY FIGURE 4
Relative and absolute abundances of commensal genera in porcine faecal microbiota. **(A)** Relative abundances of bacterial families obtained by standard analysis of 16S rRNA gene sequencing. **(B)** Same data as in panel A after GCN correction. **(C)** Same data as in panel B after integrating total cell counts obtained from flow cytometry and **(D)** after calculating absolute abundances of bacterial genera from spike-in DNA after sequencing. Significantly changed relative and absolute abundances of single genera are shown in boxplots. Mean values over all six animals are indicated. Cumulative abundances were calculated from all single ASVs classified within one genus as per the best possible taxonomy using both RDP and SILVA (# $p < 0.05$ after Paired Wilcoxon Signed Rank Sum Test, $n = 6$).

References

Abellan-Schneyder, I., Matchado, M. S., Reitmeier, S., Sommer, A., Sewald, Z., Baumbach, J., et al. (2021). Primer, pipelines, parameters: issues in 16S rRNA gene sequencing. *mSphere* 6:e01202-20. doi: 10.1128/mSphere.01202-20

Acinas, S. G., Marcelino, L. A., Klepac-Ceraj, V., and Polz, M. F. (2004). Divergence and redundancy of 16S rRNA sequences in genomes with multiple rrn operons. *J. Bacteriol.* 186, 2629–2635. doi: 10.1128/JB.186.9.2629-2635.2004

Angly, F. E., Dennis, P. G., Skarshewski, A., Vanwonterghem, I., Hugenholtz, P., and Tyson, G. W. (2014). Copy righter: a rapid tool for improving the accuracy of microbial community profiles through lineage-specific gene copy number correction. *Microbiome* 2:11. doi: 10.1186/2049-2618-2-11

Atzeni, A., Bastiaanssen, T. F. S., Cryan, J. F., Tinahones, F. J., Vioque, J., Corella, D., et al. (2022). Taxonomic and functional fecal microbiota signatures associated with insulin resistance in non-diabetic subjects with overweight/obesity within the frame of the PREDIMED-plus study. *Front. Endocrinol. (Lausanne).* 13:804455. doi: 10.3389/fendo.2022.804455

Barbera, P., Kozlov, A. M., Czech, L., Morel, B., Darriba, D., Flouri, T., et al. (2018). EPA-ng: massively parallel evolutionary placement of genetic sequences. *Syst. Biol.* 68, 365–369. doi: 10.1093/sysbio/syy054

Bin, P., Tang, Z., Liu, S., Chen, S., Xia, Y., Liu, J., et al. (2018). Intestinal microbiota mediates enterotoxigenic *Escherichia coli*-induced diarrhea in piglets. *BMC Vet. Res.* 14:385. doi: 10.1186/s12917-018-1704-9

Bonardi, S. (2017). Salmonella in the pork production chain and its impact on human health in the European Union. *Epidemiol. Infect.* 145, 1513–1526. doi: 10.1017/S095026881700036X

Bonk, F., Popp, D., Harms, H., and Centler, F. (2018). PCR-based quantification of taxa-specific abundances in microbial communities: quantifying and avoiding common pitfalls. *J. Microbiol. Methods* 153, 139–147. doi: 10.1016/j.mimet.2018.09.015

Boshuizen, H. C., and Te Beest, D. E. (2023). Pitfalls in the statistical analysis of microbiome amplicon sequencing data. *Mol. Ecol. Resour.* 23, 539–548. doi: 10.1111/1755-0998.13730

Bublitz, A., Brauer, M., Wagner, S., Hofer, W., Musken, M., Deschner, F., et al. (2023). The natural product chlorotonil a preserves colonization resistance and prevents relapsing Clostridioides difficile infection. *Cell Host Microbe* 31, 734–750.e8. doi: 10.1016/j.chom.2023.04.003

Callahan, B. J., McMurdie, P. J., Rosen, M. J., Han, A. W., Johnson, A. J., and Holmes, S. P. (2016). DADA2: high-resolution sample inference from Illumina amplicon data. *Nat. Methods* 13, 581–583. doi: 10.1038/nmeth.3869

Candon, S., Perez-Arroyo, A., Marquet, C., Valette, F., Foray, A. P., Pelletier, B., et al. (2015). Antibiotics in early life alter the gut microbiome and increase disease incidence in a spontaneous mouse model of autoimmune insulin-dependent diabetes. *PLoS One* 10:e0125448. doi: 10.1371/journal.pone.0125448

Chen, J., Bittinger, K., Charlson, E. S., Hoffmann, C., Lewis, J., Wu, G. D., et al. (2012). Associating microbiome composition with environmental covariates using generalized Uni Frac distances. *Bioinformatics* 28, 2106–2113. doi: 10.1093/bioinformatics/bts342

Collington, G. K., Parker, D. S., Ellis, M., and Armstrong, D. G. The influence of probios or tylosin on growth of pigs and development of the gastrointestinal tract. Proceedings of the British Society of Animal Production. (1972); 1988: 128. doi: 10.1017/S0308229600017657

Contijoch, E. J., Britton, G. J., Yang, C., Mogno, I., Li, Z., Ng, R., et al. (2019). Gut microbiota density influences host physiology and is shaped by host and microbial factors. *eLife* 8:e40553. doi: 10.7554/eLife.40553

Czech, L., and Stamatakis, A. (2019). Scalable methods for analyzing and visualizing phylogenetic placement of metagenomic samples. *PLoS One* 14:e0217050. doi: 10.1371/journal.pone.0217050

De La Cochetiere, M. F., Durand, T., Lepage, P., Bourreille, A., Galmiche, J. P., and Dore, J. (2005). Resilience of the dominant human fecal microbiota upon short-course antibiotic challenge. *J. Clin. Microbiol.* 43, 5588–5592. doi: 10.1128/JCM.43.11.5588-5592.2005

Dethlefsen, L., and Relman, D. A. (2011). Incomplete recovery and individualized responses of the human distal gut microbiota to repeated antibiotic perturbation. *Proc. Natl. Acad. Sci. USA* 108, 4554–4561. doi: 10.1073/pnas.1000087107

Douglas, G. M., Maffei, V. J., Zaneveld, J. R., Yurgel, S. N., Brown, J. R., Taylor, C. M., et al. (2020). PICRUSt2 for prediction of metagenome functions. *Nat. Biotechnol.* 38, 685–688. doi: 10.1038/s41587-020-0548-6

Ericson, U., Brunkwall, L., Hellstrand, S., Nilsson, P. M., and Orho-Melander, M. (2020). A health-conscious food pattern is associated with prediabetes and gut microbiota in the Malmö offspring study. *J. Nutr.* 150, 861–872. doi: 10.1093/jn/nxz293

Euzéby, J. P. (1997). List of bacterial names with standing in nomenclature: a folder available on the internet. *Int. J. Syst. Evol. Microbiol.* 47, 590–592. doi: 10.1099/00207713-47-2-590

Galazzo, G., van Best, N., Benedikter, B. J., Janssen, K., Bervoets, L., Driessen, C., et al. (2020). How to count our microbes? The effect of different quantitative microbiome profiling approaches. *Front. Cell. Infect. Microbiol.* 10:10. doi: 10.3389/fcimb.2020.00403

Göker, M., and Oren, A. (2024). Valid publication of names of two domains and seven kingdoms of prokaryotes. *Int. J. Syst. Evol. Microbiol.* 74:006242. doi: 10.1099/ijsem.0.006242

Greening, R. C., and Leedle, J. A. Z. (1989). Enrichment and isolation of *Acetitomaculum ruminis*, gen. Nov., sp. nov.: acetogenic bacteria from the bovine rumen. *Arch. Microbiol.* 151, 399–406. doi: 10.1007/BF00416597

Haider, D., Hall, M. W., LaRoche, J., and Beiko, R. G. (2024). Mock microbial community meta-analysis using different trimming of amplicon read lengths. *Environ. Microbiol.* 26:e16566. doi: 10.1111/1462-2920.16566

Hu, C., Niu, X., Chen, S., Wen, J., Bao, M., Mohyuddin, S. G., et al. (2021). A comprehensive analysis of the colonic flora diversity, short chain fatty acid metabolism, transcripts, and biochemical indexes in heat-stressed pigs. *Front. Immunol.* 12:717723. doi: 10.3389/fimmu.2021.717723

Jian, C., Luukkonen, P., Yki-Järvinen, H., Salonen, A., and Korpela, K. (2020). Quantitative PCR provides a simple and accessible method for quantitative microbiota profiling. *PLoS One* 15:e0227285. doi: 10.1371/journal.pone.0227285

Jost, L. (2007). Partitioning diversity into independent alpha and beta components. *Ecology* 88, 2427–2439. doi: 10.1890/06-1736.1

Kamiya, E., Izumiyama, S., Nishimura, M., Mitchell, J. G., and Kogure, K. (2007). Effects of fixation and storage on flow cytometric analysis of marine bacteria. *J. Oceanogr.* 63, 101–112. doi: 10.1007/s10872-007-0008-7

Kenny, M., Smidt, H., Mengheri, E., and Miller, B. (2011). Probiotics – do they have a role in the pig industry? *Animal* 5, 462–470. doi: 10.1017/S175173111000193X

Kim, H. B., Borewicz, K., White, B. A., Singer, R. S., Sreevatsan, S., Tu, Z. J., et al. (2012). Microbial shifts in the swine distal gut in response to the treatment with antimicrobial growth promoter, tylosin. *Proc. Natl. Acad. Sci. USA* 109, 15485–15490. doi: 10.1073/pnas.1205147109

Kim, J., Guevarra, R. B., Nguyen, S. G., Lee, J. H., Jeong, D. K., and Unno, T. (2016). Effects of the antibiotics growth promoter tylosin on swine gut microbiota. *J. Microbiol. Biotechnol.* 26, 876–882. doi: 10.4014/jmb.1512.12004

Lagkouvardos, I., Fischer, S., Kumar, N., and Clavel, T. (2017). Rhea: a transparent and modular R pipeline for microbial profiling based on 16S rRNA gene amplicons. *PeerJ* 5:e2836. doi: 10.7717/peerj.2836

Lambrecht, J., Cichocki, N., Hübschmann, T., Koch, C., Harms, H., and Müller, S. (2017). Flow cytometric quantification, sorting and sequencing of methanogenic archaea based on F420 autofluorescence. *Microb. Cell Factories* 16:180. doi: 10.1186/s12934-017-0793-7

Lin, Y., Gifford, S., Ducklow, H., Schofield, O., and Cassar, N. (2019). Towards quantitative microbiome community profiling using internal standards. *Appl. Environ. Microbiol.* 85:e02634-18. doi: 10.1128/AEM.02634-18

Lin, H., and Peddada, S. D. (2020). Analysis of microbial compositions: a review of normalization and differential abundance analysis. *NPJ Biofilms Microbiomes* 6:60. doi: 10.1038/s41522-020-00160-w

Ma, E., Maskarinec, G., Lim, U., Boushey, C. J., Wilkens, L. R., Setiawan, V. W., et al. (2021). Long-term association between diet quality and characteristics of the gut microbiome in the multiethnic cohort study. *Br. J. Nutr.* 128, 93–102. doi: 10.1017/S0007114521002968

Martin, R., Rios-Covian, D., Huillet, E., Auger, S., Khazaal, S., Bermudez-Humaran, L. G., et al. (2023). Faecalibacterium: a bacterial genus with promising human health applications. *FEMS Microbiol. Rev.* 47:fuad039. doi: 10.1093/femsre/fuad039

McDonnell, L., Gilkes, A., Ashworth, M., Rowland, V., Harries, T. H., Armstrong, D., et al. (2021). Association between antibiotics and gut microbiome dysbiosis in children: systematic review and meta-analysis. *Gut Microbes* 13, 1–18. doi: 10.1080/19490976.2020.1870402

Morjaria, S., Schluter, J., Taylor, B. P., Littmann, E. R., Carter, R. A., Fontana, E., et al. (2019). Antibiotic-induced shifts in fecal microbiota density and composition during hematopoietic stem cell transplantation. *Infect. Immun.* 87:e00206-19. doi: 10.1128/IAI.00206-19

Morton, J. T., Marotz, C., Washburne, A., Silverman, J., Zaramela, L. S., Edlund, A., et al. (2019). Establishing microbial composition measurement standards with reference frames. *Nat. Commun.* 10:2719. doi: 10.1038/s41467-019-10656-5

Parte, A. C. (2013). LPSN—list of prokaryotic names with standing in nomenclature. *Nucleic Acids Res.* 42, D613–D616. doi: 10.1093/nar/gkt1111

Parte, A. C. (2018). LPSN–List of prokaryotic names with standing in nomenclature (bacterio.net), 20 years on. *Int. J. Syst. Evol. Microbiol.* 68, 1825–1829. doi: 10.1099/ijsem.0.002786

Parte, A. C., Sardà Carbasse, J., Meier-Kolthoff, J. P., Reimer, L. C., and Göker, M. (2020). List of prokaryotic names with standing in nomenclature (LPSN) moves to the DSMZ. *Int. J. Syst. Evol. Microbiol.* 70, 5607–5612. doi: 10.1099/ijsem.0.004332

Prax, N., Wagner, S., Schardt, J., Neuhaus, K., Clavel, T., and Fuchs, T. M. (2021). A diet-specific microbiota drives *Salmonella Typhimurium* to adapt its in vivo response to plant-derived substrates. *Anim. Microbiome* 3:24. doi: 10.1186/s42523-021-00082-8

Prest, E. I., Hammes, F., Kotzsch, S., van Loosdrecht, M. C., and Vrouwenvelder, J. S. (2013). Monitoring microbiological changes in drinking water systems using a fast and reproducible flow cytometric method. *Water Res.* 47, 7131–7142. doi: 10.1016/j.watres.2013.07.051

Pruesse, E., Peplies, J., and Glöckner, F. O. (2012). SINA: accurate high-throughput multiple sequence alignment of ribosomal RNA genes. *Bioinformatics* 28, 1823–1829. doi: 10.1093/bioinformatics/bts252

Rao, C., Coyte, K. Z., Bainter, W., Geha, R. S., Martin, C. R., and Rakoff-Nahoum, S. (2021). Multi-kingdom ecological drivers of microbiota assembly in preterm infants. *Nature* 591, 633–638. doi: 10.1038/s41586-021-03241-8

Reitmeier, S., Hitch, T. C. A., Treichel, N., Fikas, N., Hausmann, B., Ramer-Tait, A. E., et al. (2021). Handling of spurious sequences affects the outcome of high-throughput 16S rRNA gene amplicon profiling. *ISME Commun.* 1:31. doi: 10.1038/s43705-021-00033-z

Reitmeier, S., Kiessling, S., Neuhaus, K., and Haller, D. (2020). Comparing circadian rhythmicity in the human gut microbiome. *STAR Protoc.* 1:100148. doi: 10.1016/j.xpro.2020.100148

Saladrigas-García, M., Durán, M., D'Angelo, M., Coma, J., Pérez, J. F., and Martín-Orúe, S. M. (2022). An insight into the commercial piglet's microbial gut colonization: from birth towards weaning. *Anim. Microbiome* 4:68. doi: 10.1186/s42523-022-00221-9

Satinsky, B. M., Gifford, S. M., Crump, B. C., and Moran, M. A. (2013). Use of internal standards for quantitative metatranscriptome and metagenome analysis. *Methods Enzymol.* 531, 237–250. doi: 10.1016/B978-0-12-407863-5.00012-5

Sawicka-Smiarowska, E., Bondarczuk, K., Bauer, W., Niemira, M., Szalkowska, A., Raczkowska, J., et al. (2021). Gut microbiome in chronic coronary syndrome patients. *J. Clin. Med.* 10:5074. doi: 10.3390/jcm10215074

Sebastià, C., Folch, J. M., Ballester, M., Estellé, J., Passols, M., Muñoz, M., et al. (2024). Interrelation between gut microbiota, SCFA, and fatty acid composition in pigs. *mSystems* 9, e01049–e01023. doi: 10.1128/msystems.01049-23

Shin, N. R., Whon, T. W., and Bae, J. W. (2015). Proteobacteria: microbial signature of dysbiosis in gut microbiota. *Trends Biotechnol.* 33, 496–503. doi: 10.1016/j.tibtech.2015.06.011

Stämmler, F., Glasner, J., Hiergeist, A., Holler, E., Weber, D., Oefner, P. J., et al. (2016). Adjusting microbiome profiles for differences in microbial load by spike-in bacteria. *Microbiome* 4:28. doi: 10.1186/s40168-016-0175-0

Stecher, B., Maier, L., and Hardt, W. D. (2013). "Blooming" in the gut: how dysbiosis might contribute to pathogen evolution. *Nat. Rev. Microbiol.* 11, 277–284. doi: 10.1038/nrmicro2989

Sun, J., Du, L., Li, X., Zhong, H., Ding, Y., Liu, Z., et al. (2019). Identification of the core bacteria in rectums of diarrheic and non-diarrheic piglets. *Sci. Rep.* 9:18675. doi: 10.1038/s41598-019-55328-y

Tkacz, A., Hortala, M., and Poole, P. S. (2018). Absolute quantitation of microbiota abundance in environmental samples. *Microbiome* 6:110. doi: 10.1186/s40168-018-0491-7

Tourlousse, D. M., Ohashi, A., and Sekiguchi, Y. (2018). Sample tracking in microbiome community profiling assays using synthetic 16S rRNA gene spike-in controls. *Sci. Rep.* 8:9095. doi: 10.1038/s41598-018-27314-3

Tourlousse, D. M., Yoshiike, S., Ohashi, A., Matsukura, S., Noda, N., and Sekiguchi, Y. (2017). Synthetic spike-in standards for high-throughput 16S rRNA gene amplicon sequencing. *Nucleic Acids Res.* 45:e23. doi: 10.1093/nar/gkw984

Valeriano, V. D., Balolong, M. P., and Kang, D. K. (2017). Probiotic roles of Lactobacillus sp. in swine: insights from gut microbiota. *J. Appl. Microbiol.* 122, 554–567. doi: 10.1111/jam.13364

Vandeputte, D., De Commer, L., Tito, R. Y., Kathagen, G., Sabino, J., Vermeire, S., et al. (2021). Temporal variability in quantitative human gut microbiome profiles and implications for clinical research. *Nat. Commun.* 12:6740. doi: 10.1038/s41467-021-27098-7

Vandeputte, D., Kathagen, G., D'Hoe, K., Vieira-Silva, S., Valles-Colomer, M., Sabino, J., et al. (2017). Quantitative microbiome profiling links gut community variation to microbial load. *Nature* 551, 507–511. doi: 10.1038/nature24460

Vetrovsky, T., and Baldrian, P. (2013). The variability of the 16S rRNA gene in bacterial genomes and its consequences for bacterial community analyses. *PLoS One* 8:e57923. doi: 10.1371/journal.pone.0057923

Wang, Q., Garrity, G. M., Tiedje, J. M., and Cole, J. R. (2007). Naive Bayesian classifier for rapid assignment of rRNA sequences into the new bacterial taxonomy. *Appl. Environ. Microbiol.* 73, 5261–5267. doi: 10.1128/AEM.00062-07

Williams, K. P., and Kelly, D. P. (2013). Proposal for a new class within the phylum Proteobacteria, Acidithiobacillia classis nov., with the type order Acidithiobacillales, and emended description of the class Gammaproteobacteria. *Int. J. Syst. Evol. Microbiol.* 63, 2901–2906. doi: 10.1099/ijs.0.049270-0

Yang, C., Du, Y., Ren, D., Yang, X., and Zhao, Y. (2021). Gut microbiota-dependent catabolites of tryptophan play a predominant role in the protective effects of turmeric polysaccharides against DSS-induced ulcerative colitis. *Food Funct.* 12, 9793–9807. doi: 10.1039/D1FO01468D

Yang, W. Y., Lee, Y., Lu, H., Chou, C. H., and Wang, C. (2019). Analysis of gut microbiota and the effect of lauric acid against necrotic enteritis in Clostridium perfringens and Eimeria side-by-side challenge model. *PLoS One* 14:e0205784. doi: 10.1371/journal.pone.0205784

Yang, Y., Zhao, X., Le, M. H., Zijlstra, R. T., and Gänzle, M. G. (2015). Reutericyclin producing *Lactobacillus reuteri* modulates development of fecal microbiota in weanling pigs. *Front. Microbiol.* 6:762. doi: 10.3389/fmicb.2015.00762

frontiers | Frontiers in Microbiology

TYPE Original Research
PUBLISHED 28 March 2025
DOI 10.3389/fmicb.2025.1530414

OPEN ACCESS

EDITED BY
Israel Nissan,
Ministry of Agriculture and Rural Development (Israel), Israel

REVIEWED BY
Harapan Harapan,
Syiah Kuala University, Indonesia
Yasmin Maor,
Wolfson Medical Center, Israel

*CORRESPONDENCE
Rasha Abdelsalam-Elshenawy
✉ r.elshenawy@herts.ac.uk

RECEIVED 18 November 2024
ACCEPTED 10 March 2025
PUBLISHED 28 March 2025

CITATION
Abdelsalam-Elshenawy R, Umaru N and Aslanpour Z (2025) Seasonal variations and the COVID-19 pandemic: impact on antimicrobial stewardship and antibiotic prescribing in a UK secondary care setting to combat antimicrobial resistance—a pilot study.
Front. Microbiol. 16:1530414.
doi: 10.3389/fmicb.2025.1530414

Seasonal variations and the COVID-19 pandemic: impact on antimicrobial stewardship and antibiotic prescribing in a UK secondary care setting to combat antimicrobial resistance—a pilot study

Rasha Abdelsalam-Elshenawy*, Nkiruka Umaru and Zoe Aslanpour

School of Health, Medicine and Life Sciences, University of Hertfordshire, Hatfield, United Kingdom

Antimicrobial resistance (AMR) remains a significant global health challenge, exacerbated by inappropriate antibiotic use, particularly during crises such as the COVID-19 pandemic. This pilot study evaluates the impact of seasonal variations and the pandemic on antimicrobial stewardship (AMS) practices in a UK secondary care setting. Using an interrupted time-series analysis, the study examined antibiotic prescribing patterns for respiratory tract infections (RTIs) during the pre-pandemic period of 2019 and the pandemic year of 2020. Among the 80 admissions reviewed, communityacquired pneumonia (CAP) was the most frequent diagnosis, with cases peaking at 15 in December 2019, illustrating the seasonal burden of RTIs. AMS interventions were assessed using the CARES framework, as recommended by the United Kingdom Health Security Agency's (UKHSA) Start Smart, Then Focus toolkit. This CARES framework consists of five key actions: Cease, which involves discontinuing antibiotics if no infection is present; Amend, modifying antibiotic therapy based on clinical response or diagnostic findings; Refer, consulting specialised services when additional expertise is required; Extend, continuing antibiotic therapy with a documented review date; and Switch, transitioning from intravenous to oral antibiotic therapy when clinically appropriate. Notable shifts in AMS practices were observed, with Cease interventions increasing from 5% in winter 2019 to 9% by early spring 2020, Amend actions briefly spiking in March 2020, and Switch interventions peaking at 6% in spring 2020, reflecting dynamic stewardship responses to the evolving pandemic landscape. While the small sample size limits statistical power, a more extensive validation sample would strengthen the robustness of the data extraction tool and enhance its credibility for broader applications. Nevertheless, these findings highlight the importance of adaptive, sustainable, and resilient AMS strategies that align with seasonal trends to mitigate AMR risks and ensure effective healthcare delivery during public health emergencies. The study highlights the value of pilot testing in ensuring feasibility and reliability, advocating for the development of robust AMS frameworks to combat AMR and build healthcare resilience during future global crises.

KEYWORDS

antimicrobial stewardship (AMS), antimicrobial resistance, COVID-19 pandemic, seasonal variation, hospital, antibiotic stewardship (ABS), antimicrobial stewardship (ASP) intervention, antibiotic prescribing

Introduction

Antimicrobial resistance (AMR) is a critical global health threat, causing an estimated 4.71 million deaths in 2021, with mortality trends varying significantly by age and region. Although AMR deaths among children under five have decreased, rates among older adults have sharply increased, driven largely by multidrug-resistant bacteria such as methicillin-resistant *Staphylococcus aureus* and carbapenem-resistant Gram-negative pathogens (Kariuki, 2024). Globally, multidrug-resistant *Acinetobacter baumannii* has also emerged, especially in Brazil, associated with invasive medical procedures, antibiotic use, and severe infections (Silva et al., 2022). AMR threatens progress towards the United Nations Sustainable Development Goals (SDGs), particularly SDG 3, which aims to ensure healthy lives and promote well-being for all (Jasovský et al., 2016).

This hidden crisis necessitates immediate and sustained action to prevent a future where common infections become untreatable and medical procedures carry increased risks (World Health Organization, 2023). The introduction of penicillin in the 1920s marked a transformative era in infection management, significantly reducing mortality rates (Elshenawy et al., 2023a,b). However, despite these advancements, inappropriate antibiotic prescriptions have driven the rise of AMR (GOV.UK, 2024). Urgent and sustainable measures are essential to combat AMR and preserve the effectiveness of antibiotics (GOV.UK, 2024).

Seasonal variations significantly impact antibiotic prescribing patterns, often resulting in higher rates of inappropriate antibiotic use, particularly for conditions where antibiotics are rarely indicated. Antibiotic prescribing increases notably during winter, frequently without clear clinical justification, thereby exacerbating the AMR crisis. Recognising these seasonal prescribing patterns provides opportunities for targeted AMS interventions aimed at reducing inappropriate antibiotic use and strengthening stewardship efforts during critical periods (Serletti et al., 2023).

Antimicrobial stewardship (AMS) is a pivotal component of the UK's five-year strategy to effectively combat antimicrobial resistance. Its implementation promotes judicious antibiotic use, optimises treatment outcomes, and minimises resistance (Elshenawy et al., 2023a,b). In 2015, Public Health England (PHE) developed the "Start Smart, Then Focus" (SSTF) toolkit, a structured, evidence-based approach guiding AMS practices in inpatient care. The toolkit provides guidance for clinicians and healthcare leaders to reduce AMR risks while maintaining high-quality patient care. In 2023, the UK Health Security Agency (UKHSA) updated the SSTF toolkit, emphasising timely and responsible antibiotic use through the rapid initiation of effective therapies. The SSTF approach consists of two key phases: Start Smart, which focuses on the prompt and appropriate initiation of antibiotic therapy, and Then Focus, which involves reviewing and adjusting therapy based on clinical progress and diagnostic results. Within the "Then Focus" phase, the toolkit outlines five essential actions for clinicians to consider: Cease, discontinuing antibiotics if there is no evidence of infection; Amend, modifying therapy to a narrower or broader spectrum based on clinical findings; Refer, consulting or referring to specialised services when necessary; Extend, continuing treatment with a documented review or specified stop date; and Switch, transitioning from intravenous to oral antibiotics when appropriate. The 2023 update further reinforces the need for mandatory reviews within 24–72 h to ensure appropriate prescribing and reduce unnecessary antibiotic use (UK Health Security Agency, 2023). These measures are designed to enhance patient outcomes, optimise antimicrobial use, and mitigate the growing threat of AMR.

The COVID-19 pandemic significantly disrupted global healthcare systems, leading to increased inappropriate antibiotic use and rising AMR rates. There remains an urgent need to understand AMS practices during crises that disrupt healthcare delivery, particularly how AMS programs adapted to challenges such as staff shortages, resource constraints, and altered clinical priorities. This understanding is crucial for enhancing emergency preparedness and ensuring healthcare systems sustain effective antibiotic prescribing during future emergencies in secondary care settings (Elshenawy et al., 2024a).

Therefore, understanding how both seasonal variations and global crises influence antibiotic prescribing is essential for ensuring the effectiveness of AMS initiatives and combating the growing threat of AMR. This insight will be vital for developing robust AMS frameworks capable of withstanding disruptions and ensuring optimal antibiotic use during emergencies.

This pilot study aimed to evaluate the impact of seasonal variations, particularly the rise in respiratory infections during winter, and the COVID-19 pandemic on antibiotic prescribing patterns and antimicrobial stewardship practices in a UK secondary care setting. By comparing data collected before and during the pandemic. By comparing AMS practices from 2019 as a baseline with those during the 2020 crisis, the study sought to understand how AMS efforts were maintained or disrupted. The ultimate goal is to provide practical solutions and strengthen AMS practices to address the ongoing threat of antimicrobial resistance.

Materials and methods

Study design and setting

This pilot study aimed to assess the combined impact of seasonal variations and the COVID-19 pandemic on AMS practices by comparing data collected before and during the pandemic. Baseline data from 2019 served as a pre-pandemic reference, with measurements taken during the first week of March, June, September, and December. The exact periods were analysed in 2020, coinciding with UK national lockdowns and the initial rollout of COVID-19 vaccines in December 2020 (Institute for UK Government, 2022). Utilising an interrupted time-series approach, the study accounted for seasonal variations in antibiotic prescribing. This retrospective medical records review was conducted from 1 August 2021 to 28 February 2023 at a single National Health Service (NHS) Foundation Trust in the East of England, which serves a population of approximately 700,000 across 742 beds. The study focused on adult patients aged 25 years and above, aiming to assess AMS implementation and antibiotic prescribing patterns in 2019 (pre-pandemic) and 2020 (during the pandemic). The evaluation included AMS strategies outlined in the "Then Focus" phase, which emphasise examine Antimicrobial review outcomes based on the CARES framework and clinical progress.

Study population (inclusion/exclusion criteria)

A stratified sampling strategy was employed to ensure maximum diversity among the included medical records. The inclusion criteria comprised adult patients aged 25 years and older, pregnant women, and immunocompromised individuals admitted to the Trust in 2019 and 2020. Only those prescribed antibiotics for RTIs, including pneumonia, were included in the study. Patients who spent less than 48–72 h in the Accident & Emergency (A&E) department were not prescribed antibiotics, or paediatric patients were excluded. This approach ensured a diverse and representative sample for evaluating antimicrobial stewardship practices.

The public and patient involvement included submitting the study protocol to the Citizens Senate, which provided valuable feedback and suggestions. This study was registered with the International Standard Randomised Controlled Trial Number (ISRCTN 14825813) and with Octopus, the global primary research registry (ISRCTN, 2022; Elshenawy, 2023). Ethical approval was granted by the University of Hertfordshire Ethics Committee and the Health Research Authority (HRA). Public and patient involvement included submission of the study protocol to the Citizens Senate, which provided valuable feedback and recommendations.

Data sources and variables

In this retrospective cross-sectional study, patients were selected using electronic health records (EHRs) based on ICD-10 codes indicative of respiratory tract infections (RTIs). This included a range of conditions, encompassing both specific and indeterminate diagnoses. Specific conditions included community-acquired pneumonia (CAP), infective exacerbation of chronic obstructive pulmonary disease (COPD), hospital-acquired pneumonia (HAP), and ventilator-associated pneumonia (VAP). In 2020, the selection criteria were expanded to incorporate cases of COVID-19 pneumonia. Additionally, indeterminate diagnoses such as upper respiratory tract infections (URTIs), lower respiratory tract infections (LRTIs), and unspecified pneumonia were categorised as "Unspecific" RTIs. The primary diagnosis of RTIs in these records was crucial in determining the initial or empirical antibiotic prescribed to patients.

Utilising Minitab Statistical Software Version 21.1.0, and based on Public Health England's estimation that 20% of all antibiotics prescribed in the UK might be inappropriate, with a 10% margin of error and a 95% confidence interval, the required sample size was determined (Public Health England, 2018). Data were randomly selected using Excel's RAND function, resulting in a total of 80 patient records (40 from 2019 and 40 from 2020). This approach streamlined the sampling process while ensuring a comprehensive representation of the patient population. The primary author (RAE) extracted data from the EHRs, strictly adhering to the established inclusion and exclusion criteria. The extracted data included demographic characteristics and antibiotic prescribing practices, evaluated using the antimicrobial stewardship "Start Smart, Then Focus" Toolkit, which served as the study's gold standard (UK Health Security Agency, 2023).

To validate the data extraction tool, two independent authors each extracted data from 10% of the sample (four patient records) per year, totalling eight records. An agreement rate of 80% or higher was required to confirm the tool's validity (Price, 2018). For reliability assessment, both authors independently extracted data from 10% (eight records), and inter-rater reliability was determined by the percentage agreement. Discrepancies were resolved through discussion.

Data collection

Data were collected from the medical records of 80 patients within the Foundation Trust in accordance with the specified inclusion and exclusion guidelines. Data were gathered from eight time points, specifically the first week of each selected month. The four pre-pandemic time points included: (i) March 2019 (Spring); (ii) June 2019 (Summer); (iii) September 2019 (Autumn); and (iv) December 2019 (Winter). Additionally, four pandemic time points were selected: (i) March 2020 (Spring)—the first wave of COVID-19; (ii) June 2020 (Summer)—the first lockdown; (iii) September 2020 (Autumn)—the second wave of the pandemic; and (iv) December 2020 (Winter)—the vaccination rollout. This approach ensured that data collection was consistent and accounted for seasonal variations and key phases of the COVID-19 pandemic.

Data extraction

The primary author developed the data extraction tool by reviewing relevant literature and the UKHSA Toolkit. The authors collaboratively discussed and agreed upon the elements to be included in the tool. To extract data from patients meeting the inclusion criteria, access to the Trust's electronic health system was necessary. Prior to commencing data extraction, the primary author completed training modules for these systems and subsequently gained access. The AMS data extraction tool encompassed demographic information, primary diagnosis, SSTF criteria, and AMS practices. This tool was employed to gather the required information from patients' medical records, with each extraction taking approximately 45 min. This structured approach ensured the accurate and efficient collection of data necessary for assessing antimicrobial stewardship practices.

Statistical methods

Descriptive analyses were conducted to summarise the data. Categorical and binary variables—including sex, age, admission speciality, patient classification, and types of AMS interventions—were presented as numbers (*n*) and proportions (%). Continuous variables with non-normal distributions were summarised using mean and standard deviation (SD). AMS implementation was assessed using the AMS Toolkit and further evaluated using the Start Smart Then Focus toolkit (UK Health Security Agency, 2023). Decisions made following this review were utilised to determine the type of AMS intervention. All statistical analyses were performed using Microsoft Excel 2019 for Windows (Microsoft, 2019).

Results

Table 1 summarises the demographic characteristics and admissions of 80 patients. The cohort included 39 males (49%) and 41

females (51%), with a mean age of 76 ± 14.8 years, ranging from 26 to 99 years. Most patients were admitted to General Medicine (39 patients) and Elderly Medicine (18), with smaller numbers in Surgery (7), Cardiology (3), Respiratory Medicine (3), Accident & Emergency (1), and Others (1). The majority were urgent admissions (76 patients), while 4 were ordinary and routine admissions.

Figure 1 illustrates the number of respiratory tract infection (RTI) admissions during the first week of March, June, September, and December in both 2019 and 2020. Notably, admissions peaked in the first week of December 2019 with 15 cases. Although December 2019 marks the initial global emergence of the COVID-19 pandemic, the first confirmed COVID-19 case in the UK was reported in January 2020. Therefore, the December 2019 peak may not be directly attributable to COVID-19 within the UK context and could instead reflect typical seasonal variations or other factors influencing RTI admissions during that period. In the first week of March 2020, admissions decreased to 10, followed by a further decline to 9 in both June and September 2020. There was a slight increase in the first week of December 2020, with admissions rising to 11 cases. This pattern indicates fluctuations in RTI admissions that correlate more closely with the early stages and progression of the COVID-19 pandemic in the UK, particularly from January 2020 onward, rather than the initial global onset in December 2019.

Table 2 below compares the length of stay (LOS) in 2019 and 2020. The average LOS was almost the same between 2019 and 2020. The SD was 16 in 2019, while in 2020, the SD was 13.

Figure 2 presents the number of respiratory tract infection (RTI) admissions from March 2019 to December 2020, categorised by diagnosis and totalling 80 admissions. Community acquired pneumonia (CAP) was the most frequent, with 24 admissions, peaking at 5 in December 2020. Non-specific diagnoses (URTI, pneumonia) followed with 23 admissions, peaking at 6 in June 2020. Hospital acquired pneumonia (HAP) had 10 admissions, with peaks of 3 in both March and June 2020. Ventilator pneumonia (VAP) had six admissions, with 3 in June 2019. Bronchiectasis also had six admissions, evenly spread. COVID-19 pneumonia accounted for five admissions, peaking at 2 in March 2020. COPD infective exacerbation had four admissions, while viral pneumonia had the lowest frequency with two admissions, one each in March and September 2019.

Figure 3 illustrates the seasonal and monthly trends in antimicrobial stewardship (AMS) practices—Cease, Amend, Refer, Extend, and Switch—from spring 2019 (March) to winter 2020 (December). During the winter of 2019 (December), Cease actions were at 5%, peaking in early spring 2020 (March) at 9%, coinciding with the onset of the COVID-19 pandemic, before sharply declining to 1% by winter 2020 (December). A similar pattern was observed with Amend actions, which rose from 7% in winter 2019 (December) to 8% in early spring 2020 (March) and then declined to 2% by the end of winter 2020 (December). Throughout all seasons, the Refer and Extend actions remained consistently low, fluctuating between 1 and 3%. The Switch category, which indicates efforts to transition patients from intravenous to oral antibiotics, reached its peak of 6% in early spring 2020 (March) before decreasing to 1% by the winter of 2020 (December).

TABLE 1 Demographic characteristics and admissions (n = 80).

Characteristics		Admissions (n = 80)
Sex	Male (%)	39 (49%)
	Female (%)	41 (51%)
Admission specialty	General medicine	39
	Elderly medicine	18
	Surgery	7
	Cardiology	3
	Respiratory medicine	3
	Accident & emergency	1
	Others[a]	1
Patient classification[b]	Ordinary and routine admission	4
	Urgent admission	76

[a]The "other" consultant specialities include endocrinology, diabetic medicine, acute internal medicine, thoracic medicine, neurology, and rheumatology.
[b]Ordinary admissions are planned and elective, while urgent admissions require immediate hospitalisation, often through accident & emergency (A&E), for acute illness or emergencies.

Discussion

The findings from this pilot study provide valuable insights into the impact of the COVID-19 pandemic on antimicrobial stewardship practices in a secondary care setting in the UK. This study utilised an interrupted time-series analysis to compare antibiotic prescribing patterns before (2019) and during (2020) the pandemic, focusing on respiratory tract infections.

With regards to the demographic characteristics and admissions, this study included 80 patient admissions, with a balanced gender distribution (49% male, 51% female) and a mean age of 76 years. The majority of admissions were for general medicine (39) and elderly medicine (18), reflecting the high vulnerability of these groups to RTIs and the critical need for effective AMS practices in these areas. The pre-dominance of urgent admissions (76 out of 80) highlights the acute nature of these cases and the necessity for prompt and appropriate antibiotic use. A meta-analysis of 59 studies from the Netherlands in 2020, involving 36,470 patients, found that men and individuals aged 70 and above face higher risks of COVID-19 infection, severe disease, ICU admission, and death. The study highlights significant age and sex disparities in COVID-19 outcomes (Pijls et al., 2021).

Findings from this study illustrate the fluctuations in RTI admissions across eight time points in 2019 and 2020. The data shows a peak in admissions in December 2019, followed by a decline throughout 2020. While December 2019 marks the initial global emergence of COVID-19, the first confirmed case in the UK was reported in January 2020 (GOV.UK, 2022). Therefore, the peak in December 2019 may not be directly attributable to COVID-19 within the UK context but could instead reflect typical seasonal variations or other factors influencing RTI admissions during that period. As COVID-19 cases surged in the UK from early 2020 onward, several factors likely influenced the decline in RTI admissions. Increased awareness and testing for respiratory symptoms, changes in patient behaviour due to lockdowns, and restricted access to healthcare services may have contributed to this downward trend (Institute for UK Government, 2022). This pattern is consistent with findings from a 2020 study in the United States, which revealed a 33.7% decrease in daily hospital admissions for urgent conditions during the COVID-19

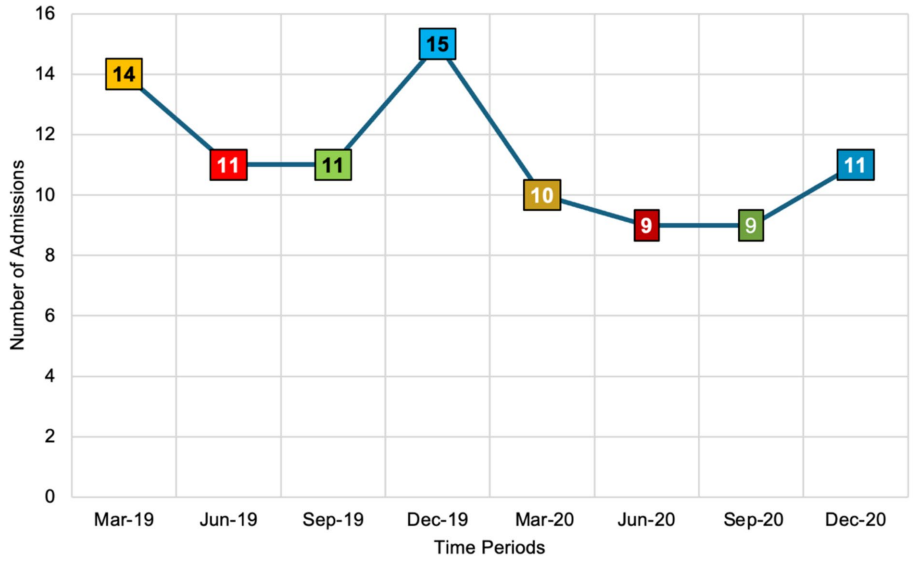

FIGURE 1
The number of respiratory tract infection admissions across eight seasonal time points in 2019 and 2020 (n = 80 admissions). This figure utilises a colour-coded scheme to illustrate the number of respiratory tract infection (RTI) admissions across different months and years. Orange, presented in both light and dark shades, represents RTI admissions in March 2019 and March 2020. Red, also in light and dark shades, denotes admissions in June 2019 and June 2020. Similarly, green, in light and dark shades, corresponds to RTI admissions in June 2019 and June 2020. Finally, blue, shown in both light and dark shades, signifies RTI admissions in December 2019 and December 2020. This colour differentiation allows for a clear visual comparison of RTI admission trends over the specified periods.

TABLE 2 Length of stay in days (2019–2020).

Length of stay in days	2019	2020
Mean	16	15
Median	11	10
Range	1–119	1–97
Standards deviation	16	13

pandemic compared to 2019. Significant declines were observed in gastroenterology (−29.6%) and cardiovascular (−44.7%) admissions. These trends emphasise the critical importance of public awareness campaigns aimed at reassuring the public about the safety of seeking necessary medical care during pandemics. Ensuring that individuals feel safe to access healthcare services is essential to prevent declines in admissions for non-COVID-19 related urgent conditions, thereby maintaining overall healthcare system effectiveness and patient safety (Oseran et al., 2020).

For the LOS, the average LOS remained consistent between 2019 and 2020, with a mean of 15–16 days. However, the standard deviation decreased from 16 in 2019 to 13 in 2020, indicating a slight reduction in the variability of hospital stays during the pandemic. This could reflect more standardised treatment protocols or the impact of pandemic-related healthcare policies on patient management. A 2022 study in China examined 563,680 emergency admissions in 2020 and 709,583 in 2019, finding that the COVID-19 pandemic increased 28-day in-hospital mortality from 2.9 to 3.6%. The first and third waves had significantly higher mortality than inter-wave periods. The average length of stay decreased by 0.40 days, notably shorter for patients with mental disorders and cerebrovascular disease (Xiong et al., 2021).

The Centers for Disease Control and Prevention (CDC) report that during the COVID-19 pandemic, antibiotic prescribing in hospitals surged, with nearly 80% of COVID-19 admissions receiving antibiotics despite low rates of bacterial co-infections. While antibiotics and antifungals are essential for saving lives, their inappropriate use significantly contributes to increasing antimicrobial resistance (Centers for Disease Control and Prevention, 2021). For example, antibiotic misuse has been linked to the global rise of multidrug-resistant *Pseudomonas aeruginosa* (MDRPA) (Hayati et al., 2023).

Although overall antibiotic use decreased by August 2021 compared to 2019, prescriptions for specific antibiotics, such as azithromycin and ceftriaxone, increased, often being prescribed together. This trend likely reflects challenges in distinguishing COVID-19 from community-acquired pneumonia upon admission (Elshenawy et al., 2023a,b). Importantly, effective AMS strategies were implemented during the pandemic, aiding in maintaining appropriate antibiotic use and mitigating AMR risks. Sustained robust AMS practices are essential to ensure appropriate antibiotic prescribing and combat AMR in ongoing and future health crises (Elshenawy et al., 2024b).

For RTI diagnoses and antibiotic use, CAP was the most common diagnosis across the study period, with significant cases of HAP and non-specific RTIs. The emergence of COVID-19 pneumonia cases in 2020 highlights the direct impact of the pandemic on respiratory infection trends. The variability in diagnoses emphasises the challenges of maintaining precise AMS during a health crisis, emphasising the need for robust diagnostic and treatment protocols. As an example of pneumonia education, a Continuing Education Activity in Australia in 2024 highlights the complexities of bacterial pneumonia, including its symptoms, complications, and long-term

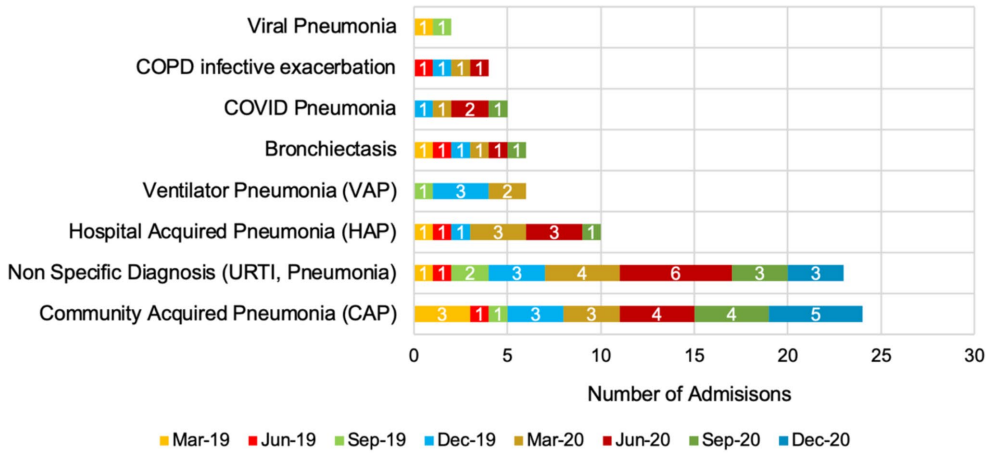

FIGURE 2
Seasonal trends in respiratory tract infection admissions in 2019 and 2020 (total number = 80 admissions).

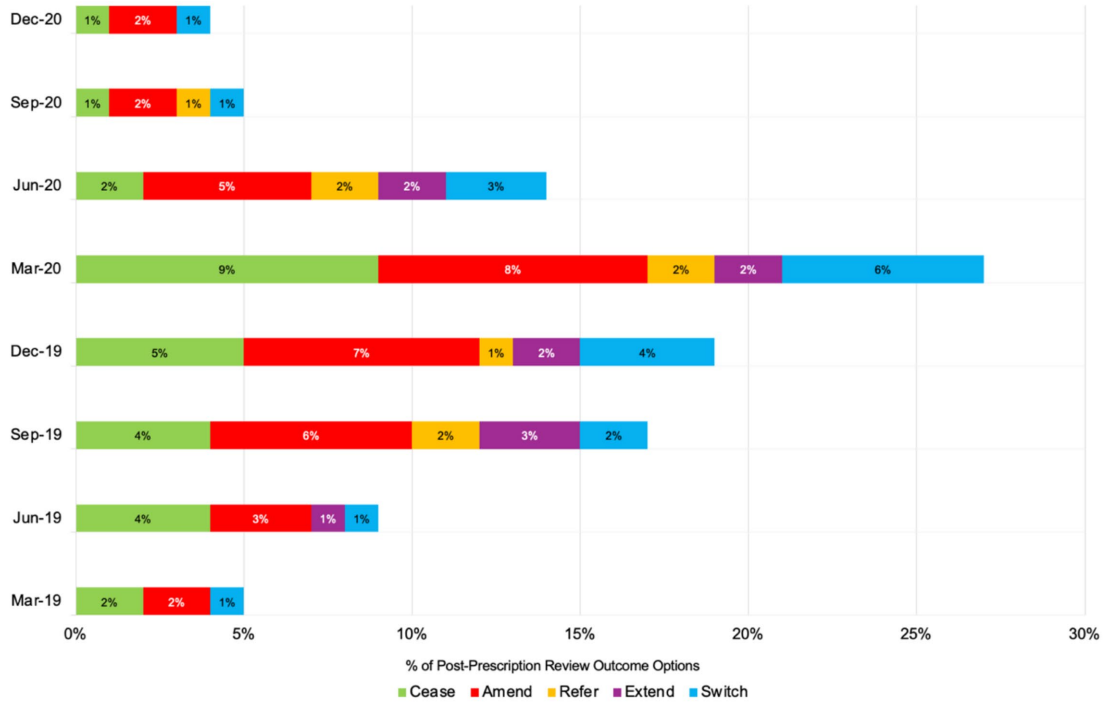

FIGURE 3
Number of post-prescription antibiotic review outcome options or AMS practices across eight seasonal time points in 2019 and 2020 (total number = 80 admissions).

impacts (Sattar et al., 2024). This module highlights a multidisciplinary approach to managing the disease, offering practical strategies for diagnosis, treatment, and patient care. It aims to enhance clinician knowledge, improve patient outcomes, and promote a cohesive healthcare approach.

Additionally, the protocol preparation adheres to national and international guidelines, including NICE guidelines, and incorporates results from local antibiograms (Sattar et al., 2024; NICE Guidelines, 2019). It is frequently updated with changes in local or national resistance patterns, clinical situations, or emergencies such as the COVID-19 pandemic. Updated protocols and antimicrobial guidelines should be properly disseminated to healthcare professionals to maintain proper antibiotic prescribing and antimicrobial stewardship practices (National Institute for Health and Care Excellence, 2023).

The COVID-19 pandemic posed significant challenges to maintaining optimal antibiotic stewardship. The consistent use of documentation for clinical indications and drug allergies is commendable, but the variability in other AMS interventions points to the need for strengthened protocols and continuous monitoring.

These findings align with the study conducted in Spain in 2021, which reported increased inappropriate antibiotic use during the COVID-19 pandemic, highlighting a significant rise in inappropriate prescriptions and exacerbating antimicrobial resistance concerns (Calderón-Parra et al., 2021).

The seasonal and monthly trends observed in AMS practices reveal notable variations, particularly in response to the COVID-19 pandemic. Figure 3 shows that Cease actions, which indicate a complete cessation of antibiotic use, peaked at 9% in March 2020 and declined to 1% by December 2020. This increase in March aligns with the pandemic's onset, reflecting heightened caution and AMS efforts during the crisis. Similarly, Amend actions peaked in March 2020 before tapering off, indicating that initial adjustments to antimicrobial treatments were made in response to the pandemic. The trends observed in this study align with findings from other studies. For example, the research on respiratory tract diagnoses in the United States found that antibiotic prescribing increased significantly during winter, driven by diagnoses where antibiotics were only sometimes or rarely indicated (Serletti et al., 2023). This pattern mirrors the peaks in AMS actions observed in the present study during the winter months of December 2019 and early spring 2020, which coincided with the pandemic onset.

Furthermore, the consistency of low Refer and Extend actions across all seasons, as seen in this study, suggests minimal referrals or extensions of treatment during the study period. A similar pattern of minimal seasonal variations in certain AMS actions was reported in the Netherlands' study, which found that antimicrobial resistance rates in *Streptococcus pneumoniae* were higher in winter due to increased antibiotic use, similar to the peaks observed in this study (Martinez et al., 2019). The increased Switch actions in early spring 2020 indicate efforts to transition patients from intravenous to oral antibiotics, aligning with AMS goals to reduce inpatient antibiotic use. However, the subsequent decline in Switch actions reflects a stabilisation of AMS efforts as healthcare providers adapted to the ongoing pandemic challenges. Seasonal peaks of antimicrobial-resistant pathogens, such as vancomycin-resistant *enterococci* (VRE) and methicillin-resistant *Staphylococcus aureus* (MRSA) peaking in spring and *Klebsiella pneumoniae* and ciprofloxacin-resistant *E. coli* in summer, suggest the need for season-specific AMS strategies (Cassone et al., 2021). These findings emphasise the importance of understanding seasonal AMS trends to enhance stewardship strategies. The findings from this pilot study revealed that AMS practices were intensified during the pandemic and exhibited seasonal variations. This highlights the importance of implementing targeted interventions to address inappropriate prescribing and enhance AMS efforts consistently across healthcare settings.

This pilot study also acknowledges that incorporating detailed virological and microbiological data would enhance the interpretation of AMS interventions. In this pilot, only 5 out of 80 (6%) admissions were documented as COVID-19 pneumonia, while many records contained incomplete virology or microbiology data, limiting the ability to establish direct correlations between specific pathogens and prescribing interventions. This constraint highlights the need for future research to integrate comprehensive PCR and microbiological testing to provide a more detailed understanding of AMS practices in response to pathogen-specific infections. However, the primary aim of this study was to assess the feasibility of the data extraction tool and evaluate broader AMS patterns, rather than conduct an in-depth microbiological analysis. These findings highlight the necessity of future large-scale studies with improved microbiological reporting to refine AMS strategies further and ensure a more targeted approach to antibiotic prescribing, particularly during global health crises such as the COVID-19 pandemic.

Strengths and limitations

This study has several strengths and limitations that influence its findings. One key strength is the role of pilot testing, which ensured feasibility, validity, and reliability in the study's design and execution. The research highlights the impact of the COVID-19 pandemic on AMS practices, particularly in relation to seasonal variations, providing valuable insights to promote resilient and sustainable AMS frameworks, support rational antibiotic use, and address the global threat of antimicrobial resistance. The use of a validated data extraction tool and interrupted time-series analysis added rigour to the understanding of changes in AMS practices during the pandemic.

The study's small sample size and single-centre scope limit generalisability. However, pilot studies play a critical role in testing feasibility and refining data collection tools before larger investigations. This study was designed as a pilot project to assess the reliability of a data extraction tool and evaluate trends in AMS practices. The manuscript explicitly identifies this as a pilot study to ensure clarity regarding its scope. Additionally, subsequent research, referenced in the Discussion, has since expanded the sample size and coverage, further addressing the feasibility findings of this pilot. Such pilot data are valuable for guiding resource allocation and justifying multi-centre or multi-year expansions. Pilot studies help optimise research methodologies, ensuring that future large-scale investigations are methodologically sound and effectively address antimicrobial stewardship challenges.

Despite these limitations, the study provides important insights into seasonal AMS variations during a global health crisis, demonstrating the necessity of tailored AMS strategies that adapt to seasonal and pandemic-driven disruptions in antibiotic prescribing. Future research should incorporate larger, multi-centre, and multi-year studies while also considering factors such as healthcare provider workload and hospital capacity, which may influence AMS adherence.

Conclusion

This pilot study highlights the significant impact of the COVID-19 pandemic on AMS practices in a UK secondary care setting, particularly in relation to seasonal variations. Using interrupted time-series analysis, it examined antibiotic prescribing patterns for respiratory infections during the pre-pandemic period in 2019 and the pandemic period in 2020. Among the 80 admissions reviewed, community-acquired pneumonia was the most frequent diagnosis, with admissions peaking at 15 cases in December 2019, reflecting the seasonal burden of RTIs. During the pandemic, AMS interventions demonstrated notable shifts: Cease actions increased from winter 2019 to early spring 2020, Amend

actions briefly spiked in March 2020, and Switch actions peaked in spring 2020. These findings highlight the need for targeted and adaptable AMS strategies to address seasonal trends and global health crises. Aligning AMS efforts with seasonal patterns and establishing robust, sustainable AMS frameworks are essential to saving lives and maintaining effective healthcare during global emergencies. Furthermore, the study emphasises the importance of pilot testing in ensuring research feasibility and reliability, ultimately advocating for sustainable AMS frameworks to combat antimicrobial resistance.

Data availability statement

The datasets presented in this article are not readily available because this data is restricted and confidential with the institution policy. Requests to access the datasets should be directed to: r.a.elshenawy@herts.ac.uk.

Ethics statement

Ethical approval for this study was granted by the Health Research Authority (HRA), with the Research Ethics Committee (REC) assigning reference number 22/EM/0161. In compliance with this approval, the study protocol underwent review and received approval from the University of Hertfordshire (UH) ethics committee under the reference LMS/PGR/NHS/02975. The authors have no conflicts of interest to disclose. The study was conducted in accordance with the local legislation and institutional requirements. Written informed consent for participation was not required from the participants or the participants' legal guardians/next of kin in accordance with the national legislation and institutional requirements.

Author contributions

RA-E: Formal analysis, Investigation, Methodology, Validation, Visualization, Writing – original draft. NU: Supervision, Visualization, Writing – review & editing. ZA: Supervision, Visualization, Writing – review & editing.

Funding

The author(s) declare that no financial support was received for the research and/or publication of this article.

Conflict of interest

The authors declare that the research was conducted in the absence of any commercial or financial relationships that could be construed as a potential conflict of interest.

Generative AI statement

The authors declare that no Generative AI was used in the creation of this manuscript.

Publisher's note

References

Calderón-Parra, J., Muiño-Miguez, A., Bendala-Estrada, A. D., Ramos-Martínez, A., Muñez-Rubio, E., Fernández Carracedo, E., et al. (2021). Inappropriate antibiotic use in the COVID-19 era: factors associated with inappropriate prescribing and secondary complications. Analysis of the registry SEMI-COVID. *PLoS One* 16, 16:e0251340. doi: 10.1371/journal.pone.0251340

Cassone, M., Mantey, J., Gontjes, K. J., Lansing, B. J., Gibson, K. E., Wang, J., et al. (2021). Seasonal patterns in incidence and antimicrobial resistance of common bacterial pathogens in nursing home patients and their rooms. *Front. Public Health* 9:671428. doi: 10.3389/fpubh.2021.671428

Centers for Disease Control and Prevention (2021). COVID-19 impacts on antibiotic use: improve the use of antibiotics wherever they are used and improve access. Available online at: https://www.cdc.gov/antimicrobial-resistance/media/pdfs/COVID19-Impacts-AR-AntibioicUse-508.pdf (Accessed October 25, 2024).

Elshenawy, R. A. (2023). How did the COVID-19 pandemic impact antibiotic prescribing and antimicrobial stewardship in acute care settings- Octopus | Built for Researchers. Octopus.ac. [online] doi: 10.57874/22e4-1t08

Elshenawy, R. A., Umaru, N., Alharbi, A. B., and Aslanpour, Z. (2023b). Antimicrobial stewardship implementation before and during the COVID-19 pandemic in the acute care settings: a systematic review. *BMC Public Health* 23:309. doi: 10.1186/s12889-023-15072-5

Elshenawy, R. A., Umaru, N., and Aslanpour, Z. (2023a). WHO AWaRe classification for antibiotic stewardship: tackling antimicrobial resistance—a descriptive study from an English NHS Foundation Trust prior to and during the COVID-19 pandemic. *Front. Microbiol.* 14:1298858. doi: 10.3389/fmicb.2023.1298858

Elshenawy, R. A., Umaru, N., and Aslanpour, Z. (2024a). Impact of COVID-19 on 'Start Smart, Then Focus' antimicrobial stewardship at one NHS Foundation Trust in England prior to and during the pandemic. *COVID* 4, 102–116. doi: 10.3390/covid4010010

Elshenawy, R. A., Umaru, N., and Aslanpour, Z. (2024b). An evaluation of the five rights antibiotic safety before and during COVID-19 at an NHS Foundation Trust in the United Kingdom. *J. Glob. Antimicrob. Resist.* 36, 188–189. doi: 10.1016/j.jgar.2023.12.019

GOV.UK (2022). COVID-19 and occupational impacts. Available at: https://www.gov.uk/government/publications/covid-19-and-occupational-impacts/covid-19-and-occupational-impacts

GOV.UK (2024). Confronting antimicrobial resistance 2024 to 2029. Available online at: https://www.gov.uk/government/publications/uk-5-year-action-plan-for-antimicrobial-resistance-2024-to-2029/confronting-antimicrobial-resistance-2024-to-2029

Hayati, Z., Ismail, Y. S., Suhartono, S., Zikra, M., Karmil, T. F., and Oktiviyari, A. (2023). Distribution and antimicrobial sensitivity pattern of multidrug-resistant *Pseudomonas aeruginosa* from the clinical specimen in Aceh, Indonesia. *Narra X* 1:e87. doi: 10.52225/narrax.v1i2.87

Institute for UK Government (2022). Timeline of UK government coronavirus lockdowns and restrictions. Available online at: https://www.instituteforgovernment.org.uk/data-visualisation/timeline-coronavirus-lockdowns (Accessed October 31, 2024).

ISRCTN (2022). Antibiotic prescribing in an English secondary care setting before and during the COVID-19 pandemic. Available at: https://www.isrctn.com/ISRCTN14825813

Jasovský, D., Littmann, J., Zorzet, A., and Cars, O. (2016). Antimicrobial resistance—a threat to the world's sustainable development. *Ups. J. Med. Sci.* 121, 159–164. doi: 10.1080/03009734.2016.1195900

Kariuki, S. (2024). Global burden of antimicrobial resistance and forecasts to 2050. *Lancet* 404, 1172–1173. doi: 10.1016/s0140-6736(24)01885-3

Martinez, E. P., Cepeda, M., Jovanoska, M., Bramer, W. M., Schoufour, J., Glisic, M., et al. (2019). Seasonality of antimicrobial resistance rates in respiratory bacteria: a systematic review and meta-analysis. *PLoS One* 14:e0221133. doi: 10.1371/journal.pone.0221133

Microsoft (2019). What's new in Excel 2019 for Windows. Available online at: https://support.microsoft.com/en-gb/office/what-s-new-in-excel-2019-for-windows-5a201203-1155-4055-82a5-82bf0994631f

National Institute for Health and Care Excellence (2023). Antimicrobial stewardship. Available online at: https://bnf.nice.org.uk/medicines-guidance/antimicrobial-stewardship/

NICE Guidelines (2019). *Pneumonia* (community-acquired): antimicrobial prescribing NICE guideline. Available online at: https://www.nice.org.uk/guidance/ng138/resources/pneumonia-communityacquired-antimicrobial-prescribing-pdf-66141726069445 (Accessed September 1, 2024).

Oseran, A. S., Nash, D., Kim, C., Moisuk, S., Lai, P. Y., Pyhtila, J., et al. (2020). Changes in hospital admissions for urgent conditions during COVID-19 pandemic. *Am. J. Manag. Care* 26, 327–328. doi: 10.37765/ajmc.2020.43837

Pijls, B. G., Jolani, S., Atherley, A., Derckx, R. T., Dijkstra, J. I. R., Franssen, G. H. L., et al. (2021). Demographic risk factors for COVID-19 infection, severity, ICU admission and death: a meta-analysis of 59 studies. *BMJ Open* 11:e044640. doi: 10.1136/bmjopen-2020-044640

Price, P. C. (2018). Reliability and validity of measurement—research methods in psychology. Available online at: https://opentextbc.ca/researchmethods/chapter/reliability-and-validity-of-measurement/

Public Health England (2018). Research reveals levels of inappropriate prescriptions in England. Available online at: https://www.gov.uk/government/news/research-reveals-levels-of-inappropriate-prescriptions-in-england

Sattar, S. B. A., Nguyen, A. D., and Sharma, S. (2024). "Bacterial pneumonia" in StatPearls (Treasure Island, FL: StatPearls Publishing).

Serletti, L., Dutcher, L., Degnan, K. O., Szymczak, J. E., Cluzet, V., David, M. Z., et al. (2023). Analysis of seasonal variation of antibiotic prescribing for respiratory tract diagnoses in primary care practices. *Antimicrob. Steward Healthc. Epidemiol.* 3:e147. doi: 10.1017/ash.2023.418

Silva, M. C., Werlang, M. H., Vandresen, D. F., Fortes, P. C., Pascotto, C. R., Lúcio, L. C., et al. (2022). Genetic, antimicrobial resistance profile and mortality rates of *Acinetobacter baumannii* infection in Brazil: a systematic review. *Narra J* 2:e68. doi: 10.52225/narra.v2i1.68

UK Health Security Agency (2023). Start smart then focus: antimicrobial stewardship toolkit for inpatient care settings. Available online at: https://www.gov.uk/government/publications/antimicrobial-stewardship-start-smart-then-focus/start-smart-then-focus-antimicrobial-stewardship-toolkit-for-inpatient-care-settings

World Health Organization (2023). Antimicrobial resistance. Available online at: https://www.who.int/news-room/fact-sheets/detail/antimicrobial-resistance

Xiong, X., Wai, A. K. C., Wong, J. Y. H., Tang, E. H. M., Chu, O. C. K., Wong, C. K. H., et al. (2021). Impact of varying wave periods of COVID-19 on in-hospital mortality and length of stay for admission through emergency department: a territory-wide observational cohort study. *Influenza Other Respir. Viruses* 16, 193–203. doi: 10.1111/irv.12919

frontiers | Frontiers in Microbiology

TYPE Original Research
PUBLISHED 28 April 2025
DOI 10.3389/fmicb.2025.1528341

OPEN ACCESS

EDITED BY
Santi M. Mandal,
Indian Institute of Technology Kharagpur, India

REVIEWED BY
Zhangyong Song,
Southwest Medical University, China
Erika Shor,
Hackensack Meridian Health, United States

*CORRESPONDENCE
Liangsheng Guo
✉ gls2135@sina.com

†These authors have contributed equally to this work

RECEIVED 14 November 2024
ACCEPTED 11 April 2025
PUBLISHED 28 April 2025

CITATION
Zheng L, Dong Y, Wang J, Zhang M, Xu Y, Ma L and Guo L (2025) Uncovering the connection between tunicamycin-induced respiratory deficiency and reduced fluconazole tolerance in *Candida glabrata*. *Front. Microbiol.* 16:1528341. doi: 10.3389/fmicb.2025.1528341

Uncovering the connection between tunicamycin-induced respiratory deficiency and reduced fluconazole tolerance in *Candida glabrata*

Lijun Zheng[1†], Yubo Dong[2†], Jing Wang[3], Maoji Zhang[4], Yi Xu[2], Linfeng Ma[4] and Liangsheng Guo[5*]

[1]Department of Ultrasound Medicine, The Second Affiliated Hospital of Soochow University, Suzhou, China, [2]Department of Pharmacy, The 960th Hospital of PLA, Jinan, China, [3]Department of Pharmacy, Zibo Zhoucun People's Hospital, Zibo, China, [4]Jinzhou Medical University Graduate Training Base (The 960th Hospital of PLA), Jinan, China, [5]Department of Obstetrics and Gynecology, The Second Affiliated Hospital of Soochow University, Suzhou, China

Introduction: *Candida glabrata* is a prevalent opportunistic fungal pathogen in humans, and fluconazole (FLC) is one of the most commonly used antifungal agents. However, the molecular mechanisms underlying FLC tolerance in *C. glabrata* remain largely unexplored.

Objective: This study aims to identify novel mechanisms regulating FLC tolerance, with a particular focus on tunicamycin (TUN)-induced respiratory deficiency.

Methods: We employed three distinct experimental approaches to investigate the impact of TUN on FLC tolerance: (1) co-treatment with TUN and FLC, (2) exclusive exposure to TUN, and (3) induction of petite formation through alternative methods. Additionally, gene expression analyses were conducted to evaluate the regulation of key genes involved in the ergosterol biosynthesis pathway.

Results: Our findings reveal that TUN exposure significantly abolishes FLC tolerance in *C. glabrata*, primarily through the induction of petite formation, which is characterized by mitochondrial dysfunction. Notably, TUN treatment resulted in the downregulation of critical ergosterol biosynthesis genes, including *ERG1* and *ERG11*, indicating a metabolic shift in response to endoplasmic reticulum (ER) stress. Furthermore, both TUN-induced and ethidium bromide-induced petites displayed cross-resistance to TUN and FLC but showed reduced tolerance to FLC.

Conclusion: These results underscore the pivotal role of TUN-induced ER stress in modulating FLC tolerance via respiratory deficiency and alterations in ergosterol metabolism. Our study emphasizes the importance of mitochondrial integrity in maintaining drug tolerance in *C. glabrata* and suggests potential therapeutic strategies targeting metabolic pathways associated with antifungal tolerance. A deeper understanding of these mechanisms may enhance our capacity to effectively combat fungal infections.

KEYWORDS

***Candida glabrata*, fluconazole tolerance, fluconazole resistance, petite, tunicamycin**

Introduction

The incidence of opportunistic fungal infections has been steadily increasing in recent years, particularly among immunocompromised individuals such as those with HIV/AIDS, cancer patients undergoing chemotherapy, and organ transplant recipients. Among these pathogens, *Candida* species are significant contributors to morbidity and mortality (Fisher et al., 2022). Epidemiological studies indicate that *C. glabrata* is one of the most frequently isolated *Candida* species in clinical settings, surpassing *C. albicans* in certain patient populations (Lamoth et al., 2018). The rise of *C. glabrata* infections is concerning, as this yeast demonstrates intrinsic resistance to many antifungal agents and exhibits an alarming capability for acquiring resistance during treatment. This shift highlights the urgent need for effective therapeutic strategies and a deeper understanding of the molecular mechanisms underlying drug tolerance and resistance (Brunke and Hube, 2013).

Fluconazole (FLC) has long been a cornerstone of antifungal therapy due to its broad-spectrum activity against various *Candida* species, including *C. glabrata*. It is widely used for both prophylactic and therapeutic purposes in treating candidiasis. However, the emergence of FLC-resistant strains poses a significant challenge to successful treatment outcomes (Lee et al., 2023).

In addition to drug resistance, characterized by elevated minimum inhibitory concentrations (MIC) of antifungal agents, a new term—antifungal tolerance—has recently been introduced to describe the ability of drug-susceptible fungal strains to grow slowly in the presence of supra-MIC concentrations of these agents (Rosenberg et al., 2018; Berman and Krysan, 2020). FLC tolerance can be assessed using disk diffusion assays, where FLC-susceptible strains exhibit an obvious zone of inhibition (ZOI). In these assays, photographs of the plates are analyzed using the *diskImageR* pipeline. The level of drug resistance is measured by the radius of ZOI (RAD), while tolerance is evaluated based on the fraction of growth (FoG) within the ZOI (Gerstein et al., 2016; Berman and Krysan, 2020). While FLC tolerance has been best studied in *C. albicans*, it is noteworthy that *C. glabrata* is more closely related to *Saccharomyces cerevisiae* than to other *Candida* species, sharing significant genetic and evolutionary similarities. This relationship sets *C. glabrata* apart within the *Candida* genus and influences our understanding of its biology, pathogenicity, and response to antifungal treatments (Roetzer et al., 2011).

We have recently demonstrated that FLC tolerance exists in wild-type *C. glabrata* isolates and can be induced by exposure to FLC. Furthermore, similar to findings in *C. albicans*, we showed that FLC tolerance in *C. glabrata* is dependent on the heat shock protein Hsp90 and calcineurin (Zheng et al., 2024b). However, the factors modulating FLC tolerance in *C. glabrata* remain largely unknown.

Tunicamycin (TUN) is a widely used inducer of endoplasmic reticulum (ER) stress. TUN inhibits UDP-N-acetylglucosamine-dolichol phosphate N-acetylglucosamine-1-phosphate transferase (GPT), thereby blocking the initial step of glycoprotein biosynthesis in the ER. This inhibition leads to the accumulation of unfolded glycoproteins in the ER, triggering ER stress (Lee, 1992). TUN has been linked to drug resistance in both mammalian and yeast cells. Specifically, the inhibition of glycosylation by TUN sensitizes multidrug-resistant (MDR) gastric cancer cells to TUN-induced cell death (Wu et al., 2018), as well as enhancing the sensitivity of MDR cell lines, such as NIH-3T3 and KB-8-5-11, to a range of chemotherapeutic agents (Hiss et al., 1996). In the diploid fungal pathogen *Candida albicans*, TUN induces amplification of chromosome 2, which results in the upregulation of several genes associated with tolerance to caspofungin, the first-line antifungal drug. This genetic adaptation potentiates cross-tolerance to both TUN and caspofungin (Yang et al., 2021). In the haploid fungal pathogen *Cryptococcus neoformans*, TUN induces formation of multiple aneuploid karyotypes, and some aneuploids, including disomy of chromosome 1 and chromosome 4, are cross-resistant to TUN and FLC (Zheng et al., 2024a). Previous studies have demonstrated that TUN can serve as an adjuvant to eliminate FLC tolerance in *C. albicans*; however, the underlying mechanism remains unexplored (Rosenberg et al., 2018). In this study, we investigated the effect of TUN on FLC tolerance in *C. glabrata* and sought to elucidate the mechanisms involved.

Materials and methods

Strains and growth conditions

The *C. glabrata* FLC-tolerant isolates CG4 and CG8, and the non-tolerant reference strain BG2 served as the progenitors for this study. The profile of FLC tolerance in CG4 has been detailed in our previous report (Zheng et al., 2024b). Stock cultures were preserved in 25% glycerol and stored at −80°C. Cells were routinely cultured in Yeast Extract-Peptone-Dextrose (YPD) medium, which contains 1% (w/v) yeast extract, 2% (w/v) peptone, and 2% (w/v) D-glucose, at 30°C using a shaking incubator set to 150–200 rpm. For YPG medium, the composition included 1% (w/v) yeast extract, 0.2% (w/v) peptone, and 3% (w/v) glycerol, with 2% (w/v) agar added for solid media. Drug solutions were prepared in dimethyl sulfoxide (DMSO) and stored at −20°C.

Disk diffusion assay

Disk diffusion assays were performed according to the protocols outlined in our previous studies (Guo et al., 2024; Zheng et al., 2024b; Zheng et al., 2024c), following the CLSI M44-A2 guidelines for antifungal disk diffusion susceptibility testing (CLSI, 2009), with minor modifications. Briefly, strains were streaked from glycerol stocks onto YPD agar plates and incubated at 30°C for 48 h. Colonies were then suspended in distilled water and adjusted to a concentration of 1×10^6 cells/mL. A volume of 100 µL of this cell suspension was evenly spread across YPD plates. An empty paper disk (6 mm diameter and 0.7 mm thickness) was saturated with 5 µL of 40 mg/mL FLC and placed at the center of each plate. The plates were subsequently incubated at 30°C and photographed after 48 h. The analysis of the disk diffusion assay was conducted using the *diskImageR* pipeline (Gerstein et al., 2016), measuring parameters such as the fraction of growth within the zone of inhibition (FoG) and the radius of inhibition (RAD).

Selection of colonies from the inhibition zone on YPD + TUN plates

For the isolation process, cells were suspended in distilled water and carefully adjusted to a concentration of 1×10^6 cells/

mL. Subsequently, 100 µL of this cell suspension was evenly spread onto a YPD plate supplemented with 1 µg/mL TUN. An empty paper disk saturated with 5 µL of 40 mg/mL FLC was placed at the center of the plate.

Following an incubation period of 48 h at 30°C, four colonies were randomly selected from within the ZOI for further examination. These chosen colonies were streaked onto fresh YPD plates and underwent an additional 48-h incubation. From each replicate, a single colony was then meticulously chosen to progress to the subsequent stage of meticulous analysis and exploration.

Acquiring adaptors through elevated tunicamycin concentrations

The cells were suspended in distilled water and adjusted to a concentration of 1×10^7 cells/mL. Subsequently, 100 µL of this cell suspension was evenly spread on YPD plates supplemented with TUN. The plates were then incubated at 30°C for a duration of 5 days, after which adaptors were randomly chosen from the drug-treated plates.

Spot assay

Cells were suspended in distilled water and adjusted to a concentration of 1×10^7 cells/mL. A volume of 3 µL of the cell suspension was spotted onto YPD or YPG plates. For testing susceptibility to TUN, 3 µL of 10-fold serial dilutions were spotted on YPD plates containing 8 µg/mL TUN. The plates were incubated at 30°C and photographed after 48 h.

Induction of petite formation using ethidium bromide

The technique for inducing petite formation with Ethidium bromide (EtBr) was adapted from Fox et al. (1991) with slight modifications. Thawed test strains were streaked onto YPD plates and incubated at 30°C for 48 h. A single colony was then inoculated into YPD broth with 25 µg/mL EtBr, followed by transfer to a second culture with the same medium. Saturated cultures were streaked onto YPD plates to isolate colonies, which were subsequently streaked onto YPD and YPG plates to confirm respiratory deficiency.

RNA extraction, synthesis of complementary DNA and quantitative real-time PCR

To compare between progenitor and petite strains, they were cultured in YPD broth until reaching the logarithmic phase (OD_{600} = 1.0). To assess the effect of TUN on gene expression, the logarithmic phase cultures were split into two groups. One group received 8 µg/mL TUN supplementation, while the other was supplemented with an equivalent amount of vehicle. After a 3-h incubation period, the cells were harvested by centrifugation.

Total RNA was extracted using YeaStar RNA kit (Zymo Research) following the manufacturer's guidelines. The RNA concentration and purity were evaluated with a spectrophotometer (NanoDrop 2000C; ThermoFisher Scientific) through absorbance measurements at 230 nm (OD_{230}), 260 nm (OD_{260}), and 280 nm (OD_{280}). Additionally, RNA integrity was confirmed by electrophoresis on 1% denaturing and non-denaturing agarose gels in selected samples.

The RNA samples were treated with DNase I (ThermoFisher Scientific) at 37°C for 30 min following the manufacturer's protocol. Approximately 1 µg of total RNA underwent reverse transcription (RT) using High Capacity cDNA Reverse Transcription Kit (ThermoFisher Scientific).

The expression of candidate genes was quantified by real-time RT-PCR using the CFX96 Touch Real-Time PCR system (Bio-Rad). The housekeeping *ACT1* was used as internal control. The relative quantification of gene expression was performed by the $2^{-\Delta\Delta CT}$ method (Schmittgen and Livak, 2008). Each reaction was performed in triplicate, and mean values of relative expression were determined for each gene. Primers are listed in Supplementary Table S1.

Measurement of FLC minimal inhibitory concentration

The experiment was performed according to the Clinical and Laboratory Standards Institute (CLSI) recommendations (CLSI, 2017) with slight modifications. Briefly, yeast cells were harvested during the logarithmic growth phase, washed twice with sterile distilled water, and resuspended in distilled water. The cell density was adjusted to a final concentration of 2.5×10^3 cells/mL in YPD broth supplemented with fluconazole (FLC) at concentrations ranging from 0.125 to 128 µg/mL. The cell suspensions were then aliquoted into 96-well microtiter plates, with each well containing 200 µL of the suspension. The plates were incubated at 30°C for 24 h under static conditions. After incubation, the optical density at 600 nm (OD600) was measured using a microplate reader to quantify cell growth. Each condition was tested in triplicate to ensure reproducibility, and control wells containing YPD broth without FLC were included to account for background growth.

Multilocus sequence typing

Multilocus sequence typing (MLST) analysis was conducted as previously described by Dodgson et al. (2003). Six loci (*FKS*, *LEU2*, *NMT1*, *TRP1*, *UGP1*, and *URA3*) were amplified using the primers specified in Dodgson et al. (2003). PCR reactions were carried out in 20-µL volumes containing 5 ng of genomic DNA, 10 µL of 2 × Phusion Green Hot Start II High-Fidelity PCR Master Mix (Fisher Scientific), and 0.1 µM of each primer. The amplified products were sequenced bidirectionally (forward and reverse) using the same primers as those employed for the PCR amplification.

Statistical analysis

All disk diffusion assays represent the average of three technical replicates, with error bars indicating the standard deviation. Statistical

analyses were conducted using a two-tailed Student's *t*-test in Microsoft Excel. A *p*-value of less than 0.05 was considered statistically significant. ** indicates $p < 0.01$, and *** indicates $p < 0.001$.

Results

Tunicamycin disrupts fluconazole tolerance in clinical isolates of *Candida glabrata* without affecting resistance

In our study, we evaluated the effects of TUN on the FLC tolerance of three clinical isolates of *C. glabrata*. Each isolate exhibited a notable tolerance to FLC, as evidenced by the presence of significant lawn growth within ZOI. In a pilot experiment, we tested the effect of various concentrations of TUN on FLC tolerance in CG4. We found that 0.5 μg/mL of TUN did not abolish FLC tolerance, whereas 1 and 2 μg/mL concentrations effectively eliminated FLC tolerance. At 4 μg/mL, the growth of most cells on the plate was inhibited (Supplementary Figure S1). Based on these results, we selected 1 μg/mL of TUN to assess its impact on FLC tolerance in CG4, as well as in two other *C. glabrata* isolates, CG8 and CG10.

Upon the supplementation of 1 μg/mL TUN, a marked change in the response was observed in all the 3 isolates: the ZOI became clear, indicating a loss of FLC tolerance (Figure 1, top panel).

Quantitative assessments revealed that a concentration of TUN at 1 μg/mL led to a significant decrease of FoG_{20} values across all three tested isolates, with statistical significance confirmed ($p < 0.001$, two-tailed Student's *t*-test). Interestingly, while TUN effectively diminished FLC tolerance, it did not appear to affect the RAD_{20} (Figure 1, bottom panel), indicating that TUN's mechanism of action primarily targets pathways associated with tolerance rather than directly impacting resistance mechanisms.

Emergence of respiratory-deficient mutants in *Candida glabrata* driven by combined stress from tunicamycin and fluconazole treatment

While TUN effectively abolished FLC tolerance in our experiments, we noted an intriguing phenomenon during the testing of the CG4 isolate; a few exceptionally large colonies were observed within ZOI, as indicated by red arrows in Figure 2A. To further investigate this anomaly, we randomly selected four of these colonies, designated as #1 through #4, for analysis.

Interestingly, although the progenitor strain CG4 was capable of growing on YPG plate—where glycerol served as the carbon source—none of the four chosen colonies exhibited growth under the same conditions. This observation suggests that these colonies may be petites, which are characterized by respiratory deficiencies due to defects in mitochondrial function (Figure 2B).

To assess the impact of TUN on these four colonies, we conducted a spot assay, which revealed that each of the four colonies demonstrated improved growth compared to the parental CG4 strain when exposed to TUN (Figure 2C). This finding indicates a possible adaptive response or compensatory mechanism in the petites that enhances their proliferation in the presence of TUN.

Furthermore, results from a disk diffusion assay using disks containing FLC showed that all four colonies exhibited clear ZOI with reduced overall size (Figure 2D). Quantitative analysis of the disk diffusion assay images confirmed that all four colonies had significantly lower values for both FoG_{20} and RAD_{20}, with statistical

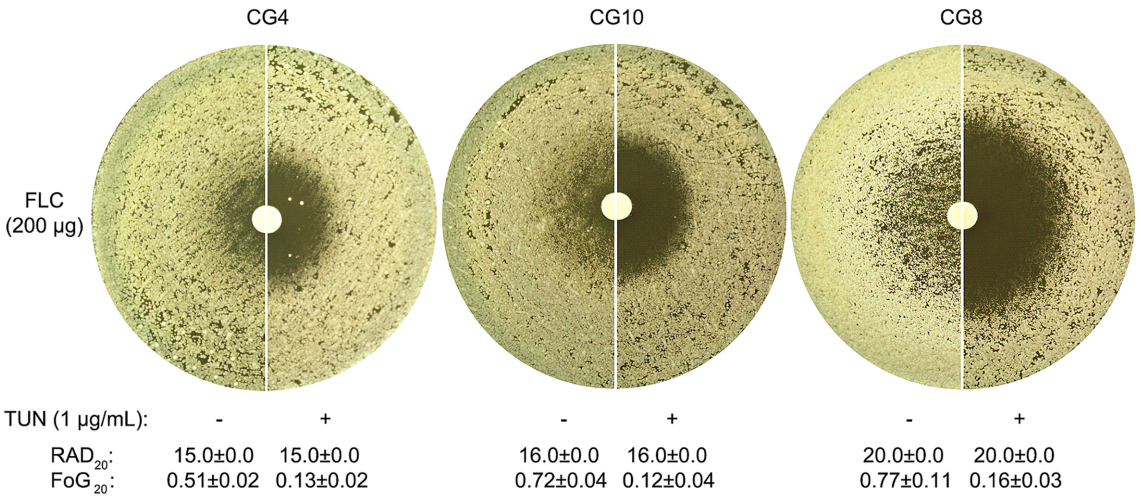

FIGURE 1
Impact of tunicamycin on fluconazole tolerance and resistance in *C. glabrata*. Top Panel: Three clinical isolates of *C. glabrata* were tested on YPD agar plates, both with and without the addition of TUN. Each disk contained 200 μg of FLC. The plates were incubated at 30°C for 48 h before being photographed to assess the growth response. Bottom Panel: Photographs were edited using ImageJ prior to quantification with the R package *diskImageR*. The images were cropped to a uniform size, colors were inverted, and brightness and contrast were adjusted using consistent parameters across all images to enhance the contrast between the white disk and black background. Susceptibility was measured as RAD_{20}, the radius where 20% reduction of growth occurs, while tolerance was measured as FoG_{20}, the fraction of growth above RAD_{20}. The RAD_{20} and FoG_{20} values shown represent the means ± standard deviation of three biological replicates for each isolate.

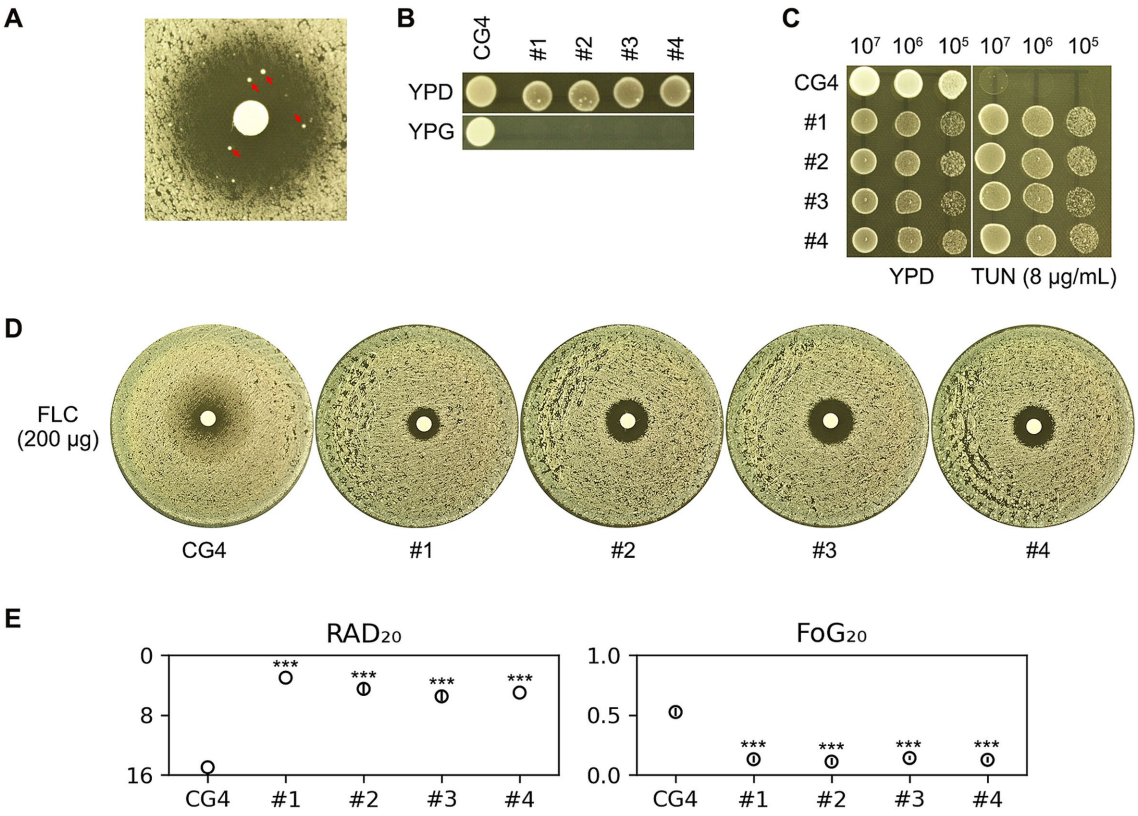

FIGURE 2
Assessment of antifungal susceptibility and growth characteristics in CG4 and derived colonies under tunicamycin and fluconazole treatment. **(A)** The CG4 isolate was subjected to a disk diffusion assay using disks containing 200 μg of FLC. The assay was conducted on YPD medium supplemented with 1 μg/mL of TUN. After a 48-h incubation period, we observed the emergence of several unusually large colonies within ZOI, which were clearly distinguishable. Four of these colonies, indicated by red arrows in the image, were selected for further analysis. **(B)** To investigate the growth characteristics of the progenitor strain CG4 and the selected four colonies (#1-#4), we performed spot assays on both YPD and YPG plates. The YPD plates utilize glucose as the carbon source, while the YPG plates utilize glycerol. This comparison allowed us to assess the respiratory capabilities of these colonies in different nutrient contexts. **(C)** A spot assay was executed on both YPD and YPD plates supplemented with 8 μg/mL TUN. For this assay, 3 μL of 10-fold serial dilutions of each strain were spotted onto the plates. This method enabled us to evaluate the growth patterns and stress responses of each isolate in the presence of TUN. **(D)** In parallel, another disk diffusion assay was performed utilizing disks impregnated with 200 μg of FLC. This experiment aimed to quantify the antifungal susceptibility of the isolates, providing further insight into their resistance profiles. **(E)** The images obtained from the disk diffusion assay plates were quantified using the *diskImageR* package. Results are presented as the mean and standard deviation from three biological replicates for each isolate. Statistical analysis was conducted using a two-tailed Student's *t*-test to determine significance. Asterisks denote statistical significance, with *** indicating $p < 0.001$ when compared to the progenitor strain CG4. For all assays, the plates were incubated at 30°C for 48 h prior to photography.

significance denoted ($p < 0.001$, two-tailed Student's *t*-test). These results collectively indicate that the four colonies not only lost FLC tolerance but also gained FLC resistance (Figure 2E).

Tunicamycin-induced petite formation alters fluconazole tolerance and resistance

In the experiments described above, the progenitor strain CG4 was exposed to a combination of TUN and FLC. In this section, we investigate the impact of TUN alone on the CG4 isolate. To assess this, CG4 cells were spread on YPD plates containing varying concentrations of TUN. Notably, on the plate with 16 μg/mL TUN, several hundred colonies emerged, which we refer to as "adaptors." In contrast, lower concentrations of TUN resulted in a uniform lawn growth across the plates (Figure 3A).

From the colonies that appeared at the highest concentration, we randomly selected 16 adaptors for further analysis. These adaptors were then compared to the progenitor strain in terms of their resistance to TUN. A spot assay demonstrated that all 16 adaptors were capable of growing in the presence of 8 μg/mL TUN, while the progenitor strain exhibited marked inhibition of growth under the same conditions (Figure 3B). Thus, all the 16 adaptors gained resistance to TUN.

Next, we evaluated the ability of these adaptors to utilize glycerol as a carbon source, which is indicative of respiratory competency. Of the 16 adaptors tested, four—specifically #9, #10, #12, and #16—were able to grow on YPG plates, suggesting that the majority of the adaptors (12 out of 16) exhibited respiratory deficiencies (Figure 3C).

Lastly, we assessed the susceptibility of the adaptors to FLC. The petite adaptors demonstrated significantly RAD_{20} and FoG_{20} compared to the progenitor strain, indicating that they had lost FLC tolerance and gained FLC resistance. In contrast, the non-petite adaptors did not show significant changes in RAD_{20} or FoG_{20} when compared to the progenitor (Figure 3D).

10.3389/fmicb.2025.1528341

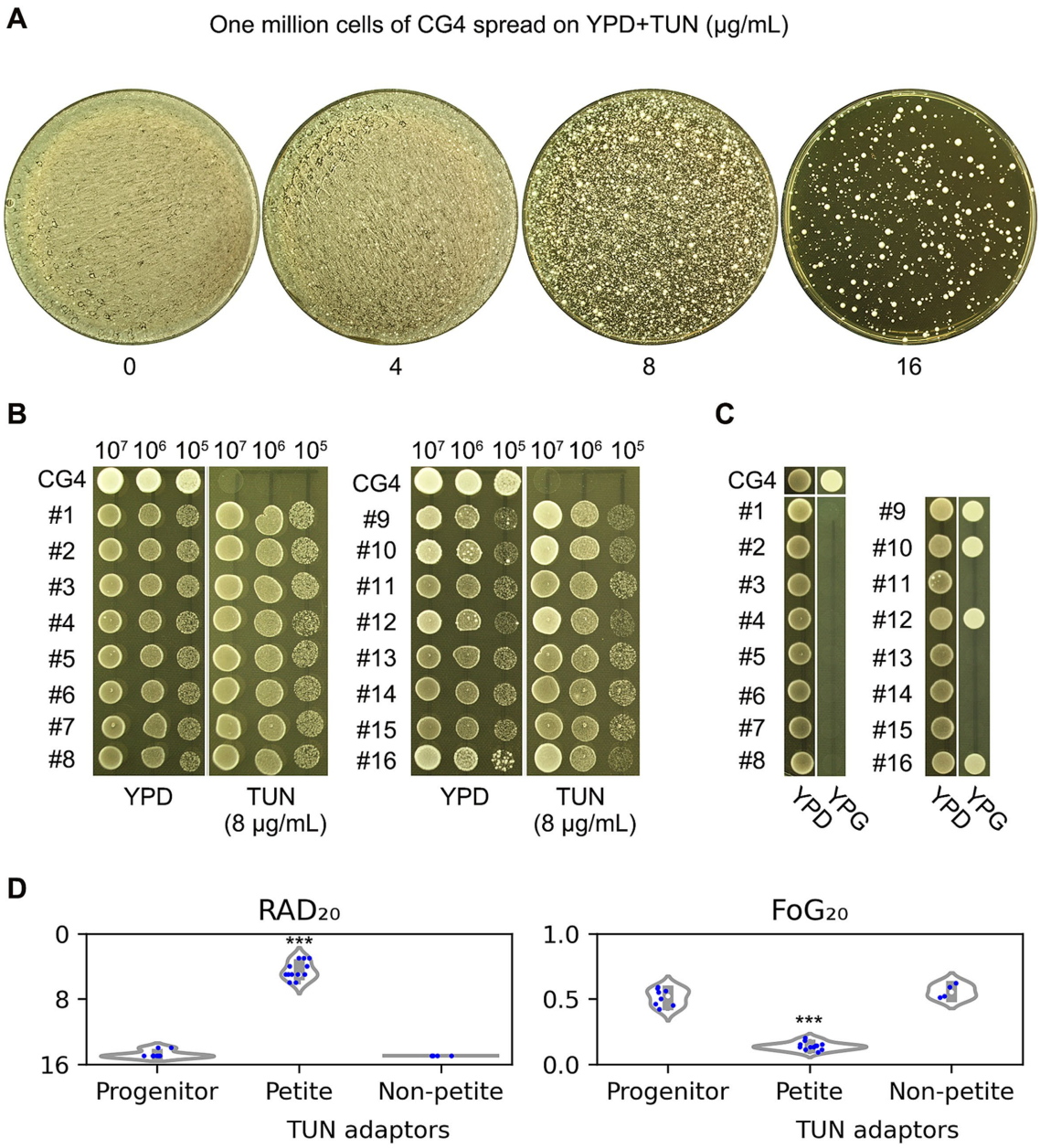

FIGURE 3
Impact of tunicamycin on fluconazole susceptibility and respiratory proficiency. **(A)** Cells of the CG4 strain were suspended in distilled water and adjusted to a concentration of 1×10^7 cells/mL. A volume of 100 μL of this cell suspension was then spread onto YPD plates supplemented with 4–16 μg/mL TUN. The plates were incubated at 30°C for 3 days before being photographed. From the plate containing 16 μg/mL TUN, 16 randomly selected colonies (referred to as "adaptors") were chosen for further analysis. **(B)** Both the progenitor strain and the TUN adaptors were evaluated for resistance to TUN using a spot assay. For each strain, cells were adjusted to 5×10^7 cells/mL. A volume of 3 μL from 10-fold serial dilutions of each strain was spotted onto YPD plates with or without 8 μg/mL TUN. The plates were incubated at 30°C for 48 h and subsequently photographed. **(C)** The adaptors were assessed for respiratory proficiency. For each strain, cells were again adjusted to 5×10^7 cells/mL using distilled water, and 3 μL were spotted onto both YPD and YPG plates. After incubation at 30°C for 48 h, the plates were photographed. Among the adaptors, four—specifically #9, #10, #12, and #16—were able to grow on YPG, while the remaining 12 adaptors were unable to do so. **(D)** To evaluate susceptibility to FLC, a disk diffusion assay was performed using disks containing 200 μg of FLC. The resulting images were analyzed using the *diskImageR* package. Results are presented as the mean of three biological replicates for each strain. Statistical analysis was conducted using a two-tailed Student's *t*-test to assess significance. Asterisks denote statistical significance, with *** indicating $p < 0.001$ when compared to the progenitor strain CG4.

Susceptibility to FLC was further assessed by determining the minimum inhibitory concentration (MIC). The progenitor strain and non-petite TUN adaptors exhibited MICs of 16 μg/mL, whereas the petite TUN adaptors showed significantly higher MICs, ranging from 64 to 128 μg/mL.

Besides CG4, another isolate, CG8, was also tested. We found that TUN at a concentration of 8 μg/mL significantly inhibited the growth of CG8 (Supplementary Figure S2A). Twelve adaptors (#1-#12) were randomly selected, and three of them (#3, #8, and #9) failed to grow on YPG plates (Supplementary Figure S2B). Disk diffusion assays

showed that the petite adaptors had significantly lower FoG_{20} and smaller RAD_{20} values compared to the wild-type ($p < 0.001$, two-tailed Student's *t*-test), while the non-petite adaptors did not exhibit significant changes in FoG_{20} or RAD_{20} ($p > 0.05$, two-tailed Student's *t*-test).

In addition to the two clinical isolates, the reference strain BG2 was also tested. We found that TUN at 8 μg/mL significantly inhibited BG2 (Supplementary Figure S3A). From a pool of randomly selected adaptors (#1-#30), eight were identified as petites (Supplementary Figure S3B). Both the progenitor BG2 strain and the non-petite TUN adaptors exhibited clear zones of inhibition (ZOI) with similar values for RAD and FoG. In contrast, the petite adaptors showed no detectable ZOI, indicating a high level of resistance to FLC (Supplementary Figures S4C,D).

Characterization of EtBr-evolved petites: similar phenotypes of altered fluconazole susceptibility

From the experiments described above, we established a connection between respiratory deficiency and resistance to TUN, as well as altered susceptibility to FLC, characterized by decreased tolerance and increased resistance. Notably, these petites were selected either through exposure to TUN alone or a combination of TUN and FLC. To explore whether petites selected under different stress conditions exhibit similar phenotypes, we turned our attention to Ethidium Bromide (EtBr). EtBr is known to inhibit mitochondrial DNA (mtDNA) synthesis and induce degradation of pre-existing mtDNA, leading to the conversion of respiratory-sufficient yeast into respiratory-deficient petites (Goldring et al., 1970).

In our study, CG4 was cultured in YPD broth supplemented with EtBr. After 24 h of incubation, the culture was diluted and subsequently spread onto YPD plates. From this plating, six randomly selected colonies were tested for their ability to grow on YPG, which serves as an indicator of respiratory competency. None of the selected colonies could grow on YPG, confirming that all were indeed petites (Figure 4A). We designated these colonies as "EtBr-evolved petites."

Further analysis using a spot assay revealed that the EtBr-evolved petites exhibited superior growth compared to the progenitor strain in the presence of 8 μg/mL TUN, indicating a level of resistance to TUN (Figure 4B). Additionally, results from a disk diffusion assay demonstrated that all six petites had clear but smaller ZOI in comparison to the progenitor strain, suggesting that they lost FLC tolerance while gaining FLC resistance (Figure 4C).

Petites have increased expression of efflux genes and reduced expression of *ERG* genes

Resistance to azoles typically arises from increased efflux and alterations in the target (Lee et al., 2023). In the *C. glabrata* genome, drug efflux is primarily mediated by ATP-binding cassette transporters, particularly through the *C. glabrata* sensitivity to 4-Nitroquinoline N-oxide (*CgSNQ2*) and *C. glabrata* Drug Resistance 1 and 2 (*CgCDR1* and *CgCDR2*) genes (Hassan et al., 2021). Moreover, *PDR1* encodes the central transcription factor that triggers the expression of *CDR1* (Moye-Rowley, 2020). Brun et al. identified that resistance in FLC-induced *C. glabrata* petites was attributed to the upregulation of efflux genes, particularly *CDR1* (Brun et al., 2004). In *Saccharomyces cerevisiae*, a model yeast closely related to *C. glabrata*, various respiratory inhibitors have diverse impacts on ergosterol biosynthesis (Adams and Parks, 1969). We hypothesize that TUN-induced and EtBr-induced petites might influence the expression of efflux and/or *ERG* genes, thereby enhancing FLC resistance while reducing FLC tolerance. Consequently, we compared the gene expressions between two petites and the parent CG4. One petite was induced by TUN exposure (TUN-induced petite, TiP), while the other was induced by EtBr exposure (EtBr-induced petite, EiP). Our findings revealed a significant increase in the expression of *CDR1* and *PDR1* compared to CG4 ($p < 0.001$, two-tailed Student's *t*-test), whereas the expression of most ERG genes, including *ERG1*, *ERG2*, *ERG3*, *ERG6*, *ERG7*, *ERG9*, *ERG11*, *ERG24*, *ERG25*, was significantly reduced ($p < 0.001$, two-tailed Student's *t*-test) in both types of petites (Figure 5A).

Next, we investigated the effect of TUN exposure on the expression of efflux and *ERG* genes. Exposure of CG4 to 8 μg/mL of TUN significantly down-regulated multiple *ERG* genes, including *ERG1*, *ERG2*, *ERG3*, *ERG9*, *ERG11*, and *ERG24* ($p < 0.001$, two-tailed Student's *t*-test). However, TUN had negligible effects on the expression of *CDR1*, *CDR2*, *SNQ2*, and *PDR1* ($p > 0.05$, two-tailed Student's *t*-test) (Figure 5B).

Discussion

Previous studies have established that azole tolerance in *C. albicans* is influenced by various physiological factors, including temperature, medium composition, and specific proteins such as Hsp90, calcineurin, V-ATPase, as well as aneuploidy (Xu et al., 2021; Kukurudz et al., 2022; Sun et al., 2023; Todd et al., 2023; Yang et al., 2023). Recently, we discovered that FLC tolerance in *C. glabrata* also depends on the heat shock protein Hsp90 and calcineurin (Zheng et al., 2024b). In the current study, we identify a novel factor—TUN-induced respiratory deficiency—that regulates FLC tolerance in *C. glabrata*, marking the first connection of this kind.

To assess the impact of TUN on FLC tolerance, we employed three distinct experimental approaches: (1) combining TUN with FLC, (2) exposing cells exclusively to TUN, and (3) utilizing an alternative method to induce petite formation. Our findings demonstrate that TUN can abolish FLC tolerance, primarily through the downregulation of ergosterol biosynthesis pathway genes.

TUN is a well-characterized inducer of ER stress, acting by inhibiting the enzyme UDP-N-acetylglucosamine: dolichol phosphate N-acetylglucosamine-1-phosphate transferase, which plays a critical role in the synthesis of N-linked glycans. Consequently, newly synthesized glycoproteins cannot undergo proper glycosylation, leading to the accumulation of misfolded or unprocessed proteins within the ER lumen. Cells have a limited capacity to manage this accumulation, prompting the activation of the unfolded protein response (UPR)—a cellular stress response mechanism aimed at restoring normal ER function (Lee, 1992).

Ergosterol, the major sterol found in fungal membranes, is synthesized in the ER through a complex pathway involving numerous enzymes encoded by the ERG genes in yeasts. In the *C. glabrata*

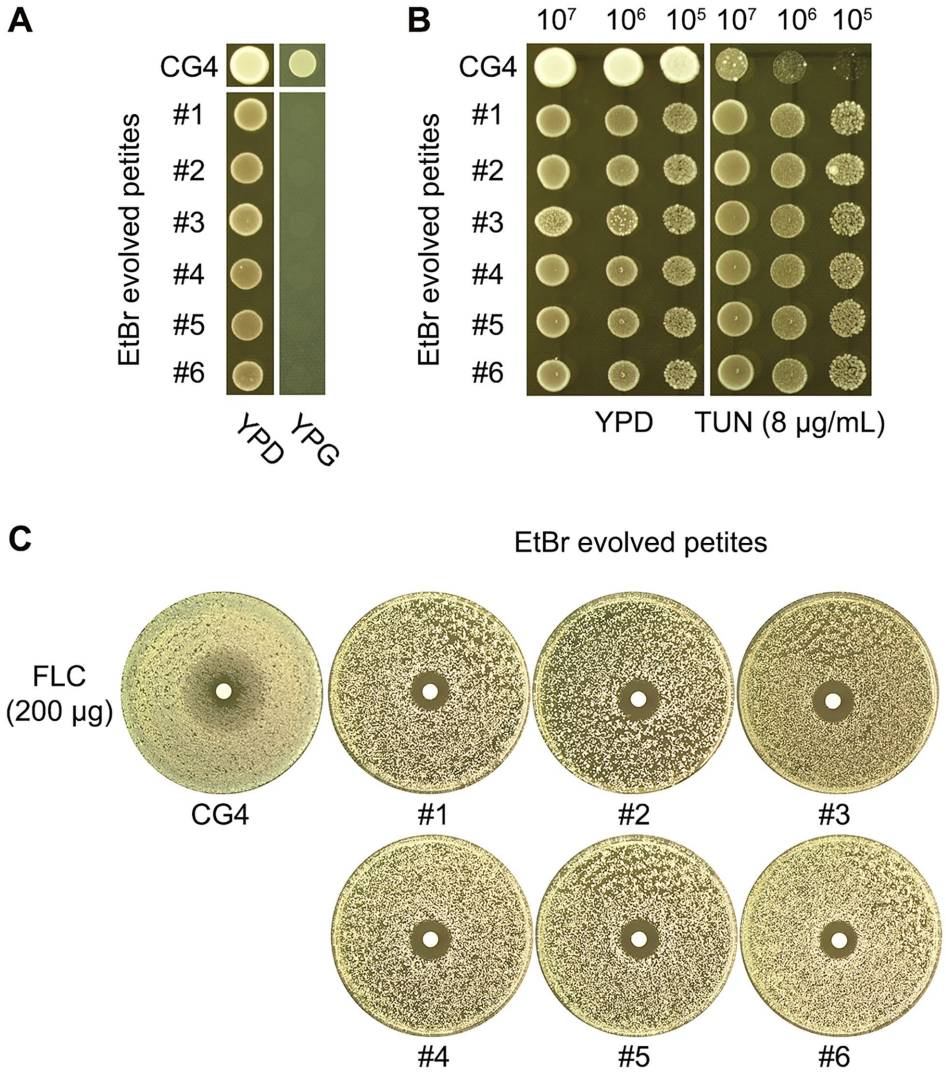

FIGURE 4
Characterization of EtBr-evolved petites: altered susceptibility to TUN and FLC. CG4 was pre-grown in YPD broth supplemented with Ethidium Bromide (EtBr) to induce the formation of respiratory-deficient petites. Six randomly selected colonies from this culture, labeled #1 through #6, were subsequently spotted onto both YPG and YPD plates to assess their respiratory proficiency **(A)**. To further investigate the phenotypic characteristics of the EtBr-evolved petites, we compared their susceptibility to TUN and FLC against the progenitor strain. Susceptibility to TUN was assessed using a spot assay **(B)**, which demonstrated that the EtBr-evolved petites (#1-#6) showed enhanced resistance to TUN compared to the progenitor CG4. Similarly, for FLC susceptibility, a disk diffusion assay was performed **(C)**. The results indicated that all six petites exhibited smaller ZOI compared to the progenitor, suggesting a loss of FLC tolerance and an increase in FLC resistance.

genome, these *ERG* genes include *ERG9/CAGL0M07095g, ERG1/CAGL0D05940g, ERG7/CAGL0J10824g, ERG11/CAGL0E04334g, ERG24/CAGL0I02970g, ERG25/CAGL0K04477g, ERG26/CAGL0G00594g, ERG27/CAGL0M11506g, ERG28/CAGL0J02684g, ERG6/CAGL0H04653g, ERG2/CAGL0L10714g, ERG3/CAGL0F01793g, ERG5/CAGL0M07656g, ERG4/CAGL0A00429g* (Eliaš et al., 2024). Notably, *ERG1* and *ERG11* represent two rate-limiting steps in the ergosterol biosynthesis pathway (Jorda and Puig, 2020).

The primary function of the UPR is to manage protein folding and restore ER homeostasis, necessitating regulatory shifts in metabolic priorities. Our study reveals that TUN-induced ER stress leads to reduced expression of ergosterol biosynthesis genes, including the key players *ERG1* and *ERG11*. This finding suggests that when the UPR is activated due to protein misfolding, the cell reallocates resources away from sterol biosynthesis to prioritize the resolution of ER stress. This supports the notion that the UPR not only oversees protein folding but also influences metabolic pathways vital for cellular integrity.

Additionally, we identified petite formation as a primary mechanism for rapid adaptation to TUN-induced ER stress in *C. glabrata*. We also evaluated petites induced by exposure to EtBr and found that both TUN-induced and EtBr-induced petites exhibited cross-resistance to TUN and FLC, albeit with a diminished tolerance to FLC. Notably, the expression of multiple *ERG* genes, including *ERG1* and *ERG11*, was lower in both types of petites compared to the wild-type strain.

Typically, petites are associated with a loss of mitochondrial function, significantly influencing cellular metabolism. The analysis of petites induced by EtBr underscores the similarity between TUN

10.3389/fmicb.2025.1528341

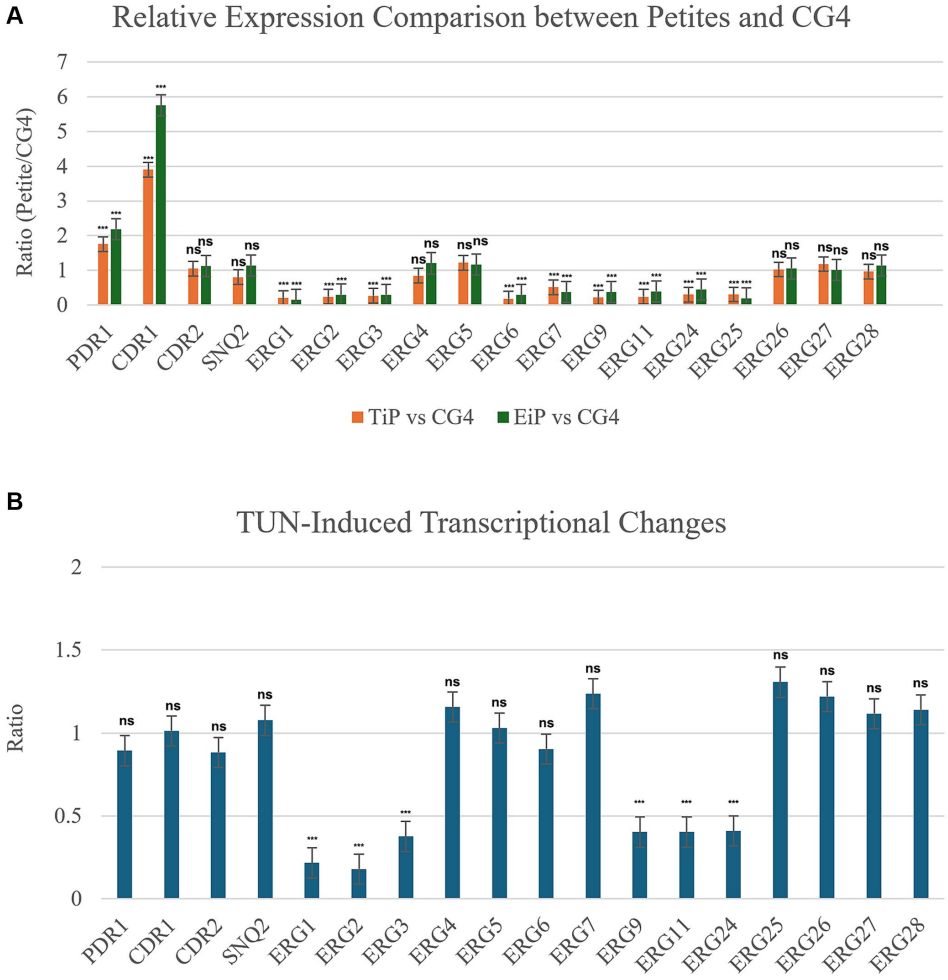

FIGURE 5
Relative expression analysis of efflux and ERG genes. **(A)** Comparison of gene expression between petite strains and progenitor CG4. Two petites were examined, TiP representing TUN-induced petite and EiP representing EtBr-induced petite. Cells were cultured to logarithmic phase, and the relative expression levels of genes in petites compared to CG4 are displayed in the figure. **(B)** Impact of TUN on gene expression. CG4 cells were grown to logarithmic phase and then treated with 8 μg/mL TUN. The graph illustrates the relative expression levels of genes in TUN-treated cells compared to vehicle-treated cells. In both A and B, the housekeeping *ACT1* was used as internal control. The relative quantification of gene expression was performed by the $2^{-\Delta\Delta CT}$ method. Each reaction was performed in triplicate, and mean values of relative expression were determined for each gene.

and EtBr in promoting cross-resistance to TUN and FLC, suggesting a shared adaptive response mechanism involving mitochondrial dysfunction and altered metabolic states. The observed reduction in the expression of multiple ergosterol biosynthesis genes in both types of petites reinforces the idea that perturbations in mitochondrial function adversely affect sterol metabolism. This reduction in key ERG gene expression implies that these petites may develop compensatory mechanisms to cope with drug stress, though this comes at the cost of FLC tolerance.

Reference to Siscar-Lewin et al.'s research highlights that deletion of the mitochondrial DNA polymerase *CgMIP1* triggers loss of mitochondrial function and petite formation, which also conveys cross-resistance to TUN and FLC (Siscar-Lewin et al., 2021). Our findings build upon this work, strengthening the hypothesis that mitochondrial integrity is essential for maintaining both ergosterol biosynthesis and drug tolerance in *C. glabrata* under stress conditions.

Notably, MLST analysis indicates that CG4 belongs to ST7, the most prevalent genotype in Asia (Meng et al., 2025). Our study demonstrates that TUN can disrupt FLC tolerance and induce FLC resistance in CG4. Given the prevalence of ST7 strains in Asia, these findings are likely to have broad applicability and relevance to other ST7 strains in this region, particularly in understanding how ER stress influences antifungal tolerance and resistance. However, further studies are needed to explore whether similar mechanisms operate in other ST7 strains. Such efforts will provide deeper insights into the epidemiology and treatment of *C. glabrata* infections, particularly in regions where ST7 is dominant.

Conclusion

In summary, our study uncovers a novel mechanism by which TUN-induced ER stress modulates FLC tolerance in *C. glabrata*. We demonstrate that this stress response leads to petite formation and reduction in ergosterol biosynthesis. This novel insight into the relationship between ER stress, mitochondrial dysfunction, antifungal

resistance and tolerance underscores potential avenues for developing more effective therapeutic strategies against resistant fungal strains.

Data availability statement

The original contributions presented in the study are included in the article/Supplementary material, further inquiries can be directed to the corresponding author.

Author contributions

LZ: Formal analysis, Investigation, Methodology, Validation, Writing – review & editing. YD: Data curation, Formal analysis, Funding acquisition, Investigation, Methodology, Validation, Writing – review & editing. JW: Data curation, Validation, Writing – review & editing. MZ: Investigation, Validation, Writing – review & editing. YX: Formal analysis, Funding acquisition, Investigation, Writing – review & editing. LM: Investigation, Validation, Writing – review & editing. LG: Conceptualization, Data curation, Funding acquisition, Project administration, Resources, Writing – original draft, Writing – review & editing.

Funding

The author(s) declare that financial support was received for the research and/or publication of this article. This study was supported by the Science and Technology Development Plan of Suzhou (SLJ2022018), and Scientific Research Project of Suzhou Commission of Health (GSWS2020028) to LG, the National Natural Science Foundation of China (81402978), Natural Science Foundation of Shandong Province (ZR2023MH227), Medical and Health Science and Technology Project of Shandong Province (202402041035) to YX, Medical and Health Science and Technology Project of Shandong Province (202302041726) to YD.

Conflict of interest

The authors declare that the research was conducted in the absence of any commercial or financial relationships that could be construed as a potential conflict of interest.

Generative AI statement

The authors declare that no Gen AI was used in the creation of this manuscript.

Publisher's note

Supplementary material

The Supplementary material for this article can be found online at: https://www.frontiersin.org/articles/10.3389/fmicb.2025.1528341/full#supplementary-material

References

Adams, B. G., and Parks, L. W. (1969). Differential effect of respiratory inhibitors on ergosterol synthesis by Saccharomyces cerevisiae during adaptation to oxygen. *J Bacteriol* 100, 370–376. doi: 10.1128/jb.100.1.370-376.1969

Berman, J., and Krysan, D. J. (2020). Drug resistance and tolerance in fungi. *Nat. Rev. Microbiol.* 18, 319–331. doi: 10.1038/s41579-019-0322-2

Brun, S., Berges, T., Poupard, P., Vauzelle-Moreau, C., Renier, G., Chabasse, D., et al. (2004). Mechanisms of azole resistance in petite mutants of *Candida glabrata*. *Antimicrob. Agents Chemother.* 48, 1788–1796. doi: 10.1128/AAC.48.5.1788-1796.2004

Brunke, S., and Hube, B. (2013). Two unlike cousins: *Candida albicans* and *C. glabrata* infection strategies. *Cell. Microbiol.* 15, 701–708. doi: 10.1111/cmi.12091

CLSI (2009). Method for antifungal disk diffusion susceptibility testing of yeasts. *2nd* Edn. Wayne, PA: C.A.L.S. Institute.

CLSI (2017). Reference method for broth dilution antifungal susceptibility testing of yeasts. *4th* Edn. CLSI standard M27. Wayne, PA: Clinical and Laboratory Standards Institute.

Dodgson, A. R., Pujol, C., Denning, D. W., Soll, D. R., and Fox, A. J. (2003). Multilocus sequence typing of *Candida glabrata* reveals geographically enriched clades. *J. Clin. Microbiol.* 41, 5709–5717. doi: 10.1128/JCM.41.12.5709-5717.2003

Eliaš, D., Tóth Hervay, N., and Gbelská, Y. (2024). Ergosterol Biosynthesis and Regulation Impact the Antifungal Resistance and Virulence of Candida spp. *Stresses* 4, 641–662.

Fisher, M. C., Alastruey-Izquierdo, A., Berman, J., Bicanic, T., Bignell, E. M., Bowyer, P., et al. (2022). Tackling the emerging threat of antifungal resistance to human health. *Nat. Rev. Microbiol.* 20, 557–571. doi: 10.1038/s41579-022-00720-1

Fox, T. D., Folley, L. S., Mulero, J. J., McMullin, T. W., Thorsness, P. E., Hedin, L. O., et al. (1991). Analysis and manipulation of yeast mitochondrial genes. *Methods Enzymol.* 194, 149–165. doi: 10.1016/0076-6879(91)94013-3

Gerstein, A. C., Rosenberg, A., Hecht, I., and Berman, J. (2016). diskImageR: quantification of resistance and tolerance to antimicrobial drugs using disk diffusion assays. *Microbiology (Reading)* 162, 1059–1068. doi: 10.1099/mic.0.000295

Goldring, E. S., Grossman, L. I., Krupnick, D., Cryer, D. R., and Marmur, J. (1970). The petite mutation in yeast. Loss of mitochondrial deoxyribonucleic acid during induction of petites with ethidium bromide. *J. Mol. Biol.* 52, 323–335. doi: 10.1016/0022-2836(70)90033-1

Guo, L., Zheng, L., Dong, Y., Wang, C., Deng, H., Wang, Z., et al. (2024). Miconazole induces aneuploidy-mediated tolerance in *Candida albicans* that is dependent on Hsp90 and calcineurin. *Front. Cell. Infect. Microbiol.* 14:1392564. doi: 10.3389/fcimb.2024.1392564

Hassan, Y., Chew, S. Y., and Than, L. T. L. (2021). *Candida glabrata*: pathogenicity and resistance mechanisms for adaptation and survival. *J. Fungi (Basel)* 7:667. doi: 10.3390/jof7080667

Hiss, D., Gabriels, G., Jacobs, P., and Folb, P. (1996). Tunicamycin potentiates drug cytotoxicity and vincristine retention in multidrug resistant cell lines. *Eur. J. Cancer* 32, 2164–2172. doi: 10.1016/s0959-8049(96)00262-6

Jorda, T., and Puig, S. (2020). Regulation of ergosterol biosynthesis in *Saccharomyces cerevisiae*. *Genes (Basel)* 11:795. doi: 10.3390/genes11070795

Kukurudz, R. J., Chapel, M., Wonitowy, Q., Adamu Bukari, A. R., Sidney, B., Sierhuis, R., et al. (2022). Acquisition of cross-azole tolerance and aneuploidy in *Candida*

albicans strains evolved to posaconazole. *G3 (Bethesda)* 12:jkac156. doi: 10.1093/g3journal/jkac156

Lamoth, F., Lockhart, S. R., Berkow, E. L., and Calandra, T. (2018). Changes in the epidemiological landscape of invasive candidiasis. *J. Antimicrob. Chemother.* 73, i4–i13. doi: 10.1093/jac/dkx444

Lee, A. S. (1992). Mammalian stress response: induction of the glucose-regulated protein family. *Curr. Opin. Cell Biol.* 4, 267–273. doi: 10.1016/0955-0674(92)90042-b

Lee, Y., Robbins, N., and Cowen, L. E. (2023). Molecular mechanisms governing antifungal drug resistance. *NPJ Antimicrob. Resist.* 1:5. doi: 10.1038/s44259-023-00007-2

Meng, Q., Wang, H., Xiao, W., Mai, W., Liu, Y., Xiao, Y., et al. (2025). Prevalence, drug resistance and genetic diversity of *Candida glabrata* in the reproductive tract of pregnant women in Hainan and comparison with global multilocus sequence data. *Mycology* 1-18, 1–18. doi: 10.1080/21501203.2025.2461725

Moye-Rowley, W. S. (2020). Linkage between genes involved in azole resistance and ergosterol biosynthesis. *PLoS Pathog.* 16:e1008819. doi: 10.1371/journal.ppat.1008819

Roetzer, A., Gabaldon, T., and Schuller, C. (2011). From *Saccharomyces cerevisiae* to *Candida glabrata* in a few easy steps: important adaptations for an opportunistic pathogen. *FEMS Microbiol. Lett.* 314, 1–9. doi: 10.1111/j.1574-6968.2010.02102.x

Rosenberg, A., Ene, I. V., Bibi, M., Zakin, S., Segal, E. S., Ziv, N., et al. (2018). Antifungal tolerance is a subpopulation effect distinct from resistance and is associated with persistent candidemia. *Nat. Commun.* 9:2470. doi: 10.1038/s41467-018-04926-x

Schmittgen, T. D., and Livak, K. J. (2008). Analyzing real-time PCR data by the comparative C(T) method. *Nat. Protoc.* 3, 1101–1108. doi: 10.1038/nprot.2008.73

Siscar-Lewin, S., Gabaldon, T., Aldejohann, A. M., Kurzai, O., Hube, B., and Brunke, S. (2021). Transient mitochondria dysfunction confers fungal cross-resistance against phagocytic killing and fluconazole. *MBio* 12:e0112821. doi: 10.1128/mBio.01128-21

Sun, L. L., Li, H., Yan, T. H., Fang, T., Wu, H., Cao, Y. B., et al. (2023). Aneuploidy mediates rapid adaptation to a subinhibitory amount of fluconazole in *Candida albicans*. *Microbiol. Spectr.* 11, e0301622–e0303022. doi: 10.1128/spectrum.03016-22

Todd, R. T., Soisangwan, N., Peters, S., Kemp, B., Crooks, T., Gerstein, A., et al. (2023). Antifungal drug concentration impacts the Spectrum of adaptive mutations in *Candida albicans*. *Mol. Biol. Evol.* 40:msad009. doi: 10.1093/molbev/msad009

Wu, J., Chen, S., Liu, H., Zhang, Z., Ni, Z., Chen, J., et al. (2018). Tunicamycin specifically aggravates ER stress and overcomes chemoresistance in multidrug-resistant gastric cancer cells by inhibiting N-glycosylation. *J. Exp. Clin. Cancer Res.* 37:272. doi: 10.1186/s13046-018-0935-8

Xu, Y., Lu, H., Zhu, S., Li, W. Q., Jiang, Y. Y., Berman, J., et al. (2021). Multifactorial mechanisms of tolerance to ketoconazole in *Candida albicans*. *Microbiol. Spectr.* 9:e0032121. doi: 10.1128/Spectrum.00321-21

Yang, F., Gritsenko, V., Slor Futterman, Y., Gao, L., Zhen, C., Lu, H., et al. (2021). Tunicamycin potentiates antifungal drug tolerance via aneuploidy in *Candida albicans*. *MBio* 12:e0227221. doi: 10.1128/mBio.02272-21

Yang, F., Scopel, E. F. C., Li, H., Sun, L. L., Kawar, N., Cao, Y. B., et al. (2023). Antifungal tolerance and resistance emerge at distinct drug concentrations and rely upon different Aneuploid chromosomes. *MBio* 14:e0022723. doi: 10.1128/mbio.00227-23

Zheng, L., Xu, Y., and Guo, L. (2024a). Unveiling genome plasticity as a mechanism of non-antifungal-induced antifungal resistance in *Cryptococcus neoformans*. *Front. Microbiol.* 15:1470454. doi: 10.3389/fmicb.2024.1470454

Zheng, L., Xu, Y., Wang, C., Dong, Y., and Guo, L. (2024b). Parallel evolution of fluconazole resistance and tolerance in *Candida glabrata*. *Front. Cell. Infect. Microbiol.* 14:1456907. doi: 10.3389/fcimb.2024.1456907

Zheng, L., Xu, Y., Wang, C., and Guo, L. (2024c). Ketoconazole induces reversible antifungal drug tolerance mediated by trisomy of chromosome R in *Candida albicans*. *Front. Microbiol.* 15:1450557. doi: 10.3389/fmicb.2024.1450557

frontiers | Frontiers in Microbiology

TYPE Original Research
PUBLISHED 29 April 2025
DOI 10.3389/fmicb.2025.1546020

OPEN ACCESS

EDITED BY
Israel Nissan,
Ministry of Agriculture and Rural Development, Israel

REVIEWED BY
Patricia Ponce-Noyola,
University of Guanajuato, Mexico
Tong-Bao Liu,
Southwest University, China

*CORRESPONDENCE
Zhenying Zhang
✉ zhangzy@hku-szh.org
Fangliang Zheng
✉ flzheng1980@163.com

†These authors have contributed equally to this work and share first authorship

RECEIVED 16 December 2024
ACCEPTED 11 April 2025
PUBLISHED 29 April 2025

CITATION
Wang Y, Wu X, Fan X, Han C, Zheng F and Zhang Z (2025) Screening and transcriptomic analysis of anti-*Sporothrix globosa* targeting AbaA.
Front. Microbiol. 16:1546020.
doi: 10.3389/fmicb.2025.1546020

Screening and transcriptomic analysis of anti-*Sporothrix globosa* targeting AbaA

Ying Wang[1†], Xiaoyan Wu[2†], Xiyuan Fan[1], Chanxu Han[2], Fangliang Zheng[1*] and Zhenying Zhang[2,3*]

[1]Academy of Life Science, Liaoning University, Shenyang, China, [2]Department of Dermatology, University of Hong Kong Shenzhen Hospital, Shenzhen, China, [3]Department of Dermatology, The Eighth Affiliated Hospital, Sun Yat-sen University, Shenzhen, China

Introduction: Sporotrichosis is a fungal disease caused by a complex of *Sporothrix schenckii*, leading to chronic infections of the epidermis and subcutaneous tissue in both humans and animals.

Methods: Through virtual screening targeting the key gene *aba*A to screen out the small-molecule drugs to treat Sporotrichosis. To further validate the antifungal activity of small-molecule drugs, growth curves, minimum bactericidal concentration (MBC), and minimum inhibitory concentration (MIC) for *Sporothrix globosa* (*S. globosa*) and *Sporothrix schenckii* (*S. schenckii*) were measured. In addition, we have done animal experiments to explore the function of the drugs. At the same time, qRT-PCR and transcriptome were used to verify the important role of *aba*A gene in *Sporothrix*.

Results: Azelastine and Mefloquine effectively inhibit S. globosa and S. schenckii. MBC, and MIC for *S. globosa* and *S. schenckii* confirmed that both Azelastine and Mefloquine inhibited the growth of *S. globosa* and *S. schenckii*. Additionally, animal experiments demonstrated that Azelastine and Mefloquine reduced skin lesions in mice; post-treatment observations revealed improvements in inflammatory infiltration and granuloma formation. Through transcriptome analysis and qRT-PCR for validation, our findings demonstrate that the *aba*A gene plays a crucial role in regulating the attachment of the *Sporothrix* cell wall to the host matrix and in melanin regulation. Notably, when the *aba*A gene was inhibited, there was a marked increase in the expression of repair genes. These results emphasize the significance of the *aba*A gene in the biology of *Sporothrix*.

Discussion: Two small-molecule drugs exhibit the ability to inhibit *Sporothrix* and treat sporotrichosis both in vitro and in murine models, suggesting their potential for development as therapeutic agents for sporotrichosis. And qRT-PCR and transcriptome results underscore the significance of the *aba*A gene in *Sporothrix*. Our results lay the foundation for the search for new treatments for other mycosis.

KEYWORDS

***Sporothrix globosa*, *abaA* gene, virtual screening, small molecule drugs, transcriptomics**

1 Introduction

Sporotrichosis is a fungal disease that leads to chronic fungal infections of the epidermis and subcutaneous tissue in both humans and animals. The pathogenic fungi involved are primarily a complex of *S. schenckii* (Chakrabarti et al., 2014; Hu et al., 2024). In the classical infection pathway, conidia initiate the fungal infection through the interaction between an implanted wound and decaying plant tissue, which results in the classification of sporotrichosis as a type of rot

(Lopes-Bezerra et al., 2018; Lv et al., 2022; Liu et al., 2024). The main pathogens responsible for sporotrichosis include *Sporothrix schenckii, Sporothrix globosa*, and *Sporothrix brasiliensis* (Zu et al., 2020). In the northeastern region of our country, the predominant pathogenic strain is *Sporothrix globose*, however, this species remains underappreciated and poorly researched. To date, there is a limited amount of literature addressing its fundamental research and clinical implications (Nava-Pérez et al., 2022; Höft et al., 2022).

Sporothrix globosa is a dimorphic fungus to which immunocompromised individuals are particularly susceptible. This organism exists as mycelium in the environment at 25°C, from which conidia are released into the air, accompanied by fragments of the mycelium through wind and soil dispersion. When a wound comes into contact with soil or inhaled spores, the pathogen can enter the host at 37°C. Temperature changes can induce the transition to a new form-the yeast phase. Yeast forms are less readily recognized by the body's immune cells compared to mycelial forms, rendering them less likely to be targeted by the immune response. Consequently, the dimorphic fungus *S. globosa* is not pathogenic in its mycelial phase but becomes pathogenic in its yeast phase. The variation in symptoms following infection is influenced by the individual's immune status and differing genotypes. Overall, *S. globosa* exhibits weak virulence and typically presents with mild symptoms (Balkrishna et al., 2022).

Gene regulatory networks (GRN) control developmental events and play an important role in species evolution (Carroll, 2008; Levine, 2010; Smith et al., 2018), three DNA transcription factors, BrlA, AbaA, and WetA, regulate the developmental program of asexual fruiting bodies. BrlA activation program. AbaA regulates the development of conidiophore. In the *ΔabaA* mutant, the developmental program halts at the formation of the peduncle base. Consequently, the mutant conidiophores deform into globular structures that are dispersed across the rod-shaped peduncle base, resembling the appearance of an abacus (Clutterbuck, 1969). WetA controls the maturation of asexual spores (Etxebeste et al., 2019; Yu, 2010). Regarding research on the DNA-binding domain of the AbaA transcription factor, Borneman et al. cloned a homolog of the *Aspergillus nidulans abaA* gene, which encodes the ATTS/TEA DNA-binding domain transcriptional regulator, and transformed it into *Penicillium marneffei* (Borneman et al. 2000). Their findings indicate that the *abaA* gene plays a crucial role in the developmental process of transitioning from the mycelial phase to the yeast phase. Additionally, Alex et al. also demonstrated that the amino acid sequence of the AbaA transcription factor contains an ATTS/TEA DNA binding motif (Andrianopoulos and Timberlake, 1994). Targeted deletion of AbaA blocks asexual development at 25°C prior to spore production, resulting in abnormal conidia with repeat terminal cells. Furthermore, the *abaA* deletion strain fails to properly switch from multinucleated filamentous forms to mononucleated yeast cells at 37°C. Many studies have found the DNA-binding domain of *abaA* gene is conserved and plays an important role in dimorphic switching (Andrianopoulos and Timberlake, 1994).

In recent years, the emergence of multi-resistant pathogens has made fungal infections increasingly difficult to treat. Consequently, strategies for managing hospital infections and opportunistic infections have garnered significant attention within the scientific community (Perlroth et al., 2007; Badiee and Hashemizadeh, 2014). Currently, treatment options for sporotrichosis are limited, and emerging resistance is a concern (Zhang et al., 2024; Brown-Elliott et al., 2001), there was no improvement observed after 16 months of treatment with terbinafine, fluconazole, and itraconazole. Consequently, there is an urgent need for new treatments for sporotrichosis.

Molecular docking is an important technology in computer-aided drug design, which is widely used in new drug development (Farha and Brown, 2019). The process of researching and developing new drugs is lengthy and requires substantial financial resources. Currently, the issue of fungal drug resistance is becoming increasingly severe. In recent years, a notable trend has emerged in the development of new drugs that involves the integration of various disciplines, particularly the combination of biology, computer science, and chemistry. With advancements in computer science, computer-aided drug design has become a prominent focus in the development of new drugs, especially through the use of molecular docking techniques (Swamidass, 2011; Jadamba and Shin, 2016). The development of new drugs is a lengthy and inefficient process, primarily due to challenges related to identifying new targets, ensuring safety, and managing significant associated costs. Consequently, repurposing drugs that have already been approved for other human conditions may offer a more expedient approach to discovering new antifungal agents. In various areas of clinical research, drug repurposing has emerged as a strategy to accelerate the development of new therapies, often utilizing drug-based phenotypic screening methods or high-throughput screening of FDA-approved drug libraries (Park, 2019). In this context, target recognition can be used to target new diseases for drug repurpose (Ma et al., 2022). So this study will look for new ways to treat sporotrichosis through a combination of bioinformatics and traditional experiments. The *abaA* gene plays a crucial role in the dimorphic switch of *Sporothrix*, and the downstream virulence factors, along with other related genes regulated by the *abaA* gene, were also investigated using bioinformatics and transcriptomic methods.

2 Materials and methods

2.1 Screening of small molecule drugs targeting AbaA protein

The target was AbaA protein, a key dimorphic switch protein of *S. schenckii*, used the Robetta[1] to predict the three-dimensional structure of AbaA, the DNA binding domain of AbaA protein was found by bioinformatics analysis. Then, the DNA-binding domain portion of the model's highest-quality three-dimensional structure was truncated for binding pocket prediction. The grid box was determined by aligning the structure of the AbaA DNA domain, and the x, y, and z-coordinates of the grid box ($x = 67.154$, $y = 85.033$, $z = -92.830$; $x = 58.693$, $y = 85.350$, $z = -82.023$) were determined. AutoDock Vina was then used to perform bulk molecular docking in the FDA-approved small molecule database, the docking results were comprehensively analyzed in terms of binding energy, price, pharmacodynamics and side effects (Moreira et al., 2021; Haozhen et al., 2023).

2.2 Fungal strain and culture conditions

The strain of *S. globosa*, *S. schenckii* used was maintained at the Research Center for Pathogenic Fungi, Liaoning University, China. To obtain a mycelial culture, the *S. globosa*, *S. schenckii* was inoculated onto Sabouraud dextrose agar (SDA) solid medium (10 g/L tryptone, 40 g/L glucose, 15 g/L agar) and incubated at 25°C. To induce the

1 https://robetta.bakerlab.org/

switch of *S. globosa* and *S. schenckii* from the mycelial phase to the yeast phase, mycelial culture was enriched and transferred to brain-heart infusion (BHI) liquid medium, which was incubated at 37°C.

2.3 *In vitro* antifungal susceptibility

Antifungal susceptibility testing was performed using the protocols described in the CLSI document. *Sporothrix* was cultured at 25°C for 4 days, followed by filtration and centrifugation. The spores were resuspended in autoclaved BHI liquid medium, adjusting the spore concentration to 1×10^5 CFU/mL. In a 96-well plate, 200 μL of the test drug working solution was added to Well 1, while 100 μL of BHI liquid medium was added to Wells 2–11. Well 12 received 200 μL of BHI liquid medium as a negative control. A 100 μL aliquot from Well 1 was transferred to Well 2 and gently mixed by pipetting up and down. This serial dilution process was repeated for Wells 3–10. After mixing Well 10, 100 μL of the supernatant was discarded. Finally, 100 μL of the prepared spore suspension (from Step 2) was added to each well. MIC and MBC results were read by visual inspection and from the readings of the cell optical density at an absorbance of 625 nm (OD_{625}) (Joao et al., 2020; Van Cutsem et al., 1994).

2.4 Measurement of growth curve

The *Sporothrix* cultured at 25°C with shaking at 150 rpm for 4 days were transferred to 50-mL sterile centrifuge tubes and centrifuged at 8,000 rpm for 5 min. The supernatant was then discarded. The mycelium was diluted in BHI medium, in groups, the final concentration of the drug was 50 μg/mL by adding quantitative *Sporothrix* suspension and DMSO-dissolved small molecule drug in groups. 37°C for 96 h, OD_{625} was measured and photographed under bright-field microscopy at 40 × magnification every 12 h, the experiment was repeated three times for each group.

2.5 Murine model of sporotrichosis

Male 8-week-old KM mice were purchased from Liaoning Changsheng Biotechnology Co. Ltd., permit No. SCXK (Liao)2020–0001. The mice in all groups were injected intraperitoneally with cortisol solution every other day for 1 week before inoculation with sporotrichosis suspension. 20 mg/kg, after 1 week it was changed to every 2 days, gavage administration was started after successful modeling (Feng et al., 2010; Boyce et al., 2011). All groups of mice had their abdominal skin shaved with a razor before being injected with *Sporothrix* suspension, 0.1 mL *Sporothrix* suspension was injected intradermically into one of the hair-removal sites with a 1 mL syringe, it contains about 1×10^7 spores.

2.6 Small molecule drugs treatment

After modeling, Daily Gavage was started. Mice were randomly assigned to two treatment cohorts: the Azelastine treatment group and Mefloquine treatment group. These cohorts were further stratified into high-dose (Azelastine: 6 mg/kg/day, Mefloquine: 20 mg/kg/day), low-dose (Azelastine: 3 mg/kg/day, Mefloquine: 3.8 mg/kg/day), and a control group receiving 0.5% carboxymethylcellulose sodium salt.

2.7 Histological examination of the skin

Following drug administration, the mice were euthanized through cervical dislocation and immersed for 5 min in a 5% phenol solution for disinfection purposes. The specimens were then rinsed three times with autoclaved sterile distilled water and placed on a sterile dissecting board under aseptic conditions. Skin lesions were excised and immediately fixed in a 4% paraformaldehyde solution for histopathological processing. Skin lesion samples were sent to Jijia for HE staining, the infiltration of inflammatory cells and the formation of granuloma were observed and analyzed.

2.8 Statistical analysis

The study groups were compared statistically using the SPSS 23.0. Significance for all statistical tests is shown in the figures for $p < 0.05$, $p < 0.01$, and $p < 0.001$.

2.9 Ethics statement

The experiment was conducted in strict accordance with the Guide for the Care and Use of Laboratory Animals.

2.10 cDNA library construction and sequencing

Total RNA was extracted from the mycelial phase of a 48-h culture, the yeast phase of 48-h induction and the liquid of 48-h culture following the addition of Azelastine. The total amount and purity of the extracted RNA were assessed. After qualification, eukaryotic mRNA was enriched using magnetic beads with Oligo (DT). Fragmentation buffer was subsequently added to cleave the mRNA into shorter fragments. Using the mRNA as a template, single-stranded cDNA was synthesized with random primers, followed by the addition of RNase H to produce double-stranded cDNA. The resulting double-stranded cDNA was purified, its ends were repaired, a tail was added, and sequencing linkers were connected. Fragments were selected using AMPure XP beads. Finally, PCR amplification and purification were performed to obtain the final library. The libraries were quality-checked, and those meeting the criteria were subjected to PE150 sequencing using the Illumina HiSeq 2,500 high-throughput sequencing platform.

2.11 Transcriptome analysis

First, the quality of sequencing data was evaluated using FASTP (Chen et al., 2018) software. Following quality control, the sequencing data were aligned with ribosome sequences from the NCBI RefSeq (Pruitt et al., 2007) and RFAM (Kalvari et al., 2021) databases utilizing Bowtie 2 (Langmead et al., 2019) software. The

alignment results were statistically processed using samtools (Danecek et al., 2021) and subsequently compared to the reference genome with Bowtie 2 (Langmead et al., 2019). Transcript assembly was performed with StringTie (Pertea et al., 2015) software, leveraging available reference information, followed by quantitative analysis of gene expression levels. Once the transcript read counts were obtained, they were converted to gene read counts using the R package maximport (Soneson et al., 2015). After acquiring read counts for all samples, we employed the differential analysis software DESEQ2 (Love et al., 2014) to conduct differential expression analysis of genes. For this analysis, we utilized the GO, KEGG, and EggNOG databases for functional annotation, functional enrichment, and GSEA analyses.

2.12 Real-time quantitative PCR

Approximately 100 mg of *S. globosa* mycelial-phase cells and yeast-phase cells were collected and rapidly frozen in liquid nitrogen. The samples were subsequently ground under continuous liquid nitrogen cooling using a mortar and pestle. Total RNA was extracted from both phases using the TRIzol Reagent Kit (Vazyme Biotech Co., Ltd., China) in accordance with the manufacturer's protocol. Quantitative real-time PCR was conducted on the StepOnePlus system. Following normalization with the 18S rDNA reference gene, the relative expression levels of the target gene between the yeast-phase and mycelial-phase were compared and analyzed using the 2^(-ΔΔCt) method.

3 Results

3.1 Discovery of anti—*S. globosa* entry inhibitors among candidates in the FDA approved drug library

The *abaA* gene sequence of *S. globosa* utilized in this study was obtained through sequencing conducted in our laboratory. The three-dimensional structure of this gene is currently unknown, prompting a search for similar proteins to facilitate further investigation. In order to search for similar proteins of AbaA, we first searched for similar genes of *abaA* (Table 1), HMPREF1624, which exhibited the highest total score and sequence similarity, was selected and subsequently searched in the UniProt database (Supplementary Table S1). This protein contains a DNA-binding domain known as TEA (Supplementary Table S2), which is identical to that of the AbaA protein. We used the RoseTTAFold module in the Robetta server to predict the three-dimensional structure of the AbaA protein (Figures 1A–E), the five predicted models are evaluated in SAVES v6.0 (Table 2), we finally chose the highest score Result-1 for follow-up processing (Moreira et al., 2021; Cho et al., 2009; Ma et al., 2022). We utilized PyMOL to truncate the AbaA protein's DNA-binding domain from the model Result-1 (Figure 1A). The binding pockets of this domain were predicted using DoGSiteScorer (Table 3, Figure 1F). We then employed AutoDock Tools to preprocess the top two pockets, setting the size and coordinates of the docking box. Subsequently, we conducted batch molecular docking using AutoDock Vina (Supplementary Table S3). We compared the binding energies and analyzed the primary efficacy and side effects of the selected small molecule drugs. Ultimately, we chose four small molecule drugs, Avodart, Eltrombopag, Azelastine, and Mefloquine, for further study (Figures 1G,H).

3.2 Azelastine and Mefloquine have *in vitro* antifungal activity against the *S. globosa* and *S. schenckii*

In our previous studies, *abaA* gene expression was upregulated during the dimorphic switch of the *S. schenckii* from the mycelial phase to the yeast phase, and the deletion of this gene causes *S. schenckii* to become less resistant to all kinds of stress, these results suggest that the gene is critical for *S. schenckii* dimorphic switch (Zheng et al., 2021). Therefore, it is reasonable to speculate that this gene is also important for the dimorphic switch of *S. globosa*. Consequently, we suspect that AbaA is also upregulated during the yeast phase of *S. globosa*. To explore the antifungal activity of Azelastine and Mefloquine, the selected drugs were administered to *S. globosa* and the *S. schenckii* phase reversal process respectively, in order to observe their effects on the dimorphic switch of *S. globosa* and *S. schenckii*. The results indicate that Avodart and Eltrombopag have no effect on either fungus (Figures 2A,B). In contrast, Azelastine and Mefloquine showed inhibitory effects on both *S. globosa* and *S. schenckii* when compared to the control group and DMSO solvent control group (Figures 2C–F). When Azelastine and Mefloquine were added, the conidia of *S. globosa* dropped off and did not grow. Both Azelastine and Mefloquine significantly inhibited the growth and spore production of *S. globosa* and *S. schenckii*. In the control and solvent control groups, dimorphic switch of *S. globosa* and *S. schenckii* occurred, there was no phase inversion in the Azelastine and Mefloquine groups. Thus, both small-molecule drugs inhibited the growth and dimorphic switch of *S. globosa* and *S. schenckii*.

3.3 Determination of fungal growth curves, MIC and MBC of Azelastine and Mefloquine

Given the subjective nature of morphological observations, we aimed to further investigate the inhibitory effects of Azelastine and

TABLE 1 BLAST comparison results.

Description	Max score Total score	Query cover	E value	Percent identity	Accession
HMPREF1624_03084	1,621	99%	0.0	94.11%	ERS99720.1
SPSK_08393	1,608	99%	0.0	93.97%	XP_016588585.1
transcription factor	1,606	99%	0.0	94.38%	XP_040619892.1

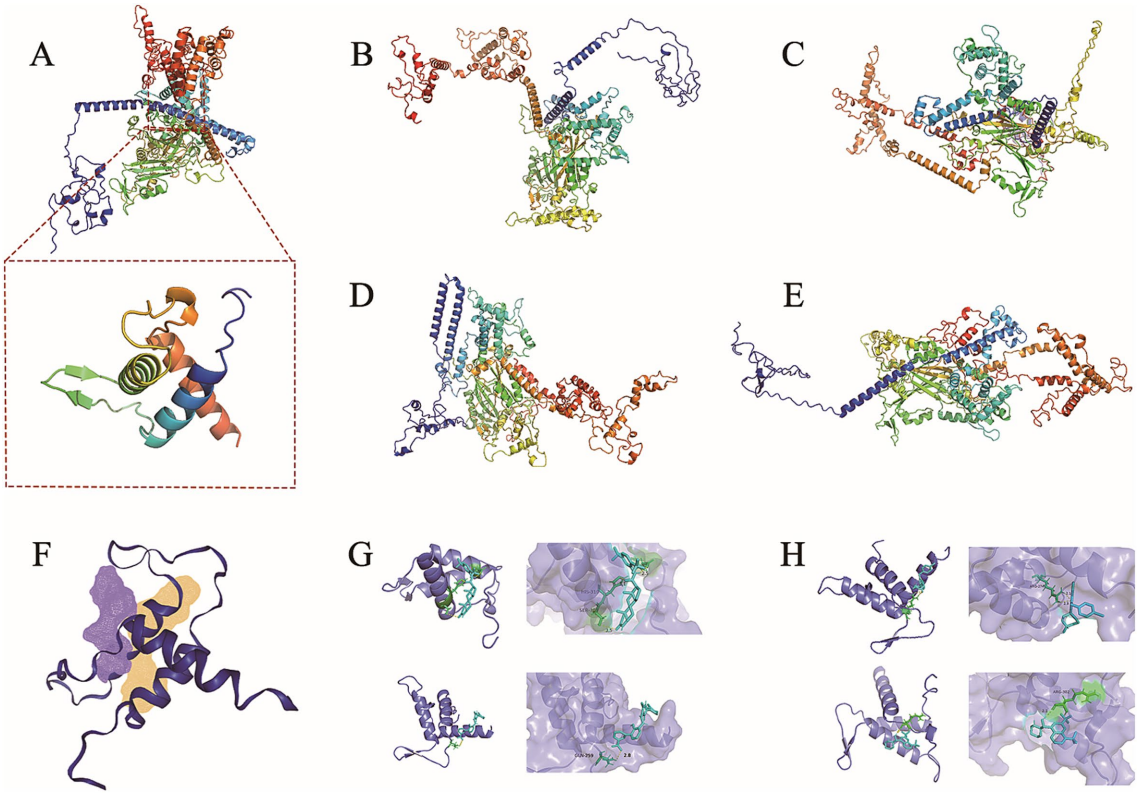

FIGURE 1
AbaA three-dimensional structure prediction and docking results display. **(A–E)** The three-dimensional structure of AbaA protein was predicted using Robetta, the three-dimensional structure of AbaA DNA-binding domain is shown under **(A)**. **(F)** Use DoGSiteScorer to predict the protein-binding pocket. **(G,H)** The four graphs are Avodart, Eltrombopag, Azelastine, Mefloquine and AbaA DNA binding domain docking results.

TABLE 2 Results of model quality evaluation.

Result	Verify 3D	Procheck	Whatcheck	Errat	Prove
1	Fail	Pass:3	Green:29	91.6514	Fail
2	Fail	Pass:3	Green:29	91.0009	Warning
3	Fail	Pass:2	Green:27	89.7179	Warning
4	Fail	Pass:2	Green:28	91.7498	Fail
5	Fail	Pass:2	Green:25	87.3733	Fail

TABLE 3 Combine pocket predictions.

Pocket number	Volume (Å^3)	Surface (Å^2)	Drug Score	Simple Score
1	499.78	912.12	0.72	0.36
2	436.16	921.93	0.76	0.34
3	227.65	316.54	0.55	0.13

Mefloquine on *S. globosa* and *S. schenckii*. To achieve this, we determined the growth curves for these small molecule drugs in relation to the inhibition of both *S. globosa* and *S. schenckii*, and we determined the MIC and MBC of the two small molecule drugs. The addition of Azelastine and Mefloquine significantly inhibited the growth of *S. globosa* and *S. schenckii* compared with the control group and DMSO solvent control group (Figure 3). Although the measured MIC and MBC values do not show a small-dose advantage over other fungicide (Table 4), these agents are considered safer than antibiotics and are administered at lower doses compared to Itraconazole alone. Both drug stents can also be optimised for the development of new small-molecule drugs to treat sporotrichosis if the clinical dose is higher than the safe range.

3.4 Azelastine and Mefloquine are effective for sporotrichosis

We verify the efficacy of Azelastine and Mefloquine in the treatment of sporotrichosis at the animal level. The model was established by intradermal injection of *Sporothrix* spore suspension in mice (Figure 4) Intradermal injection of spore into the abdomen of mice produced varying degrees of skin lesions, some grow nodules, some ulcers, or cysts. For some nodules, the pus was collected by gastric perfusion. The pus was dipped into a high-temperature sterilized cotton swab and diluted

10.3389/fmicb.2025.1546020

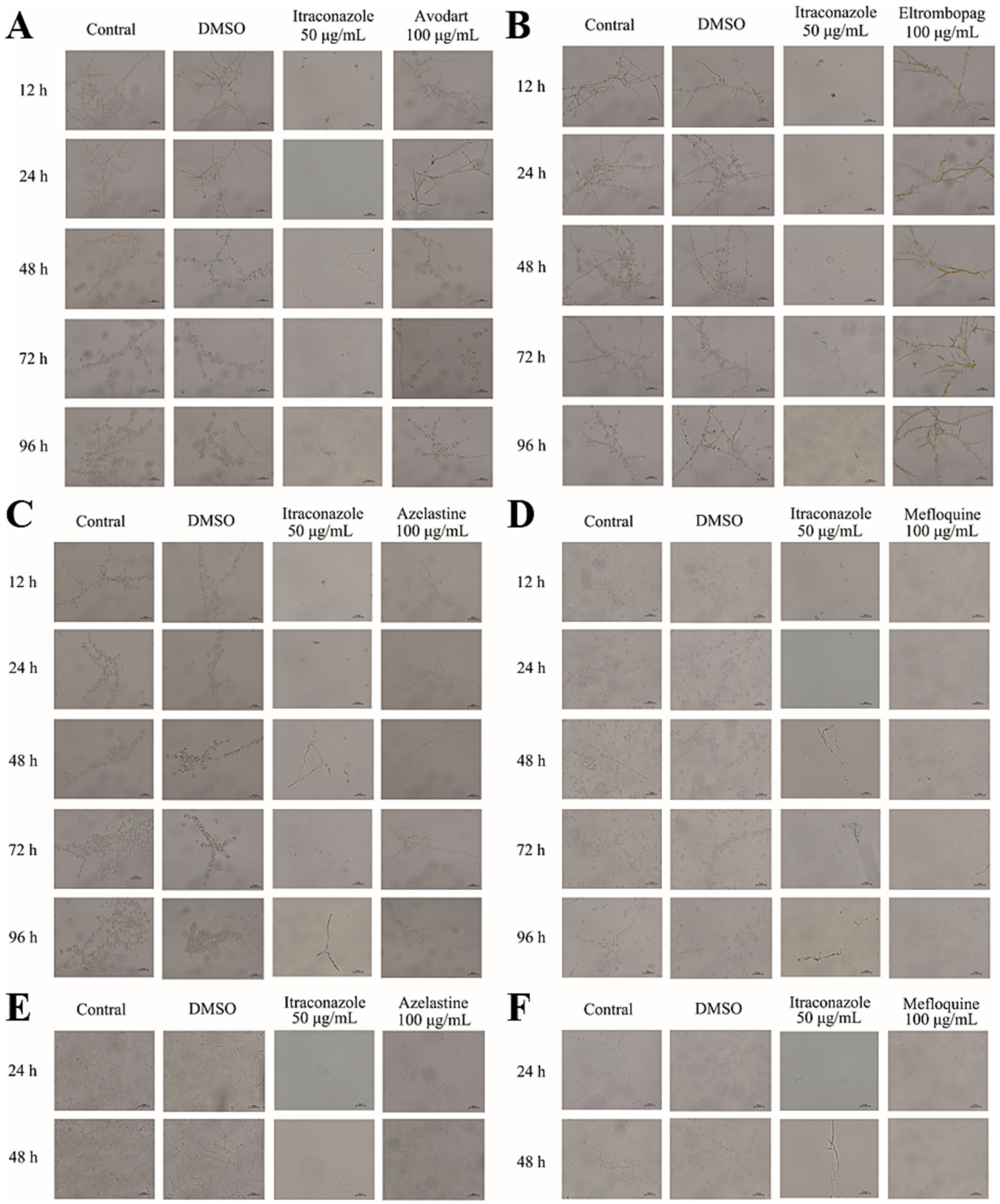

FIGURE 2
Antifungal activity of the candidate against *Sporothrix globose* and *Sporothrix schenckii* under bright-field microscopy at 40 × magnification. **(A)** *In vitro* antifungal activity of Avodart against *Sporothrix globose*. **(B)** In vitro antifungal activity of Eltrombopag against *Sporothrix globose*. **(C)** In vitro antifungal activity of Azelastine against *Sporothrix globose*. **(D)** In vitro antifungal activity of Mefloquine against *Sporothrix globose*. **(E)** In vitro antifungal activity of Azelastine against *Sporothrix schenckii*. **(F)** In vitro antifungal activity of Mefloquine against *Sporothrix schenckii*. The test concentration was 50 μg/mL, 100 μg/mL, and the selected concentration was 100 μg/mL. The amount of DMSO is the amount of candidate drugs.

with sterile distilled water. 40 μL of pus was spread evenly on SDA medium and cultured at 25°C for 4 days, microscopy confirmed *S. schenckii* (Supplementary Figure S1). Inflammatory ulcers and nodules began to appear in the skin of mice 1 week after intradermal injection, the morphology of the lesions was analyzed by reviewing the literature, and the pus was purified and cultured, microscopic observation showed that the lesions were Sporotrichosis. The Sporotrichosis was most severe in the third week, when the drug was given intragastrically for 10 days,

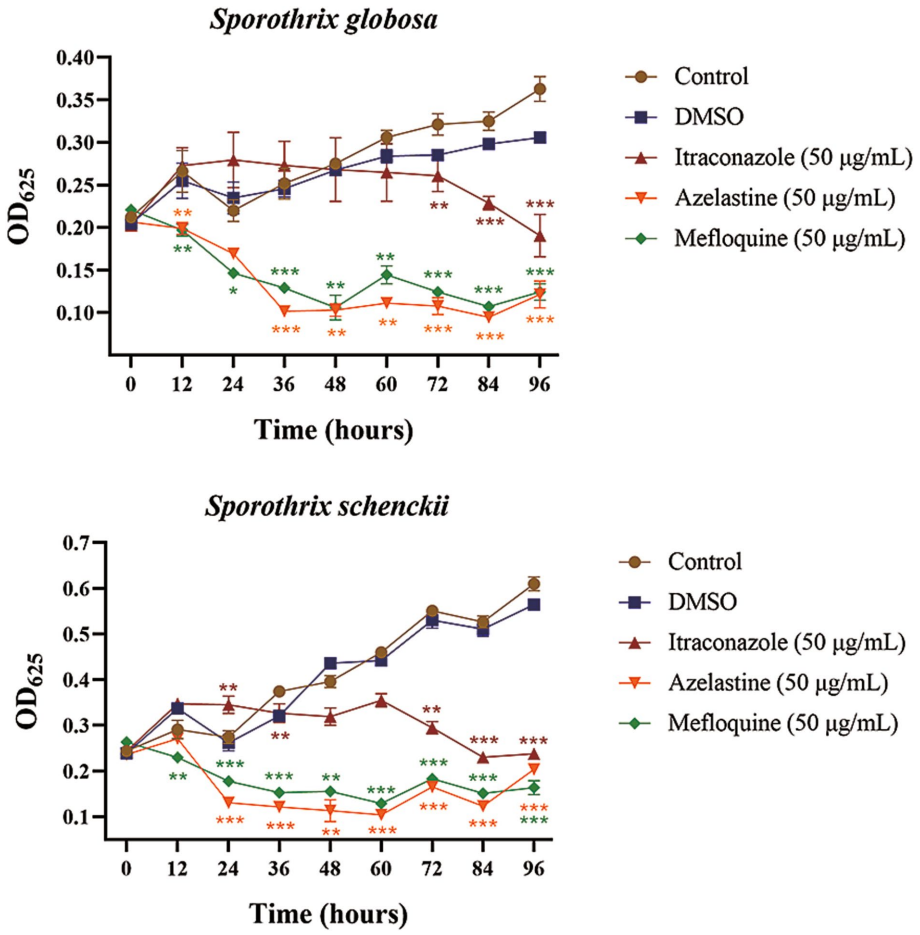

FIGURE 3
The growth curves of *Sporothrix globose* and *Sporothrix schenckii* were inhibited by small molecule drugs. **(A)** The growth curves of the small molecule drugs for the inhibition of *Sporothrix globosa*. **(B)** The growth curves of the small molecule drugs for the inhibition of and *Sporothrix schenckii*. DMSO group was solvent control group and Itraconazole group was positive control group. *, $p < 0.05$; **, $p < 0.01$; ***, $p < 0.001$. Data processing used SPSS 23.0 for Ducan's multiple comparison test to analyze its significance.

TABLE 4 **Azelastine and Mefloquine inhibited MIC and MBC of *Sporothrix globose, Sporothrix schenckii*.**

Drug	MIC (μg/mL)	MBC (μg/mL)
Azelastine-*Sporothrix globose*	25	50
Mefloquine-*Sporothrix globose*	12.5	25
Azelastine-*Sporothrix schenckii*	6.25	50
Mefloquine-*Sporothrix schenckii*	6.25	25

the nodules in the Itraconazole positive control group and the Azelastine and Mefloquine groups became smaller and the crusts were improved (Figure 5). In comparison to the mock group, the control group exhibited larger granulomas and a greater infiltration of inflammatory cells. Notably, the granulomas in the positive control group were smaller than those in the control group. The granulomas observed in both the low and high dose Azelastine groups were wider than those in the positive control group, yet smaller than those in the control group; they were dispersed and did not form a cohesive mass, with milder inflammatory cell infiltration compared to the control group. In contrast, the inflammatory infiltration in both the low and high dose Mefloquine groups did not show improvement relative to the control group; however, the granulomas were significantly smaller, with the inflammatory cells remaining dispersed and not coalescing (Figure 6). The granuloma width of the control group was significantly different from that in both the positive control group and the treatment group (Table 5). Statistical analysis of inflammatory cell statistics showed that there were significant differences between the control group and the positive control group (Table 6).

3.5 The regulatory effect of the *abaA* gene on downstream virulence factors was analyzed using bioinformatics

To further investigate the regulation of the *abaA* gene on these virulence factors, we reviewed the literature to identify the downstream virulence factors associated with *Sporothrix* (García-Carnero and Martínez-Álvarez, 2022; Teixeira et al., 2014; Félix-Contreras et al., 2020). We downloaded the gene sequences of these virulence factors from the NCBI and utilized the JASPAR database[2]

2 https://JASPAR.elixir.no/

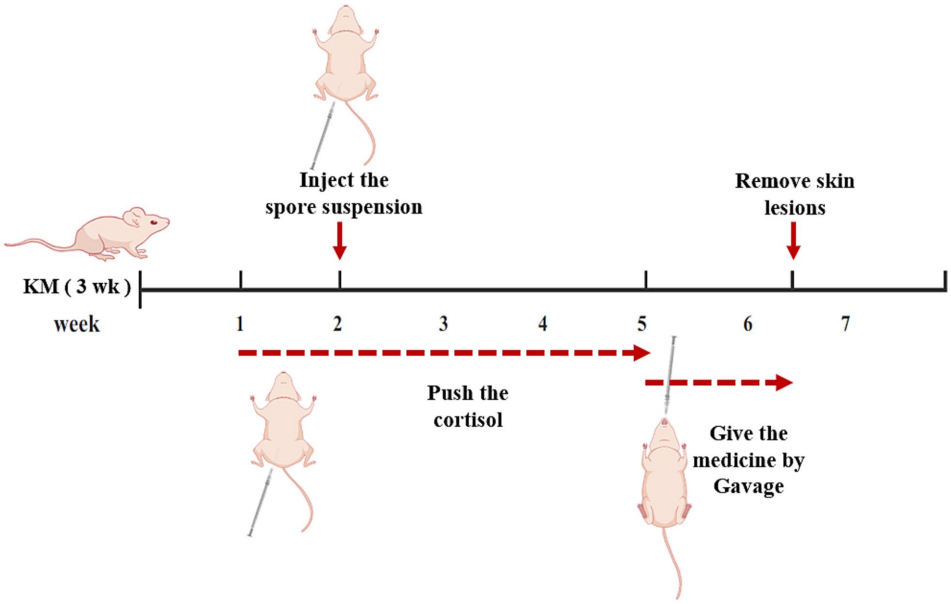

FIGURE 4
Mouse model and treatment process. After a week of acclimation, the mice were injected with a cortisol solution for immunosuppression, after 1 week of inhibition, the mold was made by injection *Sporothrix* suspension, meanwhile, immunosuppression was continued. Three weeks after successful modeling, the rats were treated with medicine. After 10 days of administration, mice were killed and skin lesions were examined.

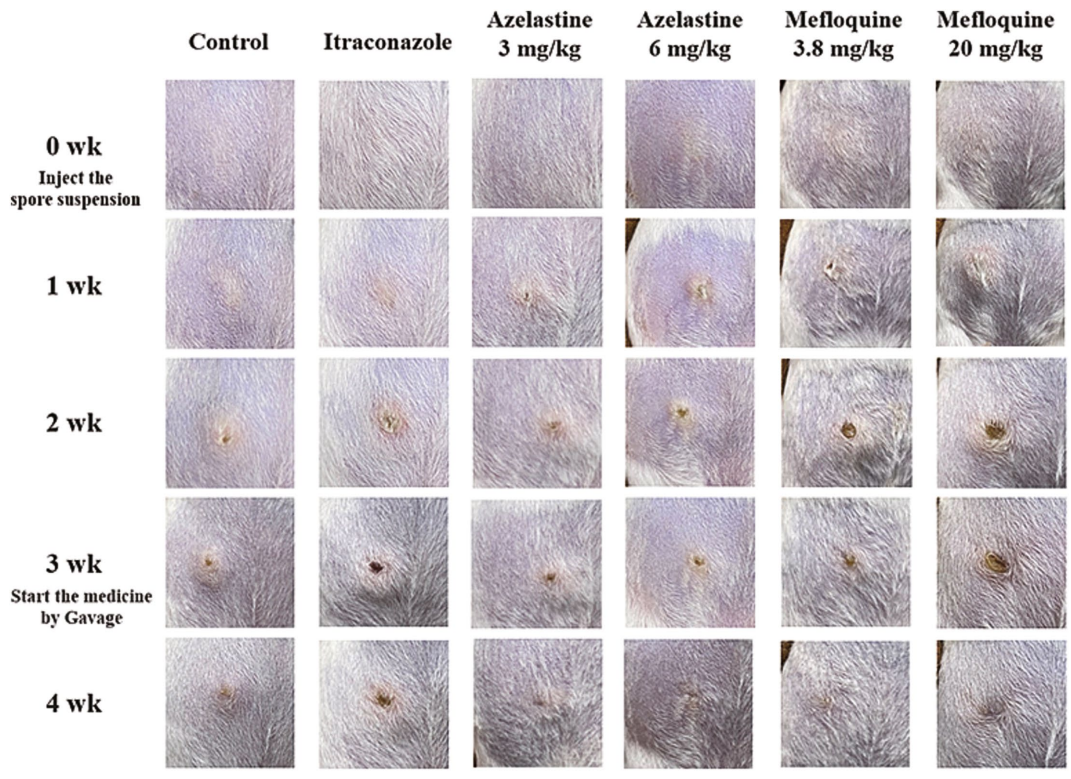

FIGURE 5
Pictures of mouse model and treatment process. Intradermal injection of *Sporothrix* suspension into the abdomen of mice produced varying degrees of skin lesions, some grow nodules, some ulcers, or cysts.

to identify virulence factors containing AbaA binding sites (Andrianopoulos and Timberlake, 1994). The sequences of the *abaA* binding sites were then compared using DANMAN sequence alignment software, allowing us to screen for virulence factors that may be regulated by the *abaA* gene. These genes are GPI-anchored cell wall beta-1,3-endoglucanase EglC, scytalone

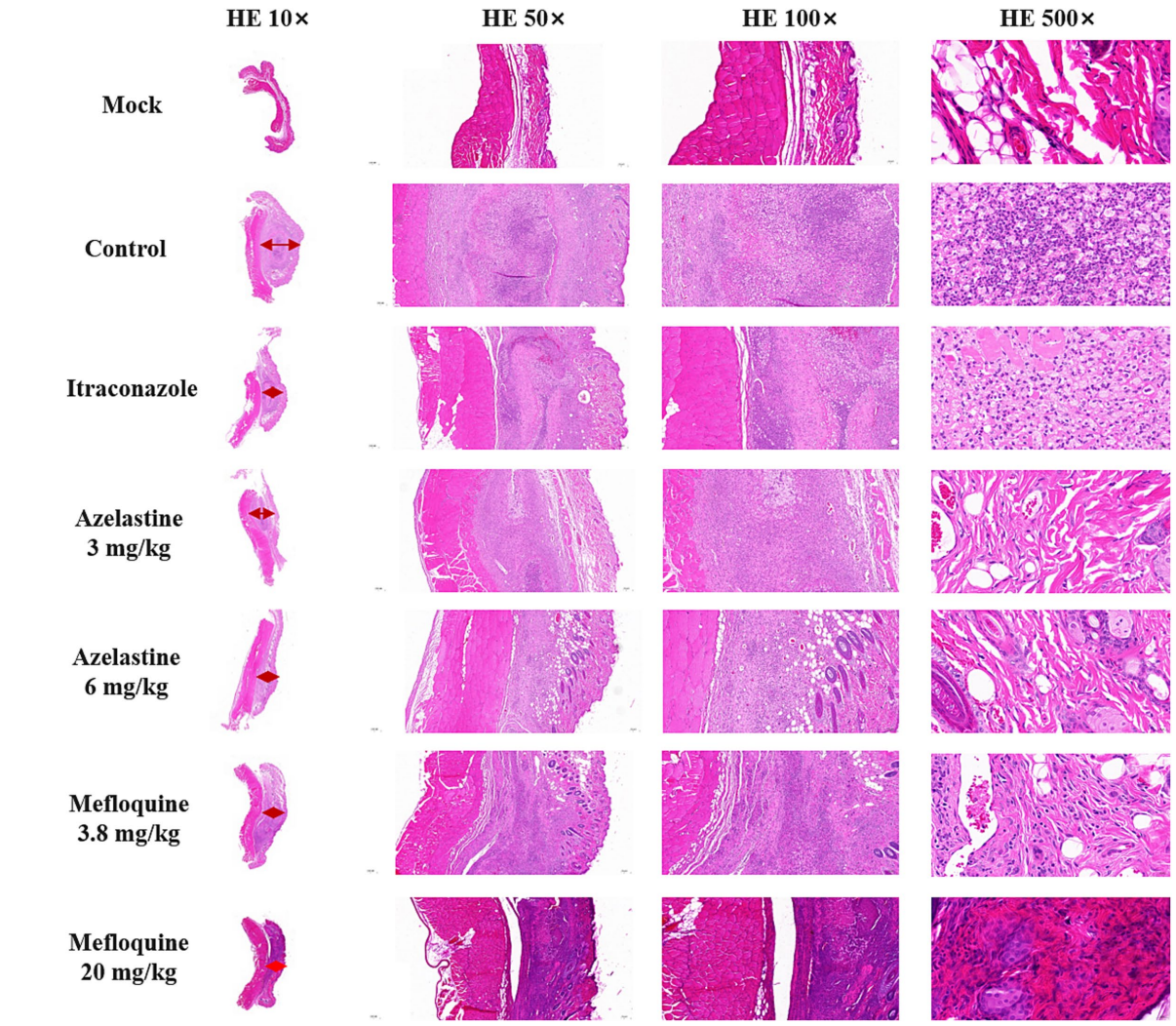

FIGURE 6
HE staining results of skin lesions in mice. The Mock group was the result of HE staining of healthy skin, the red arrow was granuloma, control group was not given medicine after successful modeling. The width of granuloma in control group was 3,320 μm; the width of granuloma in Itraconazole group was 1,460 μm; the width of granuloma in Azelastine 3 mg/kg group was 1,880 μm; the width of granuloma in Azelastine 6 mg/kg group was 1,480 μm; the width of granuloma in Mefloquine 3.8 mg/kg group was 1,940 μm; the width of granuloma in Mefloquine 20 mg/kg group was 1,251 μm. (Granuloma width was measured by software CaseViewer).

TABLE 5 Results of granuloma width statistical analysis.

Group	Granuloma width (μm)
Control	2588.9 ± 423.4[b]
Itraconazole	1446.7 ± 418.5[a]
Azelastine 3 mg/kg	1059.3 ± 699.8[a]
Azelastine 6 mg/kg	1136.9 ± 224.4[a]
Mefloquine 3.8 mg/kg	1054.7 ± 138.6[a]
Mefloquine 20 mg/kg	911.4 ± 253.2[a]

Different lowercase letters indicate significant difference ($P < 0.05$). SPSS 23.0 was used to analyze the significance of Ducan multiple comparison test.

TABLE 6 Results of inflammatory cell count were analyzed statistically.

Group	Inflammatory cell count
Control	566.9 ± 72.3[b]
Itraconazole	255.2 ± 29.7[a]
Azelastine 3 mg/kg	263.1 ± 93.4[a]
Azelastine 6 mg/kg	273.6 ± 85.5[a]
Mefloquine 3.8 mg/kg	333.1 ± 71.7[a]
Mefloquine 20 mg/kg	222.8 ± 11.9[a]

Different lowercase letters indicate significant difference ($p < 0.05$). SPSS 23.0 was used to analyze the significance of Ducan multiple comparison test. Inflammatory cells were counted using software Image-J.

dehydratase, CFEM domain protein, laccase precursor, molecular chaperone HTPG, DNA mismatch repair protein. This screening was subsequently validated through transcriptome analysis. To validate the reliability of the bioinformatics analysis, we subsequently conducted transcriptome analysis and qRT-PCR for verification.

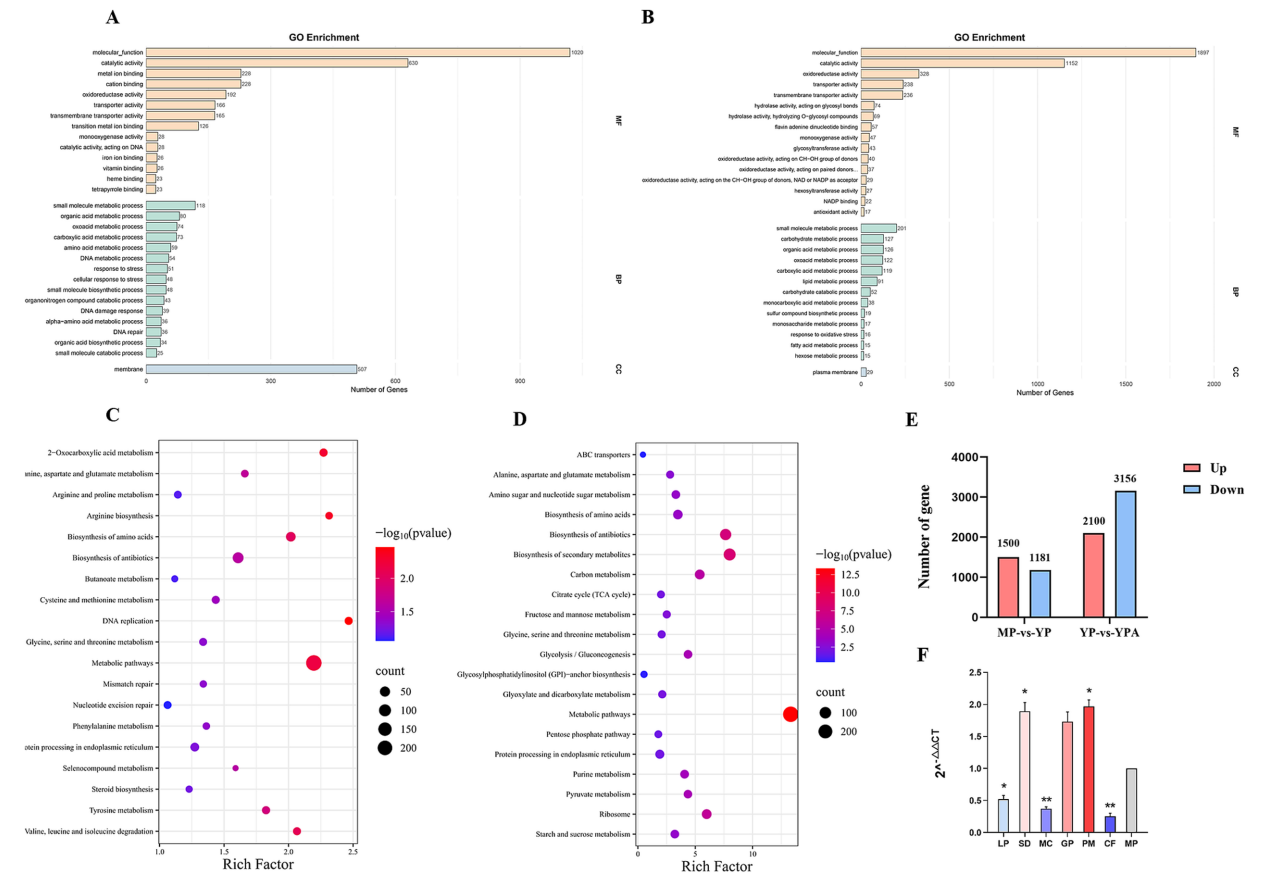

FIGURE 7
Transcriptome data analysis. **(A)** Gene Ontology Enrichment Analysis of MP and YP differentially expressed genes. **(B)** Gene Ontology Enrichment Analysis of YP and YPA differentially expressed genes. **(C)** Histogram of the Kyoto Encyclopedia of Genes and Genomes pathway classification of differentially-expressed genes of MP and YP. **(D)** Histogram of the Kyoto Encyclopedia of Genes and Genomes pathway classification of differentially-expressed genes of YP and YPA. **(E)** Histograms of differentially expressed genes. There were 2,681 genes differing between MP and YP, and 5,256 genes differing between YP and YPA. **(F)** qRT-PCR showed that *abaA* regulated virulence factor gene was expressed in yeast phase and mycelial phase with other genes. The expression of each gene was expressed as 2^-△△ CT value (mean ± SEM), and the expression of each gene in the mycelial phase was constant as 1, which served as a baseline comparison with other genes in the yeast phase. Gene: LP: laccase precursor; SD: scytalone dehydratase; MC: molecular chaperone HtpG; GP: GPI-anchored cell wall beta-1,3-endoglucanase EglC; PM: DNA mismatch repair protein. CF: CFEM domain protein. The significance was analyzed by independent sample *t* test (*, $p < 0.05$; **, $p < 0.01$). MP: mycelial phase baseline.

3.6 Transcriptome sequencing data processing and assembly result statistics

RNA-Seq sequencing yielded between 41,934,980 and 47,331,900 raw reads from nine libraries, with raw bases ranging from 6.29 G to 7.02 G. The number of clean reads varied from 43,514,694 to 8,516,234. The GC content ranged from 54.26 to 56.27%. The Q30(%), which represents the percentage of bases with an accuracy exceeding 99.9%, the Q30 value was greater than 92% in this experiment, indicating that the sequencing quality was reliable (Supplementary Table S5).

Gene expression was analyzed using DESeq, with the criteria for screening differentially expressed genes set at |log2foldchange| > 1 and significance $p < 0.05$. A total of 2,681 genes were found to be differentially expressed between the Mycelial Phase (MP) and Yeast Phase (YP), of which 1,500 genes were up-regulated and 1,181 genes were down-regulated. Additionally, 5,256 genes were differentially expressed between Yeast Phase + Azelastine (YPA) and Yeast Phase (YP), with 2,100 genes up-regulated and 3,156 genes down-regulated (Figure 7E).

We utilized the Gene Ontology (GO) and Kyoto Encyclopedia of Genes and Genomes (KEGG) databases to analyze significantly differentially expressed genes between the MP and YP, as well as between the YP and YPA. The GO functional enrichment analysis for the comparison of the MP versus YP (Figure 7A) revealed that 1,020 differentially expressed genes were enriched in molecular functions, with 630 genes enriched in catalytic activity and 507 genes enriched in membrane functions. The KEGG pathway enrichment analysis (Figure 7C) indicated that the differentially expressed genes in the treatment group were significantly enriched in metabolic and biosynthetic pathways, such as valine, leucine, and isoleucine degradation (KEGG: ko00280) and amino acid biosynthesis (KEGG: ko01230). The enrichment of these differential genes in the aforementioned functions and pathways suggests potential changes in cell membrane structure and the production of virulence factors during the dimorphic transformation of *Sporothrix*. Notably, serine metabolism can generate precursors for glutathione, enhancing the fungus's ability to cope with reactive oxygen species (ROS) produced by the host's immune response,

thereby aiding its survival following macrophage phagocytosis (Cheng et al., 2019).

For the YP and YPA, GO functional enrichment analysis (Figure 7B) revealed that 1,897 differentially expressed genes were enriched in molecular functions, with 1,152 genes enriched in catalytic activity and 328 genes enriched in oxidative activity. Additionally, KEGG pathway enrichment analysis (Figure 7D) demonstrated that the differentially expressed genes in this treatment group were enriched in the biosynthesis of secondary metabolites (KEGG: ko01110) and metabolic pathways. The significant enrichment of differentially expressed genes in molecular functions, catalytic activity, and metabolic pathways indicates that the drug had a substantial impact on the original metabolic activities of the strain. Furthermore, the functional enrichment of differentially expressed genes in oxidative activity and the biosynthesis of secondary metabolites pathway suggests that the drug may have exerted specific effects on the synthesis of secondary metabolites and the oxidative stress system in the fungal. This further implies potential disturbances in the synthesis of virulence factors and the mechanisms of host immune evasion in the fungal. Transcriptome results indicated that several virulence factors regulated by *abaA*, including GPI-anchored cell wall beta-1,3-endoglucanase (EGLC), dehydratase, and CFEM domain protein, were significantly down-regulated. Conversely, genes associated with fungal growth and repair, such as laccase precursor, molecular chaperone HTPG, and DNA mismatch repair protein, exhibited significant up-regulation. Further validation and functional analyses of these candidate genes will be performed.

3.7 The results of qRT-PCR were consistent with those of transcriptome

To verify the reliability of the transcriptome results, we performed qRT-PCR validation. (Figure 7F). The primers used are shown in Supplementary Table S4. The results of qRT-PCR were consistent with those of transcriptome analysis (Figure 8). Interestingly, among the screened genes, genes related to the cell wall structure of *Sporothrix* (GPI-anchored cell wall beta-1,3-endoglucanase EglC, CFEM domain protein) were significantly down-regulated; and genes related to melanin (scytalone dehydratase) were significantly down-regulated. Other genes such as DNA repair-related genes (molecular chaperone HtpG, DNA mismatch repair protein) and fungal adaptability-related genes (laccase precursor) were significantly up-regulated. This suggests that the *abaA* gene plays a crucial role in regulating the anchoring of the *Sporothrix* cell wall to the host matrix and in the regulation of melanin. Furthermore, inhibition of the *abaA* gene results in a significant expression of repair genes, highlighting its importance to *Sporothrix*. We analyzed the transcriptome data of the virulence factors regulated by the *abaA* gene and observed that the expression levels of these virulence factors were inversely correlated with those of yeast following the addition of Azelastine (Figure 8). This finding further confirms that the expression level of *abaA* is down-regulated upon the introduction of small molecule drugs, indicating that the *abaA* gene serves a regulatory function in these virulence factors.

4 Discussion

Currently, the issue of drug resistance in invasive fungal diseases is becoming increasingly serious, with emerging resistance also observed in sporotrichosis. Therefore, there is an urgent need to search for new small-molecule drugs to treat sporotrichosis and to explore innovative methods for drug discovery. If we want to find new small molecule drugs, we have to find new targets (Ortiz-Ramírez et al., 2022; Cortés Juan Carlos et al., 2019). *S. globosa* is a dimorphic fungus that exists in the mycelial form in the environment at 25°C, where it is non-pathogenic. Upon entering the body at 37°C, *S. globosa* transforms into its yeast phase, at which point it becomes pathogenic. The AbaA gene, which is involved in the dimorphic switching process, can influence the virulence of *S. globosa*, making it a key target for selection. The *abaA* gene, which plays a crucial role in the dimorphic switch process, can influence the virulence of *S. globosa*, making it a focal point for target selection. The *abaA* gene is essential for dimorphic switch; in *Talaromyces marneffei*, deletion of the *abaA* gene impacts dimorphic switch (Borneman et al., 2000), while in *S. schenckii*, deletion of the *abaA* gene affects virulence. Consequently, we chose *abaA* gene as a novel drug target.

We employed molecular docking techniques to screen for small molecules that could inhibit *S. globosa* and *S. schenckii*. The literature review revealed that almost all invasive mycoses can lead to central nervous system diseases when they are severe (Krysan, 2016). Consequently, it is essential for fungicides to penetrate the blood–brain barrier and achieve elevated serum and tissue concentrations (Bing et al., 2012; Karbwang and Harinasuta, 1992). Through the analysis and screening of molecular docking results, we eliminated the side effects associated with drugs used for treating cancer and psychiatric diseases. Subsequently, we combined considerations of price, efficacy, and *in vitro* antifungal tests to identify two small-molecule drugs.

Two small-molecule drugs demonstrated a tendency to inhibit the growth of *Sporothrix* in antifungal experiments. The proposed mechanism involves the regulation of conidiophore development by AbaA. In *ΔabaA* mutants, the formation of the peduncle is associated with inhibited growth of *Sporothrix*, leading to the cessation of the developmental program. Furthermore, the molecular structures of the drugs Azelastine and Mefloquine interact with AbaA, resulting in the inhibition of both mycelial and spore development of *Sporothrix*, as evidenced by a decrease in OD_{625}.Azelastine is a histamine 1 receptor blocker, its role is not an antagonist, but a reverse agonist, reduce the H1 receptor component activity (Watts et al., 2019). Azelastine has few side effects, is low-cost, can be taken for long periods of time and is safe for children over 6 years of age (Konrat et al., 2022). The drug has also been shown to have in vitro antiviral activity against the coronavirus (Lythgoe and Middleton, 2020). In addition, Azelastine also has anti-inflammatory effects, mainly by stabilizing mast cells and inhibiting the production of leukotrienes and proinflammatory cytokine (Watts et al., 2019). It can also down-regulate the expression of intercellular adhesion molecule-1 and reduce the migration of inflammatory cells. However, the effects of Azelastine on fungi have been poorly studied. Azelastine, a cationic amphiphilic drug belonging to a pharmacologically diverse class of compounds with distinct target molecules (Tummino et al., 2021), has been shown to induce phospholipidosis at the submicron scale. This property suggests that

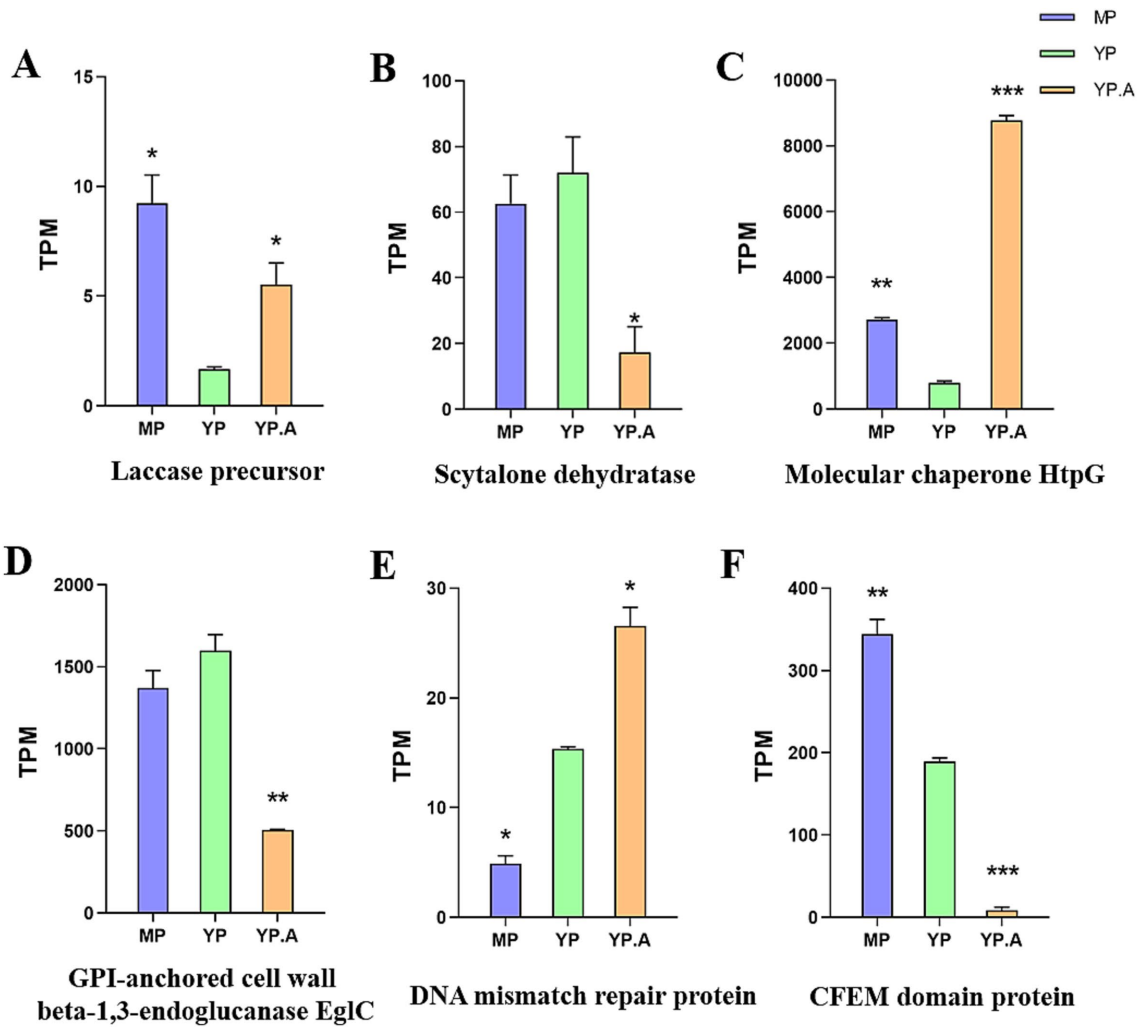

FIGURE 8
(A-F) The transcriptome shows the ratio of *abaA*-regulated virulence factors to other genes in mycelial phase, yeast phase, and yeast phase + Azelastine, with results presented as TPM values (mean ± SEM), significance was tested by independent-sample *T*-test with yeast phase as baseline (*, $p < 0.05$; **, $p < 0.01$; ***, $p < 0.001$).

its antifungal activity against *Sporothrix* may result from a combination of direct fungal growth inhibition and host-mediated mechanisms. Furthermore, Azelastine remains effective when administered as a nasal spray for the treatment of rhinitis, indicating its significant potential as a nasal spray for the treatment of sporotrichosis (Konrat et al., 2022).

The results of pharmacological studies of Mefloquine show that Mefloquine has many useful features in the treatment of fungal infections. First, when taken orally, it can be well absorbed and establishes high serum and tissue levels, second, it can penetrate the blood–brain barrier to high nerve concentrations relative to plasma, Mefloquine has a long half-life, so it can be used as a prophylactic regimen (Montoya et al., 2020). In addition, some studies have shown that Mefloquine has certain antifungal activity against *Candida*, *Cryptococcus* and *Aspergillus* (Montoya et al., 2020). Mefloquine has been shown to inhibit the formation of egg granulomas in *Schistosoma japonicum*, suggesting that it may play a role in modulating the host immune system *in vivo* (Huang et al., 2011). Furthermore Mefloquine may inhibits *Sporothrix* through two mechanisms, in addition to binding to key target proteins of *Sporothrix*, it may also influence the host immune response. The underlying mechanisms of this interaction will be explored in further studies. The selection of dosing concentration was informed by a review of pertinent literature, indicating that both Azelastine and Mefloquine are capable of penetrating the blood–brain barrier and possess potential therapeutic effects against fungal infections. With regard to Azelastine, The pharmacokinetic results of the drug demonstrated Azelastine 16 mg did not increase side effects, and the maximum dose for adults was 40 mg, through the above pharmacokinetics analysis, combined with mouse and human drug delivery conversion formula, we selected two dosing concentrations of 3 mg/kg and 6 mg/kg, to conduct animal experiments (McTavish and Sorkin, 1989). About Mefloquine, adults were given 18–20 mg/kg, or (750–1,250 mg) a day, the clinical pharmacokinetics of Mefloquine showed that the peak time of Mefloquine administration was 6–24 h in healthy subjects, the maximum blood concentration

of the drug was 1,000 μg/mL after taking 1,000 mg. Based on the above pharmacokinetics analysis, we selected a dosing concentration of 3.8 mg/kg; we also found that many studies treated neuropathic pain by intraperitoneal administration of Mefloquine at a dose of 20 mg/kg, so we chose a larger concentration of 20 mg/kg to study the effect of Mefloquine on sporotrichosis. As for the choice of the positive itraconazole concentration, the final choice was 60 mg/kg according to the conversion of doses between human and mice (Bonifaz and Vázquez-González, 2010; Saraiva et al., 2012; Moreira et al., 2015).

The *abaA* gene is crucial for the dimorphic switch of *Sporothrix* and influences the virulence of certain fungi. In this study, several genes regulated by *abaA*, including various virulence factors and functional genes, were identified through a combination of bioinformatics predictions and experimental approaches. GPI-anchored cell wall beta-1,3-endoglucanase EGLC functions as a GPI-anchored protein. Its biosynthesis is crucial for maintaining the integrity of fungal cell walls and is recognized as a significant virulence factor in various pathogenic fungi, including *Candida albicans*, where it plays an adhesive role in the process of host cell infection (Martinez-Lopez et al., 2004; Cormack et al., 1999). It is also an important target for many fungicide. The CFEM domain protein, characterized by its unique cell wall structure in fungi, is associated with glycosylphosphatidylinositol (GPI)-anchored proteins. This protein can bind to virulence factor effectors that contain the CFEM domain, thereby playing a critical role in the formation and enhancement of adhesion and virulence (Choi and Dean, 1997; Wang et al., 2022). As a classical virulence factor of pathogenic fungi, melanin plays a significant role in the immune evasion of these organisms, particularly in their resistance to oxidative attacks from immune cells, such as reactive oxygen species (ROS) (García-Carnero and Martínez-Álvarez, 2022; Wang et al., 1995). Scytalone dehydratase has been implicated in the formation of melanin virulence factors in fungi. After Wang et al. expressed the gene for scytalone dehydratase, which encodes the sickle dehydratase, in melanin-deficient, nonpathogenic *Colletotrichum lagenarium* (OSD1), it restored both melanin production and pathogenicity in this species (Wang et al., 2001). Furthermore, scytalone dehydratase has been utilized as a target for antifungal drug development aimed at inhibiting melanin synthesis (Eisenman et al., 2009). Laccase precursor is a precursor of laccase (Motoyama et al., 2022), a virulence-related cell wall enzyme associated with the blackening of *Cryptococcus neoformans* and the acquisition of resistance to polyene and echinocandins (Eisenman et al., 2009). The DNA mismatch repair protein- PMS2 is responsible for recognizing and repairing erroneous insertions, deletions, and base misincorporations that occur during DNA replication and recombination, as well as for addressing certain types of DNA damage (Iyer et al., 2006). Its absence contributes to the evolution of fungal resistance (Legrand et al., 2007; Dos Reis et al., 2019). Molecular Chaperone HTPG, a member of the Hsp90 family, is an important chaperone whose overexpression enhances the virulence of *Candida* in mice (Hodgetts et al., 1996). It is also considered central to the buffering effect known as pipelization (Burnie et al., 2006). HTPG has been described as suppressing phenotypic variation under normal conditions, yet it releases such variation when its function is impaired (Bergman and Siegal, 2003). Therefore, these genes may serve as new targets for future research.

5 Conclusion

In this study, we employ bioinformatics to identify new therapeutic targets for Sporotrichosis. To further predict these targets, selected small molecule drugs were tested *in vitro* and *in vivo*. The results concluded that Azelastine and Mefloquine are effective in treating Sporotrichosis. Furthermore, our study indicates that these small molecule drugs may possess a broad-spectrum antifungal effect, potentially providing new insights for the treatment of other invasive fungal diseases. At the same time, we investigated the virulence factors and growth repair-related genes regulated by *abaA* through transcriptomics and qRT-PCR. The results indicated that *abaA* is crucial for the toxicity, growth, and development of *Sporothrix*. The methodology employed in this research establishes a foundation for the investigation of drug resistance in other fungi, and the regulation of downstream related factors by *abaA* offers a robust basis for future studies.

Data availability statement

The datasets presented in this study can be found in online repositories. The names of the repository/repositories and accession number(s) can be found at: NCBI PRJNA1163991.

Ethics statement

The animal study was approved by Liaoning University Research Integrity and Academic Ethics Committee. The study was conducted in accordance with the local legislation and institutional requirements.

Author contributions

YW: Data curation, Writing – original draft. XW: Investigation, Writing – review & editing. XF: Validation, Writing – original draft. CH: Investigation, Writing – review & editing. FZ: Methodology, Writing – review & editing. ZZ: Funding acquisition, Writing – review & editing.

Funding

The author(s) declare that financial support was received for the research and/or publication of this article. This study was supported by Shenzhen Science and Technology Innovation Commission Project (grant no. JCYJ20210324114612034) which were distributed to Hong Kong University Shenzhen Hospital.

Conflict of interest

The authors declare that the research was conducted in the absence of any commercial or financial relationships that could be construed as a potential conflict of interest.

Generative AI statement

The authors declare that no Gen AI was used in the creation of this manuscript.

Publisher's note

Supplementary material

The Supplementary material for this article can be found online at: https://www.frontiersin.org/articles/10.3389/fmicb.2025.1546020/full#supplementary-material

References

Andrianopoulos, A., and Timberlake, W. E. (1994). The aspergillus Nidulans Abaa gene encodes a transcriptional activator that acts as a genetic switch to control development. *Mol. Cell. Biol.* 14, 2503–2515. doi: 10.1128/MCB.14.4.2503

Badiee, P., and Hashemizadeh, Z. (2014). Opportunistic invasive fungal infections: diagnosis and clinical management. *Indian J. Med. Res.* 139, 195–204

Balkrishna, A., Verma, S., Mulay, V. P., Gupta, A. K., Haldar, S., and Varshney, A. (2022). *Withania somnifera* (L.) Dunal whole-plant extracts exhibited anti-Sporotrichotic effects by destabilizing peripheral integrity of Sporothrix Globosa yeast cells. *PLoS Negl. Trop. Dis.* 16:e0010484. doi: 10.1371/journal.pntd.0010484

Bergman, A., and Siegal, M. L. (2003). Evolutionary capacitance as a general feature of complex gene networks. *Nature* 424, 549–552. doi: 10.1038/nature01765

Bing, Z., Cheng, W., Linqi, W., Sachs Matthew, S., and Xiaorong, L. (2012). The antidepressant sertraline provides a promising therapeutic option for neurotropic Cryptococcal infections. *Antimicrob. Agents Chemother.* 56:212. doi: 10.1128/aac.00212-12

Bonifaz, A., and Vázquez-González, D. (2010). Sporotrichosis: an update. *Giornale Italiano Dermatol. Venereol.* 145, 659–673. doi: 10.1016/j.fgb.2012.03.005

Borneman, A. R., Hynes, M. J., and Andrianopoulos, A. (2000). The Abaa homologue of Penicillium Marneffei participates in two developmental Programmes: Conidiation and dimorphic growth. *Mol. Microbiol.* 38, 1034–1047. doi: 10.1046/j.1365-2958.2000.02202.x

Boyce, K. J., Schreider, L., Kirszenblat, L., and Andrianopoulos, A. (2011). The two-component histidine kinases Drka and Slna are required for in vivo growth in the human pathogen Penicillium Marneffei. *Mol. Microbiol.* 82, 1164–1184. doi: 10.1111/j.1365-2958.2011.07878.x

Brown-Elliott, B. A., Wallace, R. J., Blinkhorn, R., Crist, C. J., and Mann, L. B. (2001). Successful treatment of disseminated *Mycobacterium chelonae* infection with linezolid. *Clin. Infect. Dis.* 33, 1433–1434. doi: 10.1086/322523

Burnie, J. P., Carter, T. L., Hodgetts, S. J., and Matthews, R. C. (2006). Fungal heat-shock proteins in human disease. *FEMS Microbiol. Rev.* 30, 53–88. doi: 10.1111/j.1574-6976.2005.00001.x

Carroll, S. B. (2008). Evo-Devo and an expanding evolutionary synthesis: a genetic theory of morphological evolution. *Cell* 134, 25–36. doi: 10.1016/j.cell.2008.06.030

Chakrabarti, A., Bonifaz, A., Gutierrez-Galhardo, M. C., Mochizuki, T., and Li, S. (2014). Global epidemiology of Sporotrichosis. *Sabouraudia* 53, 3–14. doi: 10.1093/mmy/myu062

Chen, S., Zhou, Y., Chen, Y., and Jia, G. (2018). Fastp: an ultra-fast all-in-one Fastq preprocessor. *Bioinformatics* 34, i884–i890. doi: 10.1093/bioinformatics/bty560

Cheng, Z. X., Guo, C., Chen, Z. G., Yang, T. C., Zhang, J. Y., Wang, J., et al. (2019). Glycine, serine and threonine metabolism confounds efficacy of complement-mediated killing. *Nat. Commun.* 10:3325. doi: 10.1038/s41467-019-11129-5

Cho, K. I., Kim, D., and Lee, D. (2009). A feature-based approach to modeling protein-protein interaction hot spots. *Nucleic Acids Res.* 37, 2672–2687. doi: 10.1093/nar/gkp132

Choi, W., and Dean, R. A. (1997). The adenylate cyclase gene Mac1 of Magnaporthe Grisea controls Appressorium formation and other aspects of growth and development. *Plant Cell* 9, 1973–1983. doi: 10.1105/tpc.9.11.1973

Clutterbuck, A. J. (1969). A mutational analysis of conidial development in aspergillus Nidulans. *Genetics* 63:317. doi: 10.1093/genetics/63.2.317

Cormack, B. P., Ghori, N., and Falkow, S. (1999). An Adhesin of the yeast pathogen Candida Glabrata mediating adherence to human epithelial cells. *Science* 285, 578–582. doi: 10.1126/science.285.5427.578

Cortés Juan Carlos, G., Curto, M. Á., Carvalho, V. S. D., Pérez, P., and Ribas, J. C. (2019). The fungal Cell Wall as a target for the development of new antifungal therapies. *Biotechnol. Adv.* 37:107352. doi: 10.1016/j.biotechadv.2019.02.008

Danecek, P., Bonfield, J. K., Liddle, J., Marshall, J., Ohan, V., Pollard, M. O., et al. (2021). Twelve years of Samtools and Bcftools. *Gigascience* 10:giab008. doi: 10.1093/gigascience/giab008

Dos Reis, T. F., Silva, L. P., de Castro, P. A., et al. (2019). The *Aspergillus fumigatus* mismatch repair Msh2 homolog is important for virulence and azole resistance. *Msphere* 4, E00416–E00419. doi: 10.1128/mSphere.00416-19

Eisenman, H. C., Frases, S., Nicola, A. M., Rodrigues, M. L., and Casadevall, A. (2009). Vesicle-associated Melanization in *Cryptococcus neoformans*. *Microbiology* 155, 3860–3867. doi: 10.1099/mic.0.032854-0

Etxebeste, O., Otamendi, A., Garzia, A., Espeso, E. A., and Cortese, M. S. (2019). Rewiring of transcriptional networks as a major event leading to the diversity of asexual multicellularity in Fungi. *Crit. Rev. Microbiol.* 45, 548–563. doi: 10.1080/1040841X.2019.1630359

Farha, M. A., and Brown, E. D. (2019). Drug repurposing for antimicrobial discovery. *Nat. Microbiol.* 4, 565–577. doi: 10.1038/s41564-019-0357-1

Félix-Contreras, C., Alba-Fierro, C. A., Ríos-Castro, E., Luna-Martínez, F., Cuéllar-Cruz, M., and Ruiz-Baca, E. (2020). Proteomic analysis of *Sporothrix schenckii* Cell Wall reveals proteins involved in oxidative stress response induced by Menadione. *Microb. Pathog.* 141:103987. doi: 10.1016/j.micpath.2020.103987

Feng, P., Xie, Z., Sun, J., Zhang, J., Li, X., Lu, C., et al. (2010). Molecular cloning, characterization and expression of Pmrsr1, a Ras-related gene from yeast form of Penicillium Marneffei. *Mol. Biol. Rep.* 37, 3533–3540. doi: 10.1007/s11033-009-9947-y

García-Carnero, L. C., and Martínez-Álvarez, J. A. (2022). Virulence factors of *Sporothrix schenckii*. *J. Fungi* 8:318. doi: 10.3390/jof8030318

Haozhen, W., Ziyin, L., Yang, L., Zhao, L., Gao, T., Lu, X., et al. (2023). Virtual screening of novel 24-Dehydroxysterol reductase (Dhcr24) inhibitors and the biological evaluation of Irbesartan in cholesterol-lowering effect. *Molecules* 28:643. doi: 10.3390/molecules28062643

Hodgetts, S., Matthews, R., Morrissey, G., Mitsutake, K., Piper, P., and Burnie, J. (1996). Over-expression of *Saccharomyces Cerevisiae* Hsp90 enhances the virulence of this yeast in mice. *FEMS Immunol. Med. Microbiol.* 16, 229–234. doi: 10.1111/j.1574-695X.1996.tb00140.x

Höft, M. A., Duvenage, L., and Claire, J. H. (2022). Key thermally dimorphic fungal pathogens: shaping host immunity. *Open Biol.* 12:210219. doi: 10.1098/rsob.210219

Hu, L., Deng, B., Wu, R., Zhan, M., Hu, X., and Huang, H. (2024). Optimized expression of peptidyl-prolyl Cis/Transisomerase Cyclophilinb with prokaryotic toxicity from Sporothrix Globosa. *J. Ind. Microbiol. Biotechnol.* 51:17. doi: 10.1093/jimb/kuae017

Huang, Y. X., Xu, Y. L., Yu, C. X., Li, H. J., Yin, X. R., Wang, T. S., et al. (2011). Effect of Praziquantel prolonged administration on granuloma formation around Schistosoma Japonicum eggs in lung of sensitized mice. *Parasitol. Res.* 109, 1453–1459. doi: 10.1007/s00436-011-2485-2

Iyer, R. R., Pluciennik, A., Burdett, V., and Modrich, P. L. (2006). DNA mismatch repair: functions and mechanisms. *Chem. Rev.* 106, 302–323. doi: 10.1002/chin.200620268

Jadamba, E., and Shin, M. (2016). A systematic framework for drug repositioning from integrated omics and drug phenotype profiles using pathway-drug network. *Biomed. Res. Int.* 2016:7147039. doi: 10.1155/2016/7147039

Joao, I., Bujdáková, H., and Jordao, L. (2020). Opportunist coinfections by nontuberculous mycobacteria and Fungi in immunocompromised patients. *Antibiotics* 9:771. doi: 10.3390/antibiotics9110771

Kalvari, I., Nawrocki, E. P., Ontiveros-Palacios, N., Argasinska, J., Lamkiewicz, K., Marz, M., et al. (2021). Rfam 14: expanded coverage of metagenomic, viral and Microrna families. *Nucleic Acids Res.* 49, D192–D200. doi: 10.1093/nar/gkaa1047

Karbwang, J., and Harinasuta, T. (1992). Overview: clinical pharmacology of Antimalarials. *Southeast Asian J. Trop. Med. Public Health* 23, 95–109

Konrat, R., Papp, H., Kimpel, J., Rössler, A., Szijártó, V., Nagy, G., et al. (2022). The anti-histamine Azelastine, identified by computational drug repurposing, inhibits infection by major variants of Sars-Cov-2 in cell cultures and reconstituted human nasal tissue. *Front. Pharmacol.* 13:861295. doi: 10.3389/fphar.2022.861295

Krysan, D. J. (2016). Challenges in the development of novel Anticryptococcal agents. *Future Med. Chem.* 8, 1375–1377. doi: 10.4155/fmc-2016-0123

Langmead, B., Wilks, C., Antonescu, V., and Charles, R. (2019). Scaling read aligners to hundreds of threads on general-purpose processors. *Bioinformatics* 35, 421–432. doi: 10.1093/bioinformatics/bty648

Legrand, M., Chan, C. L., Jauert, P. A., and Kirkpatrick, D. T. (2007). Role of DNA mismatch repair and double-Strand break repair in genome stability and antifungal drug resistance in *Candida albicans*. *Eukaryot. Cell* 6, 2194–2205. doi: 10.1128/EC.00299-07

Levine, M. (2010). Transcriptional enhancers in animal development and evolution. *Curr. Biol.* 20, R754–R763. doi: 10.1016/j.cub.2010.06.070

Liu, Z., Li, S. S., Zhang, G. Y., Lv, S., Wang, S., and Li, F. Q. (2024). Whole transcriptome sequencing for revealing the pathogenesis of Sporotrichosis caused by Sporothrix Globosa. *Sci. Rep.* 14:359. doi: 10.1038/s41598-023-50728-7

Lopes-Bezerra, L. M., Mora-Montes, H. M., and Zhang, Y. (2018). Sporotrichosis between 1898 and 2017: the evolution of knowledge on a changeable disease and on emerging etiological agents. *Med. Mycol.* 56, 126–143. doi: 10.1093/mmy/myx103

Love, M. I., Huber, W., and Anders, S. (2014). Moderated estimation of fold change and dispersion for Rna-Seq data with Deseq2. *Genome Biol.* 15, 1–21. doi: 10.1186/s13059-014-0550-8

Lv, S., Xin, H., Liu, Z., Lin, Y., Hanfei, W., and Li, F. (2022). Clinical epidemiology of Sporotrichosis in Jilin Province, China (1990–2019): a series of 4969 cases. *Infect. Drug Resist.* 15, 1753–1765. doi: 10.2147/IDR.S354380

Lythgoe, M. P., and Middleton, P. (2020). Ongoing clinical trials for the Management of the Covid-19 pandemic. *Trends Pharmacol. Sci.* 41, 363–382. doi: 10.1016/j.tips.2020.03.006

Ma, X., Zhao, Y., Yang, T., Gong, N., Chen, X., Liu, G., et al. (2022). Integration of network pharmacology and molecular docking to explore the molecular mechanism of Cordycepin in the treatment of Alzheimer's disease. *Front. Aging Neurosci.* 14:1058780. doi: 10.3389/fnagi.2022.1058780

Martinez-Lopez, R., Monteoliva, L., Diez-Orejas, R., Nombela, C., and Gil, C. (2004). The Gpi-anchored protein Caecm33p is required for Cell Wall integrity, morphogenesis and virulence in *Candida albicans*. *Microbiology* 150, 3341–3354. doi: 10.1099/mic.0.27320-0

McTavish, D., and Sorkin, E. M. (1989). Azelastine. A review of its Pharmacodynamic and pharmacokinetic properties, and therapeutic potential. *Drugs* 38, 778–800. doi: 10.2165/00003495-198938050-00005

Montoya, M. C., Beattie, S., Alden, K. M., and Krysan, D. J. (2020). Derivatives of the antimalarial drug Mefloquine are broad-Spectrum antifungal molecules with activity against drug-resistant clinical isolates. *Antimicrob. Agents Chemother.* 64, e02331–e02319. doi: 10.1128/AAC.02331-19

Moreira, M. H., Almeida, F. C. L., Domitrovic, T., and Palhano, F. L. (2021). A systematic structural comparison of all solved small proteins deposited in Pdb. The effect of disulfide bonds in protein fold. *Comput. Struct. Biotechnol. J.* 19, 6255–6262. doi: 10.1016/j.csbj.2021.11.015

Moreira, J. A. S., Freitas, D. F. S., and Lamas, C. C. (2015). The impact of Sporotrichosis in Hiv-infected patients: a systematic review. *Infection* 43, 267–276. doi: 10.1007/s15010-015-0746-1

Motoyama, T., Kondoh, Y., Shimizu, T., Hayashi, T., Honda, K., Uchida, M., et al. (2022). Identification of Scytalone dehydratase inhibitors effective against melanin biosynthesis dehydratase inhibitor-resistant *Pyricularia oryzae*. *J. Agric. Food Chem.* 70, 3109–3116. doi: 10.1021/acs.jafc.1c04984

Nava-Pérez, N., Neri-García, L. G., Romero-González, O. E., Terrones-Cruz, J. A., García-Carnero, L. C., and Mora-Montes, H. M. (2022). Biological and clinical attributes of Sporothrix Globosa, a causative agent of Sporotrichosis. *Infect. Drug Resist.* 15:2067. doi: 10.2147/IDR.S362099

Ortiz-Ramírez, J. A., Cuéllar-Cruz, M., and López-Romero, E. (2022). *Sporothrix Schenckii*cell compensatory responses of Fungi to damage of the Cell Wall induced by Calcofluor white and Congo red with emphasis on and a review. *Front. Cell. Infect. Microbiol.* 12:976924. doi: 10.3389/fcimb.2022.976924

Park, K. (2019). A review of computational drug repurposing. *Transl. Clinic. Pharmacol.* 27, 59–63. doi: 10.12793/tcp.2019.27.2.59

Perlroth, J., Choi, B., and Spellberg, B. (2007). Nosocomial fungal infections: epidemiology, diagnosis, and treatment. *Med. Mycol.* 45, 321–346. doi: 10.1080/13693780701218689

Pertea, M., Pertea, G. M., Antonescu, C. M., Chang, T.-C., Mendell, J. T., and Salzberg, S. L. (2015). Stringtie enables improved reconstruction of a transcriptome from Rna-Seq reads. *Nat. Biotechnol.* 33, 290–295. doi: 10.1038/nbt.3122

Pruitt, K. D., Tatusova, T., and Maglott, D. R. (2007). Ncbi reference sequences (Refseq): a curated non-redundant sequence database of genomes, transcripts and proteins. *Nucleic Acids Res.* 35, D61–D65. doi: 10.1093/nar/gkl842

Saraiva, F. D. F., Hoagland, B. D. S., Do Valle, A. C. F., Fraga, B. B., de Barros, M. B., de Oliveira Schubach, A., et al. (2012). Sporotrichosis in Hiv-infected patients: report of 21 cases of endemic Sporotrichosis in Rio De Janeiro, Brazil. *Sabouraudia* 50, 170–178. doi: 10.3109/13693786.2011.596288

Smith, S. J., Rebeiz, M., and Davidson, L. (2018). From pattern to process: studies at the Interface of gene regulatory networks, morphogenesis, and evolution. *Curr. Opin. Genet. Dev.* 51, 103–110. doi: 10.1016/j.gde.2018.08.004

Soneson, C., Love, M. I., and Robinson, M. D. (2015). Differential analyses for Rna-Seq: transcript-level estimates improve gene-level inferences. *F1000Research* 4:1521. doi: 10.12688/f1000research.7563.2

Swamidass, S. J. (2011). Mining small-molecule screens to repurpose drugs. *Brief. Bioinform.* 12, 327–335. doi: 10.1093/bib/bbr028

Teixeira, M. M., de Almeida, L. G. P., Kubitschek-Barreira, P., Alves, F. L., Kioshima, E. S., Abadio, A. K., et al. (2014). Comparative genomics of the major fungal agents of human and animal Sporotrichosis: Sporothrix Schenckii and Sporothrix Brasiliensis. *BMC Genomics* 15:943. doi: 10.1186/1471-2164-15-943

Tummino, T. A., Rezelj, V. V., Fischer, B., Fischer, A., O'Meara, M. J., Monel, B., et al. (2021). Drug-induced Phospholipidosis confounds drug repurposing for Sars-Cov-2. *Science* 373, 541–547. doi: 10.1126/science.abi4708

Van Cutsem, J., Kurata, H., Matsuoka, H., Mikami, Y., Pfaller, M. A., Scalarone, G. M., et al. (1994). Antifungal drug susceptibility testing. *J. Med. Vet. Mycol.* 32, 267–276. doi: 10.1080/02681219480000891

Wang, Y., Aisen, P., and Casadevall, A. (1995). *Cryptococcus Neoformans* melanin and virulence: mechanism of action. *Infect. Immun.* 63, 3131–3136. doi: 10.1016/1380-2933(95)00016-X

Wang, H.-L., Kim, S., and Breuil, C. (2001). A Scytalone dehydratase gene from Ophiostoma Floccosum restores the Melanization and pathogenicity phenotypes of a melanin-deficient Colletotrichum Lagenarium mutant. *Mol. Gen. Genomics.* 266, 126–132. doi: 10.1007/s004380100534

Wang, D., Zhang, D.-D., Song, J., Li, J. J., Wang, J., Li, R., et al. (2022). Verticillium Dahliae Cfem proteins manipulate host immunity and differentially contribute to virulence. *BMC Biol.* 20:55. doi: 10.1186/s12915-022-01254-x

Watts, A. M., Cripps, A. W., West, N. P., and Cox, A. J. (2019). Modulation of allergic inflammation in the nasal mucosa of allergic rhinitis sufferers with topical pharmaceutical agents. *Front. Pharmacol.* 10:294. doi: 10.3389/fphar.2019.00294

Yu, J.-H. (2010). Regulation of development in aspergillus Nidulans and *Aspergillus fumigatus*. *Mycobiology* 38, 229–237. doi: 10.4489/MYCO.2010.38.4.229

Zhang, Z., Li, L., and Wang, H. (2024). Sporothrix globosadisasters pile up on the rubbing heel: as secondary infection to infection. *Emerg. Microb. Infect.* 13:2358073. doi: 10.1080/22221751.2024.2358073

Zheng, F., Gao, W., and Wang, Y. (2021). *Sporothrix schenckii* map of dimorphic switching-related signaling pathways in based on its transcriptome. *Mol. Med. Rep.* 24:12285. doi: 10.3892/mmr.2021.12285

Zu, J., Yao, L., and Song, Y. (2020). Sporothrix Globosath2 biased immunity with altered B cell profiles in circulation of patients with Sporotrichosis caused by. *Front. Immunol.* 11:570888. doi: 10.3389/fimmu.2020.570888

frontiers | Frontiers in Microbiology

TYPE Original Research
PUBLISHED 01 May 2025
DOI 10.3389/fmicb.2025.1580450

OPEN ACCESS

EDITED BY
Rosa Alduina,
University of Palermo, Italy

REVIEWED BY
Jun Zhao,
Nanjing Normal University, China
Thi Thuy Do,
Department of Agriculture Food and the Marine, Ireland

*CORRESPONDENCE
Yadong Yang
✉ yadong_tracy@cau.edu.cn

RECEIVED 20 February 2025
ACCEPTED 14 April 2025
PUBLISHED 01 May 2025

CITATION
Yu T, Cheng L, Zhang Q, Yang J, Zang H, Zeng Z and Yang Y (2025) Characterization of antibiotic resistance genes and virulence factors in organic managed tea plantation soils in southwestern China by metagenomics.
Front. Microbiol. 16:1580450.
doi: 10.3389/fmicb.2025.1580450

Characterization of antibiotic resistance genes and virulence factors in organic managed tea plantation soils in southwestern China by metagenomics

Taobing Yu[1,2], Lang Cheng[1,2], Qing Zhang[3], Jida Yang[3], Huadong Zang[1,2], Zhaohai Zeng[1,2] and Yadong Yang[1,2]*

[1]State Key Laboratory of Maize Bio-breeding, China Agricultural University, Beijing, China, [2]College of Agronomy and Biotechnology, China Agricultural University, Beijing, China, [3]Agricultural Environment and Resources Institute, Yunnan Academy of Agricultural Sciences, Kunming, China

Sustainable organic management practices have gained significant attentions for its potential health and environmental benefits. However, the spread of antibiotic resistance genes (ARGs) and virulence factors (VFs) in soils, plants, and agricultural products has severely limited the development of organic managements on agriculture. At present, the distribution and assembly of ARGs and VFs in organic managed tea plantation systems remains largely unknown. Here, we used metagenomic analysis to explore soil microbial taxa, ARGs and VFs in 20 years of conventional managed (CM) and organic managed (OM) tea plantation soils. Results showed that total abundance of ARGs in OM was 16.9% ($p < 0.001$) higher than that in CM, and the increased ARGs were *rpoB2*, *evgS*, *MuxB*, *TaeA*, and *efrA*. As for VFs, OM significantly increased the abundance of adherence, stress protein and actin-based motility compared to CM. Moreover, OM increased the relative abundance of soil microbial taxa harboring ARGs and VFs, which were *Streptomyces*, *Pseudomonas*, and *Terrabacter*, compared to CM. Network analysis suggested that OM increased the positive interactions of microbial taxa-ARGs, microbial taxa-VFs and ARGs-VFs compared to CM. Impact of stochastic process on the assembly of soil microbial taxa, ARGs and VFs in OM was stronger than that in CM. Overall, these findings provide a basis for integrating ARGs, VFs and pathogen hosts to assess the ecological and health risks in long-term organic managed soils, and increased efforts need to be done in reducing ARGs, VFs and bacterial pathogens in fertilizers for organic managements on agriculture.

KEYWORDS

organic management, antibiotic resistance genes, virulence factors, assembly process, soil microorganisms

1 Introduction

In last decades, the widespread use and misuse of antibiotics in medical has led to the prevalence of antibiotic resistance genes (ARGs) in microbial communities (Kuppusamy et al., 2018; Wang J. H. et al., 2022). With the increase of ARGs and antibiotic resistant bacteria (ARBs) in the environment, antibiotic resistance poses a serious threat to ecological security and public health (Tiedje et al., 2019; Zhang et al., 2022). Soils are probably the most important hosts of ARGs, and a large number and diversity of ARGs have been found in soils around the world (Xiao et al., 2016; Braga et al., 2017). The ARGs in farmland soils can enter to plant

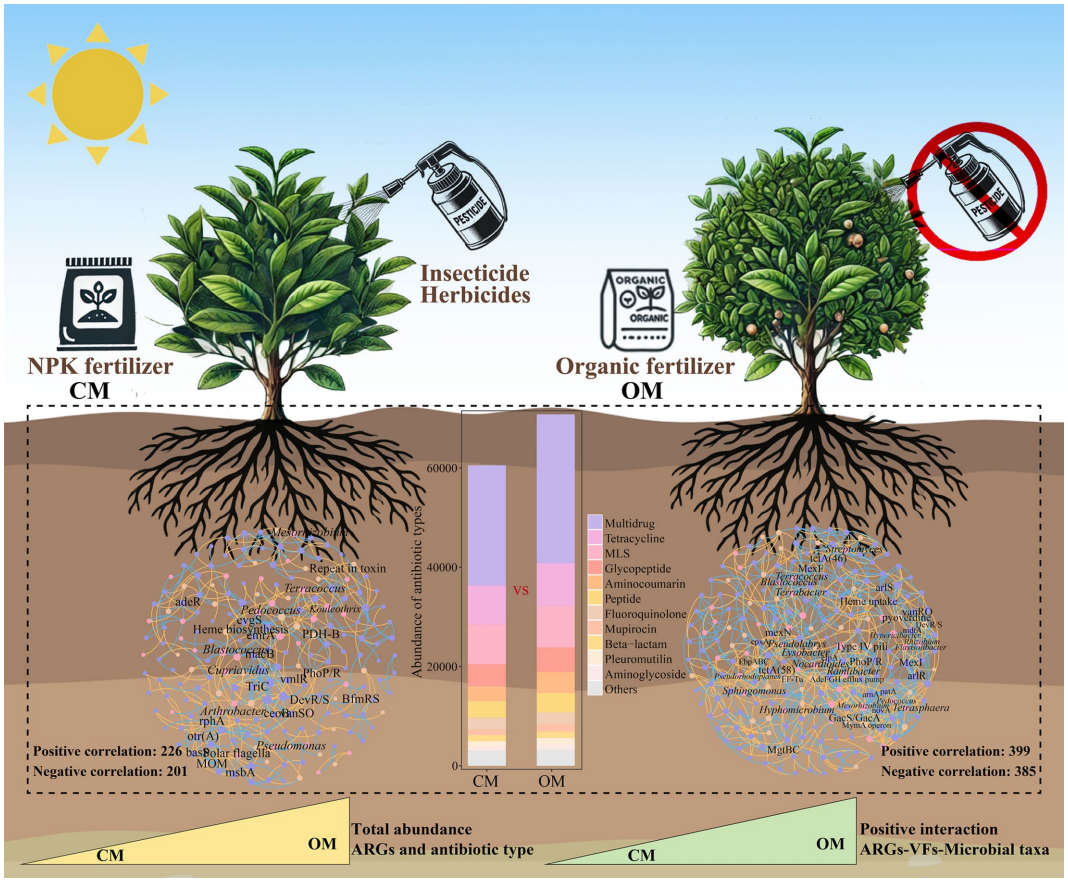

GRAPHICAL ABSTRACT

stems, leaves and agricultural products, and further spread to humans along the food chain, posing a major threat to human health (Zhang et al., 2019; Song et al., 2023). Besides, the virulence factors (VFs) enable pathogenic bacteria to colonize a host, establish infection and confer virulence, thereby enabling its bacterial hosts to invade humans or animals and cause disease (Wu H. J. et al., 2008; Liang et al., 2020). When the ARGs coexist with VFs in the genome, the risk of the genome to humans or animals will increase (Liang et al., 2020). Many studies have reported that anthropogenic activities (such as irrigation, landfilling of waste, fertilization and cropping practices, especially organic fertilization) significantly enriched the abundance of ARGs in soils (Wang et al., 2014; Wu et al., 2017; Wang et al., 2018). Hence, it is urgent to assess to distribution and interaction of ARGs and VFs in organic managed farmland systems.

Tea (*Camellia sinensis* L.) plantations are widely distributed in tropical and subtropical acidic soils (Wang et al., 2016). Normally, high nitrogen fertilization rate was applied to obtain high yield in tea plantations (Yang et al., 2023), but its misuse may trigger negative environmental impacts (Wang L. L. et al., 2020). Organic management, such as using livestock manure, can reduce chemical fertilizer application, maintain soil fertility and improve soil biodiversity (Guo et al., 2017; Ekman et al., 2020). However, inputs of livestock-derived organic fertilizers may introduce ARGs and ARBs into farmland soils (Han et al., 2018; Sanz et al., 2022). Therefore, antibiotic resistance may spread from organically amended soils to crops, products and ultimately to consumers (Yang et al., 2018). Recent findings shown that the coexistence and convergence of ARGs and VFs in pathogenic bacteria significantly increased the risk of microbial contaminants in the environment (Yang et al., 2018; Liang et al., 2020; Li et al., 2023). Therefore, it is necessary to understand the characteristics of ARGs and VFs in long-term organic managed soils.

Studies have demonstrated that soil properties and microbial diversity are the main drivers that influence ARGs and VFs distribution (Nõlvak et al., 2016; Wei et al., 2022; Wu et al., 2023a; Wang L. et al., 2024). It is found that abundance and diversity of ARGs in soil are related to soil type and nutrient content in organic farming systems (Wang L. et al., 2022). Besides, soil physicochemical variables, such as soil organic carbon (SOC), total nitrogen (TN), soil TN:TP ratio and microbiomass-P, are strongly associated with the distribution and prevalence of ARGs or VFs in soils (Guo et al., 2020; Wang L. et al., 2020; Kang et al., 2023). Furthermore, soil microorganisms carrying ARGs can influence plant-associated microbiota through direct contact between the plant rhizosphere and bulk soil environment, and ultimately accelerate the evolution of ARGs in plant compartments (Chen et al., 2018). Environmental heterogeneity has been shown to determine the diversity and distribution of bacterial communities, and soil property variables induced by fertilization may indirectly influence ARGs distribution by shaping soil bacterial communities (Li H. et al., 2022; Wu et al., 2023b). Therefore, it is essential to elucidate the complexity and correlation of microbial communities and soil properties impacts on ARGs and VFs distribution in long-term organic managed soils.

Here, we used macrogenomic sequencing to analyze soil microbial communities, antibiotic resistance genes (ARGs) and Virulence factors (VFs) in conventional and organic managed tea plantation soils after 20 years. The aims of this study were (I) to investigate the effects of conventional and organic managements on soil microbial communities, ARGs and VFs; (II) to explore the biotic and abiotic factors that affect the composition and distribution of ARGs and VFs.

2 Materials and methods

2.1 Study site and soil sampling

Soil samples of the 0–20 cm layer were collected in July 2023 from a 20-year managed tea plantation (22.48°N, 100.58°E) in Pu'er City, Yunnan Province, China. The study site has a typical subtropical monsoon climate, with an annual mean precipitation of 1,311 mm and annual mean temperature of 21.5°C. Two treatments: conventional managed (CM, only NPK fertilizer) or organic managed (OM, livestock organic fertilizer) tea plantation soils with 20 years were selected in this study. The tea variety in the experimental area is Yunkang 10. The long-term experimental field was managed according to local practices, which usually received NPK fertilizer or sheep manure compost for the past two decades. The organic management fertilization method includes basal fertilizer (November to December every year) and topdressing (May of the following year). The basal fertilizer was 12,000 kg ha^{-1} and the topdressing was 3,000 kg ha^{-1}. The organic matter content, total nutrient content and pH of the organic fertilizer were 60, 5% and 7.5, respectively. In conventional management, the compound fertilizer (1,050 kg ha^{-1}; N-P-K: 22-5-5) was applied in June each year, and Glyphosate and Diafenthiuron were used for weeding and pest extermination, respectively. In order to ensure the representativeness of the soil samples, we established 6 plots (20 m × 5 m) for each fertilization treatment to collect soil. Each plot used a five-point sampling method to collect soil, and five individual samples were mixed to obtain a duplicate sample. In total, 12 soil samples (2 treatments × 6 replicates) were obtained, then the soil samples were stored at 4°C and −80°C, respectively.

2.2 Analysis of soil properties and enzyme activities

Soil pH was determined using a pH meter (1:2.5, w/v). Soil organic carbon (SOC) and total nitrogen (TN) were determined by the $K_2Cr_2O_7$ oxidation–reduction titration and Kjeldahl digestion methods (Bao, 2000), respectively. Soil ammonium nitrogen (NH_4^+-N) and nitrate nitrogen (NO_3^--N) were determined using a microplate spectrophotometer (Thermo1510, Multiskan Go; Thermo Scientific Inc., Waltham, MA, United States). Activity of β-1, 4-glucosidase (BG), β-cellobiohydrolase (CE), β-xylosidase (BX), β-1,4-N-acetylglucosaminidase (NAG) and L-leucine aminopeptidase (LAP) were determined by a microplate spectrophotometer (Ex. 360 nm; Em. 450 nm; Thermo Scientific Inc., Waltham, MA, United States) using 4-methylumbelliferone (MUF) and 7-amino-4-methylcoumarin (AMC) coupled substrates (Marx et al., 2001).

2.3 DNA extraction, metagenomics sequencing and data analysis

Total microbial genomic DNA was extracted from 0.5 g soil using the E.Z.N.A.® soil DNA Kit (Omega Bio-tek, Norcross, GA, United States), and the quality of extracted DNA was measured using NanoDrop® ND-2000 spectrophotometer (Thermo Scientific Inc., Waltham, MA, United States). The shotgunmetagenomic sequencing were performed using Novaseq6000 (Shanghai Majorbio Bio-pharm Technology Co., Ltd., Shanghai, China).

Raw sequences were trimmed and filtered using fastp version 0.20.0 software. Reads with average quality score lower than 20, containing more than three "N," with length shorter than 50 bp and those reads matching the Illumina background sequences (artifact, spike-ins or phiX) were all removed. CD-HIT version 4.6.1 software was used for clustering, and the longest gene was selected as the representative sequence to construct a non-redundant gene set. Use BLASTP version 2.3.0 software to compare the non-redundant gene set with the NR database version 20,200,604, and obtain the species annotation results through the taxonomic information database corresponding to the NR database (Altschul et al., 1997).

2.4 ARGs and VFs analysis

We use the Comprehensive Antibiotic Resistance Database (CARD version 3.0.9) with Antibiotic Resistance Ontology (ARO) as its core for annotation of antibiotic resistance genes (ARGs) (Yang et al., 2022). The non-redundant gene sets were compared to the CARD database using BLASTP version 2.3.0 software, and the annotation of E to $1e^{-5}$ was selected. The setting parameters for ARGs annotation were ≥90% of sequence identity and ≥25 amino acids of alignment length. The ARGs obtained were classified by type (antibiotics to which the genes are resistant) and subtype (antibiotic resistance genes). To identify virulence factors (VFs) sequences in our data, open reading frames (ORFs) were compared against the virulence factor database (VFDB version 2020.07.03) using blastx with the *E*-value to $1e^{-5}$. The ORF with identity ≥90% and coverage ≥ 90% was annotated as a VFs (Liu B. et al., 2022; Liu W. B. et al., 2022). In addition, we annotated the species of ARGs or VFs to identify host bacteria.

2.5 Statistical analysis

Unpaired t tests were performed for significance analysis of two groups, and *p* values were adjusted by the false discovery rate test. Heatmap, boxplot and stacked chart were created using the OmicStudio.[1] Principal coordinate analysis (PCoA) and redundancy analysis (RDA) were performed using the "vegan" package in R version 4.2.2 (Oksanen et al., 2013). Procrustes analysis was

1 https://www.omicstudio.cn/tool

performed to examine the correlations between soil microbial communities, ARGs and VFs, and the sum of squares (M^2) and *p*-value were used to determine the consistency of two datasets. The neutral community model (NCM) was performed using the "hmisc" and "minpack.lm" packages in R version 4.2.2 to evaluate the impact of stochastic dispersal on the assembly of soil microbial communities, ARGs and VFs (Ning et al., 2019). We selected soil microbial taxa, ARGs and VFs with relative abundance greater than 0.1% to construct the co-occurrence network. The correlations were computed using the "Hmisc" package in R version 4.2.2, with a strict absolute value threshold set to 0.9. To increase the credibility of the network analysis, only correlations with adjusted *p* values less than 0.01 were retained. Network visualization was performed using the Gephi version 0.9.2 software (Bastian et al., 2009; Yu et al., 2023).

3 Results

3.1 Soil properties and enzyme activities

Soil properties and enzyme activities varied greatly in OM and CM soils (Supplementary Table S1). The soil pH, TN content and SOC content in OM was 29.9, 9.3 and 6.6% ($p < 0.05$) higher than that in CM. The soil activities of NAG and LAP in OM was 26.8 and 184.1% ($p < 0.05$) higher than that in CM. However, no difference was detected in content of NO_3^--N and NH_4^+-N, and activity of BG and CE between OM and CM (Supplementary Table S1).

3.2 Microbial diversity and community composition

A total of 6.1–7.6 Gb high quality clean reads was obtained after quality control for each sample (Supplementary Table S2). The filtered sequences were assembled *de novo* and 233,226 to 550,838 sequences were obtained, with a 481–598 bp for N50 and 332–345 bp for N90, for each sample. Each sample has 264,897–678,746 ORFs with a mean 373–419 bp per sample (Supplementary Table S3). Furthermore, bacteria and archaea dominated in total sequences with proportion of 65.3 and 19.5%, respectively (Supplementary Table S4).

The Shannon index of soil microbial communities in OM was 3.6% higher than that in CM (Figure 1a, $P < 0.001$). Similarly, OM significantly altered soil microbial community composition compared to CM (Figure 1). Actinobacteria, Proteobacteria, Acidobacteria, and Chloroflexi dominanted in abundance at the phylum level, with relative abundance of 31.9–40.7%, 27.7–36.5%, 10.8–14.9%, and 6.8–10.7%, respectively (Figure 1b). OM increased relative abundance of Proteobacteria, Gemmatimonadetes and Bacteroidota by 24.1, 56.6 and 37.4%, while reduced relative abundance of Actinobacteria and Chloroflexi by 12.6 and 34.2% compared to CM (Figure 1b, $P < 0.001$). Further analysis showed OM significantly increased relative abundance of the genera *Nocardioides*, *Terrabacter*, *Rhodococcus*, *Arthrobacter*, *Streptomyces*, *Sphingomonas*, *Pseudolabrys*, *Lysobacter*, and *Pseudomonas* within the changed phyla compared to CM (Figure 1c; Supplementary Table S5, $p < 0.001$).

3.3 Abundance and composition of ARGs and VFs

PCoA demonstrated that composition of ARGs were significantly separated in OM and CM (Figure 2a, $P = 0.004$). The total abundance of ARGs in OM was 16.9% higher than that in CM (Figure 2b, $P < 0.001$). A total of 21 ARGs and 945 subtypes were detected in OM and CM. Multidrug, Tetracycline, MLS and Glycopeptide were the major ARGs components in all samples, with abundance of 23788.9–30589.7, 7709.7–8851.8, 7681.3–8466.5 and 4324.6–5001.8, respectively (Figure 2c). Among them, OM significantly enriched the abundance of 13 antibiotics (i.e., Multidrug, Tetracycline, MLS, Glycopeptide, Aminocoumarin, Peptide, Mupirocin, Beta-lactam, Pleuromutilin, Fosfomycin, Triclosan, Diaminopyrimidine, and Bicyclomycin), while decreased the abundance of 5 antibiotics (Fluoroquinolone, Aminoglycoside, Rifamycin, Elfamycin, and Nucleoside), compared to CM (Supplementary Table S6). Subsequently, differential analysis on the top abundant 30 subtypes showed that OM enriched relative abundance of 10 subtypes (*rpoB2*, *evgS*, *TaeA*, *MuxB*, *efrA*, *otr(A)*, *tetB(P)*, *mdtC*, *efrB*, and *vanRM*), while decreased relative abundance of 16 subtypes (*macB*, *tetA(58)*, *oleC*, *bcrA*, *mtrA*, *msbA*, *efpA*, *arlR*, *kdpE*, *tlrC*, *baeS*, *facT*, *patA*, *evgA*, *patB*, and *lmrC*), compared to CM (Figure 2d; Supplementary Table S7). Furthermore, the potential host test of ARGs showed that *Mycobacterium* (Unclassified), *Bradyrhizobium* (B. sp._*35–63-5*), *Streptomyces* (S. sp._*CEV_2–1*, S. sp._*ADI95-17*, *S. chartreusis*, S. sp._*LAM7114* and *S. rishiriensis*), *Saccharopolyspora* (*S. shandongensis* and *S. hirsuta*) and *Actinomadura* (*A. amylolytica* and *A. hibisca*) were shared hosts for both CM and OM. A total of 23 unique hosts were detected in CM, such as *Bacillus* (*B. cereus*), *Dictyobacter* (D. *kobayashii* and *D. aurantiacus*), *Bradyrhizobium* (B. sp._*35–63-5*) and *Amycolatopsis* (A. *vastitatis* and *A. kentuckyensis*), while 10 unique hosts were detected in OM, such as *Terrabacter* (Terrabacter. sp._*3264*), *Pseudomonas* (*P. aeruginosa*), *Pseudonocardia* (P. *hierapolitana*), *Tetrasphaera* (T. sp._*HKS02*) and *Microbispora* (M. sp._*GKU_823*) (Supplementary Table S8).

PCoA demonstrated that composition of VFs were significantly separated between OM and CM (Figure 3a, $P = 0.003$). Iron uptake system, adherence, secretion systems, regulation, toxin and antiphagocytosis were the dominant encoded functions for both OM and CM, with relative abundance of 23.61–26.55, 16.44–18.67, 12.16–12.71, 11.32–12.26, 9.82–11.21, and 9.53–9.94, respectively (Figure 3b). Among them, OM enriched the relative abundance of adherence, stress protein, serum resistance, phase variation, complement protease, exoenzyme and actin-based motility, while decreased the relative abundance of iron uptake system, secretion system, regulation, toxin and magnesium uptake system, compared to CM (Supplementary Table S9). Further analysis of the top abundant 40 VFs showed that OM significantly increased VFs related to the putative hosts of *Acinetobacter baumannii* (AdeFGH), *Francisella tularensis subsp.* (repeat in toxin and EF-Tu), *Pseudomonas aeruginosa* (HSI-I and alginate), *Legionella pneumophila subsp.* (Hsp60), *Pseudomonas stutzeri* (pyridine-2,6-dithiocarboxylic acid), *Pseudomonas syringae pv* (GacS/GacA), *Mycobacterium smegmatis str* (proteasome-associated proteins) (Figure 3c; Supplementary Table S10). However, OM significantly decreased VFs associated with *Aeromonas hydrophila subsp.* (Polar flagella and repeat in toxin), *Mycobacterium sp.* (MymA operon), *Mycobacterium tuberculosis* (PDIM, PhoP/R and PhoP), *Mycobacterium ulcerans* (GPL locus) (Figure 3c; Supplementary Table S10).

10.3389/fmicb.2025.1580450

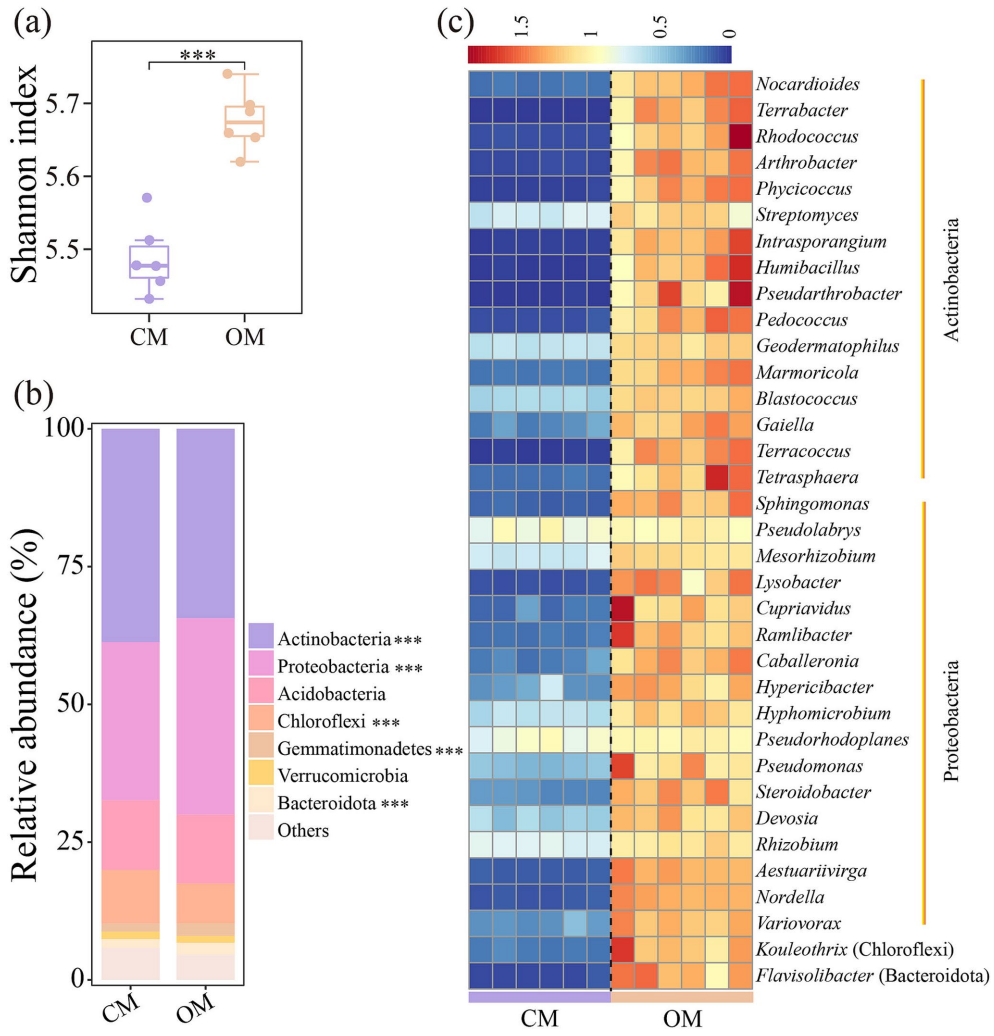

FIGURE 1
Shannon index **(a)**, relative abundance of abundant phyla **(b)**, and genera with significant differences in relative abundance **(c)** of soil bacterial community in conventional managed (CM) and organic managed (OM) tea plantation soils. Values are means (n = 6). ***p < 0.001.

3.4 Assembly processes and environmental drivers of microbial taxa, ARGs and VFs

The neutral community model fitting results showed that the explained variance of soil microbial communities (R^2_{OM} = 0.906, R^2_{CM} = 0.871), ARGs (R^2_{OM} = 0.925, R^2_{CM} = 0.775) and VFs (R^2_{OM} = 0.936, R^2_{CM} = 0.706) in OM was higher than that in CM (Figure 4). These results underscore the important role played of stochastic processes in shaping assembly of soil microbial communities, ARGs and VFs, particularly in OM. We found that OM decreased the m value (the migration rate of community) of soil microbial communities, ARGs and VFs, indicating that the species and gene dispersal was lower, compared to CM (Figure 4).

Soil properties and enzyme activities correlated significantly with composition of soil microbial communities (F = 5.33, p = 0.004), ARGs (F = 15.01, p = 0.003) and VFs (F = 21.30, p = 0.003). RDA result illustrated that RDA1 and RDA2 explained 48.2% of the microbial variations (Figure 5a), 83.2% of the ARGs variations (Figure 5b) and 79.9% of the VFs variations (Figure 5c). Furthermore, soil pH, TN, SOC, NAG and LAP were the main environmental factors driving the composition of soil microbial communities, ARGs and VFs (Supplementary Table S11).

3.5 Relationships between microbial taxa, ARGs and VFs

The Procrustes analysis showed that ARGs and VFs of soil exhibited goodness-of-fit based on the Bray–Curtis dissimilarity metrics (M^2 = 0.116, p < 0.001, permutations = 999), indicating significant correlations between ARGs and VFs (Figure 6a). Similarly, Procrustes analysis showed that ARGs (M^2 = 0.182, p < 0.002, permutations = 999; Figure 6b) and VFs (M^2 = 0.157, p < 0.001, permutations = 999; Figure 6c) correlated significantly with microbial communities, respectively. Networks showed that OM increased the number of node, edge, correlation, average degree, graph density, modularity and average clustering coefficient of the network, while reduced the average path length, compared to CM (Figures 6d,e; Supplementary Table S12). These results suggested that organic management leads to tighter relationships

10.3389/fmicb.2025.1580450

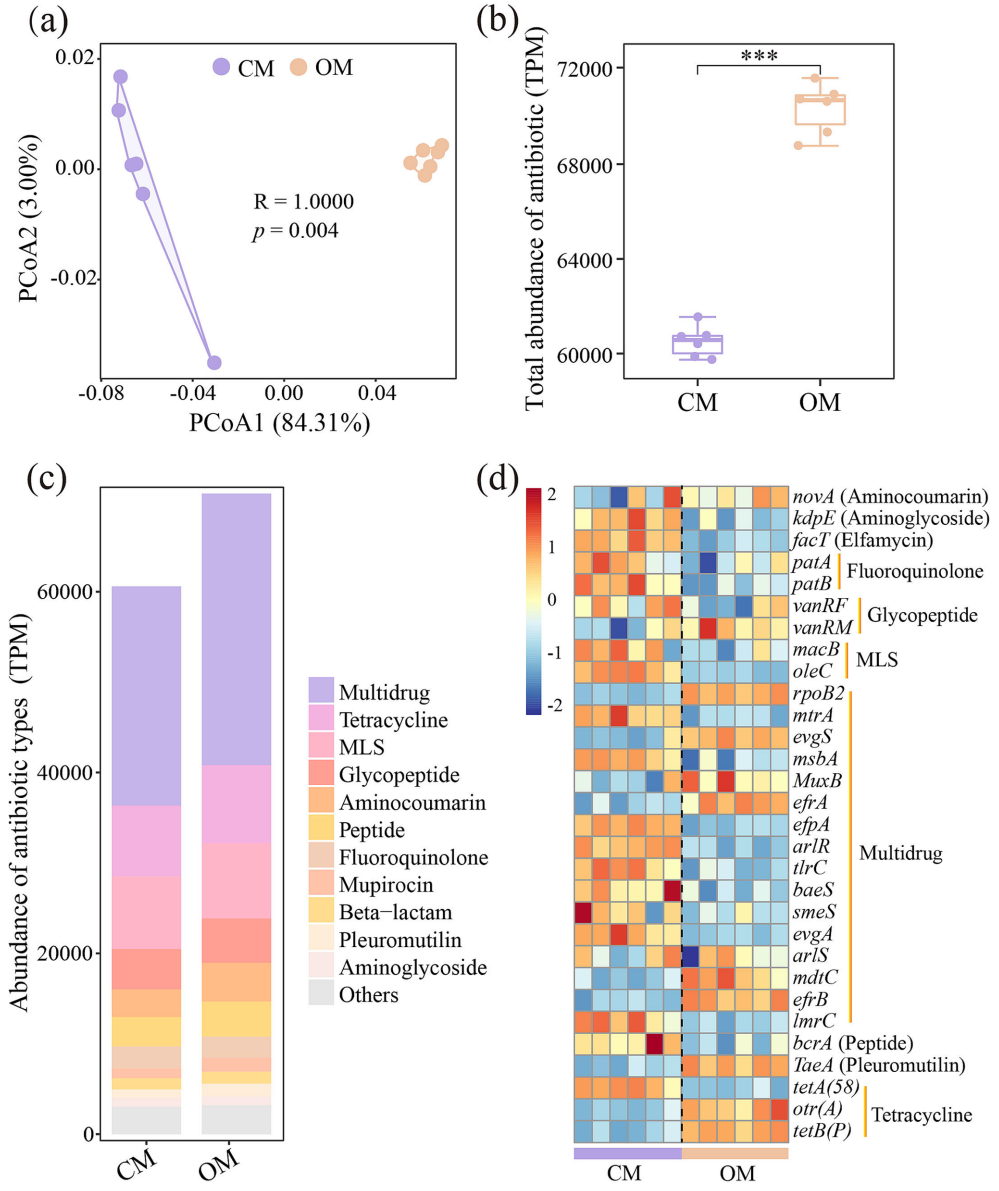

FIGURE 2
Differences in soil antibiotics resistance genes (ARGs) composition **(a)**, total abundance of ARGs **(b)**, abundance of main antibiotic types identified **(c)**, and differences in abundance of top 30 abundant ARGs subtypes **(d)** in conventional managed (CM) and organic managed (OM) tea plantation soils. Values are means (n = 6). ***p < 0.001. The data were standardized (z-score).

between microbial taxa, ARGs and VFs. Furthermore, OM increased the positive interaction of microbial taxa-ARGs (116 vs. 35), microbial taxa-VFs (40 vs. 21), and ARGs-VFs (119 vs. 57) compared to CM (Supplementary Table S13). Within the network of CM, *Mesorhizobium* (6 subtypes), *Kouleothrix* (5 subtypes) and *Blastococcus* (4 subtypes) were highly correlated with ARGs, and *Cupriavidus* (3 VFs), *Blastococcus* (2 VFs) and *Kouleothrix* (2 VFs) were highly correlated with VFs. Within the network of OM, *Streptomyces* (11 subtypes), *Flavisolibacter* (9 subtypes), *Rhizobium* (8 subtypes) *Blastococcus* (8 subtypes), *Terrabacter* (8 subtypes) and *Nocardioides* (7 subtypes) were highly correlated with ARGs, and *Pseudomonas* (5 VFs), *Hypericibacter* (4 VFs), *Ramlibacter* (4 VFs) and *Hyphomicrobium* (3 VFs) were highly correlated with VFs (Figures 6d,e).

4 Discussion

The composition of microbial communities and antibiotic resistance in agricultural soils was closely related to soil health, food production safety and human welfare (Tshikantwa et al., 2018; Bertola et al., 2021). Organic management was reported to increase soil microbial community diversity and change its community structure (Schmidt et al., 2019; Li J. et al., 2022; Shu et al., 2022). This may be attributed to organic matter addition increased organic carbon and available nitrogen contents in the soils (Wu T. et al., 2008), which provided a favorable nutritional environment for microorganisms. On the other hand, organic fertilizer can effectively regulate soil acidification and improve the living environment for soil microorganisms (Chepkorir et al., 2018; Ye

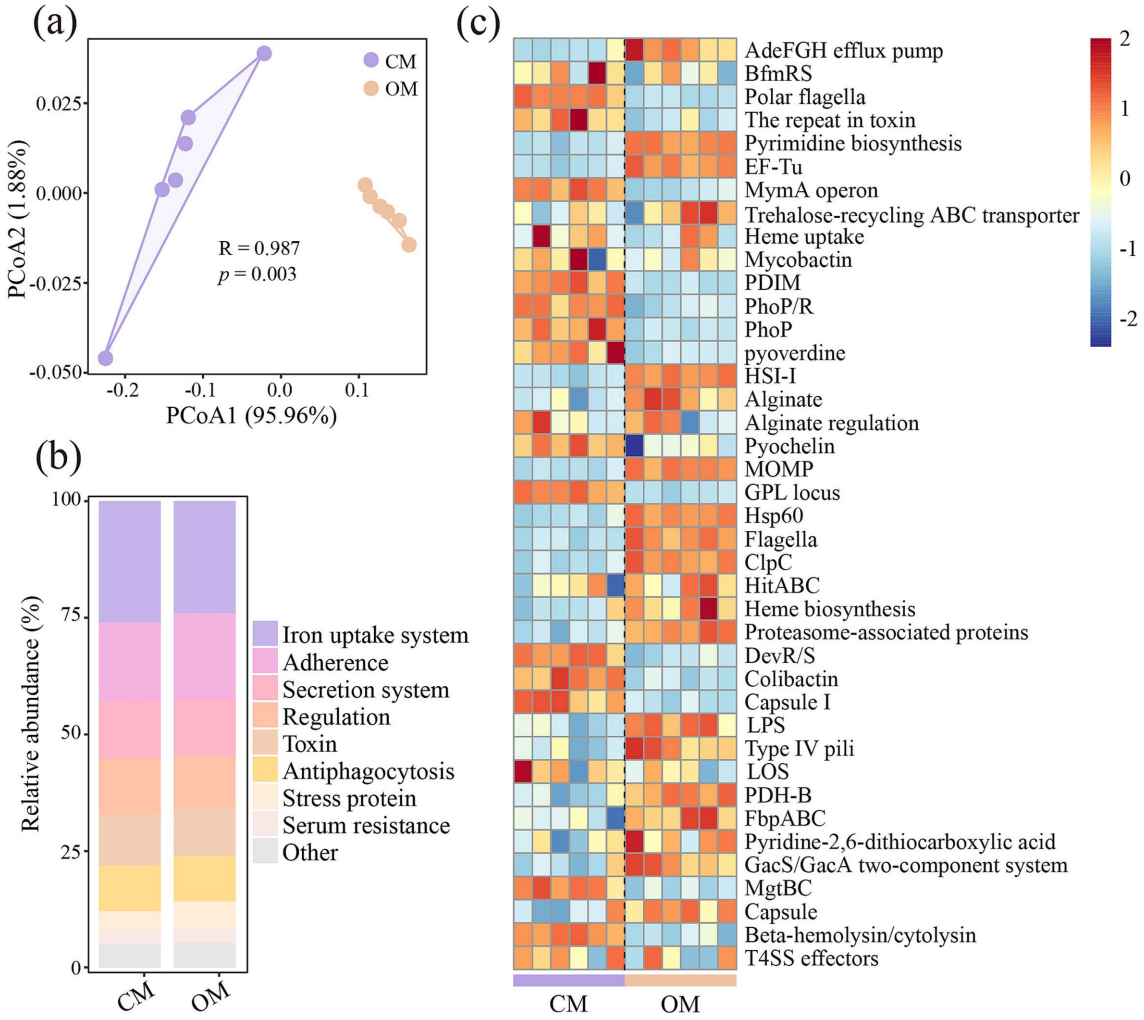

FIGURE 3
Differences in soil virulence factors (VFs) composition **(a)**, relative abundance of main VFs functions identified **(b)**, and difference in relative abundance of VFs **(c)** in conventional managed (CM) and organic managed (OM) tea plantation soils. Values are means (n = 6). The data were standardized (z-score).

et al., 2022), especially in tea plantations. Although organic fertilizer input brings many benefits to the soils, the application of livestock derived organic fertilizers also has the risk of contamination with antibiotics, virulence factors and pathogenic bacteria (Bloem et al., 2017).

In this study, OM significantly changed the ARGs composition and increased its abundance, which was consistent with previous findings (Chen et al., 2016; Sun et al., 2019). Livestock manure contains high levels of antibiotics, ARBs and ARGs (Fang et al., 2014; Wang X. R. et al., 2024), which can potentially spread into the environment when applied to agricultural fields (Joy et al., 2013). We found OM enriched the abundant of Multidrug, Tetracycline, MLS and Glycopeptide antibiotic types compared to CM. Previous studies have confirmed that application of manure introduced extra antibiotics into the agricultural ecosystems (Wang L. et al., 2020; Zhu et al., 2022; Xiao et al., 2023). Further, we explore the differences of main subtypes of the microbial risk genes and OM significantly enriched resistance genes affiliated to multidrug (*rpoB2*, *evgS*, *MuxB* and *efrA*) and Pleuromutilin (*TaeA*). These genes may increase soil resistance to multidrug and Pleuromutilin by encoding efflux pump or antibiotic target alteration (Alcock et al., 2020). In contrast, resistance genes significantly enriched in CM included MLS (*macB* and *oleC*), Tetracycline (*tetA(58)*), Aminocoumarin (*novA*) and Peptide (*bcrA*), and these genes were closely related to antibiotic efflux (Alcock et al., 2020). Virulence factors related to adherence, stress protein, serum resistance, phase variation, complement protease, exoenzyme and actin-based motility were significantly enriched in OM. Bacterial pathogens are able to adhere to host cells by produce a protein or polysaccharide surface layer, and specific enzymes participate in the invasion of host cells and tissues after adhesion (Huang et al., 2016). For intracellular survival, stress proteins affected their persistence and survival (Hingley-Wilson et al., 2010). The significant enrichment of these virulence factors in organically managed agricultural systems suggests that bacterial pathogens may have an enhanced ability to colonize and persist in these environments. Taken together, these results indicated that organic management increased some of ARGs and VFs, which

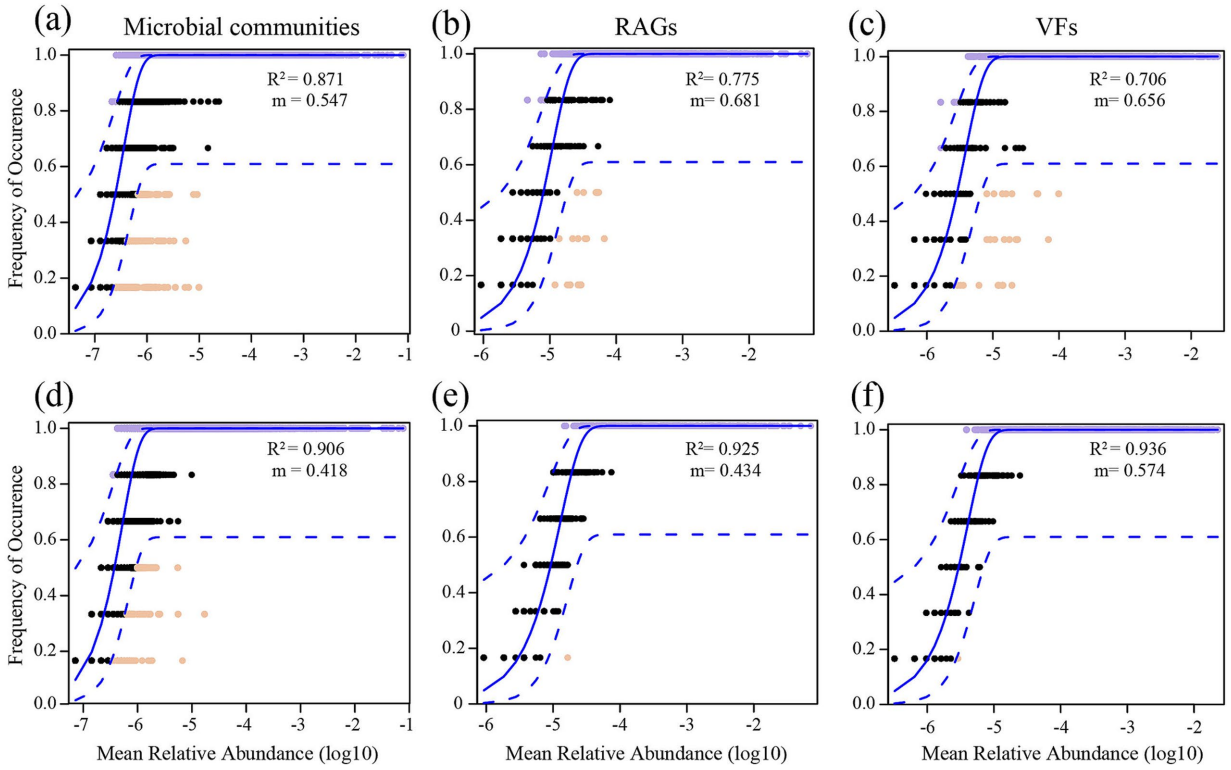

FIGURE 4
The neutral community model (NCM) of soil microbial communities **(a,d)**, antibiotics resistance genes (ARGs; **b,e**) and virulence factors (VFs; **c,f**) in conventional managed (CM) and organic managed (OM) tea plantation soils. The R^2 value signifies the fitness to the model, and m denotes the migration rate. Solid blue lines indicate optimal fits to the models, with dashed lines representing 95% confidence intervals surrounding the model prediction. Genes deviating from predictions, either occurring more or less frequently, are highlighted in distinct colors.

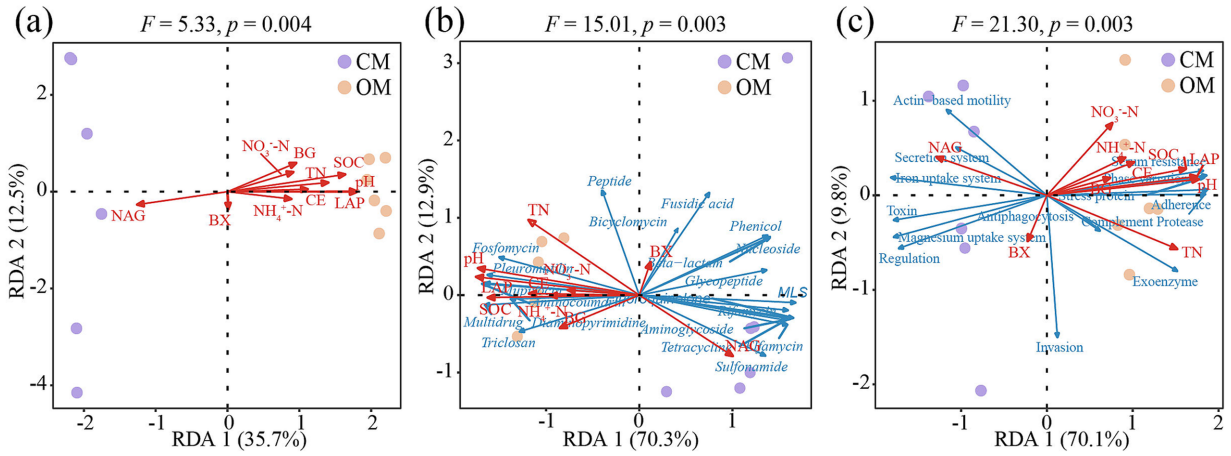

FIGURE 5
The redundancy analysis (RDA) shows the correlations between soil microbial communities **(a)**, antibiotics resistance genes (ARGs; **b**) and virulence factors (VFs; **c**) with soil properties and enzyme activities in conventional managed (CM) and organic managed (OM) tea plantation soils. Soil properties and enzyme activities are marked with red arrows. Antibiotic types and VFs functions are marked with blue arrows. pH, soil pH; NO_3^--N, nitrate nitrogen; NH_4^+-N, ammonium nitrogen; TN, total nitrogen; SOC, soil organic carbon; BG, β-1, 4-glucosidase; NAG, β-1,4-N-acetylglucosaminidase; BX, β-xylosidase; CE, β-cellobiohydrolase; and LAP, L-leucine aminopeptidase.

may pose a serious threat to public health (Carmeli et al., 2016; Coll et al., 2018).

Microbial risk depends not only on diversity and abundance of microbial communities, ARGs and VFs, but also on their patterns of coexistence in the same niche (Martínez et al., 2015; Liang et al., 2020). Procrustes analysis and network analysis found significant correlations between microbial communities, ARGs and VFs (Che et al., 2019; Li et al., 2023), and OM increased

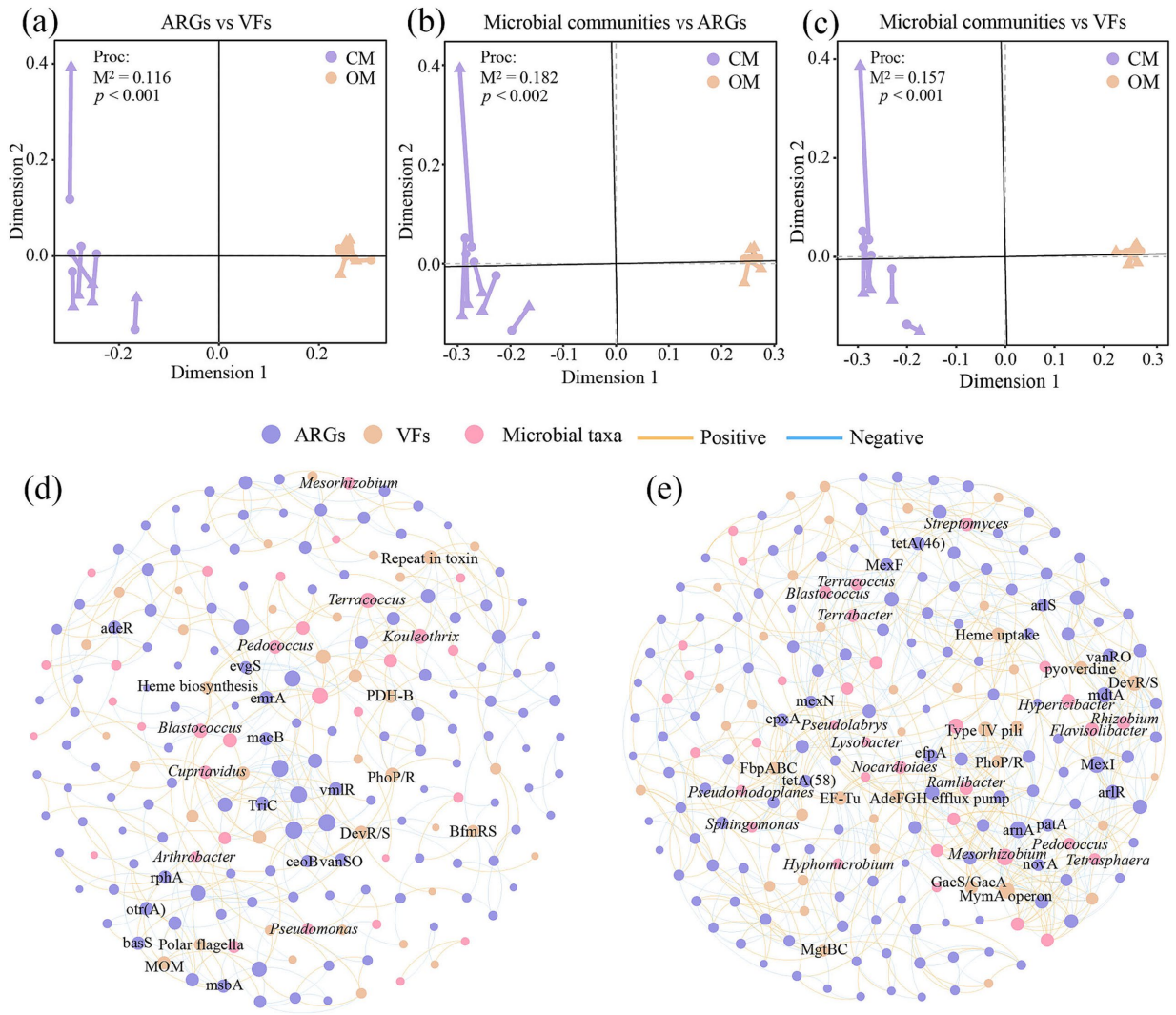

FIGURE 6
Procrustes analysis based on Bray-Curtis distance reveals the correlations between soil microbial communities **(a)**, antibiotics resistance genes (ARGs; **b**) and virulence factors (VFs; **c**), and co-occurrence network analysis shows the correlations between microbial taxa, ARGs and VFs in conventional managed (CM; **d**) and organic managed (OM; **e**) tea plantation soils based on Pearson coefficient. Nodes with different colors represent different microbial taxa, ARGs and VFs. Orange and blue edges represent positive and negative correlations, respectively.

network complexity (Xie et al., 2018), which may promote the coexistence of microbial taxa, ARGs and VFs thereby increase the risk of microbial contamination (Liang et al., 2020; Zhu et al., 2022). We found that OM increased more positive interactions of microbial taxa-ARGs, microbial taxa-VFs and ARGs-VFs which further supported this conclusion. Within the network, species in CM (such as *Kouleothrix* and *Blastococcus*) and OM (such as *Streptomyces*, *Blastococcus*, *Flavisolibacter*, *Terrabacter*, *Pseudomonas*) were significantly associated with many ARGs and VFs, suggesting that microbial taxa may carry various ARG subtypes and VFs (Yin et al., 2022). It is worth noting that *Streptomyces* (*S. rishiriensis*), *Pseudomonas* (*P. aeruginosa*) and *Terrabacter* (T. sp._*3264*) with significantly higher relative abundance in OM were identified as potential hosts carrying ARGs, which was consistent with previous findings (Ye et al., 2018; Sheam et al., 2020; Song et al., 2022). Meanwhile, several species affiliated to *Pseudomonas* were potential hosts of VFs in OM, including *P. aeruginosa*, *P. stutzeri* and *P. syringae pv*. The *P. aeruginosa* was a significant pathogen which increased risks of mortality and zoonotic diffusion among patients with sepsis (Dulger, 2020). These results indicate that close links existed between microbial taxa, ARGs and VFs in organic managed tea plantation soils, indicating the significance roles of microbial community succession in growth and spread of ARGs and VFs in soils.

Deterministic and stochastic processes play important roles in assembly of soil microbial communities, ARGs and VFs (Evans et al., 2017; Wang L. et al., 2024; Wang M. M. et al., 2024). Our results support the prominent role of stochastic processes in shaping the assembly of soil microbial communities, ARGs and VFs, particularly in organic managed systems. The higher stochastic assembly from ARGs and VFs in organic managed soils resulted in a more stable antibiotic resistome and virulence factor than that from conventional managed soils (Hou et al., 2021). For soil

microbial communities, long-term organic management increased resource availability to reduce resource competitiveness, which resulted in the dominance of stochasticity in soil microbial community assembly process (Badri et al., 2013; Chaparro et al., 2013). To some extent, the regulation principle of ARGs and VFs assembly by environmental stress is similar to regulation of soil microbial community assembly by resources (Liu B. et al., 2022; Liu W. B. et al., 2022). The importance of soil properties on soil microbial communities, ARGs and VFs varies under different management strategies (Cycon et al., 2019; Tang et al., 2023; Wu et al., 2023a). In this study, soil microbial communities, ARGs and VFs were strongly influenced by soil pH, TN, SOC, NAG, and LAP, as proved by previous findings (Zhu et al., 2022; Wu et al., 2023c; Shen et al., 2024). It has been reported that soil pH strongly affected the adsorption and desorption behavior of ARGs (Liu et al., 2010) and organic carbon, total nitrogen, and available potassium altered the distribution of ARGs in soils (Zhu et al., 2022). Furthermore, considering that ARGs and VFs are existed in microbial potential hosts, and the strong correlation between soil properties, enzyme activities and the resistance group may be mediated by soil microbial communities (Li T. T. et al., 2022).

5 Conclusion

Our study found that ARGs and VFs could be transferred into soils by agricultural managements in tea plantation. Organic management significantly increased diversity and abundance of ARGs and VFs, and increased relative abundance of microbial hosts harboring ARGs and VFs have significant impacts on soil and human health compared to conventional management. The assembly of microbial communities, ARGs and VFs in organic managed soils was more driven by stochastic processes than that in conventional managed soils. Furthermore, organic management increased the coexistence of microbial taxa-ARGs, microbial taxa-VFs and ARGs-VFs. Taken together, these findings provide more comprehensive insights into the spread, ecological processes and coexistence patterns of ARGs and VFs in tea plantation soils under long-term organic management.

Data availability statement

The datasets presented in this study can be found in online repositories. The names of the repository/repositories and accession number(s) can be found at: https://www.ncbi.nlm.nih.gov/, PRJNA1139650.

Author contributions

TY: Conceptualization, Data curation, Formal analysis, Writing – original draft, Writing – review & editing. LC: Data curation, Formal analysis, Writing – review & editing. QZ: Writing – review & editing. JY: Writing – review & editing. HZ: Writing – review & editing. ZZ: Writing – review & editing. YY: Conceptualization, Data curation, Funding acquisition, Project administration, Writing – review & editing.

Funding

The author(s) declare that financial support was received for the research and/or publication of this article. This work was supported by the Major Science and Technology Program in Yunnan Province (202202AE090029) and the National Natural Science Foundation of China (31901470).

Conflict of interest

The authors declare that the research was conducted in the absence of any commercial or financial relationships that could be construed as a potential conflict of interest.

Generative AI statement

The authors declare that no Gen AI was used in the creation of this manuscript.

Publisher's note

Supplementary material

The Supplementary material for this article can be found online at: https://www.frontiersin.org/articles/10.3389/fmicb.2025.1580450/full#supplementary-material

References

Alcock, B. P., Raphenya, A. R., Lau, T. T., Tsang, K. K., Bouchard, M., Edalatmand, A., et al. (2020). CARD 2020: antibiotic resistome surveillance with the comprehensive antibiotic resistance database. *Nucleic Acids Res.* 48, D517–D525. doi: 10.1093/nar/gkz935

Altschul, S. F., Madden, T. L., Schäffer, A. A., Zhang, J. H., Zhang, Z., Miller, W., et al. (1997). Gapped BLAST and PSI-BLAST: a new generation of protein database search programs. *Nucleic Acids Res.* 25, 3389–3402. doi: 10.1093/nar/25.17.3389

Badri, D. V., Chaparro, J. M., Zhang, R., Shen, Q., and Vivanco, J. M. (2013). Application of natural blends of phytochemicals derived from the root exudates of Arabidopsis to the soil reveal that phenolic-related compounds predominantly modulate the soil microbiome. *J. Biol. Chem.* 288, 4502–4512. doi: 10.1074/jbc.M112.433300

Bao, S. D. (2000). Soil agro-chemistrical analysis. *3rd Edn*. Beijing: China Agricultural Press.

Bastian, M., Heymann, S., and Jacomy, M. (2009). Gephi: an open source software for exploring and manipulating networks. *Proceedings of the International AAAI Conference on Web and Social Media* 3, 361–362.

Bertola, M., Ferrarini, A., and Visioli, G. (2021). Improvement of soil microbial diversity through sustainable agricultural practices and its evaluation by-omics

approaches: a perspective for the environment, food quality and human safety. *Microorganisms* 9:1400. doi: 10.3390/microorganisms9071400

Bloem, E., Albihn, A., Elving, J., Hermann, L., Lehmann, L., Sarvi, M., et al. (2017). Contamination of organic nutrient sources with potentially toxic elements, antibiotics and pathogen microorganisms in relation to P fertilizer potential and treatment options for the production of sustainable fertilizers: a review. *Sci. Total Environ.* 607-608, 225–242. doi: 10.1016/j.scitotenv.2017.06.274

Braga, L. P. P., Alves, R. F., Dellias, M. T. F., Navarrete, A. A., Basso, T. O., and Tsai, S. M. (2017). Vinasse fertirrigation alters soil resistome dynamics: an analysis based on metagenomic profiles. *Biodata Min.* 10:17. doi: 10.1186/s13040-017-0138-4

Carmeli, Y., Armstrong, J., Laud, P. J., Newell, P., Stone, G., Wardman, A., et al. (2016). Ceftazidime-avibactam or best available therapy in patients with ceftazidimeresistant Enterobacteriaceae and *Pseudomonas aeruginosa* complicated urinary tract infections or complicated intra-abdominal infections (REPRISE): a randomised, pathogen-directed, phase 3 study. *Lancet Infect. Dis.* 16, 661–673. doi: 10.1016/S1473-3099(16)30004-4

Chaparro, J. M., Badri, D. V., Bakker, M. G., Sugiyama, A., Manter, D. K., and Vivanco, J. M. (2013). Root exudation of phytochemicals in Arabidopsis follows specific patterns that are developmentally programmed and correlate with soil microbial functions. *PLoS One* 8:e55731. doi: 10.1371/journal.pone.0055731

Che, Y., Xia, Y., Liu, L., Li, A. D., Yang, Y., and Zhang, T. (2019). Mobile antibiotic resistome in wastewater treatment plants revealed by Nanopore metagenomic sequencing. *Microbiome* 7, 1–13. doi: 10.1186/S40168-019-0663-0/FIGURES/5

Chen, Q. L., An, X. L., Li, H., Su, J. Q., Ma, Y. B., and Zhu, Y. G. (2016). Long-term field application of sewage sludge increases the abundance of antibiotic resistance genes in soil. *Environ. Int.* 92-93, 1–10. doi: 10.1016/j.envint.2016.03.026

Chen, Q. L., An, X. L., Zheng, B. X., Ma, Y. B., and Su, J. Q. (2018). Long-term organic fertilization increased antibiotic resistome in phyllosphere of maize. *Sci. Total Environ.* 645, 1230–1237. doi: 10.1016/j.scitotenv.2018.07.260

Chepkorir, B. M., Ann, S., and Mbira, K. G. (2018). Effect of enriched sheep manure rates on physico-chemical parameters of tea soil in timbilil tea estate, Kericho, Kenya. *Int. J. Plant Soil Sci.* 25, 1–7. doi: 10.9734/IJPSS/2018/44866

Coll, F., Phelan, J., Hill-Cawthorne, G. A., Nair, M. B., Mallard, K., Ali, S., et al. (2018). Genome-wide analysis of multi-and extensively drug-resistant *Mycobacterium tuberculosis*. *Nat. Genet.* 50:764. doi: 10.1038/s41588-017-0029-0

Cycon, M., Mrozik, A., and Piotrowska-Seget, Z. (2019). Antibiotics in the soil environmentdegradation and their impact on microbial activity and diversity. *Front. Microbiol.* 10:412419. doi: 10.3389/fmicb.2019.00338

Dulger, D. (2020). Statistical analysis of the relationship between mortality and nosocomial factors in patients with septicemia and the importance of *Pseudomonas aeruginosa*. *Turk. J. Vet. Anim. Sci.* 44, 573–580. doi: 10.3906/vet-1912-13

Ekman, J., Goldwater, A., Bradbury, M., Matthews, J., and Rogers, G. (2020). Persistence of human pathogens in manure-amended Australian soils used for production of leafy vegetables. *Agriculture* 11:14. doi: 10.3390/agriculture11010014

Evans, S., Martiny, J. B., and Allison, S. D. (2017). Effects of dispersal and selection on stochastic assembly in microbial communities. *ISME J.* 11, 176–185. doi: 10.1038/ismej.2016.96

Fang, H., Wang, H. F., Cai, L., and Yu, Y. L. (2014). Prevalence of antibiotic resistance genes and bacterial pathogens in long-term manured greenhouse soils as revealed by metagenomic survey. *Environ. Sci. Technol.* 49, 1095–1104. doi: 10.1021/es504157v

Guo, J., Liu, W., Zhu, C., Luo, G., Kong, Y., Ling, N., et al. (2017). Bacterial rather than fungal community composition is associated with microbial activities and nutrient-use efficiencies in a paddy soil with short-term organic amendments. *Plant Soil* 424, 335–349. doi: 10.1007/s11104-017-3547-8

Guo, X. P., Zhao, S., Chen, Y. R., Yang, J., Hou, L. J., Liu, M., et al. (2020). Antibiotic resistance genes in sediments of the Yangtze estuary: from 2007 to 2019. *Sci. Total Environ.* 744:140713. doi: 10.1016/j.scitotenv.2020.140713

Han, X. M., Hu, H. W., Chen, Q. L., Yang, L. Y., Li, H. L., Zhu, Y. G., et al. (2018). Antibiotic resistance genes and associated bacterial communities in agricultural soils amended with different sources of animal manures. *Soil Biol. Biochem.* 126, 91–102. doi: 10.1016/j.soilbio.2018.08.018

Hingley-Wilson, S. M., Lougheed, K. E. A., Ferguson, K., Leiva, S., and Williams, H. D. (2010). Individual *Mycobacterium tuberculosis* universal stress protein homologues are dispensable in vitro. *Tuberculosis* 90, 236–244. doi: 10.1016/j.tube.2010.03.013

Hou, L. Y., Wang, H. J., Chen, Q. F., Su, J. Q., Gad, M., Li, J. W., et al. (2021). Fecal pollution mediates the dominance of stochastic assembly of antibiotic resistome in an urban lagoon (Yundang lagoon), China. *J. Hazard. Mater.* 417:126083. doi: 10.1016/j.jhazmat.2021.126083

Huang, Y., Wang, Q. L., Cheng, D. D., Xu, W. T., and Lu, N. H. (2016). Adhesion and invasion of gastric mucosa epithelial cells by *Helicobacter pylori*. *Front. Cell. Infect. Microbiol.* 6:159. doi: 10.3389/fcimb.2016.00159

Joy, S. R., Bartelt-Hunt, S. L., Snow, D. D., Gilley, J. E., Woodbury, B. L., Parker, D. B., et al. (2013). Fate and transport of antimicrobials and antimicrobial resistance genes in soil and runoff following land application of swine manure slurry. *Environ. Sci. Technol.* 47, 12081–12088. doi: 10.1021/es4026358

Kang, J., Qiu, W., Zhang, W., Liu, J., Yang, Z., Wu, Z., et al. (2023). Understanding how various forms of phosphorus stress affect microbiome functions and boost plant disease resistance: insights from metagenomic analysis. *Sci. Total Environ.* 904:166899. doi: 10.1016/j.scitotenv.2023.166899

Kuppusamy, S., Kakarla, D., Venkateswarlu, K., Megharaj, M., Yoon, Y. E., and Lee, Y. B. (2018). Veterinary antibiotics (VAs) contamination as a global agro-ecological issue: a critical view. *Agric. Ecosyst. Environ.* 257, 47–59. doi: 10.1016/j.agee.2018.01.026

Li, Y., Kong, F. G., Li, S., Wang, J., Hu, J. R., Chen, S., et al. (2023). Insights into the driving factors of vertical distribution of antibiotic resistance genes in long-term fertilized soils. *J. Hazard. Mater.* 456:131706. doi: 10.1016/j.jhazmat.2023.131706

Li, T. T., Li, R. C., Cao, Y. F., Tao, C. Y., Deng, X. H., Ou, Y. N., et al. (2022). Soil antibiotic abatement associates with the manipulation of soil microbiome via long-term fertilizer application. *J. Hazard. Mater.* 439:129704. doi: 10.1016/j.jhazmat.2022.129704

Li, J., Yang, Y., Wen, J., Mo, F., and Liu, Y. (2022). Continuous manure application strengthens the associations between soil microbial function and crop production: evidence from a 7-year multisite field experiment on the Guanzhong plain. *Agric. Ecosyst. Environ.* 338:108082. doi: 10.1016/j.agee.2022.108082

Li, H., Zheng, X., Tan, L., Shao, Z., Cao, H., and Xu, Y. (2022). The vertical migration of antibiotic-resistant genes and pathogens in soil and vegetables after the application of different fertilizers. *Environ. Res.* 203:111884. doi: 10.1016/j.envres.2021.111884

Liang, J. S., Mao, G. N., Yin, X. L., Ma, L. P., Liu, L., Bai, Y. H., et al. (2020). Identification and quantification of bacterial genomes carrying antibiotic resistance genes and virulence factor genes for aquatic microbiological risk assessment. *Water Res.* 168:115160. doi: 10.1016/j.watres.2019.115160

Liu, W. B., Cheng, Y. F., Guo, J. J., Duan, Y. H., Wang, S., Xu, Q. C., et al. (2022). Long-term manure inputs induce a deep selection on agroecosystem soil antibiotic resistome. *J. Hazard. Mater.* 436:129163. doi: 10.1016/j.jhazmat.2022.129163

Liu, Y., Xu, Z., Wu, X., Gui, W., and Zhu, G. (2010). Adsorption and desorption behavior of herbicide diuron on various Chinese cultivated soils. *J. Hazard. Mater.* 178, 462–468. doi: 10.1016/j.jhazmat.2010.01.105

Liu, B., Zheng, D., Zhou, S., Chen, L., and Yang, J. (2022). VFDB 2022: a general classification scheme for bacterial virulence factors. *Nucleic Acids Res.* 50, D912–D917. doi: 10.1093/nar/gkab1107

Martínez, J. L., Coque, T. M., and Baquero, F. (2015). What is a resistance gene? Ranking risk in resistomes. *Nat. Rev. Microbiol.* 13, 116–123. doi: 10.1038/nrmicro3399

Marx, M. C., Wood, M., and Jarvis, S. C. (2001). A microplate fluorimetric assay for the study of enzyme diversity in soils. *Soil Biol. Biochem.* 33, 1633–1640. doi: 10.1016/S0038-0717(01)00079-7

Ning, D. L., Deng, Y., Tiedje, J. M., and Zhou, J. Z. (2019). A general framework for quantitatively assessing ecological stochasticity. *Proc. Natl. Acad. Sci. USA* 116, 16892–16898. doi: 10.1073/pnas.1904623116

Nõlvak, H., Truu, M., Kanger, K., Tampere, M., Espenberg, M., Loit, E., et al. (2016). Inorganic and organic fertilizers impact the abundance and proportion of antibiotic resistance and integron-integrase genes in agricultural grassland soil. *Sci. Total Environ.* 562, 678–689. doi: 10.1016/j.scitotenv.2016.04.035

Oksanen, J., Blanchet, F. G., Kindt, R., Legendre, P., Minchin, P., O'Hara, R. B., et al. (2013). Vegan: community ecology package. R Package Version 2.0–10.

Sanz, C., Casado, M., Navarro-Martin, L., Cañameras, N., Carazo, N., Matamoros, V., et al. (2022). Implications of the use of organic fertilizers for antibiotic resistance gene distribution in agricultural soils and fresh food products. A plot-scale study. *Sci. Total Environ.* 815:151973. doi: 10.1016/j.scitotenv.2021.151973

Schmidt, J. E., Vannette, R. L., Igwe, A., Blundell, R., Casteel, C. L., and Gaudin, A. C. (2019). Effects of agricultural management on rhizosphere microbial structure and function in processing tomato plants. *Appl. Environ. Microbiol.* 85, e01064–e01019. doi: 10.1128/AEM.01064-19

Sheam, M., Haque, Z., and Nain, Z. (2020). Towards the antimicrobial, therapeutic and invasive properties of *Mikania micrantha* Knuth: a brief overview. *J. Adv. Biotechnol. Exp. Ther.* 3, 92–101. doi: 10.5455/jabet.2020.d112

Shen, C., He, M., Zhang, J., Liu, J., and Wang, Y. (2024). Response of soil antibiotic resistance genes and bacterial communities to fresh cattle manure and organic fertilizer application. *J. Environ. Manag.* 349:119453. doi: 10.1016/j.jenvman.2023.119453

Shu, X. Y., He, J., Zhou, Z. H., Xia, L. L., Hu, Y. F., Zhang, Y. L., et al. (2022). Organic amendments enhance soil microbial diversity, microbial functionality and crop yields: a meta-analysis. *Sci. Total Environ.* 829:154627. doi: 10.1016/j.scitotenv.2022.154627

Song, R., Sun, Y., Li, X., Ding, C., Huang, Y., Du, X., et al. (2022). Biodegradable microplastics induced the dissemination of antibiotic resistance genes and virulence factors in soil: a metagenomic perspective. *Sci. Total Environ.* 828:154596. doi: 10.1016/j.scitotenv.2022.154596

Song, D., Tang, X., Tariq, A., Pan, K., and Li, D. (2023). Regional distribution and migration potential of antibiotic resistance genes in croplands of Qinghai Tibet plateau. *Environ. Res.* 231:116233. doi: 10.1016/j.envres.2023.116233

Sun, Y. M., Qiu, T. L., Gao, M., Shi, M. M., Zhang, H. F., and Wang, X. M. (2019). Inorganic and organic fertilizers application enhanced antibiotic resistome in greenhouse soils growing vegetables. *Ecotoxicol. Environ. Saf.* 179, 24–30. doi: 10.1016/j.ecoenv.2019.04.039

Tang, S., Ma, Q., Marsden, K. A., Chadwick, D. R., Luo, Y., Kuzyakov, Y., et al. (2023). Microbial community succession in soil is mainly driven by carbon and nitrogen contents rather than phosphorus and Sulphur contents. *Soil Biol. Biochem.* 180:109019. doi: 10.1016/j.soilbio.2023.109019

Tiedje, J. M., Fang, W., Manaia, C. M., Virta, M., Sheng, H., Liping, M., et al. (2019). Antibiotic resistance genes in the human-impacted environment: a one health perspective. *Pedosphere* 29, 273–282. doi: 10.1016/S1002-0160(18)60062-1

Tshikantwa, T. S., Ullah, M. W., He, F., and Yang, G. (2018). Current trends and potential applications of microbial interactions for human welfare. *Front. Microbiol.* 9:1156. doi: 10.3389/fmicb.2018.01156

Wang, Y. C., Hao, X. Y., Wang, L., Xiao, B., Wang, X. C., and Yang, Y. J. (2016). Diverse Colletotrichum species cause anthracnose of tea plants (Camellia sinensis (L.) O. Kuntze) in China. *Sci. Rep.* 6:35287. doi: 10.1038/srep35287

Wang, L. L., Li, Q., Coulter, J. A., Xie, J. H., Luo, Z. Z., Zhang, R. Z., et al. (2020). Winter wheat yield and water use efficiency response to organic fertilization in northern China: a meta-analysis. *Agric. Water Manag.* 229:105934. doi: 10.1016/j.agwat.2019.105934

Wang, L., Li, Y., Zhao, Z., Zhu, M., and Hu, T. (2022). Tidal flat aquaculture pollution governs sedimentary antibiotic resistance gene profiles but not bacterial community based on metagenomic data. *Sci. Total Environ.* 833:155206. doi: 10.1016/j.scitotenv.2022.155206

Wang, F. H., Qiao, M., Su, J. Q., Chen, Z., Zhou, X., and Zhu, Y. G. (2014). High throughput profiling of antibiotic resistance genes in urban park soils with reclaimed water irrigation. *Environ. Sci. Technol.* 48, 9079–9085. doi: 10.1021/es502615e

Wang, L., Wang, J. H., Wang, J., Zhu, L., Conkle, J. L., and Yang, R. (2020). Soil types influence the characteristic of antibiotic resistance genes in greenhouse soil with long-term manure application. *J. Hazard. Mater.* 392:122334. doi: 10.1016/j.jhazmat.2020.122334

Wang, J. H., Wang, L., Zhu, L., Wang, J., and Xing, B. (2022). Antibiotic resistance in agricultural soils: source, fate, mechanism and attenuation strategy. *Crit. Rev. Environ. Sci. Technol.* 52, 847–889. doi: 10.1080/10643389.2020.1835438

Wang, F., Xu, M., Stedtfeld, R. D., Sheng, H., Fan, J., Liu, M., et al. (2018). Long-term effect of different fertilization and cropping systems on the soil antibiotic resistome. *Environ. Sci. Technol.* 52, 13037–13046. doi: 10.1021/acs.est.8b04330

Wang, X. R., Zhang, X., Li, N., Yang, Z. Z., Li, B. X., Zhang, X. L., et al. (2024). Prioritized regional management for antibiotics and heavy metals in animal manure across China. *J. Hazard. Mater.* 461:132706. doi: 10.1016/j.jhazmat.2023.132706

Wang, L., Zhang, T. L., Xiang, Q., Fu, C. X., Qiao, M., Ding, L. J., et al. (2024). Selective enrichment of virulence factor genes in the plastisphere under antibiotic and heavy metal pressures. *J. Hazard. Mater.* 465:133319. doi: 10.1016/j.jhazmat.2023.133319

Wang, M. M., Zhao, J. Y., Liu, Y., Huang, S. J., Zhao, C. Y., Jiang, Z. K., et al. (2024). Decipher soil resistance and virulence gene risks in conventional and organic farming systems. *J. Hazard. Mater.* 468:133788. doi: 10.1016/j.jhazmat.2024.133788

Wei, Z., Shen, W., Feng, K., Feng, Y., He, Z., Li, Y., et al. (2022). Organic fertilizer potentiates the transfer of typical antibiotic resistance gene among special bacterial species. *J. Hazard. Mater.* 435:128985. doi: 10.1016/j.jhazmat.2022.128985

Wu, T., Chellemi, D. O., Graham, J. H., Martin, K. J., and Rosskopf, E. N. (2008). Comparison of soil bacterial communities under diverse agricultural land management and crop production practices. *Microb. Ecol.* 55, 293–310. doi: 10.1007/s00248-007-9276-4

Wu, J., Guo, S., Li, K., Li, Z., Xu, P., Jones, D. L., et al. (2023b). Effect of fertilizer type on antibiotic resistance genes by reshaping the bacterial community and soil properties. *Chemosphere* 336:139272. doi: 10.1016/j.chemosphere.2023.139272

Wu, J., Guo, S., Lin, H. Y., Li, K. J., Li, Z. T., Wang, J. Y., et al. (2023c). Uncovering the prevalence and drivers of antibiotic resistance genes in soils across different land-use types. *J. Environ. Manag.* 344:118920. doi: 10.1016/j.jenvman.2023.118920

Wu, D., Huang, X. H., Sun, J. Z., Graham, D. W., and Xie, B. (2017). Antibiotic resistance genes and associated microbial community conditions in aging landfill systems. *Environ. Sci. Technol.* 51, 12859–12867. doi: 10.1021/acs.est.7b03797

Wu, H. J., Wang, A. H., and Jennings, M. P. (2008). Discovery of virulence factors of pathogenic bacteria. *Curr. Opin. Chem. Biol.* 12, 93–101. doi: 10.1016/j.cbpa.2008.01.023

Wu, J., Wang, J., Li, Z., Guo, S., Li, K., Xu, P., et al. (2023a). Antibiotics and antibiotic resistance genes in agricultural soils: a systematic analysis. *Crit. Rev. Environ. Sci. Technol.* 53, 847–864. doi: 10.1080/10643389.2022.2094693

Xiao, R. H., Huang, D. L., Du, L., Song, B., Yin, L. S., Chen, Y. S., et al. (2023). Antibiotic resistance in soil-plant systems: a review of the source, dissemination, influence factors, and potential exposure risks. *Sci. Total Environ.* 869:161855. doi: 10.1016/j.scitotenv.2023.161855

Xiao, K. Q., Li, B., Ma, L. P., Bao, P., Zhou, X., Zhang, T., et al. (2016). Metagenomic profiles of antibiotic resistance genes in paddy soils from South China. *FEMS Microbiol. Ecol.* 92:fiw023. doi: 10.1093/femsec/fiw023

Xie, W. Y., Yuan, S. T., Xu, M. G., Yang, X. P., Shen, Q. R., Zhang, W. W., et al. (2018). Long-term effects of manure and chemical fertilizers on soil antibiotic resistome. *Soil Biol. Biochem.* 122, 111–119. doi: 10.1016/j.soilbio.2018.04.009

Yang, L., Liu, W., Zhu, D., Hou, J., Ma, T., Wu, L., et al. (2018). Application of biosolids drives the diversity of antibiotic resistance genes in soil and lettuce at harvest. *Soil Biol. Biochem.* 122, 131–140. doi: 10.1016/j.soilbio.2018.04.017

Yang, X. D., Ni, K., Shi, Y. Z., Yi, X. Y., Ji, L. F., Wei, S. R., et al. (2023). Metagenomics reveals N-induced changes in carbon-degrading genes and microbial communities of tea (*Camellia sinensis* L.) plantation soil under long-term fertilization. *Sci. Total Environ.* 856:159231. doi: 10.1016/j.scitotenv.2022.159231

Yang, C., Zhao, Y., Cao, W., Xing, M., Xu, X., Wang, Z., et al. (2022). Metagenomic analysis reveals antibiotic resistance genes and virulence factors in the saline-alkali soils from the Yellow River Delta, China. *Environ. Res.* 214:113823. doi: 10.1016/j.envres.2022.113823

Ye, M., Sun, M., Zhao, Y., Jiao, W., Xia, B., Liu, M., et al. (2018). Targeted inactivation of antibiotic-resistant Escherichia coli and *Pseudomonas aeruginosa* in a soil-lettuce system by combined polyvalent bacteriophage and biochar treatment. *Environ. Pollut.* 241, 978–987. doi: 10.1016/j.envpol.2018.04.070

Ye, J., Wang, Y., Jia, X., Wu, Z., and Wang, H. (2022). Improvement of soil acidification in tea plantations by long-term use of organic fertilizers and its effect on tea yield and quality. *Front. Plant Sci.* 13:1055900. doi: 10.3389/fpls.2022.1055900

Yin, Y., Zhu, D., Yang, G., Su, J., and Duan, G. (2022). Diverse antibiotic resistance genes and potential pathogens inhabit in the phyllosphere of fresh vegetables. *Sci. Total Environ.* 815:152851. doi: 10.1016/j.scitotenv.2021.152851

Yu, T. B., Fang, X. Y., Liu, Y., Zang, H. D., Zeng, Z. H., and Yang, Y. D. (2023). Irrigation rather than fertilization drives the abundance, community structure and assembly process of soil denitrifiers. *Agric. Ecosyst. Environ.* 357:108688. doi: 10.1016/j.agee.2023.108688

Zhang, Y. J., Hu, H. W., Chen, Q. L., Singh, B. K., Yan, H., Chen, D., et al. (2019). Transfer of antibiotic resistance from manure-amended soils to vegetable microbiomes. *Environ. Int.* 130:104912. doi: 10.1016/j.envint.2019.104912

Zhang, Z., Zhang, Q., Wang, T., Xu, N., Lu, T., Hong, W., et al. (2022). Assessment of global health risk of antibiotic resistance genes. *Nat. Commun.* 13:1553. doi: 10.1038/s41467-022-29283-8

Zhu, L., Lian, Y., Lin, D., Huang, D., Yao, Y., Ju, F., et al. (2022). Insights into microbial contamination in multi-type manure-amended soils: the profile of human bacterial pathogens, virulence factor genes and antibiotic resistance genes. *J. Hazard. Mater.* 437:129356. doi: 10.1016/j.jhazmat.2022.129356

frontiers | Frontiers in Microbiology

TYPE Original Research
PUBLISHED 14 May 2025
DOI 10.3389/fmicb.2025.1546805

OPEN ACCESS

EDITED BY
Hemda Garelick,
Middlesex University, United Kingdom

REVIEWED BY
Okon Okwong Kenneth,
Federal University, Wukari, Nigeria
Pedro Teixeira,
National Institute of Health Dr. Ricardo Jorge, Portugal

*CORRESPONDENCE
Qingcao Li
lqc_lab@163.com

†These authors have contributed equally to this work and share first authorship

RECEIVED 17 December 2024
ACCEPTED 30 April 2025
PUBLISHED 14 May 2025

CITATION
Qiu X, Jiang M, Xu J, Wu Q, Lin C, Li W and Li Q (2025) Molecular characterization of carbapenem resistance mechanisms and phenotypic correlations in clinical *Klebsiella pneumoniae* isolates from Ningbo, China. *Front. Microbiol.* 16:1546805. doi: 10.3389/fmicb.2025.1546805

Molecular characterization of carbapenem resistance mechanisms and phenotypic correlations in clinical *Klebsiella pneumoniae* isolates from Ningbo, China

Xuedan Qiu[1†], Min Jiang[1†], Jianqiang Xu[1], Qiaoping Wu[1], Chenyao Lin[1], Weiying Li[2] and Qingcao Li[1*]

[1]Department of Clinical Laboratory, The Affiliated Li Huili Hospital of Ningbo University, Ningbo, China, [2]Department of Clinical Laboratory, Langxia Street Health Service Center, Ningbo, China

Objective: The purpose of this study is to understand the antimicrobial susceptibility and molecular distribution characteristics of carbapenem-resistant *Klebsiella pneumoniae* (CRKP) in the region, and to evaluate their correlation. Additionally, the study aims to investigate the transmission status of these strains.

Methods: A total of 150 CRKP collected from January 2019 to December 2021 in the Ningbo region were included in this study. Antimicrobial susceptibility testing was performed using broth microdilution method following CLSI guidelines (CLSI, 2023). The tested agents included: (1) basic antimicrobials (tigecycline, polymyxin B, ceftazidime-avibactam); and (2) combination therapy candidates (ertapenem, imipenem, levofloxacin, piperacillin-tazobactam, ceftriaxone, cefepime, trimethoprim-sulfamethoxazole, fosfomycin, amikacin, aztreonam, chloramphenicol, amoxicillin-clavulanate, ceftazidime). Resistance genes were detected using polymerase chain reaction (PCR). Multi-locus sequence typing (MLST) was employed to analyze the molecular characteristics and evolutionary trends of the strains to determine their clonal relationships.

Results: The 150 strains of CRKP exhibit high resistance rates to various conventional drugs; The sensitivity rates to tigecycline, polymyxin B, and ceftazidime-avibactam were 98.7, 98.0, and 68%, respectively; Conversely, the sensitivity rates to fosfomycin, amikacin, and chloramphenicol were 72.0, 40.0, and 16.7%, respectively; The main proportions of carbapemen genes producing in CRKP are as follows: *KPC-2* (61.3%), *NDM-5* (14.7%), *IMP-4* (8.0%), *OXA-232* (6.0%), and *OXA-181* (1.3%); The main proportions of β-lactamase resistance genes are as follows: *CTX-M-1* (13.33%), *CTX-M-3* (25.33%), *CTX-M-9* (17.33%), *CTX-M-14* (34.67%), *SHV-1* (26.66%), *SHV-11* (66.66%), *SHV-12* (18.66%), and *SHV-28* (10.00%); CRKP carrying class A, B, and D carbapenemases had a sensitivity rate greater than 96% for tigecycline and polymyxin B, while their sensitivities to ceftazidime-avibactam, aztreonam, and amikacin varied significantly ($p < 0.01$). Analysis of the MLST results for CRKP revealed that ST11 strains were predominant in the region. There was a significant difference in the resistance genes carried by ST11 strains compared to non-ST11 strains. While different healthcare institutions exhibited variations in ST types, the strains generally showed high homogeneity.

Conclusion: In the region, CRKP showed high sensitivity to tigecycline, polymyxin B, ceftazidime-avibactam, fosfomycin, amikacin, and chloramphenicol. The main carbapenemase genes identified were *KPC-2* and *NDM-5*. The inhibitory effects of ceftazidime-avibactam, aztreonam, and amikacin varied for CRKP carrying different enzyme types. ST11 strains were predominant in the region. There was a significant difference in the resistance genes carried by ST11 strains compared to non-ST11 strains. Clonal dissemination was observed both within the same healthcare institution and between different institutions.

KEYWORDS

***Klebsiella pneumoniae*, carbapenem-resistant, antibacterial susceptibility, resistance genes, MLST**

1 Introduction

Klebsiella pneumoniae (KP) commonly colonizes the human nasopharynx, skin, and intestines and is one of the main pathogens causing hospital-acquired infections. It poses significant risks and can lead to multiple systemic infections such as meningitis, pneumonia, abdominal infections, and bloodstream infections (Jiang et al., 2024). In recent years, the emergence of carbapenem-resistant *Klebsiella pneumoniae* (CRKP) has become a significant public health concern, particularly in China. The widespread use of carbapenem antibiotics has led to a steady increase in CRKP detection rates (Hu et al., 2020). According to data from the China Antimicrobial Resistance Surveillance System (CARSS, 2014–2023),[1] the prevalence of CRKP has shown a consistent upward trend in Zhejiang Province, with the Ningbo region being particularly affected (Gao et al., 2024). In healthcare settings in Ningbo, CRKP infections have exhibited a marked increase, reflecting a growing challenge in the management of antimicrobial resistance in the area. CRKP possesses significant pathogenicity, with mortality rates for bloodstream infections caused by it reaching as high as 45–75% (Venugopalan et al., 2017; Wang et al., 2018; Soares de Moraes et al., 2022). CRKP exhibits high resistance to commonly used antimicrobial drugs in clinical practice, resulting in a gradual reduction in available sensitive medications. Its broad transmission routes significantly increase the difficulty of treatment. In recent years, experts (Rodríguez-Baño et al., 2015; Guan et al., 2016) both domestically and internationally have reported reaching a consensus recommending a combination therapy approach for the treatment of CRKP infections. This approach is based on a combination of tigecycline, polymyxin B, imipenem, and ceftazidime-avibactam. Additional drugs included in the combination may be aminoglycosides, fosfomycin, and amoxicillin-clavulanic acid. Indeed, there are discrepancies in the reported sensitivity of these foundational antimicrobial agents for multidrug-resistant organisms and combination therapy drugs, including CRKP. Currently, there is a lack of systematic testing and evaluation in this regard. The mechanism of carbapenem resistance in CRKP is complex, with the most common being the production of carbapenemases (Sarva et al., 2023). Currently, carbapenemases are classified into three classes, A, B, and D, according to the Ambler classification system. Class A enzymes are mainly represented by *KPC* and *GES*, Class B enzymes are mainly represented by *IMP, VIM, GIM, SPM, SIM*, and *NDM*, and Class D enzymes are mainly represented by *OXA-48* (Çalık et al., 2022). The distribution of these carbapenemase genes varies significantly among CRKP strains across different regions (Angles-Yanqui et al., 2020; García-Betancur et al., 2021; Ge et al., 2024; Guo et al., 2024). In China, among CRKP clinical isolates, the primary carbapenemase types are *KPC* and *NDM*, with a small proportion of strains carrying *OXA-48* or *IMP-type* carbapenemase genes (Han et al., 2020; Li et al., 2021). Notably, several studies have reported that KPC-2 and NDM-1 are the most prevalent carbapenemases among CRKP clinical isolates in Eastern China, including the Ningbo region (Ding et al., 2024; Zhao et al., 2021), reflecting both regional epidemiological characteristics. Furthermore, strains producing different types of enzymes exhibit significant differences in resistance characteristics. The sensitivity of CRKP carrying different carbapenemase genes to antimicrobial drugs also varies, thereby affecting drug selection. Clearly identifying the distribution of carbapenemase types among CRKP strains in the local region is crucial for various aspects, including early intervention in CRKP infections, selecting empiric therapy, and enhancing treatment success rates. This study aims to understand the corelation between molecular and phenotype of CRKP in the Ningbo region, and to evaluate their correlation to lay a foundation for the treatment of CRKP infections. Additionally, it seeks to map the dissemination patterns of these strains, providing a scientific basis for the prevention and control of hospital-acquired infections in the region. By integrating epidemiological data with molecular insights, this research will contribute to the development of targeted interventions and improved management strategies for CRKP infections in healthcare settings.

2 Materials and methods

2.1 Bacterial strains and specimen source

In this study, a total of 150 strains of CRKP were selected from multiple hospitals located in Ningbo, Zhejiang Province, China, from January 2019 to December 2021. The hospitals included Hospital A (with two campuses: Campus I and Campus II), Hospital B, Hospital C, Hospital D, and Hospital E. The distribution of strains across hospitals, patient age, gender and departments was analyzed. This study was approved by the Ethics Committee of Ningbo Medical Centre Lihuili Hospital, Ningbo University (KY2023SL347-01). The specimen types included sputum, bronchoalveolar lavage fluid, urine,

1 http://www.carss.cn/

blood, puncture fluid, drainage fluid, pleural/peritoneal fluid, and bile, and strain identification was conducted using a mass spectrometer (Zhongyuan Huji, China). *Escherichia coli* ATCC 25922 served as the quality control strain for strain identification and antimicrobial susceptibility testing, and purchased from the National Center for Clinical Laboratories, Ministry of Health.

2.2 Drug susceptibility test

Antimicrobial susceptibility testing was performed using the broth microdilution method following CLSI guidelines (CLSI 2023). Briefly, bacterial suspensions were adjusted to 0.5 McFarland standard and diluted 1:200 in cation-adjusted Mueller-Hinton broth, with 100 μL aliquots dispensed into microdilution plates containing graded antimicrobial concentrations. After incubation at 35°C for 16–20 h, the minimum inhibitory concentration (MIC) was determined as the lowest concentration showing complete growth inhibition. The susceptibility results for ertapenem, imipenem, levofloxacin, piperacillin-tazobactam, ceftriaxone, cefepime, trimethoprim-sulfamethoxazole, ceftazidime-avibactam, amoxicillin-clavulanic acid, fosfomycin, ceftazidime, aztreonam, amikacin, and chloramphenicol were interpreted according to Clinical and Laboratory Standards Institute (CLSI) 2023 standards. Polymyxin B susceptibility was evaluated using European Committee on Antimicrobial Susceptibility Testing (EUCAST) version 10.0 criteria, while tigecycline breakpoints were determined based on standards from both the U.S. Food and Drug Administration (FDA) and China's National Medical Products Administration (NMPA).

2.3 Screening of antibiotic resistance genes and whole-genome sequencing

In order to identify the presence of carbapenemase resistance genes, we conducted PCR amplification using specific primers targeting *KPC-2, NDM-1, NDM-5, VIM, IMP-1, IMP-2, IMP-4, OXA-232, OXA-181, IMI, SME, GES, GIM, SIM, SPM, AIM*, and *DIM*. These primers, designed to detect markers for carbapenemase resistance genes (refer to Supplementary Table 1), were utilized to screen for the presence of these genes in the template DNA of bacterial isolates. The PCR mixture consisted of a total volume of 25 μL, comprising 1 μL of genomic DNA template, 1 μL of each primer, 12.5 μL of Premix-rTaq PCR solution (manufactured by TaKaRa, Japan), and 9.5 μL of distilled water. The PCR procedure was conducted utilizing an ABI Veriti Thermal Cycler (Applied Biosystems, Singapore). The template was initially subjected to denaturation at a temperature of 94°C for a duration of 5 min. This was followed by 30 cycles consisting of denaturation at 94°C for 45 s, annealing at 55°C for 45 s, and extension at 72°C for 1 min. A final extension step was performed at 72°C for 10 min. The reaction conditions for β-lactamase genes (*DHA, CIT, EBC, MOX, ACC, FOX, CMY, TEM, SHV, CTX-M-1, CTX-M-2, CTX-M-3, CTX-M-8, CTX-M-9, CTX-M-10, CTX-M-14*, and *CTX-M-25*), outer membrane protein genes (*OmpK35* and *OmpK36*), and efflux pump genes (*acrA, oqxB, kexD, kdeA, kpnE, emrB, oqxA*, and *qacEΔ1*) may vary slightly. The PCR products were subsequently confirmed through electrophoresis and sequencing. The presence of carbapenemase genes was confirmed by aligning assembled contigs against the CARD database using BLASTn (Alcock et al., 2020). The primer sequences for other antibiotic resistance genes are provided in Supplementary Table 1, which were used to screen whether these genes are present in the template DNA of bacterial isolates. Due to limited funds, we selected 47 strains of CRKP from a total of 150 isolates for whole genome sequencing (WGS) using next-generation sequencing (NGS). The selection criteria were based on the following factors: (1) the distribution of resistance genes, particularly carbapenem resistance genes, to ensure that all major resistance genotypes were represented; (2) antimicrobial susceptibility profiles, with strains exhibiting diverse resistance patterns prioritized to capture the full spectrum of resistance mechanisms; and (3) the epidemiological distribution of strains across hospitals, patient demographics (age, gender), and clinical departments (e.g., ICU, respiratory, surgery). Genomic DNA was extracted and sent to Novogene (Beijing Novogene Bioinformatics Co., Ltd., Beijing, China) for WGS, which was performed using the Illumina HiSeq 4000 platform (Illumina, San Diego, CA, United States). Raw sequencing data obtained from the Illumina HiSeq 4000 platform were subjected to quality control using FastQC (v0.11.9) to assess read quality (de Sena Brandine and Smith, 2019). Low-quality reads and adapters were trimmed using Trimmomatic (v0.39) with the following parameters: SLIDINGWINDOW:4:20 and MINLEN:50 (Bolger et al., 2014). Clean reads were then assembled *de novo* using SPAdes (v3.15.4) with default parameters to generate draft genomes (Bankevich et al., 2012). The quality of the assemblies was evaluated using QUAST (v5.0.2) (Gurevich et al., 2013).

2.4 Determination of phylogenetic groups of *Klebsiella pneumoniae* by MLST

MLST analysis was performed to determine the sequence types (STs) of 150 CRKP isolates by amplifying seven housekeeping genes (gapA, infB, mdh, pgi, phoE, rpoB, and tonB). The sequences were compared with the *Klebsiella pneumoniae* MLST database (Jolley et al., 2018)[2] to assign STs. A minimum spanning tree (MST) was constructed using PHYLOViZ Online (Nascimento et al., 2017)[3] by uploading FASTA files containing housekeeping gene sequences and strain metadata. The MST was visualized with adjustments to node size, color, and other parameters.

2.5 Statistical analysis

Statistical analyses were performed using SPSS 26.0. Differences in resistance gene distribution and antimicrobial susceptibility profiles among ST types and carbapenemase gene carriers were evaluated using the chi-square test or Fisher's exact test, with a significance level of $p < 0.01$.

2 Available at: https://bigsdb.pasteur.fr/cgi-bin/bigsdb/bigsdb.pl?db=pubmlst_klebsiella_seqdef.

3 http://www.phyloviz.net/

2.6 Data availability

The complete genome sequences of 47 strains of CRKP were deposited in GenBank with accession numbers PRJNA1241480.

3 Results

3.1 Analysis of strain origin

The distribution of CRKP strains across hospitals revealed that Hospital A Campus I accounted for the highest proportion of cases (36.7%, 55/150), followed by Hospital A Campus II (24.6%, 37/150), Hospital B (14.0%, 21/150), Hospital C (10.7%, 16/150), Hospital D (8.0%, 12/150), and Hospital E (6.0%, 9/150). In terms of patient demographics, the majority of CRKP infections occurred in individuals aged 55 years or older, accounting for 72.0% (108/150) of the cases. The median age of patients was 65 years, with an age range of 18 to 92 years. Gender distribution was relatively balanced, with male patients representing 52.0% (78/150) and female patients representing 48.0% (72/150) of the cases. Regarding departmental distribution, the intensive care unit (ICU) had the highest proportion of CRKP cases, representing 30.0% (45/150) of the isolates. This was followed by the respiratory department (23.3%, 35/150), general surgery (16.7%, 25/150), nephrology (13.3%, 20/150), and other departments (16.7%, 25/150). Notably, Hospital B had a concentration of cases in the hepatobiliary-pancreatic surgery department, while Hospital E primarily reported cases from the burn unit.

3.2 The sensitivity of antimicrobial drugs

The MIC results obtained through instrumental methods and the broth microdilution method reveal that 150 CRKP strains had relatively high sensitivity to the basic drugs tigecycline, polymyxin B, and ceftazidime-avibactam. Additionally, the sensitivity to combination therapy drugs fosfomycin, amikacin, and chloramphenicol was also relatively high, with rates of 72, 40, and 16.7%, respectively. Furthermore, a certain proportion of the strains exhibited intermediate sensitivity to fosfomycin and chloramphenicol, at 9.3 and 8.7%, respectively. The resistance rates for the remaining drugs were all above 90% (Table 1).

3.3 The screening results for antibiotic resistance genes

The main proportions of carbapemen genes producing in CRKP are as follows: *KPC-2* (61.3%), *NDM-5* (14.7%), *IMP-4* (8.0%), *OXA-232* (6.0%), and *OXA-181* (1.3%), respectively. No strains expressed *IMP-2, VIM, IMI, SME, GES, GIM, SIM, SPM, AIM*, or *DIM* genes were detected. The distribution of β-lactamase resistance genes in the analyzed isolates was as follows: *CTX-M-1* (13.33%), *CTX-M-3* (25.33%), *CTX-M-9* (17.33%), *CTX-M-14* (34.67%), and *SHV* (93.33%) were the most prevalent. Subsequent sequencing of the *SHV*-positive isolates revealed seven variants: *SHV-1* (16.66%), *SHV-11* (52.66%), *SHV-12* (18.66%), *SHV-28* (10.00%), *SHV-65* (0.66%), *SHV-103* (0.66%) and *SHV-33* (0.6%). For additional details on the distribution of other resistance genes, please refer to Figure 1.

TABLE 1 Resistance and sensitivity profiles of 150 CRKP strains to antimicrobial agents.

Antibacterial agents	Break point (MIC, μg/mL)		Sensitive		Intermediary		Resistance	
	R[a]	S[b]	N[c]	P[d] (%)	N[c]	P[d] (%)	N[c]	P[d] (%)
Ertapenem	≥2	≤0.5	0	0.0	0	0.0	150	100.0
Imipenem	≥4	≤1	2	1.3	1	0.7	147	98.0
Levofloxacin	≥2	≤0.5	8	5.3	15	10.0	127	84.7
Piperacillin-Tazobactam	≥32/4	≤8/4	0	0.0	0	0.0	150	100.0
Ceftriaxone	≥4	≤1	0	0.0	0	0.0	150	100.0
Cefepime	≥32	≤8	0	0.0	1	0.7	149	99.3
SMZ-TMP	≥4/76	≤2/38	70	46.7	7	4.6	73	48.7
Ceftazidime	≥16	≤4	3	2.0	2	1.3	145	96.7
Amikacin	≥64	≤16	60	40.0	4	2.7	86	57.3
Amoxicillin-clavulanate	≥32/16	≤8/4	2	1.3	0	0.0	148	98.7
Fosfomycin	≥256	≤64	108	72.0	14	9.3	28	18.7
Aztreonam	≥16	≤4	13	8.7	1	0.6	136	90.7
Chloramphenicol	≥32	≤8	25	16.6	13	8.7	112	74.7
Tigecycline	≥8	≤2	148	98.7	2	1.3	0	0.0
Polymyxin B	>2	≤2	147	98.0	0	0.0	3	2.0
ceftazidime-avibactam	≥16/4	≤8/4	102	68.0	0	0.0	48	32.0

[a]Resistance breakpoint.
[b]Sensitivelass breakpoint.
[c]Number.
[d]Proportion.

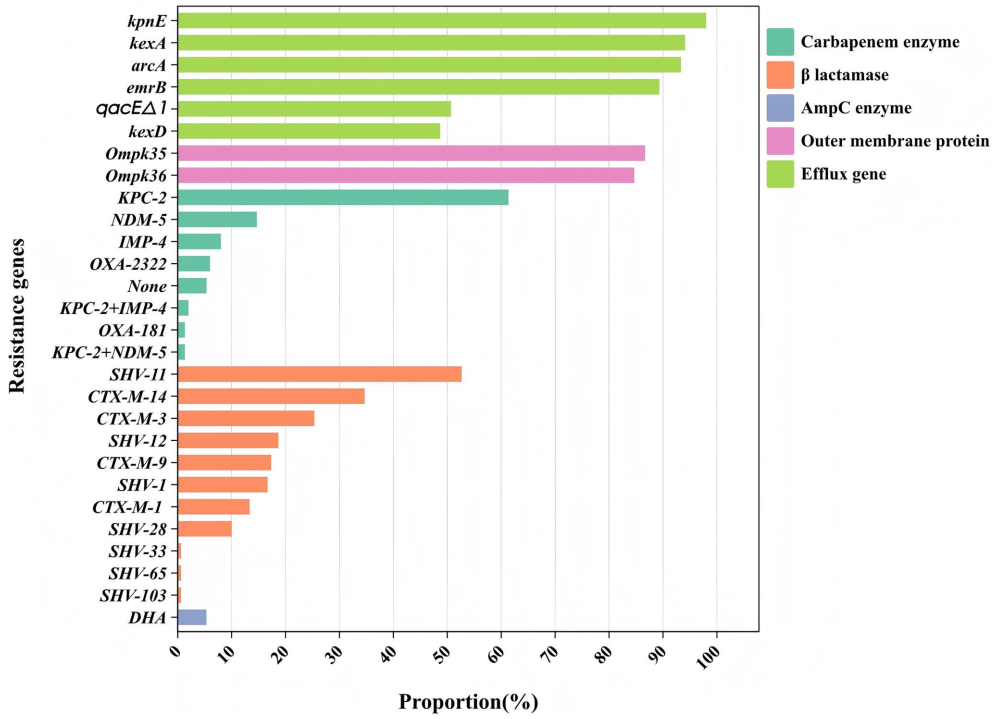

FIGURE 1
Classification of the resistance genes. Different colors represent different types of drug resistance genes.

The genome of strain 111 (Figure 2) was selected for display because it carries *KPC-2*, the most prevalent carbapenemase gene in CRKP, and represents a comprehensive and typical profile of carbapenemase genes observed in CRKP. Strain 111 was chosen because it carries *KPC-2*, the most prevalent carbapenemase gene in CRKP. This combination of genes makes strain 111 highly representative of the resistance patterns observed in the studied population. Furthermore, the whole genome sequencing results of strain 111were consistent with the PCR-based detection of resistance genes, confirming the accuracy and reliability of the data. Its genomic profile not only reflects the dominant resistance mechanisms but also provides a clear example of the genetic diversity and complexity of CRKP strains.

3.4 Correlation analysis of the sensitivity of basic antimicrobial drugs and combination therapy drugs with different enzyme types

Analysis of the sensitivity of basic antimicrobial drugs in relation to the three main carbapenemase enzyme types revealed that CRKP producing class A, class B, and class D enzymes had sensitivity rates of 97.8, 100, and 100% to tigecycline, and 96.7, 100, and 100% to polymyxin B, respectively, indicating relatively high sensitivity rates. Specifically, CRKP producing class A enzymes exhibited a sensitivity rate of 100% to ceftazidime-avibactam, while CRKP producing class B and class D enzymes had sensitivity rates of only 0 and 18.2%, respectively (Figure 3). Ceftazidime-avibactam exhibited better inhibitory effects against CRKP strains producing class A enzymes ($p < 0.01$). The study on the differences in sensitivity to combination therapy drugs among the three main enzyme types of strains showed that the sensitivity rates of CRKP producing class A, class B, and class D enzymes to fosfomycin were 76.1, 73.5, and 45.5%, respectively. The sensitivity rates to amikacin were 29.3, 61.8, and 27.3%, respectively, and to chloramphenicol were 13, 23.5, and 18.2%, respectively. The sensitivity rates to aztreonam were 0.0, 29.4, and 0.1%, respectively. Aztreonam and amikacin exhibited a more significant inhibitory effect against CRKP producing class B enzymes ($p < 0.01$). The resistance rates with the remaining combination therapy drugs were relatively high, and no comparison of drug sensitivity rates was conducted (Figure 3).

3.5 The subtyping results for the MLST

According to the MLST typing method, the 150 CRKP were classified into 19 ST (sequence type) types. Among them, ST11 was the dominant clone (75/150, 50.00%), followed by ST437 (22/150, 14.67%), ST15 (16 strains, 10.67%), ST290 (11 strains, 7.33%), ST307 (5 strains, 3.33%), ST4 and ST37 (3 strains each, 2.00%), ST35, ST412, and ST3113 (2 strains each, 1.33%), and ST5734, ST86, ST519, ST2370, ST1203, ST2189, ST2668, ST43, and ST193 (1 strain each, 1/60, 1.67%). Among them, ST11, ST437, and ST2189 are phylogenetically related, while ST2370 and ST37 are also phylogenetically related. The minimum spanning tree is shown in Figure 4.

3.6 Difference in antibiotic resistance genes by different ST types

Analyzing the antibiotic resistance genes carried by different ST strains revealed that ST11 strains carry a higher number of resistance

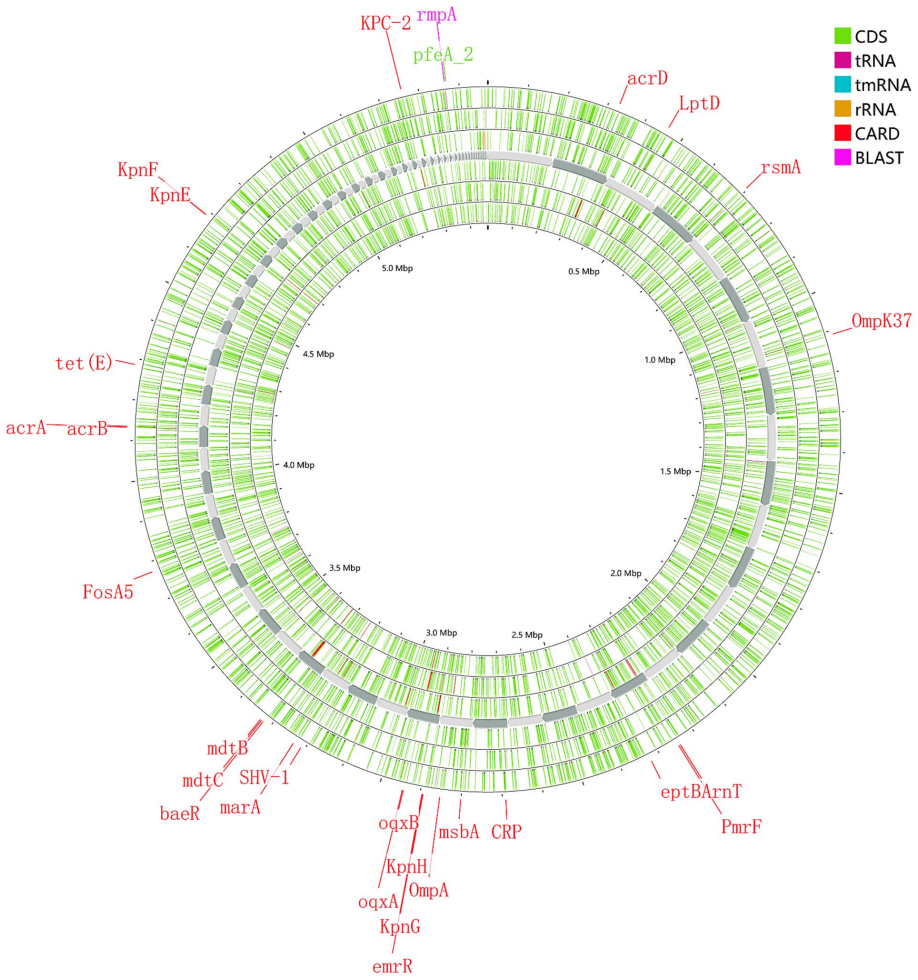

FIGURE 2
Whole genome sequencing of resistance and virulence genes of strain 111.

genes. Other strains, particularly those of ST437, exhibit a wide distribution in the number of resistance genes and, comparatively, carry fewer resistance genes (Figure 5). Comparison between ST11 and non-ST11 strains revealed that ST11 strains primarily carry the *KPC-2* carbapenemase gene, whereas other carbapenemase genes are predominantly carried by non-ST11 strains ($p < 0.01$). The presence of β-lactamase resistance genes *CTX-M-14*, *SHV-11*, and *SHV-12* types is mainly observed in ST11 strains, while the *CTX-M-1*, *SHV-1*, and *SHV-28* β-lactamase resistance gene is primarily found in non-ST11 strains ($p < 0.05$). Additionally, the presence of outer membrane protein genes *Ompk35* and *Ompk36* is predominantly associated with ST11 strains ($p < 0.01$). Similarly, the presence of efflux pump genes *arcA*, *kexD*, *kexA*, *emrB*, and *qacE△1* types is mainly observed in ST11 strains ($p < 0.01$), indicating statistically significant differences (Table 2).

3.7 The distribution of carbapenemase genes and ST types in different medical institutions

In hospitals A, B, C, and D, the *KPC-2* gene predominated, accounted for 78.2, 43.3, 85.7, and 75.0%, respectively. Additionally, the *IMP-4* gene also constituted a significant proportion in hospital B, at 21.6%. In hospital E, the *NDM-5* gene was the most prevalent, accounted for 91.7%. There were notable differences in the distribution of ST types among different resistance gene types. Among the isolates carrying the *KPC-2* gene, the most common ST type was ST11 ($n = 70$, 76.1%), followed by ST15 ($n = 10$, 10.9%). In the *NDM-5* gene isolates, the most common ST type was ST290 ($n = 11$, 50.0%), followed by ST307 ($n = 5$, 22.7%). The *IMP-4* and *OXA-232* types were mainly associated with ST437. More details can be found in Figure 6.

4 Discussion

The emergence and rapid dissemination of carbapenem-resistant *Klebsiella pneumoniae* (CRKP) have become a global public health crisis, particularly in regions with high antibiotic consumption such as China (Hu et al., 2020; Ge et al., 2024). This study provides a comprehensive analysis of the antimicrobial susceptibility profiles, carbapenemase gene distribution, and molecular epidemiology of CRKP strains isolated from multiple hospitals in the Ningbo region. By integrating phenotypic and genotypic data, our findings not only elucidate the local resistance patterns but also offer valuable insights

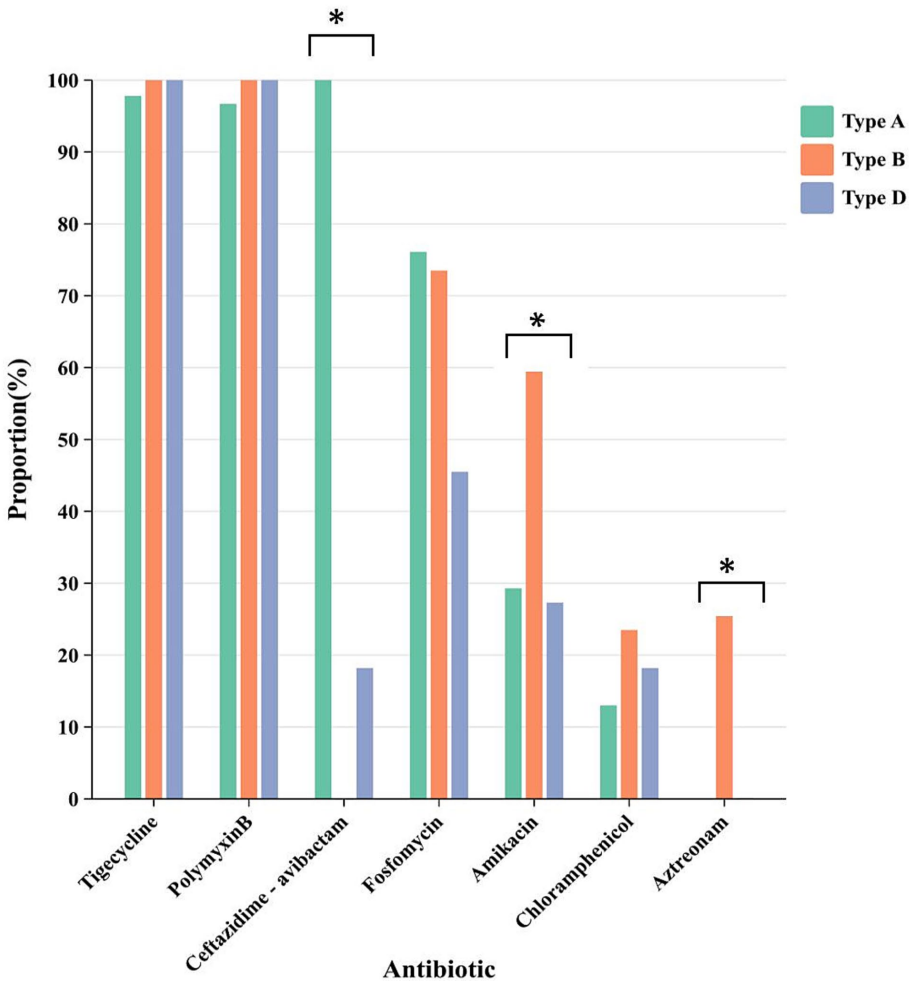

FIGURE 3
The differences in sensitivity of CRKP carrying different enzyme types to different drugs. Different colors represent different carbapenem enzyme types. * represents comparison of sensitivity rates, $p < 0.01$.

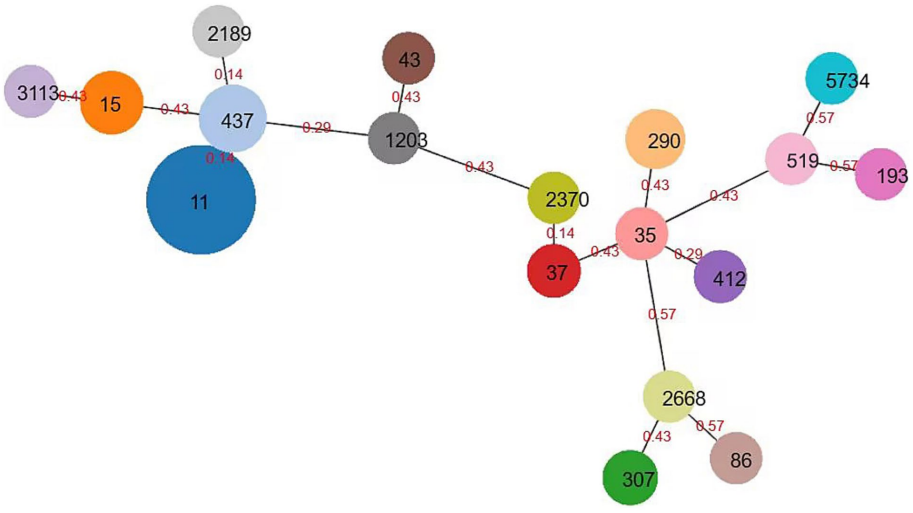

FIGURE 4
Minimum spanning tree of *Klebsiella pneumoniae*. The minimum spanning tree is constructed using seven allelic genes (gapA, infB, mdh, pgi, phoE, rpoB, tonB) of *Klebsiella pneumoniae*. The size of the nodes is proportional to the number of isolates, and the red number represents affinity, and the smaller the number, the closer the two ST types are.

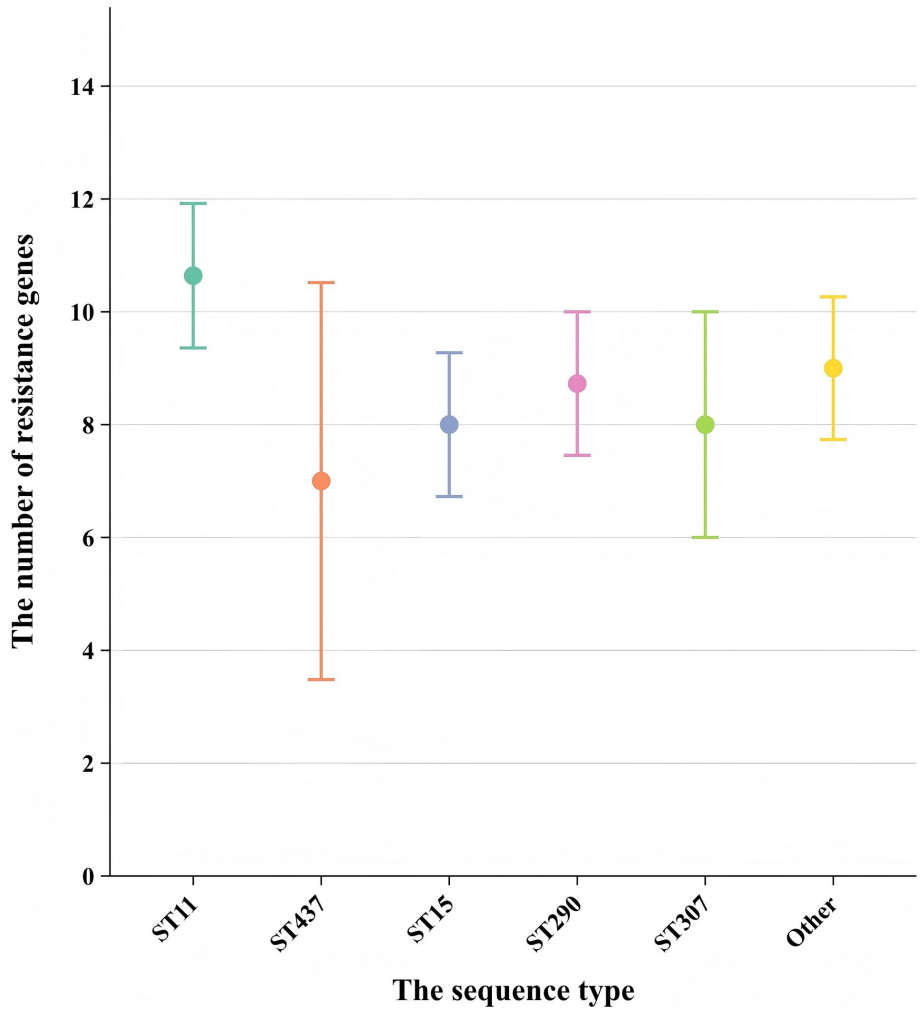

FIGURE 5
Comparison of the number of resistance genes carried among different sequence types (STs). Each point represents the mean number of resistance genes carried by strains of a specific ST. Error bars indicate the standard deviation (SD) derived from strains per ST. The x-axis shows the sequence type (ST), and the y-axis shows the number of resistance genes.

for optimizing treatment strategies and infection control measures in the context of global CRKP epidemiology.

The high resistance rates of CRKP to most commonly used antibiotics observed in our study are consistent with reports from other regions in China, such as Changsha (Jia et al., 2023) and Beijing (Wang et al., 2018), as well as globally (Jean et al., 2022). However, the relatively high sensitivity to tigecycline, polymyxin B, and ceftazidime-avibactam aligns with their recommended use as first-line treatments for CRKP infections (Zhuang et al., 2025). In comparison to other regions in China, the resistance rates observed in Ningbo are similar to those reported in Henan Province, where *KPC-2*-producing CRKP strains also exhibit high resistance to carbapenems but remain sensitive to polymyxin B and ceftazidime-avibactam (Wang et al., 2023). These differences may be attributed to variations in antibiotic usage patterns, infection control practices, and the prevalence of specific resistance mechanisms. Notably, the sensitivity of CRKP to combination therapy drugs such as fosfomycin, amikacin, and chloramphenicol was higher than expected, suggesting their potential utility in tailored treatment regimens. This contrasts with reports from some countries, where fosfomycin resistance rates are significantly higher due to its widespread use in urinary tract infections (Hurwitz et al., 2024). The regional differences highlight the importance of local antimicrobial resistance surveillance in guiding empirical therapy. Additionally, CRKP shows low resistance rates to levofloxacin and amikacin. The reason for this is that in clinical practice, these three drugs are typically not used individually but rather as components of combination therapy. This approach can enhance treatment efficacy and mitigate the development of bacterial resistance to medications. The lower resistance rates to SMZ-TMP compared to β-lactam antibiotics can be attributed to their different mechanisms of action (Li et al., 2020). However, while SMZ-TMP demonstrates sensitivity *in vitro*, its efficacy *in vivo* may be limited.

CRKP exhibits a complex mechanism of resistance to carbapenem antibiotics, with the most common mechanism being the production of carbapenemases. The *KPC-2* gene was predominant in hospitals A, C, and D (78.2, 85.7, and 75.0%, respectively), consistent with its high prevalence in eastern China (Kong et al., 2020; Li et al., 2025). *NDM* and *VIM* are more prevalent in South Asia and Europe, respectively

10.3389/fmicb.2025.1546805

TABLE 2 Comparison of drug resistance genes between ST11 type and non-ST11 type CRKP strains.

Resistance mechanism	Genotype	ST11 type (n = 75)	Non-ST11 type (n = 75)	χ^2	P
Carbapenemase	*KPC-2*	70	22	67.768	<0.01
	NDM-5	0	22	25.781	<0.01
	IMP-4	1	11	9.058	<0.01
	OXA-232	0	9	9.574	<0.01
	OXA-181	0	2	2.027	0.16
	KPC-2+NDM-1	2	0	2.027	0.16
	KPC-2+IMP-4	2	1	0.340	0.56
β lactamase	*CTX-M-1*	2	18	14.769	<0.01
	CTX-M-3	16	22	1.269	0.26
	CTX-M-9	21	7	8.607	<0.01
	CTX-M-14	43	9	34.027	<0.01
	SHV-1	0	25	38.368	<0.01
	SHV-11	64	15	3.930	0.047
	SHV-12	28	0	10.465	0.0012
	SHV-28	0	15	55.4112	<0.01
AmpC enzyme	*DHA*	3	5	0.528	0.467
Outer membrane protein	*Ompk35*	75	55	23.077	<0.01
	Ompk36	71	56	11.554	<0.01
Efflux gene	*arcA*	75	65	10.714	<0.01
	kexD	56	17	40.589	<0.01
	kexA	75	66	9.574	<0.01
	kpnE	75	72	3.063	0.08
	emrB	74	60	13.713	<0.01
	qacEΔ1	54	22	27.312	<0.01

(Gajdács et al., 2020). For example, in India, *NDM* is the dominant carbapenemase gene, accounting for over 70% of CRKP isolates (Kumarasamy et al., 2010), while in Poland, *VIM* is the most common carbapenemase gene (Izdebski et al., 2023). However, the high proportion of *IMP-4* (21.6%) in hospital B and *NDM-1* (91.7%) in hospital E suggests localized outbreaks driven by specific resistance genes. The occurrence of CRKP strains with identical resistance genes across different hospitals or departments may be attributed to nosocomial cross-transmission, patient referrals, or healthcare worker-mediated spread. Furthermore, factors such as antibiotic prescribing practices, environmental contamination levels, and the frequency of invasive procedures can significantly influence bacterial colonization and dissemination, leading to the clustering of resistant strains in high-risk units. These findings underscore the importance of tailored infection control strategies that consider the unique risks and patient populations in different hospital departments. Enhanced surveillance, strict adherence to hand hygiene, and targeted decolonization efforts may help mitigate the spread of CRKP within high-risk departments. Additionally, further research into the molecular epidemiology of CRKP strains within specific departments could provide valuable insights into their transmission dynamics and inform more effective intervention strategies. The co-occurrence of *KPC-2* and *NDM-1* genes in some strains is particularly concerning, as it may limit treatment options and facilitate the spread of multidrug resistance. In our study, carrying both *KPC-2* and *NDM-1* types, as well as *KPC-2* and *IMP-4* types, were found. This phenomenon has also been reported in other regions, such as India and the Middle East, where the co-production of multiple carbapenemases is increasingly common (Kumarasamy et al., 2010). These regional differences highlight the importance of tailoring infection control strategies to local epidemiological patterns. Further investigation into other patient information revealed that patients infected with CRKP are mainly concentrated in the elderly population aged 55 years and older, who generally have relatively weakened immune systems and are more susceptible to superbug infections. However, the gender distribution is relatively balanced. Analysis indicates that there is no significant correlation between enzyme type distribution and patient age or gender.

Strains carrying different β-lactamase enzyme types (class A, B, and D) exhibit distinct resistance profiles, leading to varying sensitivities to antimicrobial agents and influencing therapeutic decisions (da Costa de Souza et al., 2022). In this study, CRKP carrying class A, B, and D enzymes exhibited high sensitivity to tigecycline and polymyxin B, consistent with previous reports highlighting these drugs as last-resort options against carbapenem-resistant Enterobacterales (CRE) (Chang et al., 2022). Regarding ceftazidime-avibactam (CZA) susceptibility, CRKP strains harboring class A enzymes (particularly KPC) showed a sensitivity rate of 100%,

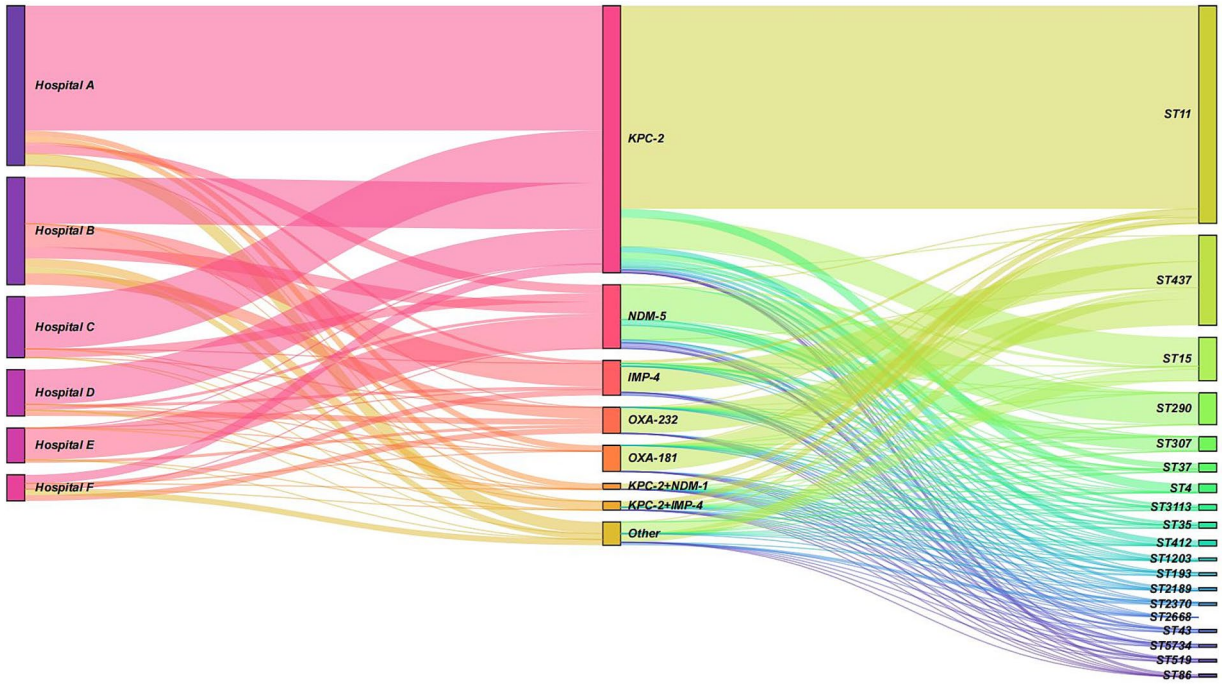

FIGURE 6
Sankey diagram illustrating the distribution of resistance genes and sequence types (STs) across hospitals. The diagram shows the flow and proportion of resistance genes (*KPC-2*, *NDM-5*, *IMP-4*, and *OXA-232*) and their associated ST types (e.g., ST11, ST15, ST290, ST307, and ST437) in hospitals A, B, C, D, and E. The width of the bands represents the relative proportion of isolates. *KPC-2* was the predominant gene in hospitals A, B, C, and D, while *NDM-5* was the most prevalent in hospital E. ST11 was the most common ST type among *KPC-2*-carrying isolates, whereas ST290 was the most frequent among *NDM-5*-carrying isolates. *IMP-4* and *OXA-232* were primarily associated with ST437.

aligning with studies confirming CZA's potent activity against KPC-producing isolates (Huang et al., 2021). In contrast, strains carrying class B and class D enzymes exhibited significantly reduced susceptibility, corroborating findings that avibactam does not inhibit metallo-β-lactamases (Xiong et al., 2022). For metalloenzyme-producing CRKP (class B), combination therapies involving aztreonam and amikacin demonstrated notable inhibition zones, likely due to aztreonam's stability against metallo-β-lactamases despite its susceptibility to serine β-lactamases (Vázquez-Ucha et al., 2023). This observation aligns with clinical studies advocating aztreonam-avibactam combinations for NDM-producing Enterobacterales (Delp et al., 2024). However, other tested combinations (e.g., ceftazidime, amoxicillin/clavulanic acid, cefepime, and rifampin) showed limited efficacy despite statistically significant differences in zone diameters, underscoring the need for tailored regimens based on enzyme type.

In addition to carbapenemase production, the loss of outer membrane proteins (e.g., *Ompk35* and *Ompk36*) and the overexpression of efflux pumps (e.g., *arcA*, *kexD*, *emrB*) were identified as key resistance mechanisms in CRKP strains. These mechanisms contribute to reduced antibiotic penetration and increased drug efflux, further complicating treatment (Alenazy, 2022; Onishi et al., 2022). The widespread distribution of *CTX-M* β-lactamase genes among CRKP strains also underscores their high resistance to β-lactam antibiotics, necessitating the use of alternative therapeutic strategies. In this study, a certain proportion of strains exhibited loss of the outer membrane protein genes *Ompk35* and *Ompk36*, with the loss rates of these genes being 13.4 and 15.4%, respectively. The loss of these outer membrane proteins can compromise the permeability of the bacterial cell wall, thereby contributing to increased antibiotic resistance. Furthermore, efflux pumps play a critical role in antibiotic resistance by actively transporting drugs from inside the cell to the outside, reducing the effective drug concentration and enhancing the resistance of the cell to drugs (Alenazy, 2022). In this study, a significant proportion of strains were found to carry efflux pump genes such as *arcA*, *kexD*, *kexA*, *kpnE*, *emrB*, and *qacE*△*1*. This enhances CRKP's ability to actively pump out antibiotics, thereby further increasing antibiotic resistance.

Multilocus sequence typing (MLST) revealed that ST11 was the dominant sequence type (50.0%) among CRKP strains in the Ningbo region, consistent with reports from other parts of China (Liao et al., 2020). The ST11 strains have broad dissemination capability and adaptability, enabling them to survive and proliferate in diverse environments. This makes them more prone to acquiring and disseminating resistance genes, leading to their high revalence in the local area. In addition, our study results further demonstrate molecular characteristic differences among different ST types of strains. For example, ST11 strains exhibited a higher prevalence of resistance genes, including *KPC-2*, *CTX-M-9*, *CTX-M-14*, and *SHV-11/SHV-12* (ESBL variants), compared to non-ST11 strains. In contrast, non-ST11 strains were more likely to carry *NDM-5* and *IMP-4* carbapenemase genes, as well as *CTX-M-1* and non-ESBL *SHV-1/SHV-28* β-lactamase genes (Talebzadeh et al., 2022). The predominance of *SHV-11* and *SHV-12* (both confirmed ESBLs) in ST11 strains suggests a lineage-specific adaptation favoring extended-spectrum resistance, whereas non-ST11 strains predominantly harbored *SHV-1* (a narrow-spectrum β-lactamase) and *SHV-28* (a rare

variant with uncertain ESBL phenotype). This divergence underscores the role of ST11 in propagating ESBL-associated resistance, potentially due to plasmid compatibility or selective pressures in clinical environments. These findings suggest that ST11 strains have a greater capacity for acquiring and disseminating resistance genes, contributing to their widespread prevalence. The high genetic homogeneity of ST11 strains within individual hospitals indicates potential intra-hospital transmission, likely facilitated by the movement of healthcare workers, contaminated medical equipment, and environmental surfaces. This is consistent with reports from other regions (Li et al., 2022).

In contrast, ST258 remains the most common sequence type in Western countries, highlighting the regional variability in CRKP epidemiology (Unlu et al., 2021). For example, in the United States, ST258 strains are responsible for the majority of CRKP infections, particularly in intensive care units (Chen et al., 2014). The genetic similarity between ST11 and ST258 suggests a possible evolutionary relationship, although further studies are needed to elucidate their origins and dissemination patterns. Other ST types may also cause outbreaks, necessitating further research, detection, and control measures for these clones. In addition, strong association of *KPC-2* with ST11 (76.1%) and *NDM-5* with ST290 (50.0%) highlights the role of high-risk clones in disseminating resistance. These findings underscore the need for tailored infection control measures. Hospitals with high *KPC-2*-producing ST11 strains should prioritize strict antibiotic stewardship, while those with *NDM-5*-producing ST290 or *IMP-4*-producing ST437 strains may require targeted interventions, such as screening high-risk patients and enhancing contact precautions. Continuous surveillance is essential to monitor emerging resistance patterns and prevent the spread of multidrug-resistant clones.

Our findings have several clinical implications. First, the high sensitivity of CRKP to tigecycline, polymyxin B, and ceftazidime-avibactam supports their continued use as first-line treatments. However, the potential for heteroresistance and toxicity associated with these drugs necessitates careful monitoring and dose optimization (Ma et al., 2019; Fang et al., 2023). Second, the observed sensitivity of CRKP to combination therapy drugs such as fosfomycin and amikacin suggests their potential utility in tailored treatment regimens. Finally, the identification of hospital-specific resistance patterns underscores the need for targeted infection control measures to prevent the spread of CRKP within healthcare facilities. Future studies should focus on longitudinal surveillance of CRKP strains to monitor emerging resistance patterns and evaluate the effectiveness of intervention strategies. The integration of epidemiological data with molecular insights will be crucial for addressing the global challenge of CRKP infections.

5 Conclusion

In summary, CRKP showed high sensitivity to tigecycline, polymyxin B, ceftazidime-avibactam, fosfomycin, amikacin, and chloramphenicol. The main carbapenemase genes identified were *KPC-2* and *NDM-5*. The inhibitory effects of ceftazidime-avibactam, aztreonam, and amikacin varied for CRKP carrying different enzyme types. ST11 strains were predominant in the region. There was a significant difference in the resistance genes carried by ST11 strains compared to non-ST11 strains. Clonal dissemination was observed both within the same healthcare institution and between different institutions.

Data availability statement

The complete genome sequences of 47 strains of CRKP were deposited in GenBank with accession number PRJNA1241480.

Author contributions

XQ: Conceptualization, Formal analysis, Methodology, Writing – original draft. MJ: Methodology, Validation, Writing – original draft. JX: Project administration, Validation, Writing – review & editing. QW: Funding acquisition, Project administration, Resources, Writing – review & editing. CL: Conceptualization, Methodology, Writing – original draft. WL: Investigation, Methodology, Validation, Writing – original draft. QL: Project administration, Supervision, Writing – review & editing.

Funding

The author(s) declare that financial support was received for the research and/or publication of this article. This study was supported by the research grants from Medical and Health Research Project of Zhejiang Province (Grant No. 2021KY1031), the Key Cultivation Disciplines Foundation of Ningbo Medical Centre Lihuili Hospital (Grant No. 2022-P04), and was partly supported by Medical and Health Research Project of Zhejiang Province (Grant No. 2024KY288, 2023KY245, 2023KY1042), and Ningbo health science and technology plan project (Grant No. 2022Y03).

Conflict of interest

The authors declare that the research was conducted in the absence of any commercial or financial relationships that could be construed as a potential conflict of interest.

Generative AI statement

The authors declare that no Gen AI was used in the creation of this manuscript.

Publisher's note

Supplementary material

The Supplementary material for this article can be found online at: https://www.frontiersin.org/articles/10.3389/fmicb.2025.1546805/full#supplementary-material

References

Alcock, B. P., Raphenya, A. R., Lau, T. T. Y., Tsang, K. K., Bouchard, M., Edalatmand, A., et al. (2020). CARD 2020: antibiotic resistome surveillance with the comprehensive antibiotic resistance database. *Nucleic Acids Res.* 48, D517–d525. doi: 10.1093/nar/gkz935

Alenazy, R. (2022). Drug efflux pump inhibitors: a promising approach to counter multidrug resistance in gram-negative pathogens by targeting AcrB protein from AcrAB-TolC multidrug efflux pump from *Escherichia coli*. *Biology (Basel)* 11:1328. doi: 10.3390/biology11091328

Angles-Yanqui, E., Huaringa-Marcelo, J., Sacsaquispe-Contreras, R., and Pampa-Espinoza, L. (2020). Panorama of carbapenemases in PeruUm panorama das carbapenemases presentes no Peru. *Rev. Panam. Salud Publica* 44:e61. doi: 10.26633/rpsp.2020.61

Bankevich, A., Nurk, S., Antipov, D., Gurevich, A. A., Dvorkin, M., Kulikov, A. S., et al. (2012). SPAdes: a new genome assembly algorithm and its applications to single-cell sequencing. *J. Comput. Biol.* 19, 455–477. doi: 10.1089/cmb.2012.0021

Bolger, A. M., Lohse, M., and Usadel, B. (2014). Trimmomatic: a flexible trimmer for Illumina sequence data. *Bioinformatics* 30, 2114–2120. doi: 10.1093/bioinformatics/btu170

Çalık, Ş., Kansak, N., and Aksaray, S. (2022). Phenotypic detection of carbapenemase production in carbapenem-resistant isolates with the rapid carbapenemase detection method (rCDM). *J. Microbiol. Methods* 200:106536. doi: 10.1016/j.mimet.2022.106536

CARSS. (2014–2023). Annual report on bacterial resistance in China. National Health Commission.

Chang, K., Wang, H., Zhao, J., Yang, X., Wu, B., Sun, W., et al. (2022). Polymyxin B/Tigecycline combination vs. Polymyxin B or Tigecycline alone for the treatment of hospital-acquired pneumonia caused by Carbapenem-resistant Enterobacteriaceae or Carbapenem-resistant *Acinetobacter baumannii*. *Front. Med. (Lausanne)* 9:772372. doi: 10.3389/fmed.2022.772372

Chen, L., Mathema, B., Pitout, J. D., Deleo, F. R., and Kreiswirth, B. N. (2014). Epidemic *Klebsiella pneumoniae* ST258 is a hybrid strain. *mBio* 5, e01355–e01314. doi: 10.1128/mBio.01355-14

da Costa de Souza, G., Roque-Borda, C. A., and Pavan, F. R. (2022). Beta-lactam resistance and the effectiveness of antimicrobial peptides against KPC-producing bacteria. *Drug Dev. Res.* 83, 1534–1554. doi: 10.1002/ddr.21990

De Sena Brandine, G., and Smith, A. D. (2019). Falco: high-speed FastQC emulation for quality control of sequencing data. *F1000Res* 8:1874. doi: 10.12688/f1000research.21142.2

Delp, H., Gibson, G. A., and Buckman, S. A. (2024). Aztreonam-avibactam for the treatment of intra-abdominal infections. *Expert. Opin. Pharmacother.* 25, 1867–1872. doi: 10.1080/14656566.2024.2409950

Ding, L., Yang, Z., and Sun, B. (2024). Understanding blaNDM-1 gene regulation in CRKP infections: toward novel antimicrobial strategies for hospital-acquired pneumonia. *Mol. Med.* 30:29. doi: 10.1186/s10020-024-00794-y

Fang, Y., Zhong, Q., Chen, Y., Hang, Y., Fang, X., Xiao, Y., et al. (2023). Ceftazidime/avibactam, Polymyxin or Tigecycline as a rescue strategy for the treatment of Carbapenem-resistant *Klebsiella pneumoniae* in bloodstream infection: a retrospective cohort study. *Infect. Drug Resist.* 16, 2963–2971. doi: 10.2147/idr.S409506

Gajdács, M., Ábrók, M., Lázár, A., Jánvári, L., Tóth, Á., Terhes, G., et al. (2020). Detection of VIM, NDM and OXA-48 producing carbapenem resistant Enterobacterales among clinical isolates in southern Hungary. *Acta Microbiol. Immunol. Hung.* 67, 209–215. doi: 10.1556/030.2020.01181

Gao, H., Tu, Y., Li, Q., and Wu, Q. (2024). Molecular prevalence and geographical variations of Carbapenem-resistant *Klebsiella pneumoniae* ST15 isolates in a tertiary Hospital in Ningbo, China. *Med. Sci. Monit.* 30:e943596. doi: 10.12659/msm.943596

García-Betancur, J. C., Appel, T. M., Esparza, G., Gales, A. C., Levy-Hara, G., Cornistein, W., et al. (2021). Update on the epidemiology of carbapenemases in Latin America and the Caribbean. *Expert Rev. Anti-Infect. Ther.* 19, 197–213. doi: 10.1080/14787210.2020.1813023

Ge, X., Zhou, Y., Jin, H., Liu, K., Zhu, K., Yu, Y., et al. (2024). Genomic insights and antimicrobial resistance profiles of CRKP and non-CRKP isolates in a Beijing geriatric medical center: emphasizing the Bla(KPC-2) carrying high-risk clones and their spread. *Front. Microbiol.* 15:1359340. doi: 10.3389/fmicb.2024.1359340

Guan, X., He, L., Hu, B., Hu, J., Huang, X., Lai, G., et al. (2016). Laboratory diagnosis, clinical management and infection control of the infections caused by extensively drug-resistant gram-negative bacilli: a Chinese consensus statement. *Clin. Microbiol. Infect.* 22, S15–S25. doi: 10.1016/j.cmi.2015.11.004

Guo, B., Li, P., Qin, B., Wang, S., Zhang, W., Shi, Y., et al. (2024). An analysis of differences in Carbapenem-resistant Enterobacterales in different regions: a multicenter cross-sectional study. *BMC Infect. Dis.* 24:116. doi: 10.1186/s12879-024-09005-9

Gurevich, A., Saveliev, V., Vyahhi, N., and Tesler, G. (2013). QUAST: quality assessment tool for genome assemblies. *Bioinformatics* 29, 1072–1075. doi: 10.1093/bioinformatics/btt086

Han, R., Shi, Q., Wu, S., Yin, D., Peng, M., Dong, D., et al. (2020). Dissemination of Carbapenemases (KPC, NDM, OXA-48, IMP, and VIM) among Carbapenem-resistant Enterobacteriaceae isolated from adult and children patients in China. *Front. Cell. Infect. Microbiol.* 10:314. doi: 10.3389/fcimb.2020.00314

Hu, Y., Liu, C., Shen, Z., Zhou, H., Cao, J., Chen, S., et al. (2020). Prevalence, risk factors and molecular epidemiology of carbapenem-resistant *Klebsiella pneumoniae* in patients from Zhejiang, China, 2008-2018. *Emerg. Microbes Infect.* 9, 1771–1779. doi: 10.1080/22221751.2020.1799721

Huang, Y., Wu, T., Perez, O., Rana, A. P., Chen, L., Kreiswirth, B. N., et al. (2021). *In vitro* optimization of Ceftazidime/avibactam for KPC-producing *Klebsiella pneumoniae*. *Front. Microbiol.* 12:618087. doi: 10.3389/fmicb.2021.618087

Hurwitz, J. S., Newton-Foot, M., Nel Van Zyl, K., and Nel, P. (2024). Fosfomycin susceptibility testing and resistance mechanisms in Enterobacterales in South Africa. *Afr. J. Lab. Med.* 13:2252. doi: 10.4102/ajlm.v13i1.2252

Izdebski, R., Biedrzycka, M., Urbanowicz, P., Żabicka, D., and Gniadkowski, M. (2023). Genome-based epidemiologic analysis of VIM/IMP Carbapenemase-producing *Enterobacter* spp Poland. *Emerg. Infect. Dis.* 29, 1618–1626. doi: 10.3201/eid2908.230199

Jean, S. S., Harnod, D., and Hsueh, P. R. (2022). Global threat of Carbapenem-resistant gram-negative Bacteria. *Front. Cell. Infect. Microbiol.* 12:823684. doi: 10.3389/fcimb.2022.823684

Jia, Y., Liu, Y., Huang, Y., Wang, J., Wang, H., Tan, S., et al. (2023). Clinical characteristics, drug resistance, and risk factors for death of *Klebsiella pneumoniae* infection in patients with acute pancreatitis: a single-center retrospective study from China. *Infect. Drug Resist.* 16, 5039–5053. doi: 10.2147/idr.S410397

Jiang, M., Qiu, X., Shui, S., Zhao, R., Lu, W., Lin, C., et al. (2024). Differences in molecular characteristics and expression of virulence genes in carbapenem-resistant and sensitive *Klebsiella pneumoniae* isolates in Ningbo, China. *Front. Microbiol.* 15:1356229. doi: 10.3389/fmicb.2024.1356229

Jolley, K. A., Bray, J. E., and Maiden, M. C. J. (2018). Open-access bacterial population genomics: BIGSdb software, the PubMLST.org website and their applications. *Wellcome Open Res.* 3:124. doi: 10.12688/wellcomeopenres.14826.1

Kong, Z., Liu, X., Li, C., Cheng, S., Xu, F., and Gu, B. (2020). Clinical molecular epidemiology of Carbapenem-resistant *Klebsiella pneumoniae* among pediatric patients in Jiangsu Province, China. *Infect. Drug Resist.* 13, 4627–4635. doi: 10.2147/idr.S293206

Kumarasamy, K. K., Toleman, M. A., Walsh, T. R., Bagaria, J., Butt, F., Balakrishnan, R., et al. (2010). Emergence of a new antibiotic resistance mechanism in India, Pakistan, and the UK: a molecular, biological, and epidemiological study. *Lancet Infect. Dis.* 10, 597–602. doi: 10.1016/s1473-3099(10)70143-2

Li, J., Bi, W., Dong, G., Zhang, Y., Wu, Q., Dong, T., et al. (2020). The new perspective of old antibiotic: *in vitro* antibacterial activity of TMP-SMZ against *Klebsiella pneumoniae*. *J. Microbiol. Immunol. Infect.* 53, 757–765. doi: 10.1016/j.jmii.2018.12.013

Li, X., Chen, S., Lu, Y., Shen, W., Wang, W., Gao, J., et al. (2025). Molecular epidemiology and genetic dynamics of carbapenem-resistant hypervirulent *Klebsiella pneumoniae* in China. *Front. Cell. Infect. Microbiol.* 15:1529929. doi: 10.3389/fcimb.2025.1529929

Li, Z., Ding, Z., Yang, J., Liu, Y., Jin, X., Xie, J., et al. (2021). Carbapenem-resistant *Klebsiella pneumoniae* in Southwest China: molecular characteristics and risk factors caused by KPC and NDM producers. *Infect. Drug Resist.* 14, 3145–3158. doi: 10.2147/idr.S324244

Li, T., Yang, Y., Yan, R., Lan, P., Liu, H., Fu, Y., et al. (2022). Comparing core-genome MLST with PFGE and MLST for cluster analysis of carbapenem-resistant *Acinetobacter baumannii*. *J. Glob. Antimicrob. Resist.* 30, 148–151. doi: 10.1016/j.jgar.2022.06.014

Liao, W., Liu, Y., and Zhang, W. (2020). Virulence evolution, molecular mechanisms of resistance and prevalence of ST11 carbapenem-resistant *Klebsiella pneumoniae* in China: a review over the last 10 years. *J. Glob. Antimicrob. Resist.* 23, 174–180. doi: 10.1016/j.jgar.2020.09.004

Ma, X., He, Y., Yu, X., Cai, Y., Zeng, J., Cai, R., et al. (2019). Ceftazidime/avibactam improves the antibacterial efficacy of Polymyxin B against Polymyxin B Heteroresistant KPC-2-producing Klebsiella pneumoniae and hinders emergence of resistant subpopulation in vitro. *Front. Microbiol.* 10:2029. doi: 10.3389/fmicb.2019.02029

Nascimento, M., Sousa, A., Ramirez, M., Francisco, A. P., Carriço, J. A., and Vaz, C. (2017). PHYLOViZ 2.0: providing scalable data integration and visualization for multiple phylogenetic inference methods. *Bioinformatics* 33, 128–129. doi: 10.1093/bioinformatics/btw582

Onishi, R., Shigemura, K., Osawa, K., Yang, Y. M., Maeda, K., Tanimoto, H., et al. (2022). Molecular characteristics and genetic analysis of the genes related to carbapenemase, efflux pump, and outer membrane proteins in carbapenem-resistant *Klebsiella pneumoniae*. *Lett. Appl. Microbiol.* 76:ovac069. doi: 10.1093/lambio/ovac069

Rodríguez-Baño, J., Cisneros, J. M., Cobos-Trigueros, N., Fresco, G., Navarro-San Francisco, C., Gudiol, C., et al. (2015). Executive summary of the diagnosis and antimicrobial treatment of invasive infections due to multidrug-resistant Enterobacteriaceae. Guidelines of the Spanish Society of Infectious Diseases and Clinical Microbiology (SEIMC). *Enferm. Infecc. Microbiol. Clin.* 33, 338–341. doi: 10.1016/j.eimc.2014.11.015

Sarva, K., Marimuthu Ragavan, R., Tadi, L. J., Raja, S., and Narasingam, A. (2023). Performance of Carbapenemase Nordmann-Poirel, modified Carbapenem inactivation, and EDTA Carbapenem inactivation methods for detecting Carbapenem-resistant

Klebsiella pneumoniae isolates. *Microb. Drug Resist.* 29, 504–509. doi: 10.1089/mdr.2023.0040

Soares De Moraes, L., Gomes Magalhaes, G. L., Material Soncini, J. G., Pelisson, M., Eches Perugini, M. R., and Vespero, E. C. (2022). High mortality from carbapenem-resistant *Klebsiella pneumoniae* bloodstream infection. *Microb. Pathog.* 167:105519. doi: 10.1016/j.micpath.2022.105519

Talebzadeh, H., Mellali, H., and Solgi, H. (2022). Association of fluoroquinolone resistance and ESBL production in hypervirulent *Klebsiella pneumoniae* ST11 and ST893 in Iran. *Acta Microbiol. Immunol. Hung.* 69, 135–143. doi: 10.1556/030.2022.01638

Unlu, O., Ersoz, B. R., Istanbullu Tosun, A., and Demirci, M. (2021). Epidemic *Klebsiella pneumoniae* ST258 incidence in ICU patients admitted to a university hospital in Istanbul. *J. Infect. Dev. Ctries.* 15, 665–671. doi: 10.3855/jidc.13430

Vázquez-Ucha, J. C., Alonso-Garcia, I., Guijarro-Sánchez, P., Lasarte-Monterrubio, C., Álvarez-Fraga, L., Cendón-Esteve, A., et al. (2023). Activity of aztreonam in combination with novel β-lactamase inhibitors against metallo-β-lactamase-producing Enterobacterales from Spain. *Int. J. Antimicrob. Agents* 61:106738. doi: 10.1016/j.ijantimicag.2023.106738

Venugopalan, V., Nogid, B., Le, T. N., Rahman, S. M., and Bias, T. E. (2017). Double carbapenem therapy (DCT) for bacteremia due to carbapenem-resistant *Klebsiella pneumoniae* (CRKP): from test tube to clinical practice. *Infect. Dis. (Lond.)* 49, 867–870. doi: 10.1080/23744235.2017.1350880

Wang, Z., Qin, R. R., Huang, L., and Sun, L. Y. (2018). Risk factors for Carbapenem-resistant *Klebsiella pneumoniae* infection and mortality of *Klebsiella pneumoniae* infection. *Chin. Med. J.* 131, 56–62. doi: 10.4103/0366-6999.221267

Wang, S., Wang, L., Jin, J., Li, G., Shao, H., Song, Y., et al. (2023). Genomic epidemiology and characterization of Carbapenem-resistant *Klebsiella pneumoniae* in ICU inpatients in Henan Province, China: a multicenter cross-sectional study. *Microbiol. Spectr.* 11:e0419722. doi: 10.1128/spectrum.04197-22

Xiong, L., Wang, X., Wang, Y., Yu, W., Zhou, Y., Chi, X., et al. (2022). Molecular mechanisms underlying bacterial resistance to ceftazidime/avibactam. *WIREs Mech. Dis.* 14:e1571. doi: 10.1002/wsbm.1571

Zhao, J. Y., Xu, W. F., and Jin, F. X. (2021). A study on the characteristics of carbapenem-resistant *Klebsiella pneumoniae* in elderly patients of Shaoxing City. *Chin. J. Health Lab. Technol.* 31, 2458–2461+2465.

Zhuang, H., Qu, Q., Long, W., Hu, Q., Wu, X. L., Chen, Y., et al. (2025). Ceftazidime/avibactam versus polymyxin B in carbapenem-resistant *Klebsiella pneumoniae* infections: a propensity score-matched multicenter real-world study. *Infection* 53, 95–106. doi: 10.1007/s15010-024-02324-8

frontiers | Frontiers in Microbiology

TYPE Original Research
PUBLISHED 19 May 2025
DOI 10.3389/fmicb.2025.1567921

OPEN ACCESS

EDITED BY
Israel Nissan,
Ministry of Agriculture and Rural Development, Israel

REVIEWED BY
Shamkant B. Badgujar,
Tulip Diagnostics Private Limited, India
Caterina Pagliarulo,
University of Sannio, Italy

*CORRESPONDENCE
Farag Bleiblo
✉ farag.bleiblo@uob.edu.ly

†These authors have contributed equally to this work and share first authorship

RECEIVED 28 January 2025
ACCEPTED 22 April 2025
PUBLISHED 19 May 2025

CITATION
Aloriby M, Elkawafi M, Aldrsy S, Sweker M, Elabdeli H, Elbarghathi A, Benhasouna A, El-Awamie M, Elsharif N, Alqabbasi O, Alshalmani S, Algazal R and Bleiblo F (2025) Overall *in vitro*, *in vivo*, and *in silico* evaluation of *Olea europaea* and *Ficus carica* leaf extracts for antimicrobial activity against multidrug-resistant pathogens. *Front. Microbiol.* 16:1567921. doi: 10.3389/fmicb.2025.1567921

Overall *in vitro*, *in vivo*, and *in silico* evaluation of *Olea europaea* and *Ficus carica* leaf extracts for antimicrobial activity against multidrug-resistant pathogens

Mahmoud Aloriby[1,2†], Mohamed Elkawafi[3†], Salem Aldrsy[1†], Mohamed Sweker[1†], Hadeel Elabdeli[1†], Aisha Elbarghathi[1†], Ahmed Benhasouna[4], Madiha El-Awamie[5], Nariman Elsharif[5], Omar Alqabbasi[6], Salmin Alshalmani[7], Rabiea Algazal[8] and Farag Bleiblo[5*]

[1]Department of Cytotechnology, Faculty of Biomedical Sciences, University of Benghazi, Benghazi, Libya, [2]Department of Pathology, Medical Center, Libyan International Medical University, Benghazi, Libya, [3]Basic Medical Sciences Program, Faculty of Medical and Health Sciences, Libyan International Medical University, Benghazi, Libya, [4]Department of Pathology, Faculty of Medicine, University of Benghazi, Benghazi, Libya, [5]Department of Microbiology, Faculty of Science, University of Benghazi, Benghazi, Libya, [6]Department of Molecular Diagnostics, Faculty of Biomedical Sciences, University of Benghazi, Benghazi, Libya, [7]Department of Pharmacognosy, Faculty of Pharmacy, University of Benghazi, Benghazi, Libya, [8]Laboratory of Immunology and Virology, Children Hospital of Benghazi, Benghazi, Libya

Introduction: Antimicrobial resistance (AMR) represents a critical global health issue, prompting the urgent exploration of alternative plant-derived antimicrobial therapies. In this context, the present study evaluates the therapeutic efficacy and safety profiles of *Olea europaea* and *Ficus carica* leaf extracts against multidrug-resistant pathogens, integrating *in vitro* antimicrobial assays, *in vivo* toxicity assessments, and *in silico* modeling approaches.

Methods: Leaf extracts from *O. europaea* and *F. carica* were prepared by solvent-based maceration using methanol, acetone, and distilled water. Their antimicrobial properties were evaluated through disk and well diffusion assays to determine the minimum inhibitory concentration (MIC) and minimum bactericidal concentration (MBC) against clinically relevant pathogens. Toxicological assessments were performed *in vivo* using the BALB/c mice model, including histopathological examinations, hematological profiling, and biochemical analyses. A complementary *in vitro* toxicogenomic screening was conducted using a cell-based reporter assay to profile nuclear receptor signaling and cellular stress responses. Furthermore, computational modeling and molecular docking were employed to predict the possible interactions of selected phytochemicals with *E. coli* cytochrome c peroxidase.

Results: Methanolic extracts of *O. europaea* exhibited potent antimicrobial activity against multidrug-resistant isolates, whereas *F. carica* extracts showed minimal efficacy across all experimental contexts. *In silico* molecular docking analyses revealed high-affinity interactions between olive-derived phenolic compounds and *E. coli* cytochrome c peroxidase, suggesting a plausible mechanistic basis for the observed antibacterial effects. *In vivo,* toxicological evaluation in BALB/c mice administered aqueous formulations of the methanolic

olive extract demonstrated dose-dependent hepatic and renal histopathological alterations, accompanied by dysregulation of the immunological profiles and elevated hepatic enzyme levels. These findings were consistent with outcomes from the cell reporter assays and computational toxicology models, which indicated potential nephrotoxic and immunotoxic risks at higher concentrations.

Discussion: These findings validate the promising antimicrobial activity of *O. europaea* and *F. carica* leaf extracts against multidrug-resistant pathogens. However, further investigations on precise dosage optimization and long-term safety evaluations are essential before these extracts are implemented in clinical practice.

KEYWORDS

***Olea europae*, *Ficus carica*, multidrug-resistant pathogens, solvent extraction, antimicrobial activities, toxicological evaluation, histopathology, *in silico* modeling and docking**

1 Introduction

Antimicrobial resistance (AMR) has become a leading cause of mortality globally, with an estimated 1.14 million deaths directly caused by drug-resistant bacterial infections in 2021. In the absence of effective interventions, this figure is anticipated to rise significantly, potentially resulting in ~2 million direct deaths annually by 2050 (Sullivan et al., 2024). Therefore, an integrated strategy emphasizing improved antimicrobial stewardship, infection control measures, and innovative therapeutic approaches is essential to effectively address this challenge (Ho et al., 2024). Recent reports highlight exploring alternative antimicrobial strategies, including plant-based pharmaceuticals, bacteriophage therapy, antimicrobial peptides, RNA-based therapies, and probiotics (Singha et al., 2024). Several plant-derived phytochemicals have shown promising activity against multidrug-resistant (MDR) pathogens as direct inhibitors or by potentiating the action of traditional antimicrobial drugs to overcome resistance mechanisms (Jubair et al., 2021). The renewed interest in plant-derived antimicrobials reflects a strategic paradigm shift in antimicrobial drug discovery, emphasizing their potential as rich reservoirs of novel, bioactive compounds to address the rising challenge of MDR. The secondary metabolites of plants offer considerable therapeutic promise due to their inherent biocompatibility.

Olive (*O. europaea*) leaf extracts exhibit broad-spectrum antibacterial properties, demonstrating significant *in vitro* efficacy against pathogens commonly associated with gastrointestinal and respiratory tract infections (de Oliveira et al., 2024). The antimicrobial efficacy of olive leaf extract is attributed to a synergistic interplay of its phenolic constituents (like oleuropein and hydroxytyrosol) and other components, such as fatty acids (de Oliveira et al., 2024). Recent studies highlight the potent antimicrobial activity of olive leaf extract, revealing an 82% inhibition of biofilm formation by MDR *Pseudomonas aeruginosa* strains at sub-inhibitory concentrations (Esfandiary et al., 2024). Furthermore, olive leaf extracts have demonstrated potent bactericidal activity against *Campylobacter* species resistant to ciprofloxacin and tetracycline (Silvan et al., 2022). Similarly, fig (*F. carica*) leaves are a potential source of diverse bioactive compounds with promising antimicrobial and therapeutic activities. Phytochemical analyses reveal that fig leaves contain various organic acids, coumarins, tannins, and flavonoids, contributing to their ethnomedicinal uses (Shiraishi et al., 2023). Notably, *F. carica* leaf extracts exhibited potent antimicrobial activity against several MDR pathogens, including carbapenem-resistant *Klebsiella pneumoniae*, *Escherichia coli*, *Staphylococcus aureus*, and *P. aeruginosa* (Shiraishi et al., 2023). The fig extract was particularly effective due to the phenolic compounds, including eugenol, acetyleugenol, and psoralen, which were demonstrated to be the essential active constituents (Kim and Lee, 2023). Collectively, *F. carica* leaf extracts demonstrate antimicrobial efficacy and pharmacological activity, underscoring their potential utility as alternative therapies in managing infections caused by MDR pathogens.

This investigation employs a comprehensive strategy to integrate *in silico* modeling, *in vitro* experiments, and *in vivo* validation to assess the antimicrobial potential and safety of *O. europaea* and *F. carica* leaf extracts. Computational techniques enable efficient prediction of interactions between phytochemicals and biological targets (Mangana et al., 2025; Mishra and Muthukaliannan, 2024), while *in vitro* analyses provide empirical evidence of efficacy against MDR organisms (Esfandiary et al., 2024). Subsequent *in vivo* studies in animal models provide critical insights into therapeutic efficacy and biosafety, enhancing the translational relevance of the findings (Shiraishi et al., 2023). Although *in silico*, *in vitro*, and *in vivo* approaches have been independently explored in previous studies, research integrating these methodologies remains limited. This study conducts a comprehensive evaluation to underscore the therapeutic potential of *O. europaea* and *F. carica* leaf extracts as plant-based interventions against antimicrobial resistance.

2 Materials and methods

2.1 *In vitro* studies

2.1.1 Antimicrobial susceptibility testing

Antimicrobial susceptibility profiles for selected clinically relevant pathogens were evaluated against a panel of antimicrobial agents. Antimicrobial susceptibility testing was performed using

the standardized disk diffusion method according to the Clinical and Laboratory Standards Institute (CLSI) guidelines (Haley et al., 2024). Bacterial and fungal isolates from clinical samples were identified using standard methods. The pathogens investigated in the study were *Escherichia coli, Klebsiella pneumoniae, Staphylococcus aureus, Enterococcus faecalis, Enterococcus faecium, Streptococcus agalactiae, Enterobacter cloacae,* and *Candida albicans*. The clinical isolates were first cultivated on appropriate selective and enriched media for optimal growth and preliminary identification. Subsequent identification of the pathogens was conducted using the Vitek2 Compact Identification System (BioMérieux, Marcy-l'Étoile, France) for confirmation. The selected antimicrobial agents included azithromycin (AZM), nitrofurantoin (NIF), trimethoprim/sulfamethoxazole (SXT), amikacin (AK), gentamicin (CN), vancomycin (VA), amoxicillin/clavulanic acid (AMC), ceftriaxone (CRO), ceftazidime (CAZ), and tobramycin (TOP; Oxoid Ltd., Basingstoke, UK). These antimicrobial agent were chosen based on their clinical relevance and therapeutic significance. Inoculum suspensions (in 0.5 McFarland unit) were plated on Mueller-Hinton agar (for bacteria) and Sabouraud Dextrose Agar (SDA) for fungi to perform the test (Kebede and Shibeshi, 2022). The inhibition zone diameters were measured in millimeters and interpreted as Susceptible (S) and Resistant (R) according to CLSI guidelines.

2.1.2 Plant material and extraction procedures

2.1.2.1 Sample collection of plant material

O. europaea leaves were collected in July 2024 from a 12-year-old Manzanilla del Litoral tree in the Abuatni district of Benghazi, Libya. Simultaneously, *F. carica* leaves were collected from a 28-year-old Moraceae tree in the Al-Laithi district of the same city. Before analysis, all plant materials were thoroughly washed with running tap water to remove superficial debris and then air-dried at ambient temperature in a shaded and well-ventilated area for 6 days. The leaves were dried in a dehydrator before being ground to a fine powder in a commercial blender (Ahmed et al., 2023).

2.1.2.2 Extraction protocol

For each plant species, 20 g of powdered olive leaves and 15 g of powdered fig leaves were accurately weighed and individually immersed in 200 mL of high-purity analytical-grade methanol or acetone (BDH Chemicals Ltd., England) or distilled water. The extraction was performed in sterile glass containers under controlled laboratory conditions to ensure reproducibility and prevent contamination. We selected methanol, acetone, and distilled water based on their efficacy in extracting polyphenolic compounds from plant materials, as supported by previous studies. The solvent-to-powder ratio was optimized following standard extraction protocols to ensure efficient recovery of bioactive constituents and allow methodological consistency across conditions. These parameters are widely used in phytochemical extraction to maximize yield and reproducibility (Cifá et al., 2018; Meziant et al., 2018; Agatonovic-Kustrin et al., 2023; Nguyen et al., 2023). The mixtures were kept at room temperature for 24 h, with occasional gentle agitation, to facilitate the extraction of bioactive compounds. After maceration, the extracts were first filtered through multiple layers of gauze and subsequently passed through 180 mL of filter paper to remove coarse particulates.

2.1.2.3 Concentration and stock solution preparation

The resulting filtrates were concentrated under reduced pressure with a rotary evaporator at 45°C for methanolic and acetone extracts and at 100°C for the distilled water extract. The acetone and methanolic residues were left at room temperature for 24 h without covering to allow residual solvents to evaporate. Meanwhile, the distilled water extract was further concentrated via Soxhlet extraction until a sufficiently dense residue was obtained. For the olive leaf extract, an approximate yield of 4 g was achieved from the initial leaf powder at a solvent-to-powder ratio of 1:5. A total of 2 g of fig leaf extract was obtained at a solvent-to-powder ratio of 1:7.5 following the extraction process, providing an adequate quantity for subsequent antimicrobial evaluation and toxicity assessment. The lower yield of *F. carica* extract may be attributed to the comparatively lower concentration of extractable bioactive compounds, mainly phenolic acids, and flavonoids, which vary depending on the plant's maturity, growing conditions, and solvent polarity. Fig leaves also possess a different cellular structure than olive leaves, which may affect solvent permeability and compound solubility (Cho et al., 2020; Khelouf et al., 2023; Zhang et al., 2024). Notably, during our preliminary experiments using different solvents under the same conditions, we did not observe significant variations in extraction yields, suggesting that the solvent type may not significantly influence the yield differences between the two plant species (Abi-Khattar et al., 2019). The dried fine powder from each extract was reconstituted in dimethyl sulfoxide (DMSO) to prepare a stock solution at 100 mg/mL concentration and transferred into dark, airtight vials for storage at room temperature until further use.

2.1.2.4 Disc and well diffusion assay

Sterile filter-paper discs were prepared by punching uniform circles (6 mm diameter) and immersing them in each extract solution for 12 h. Standardized Muller-Hinton agar plates were bored with 6 mm wells and filled with the corresponding volumes or concentrations of olive or fig leaf extract for well-diffusion assays. All prepared plates were subsequently sealed and stored at 4°C in sterile amber glass vials, protected from light and moisture until antimicrobial testing commenced within 7–10 days of preparation to ensure chemical stability and preserve bioactivity (Sa and Bradford, 2008; Ahmad-Qasem et al., 2016; Khelouf et al., 2023).

2.1.3 Cultivation and standardization of microbial strains

2.1.3.1 Bacterial cultures

The clinical samples used in this study were collected from hospitalized patients with confirmed bacterial infections. Isolates of Gram-positive and Gram-negative bacteria were collected from various clinical specimens from patients of different ages and sexes, including stool, blood, cerebrospinal fluid (CSF), urine, and swab cultures. All isolates were obtained with informed patient consent and approved by the institutional ethics committee to ensure compliance with ethical research standards. Bacterial identification was performed using the Vitek2 compact

system (BioMérieux, Marcy-l'Étoile, France). The Gram-positive isolates included *Staphylococcus aureus, Streptococcus agalactiae,* and *Enterococcus faecalis*, while the Gram-negative isolates comprised *Escherichia coli, Pseudomonas aeruginosa,* and *Klebsiella pneumoniae*. All bacterial isolates were routinely maintained on Mueller-Hinton agar (HIMEDIA, India) and subcultured onto fresh nutrient agar plates as required to ensure viability and purity throughout the study. Antimicrobial susceptibility testing was assessed using disc diffusion and well-diffusion assays, following Clinical and Laboratory Standards Institute (CLSI) guidelines. Broth microdilution and Mueller-Hinton agar plating methods determined minimum inhibitory (MIC) and minimum bactericidal concentration (MBC).

2.1.3.2 Inoculum standardization

Bacterial isolates were standardized to a 0.5 McFarland turbidity, approximately equivalent to $\sim 1 \times 10^8$ CFU/mL. In brief, a single loopful of the respective colony was transferred to 10 mL of sterile distilled water in a glass tube, ensuring that the optical density matched the 0.5 McFarland reference (Haley et al., 2024).

2.1.3.3 Fungal culture

A clinical isolate of *Candida albicans* from the sputum of the 35-year-old male patient was obtained and cultured on Sabouraud Dextrose Agar (SDA) at 37°C. Following initial growth, the isolate was subcultured as required for antifungal evaluation.

2.1.4 Antimicrobial assays

2.1.4.1 Determination of MIC and MBC/MFC

The antimicrobial efficacy of the plant extracts was assessed using standardized broth microdilution and agar diffusion techniques following Clinical and Laboratory Standards Institute (CLSI) recommendations (Haley et al., 2024). Serial two-fold dilutions of each plant extract were prepared in Mueller-Hinton Broth (MHB) to obtain final 100, 50, 25, and 12.5 mg/mL concentrations. Each sterile 96-well microtiter plate received 100 µL of the diluted extract and 100 µL of a bacterial suspension standardized to a 0.5 McFarland turbidity. The following experimental controls were included to ensure assay reliability: a growth control (MHB and bacterial inoculum), a sterility control (MHB and extract without bacterial inoculum), a DMSO control (MHB, bacterial inoculum, and DMSO), and a solvent control (MHB, bacterial inoculum, and either methanol or acetone), to account for potential solvent effects. Following incubation at 37°C for 18–24 h, the minimum inhibitory concentration (MIC) was defined as the lowest concentration of extract that inhibited visible microbial growth. To determine the minimum bactericidal concentration (MBC), 10 µL aliquots from wells showing no turbidity were subcultured onto Mueller-Hinton Agar (MHA), and the lowest concentration at which no colonies were observed after incubation was considered as the MBC (Liu et al., 2017; Sánchez-Gutiérrez et al., 2021; Kebede and Shibeshi, 2022; Esfandiary et al., 2024).

For the disc diffusion assay, MHA plates were uniformly inoculated with a 0.5 McFarland bacterial suspension using sterile cotton swabs. Sterile 6 mm filter paper discs were saturated with plant extracts (100, 50, 25, and 12.5 mg/mL) prepared in DMSO or sterile water. Positive control discs were antimicrobial agents (e.g., Levofloxacin 5 µg/disc was used as an antibacterial agent, Sulconazole 25 µg disc was used as the antifungal control), while negative control discs contained only the solvent (methanol, acetone, or DMSO). After air-drying the discs for ~5 min to ensure complete solvent evaporation, the discs were aseptically placed on the surface of the inoculated plates, maintaining a minimum spacing of 24 mm. Plates were incubated at 37°C for 18–24 h, after which inhibition zones (including the disc diameter) were measured in millimeters and compared to the standard antibiotic controls (Liu et al., 2017; Sánchez-Gutiérrez et al., 2021; Kebede and Shibeshi, 2022; Esfandiary et al., 2024).

Similarly, MHA plates were inoculated in the well diffusion assay as described above. Wells of 6–8 mm diameter were aseptically made using a sterile cork borer, and 100 µL of each plant extract concentration (100, 50, 25, and 12.5 mg/mL) was loaded into individual wells. Solvent and antibiotic controls were also applied. Plates were left at room temperature for 10 min to facilitate initial diffusion, followed by incubation at 37°C for 18–24 h. The inhibition zone surrounding each well was measured and recorded (Liu et al., 2017; Sánchez-Gutiérrez et al., 2021; Kebede and Shibeshi, 2022; Esfandiary et al., 2024).

2.1.4.2 Control measures

Levofloxacin (5 µg/disc) was used as the positive control for antibacterial activity, whereas Sulconazole (25 µg) was used as the antifungal control. To ensure appropriate negative controls, both the extraction solvents (methanol, ethanol, and aqueous media) and a 10% DMSO solution were tested to ensure appropriate negative controls. DMSO was included based on its frequent use as a solvent for plant extracts and bioactive compounds. However, to mitigate its potential antimicrobial effect, we ensured that the DMSO final concentration in microbial assays remained below inhibitory levels, as previously reported in the literature (Gonelimali et al., 2018; Ratananikom and Srikacha, 2020; Summer et al., 2022). Furthermore, methanol, ethanol, and aqueous media were individually tested as standalone negative controls to eliminate the possibility of solvent-induced antimicrobial effects. These tests confirmed that the extraction solvents did not exhibit antimicrobial activity at the concentrations used in the experiments, validating their appropriateness as controls.

2.1.5 *In vitro* reporter-gene profiling of toxicity pathways

We employed toxicological assay software (Attagene, Inc., Morrisville, NC, USA) to evaluate critical toxicological endpoints encompassing nuclear receptor signaling pathways, stress response pathways, molecular initiating events (MIEs), and metabolism. Unless otherwise noted, all procedures were performed according to the manufacturer's instructions (which included guidelines for plate preparation, reagent handling, incubation conditions, and normalization of data). Although the Attagene platform employs automated software analytics, the TF-CIS/NRF assay is a cell reporter-gene *in vitro* screening system; therefore, all pathway data reported here originate from cultured HepG2-derived cells rather than purely computational (*in silico*) simulations. We evaluated three plant extracts: *O. europaea* methanolic fraction, *O. europaea*

aqueous fraction, and *F. carica* methanolic fraction. Each extract was tested at five concentrations: 6.25, 12.5, 25, 50, and 100 mg/mL, with 0.5% DMSO as the constant vehicle.

The Tox21 software was used to determine the activity of the following nuclear receptor signaling pathways: aryl hydrocarbon receptor (AhR), androgen receptor (AR), androgen receptor ligand binding domain (AR-LBD), aromatase, estrogen receptor alpha (ER), and estrogen receptor ligand binding domain (ER-LBD), and peroxisome proliferator-activated receptor gamma (PPAR-Gamma). Using the same platform, stress response pathways were detected by assessing the activity of key stress-related factors: nuclear factor (erythroid-derived 2)-like 2/antioxidant responsive element (nrf2/ARE); heat shock factor response element (HSE); mitochondrial membrane potential (MMP); phosphoprotein (tumor suppressor) p53; and ATPase family AAA domain-containing protein 5 (ATAD5). Reporter cells or assays specific to each stress factor were employed according to the manufacturer's guidelines, which included protocol-driven cell seeding, compound exposure, and post-treatment incubation. The resulting signals were detected and analyzed according to the software's instructions. Positive-control agonists for each pathway (e.g., TCDD for AhR, 17β-estradiol for ERα, rosiglitazone for PPAR-γ, and tBHQ for Nrf2/ARE) were run in parallel to validate assay performance. At the same time, vehicle-only wells served as baselines for fold-induction calculations.

To further identify molecular initiating events, the assay software was further applied to measure the activity of the following receptors and enzymes: thyroid hormone receptor alpha (THRα), thyroid hormone receptor beta (THRβ), transthyretin (TTR), ryanodine receptor (RYR), GABA receptor (GABAR), glutamate N-methyl-D-aspartate receptor (NMDAR), alpha-amino-3-hydroxy-5-methyl-4-isoxazole-propionate receptor (AMPAR), kainate receptor (KAR), acetylcholinesterase (AChE), constitutive androstane receptor (CAR), pregnane X receptor (PXR), NADH-quinone oxidoreductase (NADHOX), voltage-gated sodium channel (VGSC), and Na^+/I^- symporter (NIS). We also expand our investigation using the Attagene platform to assess metabolic activity by measuring the activity of the following cytochrome P450 enzymes: cytochrome CYP1A2, CYP2C19, CYP2C9, CYP2D6, CYP3A4, and CYP2E1. A reporter was classified as "active" when the fold-induction exceeded 1.5× vehicle control in at least two adjacent concentrations and demonstrated a concentration-dependent trend with Hill-fit $R^2 \geq 0.9$; otherwise, it was deemed inactive.

2.2 *In vivo* studies

2.2.1 Animal model

All animal experiments were carried out in accordance with institutional guidelines and international regulations for the care and use of laboratory animals, following the ARRIVE 2.0 guidelines (Percie du Sert et al., 2020). Fifteen healthy male BALB/c mice were purchased from the University of Benghazi, Faculty of Medicine Animal House. Individual mice were 1–2 months old, with an average weight of 25–30 g. Animals were maintained at a 12-h light/dark cycle at 24–25°C, receiving unrestricted access to tap water and a standard commercial rodent diet throughout both the acclimation and experimental phases. The mice were randomly assigned to three experimental groups ($n = 5$ per group). The selection of five mice per group was guided by considerations of scientific rigor, ethical responsibility, and consistency with prior *in vivo* studies. A sample size of $n = 5$ is commonly employed in murine models investigating plant extracts, as it provides adequate statistical power while reducing excessive animal use (Charan and Kantharia, 2013). Moreover, this selection aligns with the principles of Reduction, Replacement, and Refinement (3Rs), ensuring ethical compliance without compromising data integrity. Moreover, established guidelines in experimental design recommend similar sample sizes for preclinical studies to balance statistical robustness and ethical responsibility (Festing and Altman, 2002; Piper et al., 2022). The first experimental group was administered intraperitoneal injections with the methanolic fraction of olive leaf extract, reconstituted in distilled water at 50 mg/kg. The second group received the same extract at 100 mg/kg dose. The control group was administered distilled water. For *in vivo* administration, the methanolic extract of *O. europaea* was reconstituted in distilled water to ensure biocompatibility and reduce solvent-related toxicity in accordance with ethical and safety standards for animal research. The doses of 50 and 100 mg/kg of *O. europaea* leaf extract were selected based on previous studies demonstrating their safety and efficacy in animal models. Oral administration of olive leaf extracts at doses up to 200 mg/kg has shown therapeutic effects without toxicity, while acute toxicity studies report no adverse effects at doses up to 2,000 mg/kg (Clewell et al., 2015; Guex et al., 2018; Hinad et al., 2021). Before sacrifice, animals were fasted but retained free access to water until 24 h before euthanasia. *In vivo* experiments were conducted exclusively with the methanolic extract of olive leaves due to its promising bioactivity observed in preliminary *in vitro* evaluations, thus warranting further investigation. In contrast, fig leaf extract was excluded from *in vivo* testing due to practical limitations, such as restricted laboratory animal availability and the necessity to optimize resource allocation to ensure a statistically significant and ethically compliant study design. All procedures were carried out in accordance with institutional guidelines for animal care and use and conformed to internationally recognized ethical standards.

2.2.2 Ethical approval

All clinical samples were anonymized prior to analysis to ensure patient confidentiality. The study was approved by the Institutional Ethics Review Board and conducted in accordance with the ethical principles outlined in the Declaration of Helsinki (approval reference number: LIMU/UMC/IRB/2024-027). The Institutional Animal Care and Use Committee, University of Benghazi, reviewed and approved animal protocols (animal ethical approval certificate number: IACUCB-MED-JY/2024/015). All experimental protocols were performed in accordance with institutional guidelines for the care and use of laboratory animals.

2.2.3 Histological techniques and sample collection

The histological methods employed in this study were conducted to assess potential tissue alterations induced by olive

and fig leaf extracts, detect cellular and inflammatory responses, evaluate safety and adverse effects, and provide microscopic evidence of physiological impacts not detected by biochemical assays alone.

2.2.3.1 Organ removal and fixation

Mice were anesthetized by diethyl ether inhalation 24 h after the injection of olive leaf extracts. These animals were then euthanized, and liver (hepatectomy) and kidney (nephrectomy) tissues were extracted in aseptic conditions. Each tissue sample was placed in 10% neutral-buffered formalin for 24 h to preserve the structure. After fixation for the first time, standard histological preparations were performed as described by Suvarna et al. (2020). Briefly, samples remained in 10% formalin to stabilize tissue architecture, and tissues were sequentially exposed to increasing ethanol concentrations (50%, 70%, 90%, and 100%) to remove residual water. Dehydrated samples were immersed in xylene for ~2 h to replace ethanol and increase tissue transparency. Tissues were infiltrated with molten paraffin wax, providing mechanical support and enabling thin sectioning, and transferred to metallic or plastic molds, which were then rapidly cooled (−6 to −4°C) to solidify the wax block, thereby fixing the tissue orientation. Blocks were trimmed into 3–5 μm sections with a rotary microtome for sectioning. Ribbon sections were floated on a 40–45°C water bath and subsequently mounted onto microscope slides pre-treated with an adhesive or 50% ethanol to facilitate adherence. The slides were then dried before staining 0.50% ethanol or adhesive is needed to perform well, and the slides were dried before staining.

2.2.3.2 Hematoxylin and eosin staining

The staining procedure was conducted according to the method described by Fischer et al. (2008), with minor modifications. For deparaffinization and rehydration, the slides were placed in xylene for about 2 min, then in descending concentrations of ethanol (96%, 90%, 70%) to rehydrate the tissue sections. Slides were then immersed in hematoxylin solution for 5 min, rinsed under running water, briefly dipped in acid alcohol (one dip) for differentiation, and thoroughly rewashed. These sections were transferred to eosin for 3 min, then lightly rinsed in water to remove excess stain and dehydrated for mounting. The slides were finally immersed in xylene to clear residual ethanol and mounted with DPX (styrene plasticizer xylene). A coverslip was gently lowered to seal the tissue sections.

2.2.3.3 Histopathological evaluation

Prepared slides were examined under an Olympus BX41 light microscope. Images were captured digitally with an Olympus DP2-BSW system. Pathological assessments focused on identifying inflammatory lesions, necrosis, and other cellular or architectural alterations relevant to olive leaf extract treatment effects.

2.2.3.4 Hematological and biochemical analysis

Blood samples were drawn via puncture using a 30-gauge needle. A portion of the blood was collected into EDTA tubes for complete blood count (CBC) analysis using a SYSMEX XN330 (Diamond Diagnostics, USA) hematology analyzer, determining red blood cells (RBCs), white blood cells (WBCs), hemoglobin, and platelets. The remaining blood sample was placed into plain tubes centrifuged at 4,000 rpm, and the resulting serum was evaluated for liver and kidney function using a Cobas Integra 400 plus platform (Roche Diagnostics, Germany). Parameters such as alanine transaminase (ALT), aspartate transaminase (AST), creatinine, and urea were measured to assess organ function (Arantes-Rodrigues et al., 2011; Clewell et al., 2015).

2.3 *In silico* studies

2.3.1 Molecular docking studies

All calculations were initiated by preparing and optimizing the ligand as *O. europaea* leaf extract with Gaussian 09 (Gaussian Inc., Wallingford, CT, USA). The quantum-chemical geometry optimizations used DFT at the B3LYP functional level with the 6-311 G++(d,p) basis set, a commonly used combination where computational load and accuracy are balanced. Subsequent vibrational-frequency analyses were conducted to ensure no imaginary frequencies were present, confirming that optimized structures corresponded to true potential-energy minima. The energy diagram (Figure 1) and the refined version of the final geometry (Figure 2A) were exported from Gaussian 09 to ensure reproducibility and clarity.

We selected the cytochrome-c peroxidase (Ccp) because it is an essential periplasmic H_2O_2-detoxifying enzyme in many of the Gram-negative MDR pathogens examined in this study. Chemical or genetic inhibition of Ccp markedly increases oxidative-stress sensitivity and attenuates virulence. The high-resolution *E. coli* Ccp structure (PDB ID 1BEK, 1.8 Å) provides a conserved, biologically relevant, and readily druggable target for our panel of Enterobacteriaceae isolates. The *E. coli* peroxidase structure was obtained from the Protein Data Bank (PDB ID: 1BEK; https://www.rcsb.org) and processed to remove any unnecessary entities, including crystallographic water and non-essential cofactors, keeping only the functional portion of the enzyme-binding site. Missing hydrogen atoms were added, and side-chain orientations were validated using the standard protein-preparation protocols. PyMOL (v 2.0; Schrödinger, LLC) was used to visualize the α-helices, β-sheets and loop regions in red, cyan, and green, respectively (Figure 2B). This color scheme and rendering style were selected to emphasize the overall fold of the protein with a focus on the structural motifs essential for enzymatic catalysis.

For the molecular docking analyses, 10 phenolic compounds were selected based on their consistent identification as major constituents in methanolic leaf extracts through recent LC-MS and HPLC-MS studies. These included oleuropein, hydroxytyrosol, tyrosol, verbascoside, luteolin-7-O-glucoside, and apigenin from *Olea europaea* (Kabbash et al., 2023; Papageorgiou et al., 2022), as well as psoralen, eugenol, acetyleugenol, and quercetin from *Ficus carica* (Kim and Lee, 2023; Tikent et al., 2024; Shiraishi et al., 2023). These compounds were selected for docking based on their well-documented antimicrobial and redox-modulatory properties, adherence to Lipinski's and Veber's criteria for drug-likeness, their substantial representation in the methanolic extract (≥5% of the total peak area), and the availability of

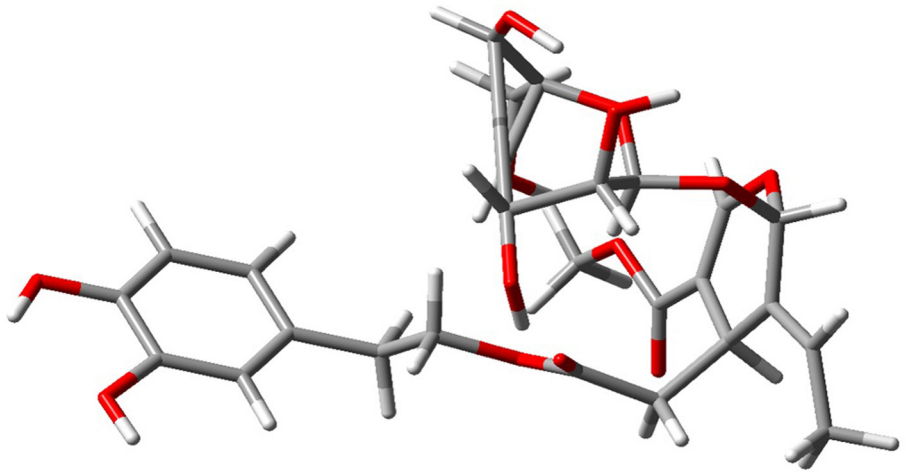

FIGURE 1
Optimized minimum-energy geometry of a representative olive leaf extract compound obtained using DFT calculations [B3LYP/6-311++G(d,p)] in Gaussian 09. The absence of imaginary vibrational frequencies in the vibrational analysis confirms that the structure corresponds to an actual local minimum on the potential energy surface.

high-quality, structurally resolved 3D coordinates enabling robust computational modeling.

Pre-docking and docking simulations were conducted using established molecular-docking software, such as AutoDock Vina and Schrödinger Glide (MOE-Dock). The optimized olive-leaf-extract ligands were converted into the appropriate docking-file formats (PDBQT) suitable for each software package. During ligand preparation, rotatable bonds, such as broken rings, were carefully defined to ensure accurate modeling of ligand flexibility. Reported catalytic residues were combined with automated pocket-detection algorithms for peroxidase active-site delineation. Multiple independent docking runs allowed for extensive exploration of the conformational landscape, resulting in various plausible ligand poses. We further examined the high-scoring solutions in detail, with a focus on hydrogen-bond formation, π-π stacking, hydrophobic contacts, and potential electrostatic clashes, particularly for functionally important residues (e.g., Ser 185, Lys 179, Arg 48).

2.4 Statistical analysis

All data were processed using Microsoft Excel 2023 and are expressed as means ± standard deviation (SD). Statistical significance across multiple experimental groups was assessed via one-way analysis of variance (ANOVA) with repeated measures, utilizing SPSS software (SPSS, Inc., Chicago, IL). Additionally, a *t*-test was conducted to determine differences between two independent group means. Furthermore, two-way ANOVA was employed to simultaneously evaluate the influence and interactions of two independent factors, providing a more comprehensive understanding of their combined effects on the results. Differences with *p*-values below 0.05 ($p < 0.05$) were considered statistically significant.

3 Results

3.1 *In vitro* studies

3.1.1 Antimicrobial susceptibility testing of the clinical isolates

We evaluated antimicrobial susceptibility profiles for the selected clinically relevant pathogens against a panel of antimicrobial agents, as shown in Table 1. Our results revealed that *E. faecium* exhibited complete resistance to all tested antimicrobial agents, suggesting a pan-resistant phenotype. *K. pneumoniae* exhibited extensive antimicrobial resistance but retained susceptibility to amoxicillin-clavulanate and ceftazidime. In contrast, *S. aureus* was sensitive to azithromycin, nitrofurantoin/fosfomycin, trimethoprim-sulfamethoxazole, and amikacin but resistant to gentamicin, vancomycin, amoxicillin-clavulanate, ceftriaxone, ceftazidime, and tobramycin. Furthermore, *E. coli* was susceptible to azithromycin, amikacin, and gentamicin but resistant to nitrofurantoin/Fosfomycin, trimethoprim-sulfamethoxazole, vancomycin, amoxicillin-clavulanate, ceftriaxone, ceftazidime, and tobramycin. *E. faecalis* exhibited a limited antimicrobial susceptibility profile, demonstrating sensitivity exclusively to trimethoprim-sulfamethoxazole while exhibiting resistance to all other agents tested. *S. agalactiae* exhibited complete resistance to all antimicrobial agents tested. *E. cloacae* remained resistant to azithromycin and amoxicillin-clavulanate but susceptible to trimethoprim-sulfamethoxazole and amikacin. Two-way ANOVA revealed statistically significant differences in antimicrobial agents efficacy ($p = 0.042$). These findings highlight the widespread occurrence of multidrug resistance in specific microbial pathogens, particularly *E. faecium* and *S. agalactiae*. Furthermore, the results emphasize the necessity of ongoing monitoring, careful antimicrobial agent selection, and responsible antimicrobial practices.

10.3389/fmicb.2025.1567921

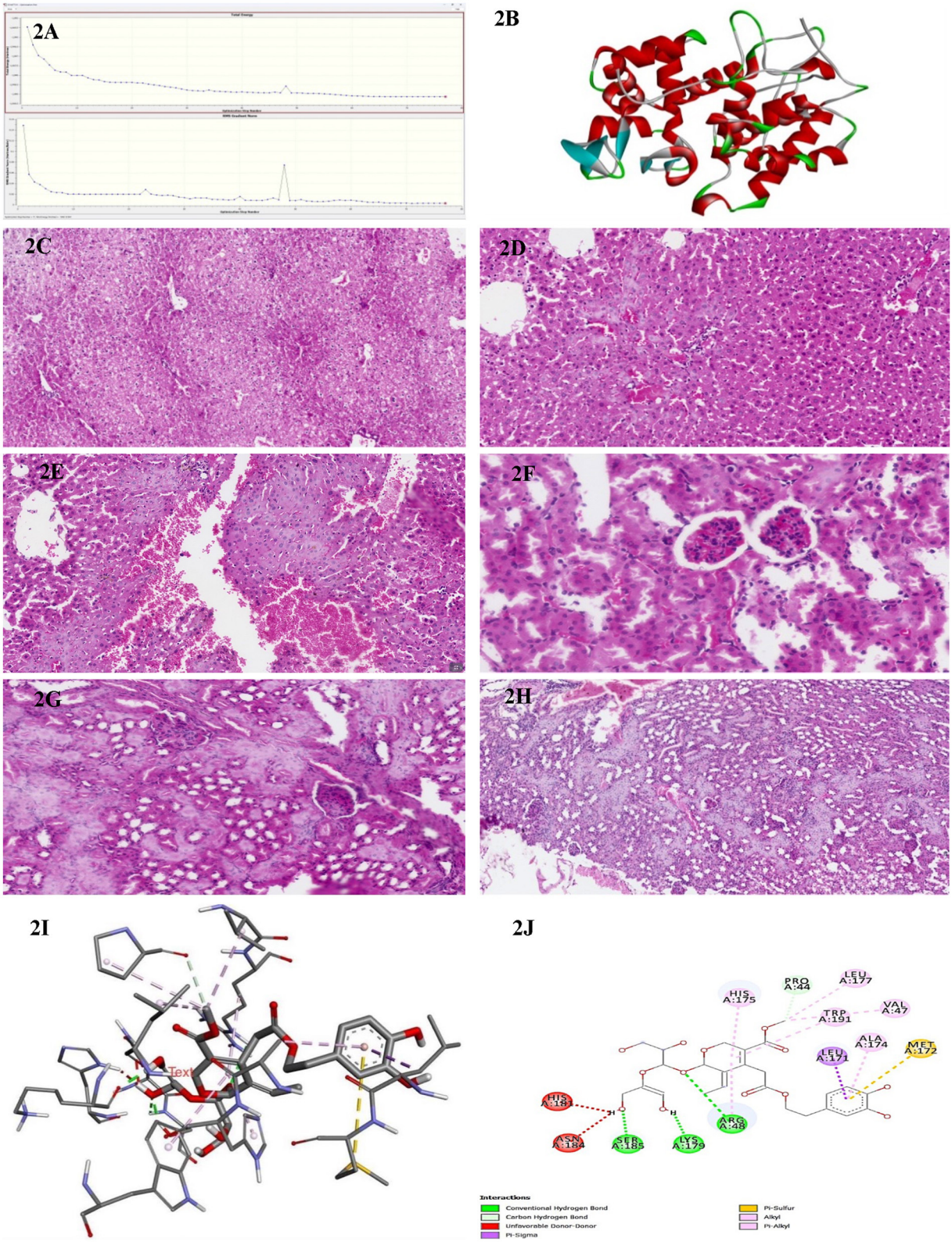

FIGURE 2
(A) Energy convergence diagram obtained during the DFT [B3LYP/6-311G++(d,p)] geometry optimization of olive leaf extract in Gaussian 09. The top panel shows the total electronic energy at each optimization step, while the bottom panel depicts the root-mean-square (RMS) gradient norm. The systematic decrease in energy and gradient norm over successive iterations indicates successful convergence to a stable local minimum on the potential energy surface. **(B)** Three-dimensional structure representation of the peroxidase enzyme from *E. coli* (PDB ID: 1BEK). Alpha-helices are depicted in red, β-sheets in cyan, and loop regions in green. This structure was obtained from the Protein Data Bank and visualized here to illustrate the overall fold and secondary structural elements characteristic of bacterial peroxidases. **(C)** A representative histological section of the liver from a

(Continued)

FIGURE 2 (Continued)
BALB/c control mouse administered an intraperitoneal injection of distilled water, stained with hematoxylin and eosin, and examined at 200× magnification. **(D)** A representative histological section of the liver from a BALB/c mouse administered an intraperitoneal dose of 50 mg/kg of the methanolic fraction of olive leaf extract reconstituted in distilled water. The tissue was stained with hematoxylin and eosin and examined at 200× magnification. **(E)** A representative histological section of the liver from a BALB/c mouse administered an intraperitoneal dose of 100 mg/kg of the methanolic fraction of olive leaf extract reconstituted in distilled water. The tissue was stained with hematoxylin and eosin and examined at 200× magnification. **(F)** A representative histological section of the kidney from a BALB/c control mouse was administered an intraperitoneal injection of distilled water. The tissue was stained with hematoxylin and eosin and examined at 200× magnification. **(G)** A representative histological section of the kidney from a BALB/c mouse following intraperitoneal injection with 50 mg/kg of the methanolic fraction of olive leaf extract reconstituted in distilled water. The tissue was stained with hematoxylin and eosin and observed at 200× magnification. The section exhibits cortical hemorrhages and focal regions of interstitial damage. **(H)** A representative histological section of the kidney from a BALB/c mouse following intraperitoneal injection with 100 mg/kg of the methanolic fraction of olive leaf extract reconstituted in distilled water. The tissue was stained with hematoxylin and eosin and observed at 200× magnification. The section exhibits cortical hemorrhages and focal regions of interstitial damage. **(I)** The three-dimensional molecular docking representation of oleuropein (olive leaf extract) bound to bacterial peroxidase. The model highlights critical tight binding interactions, including hydrogen bonds and hydrophobic contacts, illustrated as dashed lines. This interaction provides insights into Oleuropein's potential mechanism of action in modulating bacterial peroxidase activity. **(J)** The two-dimensional interaction map of Oleuropein (olive leaf extract) with bacterial peroxidase highlights the key molecular interactions. The diagram illustrates hydrogen bonds (green and red dashed lines), carbon-hydrogen bonds, and various hydrophobic interactions, such as π-alkyl, π-sulfur, and π-π stacking, which contribute to the binding stability. Residues involved in these interactions are labeled, providing a detailed view of the compound's binding orientation and affinity for peroxidase.

3.1.2 Antimicrobial efficacy of *O. europaea* and *F. carica* leaf extracts using different solvents

In parallel, a range of *in vitro* assays was performed on *O. europaea* and *F. carica* leaf extracts against the previously described pathogenic bacterial strains and *C. albicans*. Extracts were prepared using three different solvents (acetone, methanol, and distilled water) at five concentrations (100, 50, 25, 12.5, 6.25 mg/mL). Antimicrobial activity was assessed using the agar well diffusion assay, with inhibition zones recorded in millimeters from three independent replicates. To ensure the specificity of the antimicrobial activity, each solvent alone was tested in parallel with the target pathogens as a solvent control. The negative control consisted of 10% DMSO, while standard antimicrobial agents were positive controls.

3.1.2.1 Acetone extracts

At 100 mg/mL concentration, *O. europaea* acetone extracts demonstrated moderate inhibitory effects against some bacterial isolates. The most significant susceptibility was observed in *K. pneumoniae* (14.67 mm) and *E. coli* (14.33 mm), followed by modest zones against *S. aureus* (11 mm) and *S. agalactiae* (10 mm), as shown in Supplementary Table 1. However, no inhibition was detected at lower extract concentrations, nor against *Enterococcus* spp., *P. aeruginosa*, or *C. albicans*. In contrast, *F. carica* acetone extracts displayed minimal activity. Only *K. pneumoniae* showed a small inhibition zone (8.67 mm) at 100 mg/mL, with no measurable effects against any other tested organism at lower concentrations.

These findings suggested that the antimicrobial efficacy of acetone extracts is notably limited. At the highest concentration, the extracts showed effectiveness only against a few Gram-positive and Gram-negative bacterial strains. Furthermore, neither extract demonstrated antifungal efficacy against *C. albicans*, indicating poor extraction of antifungal constituents using acetone.

Overall, both acetone extracts demonstrated narrower spectra and smaller inhibition zones relative to the positive controls (e.g., up to 32.33 mm for *K. pneumoniae*). These results suggest that acetone-based extracts exhibit limited antimicrobial efficacy, particularly at lower concentrations. Consequently, acetone appears to be a less effective solvent for extracting pharmacologically active antimicrobial constituents from these plant sources.

3.1.2.2 Methanol extracts

Methanol emerged as the most effective solvent for extracting bioactive compounds from *O. europaea* (Supplementary Table 2). The methanolic extract exhibited potent antibacterial activity at the highest tested concentration (100 mg/mL), notably against *S. agalactiae* (29 mm) and *E. cloacae* (39.33 mm). Even at 50%, considerable inhibition zones were observed, particularly for *S. agalactiae* (20.67 mm) and *K. pneumoniae* (20.33 mm). A moderate antifungal effect was also evident at 100% against *C. albicans* (19.66 mm). However, moderate fungal inhibition was observed at lower concentrations.

In contrast, the methanolic extract of *F. carica* exhibited comparable antimicrobial potency. At 100 mg/mL, the extract exhibited wider inhibition zones: 20 mm for *S. aureus*, 8 mm for *K. pneumoniae*, 9.33 mm for *E. coli*, and 13.67 mm for *S. agalactiae*. At lower concentrations, the extracts exhibited minimal to no detectable antimicrobial activity, and *C. albicans* showed complete resistance across all tested concentrations.

These findings suggest that methanol is highly efficient in extracting antimicrobial phytochemicals from *O. europaea*, presumably due to its strong capacity to solubilize polar compounds such as polyphenols and flavonoids. The observed concentration-dependent activity further highlights the importance of solvent selection and dosage in optimizing the recovery of pharmacologically active constituents. The broad-spectrum efficacy of *O. europaea* methanolic extracts against multiple bacterial strains underscores its potential for further investigation as a plant-derived antimicrobial agent.

3.1.2.3 Water extracts

The experimental findings revealed that at 100 mg/mL concentration, aqueous extracts of *O. europaea* exhibited moderate to potent antimicrobial activity, particularly against *E. cloacae* (23.10 mm), *S. aureus* (20.3 mm), *P. aeruginosa* (27 mm), and *E. faecium* (17.7 mm) as shown in Supplementary Table 3. *K. pneumoniae* and *E. coli* exhibited limited susceptibility to the aqueous extracts, each showing inhibition zones of 14.7 mm. In contrast, *S. agalactiae*, *E. faecalis*, and *C. albicans* were

10.3389/fmicb.2025.1567921

TABLE 1 Zone of inhibition diameters (in mm, presented as mean ± standard deviation) for various clinically relevant pathogens tested against a panel of antimicrobial agents.

Pathogen	AZM	NI/F	SXT	AK	CN	VA	AMC	CRO	CAZ	TOP
E. faecium	17.00 ±1.00	10.67 ±0.57	8.33 ±0.57	15.00 ±1.00	16. ±0.57	9.33 ±0.57	9.33 ±1.15	8.67 ±0.57	9.00 ±1.00	9.33 ±1.52
K. pneumoniae	17.00 ±1.00	9.66 ±1.15	10.66 ±0.57	10.66 ±0.57	9.66 ±1.52	8.66 ±0.57	27.34 ±1.15	10.33 ±1.15	26.00 ±0.00	8.33 ±1.15
S. aureus	32.00 ±1.00	30.33 ±1.155	30.66 ±0.57	26.66 ±0.57	10.00 ±1.00	11.00 ±1.00	11.000 ±1.00	9.66 ±0.57	9.00 ±1.00	9.66 ±0.57
E. coli	30.33 ±1.15	10.66 ±0.57	10.33 ±0.57	25.66 ±0.57	26.00 ±0.00	9.66 ±0.57	9.33 ±1.15	13.66 ±0.57	10.66 ±1.52	9.33 ±1.15
E. faecalis	12.66 ±1.15	8.66 ±0.57	33.33 ±1.155	16.33 ±0.57	17.66 ±0.57	11.33 ±0.57	8.66 ±0.57	10.33 ±0.57	9.33 ±0.57	11.66 ±0.57
S. agalactiae	10.33 ±0.57	9.66 ±0.57	11.00 ±1.00	11.33 ±0.57	11.00 ±1.00	11.67 ±1.15	12.67 ±0.57	11.67 ±0.57	9.67 ±0.57	10.00 ±1.00
E. cloacae	10.33 ±0.57	10.00 ±0.00	32.00 ±1.00	38.00 ±1.73	9.67 ±0.57	6.00 ±0.00	12.67 ±0.57	10.00 ±1.00	6.00 ±0.00	6.00 ±0.00

Measurements were obtained following the Clinical and Laboratory Standards Institute (CLSI) guidelines. AZM, Azithromycin; NI/F, Nitrofurantoin; SXT, Trimethoprim/Sulfamethoxazole; AK, Amikacin; CN, Gentamicin; VA, Vancomycin; AMC, Amoxicillin/Clavulanic Acid; CRO, Ceftriaxone; CAZ, Ceftazidime; and TOP, Tobramycin.

entirely resistant with no observable inhibitory effect. Notably, a moderate level of antimicrobial activity remained detectable at 50 and 25 mg/mL concentrations, particularly against *S. aureus* (12.7 and 7.3 mm, respectively) and *E. coli* (14.3 mm at 50%). However, no measurable inhibitory effects were observed at lower concentrations or against the remaining tested isolates. Consistent with its limited activity in other solvents, *F. carica* aqueous extracts exhibited only weaker antimicrobial activity. Inhibition was observed sporadically at 100 mg/mL, specifically against *S. aureus* (11.33 mm). However, most other bacterial isolates and *C. albicans* showed complete resistance. These findings suggest water is a suboptimal solvent for extracting bioactive antimicrobial constituents from *F. carica*. These findings suggest that although aqueous extracts of *O. europaea* display moderate antibacterial activity, their overall efficacy remains markedly lower than that of the methanolic extracts. Nevertheless, due to the absence of organic solvents, their non-toxic nature and compatibility with *in vivo* applications underscore their relevance in specific therapeutic contexts. These findings further underscore the critical importance of solvent selection in enhancing the antimicrobial efficacy and potential clinical utility of plant-based therapeutics.

In conclusion, these findings demonstrate that the antimicrobial effectiveness differs considerably based on the solvent type and the tested plant species. Methanol proved to be the most effective solvent for extracting bioactive compounds from *O. europaea*, demonstrating potent broad-spectrum antibacterial activity and moderate antifungal efficacy at the highest concentration tested. In contrast, extracts from *F. carica* exhibited limited antimicrobial potency against specific bacterial strains at the highest methanolic concentration. Moreover, aqueous extracts of *O. europaea* showed moderate antibacterial activity against particular pathogens, whereas acetone extracts exhibited more limited activity even at higher concentrations. These observations emphasize the significant role of solvent selection in effectively extracting bioactive compounds. Therefore, methanolic extracts of *O. europaea* represent a promising candidate for future antimicrobial research to combat agents-resistant pathogens.

3.1.3 Comparison of plant extracts and conventional antimicrobial agents against MDR pathogens

A comparison of the antimicrobial agent susceptibility data with the current plant extract results shows several noteworthy similarities and differences. Most prominently, *E. faecium* and *S. agalactiae* exhibited pan-resistance to all conventional antimicrobial agents tested, yet both demonstrated appreciable inhibition zones in response to methanolic extracts of *O. europaea*. In contrast, S. *agalactiae*, which exhibited no susceptibility to standard antimicrobial agents, displayed an inhibition zone of up to 45 mm with *O. europaea* methanol extract at 100 mg/mL concentration, suggesting that these phytochemical constituents can inhibit pathogens. Similarly, *E. faecium*—entirely resistant under antimicrobial conventional testing—was also inhibited by *O. europaea* methanolic extracts at 100 mg/mL, whereas *F. carica* extracts remained largely ineffective.

A similar pattern was observed in the cases of *S. aureus* and *K. pneumoniae*. In our analyses, both isolates displayed

variable susceptibility or partial resistance to selected antimicrobial agents but showed clear zones of inhibition upon exposure to methanolic extracts of *O. europaea*. Moreover, inhibition zone for *S. aureus* and *K. pneumoniae* at 100% concentration highlight the broad-spectrum potential of *O. europaea* under these conditions. By contrast, *F. carica* extracts displayed comparatively modest or negligible antimicrobial activity against the same organisms, particularly at lower concentrations and with acetone or water extractions. For *E. coli* which was susceptible to a limited number of standard antimicrobial agents, the methanol-based *O. europaea* extract demonstrated consistent inhibition, reflecting the partial efficacy observed in the antimicrobial drug profile. *E. cloacae* also followed a similar pattern, showing high-level inhibition with *O. europaea* methanol extracts despite exhibiting limited susceptibility to conventional antimicrobial agents.

Taken together, these comparative findings highlight some key observations. First, methanol appears most effective in extracting antimicrobial compounds from *O. europaea*, as evidenced by the larger inhibition zones against pathogens that significantly resisted conventional antimicrobial agents. Secondly, *F. carica* extracts generally showed lower activity across the tested organisms, suggesting that its extracts may lack the same potency against multidrug-resistant pathogens. The fact that certain strains were resistant to multiple standard antimicrobial agents but showed susceptibility to *O. europaea* extracts underscores the potential clinical relevance of plant-derived antimicrobials. Consequently, solvent choice (particularly methanol) and plant species selection (notably O. europaea) emerge as key factors in maximizing the inhibitory efficacy against bacterial and fungal pathogens.

3.1.4 *In vitro* high-content reporter-gene profiling of toxicity pathways

Toxicity prediction using *in silico* models has gained widespread application in pharmacology and toxicology, offering a rapid and efficient means of screening compounds for potential safety concerns (Wichard, 2017). These computational tools provide notable benefits in early-stage drug development by reducing time and cost while avoiding the ethical challenges posed by animal experimentation. Increasingly, regulatory bodies are recognizing the validity of *in silico* approaches for specific evaluations; for instance, the ICH M7 guideline endorses the use of QSAR models as acceptable alternatives to laboratory testing for detecting DNA-reactive impurities (Raies and Bajic, 2016; Wichard, 2017).

Using Attagene's toxicological assay software (Attagene, Inc., Morrisville, NC, USA), we evaluated olive leaf extract at doses up to 2,000 mg/kg for potential organ-specific toxicity, effects on nuclear receptors and stress response pathways, molecular initiating events, and metabolic enzymes. As presented in Supplementary Table 4, the predictive models indicated low probabilities of hepatotoxicity (0.85), neurotoxicity (0.88), and respiratory toxicity (0.54). However, relatively moderate probabilities were observed for nephrotoxicity (0.75) and cardiotoxicity (0.77), signaling potential renal and cardiovascular concerns. Additionally, the algorithm categorized olive leaf extracts as active for immunotoxicity (0.98). Clinical toxicity (0.64) refers to the potential for adverse physiological effects, such as organ toxicity, biochemical imbalances, or systemic inflammatory responses, that could arise from prolonged exposure or high doses of the studied compound. On the other hand, nutritional toxicity (0.54) denotes the possibility of disruptions in nutrient metabolism, absorption, or utilization, which may lead to deficiencies, metabolic stress, or unintended immune modulation. In contrast, *in silico* analyses predicted no significant activity for carcinogenicity (0.79), mutagenicity (0.84), cytotoxicity (0.70), and ecotoxicity (0.70), indicating a low risk of malignancy, genotoxicity, direct cellular toxicity, or environmental hazard. However, a moderate probability of blood-brain barrier (BBB) penetration (0.52) underscores the need for further pharmacokinetic investigations to evaluate potential central nervous system (CNS) exposure.

Subsequent Tox21-focused evaluations (Supplementary Table 5) indicated no significant activity against key nuclear receptors including, the aryl hydrocarbon receptor (AHR, 0.94), androgen receptor (AR, 0.97), aromatase (0.86), estrogen receptor alpha (0.75), and PPAR-gamma (0.92), suggesting minimal potential for endocrine pathway disruption. Similarly, data presented in Supplementary Table 6 indicate that olive leaf extracts did not significantly induce activation of stress response pathways such as nrf2/ARE (0.92), heat shock factor (HSE, 0.92), mitochondrial membrane potential disruption (MMP, 0.82), or p53 (0.79). Moreover, molecular initiating event (MIE)-based analyses (Supplementary Table 7) revealed consistent inactivity across several key receptor sites, including thyroid hormone receptors (THRα and THRβ), ryanodine receptors (RYR), and key neurotransmitter-gated ion channels such as GABA, NMDAR, AMPAR, and KAR. The extracts exhibited low interaction potential with key xenobiotic-sensing receptors, including CAR and PXR. Cytochrome P450 interaction predictions (CYP1A2, CYP2C19, CYP2C9, CYP2D6, CYP3A4, and CYP2E1) also revealed a minimal likelihood of inducing significant metabolic disruptions or drug-drug interactions. The *in silico* analyses suggested that olive leaf extracts exhibit minimal or no activity across several pathways and stress response mechanisms. However, this analysis suggests possible immunotoxic, nephrotoxic, and cardiotoxic effects. Supporting these predictions, our *in vivo* hematological data (Section 3.2.2) also revealed immune-related alterations, such as decreases in white blood cells and platelet counts. These findings underscore the requirements for further investigation into the potential immunotoxic effects of the extracts. Accordingly, advanced cellular assays and targeted histopathological analyses are crucial to substantiate the computational predictions and determine whether the immunomodulatory effects of olive leaf extracts are beneficial or adverse across different dosage levels.

3.1.5 Toxicological evaluation of oleuropein

Oleuropein, the principal bioactive constituent of olive leaf extracts, was evaluated using the ProTox-3 modeling platform (IUPAC Food ID) to generate a comprehensive toxicity profile. As shown in Table 2, the predicted LD50 for oleuropein is 2,000 mg/kg, classifying it within Toxicity Class 4, corresponding to low acute toxicity. This suggests that while moderate oral doses may be considered relatively safe, higher concentrations

require careful consideration. *In silico* predictions also revealed low mutagenic and carcinogenic potential. These findings are consistent with the reported absence of carcinogenic and mutagenic effects associated with olive leaf extracts, as shown in Table 2. In contrast, oleuropein demonstrated a high immunotoxicity score. This suggests a potential for immunomodulatory activity, which is partially supported by our *in vivo* evidence showing alterations in leukocyte and platelet counts.

Mild, statistically non-significant elevations in urea levels observed in both *in vivo* biochemical analyses and *in silico* predictions suggest potential nephrotoxic effects, warranting further detailed renal investigations. In contrast, predicted low hepatotoxicity aligns with the absence of histopathological liver abnormalities in experimental animals. However, the elevation of AST levels at higher doses may indicate mild hepatic stress, highlighting the requirements for continued monitoring in long-term studies. As presented in Table 2, oleuropein's physicochemical properties-specifically its pronounced hydrophilicity (logP = −0.63) and extensive hydrogen-bonding potential (6 donors and 13 acceptors)-are likely to impact its absorption, distribution, and overall metabolic behavior. Therefore, detailed pharmacokinetic assessments are significant in accurately establishing oleuropein's safety thresholds. Evidence from our computational modeling and *in vivo* investigations underscores its potent antimicrobial and antioxidant properties. However, these benefits are accompanied by critical safety concerns, particularly regarding potential nephrotoxicity and immunotoxicity. For effective clinical translation, further investigations are essential, particularly those addressing chronic toxicity, immunophenotypic profiling, and detailed renal function assessment.

TABLE 2 The structural and physicochemical properties of oleuropein illustrate key molecular characteristics such as molecular weight, hydrogen bonding potential, polarity, and partition coefficient.

Molecular structure of oleuropein	Properties of oleuropein	Value
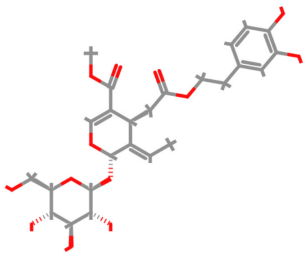	Molecular weight	540.51 g/mol
	Hydrogen bond acceptors	13
	Hydrogen bond donors	6
	Number of atoms	38
	Number of bonds	40
	Number of rotatable bonds	11
	Molecular refractivity	127.28
	Topological polar surface area	201.67 Å²
	Octanol/water partition coefficient (logP)	−0.63

These properties highlight the compound's chemical nature and potential interactions in biological systems. The molecular structure is shown for reference.

3.2 *In vivo* studies

3.2.1 Histopathological observations

Initial histological assessment of hepatic and renal tissues from mice treated with 50 and 100 mg/kg doses revealed no overt necrosis, marked inflammation, or notable degenerative alterations. These findings correlate well with the predicted "Inactive" hepatotoxic and neurotoxic profiles from the *in silico* toxicological studies (discussed later), suggesting minimal structural compromise at the doses tested.

Microscopic sections of the liver revealed well-preserved architecture. Hepatocytes were organized in one to two thick cell plates, with uniform cytoplasm and round nuclei that were centrally located, without atypia or pleomorphism. They showed patent sinusoids and organized portal tracts containing bile ducts, portal veins, and hepatic arteries without fibrosis, inflammation, or cell infiltration. Biliary morphologic structures were also typical; the Kupffer cell population had a uniform distribution from portal to center of the lobule, and the connective tissue framework of the Globus was intact with no evidence of cirrhosis or other architectural abnormalities. Liver sections from the control group (Figure 2C) exhibited no notable signs of inflammation, necrosis, or fibrosis. In contrast, hepatic tissues from the 50 mg/kg olive leaf extract group treatment (Figure 2D) exhibited notable alterations in hepatocyte nuclear morphology and more pronounced hemorrhagic manifestations. Sections from the 100 mg/kg olive leaf extracts group treatment (Figure 2E) revealed increased hepatocellular necrosis, nuclear enlargement, and widespread hemorrhage, indicating a dose-related intensification of hepatic injury.

Renal tissues from both the right and left sides showed preserved cortical and medullary organization. The glomeruli appeared normocellular with intact capillary loops, without sclerosis or basement membrane alterations. No atrophy, degeneration, or necrosis was observed in renal tubules with normal epithelial morphology. Interstitium appeared unremarkable, while vascular structures were free of vasculitis, hyaline arteriosclerosis, or thrombosis. The collecting ducts and renal pelvic components were structurally unremarkable, with no evidence of epithelial proliferation or inflammatory changes. The kidneys from the control treatment (Figure 2F) were histologically normal aside from isolated interstitial hemorrhage. In contrast, tissues from the 50 mg/kg olive leaf extracts group (Figure 2G) exhibited more extensive interstitial hemorrhage and occasional glomerular atrophy with localized tubular atrophy. At the 100 mg/kg dose treatment, hemorrhagic changes were more prominent, accompanied by marked glomerular atrophy, suggesting a dose-related progression of renal pathology (Figure 2H).

3.2.2 Hematological findings

The administration of olive leaf extract at 50 and 100 mg/kg in BALB/c mice results in several prominent changes in white blood cell (WBC) counts and platelet levels (Table 3). Both groups experienced a significant reduction in total WBC count ($p < 0.05$) compared to control, suggesting that these doses may induce an immunomodulatory response. In addition, differential leukocyte

10.3389/fmicb.2025.1567921

TABLE 3 Hematological parameters in BALB/c mice ($n = 5$) following intraperitoneal administration of the methanolic fraction of olive leaf extract, reconstituted in distilled water, at doses of 50 and 100 mg/kg, compared to a control group administered distilled water.

Parameter	Control	Group A (50 mg/kg)	Group B (100 mg/kg)
WBC	8.02 ± (0.45)	6.48 ± (0.73)*	5.52 ± (0.41)*
Neutrophils	20.17 ± (0.90)	12.17 ± (1.59)*	15.40 ± (0.61)*
Eosinophils	1.57 ± (0.55)	0.97 ± (0.59)	1.30 ± (0.26)
Basophils	0.33 ± (0.25)	0.50 ± (0.53)	1.63 ± (0.25)*
Lymphocyte	24.63 ± (2.28)	42.23 ± (2.25)*	62.07 ± (10.94)*
Monocyte	5.57 ± (0.50)	4.47 ± (0.35)	6.23 ± (1.33)
RBC	6.37 ± (0.50)	7.82 ± (2.19)	5.07 ± (2.40)
HGB	11.63 ± (1.53)	13.98 ± (2.15)	9.63 ± (5.23)
HTC	43.70 ± (3.20)	44.70 ± (4.10)	11.90 ± (0.72)*
MCV	56.23 ± (3.49)	51.74 ± (2.99)	50.17 ± (1.85)
MCH	12.10 ± (0.61)	16.63 ± (1.33)*	15.43 ± (0.25)*
MCHC	30.67 ± (0.57)	31.70 ± (2.55)	33.17 ± (0.68)
Platelet	373.33 ± (40.41)	157.00 ± (8.19)*	213.33 ± (20.82)*

Data are presented as mean ± standard deviation (SD). Asterisks indicate statistically significant differences relative to the control group ($p < 0.05$).

TABLE 4 Biochemical parameters in BALB/c mice ($n = 5$) following intraperitoneal administration of the methanolic fraction of olive leaf extract, reconstituted in distilled water, at doses of 50 and 100 mg/kg, compared to a control group receiving distilled water.

Parameters	Control	Group A (50 mg/kg)	Group B (100 mg/kg)
Urea	40.67 ± (13.03)	55 ± (21.9)	61.7 ± (6.9)
B.U.N	52.43 ± (2.58)	41 ± (7.1)	53.8 ± (3.1)
Creatinine	0.41 ± (0.13)	0.4 ± (0.1)	0.2 ± (0.1)
ALT	28.83 ± (1.24)	24.1 ± (2.7)	35.7 ± (3.2)
AST	56.25 ± (1.15)	74.9 ± (16.5)	91.4 ± (5.4)*
ALP	22.15 ± (1.78)	4.0 ± (0.8)*	2.5 ± (1.3)*
BIL IND	0	0	0.1
BIL DIR	0	0	0.1

Data are presented as mean ± standard deviation (SD). Asterisks denote statistically significant differences compared to the control group ($p < 0.05$). B.U.N., blood urea nitrogen; ALT, alanine aminotransferase; AST, aspartate aminotransferase; ALP, alkaline phosphatase; BIL IND, indirect bilirubin; BIL DIR, direct bilirubin.

analysis showed a notable increase in lymphocyte percentages in these animal groups ($p < 0.05$), along with a corresponding decrease in neutrophils ($p < 0.05$). This shift could signify alterations in immune cell populations caused by olive leaf extract. A slight but statistically significant increase in basophils was also observed in BALB/c mice administered with 100 mg/kg dose ($p < 0.05$).

Regarding red blood cell (RBC) parameters, neither treatment group exhibited a significant change in RBC count or hemoglobin (HGB) compared to controls ($p > 0.05$). However, according to *T*-test comparisons, Group B mice showed a pronounced reduction in hematocrit (HTC; $p < 0.05$). The mean corpuscular volume (MCV), mean corpuscular hemoglobin (MCH), and mean corpuscular hemoglobin concentration (MCHC) values remained within their normal ranges. Nevertheless, there was a minor yet significant rise in MCH among both treated groups ($p < 0.05$). Alterations in RBC parameters may suggest altered erythropoiesis or RBC turnover, but no clear pattern of dose-related toxicity was evident.

In both treated groups, platelet counts significantly declined ($p < 0.05$) compared to control animals, suggesting either reduced platelet production in the bone marrow or enhanced peripheral consumption (e.g., destruction or sequestration). These hematological changes highlight the importance of further investigations, including bone marrow histopathology and broader immunological evaluations, to detect whether olive leaf extract exerts immunomodulatory effects or specifically targets thrombocytes.

3.2.3 Biochemical findings

Biochemical analyses revealed several notable alterations in hepatic and renal biomarkers following the administration of aqueous *Olea europaea* leaf extract (Table 4). A significant elevation in AST (Aspartate Aminotransferase) was observed in Group B (100 mg/kg), potentially suggesting possible hepatocellular injury or muscular stress associated with higher olive leaf extract exposure. Meanwhile, ALT (Alanine Aminotransferase) in the same group displayed a slight, though statistically non-significant, increase, suggesting possible hepatic involvement but no definitive proof of liver injury. *T*-test analysis also indicated that Alkaline Phosphatase (ALP) was moderately lower in Group B ($p = 0.085$) than in controls, suggesting a potential regulatory shift in liver or bone enzyme production. Animals in both Groups A and B exhibited moderate increases in urea levels; however, these changes did not reach statistical significance ($p > 0.05$). Creatinine and blood urea nitrogen (B.U.N.) remained stable across all experimental groups, suggesting minimal or no kidney impairment under the examined conditions. Furthermore, direct and indirect bilirubin levels were unaffected, implying that bilirubin metabolism remained intact. Although the slight elevation in urea may suggest mild renal or metabolic disturbances, the lack of associated changes in B.U.N. and creatinine makes definitive conclusions challenging. Therefore, additional histopathological and mechanistic studies are required to validate these findings and determine the long-term safety profile of olive leaf extract.

3.3 *In silico* studies

3.3.1 Molecular docking results

Molecular docking simulations targeting bacterial peroxidase (Figure 2I) identified robust non-covalent interactions between olive leaf extract constituents and the enzyme. These interactions included classical hydrogen bonding with Ser185, Lys179, and Arg48 and carbon-hydrogen bonding involving Pro44. Donor-donor repulsion observed at His181 and Asn184 suggested potential steric or electronic interference. At the same time, π-σ interactions with Leu171 and π-sulfur contacts at Met172 further characterized the complex binding architecture at the

active site (Figure 2J). This intricate binding network likely contributes to the pronounced antibacterial activity associated with methanolic olive leaf extracts. It highlights the critical role of solvent choice in maximizing phytochemical recovery and bioactivity.

Although this study identified limited antifungal activity, the docking analyses provide evidence for an antibacterial mechanism involving peroxidase inhibition or disrupting bacterial redox homeostasis. Although *in silico* toxicity assessments (Supplementary Table 4) suggest potential immunotoxic risks, they highlight the requirement for cautious dosing and further mechanistic investigations to differentiate between desirable immunomodulatory effects and unintended immune suppression or hyperactivation. Future investigations should incorporate integrated pharmacokinetic and pharmacodynamic assessments alongside advanced omics-driven approaches to elucidate the comprehensive therapeutic potential of olive leaf extracts in addressing MDR pathogens.

4 Discussion

This study presents novel findings on the antimicrobial efficacy of *O. europaea* and *F. carica* leaf extracts against MDR pathogens. Notably, *O. europaea* leaf extracts, particularly the methanolic fraction, demonstrated potent inhibitory activity against several MDR strains, including *E. faecium* and *S. agalactiae*, which exhibited high levels of resistance to conventional antimicrobial agents. This inhibitory effect is consistent with previous reports emphasizing the potency of olive-derived phenolics, including oleuropein hydroxytyrosol and rutin, in inhibiting both Gram-positive and Gram-negative bacteria (Sudjana et al., 2009; Lee and Lee, 2010; Zorić and Kosalec, 2022). Interestingly, our findings revealed that even pan-resistant pathogens exhibited susceptibility to these polyphenolic compounds, supporting existing evidence that plant-derived antimicrobials may act through alternative mechanisms such as disrupting membrane integrity, modulating redox homeostasis, or impairing stress-response pathways (Borjan et al., 2020). The antimicrobial mechanism of olive leaf extracts against Gram-positive and Gram-negative pathogens resembles that of other plant-derived biomolecules such as green tea, oregano, and thyme, which typically exert their effects by inducing oxidative stress or disrupting microbial membrane integrity (Magyari-Pavel et al., 2024).

In contrast, the *F. carica* leaf extracts investigated in this study showed comparatively modest inhibition zones, consistent with reports suggesting that fig preparations may exhibit reduced antimicrobial activity depending on the solvent used and the extraction method (Rahmani and Aldebasi, 2017; Abdel-Rahman et al., 2021). The antimicrobial activity observed in *F. carica* extracts has been attributed to phenolic acids such as caftaric, gallic, and quercetin (Abdel-Aziz et al., 2020). Previous studies have indicated that the antimicrobial efficacy of *F. carica* may vary depending on the specific plant part utilized and the extraction solvent employed, suggesting that fig leaves contain a diverse array of bioactive compounds whose activity is significantly influenced by the extraction methodology (Abubakar and Haque, 2020). The discrepancies between our results and those reported in previous studies underscore the critical influence of variables such as solvent polarity, chemical composition, extraction temperature, and extract concentration on the antimicrobial efficacy of plant-derived bioactive compounds (Papageorgiou et al., 2022; Barolo et al., 2023; Agatonovic-Kustrin et al., 2023). Our findings are consistent with the expanding body of research on phytochemicals, including those derived from *Nigella sativa*, *Cinnamomum verum*, and other phenolic-rich plants (Papageorgiou et al., 2022). Furthermore, studies on green tea catechins and oregano oils suggested that combining plant phenolics with conventional antimicrobial agents may exert synergistic effects that enable dose reduction while minimizing toxicity-related concerns (Somerville et al., 2019). Regarding *F. carica*, the present findings may support the development of synergy approaches by refining extraction techniques or using combined formulations to enhance its antimicrobial potency.

Consistent with our findings, a broad range of *in vivo* and *in vitro* studies suggested that olive leaf extract is generally safe at low doses. Oleuropein, the predominant phenolic constituent of the olive leaf, has not produced adverse or low effects in animal models, even at doses as high as 1,000 mg/kg (Gonzalez-Pastor et al., 2023). In addition, human clinical data further support this favorable safety profile. In a pilot study, healthy subjects consuming olive leaf extract daily for 8 weeks displayed no notable alterations in hepatic or renal biomarkers. Interestingly, the study documented a slight increase in red blood cell counts and no reports of severe adverse reactions (Kondo et al., 2023). However, adverse effects have been reported with excessive intake or prolonged administration of olive leaf extract. It has also been demonstrated that mice fed diets containing 0.7%−0.9% olive leaf extract for 6 weeks exhibited significant elevations in liver enzyme activity and bilirubin levels, accompanied by histopathological evidence of hepatocellular vacuolation and focal necrosis (Omer et al., 2012). Moreover, prolonged consumption of olive leaf extract at dietary concentrations ranging from 0.5% to 0.75% over 14 weeks resulted in hepatic alterations, including bile duct proliferation, cholestasis, inflammatory cell infiltration, and early fibrotic changes. These pathological effects were linked to mitochondrial dysfunction, reduced membrane potential, and compromised respiratory capacity. Importantly, such effects were absent at a lower dose of 0.25%, indicating a clear threshold beyond which toxicity becomes apparent (Arantes-Rodrigues et al., 2011). The evidence suggests that while olive leaf extract is generally considered safe at conventional therapeutic doses, prolonged or high-dose administration may elicit notable hepatic, renal, and hematopoietic toxicities.

A fundamental aspect of this study is integrating *in silico* toxicity predictions with *in vitro* and *in vivo* experiments to evaluate the efficacy and safety profiles of olive leaf extracts. *In silico* approaches, including molecular docking and computational toxicity prediction, have become essential tools in antimicrobial drug discovery. They offer a rapid method of screening plant-derived compounds for potential bioactivity. Recent computational studies on *O. europaea* and *F. carica* leaf extracts illustrate the utility of these approaches. Molecular docking simulations have revealed that hydroxytyrosol, a key olive leaf phytochemical, binds

to bacterial DNA gyrase and penicillin-binding protein 3 (PBP3), enzymes critical for DNA replication and cell wall synthesis (Ben Hassena et al., 2024). Notably, olive leaf phytochemicals appear to target similar pathways as conventional drugs (e.g., gyrase, a target of fluoroquinolones, and PBPs, targets of β-lactams), suggesting a mechanism for synergizing with or alternating conventional antimicrobial agents. Phenolic compounds such as oleuropein and hydroxytyrosol of olive leaves are considered safe bioactive dietary compounds. However, our computational models suggested low potential acute toxicity of *O. europaea* extracts. This finding aligns with both *in silico* toxicity assessments and *in vivo* studies consistently validating their low acute toxicity profiles (Arantes-Rodrigues et al., 2011; Guex et al., 2018; Wylie and Scott Merrell, 2022).

Similarly, *F. carica* leaf extracts have demonstrated promising *in silico* profiles. A recent study of Moroccan fig leaves identified several bioactive constituents with strong predicted binding affinities to microbial targets, including bacterial β-ketoacyl-ACP synthase (involved in fatty acid biosynthesis), nucleoside diphosphate kinase, and the fungal sterol 14α-demethylase (CYP51; Tikent et al., 2024). These findings suggest a potential for broad-spectrum antimicrobial activity, evidenced by *in vitro* activity against bacteria and *C. albicans*. Regarding safety, both experimental cytotoxicity assays and computational models suggest low to moderate toxicity, revealing selective toxicity against pathogens over host cells (Tikent et al., 2024).

Generally, *in silico* findings of olive and fig leaf extracts follow similar patterns commonly observed in other medicinal plant investigations. Molecular docking studies consistently highlight microbial proteins such as DNA gyrase, topoisomerases, transpeptidases, and virulence regulators as common targets. For example, phytochemicals from *Azadirachta indica* (neem) and *Curcuma longa* (turmeric) have shown high binding affinities to bacterial DNA replication and quorum-sensing machinery (Wylie and Scott Merrell, 2022; Dai et al., 2022). Likewise, *Snapdragon* flower extracts and garlic-derived compounds have demonstrated multitarget binding affecting enzymes such as CYP51 and proteins involved in biofilm formation (Saqallah et al., 2022). A consistent observation across these studies is the pharmacological nature of plant-derived compounds. Unlike several synthetic antimicrobial drugs that act on a single molecular target, phytochemicals often exhibit moderate affinity for multiple microbial proteins, which may contribute to their broad-spectrum or synergistic antimicrobial activity.

Overall, recent comparative studies on plant extracts highlight the significance of *in silico* methods in antimicrobial research. These approaches reliably identify bioactive plant compounds capable of binding key microbial targets and prioritize candidates with the most favorable efficacy-to-toxicity profiles for further investigation (Ben Hassena et al., 2024; Dai et al., 2022). Although these *in silico* predictions provide valuable insights, experimental *in vitro* and *in vivo* validations are essential. For instance, a recent phytochemical screening study identified several plant-derived compounds as drug-like and emphasized extensive *in vitro* and *in vivo* validation to confirm their clinical relevance (Belitibo et al., 2024). This observation is consistent with our findings, demonstrating that computational predictions require empirical validation to ensure their reliability and biological significance.

5 Conclusion

This study highlights the significant antimicrobial properties of *O. europaea* and *F. carica* leaf extracts against MDR pathogens. Remarkably, *O. europaea* extracts, especially those derived using methanol, demonstrated potent antimicrobial activity against several pathogens. These findings are consistent with existing research, confirming that plant-derived compounds commonly exhibit antimicrobial properties by targeting microbial proteins. Nevertheless, this study identified certain limitations. *F. carica* extracts exhibited relatively narrow antimicrobial efficacy, aligning with previous evidence that factors such as extraction methodology, solvent system, the concentration of bioactive constituents, and overall phytochemical profile critically influence the therapeutic potential of plant-derived extracts. Although *O. europaea* extracts demonstrated encouraging therapeutic promise, *in vivo* studies revealed subtle signs of toxicity at higher doses, such as liver and kidney alterations, underscoring the importance of careful dose optimization. Although computational models predicted low risks for organ toxicity, notable discrepancies emerged when compared with experimental biological outcomes. This divergence between computational predictions and experimental findings underscores the limitation of *in silico* approaches. Although such models are valuable for early toxicity screening and microbial target identification, their utility must be integrated with *in vivo* and *in vitro* experiments. In conclusion, this study provided evidence supporting the antimicrobial potential of plant-derived phytochemicals against MDR pathogens while emphasizing the importance of therapeutic efficacy with rigorous safety evaluation. Further investigations are essential to establish optimal dosing strategies and to elucidate the molecular mechanisms underlying their biological activity before translation into clinical practice.

Data availability statement

The datasets presented in this study can be found in online repositories. The names of the repository/repositories and accession number(s) can be found in the article/Supplementary material.

Ethics statement

The studies involving humans were approved by BioEthical Committee at the Benghazi Medical Center. The studies were conducted in accordance with the local legislation and institutional requirements. The participants provided their written informed consent to participate in this study. The animal study was approved by Prof. Dr. Gumma Al-Orify, Prof. Dr. Mohamed Bumedian, Prof. Dr. Ismael Buzakouk, Bioethics and Institutional Board at University of Benghazi. The study was conducted in accordance with the local legislation and institutional requirements.

Author contributions

MA: Investigation, Methodology, Writing – original draft. ME: Investigation, Conceptualization, Methodology, Writing – original draft. SA: Investigation, Methodology, Writing – original draft. MS: Investigation, Methodology, Writing – original draft. HE: Investigation, Methodology, Writing – original draft. AE: Investigation, Methodology, Writing – original draft. AB: Conceptualization, Formal analysis, Investigation, Methodology, Writing – original draft. ME-A: Conceptualization, Writing – original draft. NE: Conceptualization, Writing – original draft. OA: Conceptualization, Writing – original draft. SA: Conceptualization, Formal analysis, Investigation, Validation, Writing – original draft. RA: Conceptualization, Investigation, Methodology, Writing – original draft. FB: Conceptualization, Formal analysis, Investigation, Project administration, Supervision, Validation, Writing – review & editing.

Funding

The author(s) declare that no financial support was received for the research and/or publication of this article.

Acknowledgments

The authors would like to acknowledge Prof. Dr. Fathi Elbraky, Prof. Dr. Souad Elawami, Prof. Dr. Farag Al-Shari, Dr. Zinab Elharash, Dr. Enas Al-Kilani, Dr. Mohammed Blhaj, Mr. Abdrahman Hwide, Mrs. Asha Eltajori, Ms. Asma Elramli, Ms. Marwa Elsenosi, for their valuable contributions and support. Special thanks are extended to the Animal House—University of Benghazi, Elsaleem Lab, Alakeed Lab, the Advanced Center, and the Faculty of Pharmacy Research Center for providing facilities and resources essential to this study.

Conflict of interest

The authors declare that the research was conducted in the absence of any commercial or financial relationships that could be construed as a potential conflict of interest.

Generative AI statement

The author(s) declare that no Gen AI was used in the creation of this manuscript.

Publisher's note

Supplementary material

The Supplementary Material for this article can be found online at: https://www.frontiersin.org/articles/10.3389/fmicb.2025.1567921/full#supplementary-material

References

Abdel-Aziz, M. E., Darwish, M. S., Mohamed, A. H., El-Khateeb, A. Y., and Hamed, S. E. (2020). Potential activity of aqueous fig leaves extract, olive leaves extract and their mixture as natural preservatives to extend the shelf life of pasteurized Buffalo milk. *Foods* 9:615. doi: 10.3390/foods9050615

Abdel-Rahman, R., Ghoneimy, E., Abdel-Wahab, A., Eldeeb, N., Salem, M., Salama, E., et al. (2021). The therapeutic effects of *Ficus carica* extract as an antioxidant and anticancer agent. *South Afr. J. Bot.* 141, 273–277. doi: 10.1016/j.sajb.2021.04.019

Abi-Khattar, A. M., Rajha, H. N., Abdel-Massih, R. M., Maroun, R. G., Louka, N., Debs, E., et al. (2019). Intensification of polyphenol extraction from olive leaves using Ired-Irrad®, an environmentally-friendly innovative technology. *Antioxidants* 8:227. doi: 10.3390/antiox8070227

Abubakar, A., and Haque, M. (2020). Preparation of medicinal plants: basic extraction and fractionation procedures for experimental purposes. *J. Phar. Bioallied Sci.* 12, 1–10. doi: 10.4103/jpbs.JPBS_175_19

Agatonovic-Kustrin, S., Wong, S., Dolzhenko, A. V., Gegechkori, V., Ku, H., Tucci, J., et al. (2023). Evaluation of bioactive compounds from *Ficus carica* L. leaf extracts via high-performance thin-layer chromatography combined with effect-directed analysis. *J. Chromatogr. A* 1706:464241. doi: 10.1016/j.chroma.2023.464241

Ahmad-Qasem, M. H., Ahmad-Qasem, B. H., Barrajón-Catalán, E., Micol, V., Cárcel, J. A., and García-Pérez, J. V. (2016). Drying and storage of olive leaf extracts. Influence on polyphenols stability. *Indus. Crops Prod.* 79, 232–239. doi: 10.1016/j.indcrop.2015.11.006

Ahmed, O. H., Abbas, A. H., and Yaseen, Y. S. (2023). GC/MS analysis of crude extract of Fig leaves naturally grown in Iraq. *J. Adv. Pharm. Educ. Res.* 13, 96–101. doi: 10.51847/TF4ouLslks

Arantes-Rodrigues, R., Henriques, A., Pires, M. J., Colaço, B., Calado, A. M., Rema, P., et al. (2011). High doses of olive leaf extract induce liver changes in mice. *Food Chem. Toxicol.* 49, 1989–1997. doi: 10.1016/j.fct.2011.05.010

Barolo, M. I., Castelli, M. V., and López, S. N. (2023). Antimicrobial properties and biotransforming ability of fungal endophytes from *Ficus carica* L. (Moraceae). *Mycol. Int. J. Fungal Biol.* 14, 108–132. doi: 10.1080/21501203.2023.2175500

Belitibo, D. B., Meressa, A., Abebe, A., Negassa, T., Endale, M., Assamo, F. T., et al. (2024). *In vitro* antibacterial activity, molecular docking, and ADMET analysis of phytochemicals from roots of *Dovyalis abyssinica*. *Molecules* 29:5608. doi: 10.3390/molecules29235608

Ben Hassena, A., Abidi, J., Miled, N., Kulinowski, Ł., Skalicka-Wozniak, K., Bouaziz, M., et al. (2024). New insights into the antibacterial activity of hydroxytyrosol extracted from olive leaves: molecular docking simulations of its antibacterial mechanisms. *Chem. Biodivers.* 22:e202401714. doi: 10.1002/cbdv.202401714

Borjan, D., Leitgeb, M., Knez, Ž., and Hrnčič, M. K. (2020). Microbiological and antioxidant activity of phenolic compounds in olive leaf extract. *Molecules* 25:5946. doi: 10.3390/molecules25245946

Charan, J., and Kantharia, N. D. (2013). How to calculate sample size in animal studies? *J. Pharmacol. Pharmacother.* 4, 303–306. doi: 10.4103/0976-500X.119726

Cho, J.-Y., Lee, H. J., and Kim, S. H. (2020). Journal of food quality evaluation of effect of extraction solvent on selected properties of olive leaf extract. *J. Food Qual.* 2020, 1–7. doi: 10.1155/2020/3013649

Cifá, D., Skrt, M., Pittia, P., Di Mattia, C., and Poklar Ulrih, N. (2018). Enhanced yield of oleuropein from olive leaves using ultrasound-assisted extraction. *Food Sci. Nutr.* 6, 1128–1137. doi: 10.1002/fsn3.654

Clewell, A. E., Béres, E., Vértesi, A., Glávits, R., Hirka, G., Endres, J. R., et al. (2015). A Comprehensive toxicological safety assessment of an extract of *Olea europaea* L. leaves (BonoliveTM). *Int. J. Toxicol.* 35, 208–221. doi: 10.1177/1091581815619764

Dai, C., Lin, J., Li, H., Shen, Z., Wang, Y., Velkov, T., et al. (2022). The natural product curcumin as an antibacterial agent: current achievements and problems. *Antioxidants* 11:459. doi: 10.3390/antiox11030459

de Oliveira, N. M., Machado, J., Chéu, M. H., Lopes, L., and Criado, M. B. (2024). Therapeutic potential of olive leaf extracts: a comprehensive review. *Appl. Biosci.* 3, 392–425. doi: 10.3390/applbiosci3030026

Esfandiary, M. A., Khosravi, A. R., and Asadi, S. (2024). Antimicrobial and anti-biofilm properties of oleuropein against Escherichia coli and fluconazole-resistant isolates of *Candida albicans* and *Candida glabrata*. *BMC Microbiol.* 24:154. doi: 10.1186/s12866-024-03305-5

Festing, M. F. W., and Altman, D. G. (2002). Guidelines for the design and statistical analysis of experiments using laboratory animals. *ILAR J.* 43, 244–258. doi: 10.1093/ilar.43.4.244

Fischer, A. H., Jacobson, K. A., Rose, J., and Zeller, R. (2008). Hematoxylin and eosin staining of tissue and cell sections. *Cold Spring Harbor Protoc.* 2008:pdb.prot4986. doi: 10.1101/pdb.prot4986

Gonelimali, F. D., Lin, J., Miao, W., Xuan, J., Charles, F., Chen, M., et al. (2018). Antimicrobial properties and mechanism of action of some plant extracts against food pathogens and spoilage microorganisms. *Front. Microbiol.* 9:1639. doi: 10.3389/fmicb.2018.01639

Gonzalez-Pastor, R., Carrera-Pacheco, S. E., Zúñiga-Miranda, J., Rodríguez-Pólit, C., Mayorga-Ramos, A., Guamán, L. P., et al. (2023). Current landscape of methods to evaluate antimicrobial activity of natural extracts. *Molecules* 28:1068. doi: 10.3390/molecules28031068

Guex, C. G., Reginato, F. Z., Figueredo, K. C., da Silva Pires, A. R. H., da Silva Jesus, F. B., and de Freitas Bauermann, L. (2018). Safety assessment of ethanolic extract of *Olea europaea* L. leaves after acute and subacute administration to Wistar rats. *Regul. Toxicol. Pharmacol.* 95, 395–399. doi: 10.1016/j.yrtph.2018.04.013

Haley, E., Cockerill, F. R., Pesano, R. L., Festa, R. A., Luke, N., Mathur, M., et al. (2024). Pooled antibiotic susceptibility testing performs within CLSI standards for validation when measured against broth microdilution and disk diffusion antibiotic susceptibility testing of cultured isolates. *Antibiotics* 13:1214. doi: 10.3390/antibiotics13121214

Hinad, I., S'hih, Y., Gui, R., Elhessni, A., Mesfioui, A., and Ouahidi, M. (2021). "Acute and subacute toxicity study of the methanolic extract of *Olea europea*. L leaves in Wistar rat," in *E3S Web Conf.* 319:01094. doi: 10.1051/e3sconf/202131901094

Ho, P. L., Tängdén, T., Pulcini, C., Fitzpatrick, J. M., Zaman, M. H., Hara, G. L., et al. (2024). Antimicrobial resistance: a concise update. *Lancet Microbe* 6:100947. doi: 10.1016/j.lanmic.2024.07.010

Jubair, N., Rajagopal, M., Chinnappan, S., Abdullah, N. B., and Fatima, A. (2021). Review on the antibacterial mechanism of plant-derived compounds against multidrug-resistant bacteria (MDR). *Evid. Based Complement. Alternat. Med.* 2021, 1–30. doi: 10.1155/2021/3663315

Kabbash, E. M., Abdel-Shakour, Z. T., El-Ahmady, S. H., Wink, M., and Ayoub, I. M. (2023). Comparative metabolic profiling of olive leaf extracts from twelve different cultivars collected in both fruiting and flowering seasons. *Sci. Rep.* 13:612. doi: 10.1038/s41598-022-27119-5

Kebede, B., and Shibeshi, W. (2022). *In vitro* antibacterial and antifungal activities of extracts and fractions of leaves of *Ricinus communis* Linn against selected pathogens. *Vet. Med. Sci.* 8, 1802–1815. doi: 10.1002/vms3.772

Khelouf, I., Karoui, I. J., Lakoud, A., Hammami, M., and Abderrabba, M. (2023). Comparative chemical composition and antioxidant activity of olive leaves *Olea europaea* L. of Tunisian and Algerian varieties. *Heliyon* 9:e22217. doi: 10.1016/j.heliyon.2023.e22217

Kim, J., and Lee, D. (2023). The natural *Ficus carica* L. (fig) extract as an effective prophylactic antibacterial agent for inflammation-related infections. *Life* 13:2356. doi: 10.3390/life13122356

Kondo, S., Ferdousi, F., Zhao, J., Suidasari, S., Yokozawa, M., Yamauchi, K., et al. (2023). Hematinic potential of olive leaf extract: evidence from an *in vivo* study in mice and a pilot study in healthy human volunteers. *Nutrients* 15:4095. doi: 10.3390/nu15194095

Lee, O.-H., and Lee, B.-Y. (2010). Antioxidant and antimicrobial activities of individual and combined phenolics in *Olea europaea* leaf extract. *Bioresour. Technol.* 101, 3751–3754. doi: 10.1016/j.biortech.2009.12.052

Liu, Y., McKeever, C. L., and Malik, N. S. A. (2017). Assessment of the antimicrobial activity of olive leaf extract against foodborne bacterial pathogens. *Front. Microbiol.* 8:113. doi: 10.3389/fmicb.2017.00113

Magyari-Pavel, I. Z., Moacă, E.-A., Avram, Ş., Diaconeasa, Z., Haidu, D., Ştefănuţ, M. N., et al. (2024). Antioxidant extracts from Greek and Spanish olive leaves: antimicrobial, anticancer and antiangiogenic effects. *Antioxidants* 13:774. doi: 10.3390/antiox13070774

Mangana, M., Lambrinidis, G., Kostakis, I. K., Kalpaktsi, I., Sagnou, M., Nicolaou, C., et al. (2025). Towards new scaffolds for antimicrobial activity—*in silico*/*in vitro* workflow introducing new lead compounds. *Antibiotics* 14:11. doi: 10.3390/antibiotics14010011

Meziant, L., Boutiche, M., and Bachir Bey, M. (2018). Standardization of monomeric anthocyanins extraction from fig fruit peels (*Ficus carica* L.) using single factor methodology. *J. Food Measure. Character.* 12, 2865–2873. doi: 10.1007/s11694-018-9901-6

Mishra, R. A. K., and Muthukaliannan, G. K. (2024). *In-silico* and *in-vitro* study of novel antimicrobial peptide AM1 from *Aegle marmelos* against drug-resistant *Staphylococcus aureus*. *Sci. Rep.* 14:25822. doi: 10.1038/s41598-024-76553-0

Nguyen, T. L., Ora, A., and Häkkinen, S. T. (2023). Innovative extraction technologies of bioactive compounds from plant by-products for textile colorants and antimicrobial agents. *Biomass Convers. Biorefinery* 14, 24973–25002. doi: 10.1007/s13399-023-04726-4

Omer, S. A., Elobeid, M. A., Elamin, M. H., Hassan, Z. K., Virk, P., Daghestani, M. H., et al. (2012). Toxicity of olive leaves (*Olea europaea* L.) in wistar albino rats. *Asian J. Anim. Vet. Adv.* 7, 1175–1182. doi: 10.3923/ajava.2012.1175.1182

Papageorgiou, C. S., Lyri, P., Xintaropoulou, I., Diamantopoulos, I., Zagklis, D. P., and Paraskeva, C. A. (2022). High-yield production of a rich-in-hydroxytyrosol extract from olive (*Olea europaea*) leaves. *Antioxidants* 11:1042. doi: 10.3390/antiox11061042

Percie du Sert, N., Hurst, V., Ahluwalia, A., Alam, S., Avey, M. T., Baker, M., et al. (2020). The ARRIVE guidelines 2.0: updated guidelines for reporting animal research. *PLoS Biol.* 18:e3000410. doi: 10.1371/journal.pbio.3000410

Piper, S. K., Zocholl, D., Toelch, U., Roehle, R., Stroux, A., Hoessler, J., et al. (2022). Statistical review of animal trials—a guideline. *Biometrical J.* 65:2200061. doi: 10.1002/bimj.202200061

Rahmani, A. H., and Aldebasi, Y. H. (2017). *Ficus carica* and its constituents role in management of diseases. *Asian J. Pharm. Clin. Res.* 10:49. doi: 10.22159/ajpcr.2017.v10i6.17832

Raies, A. B., and Bajic, V. B. (2016). *In silico* toxicology: computational methods for the prediction of chemical toxicity. *Wiley Interdiscipl. Rev. Comput. Mol. Sci.* 6, 147–172. doi: 10.1002/wcms.1240

Ratananikom, K., and Srikacha, N. (2020). Antibacterial activity of plant extracts in different solvents against pathogenic bacteria: an *in vitro* experiment. *J. Acute Dis.* 9:223. doi: 10.4103/2221-6189.291288

Sa, N., and Bradford, J. (2008). Recovery and stability of oleuropein and other phenolic compounds during extraction and processing of olive (*Olea europaea* L.) leaves. *J. Food Agric. Environ.* 6, 8–13.

Sánchez-Gutiérrez, M., Isabel, B., Alejandro, R., Fernando, P., África, F., Antonio, R., et al. (2021). Valorisation of *Olea europaea* L. olive leaves through the evaluation of their extracts: antioxidant and antimicrobial activity. *Foods* 10:966. doi: 10.3390/foods10050966

Saqallah, F. G., Hamed, W. M., Talib, W. H., Dianita, R., and Wahab, H. A. (2022). Antimicrobial activity and molecular docking screening of bioactive components of antirrhinum majus (Snapdragon) aerial parts. *Heliyon* 8:e10391. doi: 10.1016/j.heliyon.2022.e10391

Shiraishi, C. S. H., Zbiss, Y., Roriz, C. L., Dias, M. I., Prieto, M. A., Calhelha, R. C., et al. (2023). Fig leaves (*Ficus carica* L.): source of bioactive ingredients for industrial valorization. *Processes* 11:1179. doi: 10.3390/pr11041179

Silvan, J. M., Guerrero-Hurtado, E., Gutierrez-Docio, A., Prodanov, M., and Martinez-Rodriguez, A. J. (2022). Olive leaf as a source of antibacterial compounds active against antibiotic-resistant strains of *Campylobacter jejuni* and *Campylobacter coli*. *Antibiotics* 12:26. doi: 10.3390/antibiotics12010026

Singha, B., Singh, V., and Soni, V. (2024). Alternative therapeutics to control antimicrobial resistance: a general perspective. *Front. Drug Discov.* 4:1385460. doi: 10.3389/fddsv.2024.1385460

Somerville, V., Moore, R., and Braakhuis, A. (2019). The effect of olive leaf extract on upper respiratory illness in high school athletes: a randomized control trial. *Nutrients* 11:358. doi: 10.3390/nu11020358

Sudjana, A. N., D'Orazio, C., Ryan, V., Rasool, N., Ng, J., Islam, N., et al. (2009). Antimicrobial activity of commercial *Olea europaea* (olive) leaf extract. *Int. J. Antimicrob. Agents* 33, 461–463. doi: 10.1016/j.ijantimicag.2008.10.026

Sullivan, C., Fisher, C. R., and Taenzer, J. (2024). *Novel Antimicrobial Drug Development and Access: U.S. Government Support and Opportunities*. Available online at: https://www.ncbi.nlm.nih.gov/books/NBK611093/ (accessed December 17, 2024).

Summer, K., Browne, J., Hollanders, M., and Benkendorff, K. (2022). Out of control: the need for standardized solvent approaches and data reporting in antibiofilm assays incorporating dimethyl-sulfoxide (DMSO). *Biofilm* 4:100081. doi: 10.1016/j.bioflm.2022.100081

Suvarna, K. S., Layton, C., and Bancroft, J. D. (2020). *Bancroft's Theory and Practice of Histological Techniques*. 8th Edn. Elsevier.

Tikent, A., Laaraj, S., Bouddine, T., Chebaibi, M., Bouhrim, M., Elfazazi, K., et al. (2024). Antioxidant potential, antimicrobial activity, polyphenol profile analysis, and cytotoxicity against breast cancer cell lines of hydro-ethanolic extracts of leaves of (*Ficus carica* L.) from Eastern Morocco. *Front Chem.* 12:1505473. doi: 10.3389/fchem.2024.1505473

Wichard, J. D. (2017). *In silico* prediction of genotoxicity. *Food Chem. Toxicol.* 106, 595–599. doi: 10.1016/j.fct.2016.12.013

Wylie, M. R., and Scott Merrell, D. (2022). The antimicrobial potential of the neem tree (*Azadirachta indica*): a review. *Front. Pharmacol.* 13:901163. doi: 10.3389/fphar.2022.891535

Zhang, Q., Peng, Y., Li, F., Xu, Y., Zhang, Q., Wu, D., et al. (2024). An updated review of composition, health benefits, and applications of phenolic compounds in *Ficus carica* L. *Food* 5:e154. doi: 10.1002/efd2.154

Zorić, N., and Kosalec, I. (2022). "The antimicrobial activities of oleuropein and hydroxytyrosol," in *Promising Antimicrobials from Natural Products* (Cham: Springer eBooks), 75–89. doi: 10.1007/978-3-030-83504-0_5

frontiers | Frontiers in Microbiology

TYPE Original Research
PUBLISHED 17 June 2025
DOI 10.3389/fmicb.2025.1567913

OPEN ACCESS

EDITED BY
Alberto Antonelli,
University of Florence, Italy

REVIEWED BY
Chamara De Silva Benthotage,
Southern Cross University, Australia
Salome N. Seiffert,
Zentrum für Labormedizin (ZLM), Switzerland

*CORRESPONDENCE
Meeri Piispa
✉ meeri.piispa@helsinki.fi

RECEIVED 28 January 2025
ACCEPTED 15 May 2025
PUBLISHED 17 June 2025

CITATION
Piispa M, Vainio A, Halkilahti J, Lyytikäinen O and Räisänen K (2025) Detecting plasmid-mediated dissemination of *bla*$_{KPC-3}$ and *bla*$_{OXA-48-like}$ genes in Enterobacterales across Finnish healthcare organizations using hybrid genome assembly. *Front. Microbiol.* 16:1567913. doi: 10.3389/fmicb.2025.1567913

Detecting plasmid-mediated dissemination of *bla*$_{KPC-3}$ and *bla*$_{OXA-48-like}$ genes in Enterobacterales across Finnish healthcare organizations using hybrid genome assembly

Meeri Piispa[1,2]*, Anni Vainio[2], Jani Halkilahti[2], Outi Lyytikäinen[2] and Kati Räisänen[2]

[1]Department of Microbiology, Faculty of Agriculture and Forestry, University of Helsinki, Helsinki, Finland, [2]Department of Public Health, Microbiology Unit, Finnish Institute for Health and Welfare (THL), Helsinki, Finland

The spread of carbapenemase-producing Enterobacterales (CPE) is a global concern. While the majority of the CPE outbreaks are due to clonal spread, recent findings highlight the transmission of carbapenemase gene-carrying plasmids across various bacterial species, exacerbated by extensive antibiotic use in hospitals. This study aimed to identify plasmid-mediated horizontal transfer of carbapenemase genes among Enterobacterales isolated from patient samples and hospital environment samples in three healthcare organizations in Finland. Using a hybrid assembly of short and long reads, we could complete the genome assembly and compare the plasmids harboring the *bla*$_{KPC-3}$ and *bla*$_{OXA-48-like}$ genes. Our findings reveal indications of interspecies and intraspecies plasmid-mediated gene transfer of *bla*$_{KPC-3}$ and *bla*$_{OXA-48-like}$, emphasizing the role of horizontal gene transfer (HGT) in outbreaks. The study underscores the need for comprehensive infection control and surveillance beyond specific species to prevent the spread of antimicrobial resistance genes. These results suggest that expanding outbreak investigations to an interspecies level could be beneficial.

KEYWORDS

hybrid assembly, horizontal plasmid-mediated gene transfer, outbreak, molecular epidemiology, plasmid, CPE, whole genome sequencing

Introduction

Carbapenems are considered last-line drugs for the treatment of infections caused by multidrug-resistant Enterobacterales (Van Duin and Doi, 2017). The continuous rise in carbapenem resistance, resulting from the acquisition of carbapenemase genes, is a global concern. Infections caused by carbapenemase-producing Enterobacterales (CPE) are commonly associated with healthcare settings, where the hospital environment often serves as a reservoir for the spread of these bacteria. In outbreak investigations, the primary focus has usually been on tracking the clonal spread of a single pathogen. However, it is essential to consider that carbapenem resistance genes are predominantly located in mobile genetic elements (MGEs), such as integrons, insertion sequences, transposons, and plasmids (Kopotsa et al., 2019). It has been estimated that up to half of the CPE transmissions could occur through plasmid-mediated mechanisms (Marimuthu et al., 2022). The ability of plasmids to harbor

multiple antibiotic resistance genes (ARGs) and facilitate their transfer between the same and different bacterial species makes them highly significant in the molecular epidemiology of CPE (Kopotsa et al., 2019). Horizontal gene transfer (HGT) of plasmids via conjugation occurs through physical contact between bacteria. This process involves plasmids carrying mobility (MOB) genes for DNA processing and a mating pair formation (MPF) complex, a type 4 secretion system (T4SS), to form the mating channel (Smillie et al., 2010; Coluzzi et al., 2022). Plasmids can be classified as conjugative (self-transmissible), mobilizable (relying on another element's MPF genes), or non-mobilizable. Conjugation begins with a relaxase enzyme nicking the plasmid DNA at the origin of transfer (oriT), thereby initiating rolling-circle replication in the donor cell (Coluzzi et al., 2022). The resulting single-stranded DNA is then transferred to the recipient cell via the T4SS, where it is circularized and replicated to restore its double-stranded form.

While the majority of the *Klebsiella pneumoniae* carbapenemase (KPC)-producing *Klebsiella pneumoniae* outbreaks reported to date are due to clonal spread (Marí-Almirall et al., 2021; Pournaras et al., 2009; van Beek et al., 2019), recent findings suggest an emerging concern regarding the transmission of KPC gene-carrying plasmids (Adler et al., 2016), facilitating their dissemination across different bacterial species and genera (Schweizer et al., 2019). Plasmid-mediated horizontal transfer of resistance genes, often exacerbated by the extensive use of antibiotics in hospitals, may play a significant role in the regional and supra-regional spread of carbapenem resistance in healthcare settings (Li et al., 2018; Marí-Almirall et al., 2021; Schweizer et al., 2019).

To date, the number of CPE cases has been relatively low in Finland, ranging from 50 to 120 cases annually (Finnish Institute for Health and Welfare, 2023). From 2017 to 2022, on average, one-third of the annual CPE strains were associated with possible local transmission, indicating that they were genetically closely related. The most common types of carbapenemases detected were bla_{KPC}, bla_{NDM}, and $bla_{OXA\text{-}48\text{-}like}$.

This study aimed to identify the interspecies and intraspecies plasmid-mediated horizontal transfer of carbapenemase genes among Enterobacterales isolated from patient samples and hospital environment samples in three healthcare organizations in Finland. The location of the $bla_{KPC\text{-}3}$ and $bla_{OXA\text{-}48\text{-}like}$ genes was investigated in the bacterial genome and plasmid components for mobility prediction. Knowing the transmission routes of the gene will provide valuable information for tackling CPE outbreaks and epidemiological surveillance.

Materials and methods

According to the Communicable Diseases Act (1227/2016) and the national guidelines for controlling multidrug-resistant microbes (Kolho et al., 2020), all Finnish clinical microbiology laboratories are required to notify the National Infectious Diseases Register of any human isolates of *Enterobacter cloacae, Escherichia coli*, and *K. pneumoniae* that exhibit reduced susceptibility to carbapenems. These bacterial strains must also be submitted to the national CPE strain collection at the Finnish Institute for Health and Welfare (THL) (Räisänen et al., 2020). In addition, other CPE species and environmental isolates obtained as a part of the outbreak investigations are sent for further characterization to THL. Species identification and antimicrobial susceptibility tests were performed in clinical microbiology laboratories, along with confirmation of carbapenemase genes for isolates with reduced susceptibility, as previously described (Räisänen et al., 2020). For short-read whole genome sequencing (WGS), 1 ng of purified DNA was used, and the library was prepared using the Nextera XT DNA Sample Preparation Kit (Illumina, SD, USA). The paired-end short reads (2× 150-bp) were sequenced using the Illumina MiSeq instrument (Illumina, SD, USA). The short-read sequences were processed and analyzed using Trimmomatic (version 0.33), fastQC (version 0.11.6), SRST2 (version 0.2.0), and SeqSphere+ (Ridom GmbH, Münster, Germany), as previously described (van Beek et al., 2019).

When selecting CPE strains for this study, patient, time, and hospital environment were noted and grouped accordingly (Table 1). KP_4 and EC_1 strains were obtained from the same patient on the same collection date, both carrying the $bla_{OXA\text{-}48\text{-}like}$ gene (group 1). The other eight strains were obtained within a close timeframe in the same or close location to each other, all carrying the $bla_{KPC\text{-}3}$ gene (groups 2A and 2B). Locations A and C were related to an outbreak caused by *K. pneumoniae* ST512 (van Beek et al., 2019) and two other *K. pneumoniae* strains (KP_1 & KP_2). *Citrobacter freundii* strain (CF_1) from a cluster *C. freundii* ST116 (Räisänen et al., 2021) was obtained from the same patient as the KP_2 strain (group 2B). The environmental strains of *Klebsiella oxytoca* (KO_1), *Citrobacter braakii* (CB_1), and *Enterobacter agglomerans* (EA_1) were obtained from the same hospital ward.

Whole genome sequencing with Oxford Nanopore

The long-read WGS was performed using the MinION Mk1B device by the R9.4.1 flow cells (FLO-MIN106) (Oxford Nanopore Technologies, UK). The bacterial isolates were cultured from frozen stocks (−70°C) on Mueller-Hinton II agar plates (containing 2 g of beef extract, 17.5 g of acid hydrolysate of casein, 1.5 g of starch, and 17 g of agar) overnight at 37°C.

The library was prepared using the Rapid Barcoding Kit 96 (SQK-RBK110.96) (Oxford Nanopore Technologies, UK) according to the manufacturer's protocol, except the eluate was incubated in the rotator mixer (1,200 rpm) for 10 min at 56°C. The total run time was 72 h.

Basecalling was performed using the Guppy basecaller (v6.3.8) in super high-accuracy mode in real time. The data were processed using the MinKNOW (v22.10.7) software with the following utility programs: Bream (v7.3.2) and Configuration (v5.3.7).

Data analysis

For the data analysis, a FullForcePlasmidAssembler (FFPA) pipeline was used,[1] which includes Trimmomatic (v0.39), QCAT (v1.1.0), UniCycler (v0.4.7), and NanoPlot (v1.30.1). The FFPA uses

1 https://github.com/MBHallgren/FullForcePlasmidAssembler#readme/ accessed 2023-2-8

TABLE 1 Characteristics of the study strains.

ID	Group	Species	Sequence type	Carbapenemase gene	Collection date	Sources	Healthcare organization
KP_4	1	*K. pneumoniae*	ST15	$bla_{\text{OXA-48-like}}$	04/2022	Human[1]	B
EC_1	1	*E. coli*	ST1170	$bla_{\text{OXA-48-like}}$	04/2022	Human[1]	B
KP_1	2A	*K. pneumoniae*	ST512	$bla_{\text{KPC-3}}$	10/2019	Hospital environment (toilet)	A
KP_3	2A	*K. pneumoniae*	ST307	$bla_{\text{KPC-3}}$	03/2020	Human	A
CF_2	2A	*C. freundii*	ST125	$bla_{\text{KPC-3}}$	08/2020	Hospital environment (floor drain)	C
KO_1	2A	*K. oxytoca*	ST21	$bla_{\text{KPC-3}}$	08/2019	Hospital environment (toilet)*	C
CB_1	2A	*C. braakii*	NT	$bla_{\text{KPC-3}}$	10/2019	Hospital environment (toilet)*	C
EA_1	2A	*E. agglomerans*	NT	$bla_{\text{KPC-3}}$	12/2019	Hospital environment (floor drain)*	C
KP_2	2B	*K. pneumoniae*	ST512	$bla_{\text{KPC-3}}$	01/2020	Human[2]	A
CF_1	2B	*C. freundii*	ST116	$bla_{\text{KPC-3}}$	01/2020	Human[2]	A

NT, non-typable; KP, *Klebsiella pneumoniae*; CF, *Citrobacter freundii*; KO, *Klebsiella oxytoca*; CB, *Citrobacter braakii*; EA, *Enterobacter agglomerans*; EC, *Escherichia coli*.
[1]Isolated from the same patient.
[2]Isolated from the same patient.
*Isolated from the same hospital ward.

Trimmomatic and QCAT for trimming long and short reads. UniCycler (using eight threads) was used to maintain the hybrid assembly of short and long reads (Wick et al., 2017) using the *de novo* assembler SPAdes (v3.13.1) for the short reads (Bankevich et al., 2012), followed by alignment of the long reads to the graph. The quality and statistics of the MinION run were confirmed using NanoPlot (De Coster et al., 2018).

A software platform, Geneious Prime (v2022.2)[2], was used to annotate and assemble the contigs found from the hybrid assembly FASTA data. The target genes ($bla_{\text{KPC-3}}$ and $bla_{\text{OXA-48-like}}$) were annotated against the contigs. The accession numbers of the genes were obtained from the ResFinder (v.4.1) (Bortolaia et al., 2020) ($bla_{\text{KPC-3}}$: HM769262 and $bla_{\text{OXA-48-like}}$: AY236073), and the corresponding gene sequences were obtained from the National Center for Biotechnology Information (NCBI) GenBank[3]. The genes were annotated against the contigs, and the target contigs were aligned using the MAFFT alignment -tool (v7.490) (Katoh and Standley, 2013). A distance matrix and a heatmap, as well as a similarity dendrogram, were built from the aligned contigs. The similarity dendrogram was built using Geneious Tree Builder with the Jukes–Cantor distance model and the neighbor-joining building method. Each target contig was compared to the NCBI[4] database using the BLAST Megablast online tool.

The draft assembly of the plasmids was analyzed and characterized by the software tool MOB-suite using default parameters (Robertson and Nash, 2018). The MOB-suite includes a set of modular tools for reconstruction and typing. In the analysis, we used MOB-typer for conjugative transferability predictions. For predicting putative conjugative transferability, the MOB-typer identifies different DNA markers needed for the transfer, including an origin of transfer (oriT), a DNA relaxase, a type IV coupling protein (T4CP), and the type IV secretion system (T4SS) (Robertson and Nash, 2018). Plasmids possessing both a relaxase and a mate-pair formation marker were categorized as "conjugative," plasmids that had either relaxase or oriT, but lacked the mate-pair formation marker, were classified as "mobilizable," and plasmids that lacked both relaxase and oriT were considered "non-mobilizable." Each plasmid replicon (rep) type was confirmed additionally using PlasmidFinder, with >95% identity and >85% coverage[5] (Camacho et al., 2009; Carattoli et al., 2014).

Ethical statement

The isolates were part of the CPE surveillance or outbreak investigations based on the Communicable Disease Act (1227/2016); therefore, patients were not contacted, and ethical permission was not needed.

Results

The $bla_{\text{OXA-48-like}}$ gene was detected in two strains (group 1), and the $bla_{\text{KPC-3}}$ gene was detected in eight strains (groups 2A and 2B) (Table 1). In Geneious Prime, hybrid assembly data were divided into 3–14 contigs, and the size of the contigs where the target gene ($bla_{\text{KPC-3}}$ or $bla_{\text{OXA-48-like}}$) was found varied between 59,633 bp and 117,396 bp (Table 2). Each of the contigs with the carbapenemase gene was

2 https://www.geneious.com
3 https://www.ncbi.nlm.nih.gov/nucleotide/ accessed 2023-8-18
4 https://blast.ncbi.nlm.nih.gov/Blast.cgi/ accessed 2023-8-18
5 http://cge.cbs.dtu.dk/services/PlasmidFinder/ accessed 2025-5-7

determined as a plasmid sequence with the grade (E-value 0) varying from 72.3 to 100%.

MOB-typer analysis revealed that 6 out of 10 (KP_3, KP_4, CF_1, CF_2, EA_1, and EC_1) plasmids were putatively conjugative and the remaining were putatively non-mobilizable (KP_1, KP_2, KO_1, and CB_1) (Table 3). The $bla_{\text{OXA-48-like}}$ gene was located in putatively conjugative plasmids in both strains of group 1. In groups 2A and 2B, only the plasmids of the strains KP_3, CF_1, CF_2, and EA_1 containing the gene $bla_{\text{KPC-3}}$ were classified as conjugative.

The similarity dendrogram and distance matrix were generated by aligning the plasmid sequences that harbor the target genes ($bla_{\text{KPC-3}}$ or $bla_{\text{OXA-48-like}}$). Analysis of the similarities unveiled the clustering of plasmids into three distinct clades (Figure 1). The plasmids of EC_1 and KP_4 belonged to group 1 and created its own clade. The plasmids of KP_1, KP_2, KP_3, CF_1, KO_1, CB_1, and EA_1 belonging to group 2A and the plasmids belonging to group 2B were all found in the same clade. One plasmid from group 2A, namely CF_2, was found in its own clade apart from the rest of the plasmids.

The distance matrix and the heat map include the sequences of the contigs containing the target genes ($bla_{\text{KPC-3}}$ or $bla_{\text{OXA-48-like}}$) (Table 4). In this matrix, a higher value indicates a greater similarity in plasmid sequences. The total range of sequence similarity varied from 11 to 100%. In the distance matrix, the similarity between the plasmids in group 1 (with KP_4 and EC_1) was 100%. Among the largest clade—containing group 2A excluding CF_2 and group 2—the similarity ranged from 17 to 97%. In group 2A, the greatest similarity was observed between the putatively conjugative plasmids of KP_3 and EA_1, with a similarity of 97%. However, the putatively conjugative plasmid from CF_2 did not demonstrate significant similarities with the plasmids of any other strains. The plasmids of CF_1 and KP_2 from group 2B showed 81% similarity, although only CF_1 was characterized as putatively conjugative. Finally, among groups 2A and 2B, the putatively conjugative plasmid of CF_1 demonstrated a relatively close similarity (87%) with the putatively conjugative plasmids of KP_3 and EA_1.

Discussion

With the hybrid assembly, we could overcome the challenge stated in the article by Zou et al. (2022), where short-read sequencing often resulted in fragmented genomes, thereby complicating the classification of chromosomal and plasmid sequences. By using the hybrid assembly, we were able to create a comprehensive assembly of the plasmids and map the target genes ($bla_{\text{KPC-3}}$ or $bla_{\text{OXA-48-like}}$). Based on the MOB-typer analysis, 6 out of 10 strains carried putatively conjugative plasmids (Table 3). By comparing the similarities between the plasmid sequences, we could predict the mobility between the strains and predict if interspecies and intraspecies plasmid-mediated HGT has occurred.

The strains KP_4 and EC_1 from group 1, isolated from the same patient, carried the $bla_{\text{OXA48-like}}$ gene on identical, putatively conjugative plasmids classified as IncL/M type (Tables 2, 3). These plasmids, found in the same clade and with 100% similarity, strongly suggest interspecies plasmid-mediated HGT (Figure 1). This finding aligns with previous research by Hamprecht et al. (2019), which demonstrated that bla_{OXA48} dissemination primarily occurs via plasmid-mediated HGT rather than clonal expansion. In addition, MOB-typer and PlasmidFinder analyses confirmed the IncL/M and IncL rep types, respectively, which was consistent with the study by Poirel et al. (2012), further supporting the notion of a common origin for $bla_{\text{OXA48-like}}$-carrying plasmids. These plasmids exhibit low fitness burden and high stability, enhancing HGT potential (Hamprecht et al., 2019).

In group 2A, only strains KP_3, CF_2, and EA_1 harbored putatively conjugative plasmids according to the MOB-typer. The plasmid sequences of KP_3 and EA_1 exhibited a high similarity (97%) (Tables 3, 4), and this high similarity strongly suggests plasmid-mediated HGT (Orlek et al., 2017; Schweizer et al., 2019). The presence of these strains in environmental and human samples supports the hypothesis that environmental contamination in hospitals contributes to the transmission of the $bla_{\text{KPC-3}}$ gene among bacteria, as previously suggested by van Beek et al. (2019). In addition, the similarity in plasmid sequences and mobility between different species implies that interspecies plasmid-mediated gene transfer of the $bla_{\text{KPC-3}}$ gene likely occurred between environmental and human isolates. Marí-Almirall et al. (2021) proposed a similar gene transmission dynamic for the $bla_{\text{KPC-2}}$ gene in their investigation of the first hospital outbreak caused by KPC-producing Enterobacterales in Catalonia, reporting intraspecies and interspecies transmission associated with

TABLE 2 Result of the BLAST search for the target contigs containing the target gene ($bla_{\text{KPC-3}}$ or $bla_{\text{OXA-48-like}}$).

ID	Carbapenemase genes	Number of contigs	Length of the target contigs (bp)	Grade % (*E*-value 0)	Type of element
KP_1	$bla_{\text{KPC-3}}$	6	117,396	72.5	Plasmid
KP_2	$bla_{\text{KPC-3}}$	6	117,058	72.5	plasmid
KP_3	$bla_{\text{KPC-3}}$	5	114,528	85.6	Plasmid
KP_4	$bla_{\text{OXA-48-like}}$	4	63,589	100	Plasmid
CF_1	$bla_{\text{KPC-3}}$	4	112,552	72.3	Plasmid
CF_2	$bla_{\text{KPC-3}}$	13	109,450	86.4	Plasmid
KO_1	$bla_{\text{KPC-3}}$	14	59,633	95.6	Plasmid
CB_1	$bla_{\text{KPC-3}}$	13	66,259	91	Plasmid
EA_1	$bla_{\text{KPC-3}}$	3	116,907	81.9	Plasmid
EC_1	$bla_{\text{OXA-48-like}}$	5	63,589	100	Plasmid

TABLE 3 Predicted mobility and rep type(s) of the plasmids containing the target gene (*bla*$_{KPC-3}$ or *bla*$_{OXA-48-like}$).

ID	Group	Predicted mobility	Rep type(s) (MOB-suite)	Rep type(s) (PlasmidFinder)
KP_4	1	Conjugative	IncL/M	IncL
EC_1	1	Conjugative	IncL/M	IncL
KP_1	2A	Non-mobilizable	IncFIB, IncFII, and rep_cluster_2183	IncFIB(pQil)
KP_3	2A	Conjugative	IncFIB, IncFII, and rep_cluster_2183	IncFIB(pQil) and IncFII(K)
CF_2	2A	Conjugative	IncFIC and IncFII	IncFII(SARC14)
KO_1	2A	Non-mobilizable	IncFIB, IncFII, and rep_cluster_2183	IncFII(K)
CB_1	2A	Non-mobilizable	IncFIB, IncFII, and rep_cluster_2183	IncFII(K)
EA_1	2A	Conjugative	IncFIB, IncFII, and rep_cluster_2183	IncFII(K)
KP_2	2B	Non-mobilizable	IncFIB, IncFII, and rep_cluster_2183	IncFIB(pQil)
CF_1	2B	Conjugative	IncFIB, IncFII, and rep_cluster_2183	IncFIB(pQil)

The last two columns are results from MOB-suite and PlasmidFinder, respectively.

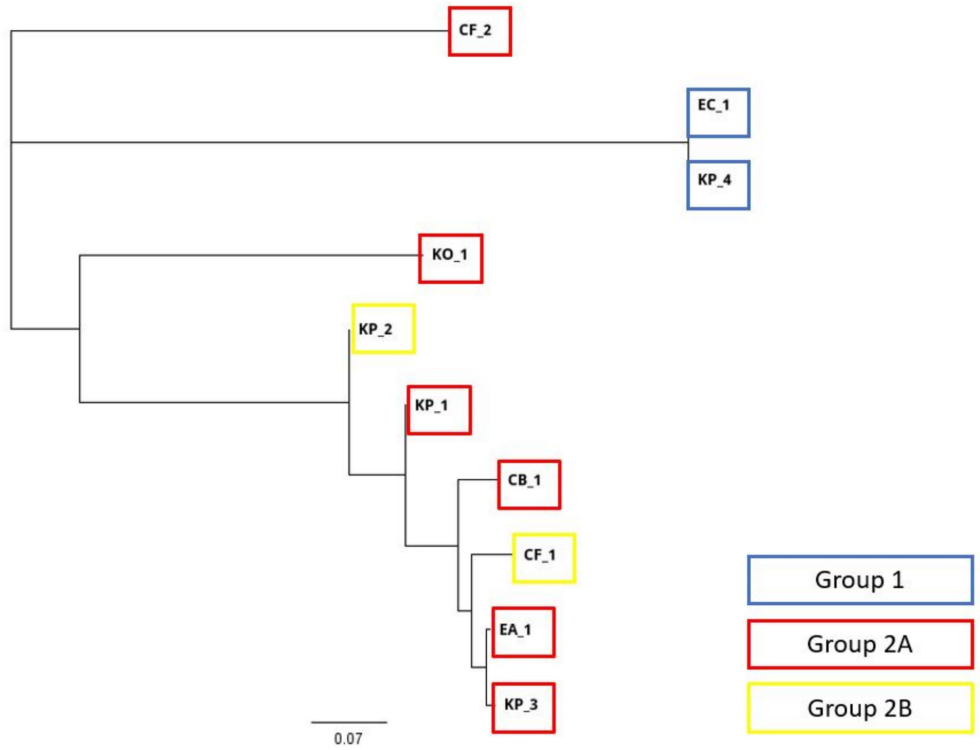

FIGURE 1
A dendrogram representing similarity of the contigs with carbapenemase gene (*bla*$_{KPC-3}$ or *bla*$_{OXA-48-like}$). The blue square marks the strains from group 1, red marks the strains from group 2A, and yellow marks the strains from group 2B.

plasmid-mediated gene transfer. They observed the plasmid overcoming genetic rearrangements in non-*K. pneumoniae* isolates, which could explain the minor differences observed in plasmid sequences in our study.

The suspected plasmid-mediated HGT between the environmental strains KO_1, CB_1, and EA_1 from the same hospital ward is difficult to confirm, as only the plasmid found in EA_1 was classified as putatively conjugative. In addition, the plasmid sequence of KO_1 exhibited low similarity with CB_1 (17%) and EA_1 (29%). The similarity between CB_1 and EA_1 was higher at 53%. Thus, confirming any conclusions would require more investigation.

Group 2B strains, isolated from the same patient within a short interval, suggested potential interspecies HGT (Evans et al., 2020). However, the plasmid of strain CF_1 was classified as conjugative; however, that of strain KP_2 was classified as non-mobilizable (Table 3), and moreover, the similarity of the plasmids was 81% (Table 4). It is possible that plasmid-mediated HGT occurred between CF_1 and KP_2, but the plasmid may have evolved and lost its autonomous conjugative ability (Coluzzi et al., 2022). Although the plasmid size of KP_2 was larger than that of CF_1 (Table 2), the observed differences may not be due to a simple deletion; instead, recombination events could have occurred, leading to the loss of genes required for

TABLE 4 Distance matrix and the heat map of the sequences of the contigs containing the target genes (*bla*$_{KPC-3}$ or *bla*$_{OXA-48-like}$).

Group		1		2A						2B	
	Isolate	**EC_1**	**KP_4**	CB_1	**CF_2**	**EA_1**	**KP_3**	KP_1	KO_1	KP_2	**CF_1**
1	**EC_1**	**x**	**100**	**13**	**22**	**20**	**20**	**21**	**25**	**21**	**20**
	KP_4	**100**	**x**	**13**	**22**	**20**	**20**	**21**	**25**	**21**	**20**
2A	CB_1	**13**	**13**	x	**11**	**53**	**54**	49	17	47	**52**
	CF_2	**22**	**22**	**11**	**x**	**25**	**24**	**29**	**28**	**29**	**24**
	EA_1	**20**	**20**	**53**	**25**	**x**	**97**	**89**	**29**	**86**	**87**
	KP_3	**20**	**20**	**54**	**24**	**97**	**x**	**88**	**29**	**85**	**87**
	KP_1	**21**	**21**	50	**30**	**89**	**88**	x	38	93	**84**
	KO_1	**25**	**25**	17	**28**	**29**	**29**	38	x	41	**29**
2B	KP_2	**21**	**21**	47	**29**	**86**	**85**	93	41	x	**81**
	CF_1	**20**	**20**	**52**	**24**	**87**	**87**	**84**	**29**	**81**	**x**

, 0–19%;

, 20–39%;

, 40–59%;

, 60–79;

, 80–100%.

Conjugative plasmid sequences are in bold.

conjugation. Confirming this would require further investigation into the plasmid sequences. Among groups 2A and 2B, all plasmids belonged to groups IncFIB and IncFII. In addition, all except CF_2 also had rep_cluster_2183. Only KP_3, CF_2, EA_1, and CF_1 were classified as containing a putatively conjugative plasmid with the target gene. The plasmid sequence of the strain CF_1 shared great similarity (>80%) with the plasmid sequences of the strains KP_3, KP_2, and EA_1. The strains CF_1 and KP_3, obtained from human samples collected 2 months apart at healthcare organization A, strongly suggest the occurrence of interspecies plasmid-mediated HGT among patients within the same healthcare organization. This finding confirms the discovery by Li et al. (2018) that isolates originating from a single hospital have the ability to spread among various species of Enterobacteriaceae, indicating a wide dissemination of the plasmids within the hospital. The connection observed between strains CF_1 and EA_1 further supports the previously mentioned pattern of interspecies plasmid-mediated HGT between environmental and human samples. No specific bacterial species was found to be more prone to plasmid-mediated HGT.

The plasmids of the strains KP_2 and KP_1, which are related to the same cluster (van Beek et al., 2019), created their own subgroup with 93% similarity as expected, as they were identified to be involved in the clonal spread based on the cgMLST analysis (by using Illumina data only) and shared a common epidemiological link. Predicted mobility analysis demonstrated their non-mobilizable status, further validating clonal spread and likely ruling out plasmid-mediated HGT between the strains.

In this study, we showed a strong indication of interspecies plasmid-mediated gene transfer of antibiotic resistance genes *bla*$_{KPC-3}$ and *bla*$_{OXA-48-like}$. This study highlights the prevalence of HGT in outbreaks and that infection control and surveillance should not only concern a specific species. In such outbreaks, extensive detection and surveillance should be designated as a prevention of the spread of the AMR genes. The plasmid-mediated *bla*$_{KPC-2}$ gene transfer in multispecies outbreaks has been reported worldwide, for example, in Germany (Schweizer et al., 2019) and China (Li et al., 2018). Based on our results, expanding the outbreak investigation to the interspecies level in Finland should be considered in the future.

Our study has several limitations. The prediction of plasmid-mediated HGT was based solely on observing the putative mobility and similarity of the plasmids. Performing a phylogenetic analysis of plasmids is challenging because they often lack conserved core genes, and sequence dissimilarity does not necessarily indicate a distant common origin (Orlek et al., 2017). Plasmids that are phylogenetically distant may share genetic content due to the insertion of similar mobile elements (Redondo-Salvo et al., 2020), while closely related plasmids can exhibit significant sequence differences after recombination with other genetic structures (Redondo-Salvo et al., 2020; Schweizer et al., 2019). Therefore, plasmid similarity might not be the best indicator of HGT. The use of MOB-typer for mobility analysis should be approached with caution and validated with another method in addition. Approximately half of the plasmids were identified as non-mobilizable, meaning that they lack relaxase and oriT, which are essential for the conjugation process. There is a possibility that these strains carry novel oriT systems in their plasmids that are not recognized. This could be explained by recent findings by Ares-Arroyo et al. (2024), which suggest that many oriTs are currently unrecognized. In addition, studies have found that plasmids with incomplete conjugation systems, lacking some essential genes, can utilize other mobile genetic elements (MGEs) such as bacteriophages or other plasmids to facilitate mobility (Ares-Arroyo et al., 2024; Coluzzi et al., 2022). To better understand this phenomenon, further investigation into other MGEs in the bacterium's genome is required.

To confirm both mobility and HGT in future studies, it would be advisable to perform plasmid dissemination tests, including conjugation assays between isolates, and investigation of the MGEs. In addition, our sample size was relatively small, limiting the ability to make definitive conclusions. Further data are required to strengthen our findings.

Conclusion

In this study, by using the hybrid assembly of short and long reads, we could successfully distinguish the bacterial genome into contigs to separate plasmid and chromosomal sequences, investigate whether the carbapenem resistance gene is in the plasmid or not, and predict whether the gene spreads horizontally between the strains. To the best of our knowledge, this is the first report where the plasmid-mediated spread of the AMR gene in Finland is investigated by using the hybrid assembly. Understanding the transmission route of the gene could yield valuable insights for addressing CPE outbreaks, as it has been assessed that 50% of them are disseminated via plasmids (Marimuthu et al., 2022). The threshold for indications of HGT is difficult to determine with such small sampling. To more precisely determine the exact threshold and other indications of the plasmid-mediated HGT, more research is required.

Data availability statement

The datasets presented in this study can be found in online repositories. The names of the repository/repositories and accession number(s) can be found at: https://www.ebi.ac.uk/ena, PRJEB84916.

Author contributions

MP: Data curation, Formal analysis, Methodology, Visualization, Writing – original draft, Writing – review & editing. AV: Conceptualization, Formal analysis, Methodology, Supervision, Writing – original draft, Writing – review & editing. JH: Data curation, Methodology, Software, Writing – original draft, Writing – review & editing. OL: Writing – review & editing. KR: Conceptualization, Data curation, Formal analysis, Investigation, Methodology, Supervision, Writing – original draft, Writing – review & editing.

Funding

The author(s) declare that financial support was received for the research and/or publication of this article. This research was supported by the European Health and Digital Executive Agency (HaDEA) funding with the Project 101112962—HaD_SinGen.

Acknowledgments

The authors acknowledge Henrik Hasman and Astrid Rasmussen from Statens Serum Institute for valuable counseling, Finnish clinical microbiology laboratories for providing the CPE isolates, and CSC-IT Centre for Science, Finland, for providing computational resources.

Conflict of interest

The authors declare that the research was conducted in the absence of any commercial or financial relationships that could be construed as a potential conflict of interest.

Generative AI statement

The authors declare that no Gen AI was used in the creation of this manuscript.

Publisher's note

References

Adler, A., Efrat, K., Paikin, S., and Carmeli, Y. (2016). Dissemination of the BlaKPC gene by clonal spread and horizontal gene transfer: comparative study of incidence and molecular mechanisms. *J. Antimicrob. Chemother.* 71, 2143–2146. doi: 10.1093/jac/dkw106

Ares-Arroyo, M., Nucci, A., and Rocha, E. P. C. (2024). Identification of novel origins of transfer across bacterial plasmids. Available online at: https://www.biorxiv.org/content/10.1101/2024.01.30.577996v1. (Accessed November 13, 2024)

Bankevich, A., Nurk, S., Antipov, D., Gurevich, A. A., Dvorkin, M., Kulikov, A. S., et al (2012). "SPAdes: a new genome assembly algorithm and its applications to single-cell sequencing." *Journal of Computational Biology: A Journal of Computational Molecular Cell Biology*, 19, 455–477. doi: 10.1089/cmb.2012.0021

Bortolaia, V., Kaas, R. S., Ruppe, E., Roberts, M. C., Schwarz, S., Cattoir, V., et al (2020). "ResFinder 4.0 for predictions of phenotypes from genotypes." *The Journal of Antimicrobial Chemotherapy*, 75, 3491–3500. doi: 10.1093/jac/dkaa345

Camacho, C., Coulouris, G., Avagyan, V., Ma, N., Papadopoulos, J., Bealer, K., et al. (2009). BLAST+: architecture and applications. *BMC Bioinformatics* 10:421. doi: 10.1186/1471-2105-10-421

Carattoli, A., Zankari, E., Garcia-Fernandez, A., Voldby Larsen, M., Lund, O., Villa, L., et al. (2014). Plasmidfinder and pMLST: in silico detection and typing of plasmids. *Antimicrob. Agents Chemother.* 58, 3895–3903. doi: 10.1128/AAC.02412-14

Coluzzi, C., Pilar Garcillán-Barcia, M., de la Cruz, F., and Rocha, E. P. C. (2022). Evolution of plasmid mobility: origin and fate of conjugative and nonconjugative plasmids. *Mol. Biol. Evol.* 39:msac115. doi: 10.1093/molbev/msac115

De Coster, W., D'Hert, S., Schultz, D. T., Cruts, M., and Van Broeckhoven, C. (2018). "NanoPack: visualizing and processing long-read sequencing data." *Bioinformatics (Oxford, England)* 34, 2666–2669. doi: 10.1093/bioinformatics/bty149

Evans, D. R., Griffith, M. P., Sundermann, A., Shutt, K. A., Saul, M. I., Mustapha, M. M., et al. (2020). Systematic detection of horizontal gene transfer across genera among multidrug-resistant bacteria in a single hospital. *eLife* 9:e53886. doi: 10.7554/eLife.53886

Finnish Institute for Health and Welfair. (2023). "CPE-Esiintyvyys Suomessa." Available online at: https://thl.fi/fi/web/infektiotaudit-ja-rokotukset/taudit-ja-torjunta/taudit-ja-taudinaiheuttajat-a-o/salmonella/salmonellan-esiintyvyys-suomessa. (Accessed June 1, 2023).

Hamprecht, A., Sommer, J., Willmann, M., Brender, C., Stelzer, Y., Krause, F., et al. (2019). Pathogenicity of clinical OXA-48 isolates and impact of the OXA-48 incL plasmid on virulence and bacterial fitness. *Front. Microbiol.* 10:2509. doi: 10.3389/fmicb.2019.02509

Katoh, K., and Standley, D. M. (2013). MAFFT multiple sequence alignment software version 7: improvements in performance and usability. *Mol. Biol. Evol.* 30, 772–780. doi: 10.1093/molbev/mst010

Kolho, E., Lyytikäinen, O., and Jalava, J. (2020). Ohje Moniresistenttien Mikrobien Tartunnantorjunnasta [National Guideline for Control of Multidrug-Resistant Microbes]. Helsinki: National Institute for Health and Welfare (THL).

Kopotsa, K., Osei Sekyere, J., and Mbelle, N. M. (2019). Plasmid evolution in Carbapenemase-producing *Enterobacteriaceae*: a review. *Ann. N. Y. Acad. Sci.* 1457, 61–91. doi: 10.1111/nyas.14223

Li, B., Feng, J., Zhan, Z., Yin, Z., Jiang, Q., Wei, P., et al. (2018). Dissemination of KPC-2-encoding IncX6 plasmids among multiple Enterobacteriaceae species in a single Chinese hospital. *Front. Microbiol.* 9:478. doi: 10.3389/fmicb.2018.00478

Marí-Almirall, M., Ferrando, N., Fernández, M. J., Cosgaya, C., Viñes, J., Rubio, E., et al. (2021). Clonal spread and intra- and inter-species plasmid dissemination associated with *Klebsiella Pneumoniae* Carbapenemase-producing Enterobacterales during a hospital outbreak in Barcelona, Spain. *Front. Microbiol.* 12:781127. doi: 10.3389/fmicb.2021.781127

Marimuthu, K., Venkatachalam, I., Koh, V., Harbarth, S., Perencevich, E., Cherng, B. P. Z., et al. (2022). Whole genome sequencing reveals hidden transmission of Carbapenemase-producing Enterobacterales. *Nat. Commun.* 13:3052. doi: 10.1038/s41467-022-30637-5

Orlek, A., Stoesser, N., Anjum, M. F., Doumith, M., Ellington, M. J., Peto, T., et al. (2017). Plasmid classification in an era of whole-genome sequencing: application in studies of antibiotic resistance epidemiology. *Front. Microbiol.* 8:182. doi: 10.3389/fmicb.2017.00182

Poirel, L., Bonnin, R. A., and Nordmann, P. (2012). Genetic features of the widespread plasmid coding for the Carbapenemase OXA-48. *Antimicrob. Agents Chemother.* 56, 559–562. doi: 10.1128/AAC.05289-11

Pournaras, S., Protonotariou, E., Voulgari, E., Kristo, I., Dimitroulia, E., Vitti, D., et al. (2009). Clonal spread of KPC-2 carbapenemase-producing *Klebsiella pneumoniae* strains in Greece. *J. Antimicrob. Chemother.* 64, 348–352. doi: 10.1093/jac/dkp207

Räisänen, K., Lyytikäinen, O., Kauranen, J., Tarkka, E., Forsblom-Helander, B., Grönroos, J. O., et al. (2020). Molecular epidemiology of Carbapenemase-producing Enterobacterales in Finland, 2012–2018. *Eur. J. Clin. Microbiol. Infect. Dis.* 39, 1651–1656. doi: 10.1007/s10096-020-03885-w

Räisänen, K., Sarvikivi, E., Arifulla, D., Pietikäinen, R., Forsblom-Helander, B., Tarkka, E., et al. (2021). Three clusters of Carbapenemase-producing *Citrobacter Freundii* in Finland, 2016–20. *J. Antimicrob. Chemother.* 76, 2697–2701. doi: 10.1093/jac/dkab209

Redondo-Salvo, S., Fernández-López, R., Ruiz, R., Vielva, L., de Toro, M., Rocha, E. P. C., et al. (2020). Pathways for horizontal gene transfer in Bacteria revealed by a global map of their plasmids. *Nat. Commun.* 11:3602. doi: 10.1038/s41467-020-17278-2

Robertson, J., and Nash, J. H. E. (2018). MOB-suite: software tools for clustering, reconstruction and typing of plasmids from draft assemblies. *Microb. Genom.* 4:e000206. doi: 10.1099/mgen.0.000206

Schweizer, C., Bischoff, P., Bender, J., Kola, A., Gastmeier, P., Hummel, M., et al. (2019). Plasmid-mediated transmission of KPC-2 carbapenemase in Enterobacteriaceae in critically ill patients. *Front. Microbiol.* 10:276. doi: 10.3389/fmicb.2019.00276

Smillie, C., Garcillán-Barcia, M. P., Francia, M. V., Rocha, E. P., and de la Cruz, F. (2010). Mobility of plasmids. *Microbiol. Mol. Biol. Rev.* 74, 434–452. doi: 10.1128/MMBR.00020-10

van Beek, J., Räisänen, K., Broas, M., Kauranen, J., Kähkölä, A., Laine, J., et al. (2019). Tracing local and regional clusters of carbapenemase-producing *Klebsiella pneumoniae* ST512 with whole genome sequencing, Finland, 2013 to 2018. *Eur. Secur.* 24:1800522. doi: 10.2807/1560-7917.ES.2019.24.38.1800522

Van Duin, D., and Doi, Y. (2017). The global epidemiology of Carbapenemase-producing Enterobacteriaceae. *Virulence* 8, 460–469. doi: 10.1080/21505594.2016.1222343

Wick, R. R., Judd, L. M., Gorrie, C. L., and Holt, K. E. (2017). "Completing bacterial genome assemblies with multiplex MinION sequencing." *Microbial Genomics*, 3. doi: 10.1099/mgen.0.000132

Zou, X., Nguyen, M., Overbeek, J., Cao, B., and Davis, J. J. (2022). Classification of bacterial plasmid and chromosome derived sequences using machine learning. *PLoS One* 17:e0279280. doi: 10.1371/journal.pone.0279280

frontiers | Frontiers in Microbiology

TYPE Original Research
PUBLISHED 14 July 2025
DOI 10.3389/fmicb.2025.1464573

OPEN ACCESS

EDITED BY
Ana P. Tedim,
Institute of Health Sciences Studies of Castilla y León (IECSCYL), Spain

REVIEWED BY
Susana Patricia Costa,
International Iberian Nanotechnology Laboratory (INL), Portugal
Tripti Nair,
University of Southern California, United States

*CORRESPONDENCE
Xueping Yu
✉ xpyu15@fudan.edu.cn
Yan Geng
✉ wsw87679358@163.com

†These authors have contributed equally to this work

RECEIVED 14 July 2024
ACCEPTED 19 June 2025
PUBLISHED 14 July 2025

CITATION
Liu Z, Cai H, Lei J, Zhang X, Yin J, Zhang Y, Yu X and Geng Y (2025) Distribution and analysis of the resistance profiles of bacteria isolated from blood cultures in the intensive care unit.
Front. Microbiol. 16:1464573.
doi: 10.3389/fmicb.2025.1464573

Distribution and analysis of the resistance profiles of bacteria isolated from blood cultures in the intensive care unit

Zeshi Liu[1†], Hehui Cai[2†], Jing Lei[1], Xue Zhang[1], Jian Yin[1], Yanping Zhang[1], Xueping Yu[3,4*] and Yan Geng[1*]

[1]Department of Clinical Laboratory, The Second Affiliated Hospital of Xi'an Jiaotong University, Xi'an, Shaanxi, China, [2]Department of Clinical Laboratory, Fujian Medical University Affiliated First Quanzhou hospital,Quanzhou, Fujian, China, [3]Department of Infection Disease, Clinical Medical Research Center for Bacterial and Fungal Infectious Diseases of Fujian province, Fujian Medical University Affiliated First Quanzhou Hospital, Quanzhou, Fujian, China, [4]Key Laboratory of Screening and Control of Infectious Diseases (Quanzhou Medical College), Fujian Provincial University, Quanzhou, Fujian, China

Purpose: To investigate the distribution characteristics and drug resistance of pathogenic bacteria in bloodstream infections, providing a basis for rational clinical treatment.

Patients and methods: Retrospective analysis of 1,282 pathogenic strains isolated from blood cultures in the intensive care unit (ICU) of the Second Affiliated Hospital of Xi'an Jiaotong University from January 1, 2019, to December 31, 2022.

Results: Gram-positive bacteria (52.0%) slightly predominated over gram-negative bacteria (48.0%). The top three gram-positive bacteria were Coagulase-negative *Staphylococcus* (28.0%), *Enterococcus faecium* (7.4%), and *Staphylococcus aureus* (6.6%). Staphylococci exhibited a high resistance rate to penicillin, oxacillin, and erythromycin; no strains resistant to vancomycin or linezolid were found. Among the Enterococci, *Enterococcus faecium* had a high resistance rate to penicillin, ampicillin, and erythromycin. Two strains of *Enterococcus faecalis* were resistant to linezolid, but none to vancomycin. The top three gram-negative bacteria were *Escherichia coli* (14.7%), *Klebsiella pneumoniae* (14.0%), and *Acinetobacter baumannii* (4.8%). The resistance rate of *Escherichia coli* to carbapenems increased from 0.0 to 2.3%. *Acinetobacter baumannii* reached 100% carbapenem resistance (up from 75.0%), while *Klebsiella pneumoniae* demonstrated 21.1-80.4% resistance to various carbapenems.

Conclusion: The isolation rate of gram-positive bacteria in patients with bloodstream infection in the ICU of the Second Affiliated Hospital of Xi'an Jiaotong University was slightly higher than that of gram-negative bacteria. The alarming carbapenem resistance among gram-negative pathogens and emerging linezolid resistance in *Enterococci* demand urgent clinical interventions, including enhanced surveillance, antimicrobial stewardship, and novel therapeutic strategies.

KEYWORDS

blood culture, drug resistance, pathogens, intensive care unit, antimicrobial susceptibility test

1 Introduction

Bloodstream infection (BSI) is a severe systemic infectious disease characterized by the invasion of pathogenic microorganisms into the body. These microorganisms circulate in the bloodstream, where they undergo transient, intermittent, or continuous reproduction, releasing toxins and metabolic products that trigger the release of cytokines, ultimately resulting in damage to organs. In severe cases, BSI can lead to shock, multiple organ failure, disseminated intravascular coagulation, and death (Tajima et al., 2021; Fabre et al., 2022). Globally, BSIs account for an estimated 20-30% of sepsis cases and are associated with mortality rates exceeding 40% in critically ill populations, particularly in intensive care units (ICUs) (Fleischmann-Struzek et al., 2020). The rising prevalence of antimicrobial resistance (AMR) has further complicated BSI management, with the World Health Organization declaring AMR one of the top 10 global public health threats, projected to cause 10 million annual deaths by 2050 if unchecked (World Health Organization [WHO], 2021).

The diagnoses of BSIs, infective endocarditis, unexplained infections, catheter-related BSIs, arthritis, and bacterial pneumonia rely on blood culture (Gonzalez et al., 2020) to identify the causative pathogens and provide antibiotic susceptibility profiles. These data are critical for guiding evidence-based antibiotic therapy, especially as multidrug-resistant (MDR) pathogens reduce treatment efficacy and increase healthcare costs (Cheng et al., 2020; Mazi et al., 2021). Recent data reveal alarming global shifts: while gram-negative bacteria historically dominated BSI etiology, gram-positive pathogens such as *Staphylococcus aureus*, coagulase-negative staphylococci, and enterococci now prevail in many regions (Lan et al., 2021). Concurrently, resistance mechanisms like methicillin resistance in S. aureus (MRSA), vancomycin resistance in enterococci (VRE), and extended-spectrum β-lactamase (ESBL)-producing Enterobacteriaceae have escalated, driven by antibiotic overuse in clinical and agricultural settings (Antimicrobial Resistance Collaborators, 2022). For instance, MRSA accounts for > 35% of S. aureus BSIs in high-income countries, while carbapenem-resistant *Klebsiella pneumoniae* infections in ICUs exceed 60% in some endemic regions (Centers for Disease Control and Prevention [CDC], 2023; European Centre for Disease Prevention and Control [ECDC], 2022).

These trends underscore the urgency of region-specific pathogen surveillance and resistance profiling. This study retrospectively analyzed the distribution of pathogens and their antibiotic resistance in blood culture specimens collected from an intensive care unit (ICU) between 2019 and 2022. By correlating our findings with global antimicrobial resistance dynamics, we aim to establish a scientific foundation for optimizing empirical antibiotic therapy, informing stewardship programs, and mitigating resistance escalation in critical care settings.

Abbreviations: CRAB, Carbapenem-resistant *Acinetobacter baumannii*; CREC, Carbapenem-resistant *Escherichia coli*; CRKP, Carbapenem-resistant *Klebsiella pneumoniae*; CRO, Carbapenem-resistant organisms; CRPA, Carbapenem-resistant *Pseudomonas aeruginosa*; ICU, Intensive care unit; KPC, *Klebsiella pneumoniae* carbapenemases; MH, Mueller-Hinton; MRCNS, Methicillin-resistant coagulase-negative *Staphylococcus*; MRSA, Methicillin-resistant *Staphylococcus aureus*; MSCNS, Methicillin-sensitive coagulase-negative Staphylococcus; MSSA, Methicillin-sensitive *Staphylococcus aureus*; KPN, *Klebsiella pneumonia*; KPL, *Raoultella planticola*; PAE, *Pseudomonas aeruginosa*; ABA, *Acinetobacter baumannii*; ECO, *Escherichia coli*; ECL, *Enterobacter cloacae*; NA, not available.

2 Materials and methods

2.1 Materials

2.1.1 Strains

Between January 1, 2019, and December 31, 2022, a total of 1,282 bacterial strains were collected from the positive blood cultures of patients in the ICU at the Second Affiliated Hospital of Xi'an Jiaotong University, with duplicate strains from the same patient excluded from the analyses. This study has been approved by the academic committee of the Stem Cell Clinical Research Institute of the Second Affiliated Hospital of Xi'an Jiaotong University and the ethics committee of the same institution (2023414). Informed consent was obtained from all study participants, and the guidelines outlined in the declaration of Helsinki were adhered to.

2.1.2 Culture media and antibiotic discs

Mueller-Hinton (MH) agar (Zhengzhou AutoBio Co., Ltd., Zhengzhou, China) was used for disc-diffusion susceptibility testing, and 5% defibrinated sheep blood MH agar was used for streptococci. Culture media were sourced from AutoBio (Co., Ltd., Zhengzhou, China), and the antibiotic discs were acquired from Oxoid, Basingstoke, UK). E-test strips were obtained from Wenzhou Kangtai Biotechnology (Co., Ltd., Wenzhou, China).

2.2 Methods

2.2.1 Bacterial identification and antimicrobial susceptibility test

The fully automated bacterial culture system BacT/ALERT 3D (Marcy l'Etoile, bioMérieux, France) was used to detect blood culture specimens. Bacterial identification and antimicrobial susceptibility tests were conducted using the VITEK 2-Compact bacterial identification system (Marcy l'Etoile, bioMérieux, France), while less common bacteria were identified using the VITEK MS system (Marcy l'Etoile, bioMérieux, France). The interpretation of antimicrobial susceptibility results followed the 2022 performance standards proposed by the Clinical and Laboratory Standards Institute (Clinical and Laboratory Standards Institute [CLSI], 2022). To exclude duplicate strains from the same patient, only the first positive blood culture with a specific pathogen per patient was included in the analysis. Subsequent isolates of the same species from the same patient within 30 days were excluded unless they exhibited distinct antimicrobial susceptibility profiles or were isolated from different anatomical sites, as recommended by international guidelines

for bloodstream infection surveillance (Magiorakos et al., 2017).

2.2.2 Phenotype testing for important drug resistance

Carbapenem-resistant Enterobacterales were defined as Enterobacterale specimens resistant to any of the carbapenem antibiotics, specifically imipenem, meropenem, or ertapenem.

2.2.3 Quality control strains

The quality control strains used in this study included *Escherichia coli* (ATCC 25922 and ATCC 8739), *Klebsiella pneumoniae* (ATCC 700603), *Staphylococcus aureus* (ATCC 25923 and ATCC 29213), *Pseudomonas aeruginosa* (ATCC 27853), *Enterococcus faecalis* (ATCC 29212), *Streptococcus pneumoniae* (ATCC 49619), and *Haemophilus influenzae* (ATCC 49247). These strains were selected based on CLSI recommendations for antimicrobial susceptibility testing (Clinical and Laboratory Standards Institute [CLSI], 2022) and represent common pathogens associated with bloodstream infections. All strains were procured from the American Type Culture Collection (ATCC) to ensure traceability and standardized phenotypic characteristics. Quality control testing was performed weekly alongside clinical isolates, with acceptable ranges defined by CLSI criteria. No deviations from standard protocols were observed during the study period, as confirmed by internal audit records.

2.3 Statistical analysis

The laboratory data analysis and statistical analyses were conducted using WHONET 5.6 software (China).[1] SPSS 24.0 software was utilized for statistical analysis. The chi-square test was employed to examine differences in categorical data.

3 Results

3.1 Bacterial distribution

Between January 2019 and December 2022, a total of 1,282 distinct pathogenic strains were isolated from the blood cultures of patients in the ICU (Table 1). Among these, 667 (52.0%) were gram-positive bacteria, while 615 (48.0%) were gram-negative bacteria. The five most prevalent bacterial species were coagulase-negative *Staphylococcus* (359 strains; 28.0%), *Escherichia coli* (189 strains; 14.7%), *Klebsiella pneumoniae* (180 strains; 14.0%), *Enterococcus faecium* (95 strains; 7.4%), and *Staphylococcus aureus* (85 strains;6.6%). Other gram-negative bacteria included *Raoultella planticola*, *Citrobacter freundii*, *Brucella*, *Haemophilus influenzae*, *Morganella morganii*, and

1 www.whonet.org.cn

TABLE 1 Distribution of 1282 pathogenic bacteria in blood cultures.

Organism	2019(*n*=156)		2020 (*n*=263)		2021 (*n*=384)		2022 (*n*=479)		Total (*n*=1282)	
	n	%	*n*	%	*n*	%	*n*	%	*N*	%
Gram-negative bacteria	98	7.6	126	9.8	173	13.5	218	17.0	615	48.0
Escherichia coli	24	1.9	15	1.2	64	5.0	86	6.7	189	14.7
Klebsiella pneumoniae	46	3.6	47	3.7	49	3.8	38	3.0	180	14.0
Acinetobacter baumannii	14	1.1	12	0.9	18	1.4	18	1.4	62	4.8
Stenotrophomonas maltophilia	0	0.0	8	0.6	13	1.0	9	0.7	30	2.3
Pseudomonas aeruginosa	4	0.3	13	1.0	4	0.3	24	1.9	45	3.5
Enterobacter cloacae	4	0.3	9	0.7	6	0.5	21	1.6	40	3.1
Klebsiella oxytoca	4	0.3	1	0.1	0	0.0	8	0.6	13	1.0
Serratia marcescens	0	0.0	0	0.0	3	0.2	6	0.5	9	0.7
Enterobacter aerogenes	0	0.0	0	0.0	5	0.4	0	0.0	5	0.4
Burkholderia cepacia	0	0.0	2	0.2	2	0.2	0	0.0	4	0.3
Other gram-negative bacteria	2	0.2	19	1.5	9	0.7	8	0.6	36	2.8
Gram -positive bacteria	58	4.5	137	10.7	211	16.5	261	20.4	667	52.0
Coagulase-negative Staphylococcus	33	2.6	53	4.1	136	10.6	137	10.7	359	28.0
Enterococcus faecium	7	0.5	26	2.0	34	2.7	28	2.2	95	7.4
Staphylococcus aureus	14	1.1	25	2.0	17	1.3	29	2.3	85	6.6
Enterococcus faecalis	1	0.1	7	0.5	4	0.3	10	0.8	22	1.7
Streptococcus pneumoniae	2	0.2	13	1.0	0	0.0	0	0.0	15	1.2
Alpha-hemolytic *Streptococcus*	1	0.1	4	0.3	4	0.3	12	0.9	21	1.6
Beta-hemolytic *Streptococcus*	0	0.0	2	0.2	0	0.0	0	0.0	2	0.2
Other gram-positive bacteria	0	0.0	7	0.5	16	1.2	45	3.5	68	5.3

Citrobacter diversus. Other streptococci mainly encompassed *Streptococcus viridans*, *Streptococcus mitis*, and *Streptococcus agalactiae*, while other gram-positive cocci included *Enterococcus gallinarum*, *Streptococcus bovis*, *Abiotrophia defectiva*, and *Gemella* species.

3.2 Antibiotic resistances of major gram-positive bacteria

3.2.1 *Staphylococcus* genus

A total of 443 strains of *Staphylococcus* genus were isolated, comprising 34.6% of all isolated pathogens. Among them, 85 strains were *Staphylococcus aureus*, and 358 strains were coagulase-negative staphylococci. The detection rates of methicillin-resistant *Staphylococcus aureus* (MRSA) in 2019, 2020, 2021, and 2022 were 2.3% (10 strains), 1.8% (8 strains), 0.0% (0 strains), and 2.7% (12 strains), respectively (Table 2). With the exception of 2021, the detection rates remained stable. MRSA exhibited a consistent decline in resistance to gentamicin, levofloxacin, moxifloxacin, trimethoprim-sulfamethoxazole, and erythromycin from 2019 to 2022. The resistance rate to gentamicin dropped from 75.0 to 0.0%, while the resistance rate to erythromycin decreased from 100.0 to 41.7%. Methicillin-sensitive *Staphylococcus aureus* displayed a constant resistance rate to penicillin G from 2019-2022 (100.0%), while the resistance rates to levofloxacin, moxifloxacin, and erythromycin decreased from 2019-2022. *Staphylococcus aureus* was not resistant to vancomycin, linezolid, or rifampicin.

Between 2019 and 2022, the detection rates of methicillin-resistant coagulase-negative Staphylococcus (MRCNS) were 7.2% (32 strains), 9.9% (44 strains), 26.2% (116 strains), and 24.8% (110 strains), respectively (Table 3). MRCNS did not show significant changes in resistance rates to gentamicin, rifampicin, levofloxacin, moxifloxacin, or erythromycin. However, the resistance rate to trimethoprim-sulfamethoxazole increased from 27.3% in 2020 to 41.8% in 2022. No instances of resistance to vancomycin or linezolid were detected among coagulase-negative Staphylococcus strains. The resistance to penicillin G and erythromycin remained relatively high among methicillin-sensitive coagulase-negative Staphylococcus strains (MSCNS). The resistance rates of MSCNS to levofloxacin, moxifloxacin, and trimethoprim-sulfamethoxazole decreased from 2019 to 2022.

3.2.2 *Enterococcus* genus

A total of 132 strains from the Enterococcus genus were isolated, including 22 strains of *Enterococcus faecalis*, 95 strains of *Enterococcus faecium*, and 15 strains of other Enterococcus species. *Enterococcus faecium* exhibited > 80.0% resistance to ampicillin, though *Enterococcus faecalis* was sensitive to the drug (Table 4). *Enterococcus faecium* displayed significantly higher antibiotic resistance rates than those displayed by *Enterococcus faecalis*. *Enterococcus faecium* demonstrated a resistance rate > 90% to penicillin, although its resistance rate to erythromycin declined from 2019-2022. In contrast, *Enterococcus faecalis* exhibited resistance rates of 20.0% and 40.0% to penicillin and erythromycin, respectively. Neither *Enterococcus faecium* nor

TABLE 2 Resistance and sensitivity rates of *Staphylococcus aureus* isolated from blood culture to antimicrobial agents from 2019 to 2022.

Antimicrobial agent	2019				2020				2021				2022			
	MRSA (*n*=10)		MSSA (*n*=4,strains)		MRSA (*n*=8,strains)		MSSA (*n*=17)		MRSA (*n*=0)		MSSA (*n*=17)		MRSA (*n*=12)		MSSA (*n*=17)	
	R	S	R	S	R	S	R	S	R	S	R	S	R	S	R	S
Penicillin G	100.0	0.0	4	0	8	0	100.0	0.0	NA	NA	100.0	0.0	100.0	0.0	100.0	0.0
Oxacillin	100.0	0.0	0	4	8	0	0.0	100.0	NA	NA	0.0	100.0	100.0	0.0	0.0	100.0
Gentamicin	0.0	100.0	0	4	6	2	0.0	100.0	NA	NA	0.0	100.0	0.0	91.7	0.0	100.0
Rifampin	0.0	100.0	0	4	0	8	0.0	100.0	NA	NA	0.0	100.0	0.0	100.0	0.0	100.0
Levofloxacin	20.0	40.0	0	4	4	4	47.1	52.9	NA	NA	0.0	100.0	16.7	83.3	11.8	88.2
Moxifloxacin	20.0	80.0	0	4	4	4	47.1	52.9	NA	NA	0.0	100.0	8.3	83.3	11.8	88.2
Trimethoprim/sulfamethoxazole	0.0	100.0	0	4	2	6	0.0	100.0	NA	NA	11.8	88.2	0.0	100.0	11.8	88.2
Erythromycin	100.0	0.0	3	1	8	0	47.1	52.9	NA	NA	70.6	29.4	41.7	58.3	41.2	58.8
Linezolid	0.0	100.0	0	4	0	8	0.0	100.0	NA	NA	0.0	100.0	0.0	100.0	0.0	100
Vancomycin	0.0	100.0	0	4	0	8	0.0	100.0	NA	NA	0.0	100.0	0.0	100.0	0.0	100

MRSA, Methicillin-resistant *Staphylococcus aureus*; MSSA, Methicillin-sensitive *Staphylococcus aureus*; Less than 10 bacterial strains, the resistance and sensitivity rates are replaced by the number of bacterial strains; NA, not available.

TABLE 3 Resistance and sensitivity rates of coagulase-negative *Staphylococcus* isolated from blood culture to antimicrobial agents from 2019 to 2022.

Antimicrobial agent	MRCNS							
	2019 (*n*=25)		2020 (*n*=44)		2021 (*n*=116)		2022 (*n*=110)	
	R	S	R	S	R	S	R	S
Penicillin G	100.0	0.0	100.0	0.0	100.0	0.0	100.0	0.0
Oxacillin	100.0	0.0	100.0	0.0	100.0	0.0	100.0	0.0
Gentamicin	28.0	68.0	18.2	68.2	6.0	75.0	20.9	70.9
Rifampin	16.0	84.0	11.4	88.6	4.3	93.1	12.7	84.5
Levofloxacin	80.0	12.0	68.2	31.8	65.5	29.3	73.6	25.5
Moxifloxacin	64.0	12.0	52.3	31.8	48.3	29.3	53.6	25.5
Trime-thoprim/sulfamethoxazole	72.0	0.0	27.3	72.7	32.8	67.2	41.8	58.2
Erythromycin	96.0	4.0	81.8	13.6	84.5	13.8	74.5	25.5
Linezolid	0.0	100.0	0.0	100	0.0	100	0.0	100.0
Vancomycin	0.0	100.0	0.0	100	0.0	100	0.0	100.0
Antimicrobial agent	MSCNS							
	2019 (*n*=6)		2020 (*n*=8)		2021(*n*=20)		2022(*n*=27)	
	R (strains)	S (strains)	R (strains)	S (strains)	R	S	R	S
Penicillin G	6	0	8	0	55.0	45.0	85.2	14.8
Oxacillin	0	6	0	8	0.0	100.0	0.0	100.0
Gentamicin	0	6	0	8	0.0	90.0	0.0	100.0
Rifampin	0	6	0	8	10.0	90.0	0.0	100.0
Levofloxacin	4	2	6	2	30.0	70.0	22.2	77.8
Moxifloxacin	2	4	3	5	15.0	70.0	0.0	77.8
Trime-thoprim/Sulfamethoxazole	2	4	3	5	25.0	75.0	12.0	88.0
Erythromycin	4	3	5	3	65.0	25.0	59.3	37.0
Linezolid	0	6	0	8	0.0	100.0	0.0	100.0
Vancomycin	0	6	0	8	0.0	100.0	0.0	100.0

MRCNS, methicillin-resistant coagulase-negative *Staphylococcus*; MSCNS, methicillin-sensitive coagulase-negative *Staphylococcus*. Less than 10 bacterial strains, the resistance and sensitivity rates are replaced by the number of bacterial strains.

Enterococcus faecalis were resistant to vancomycin, though two strains of *Enterococcus faecium* were found to be resistant to linezolid.

3.3 Antibiotic resistances of enterobacterales

3.3.1 *Escherichia coli*

Escherichia coli exhibited increased carbapenem resistance rising from 0.0% in 2019 to 2.3% in 2022 (Table 5). The resistance rates of *Escherichia coli* to cefazolin, ceftazidime, and ceftriaxone exceeded 20.0%, with resistance to cefazolin and ceftriaxone increasing each year. However, resistance rates to amikacin and piperacillin-tazobactam remained relatively low. No strains were found resistant to imipenem, meropenem, tigecycline, or polymyxin B. Resistance to ampicillin-Sulbactam, Cefazolin, Cefepime, Levofloxacin, and Trime-thoprim/sulfamethoxazole varied significantly each year, demonstrating statistical significance.

3.3.2 *Klebsiella pneumoniae*

Klebsiella pneumoniae demonstrated resistance rates to carbapenem antibiotics that were consistently exceeding 20.0% from 2019 to 2022 (Table 6). The resistance rates of cefazolin, ceftazidime, ceftriaxone, and cefepime exceeded 20.0%. *Klebsiella pneumoniae* demonstrated slightly higher resistance rates than *Escherichia coli*. Both bacteria exhibited their highest resistance rates in 2021, with some declines observed in 2022. Significant annual variations in resistance rates were observed for all tested antibiotics ($p < 0.05$).

The comparison of antibiotic resistance rates between *E. coli* and *K. pneumoniae* from 2019 to 2022 is shown in Figure 1.

3.3.3 *Enterobacter cloacae*

Enterobacter cloacae exhibited a rising trend in resistance rates to carbapenem antibiotics, increasing from 0.0% in 2019 to 19.0% in 2022 (Table 7). The resistance rates to piperacillin, cefotiam, and ceftriaxone all exceeded 80.0%. The resistance rate to piperacillin-tazobactam decreased from 75.0 to 38.1%, and the resistance rate to amikacin decreased from 100 to 52.4%. There were no significant changes in resistance rates to gentamicin, levofloxacin,

TABLE 4 Resistance and sensitivity rates of *Enterococcus* spp. isolated from blood culture to antimicrobial agents from 2019 to 2022.

Antimicrobial agent	Entercocccus faecium							
	2019 (*n*=1)		2020 (*n*=26)		2021 (*n*=34)		2022 (*n*=28)	
	R(strains)	S(strains)	R	S	R	S	R	S
Penicillin G	0	1	100.0	0.0	91.2	8.8	100.0	0.0
Ampicillin	0	1	100.0	0.0	88.2	11.8	100.0	0.0
Gentamicin-high	0	1	34.6	61.5	32.4	67.6	39.3	60.7
Erythromycin	1	0	96.2	0.0	82.4	0.0	50.0	50.0
Levofloxacin	1	0	69.2	30.8	64.7	29.4	55.9	28.6
Linezolid	0	1	0.0	100.0	0.0	100.0	0.0	100.0
Vancomycin	0	1	0.0	100.0	0.0	100.0	0.0	100.0
Antimicrobial agent	Entercocccus faecalis							
	2019 (*n*=7)		2020 (*n*=7)		2021 (*n*=4)		2022 (*n*=10)	
	R (strains)	S (strains)	R (strains)	S (strains)	R (strains)	S (strains)	R	S
Penicillin G	3	4	3	4	2	2	20.0	80.0
Ampicillin	0	7	0	7	0	4	0.0	100.0
Gentamicin-high	3	4	2	5	1	3	20.0	80.0
Erythromycin	7	0	7	0	3	1	40.0	0.0
Levofloxacin	2	4	1	6	1	3	10.0	90.0
Linezolid	0	7	0	7	0	4	20.0	80.0
Vancomycin	0	7	0	7	0	4	0.0	100.0

Less than 10 bacterial strains, the resistance and sensitivity rates are replaced by the number of bacterial strains.

TABLE 5 Resistance and sensitivity rates of *Escherichia Coli* isolated from blood culture to antimicrobial agents from 2019 to 2022.

Antimicrobial agent	2019(*n*=24)		2020 (*n*=15)		2021 (*n*=64)		2022 (*n*=86)		χ^2	*P*
	R	S	R	S	R	S	R	S		
Ampicillin	79.2	20.8	93.3	6.7	79.7	12.5	90.7	9.3	5.194	0.158
Piperacillin	54.2	45.8	60.0	33.3	78.1	20.3	74.4	19.8	6.292	0.098
Ampicillin-Sulbactam	33.3	50.0	80.0	6.7	64.1	28.1	59.3	25.6	9.966	0.019
Piperacillin-Tazobactam	0.0	100.0	0.0	100.0	1.6	96.9	4.7	94.2	2.694	0.441
Cefazolin	45.8	54.2	46.7	53.3	87.5	12.5	69.7	30.2	20.180	< 0.001
Ceftazidime	26.3	73.7	26.7	73.3	32.8	65.6	32.6	67.4	0.725	0.867
Ceftriaxone	58.3	41.7	46.7	53.3	60.9	39.1	58.1	41.9	1.018	0.797
Cefepime	41.7	50.0	35.8	60.3	34.4	59.4	7.0	86.0	22.938	< 0.001
Cefotetan	0.0	100.0	0.0	100.0	0	100	2.3	96.5	–	–
Aztreonam	33.3	66.7	46.7	53.3	48.4	51.6	37.2	62.8	2.746	0.433
Imipenem	0.0	100.0	0.0	100.0	0	100	2.3	97.7	–	–
Meropenem	0.0	100.0	0.0	100.0	0	100	2.3	97.7	–	–
Amikacin	0.0	100.0	0.0	100.0	1.6	98.4	0.0	100	–	–
Gentamicin	20.8	79.2	33.3	66.7	43.8	53.1	37.2	62.8	4.028	0.258
Tobramycin	16.7	66.7	20.0	66.7	21.9	50.0	15.1	67.4	1.344	0.726
Ciprofloxacin	45.8	54.2	73.3	26.7	51.6	45.3	62.8	37.2	4.787	0.188
Levofloxacin	25.0	66.7	73.3	26.7	51.6	48.4	60.5	33.7	11.982	0.007
Trime-thoprim/sulfamethoxazole	33.3	66.7	26.7	73.3	56.2	43.8	55.8	44.2	8.051	0.045
Tigecycline	0.0	100.0	0.0	100.0	0.0	100	0.0	100	–	–
Polymyxin B	0.0	100.0	0.0	100.0	0.0	100	0.0	100	–	–

10.3389/fmicb.2025.1464573

TABLE 6 Resistance and sensitivity rates of *Klebsiella pneumoniae* isolated from blood culture to antimicrobial agents from 2019 to 2022.

Antimicrobial agent	2019(n = 46)		2020 (*n* = 47)		2021 (*n* = 49)		2022 (*n* = 38)		χ^2	*P*
	R	S	R	S	R	S	R	S		
Piperacillin	23.4	76.6	38.3	61.7	55.1	22.4	15.8	81.6	17.685	0.001
Ampicillin-Sulbactam	24.5	72.7	59.6	40.4	79.6	20.4	14.4	83.2	45.287	< 0.001
Piperacillin-Tazobactam	20.2	77.8	29.8	70.2	49.0	49.0	11.1	88.9	16.170	0.001
Cefazolin	50.2	48.7	53.2	44.8	81.6	17.4	53.2	41.1	13.947	0.003
Ceftazidime	24.9	69.1	38.3	53.2	59.2	36.7	23.7	76.3	13.695	0.003
Ceftriaxone	23.1	68.9	40.4	58.6	65.3	34.7	26.3	73.7	18.130	<0.001
Cefepime	22.4	72.6	29.8	70.2	59.2	40.8	21.1	73.7	17.973	<0.001
Cefotetan	28.1	71.7	19.1	63.8	14.3	85.7	2.6	97.4	10.250	0.017
Aztreonam	28.7	71.3	38.3	61.7	63.3	36.7	28.9	71.1	13.317	0.004
Imipenem	19.6	80.4	29.8	70.2	49.0	51.0	21.1	78.9	10.480	0.015
Meropenem	19.6	80.4	29.8	70.2	49.0	51.0	21.1	78.9	10.480	0.015
Amikacin	19.6	80.4	29.8	70.2	44.9	55.1	13.2	86.8	11.357	0.010
Gentamicin	15.2	84.8	29.3	70.7	40.8	59.2	10.5	89.5	11.905	0.008
Tobramycin	19.6	80.4	38.3	61.7	44.9	40.8	31.6	60.5	7.408	0.060
Ciprofloxacin	10.9	89.1	38.3	61.7	69.4	26.5	55.3	44.7	44.249	<0.001
Levofloxacin	10.9	89.1	38.3	61.7	65.3	30.6	52.6	44.7	39.089	<0.001
Trimethoprim/sulfamethoxazole	0.0	93.5	25.5	74.5	59.2	40.8	52.6	47.4	55.966	<0.001
Tigecycline	0.0	100.0	0.0	100.0	0.0	100.0	0.0	100	–	–
Polymyxin B	0.0	100.0	0.0	100.0	0.0	100.0	0.0	100	–	–

and ciprofloxacin. However, the resistance rate to trimethoprim-sulfamethoxazole increased from 25.0 to 61.9%.

3.4 Antibiotic resistances of non-fermenting gram-negative bacteria

3.4.1 *Pseudomonas aeruginosa*

The resistance rates of *Pseudomonas aeruginosa* to imipenem and meropenem ranged from 73.7 to 84.6%, with a noticeable decrease from 2019 to 2022 (Table 8). The resistance rates to piperacillin-tazobactam, cefotiam, cefepime, amikacin, and tobramycin were steady at approximately 10.0%. The resistance rate to ciprofloxacin decreased from 84.6% in 2019 to 0.0% in 2022, as did the resistance rate to levofloxacin, which decreased from 84.6% in 2019 to 29.2% in 2022. *Pseudomonas aeruginosa* did not display any resistance to polymyxin B.

3.4.2 *Acinetobacter baumannii*

Acinetobacter baumannii displayed a notable resistance to multiple antibiotics (Table 9). The resistance rate to amikacin increased from 16.7 to 72.2% in 2022, while resistance rates to imipenem and meropenem were consistently > 75.0%. The resistance rates to other antibiotics also exhibited a rising trend from 2019 to 2022. *Acinetobacter baumannii* did not display any resistance to tigecycline or polymyxin B. Resistance to ampicillin-Sulbactam, piperacillin-tazobactam, imipenem, meropenem, amikacin, tobramycin and Trime-thoprim/sulfamethoxazole varied significantly each year, demonstrating statistical significance ($p < 0.05$).

3.5 Carbapenem-resistant gram-negative bacilli

Between 2019 and 2022, the detection rates of carbapenem-resistant organisms (CRO) among gram-negative bacilli varied (Table 10). In 2019, CRO accounted for 4.1% (52 strains) of gram-negative bacilli, including 37 strains of *Klebsiella pneumoniae*, 2 strains of *Pseudomonas aeruginosa*, and 13 strains of *Acinetobacter baumannii*. In 2020, CRO accounted for 3.1% (40 strains) of gram-negative bacilli, including 14 strains of *Klebsiella pneumoniae*, 6 strains of *Raoultella planticola*, 11 strains of *Pseudomonas aeruginosa*, and 9 strains of *Acinetobacter baumannii*. In 2021, the CRO detection rate was 3.3% (42 strains), including 24 strains of *Klebsiella pneumoniae* and 18 strains of *Acinetobacter baumannii*. In 2022, the CRO detection was 3.8% (49 strains), including 2 strains of *Escherichia coli*, 8 strains of *Klebsiella pneumoniae*, 4 strains of *Enterobacter cloacae*, 17 strains of *Pseudomonas aeruginosa*, and 18 strains of *Acinetobacter baumannii*. Carbapenem-resistant *Klebsiella pneumoniae* (CRKP) and Carbapenem-resistant *Acinetobacter baumannii* (CRAB) were consistently identified from 2019 to 2022. CRKP showed a decreasing resistance to aminoglycosides but an increasing resistance to trimethoprim-sulfamethoxazole. Conversely, CRAB exhibited increasing resistance rates to amikacin and gentamicin,

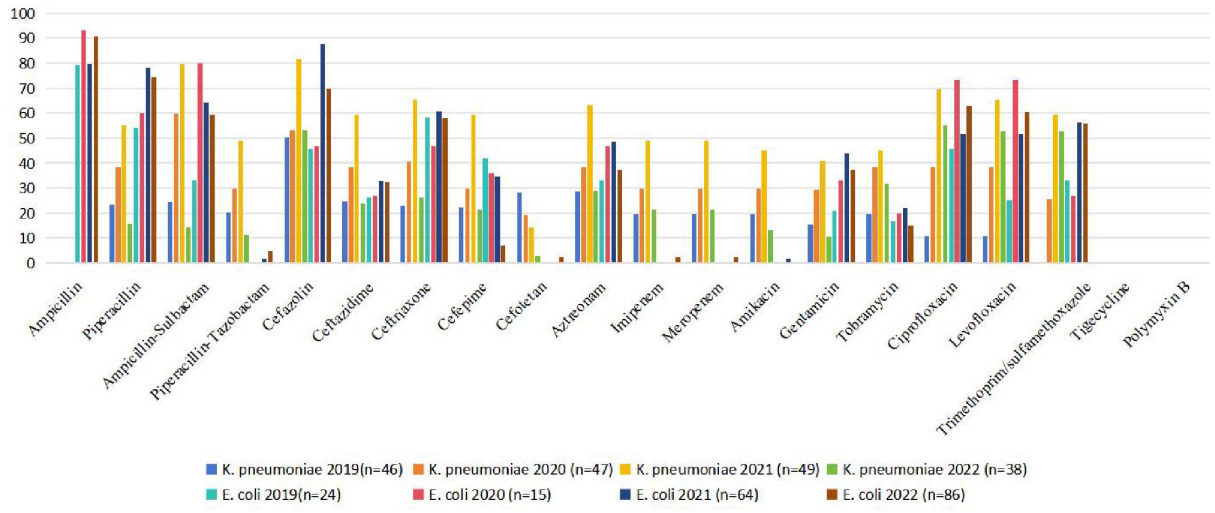

FIGURE 1
Comparison of antibiotic resistance rates of *E. coli* and *K. pneumoniae* (2019–2022). *E. coli, Escherichia coli*; *K. pneumoniae, Klebsiella pneumoniae*.

TABLE 7 Resistance and sensitivity rates of *Enterobacter cloacae* isolated from blood culture to antimicrobial agents from 2019 to 2022.

Antimicrobial agent	2019 (*n*=4)		2020 (*n*=9)		2021 (*n*=6)		2022 (*n*=21)	
	R(strains)	S (strains)	R (strains)	S (strains)	R (strains)	S (strains)	R	S
Piperacillin	4	0	9	0	6	0	85.7	0.0
Piperacillin-tazobactam	3	1	6	3	0	6	38.1	61.9
Ceftazidime	4	0	9	0	6	0	90.5	9.5
Ceftriaxone	4	0	9	0	6	0	100.0	0.0
Cefepime	1	3	3	6	0	6	33.3	47.6
Aztreonam	4	0	9	0	0	6	52.4	28.6
Imipenem	0	4	0	9	0	6	19.0	81.0
Meropenem	0	4	0	9	0	6	19.0	81.0
Amikacin	0	4	0	9	0	6	0.0	100.0
Gentamicin	1	3	3	6	0	6	47.6	52.4
Tobramycin	1	3	3	6	0	6	14.3	66.7
Ciprofloxacin	1	3	3	6	0	6	42.9	57.1
Levofloxacin	1	3	3	6	0	6	42.9	57.1
Trime-thoprim/sulfamethoxazole	1	3	3	6	0	6	61.9	38.1
Tigecycline	0	4	0	9	0	6	0.0	100.0
Polymyxin B	0	4	0	9	0	6	0.0	100.0

Less than 10 bacterial strains, the resistance and sensitivity rates are replaced by the number of bacterial strains.

from 16.7% in 2019 to 77.8% in 2022 and from 66.7% in 2019 to 94.4% in 2022, respectively. The resistance to trimethoprim-sulfamethoxazole increased from 61.5% in 2019 to 69.1% in 2022, while resistance to levofloxacin decreased from 100.0% in 2019 to 66.7% in 2022. Carbapenem-resistant *Enterobacter cloacae* (CREC) was only detected in 2022 and was sensitive to tigecycline, polymyxin B, and aminoglycoside antibiotics. Carbapenem-resistant *Pseudomonas aeruginosa* (CRPA) was identified in 2019, 2020, and 2022, with resistance rates to ceftazidime and cefepime increasing from 0.0% in 2019 to 70.6% in 2022 and from 0.0% in 2019 to 52.7% in 2022, respectively. The resistance rates of CRPA to ciprofloxacin and levofloxacin decreased from 100.0% in 2019 to 41.2% and 52.9% in 2022, respectively.

4 Discussion

Blood culture remains the gold standard for diagnosing bloodstream infections (BSIs) due to its accessibility, clinical utility, and ability to guide antibiotic susceptibility testing (Bai et al., 2022). While emerging molecular diagnostics (e.g.,

TABLE 8 Resistance and sensitivity rates of *Pseudomonas aeruginosa* isolated from blood culture to antimicrobial agents from 2019 to 2022.

Antimicrobial agent	2019 (*n*=4)		2020 (*n*=13)		2021 (*n*=4)		2022 (*n*=24)	
	R(strains)	S(strains)	R(strains)	S(strains)	R(strains)	S(strains)	R	S
Piperacillin-tazobactam	0	4	15.4	69.2	0	4	12.5	70.8
Ceftazidime	0	4	7.7	76.9	0	4	10.0	79.2
Cefepime	0	4	7.7	84.6	0	4	8.3	83.3
Imipenem	0	4	84.6	15.4	0	4	75.0	20.8
Meropenem	0	4	84.6	15.4	0	4	70.8	29.2
Amikacin	0	4	0.0	100	0	4	4.2	95.8
Tobramycin	0	4	7.7	92.3	0	4	0.0	100
Ciprofloxacin	2	2	84.6	15.4	2	2	0.0	100
Levofloxacin	2	2	84.6	15.4	2	2	29.2	62.5
Polymyxin B	0	4	0.0	100.0	0	4	0.0	100.0

Less than 10 bacterial strains, the resistance and sensitivity rates are replaced by the number of bacterial strains.

TABLE 9 Resistance and sensitivity rates of *Acinetobacter baumannii* isolated from blood culture to antimicrobial agents from 2019 to 2022.

Antimicrobial agent	2019 (*n*=14)		2020 (*n*=12)		2021 (*n*=18)		2022 (*n*=18)		χ^2/F	*P*
	R	S	R	S	R	S	R	S		
Piperacillin	100.0	0.0	100.0	0.0	100	0.0	100.0	0.0	–	–
Ampicillin/Sulbactam	42.9	57.1	58.3	25.0	72.2	11.1	77.8	5.6	13.328	0.021
Piperacillin-tazobactam	92.9	7.1	75.0	25.0	100	0.0	100.0	0.0	9.528	0.014
Ceftazidime	92.9	7.1	66.7	16.7	83.3	0.0	88.9	0.0	6.949	0.243
Cefepime	92.9	7.1	66.7	25.0	77.8	0.0	83.3	0.0	9.719	0.056
Imipenem	92.9	7.1	75.0	25.0	100	0.0	100.0	0.0	6.530	0.019
Meropenem	92.9	7.1	75.0	25.0	100	0.0	100.0	0.0	6.530	0.019
Amikacin	42.9	57.1	16.7	83.3	55.6	38.9	72.2	22.2	35.209	< 0.001
Gentamicin	42.9	57.1	50.0	33.3	66.7	16.7	77.8	11.1	10.674	0.069
Tobramycin	42.9	57.1	75.0	25.0	72.2	11.1	100.0	0.0	19.706	< 0.001
Ciprofloxacin	57.1	42.9	58.3	41.7	61.1	16.7	88.9	5.6	12.554	0.023
Levofloxacin	50.0	50.0	50.0	50.0	66.7	22.2	66.7	16.7	8.076	0.180
Trime-thoprim/sulfamethoxazole	21.4	78.6	33.3	66.7	55.6	44.4	83.3	16.7	14.186	0.002
Tigecycline	0.0	100.0	0.0	100.0	0.0	100.0	0.0	100.0	-	-
Polymyxin B	0.0	100.0	0.0	100.0	0.0	100.0	0.0	100.0	-	-

PCR-based assays) offer rapid pathogen identification, blood culture remains indispensable for capturing viable pathogens and resistance profiles, particularly in critically ill ICU patients requiring timely targeted therapy (El Haddad et al., 2018). The isolation of clinically-relevant pathogens via blood culture indicates that the defense mechanisms of the host and/or prior clinical interventions were unsuccessful in eradicating the infecting pathogens at the primary infection site. Moreover, the specific types of pathogens identified via blood culture offer important prognostic insights (El Haddad et al., 2018; Wildenthal et al., 2023). When multidrug-resistant organisms are identified in blood cultures, the patient mortality rate is as high as 35% (Abu-Saleh et al., 2018; GBD 2019 Antimicrobial Resistance Collaborators, 2022).

From 2019 to 2022, a total of 1,282 distinct strains were isolated from the positive blood cultures of patients in the ICU at the Second Affiliated Hospital of Xi'an Jiaotong University. gram-positive bacteria (52.0%) slightly outnumbered gram-negative isolates (48.0%), aligning with global ICU trends (Li et al., 2022; Van An et al., 2023). However, the data in this study may be biased due to a lower number of strains in 2021. Among the gram-positive bacteria, coagulase-negative staphylococci were the most common, followed by *Enterococcus faecalis* and *Staphylococcus aureus*. MRSA displayed a decreasing resistance to gentamicin, levofloxacin, moxifloxacin, trimethoprim-sulfamethoxazole, and erythromycin from 2019 to 2022. No resistance to vancomycin, linezolid, or rifampicin was observed in *Staphylococcus aureus*. However, coagulase-negative staphylococci (CoNS) accounted for 28.0% of isolates, raising questions about their clinical significance. While CoNS are frequent blood culture contaminants due to improper skin disinfection (Wang et al., 2023), they may

TABLE 10 Resistance rate and sensitivity rate of carbapenem resistant gram-negative bacteria isolated from blood culture to antimicrobial agents from 2019 to 2022.

Antimicrobial agents	2020(*n*=40)								2021(*n*=42)				2022(*n*=49)									
	kpn(*n* = 14)		kpl(*n*=6)		pae(*n*=11)		aba(*n*=9)		kpn(*n*=24)		aba(*n*=18)		eco(*n*=2)		kpn(*n*=8)		ecl(*n*=4)		pae(*n*=17)		aba(*n*=18)	
	R	S	R	S	R	S	R	S	R	S	R	S	R	S	R	S	R	S	R	S	R	S
Ampicillin	NA	NA	NA	NA	NA	NA	NA	NA	NA	NA	NA	NA	100.0	0.0	NA	NA	NA	NA	NA	NA	NA	NA
Piperacillin	100.0	0.0	100.0	0.0	NA	NA	100.0	0.0	100.0	0.0	100.0	0.0	100.0	0.0	100.0	0.0	NA	NA	NA	NA	100.0	0
Ampicillin/Sulbactam	100.0	0.0	100.0	0.0	NA	NA	100.0	0.0	100.0	0.0	100.0	0.0	100.0	0.0	100.0	0.0	NA	NA	NA	NA	100.0	0
Piperacillin-tazobactam	100.0	0.0	100.0	0.0	0.0	90.9	100.0	0.0	100.0	0.0	100.0	0.0	100.0	0.0	100.0	0.0	100.0	0.0	0.0	100.0	100.0	0
Cefazolin	100.0	0.0	100.0	0.0	NA	NA	NA	NA	100.0	0.0	NA	NA	100.0	0.0	100.0	0.0	NA	NA	NA	NA	NA	NA
Ceftazidime	100.0	0.0	100.0	0.0	0.0	81.8	100.0	0.0	100.0	0.0	100.0	0.0	100.0	0.0	100.0	0.0	100.0	0.0	70.6	11.8	100.0	0
Ceftriaxone	100.0	0.0	100.0	0.0	NA	NA	100.0	0.0	100.0	0.0	100.0	0.0	100.0	0.0	100.0	0.0	100.0	0.0	NA	NA	100.0	0
Cefepime	100.0	0.0	100.0	0.0	0.0	90.9	100.0	0.0	100.0	0.0	100.0	0.0	100.0	0.0	100.0	0.0	100.0	0.0	52.9	29.4	100.0	0
Cefotetan	100.0	0.0	100.0	0.0	NA	NA	NA	NA	100.0	0.0	NA	NA	100.0	0.0	100.0	0.0	NA	NA	NA	NA	NA	NA
Aztreonam	100.0	0.0	0.0	100.0	NA	NA	NA	NA	100.0	0.0	NA	NA	100.0	0.0	100.0	0.0	0.0	100.0	NA	NA	NA	NA
Imipenem	100.0	0.0	100.0	0.0	100.0	0.0	100.0	0.0	100.0	0.0	100.0	0.0	100.0	0.0	100.0	0.0	100.0	0.0	100.0	0.0	100.0	0
Meropenem	100.0	0.0	100.0	0.0	100.0	0.0	100.0	0.0	100.0	0.0	100.0	0.0	100.0	0.0	100.0	0.0	100.0	0.0	88.2	11.8	100.0	0
Amikacin	100.0	0.0	0.0	100.0	0.0	100.0	22.2	77.8	83.3	16.7	16.7	83.3	0.0	100.0	50.0	50.0	0.0	100.0	0.0	100.0	77.8	22.2
Gentamicin	100.0	0.0	100.0	0.0	NA	NA	66.7	11.1	100.0	0.0	66.7	33.3	0.0	100.0	62.5	37.5	0.0	100.0	NA	NA	94.4	0
Tobramycin	100.0	0.0	100.0	0.0	9.1	90.9	100.0	0.0	83.3	16.7	100.0	0.0	0.0	100.0	50.0	50.0	0.0	100.0	0.0	100.0	100.0	0
Ciprofloxacin	100.0	0.0	100.0	0.0	100.0	0.0	100.0	0.0	100.0	0.0	100.0	0.0	100.0	0.0	100.0	0.0	0.0	100.0	41.2	47.1	100.0	0
Levofloxacin	100.0	0.0	100.0	0.0	100.0	0.0	100.0	0.0	100.0	0.0	83.3	11.1	100.0	0.0	100.0	0.0	0.0	100.0	52.9	23.5	66.7	33.3
Trime-thoprim/sulfamethoxazole	28.6	71.4	100.0	0.0	NA	NA	44.4	55.6	100.0	0.0	61.1	38.9	100.0	0.0	62.5	37.5	100.0	0.0	NA	NA	77.8	22.2
Tigecycline	0.0	100.0	0.0	100.0	NA	NA	0.0	100.0	0.0	100.0	0.0	100.0	0.0	100.0	0.0	100.0	0.0	100.0	NA	NA	0.0	100.0
Polymyxin B	0.0	100.0	0.0	100.0	0.0	100.0	0.0	100.0	0.0	100.0	0.0	100.0	0.0	100.0	0.0	100.0	0.0	100.0	0.0	100.0	0.0	100.0

Kpn, *Klebsiella pneumoniae*; kpl, *Raoultella planticola*; pae, *Pseudomonas aeruginosa*; aba, *Acinetobacter baumannii*; eco, *Escherichia coli*; ecl, *Enterobacter cloacae*; NA, not available.

10.3389/fmicb.2025.1464573

represent true pathogens in immunocompromised patients or those with indwelling devices (Heilmann et al., 2019). In our cohort, standardized blood culture collection were followed, yet persistent CoNS isolation underscores the need for rigorous clinical correlation to distinguish contamination from true infection. The resistance rates of MRCNS to gentamicin, rifampicin, levofloxacin, moxifloxacin, and erythromycin did not change significantly throughout the study period, though the resistance of MRCNS to trimethoprim-sulfamethoxazole increased slightly. MRCNS were not resistant to vancomycin or linezolid; therefore, these are the preferred antibiotics for clinical Staphylococcus infections. The Enterococcus genus constituted 11.0% of the isolated strains in our hospital, with *Enterococcus faecium* displaying higher resistance rates than *Enterococcus faecalis*. More specifically, *Enterococcus faecium* exhibited high resistance to ampicillin, while *Enterococcus faecalis* was sensitive to ampicillin. The resistance of *Enterococcus faecium* decreased from 2019 to 2022, while *Enterococcus faecalis* was slightly resistant to penicillin and erythromycin. Neither *Enterococcus faecium* nor *Enterococcus faecalis* displayed resistance to vancomycin, though two *Enterococcus faecium* strains were resistant to linezolid.

The rising carbapenem resistance in Enterobacterales is alarming. *Escherichia coli* exhibited a carbapenem resistance increase from 0% (2019) to 2.3% (2022), while *Klebsiella pneumoniae* maintained resistance rates exceeding 20% throughout the study period. Nevertheless, the overall resistance rates decreased from 2019 to 2022. According to the 2023 CHINET China Bacterial Resistance Surveillance data, *Klebsiella pneumoniae* had resistance rates of 26.2 and 27.1% to imipenem and meropenem, respectively, which are similar to the national resistance levels (Hu et al., 2022). These trends are likely driven by horizontal gene transfer of blaKPC carbapenemases (Han et al., 2021) and prolonged carbapenem use in critically ill patients. *Enterobacter cloacae* demonstrated an increase in resistance rates to carbapenem antibiotics from 2019 to 2022. No resistance to tigecycline or polymyxin B was observed among bacteria in Enterobacterales. Therefore, it is imperative to prioritize the identification and management of risk factors associated with carbapenemase-induced nosocomial infections.

Among non-fermenting gram-negative bacteria, *Pseudomonas aeruginosa* displayed relatively high sensitivity to piperacillin-tazobactam, cefotiam, cefepime, amikacin, and tobramycin. However, its resistance rates to imipenem and meropenem decreased during the study period. *Pseudomonas aeruginosa* did not display resistance to polymyxin B. In contrast, *Acinetobacter baumannii* remained sensitive to tigecycline and polymyxin B. However, resistance rates to imipenem and meropenem were high from 2019 to 2022. The rise in carbapenem resistance aligns with global trends (GBD 2019 Antimicrobial Resistance Collaborators, 2022), particularly in A. baumannii (100% resistance in 2022), surpassing national averages reported by CHINET (26od.%) (Hu et al., 2022). It is likely due to various factors, including compromised immunity in patients in the ICU and prolonged use of broad-spectrum antibiotics (Teerawattanapong et al., 2018; Kaye et al., 2023). This phenomenon may also be linked to the production of carbapenemase hydrolytic enzymes, decreased outer membrane permeability or loss of porins, reduced affinity of penicillin-binding proteins, and overexpression of efflux pumps (Abdi et al., 2020; Somily et al., 2022).

The ICU is a high-incidence area of multidrug-resistant organisms and carries a considerable disease burden. Research shows that the six leading pathogens for deaths associated with resistance-related deaths—*Escherichia coli*, *Staphylococcus aureus*, *Klebsiella pneumoniae*, *Streptococcus pneumoniae*, *Acinetobacter baumannii*, and *Pseudomonas aeruginosa*—were responsible for approximately 929,000 (660,000–1,270,000) deaths ascribed to AMR and 3.57 million (2.62–4.78) deaths associated with AMR in 2019. Due to various factors, the number of detected strains in individual years is relatively small, and some drug resistance rates may be skewed.Clinical implications of resistance patterns demand urgent action. For gram-positive infections, vancomycin and linezolid remain effective against *staphylococci* and *enterococci*, though two *Enterococcus faecium* linezolid-resistant strains highlight emerging threats. For gram-negative infections, carbapenem-sparing regimens (e.g., ceftazidime-avibactam for *K. pneumoniae*) should be prioritized where susceptibility permits, while polymyxins and tigecycline serve as last-resort options. For critically ill patients in the ICU, who often undergo invasive medical procedures and have multiple underlying conditions and compromised immune function, the detection of CRO in blood specimens is associated with an increased risk of mortality, emphasizing the need for prompt, effective, and precise treatment (Yi and Kim, 2021; Martínez et al., 2023).

Study limitations include its single-center, retrospective design and small annual sample sizes (e.g., 2021), which may skew resistance rates due to stochastic variation. To mitigate this, we aggregated data across the 4-year period to identify overarching trends. Additionally, infection control measures (e.g., enhanced environmental decontamination, antimicrobial stewardship programs) were implemented during the study period, potentially influencing resistance dynamics. Future multicenter studies with larger cohorts are needed to validate these findings.

5 Conclusion

The pathogens responsible for BSI and their antimicrobial resistance profiles are constantly changing. Timely surveillance of pathogen distribution and resistance trends in blood cultures remain indispensable for guiding empirical antibiotic choices in ICU patients with infections. The resistance patterns reported here offer actionable insights to optimize treatment regimens and inform antimicrobial stewardship efforts in critical care settings.

Data availability statement

The original contributions presented in the study are included in the article/supplementary material,

further inquiries can be directed to the corresponding authors.

Ethics statement

The studies involving humans were approved by Ethics Committee of the Second Affiliated Hospital of Xi'an Jiaotong University School of Medicine. The studies were conducted in accordance with the local legislation and institutional requirements. The participants provided their written informed consent to participate in this study. The manuscript presents research on animals that do not require ethical approval for their study.

Author contributions

ZL: Data curation, Funding acquisition, Writing – original draft, Writing – review & editing. HC: Methodology, Writing – review & editing. JL: Data curation, Formal Analysis, Writing – review & editing. XZ: Formal Analysis, Writing – original draft. JY: Data curation, Writing – review & editing. YZ: Funding acquisition, Writing – review & editing. XY: Funding acquisition, Validation, Writing – review & editing. YG: Supervision, Validation, Writing – review & editing.

Funding

The author(s) declare that financial support was received for the research and/or publication of this article. This study was supported by the Key Research and Development Plan of Shaanxi Province (2024SF-YBXM-160), the Key Research and Development Program of Shaanxi Province (2020SF-173), the National Natural Science Foundation of China (82370604), and Natural Science Foundation of Fujian Province (2023J01239).

Conflict of interest

The authors declare that the research was conducted in the absence of any commercial or financial relationships that could be construed as a potential conflict of interest.

Publisher's note

References

Abdi, S. N., Ghotaslou, R., Ganbarov, K., Mobed, A., Tanomand, A., Yousefi, M., et al. (2020). *Acinetobacter baumannii* efflux pumps and antibiotic resistance. *Infect. Drug Resist.* 13, 423–434. doi: 10.2147/IDR.S228089

Abu-Saleh, R., Nitzan, O., Saliba, W., Colodner, R., Keness, Y., Yanovskay, A., et al. (2018). Bloodstream infections caused by contaminants: Epidemiology and risk factors: A 10-year surveillance. *Isr. Med. Assoc. J.* 20, 433–437.

Antimicrobial Resistance Collaborators (2022). Global burden of bacterial antimicrobial resistance in 2019: A systematic analysis. *Lancet* 399, 629–655. doi: 10.1016/S0140-6736(21)02724-0

Bai, A. D., Lo, C. K. L., Komorowski, A. S., Suresh, M., Guo, K., Garg, A., et al. (2022). Staphylococcus aureus bacteraemia mortality: A systematic review and meta-analysis. *Clin. Microbiol. Infect.* 28, 1076–1084. doi: 10.1016/j.cmi.2022.03.015

Centers for Disease Control and Prevention [CDC] (2023). *Antibiotic resistance threats in the United States*. Atlanta, GA: Centers for Disease Control and Prevention.

Cheng, M. P., Stenstrom, R., Paquette, K., Yansouni, C., and Sweet, D. (2020). Blood culture results before and after antimicrobial administration. *Ann. Intern. Med.* 172, 440–441. doi: 10.7326/L19-0796

Clinical and Laboratory Standards Institute [CLSI] (2022). *Performance standards for antimicrobial susceptibility testing*. Wayne, PA: CLSI.

El Haddad, H., Chaftari, A. M., Hachem, R., Chaftari, P., and Raad, I. I. (2018). Biomarkers of sepsis and bloodstream infections: The role of procalcitonin and proadrenomedullin with emphasis in patients with cancer. *Clin. Infect. Dis.* 67, 971–977. doi: 10.1093/cid/ciy331

European Centre for Disease Prevention and Control [ECDC] (2022). *Surveillance of antimicrobial resistance in Europe*. Sweden: European Centre for Disease Prevention and Control.

Fabre, V., Carroll, K. C., and Cosgrove, S. E. (2022). Blood culture utilization in the hospital setting: A call for diagnostic stewardship. *J. Clin. Microbiol.* 60:e0100521. doi: 10.1128/JCM.01005-21

Fleischmann-Struzek, C., Mellhammar, L., Rose, N., Cassini, A., Rudd, K. E., Schlattmann, P., et al. (2020). Incidence and mortality of hospital- and ICU-treated sepsis: Results from an updated and expanded systematic review and meta-analysis. *Intensive Care Med.* 46, 1552–1562. doi: 10.1007/s00134-020-06151-x

GBD 2019 Antimicrobial Resistance Collaborators (2022). Global mortality associated with 33 bacterial pathogens in 2019: A systematic analysis for the Global Burden of Disease Study 2019. *Lancet* 400, 2221–2248. doi: 10.1016/S0140-6736(22)02185-7

Gonzalez, M. D., Chao, T., and Pettengill, M. A. (2020). Modern blood culture: Management decisions and method options. *Clin. Lab. Med.* 40, 379–392. doi: 10.1016/j.cll.2020.07.001

Han, R. R., Guo, Y., Peng, M. J., Shi, Q., Wu, S., Yang, Y., et al. (2021). Evaluation of the immunochromatographic NG-test carba 5, RESIST-5 O.O.K.N.V., and IMP K-SeT for rapid detection of KPC-, NDM-, IMP-, VIM-type, and OXA-48-like carbapenemase among *Enterobacterales*. *Front. Microbiol.* 11:609856. doi: 10.3389/fmicb.2020.609856

Heilmann, C., Ziebuhr, W., and Becker, K. (2019). Are coagulase-negative staphylococci virulent? *Clin. Microbiol. Infect.* 25, 1071–1080. doi: 10.1016/j.cmi.2018.11.012

Hu, F., Yuan, L., Yang, Y., Xu, Y., Huang, Y., Hu, Y., et al. (2022). A multicenter investigation of 2,773 cases of bloodstream infections based on China antimicrobial surveillance network (CHINET). *Front. Cell. Infect. Microbiol.* 12:1075185. doi: 10.3389/fcimb.2022.1075185

Kaye, K. S., Shorr, A. F., Wunderink, R. G., Du, B., Poirier, G. E., Rana, K., et al. (2023). Efficacy and safety of sulbactam-durlobactam versus colistin for the treatment of patients with serious infections caused by *Acinetobacter baumannii*-calcoaceticus complex: A multicentre, randomised, active-controlled, phase 3, non-inferiority clinical trial (ATTACK). *Lancet Infect. Dis.* 23, 1072–1084. doi: 10.1016/S1473-3099(23)00184-6

Lan, P., Jiang, Y., Zhou, J., and Yu, Y. (2021). A global perspective on the convergence of hypervirulence and carbapenem resistance in *Klebsiella pneumoniae*. *J. Glob. Antimicrob. Resist.* 25, 26–34. doi: 10.1016/j.jgar.2021.02.020

Li, J., Jiang, F., Xie, A., and Jiang, Y. (2022). Analysis of the distribution and drug resistance of pathogens in patients with urinary tract infection in the eastern Chongming area of shanghai from 2018 to 2020. *Infect. Drug Resist.* 15, 6413–6422. doi: 10.2147/IDR.S384515

Magiorakos, A. P., Burns, K., Rodríguez-Baño, J., Borg, M., Daikos, G., Dumpis, U., et al. (2017). Infection prevention and control measures and tools for the prevention of entry of carbapenem-resistant *Enterobacteriaceae* into healthcare settings: Guidance from the European Centre for Disease Prevention and Control. *Antimicrob. Resist. Infect. Control.* 6:113. doi: 10.1186/s13756-017-0259-z

Martínez, D. A., Cai, J., Lin, G., Goodman, K. E., Paul, R., Lessler, J., et al. (2023). Modelling interventions and contact networks to reduce the spread of carbapenem-resistant organisms between individuals in the ICU. *J. Hosp. Infect.* 136, 1–7. doi: 10.1016/j.jhin.2023.02.016

Mazi, W. A., Abdulwahab, M. H., Alashqar, M. A., Aldecoa, Y. S., Bahat, Z. R., Suaking, J. L., et al. (2021). Sustained low incidence rates of central line-associated blood stream infections in the intensive care unit. *Infect. Drug Resist.* 14, 889–894. doi: 10.2147/IDR.S290791

Somily, A., Balkhy, H. H., Enani, M. A. S., Althawadi, S. I., Alawi, M., Al Johani, S. M., et al. (2022). Antimicrobial resistance trends of non-fermenter Gram negative bacteria in Saudi Arabia: A six-year national study. *J. Infect. Public Heal.* 14, 1144–1150. doi: 10.1016/j.jiph.2021.07.007

Tajima, T., Asai, Y., Endo, M., Suzuki, T., Matsunaga, N., Tsuzuki, S., et al. (2021). Rate of blood culture submissions in Japan as an indicator of bloodstream infections. *J. Infect. Chemother.* 27, 1270–1272. doi: 10.1016/j.jiac.2021.04.019

Teerawattanapong, N., Panich, P., Kulpokin, D., Na Ranong, S., Kongpakwattana, K., Saksinanon, A., et al. (2018). A systematic review of the burden of multidrug-resistant healthcare-associated infections among intensive care unit patients in Southeast Asia:the rise of multidrug-resistant *Acinetobacter baumannii*. *Infect. Control Hosp. Epidemiol.* 39, 525–533. doi: 10.1017/ice.2018.58

Van An, N., Hoang, L. H., Le, H. H. L., Thai Son, N., Hong, L. T., Viet, T. T., et al. (2023). Distribution and antibiotic resistance characteristics of bacteria isolated from blood culture in a teaching hospital in Vietnam during 2014–2021. *Infect. Drug Resist.* 16, 1677–1692. doi: 10.2147/IDR.S402278

Wang, S., Song, Y., Shi, N., Yin, D., Kang, J., Cai, W., et al. (2023). Characteristics, outcomes, and clinical indicators of bloodstream infections in neutropenic patients with hematological malignancies: A 7-year retrospective study. *Infect. Drug Resist.* 16, 4471–4487. doi: 10.2147/IDR.S413454

Wildenthal, J. A., Atkinson, A., Lewis, S., Sayood, S., Nolan, N. S., Cabrera, N. L., et al. (2023). Outcomes of partial oral antibiotic treatment for complicated Staphylococcus aureus bacteremia in people who inject drugs. *Clin. Infect. Dis.* 76, 487–496. doi: 10.1093/cid/ciac714

World Health Organization [WHO] (2021). *Antimicrobial resistance: Global report on surveillance*. Geneva: WHO.

Yi, J., and Kim, K. H. (2021). Identification and infection control of carbapenem-resistant *Enterobacterales* in intensive care units. *Acute Crit. Care* 36, 175–184. doi: 10.4266/acc.2021.00409

frontiers | Frontiers in Microbiology

TYPE Original Research
PUBLISHED 30 July 2025
DOI 10.3389/fmicb.2025.1608243

OPEN ACCESS

EDITED BY
Lucinda Janete Bessa,
Egas Moniz Center for Interdisciplinary Research (CiiEM), Portugal

REVIEWED BY
Thomas Maskow,
Helmholtz Association of German Research Centres (HZ), Germany
María Guembe,
Gregorio Marañón Hospital, Spain

*CORRESPONDENCE
Olivier Braissant
✉ olivier.braissant@unibas.ch

RECEIVED 08 April 2025
ACCEPTED 07 July 2025
PUBLISHED 30 July 2025

CITATION
Lafranca T, Bonkat G, Rieken M and Braissant O (2025) Efficacy of a commercial bacteriophage cocktail against planktonic cells and both thin and thick biofilms of skin pathogens, measured using isothermal microcalorimetry.
Front. Microbiol. 16:1608243.
doi: 10.3389/fmicb.2025.1608243

Efficacy of a commercial bacteriophage cocktail against planktonic cells and both thin and thick biofilms of skin pathogens, measured using isothermal microcalorimetry

Tecla Lafranca[1], Gernot Bonkat[1,2], Malte Rieken[1,2] and Olivier Braissant[1]*

[1]Department of Biomedical Engineering, University of Basel, Basel, Switzerland, [2]alta uro AG, Basel, Switzerland

Introduction: Skin and soft tissue infections are frequent and often require antibiotic treatment. However, for mild and self-limiting lesions, bacteriophage therapy could be an interesting treatment option that limits the use of antimicrobials and helps avoid the development of resistance. Still, very little is known about the efficacy of commercial phage cocktails against the biofilms encountered in these lesions. In this study, we investigated the use of a commercial phage cocktail against Staphylococci and Streptococci grown planktonically in thin and thick biofilms.

Methods: Isothermal microcalorimetry was used to monitor the metabolic activity of planktonic cells, as well as cells grown in thin or thick biofilms of common skin pathogens (*Staphylococcus aureus*, *Staphylococcus epidermidis*, and *Streptococcus agalactiae*), when exposed to the commercial phage cocktail.

Results: The use of phages against sensitive strains showed a rapid decrease in metabolic activity in planktonic cells. However, when applied to a thin biofilm, the effect was already less, although it was still important. Finally, no effect was visible on thick and mature biofilms.

Conclusion: The efficacy of bacteriophage cocktails is limited by the thickness and maturation of biofilms. In the case of skin and soft tissue infections, especially for chronic wounds, it might be necessary to mechanically remove and disrupt the biofilm through mechanical debridement to enable the phage product to be effective.

KEYWORDS

phage (bacteriophage), isothermal calorimetry, biofilms, *Staphylococcus*, phage therapies

Introduction

Skin and soft tissue infections (SSTIs) present a broad clinical spectrum, ranging from mild, self-limiting lesions, such as cellulitis, to serious, life-threatening conditions such as necrotizing fasciitis (Hatlen and Miller, 2021). The foot and lower leg are the most frequently affected body parts, particularly in diabetic patients (Shittu and Lin, 2006). A large proportion

of patients require medical treatment and hospitalization, and in some cases, the outcome is fatal (Moffarah et al., 2016). Current treatment options involve antibiotics and, if necessary, surgery (Hatlen and Miller, 2021). The bacterium responsible for most SSTIs is *Staphylococcus aureus* (*S. aureus*), which is a ubiquitous gram-positive bacterium (Hatlen and Miller, 2021). It is generally part of the natural flora but might become an opportunistic pathogen (Paharik and Horswill, 2016). *Staphylococcus aureus* is also the leading cause of various other serious infections, including bacteremia, meningitis, endocarditis, osteomyelitis, and pneumonia (Tong et al., 2015), and a leading cause of both hospital- and community-acquired infections worldwide (Lowy, 1998; Whittard et al., 2021).

Increasing evidence has confirmed the importance of biofilms in various skin conditions, such as diabetic and venous stasis ulcers, necrotizing fasciitis, pressure ulcers, cellulitis, atopic dermatitis, erythema nodosum, and erysipelas (Severn and Horswill, 2023). Indeed, biofilm formation in chronic wounds inhibits healing by delaying re-epithelialization (Schierle et al., 2009). Biofilms are communities of micro-organisms embedded in a matrix of polymeric substances characterized by three major growth phases: (1) attachment to the surface [in our field, e.g., on the soft tissues or the epidermal layer of the skin (Kumar et al., 2019)], (2) maturation, and (3) dispersion. Biofilms act as a protective layer against hostile physical and chemical hostile conditions, including antibacterial drugs. The induction and spread of resistant strains, such as methicillin- or vancomycin-resistant *S. aureus* (MRSA or VRSA) (Whittard et al., 2021), are of increasing concern. The continuous emergence of new resistance not only against penicillin but also against new agents such as linezolid (Tsiodras et al., 2001) highlights an urgent need to find new effective therapies. This situation necessitates increasing the antimicrobial dosage in response to rising minimal inhibitory concentration (MIC) or combining multiple antibiotics (Presterl et al., 2009).

Bacteriophage therapy is an option already used in some countries and is gaining popularity in Europe. Bacteriophages, or phages, are viruses that use bacterial hosts for replication, ultimately leading to the destruction of these bacteria (Kiani et al., 2021; Kim et al., 2021; Gündoğdu et al., 2016). Their discovery dates back to 1915, but after the discovery of penicillin, interest in phages waned in Western Europe and is only now resurfacing due to the emergence of antibiotic resistance (Clokie et al., 2011). However, in Russia and Georgia, research has been ongoing, and phage products are used in clinical settings and readily found in online pharmacies (Clokie et al., 2011). Western European agencies, on the other hand, require further research into these products; thus, phage therapy has not yet been accepted (Gordillo Altamirano and Barr, 2019).

Products found online are often a mix of different phage strains (or phage types) and are known as a cocktail. Indeed, phages exhibit high host specificity; therefore, using several phages in the same product broadens the spectrum of activity and increases the chance of therapy being efficient. It is also hypothesized to reduce the emergence of resistant variants (Chan and Abedon, 2012). For example, the cocktail used in this study (see later), called "Fersisi," can be found in an online pharmacy. The indications for such a product are broad, ranging from skin infections to otolaryngological diseases, surgical diseases, inflammations of the oral cavity, eye diseases, secondary infections of thermal burns, urogenital and gynecological infections, or enteric infections.[1] Although Russian literature on the use of phages cannot be assessed in detail, the results obtained to date are promising (Morozova et al., 2018). Phages appear to be a valid alternative to antibiotics (Jiang et al., 2021), as they are effective against several bacteria, including *S. aureus* in skin diseases (Kiani et al., 2021), and prevent or reduce the formation of their biofilm (Tan et al., 2020; Kelly et al., 2012; Alves et al., 2014). It has also been shown that the bacteria's virulence is decreased as sensitivity to certain antibiotics increases through the use of phages (León and Bastías, 2015). Similarly, combining phages with anitibiotics has been shown to be even more effective (Jiang et al., 2021; Łusiak-Szelachowska et al., 2020). However, the lack of validated clinical trials poses a challenge that needs to be addressed in the coming years (Parracho et al., 2012).

Analysis and testing of commercial phage products remain a challenge as culture-based conventional methods require a significant amount of time, resources, and laboratory staff. Similarly, optical density-based methods are also limited because some processes cannot be distinguished from others. Moreover, such methods perform poorly on solid and/or opaque substrates or media, making assessment of anti-biofilm activity an even bigger challenge. Therefore, this study utilizes an isothermal microcalorimeter (IMC) to investigate the use of these cocktails against *S. aureus* and assess the metabolic activity of planktonic cells, as well as thin and thick biofilms. IMC records the metabolic heat produced during bacterial growth in real-time, resulting in a heat flow curve that is directly comparable to the metabolic activity (see details in Bonkat et al., 2012; Nykyri et al., 2019; Braissant et al., 2020). IMC has been previously used to investigate the growth of Staphylococci and the effect of phages. For example, Molendijk et al. (2023) used different methods, including IMC, to assess the susceptibility of *S. aureus* to phage mixes and single phages. The antimicrobial efficacy and antibiofilm activity of phages against *Staphylococcus epidermidis* (*S. epidermidis*) were also demonstrated using IMC (Fanaei Pirlar et al., 2022). Similarly, the effect of antibiotics or phages on *S. aureus* biofilms was also investigated using a microcalorimeter (Butini et al., 2019; Sultan et al., 2022). This study aimed to analyze the effect of bacteriophages on planktonic cells in liquid cultures, on thin biofilms previously grown in a well plate calorimeter, and on thick biofilms using semi-permeable filters that can be easily transferred to fresh medium to allow further growth (Solokhina et al., 2018; Merritt et al., 2011; Solokhina et al., 2019).

Materials and methods

Microorganisms and phage products used

The bacteriophage used was the Fersisi (Eliava Biopreparations, Tbilisi, 0160, Georgia). The product was obtained from an online pharmacy as a box of five ampoules of phages with titers against Staphylococci (*S. aureus*, *S. epidermidis*) of no $<10^5$ mL^{-1}, and titers against Streptococci (*S. pyogenes*, *S. sanguis*, *S. salivarius*, *S. agalactiae*) of no $<10^4$ mL^{-1} (as indicated by the manufacturer). The Fersisi

1 https://mybacteriophage.net/products/fersisi-bakteriophagen-1-box-5-ampullen-x-10ml

bacteriophage cocktail was described in detail through previous metagenomic analysis (McCallin et al., 2018). *S. aureus* (ATCC 29213, ATCC 43300, and ATCC 25923), *S. epidermidis* (ATCC 49461), and *S. agalactiae* (DSM 6784) were obtained from the ATCC culture collection.

Calorimetry of liquid culture

The bacterial strains used were stored at −80°C. Before each experiment, purity was visually checked after overnight culture on agarized brain-heart infusion (BHI composition: calf brains, beef heart, peptone, sodium chloride, D-glucose, disodium hydrogen phosphate) at 37°C. After the initial purity check, one colony was taken and dissolved in 25 mL of liquid BHI. This liquid culture was incubated overnight until the stationary phase. This culture was diluted 20x in fresh BHI, and 7.5 mL of this inoculum was transferred to 20 mL glass ampoules. Two ampoules were added with 150 µL of bacteriophages from the beginning using a pipette. Two others were added with 150 µL of bacteriophages using the TAM admix ampoule injection system at different time points (between 1 and 3 h, corresponding to the early exponential phase). Finally, two ampoules without the addition of bacteriophages served as growth controls. After preparation, the samples were sealed and introduced into a TAM Air calorimeter (Waters/TA Instruments) that had been previously equilibrated at a temperature of 37°C ± 0.01°C. This device has eight measuring channels and eight slots for inert thermal references of the same heat capacity and conductivity as the samples, which were prepared with equal amounts of sterile PBS. Negative controls were prepared using two ampoules filled with uninoculated media. All measurements were performed in duplicates, and experiments were repeated twice.

Calorimetry of thin biofilm

Eight plastic inserts were prepared with 250 µL of solution prepared with 100x diluted overnight cultures, as described above. The inserts were then placed in titanium calorimetry vials and sealed. Following closure, they were placed in the Calscreener calorimeter (Symcel Sverige AB), according to the manual 3-step equilibration procedure. The Calscreener was previously equilibrated at 37°C for at least 2 days. After 1 day of incubation and once heat production returned to baseline, the planktonic cells were removed by pipetting. The non-adherent cells were removed by washing with BHI media, and finally, the insert containing the biofilm was refilled with the same amount of medium with or without bacteriophages. The phage treatment medium contained 10% phage product diluted in BHI. The growth controls were made with BHI only. Sterility controls were made with uninoculated BHI. All measurements were performed in four replicates.

Calorimetry of thick biofilm on nylon membrane

Previously sterilized nylon filters (1 cm × 3 cm–0.2 µm, Millipore, Burlington, MA, USA) were placed on BHI agar. A stationary-phase overnight culture of Staphylococci strains was spread on those filters using a 10 µL sterile inoculating loop. The plates with the biofilm were incubated at 37°C overnight. After biofilm formation under these conditions, the filters were transferred to fresh BHI agar until a mature biofilm state was achieved. Biofilms were considered mature when no visible changes could be seen in their size (surface and thickness on the filter) or appearance. This ensured that any changes detected in metabolic heat production were due to changes in metabolic activity induced by the antimicrobial treatment and not to further growth or extension of the biofilm on the membrane. All media and materials (including the cut nylon filters) were sterilized by autoclaving for 20 min at 121°C.

To detect biofilm heat production with IMC, mature biofilms grown on nylon filters were placed in 20 mL calorimetry glass vials (Waters/TA Instruments) containing slanted BHI agar. After sealing the ampoule, the sample was placed in the microcalorimeter (TAM3 - Waters/TA Instruments), and metabolic heat production was recorded in real-time. When metabolic heat production returned close to baseline, the vials were recovered from the calorimeter, and the same mature biofilms were exposed to bacteriophages. For this, 250 µL of phage product was applied to the biofilm until the solution was fully absorbed (within 5–10 min). After bacteriophage exposure, the nylon membranes bearing biofilms were transferred to fresh BHI agar vials to measure the heat flow again, following the same procedure. At the end of the experiment, the biofilms were heat-killed, and metabolic heat production was collected for the last time to establish a baseline signal. All measurements were performed in triplicate.

Data analysis

Each experiment was performed in at least duplicate. The data analysis was performed using the statistical program R (R Core Team, 2019) and the grofit package (Kahm et al., 2010). Heat flow curves were integrated to obtain the heat over time curves. The Gompertz growth model was used to fit the heat curves and further calculate the maximal growth rate (μ), the lag phase (λ), and the maximum heat (Q max). When several overlapping peaks were observed, those peaks were convoluted with Fityk (Wojdyr et al., 2004) using the Pearson VII model. Then, each individual peak of the data was analyzed as described above.

Results

Clear differences in phage product sensitivity were observed between planktonic cell cultures, thin biofilms, and thick biofilms (Table 1). Planktonic cells were the most affected, and a clear decrease of growth indicators μ and Q was observed in conjunction with an extension of the lag phase (λ). This effect on the lag phase was no longer visible for biofilm, as it had previously grown and already had a large active population of bacterial cells. With the increase in biofilm thickness, all effects were lost. All the details are provided in the specific sections.

Effect of bacteriophages on planktonic cells in liquid culture

The effect of the bacteriophages was tested for bacteria in planktonic form by adding the phage product from the beginning or

TABLE 1 Growth parameter [growth rate (μ), lag phase duration (λ), total heat produced (Q)] calculated from the calorimetric data.

Condition / Microorganism	Liquid culture*			Thin biofilm			Thick biofilm		
	% μ	Δ λ	% Q	% μ	Δ λ	% Q	% μ	delta λ	% Q
SE 49461	36.9 ± 9.9	12.2 ± 15.1	91.9 ± 4.0	49.2 ± 3.1	0.0 ± 0.4	110.3 ± 2.5	100.9 ± 22.7	1.7 ± 1.5	111.0 ± 32.4
SA 43300	30.2 ± 12.5	0.0 ± 0.5	24.2 ± 9.3	49.0 ± 7.0	0.0 ± 0.3	59.2 ± 7.8	123.1 ± 15.5	1.4 ± 0.2	108.7 ± 3.3
SA 25923	46.6 ± 27.8	13.5 ± 15.8	47.7 ± 13.5	70.7 ± 20.6	0.0 ± 1.5	78.0 ± 15.7	146.4 ± 14.2	0.0 ± 0.3	107.3 ± 3.9
SA 29213	97.0 ± 1.1	0.0 ± 0.2	101.9 ± 1.7	80.1 ± 4.0	0.4 ± 0.4	125.1 ± 9.9	ND	ND	ND
SAg 6,784	98.7 ± 2.9	0.1 ± 0.1	96.7 ± 1.2	ND	ND	ND	ND	ND	ND

SE, *Staphylococcus epidermidis*; SA, *Staphylococcus aureus*; Sag, *Streptococcus agalactiae*; numbers refer to the ATCC or DSM culture collection number. The growth rate (μ) and the total heat (Q) are expressed as a percentage of the growth control. The lag phase duration (λ) is expressed in additional lag hours. *Only data for phage addition at time = 0 are shown.

later in the early exponential phase (between 1 and 5 h; corresponding to 300 and 800 μW), with an injection system, in comparison with growth without inhibition (see Table 1 and Figure 1).

Staphylococcus epidermidis (ATCC 49461) and *S. aureus* (ATCC 43300, ATCC 25923) appeared sensitive to the phage product showing a rapid decline in metabolic heat production when the phage was added at the beginning of the experiment or early enough (up to 2 h after measurement started) (Table 1; see example in Figure 1). On the other hand, *S. aureus* ATCC 29213 and *Streptococcus agalactiae* (*S. agalactiae*) DSM 6784 displayed complete resistance (Table 1) irrespective of the phage addition time. Looking in more detail, delaying phage addition significantly reduced their inhibitory effect (see example in Figure 1). This was quite clear for all sensitive Staphylococci. In addition, once the bacterial load was too high (and consequently multiplicity of infection (MOI) too low), the addition of phages did not show any effect on the metabolic heat. Overall, in our conditions, injection after 2 h still produced a weak inhibition; however, after 3 h, no effect was visible for any of the tested strains.

In two cases (*S. epidermidis* ATCC 49461 and *S. aureus* ATCC 25923), regrowth could be observed after 15–30 h following initial phage-induced suppression, which occurred immediately after phage injection (see example in Figure 1). We assumed that phage-resistant Staphylococci have emerged or that the bacteriophages have been inactivated, allowing bacterial growth to resume using the remaining nutrients.

Effect of bacteriophages on thin biofilms

Thin biofilms grown in calorimetry inserts were analyzed after removal of the planktonic cells and non-adherent cells. For this part, we focused on the strains that proved to be sensitive in the first part of the experiment (*S. epidermidis* ATCC 49461, *S. aureus* ATCC 43300 and 25,923) and the resistant one (ATCC 29213) as a control (Figure 2).

For *S. epidermidis*, a lower maximum growth rate (μ) was observed with phages, although the peak heat production (Q max) was higher (Figure 2A). This suggests that a high metabolic activity was sustained for a longer period, likely due to slower nutrient depletion in the medium. *S. aureus* ATCC 43300 (Figure 2B) and *S. aureus* ATCC 25923 (Figure 2C) exhibited significant inhibition of both growth and heat production, indicating effective phage activity. Meanwhile, *S. aureus* ATCC 29213 (Figure 2D) showed no significant change, consistent with its previously observed resistance to phages in liquid cultures (Figure 1).

Effect of bacteriophages on thick biofilms

For this part of the experiment, we only analyzed the three sensitive *Staphylococcus* strains. In this part of the experiment, the same biofilm was measured both with and without phage insertion and in new BHI medium. No significant effect from bacteriophages was detected on any of the strains tested. The biofilm was most likely too thick and therefore resistant. No heat production was observed after heat killing (Figure 3). It must be noted that the growth indicator (μ, λ, and Q) used here reflects more the medium consumption rather than the net growth of the biofilm. Still, for ease of comparison, these indicators were calculated in the same manner.

Discussion

Observation of the heat flow curves reveals interesting phenomena such as the appearance of secondary peaks after returning to baseline for the planktonic cells in liquid medium, the prolonged maintenance of stable metabolic levels in thin biofilms, and finally, the complete resistance of thick and mature biofilms to isothermal microcalorimetry. Indeed, in planktonic cultures, resistant bacterial mutants might be selected, enabling regrowth as long as the nutrients are not depleted. Furthermore, recent studies outlined the fact that phages can lead to the production of persisters host cells (Fernández-García et al., 2024). This certainly deserves more attention in future studies. For thin biofilms, with thicknesses usually ranging between 9 and 40 μm, according to the literature, which uses closely similar preparations (Shi et al., 2016; Di Stefano et al., 2009; Shukla and Rao, 2013; Liu et al., 2015), it appears that part of the biofilm remains active. Still, thin biofilms are unable to regrow and disperse in the liquid phase. Most likely, the phage is preventing microbes from dispersing in the liquid medium, but cannot penetrate the entire biofilm and thus eliminate all microbes. Staphylococci protected in a biofilm can then survive using the remaining nutrients from the medium. In our study, mature biofilms appeared particularly resistant. When prepared on membranes, Staphylococci biofilms have a thickness varying between 270 and 311 μm; however, some studies have reported thicknesses up to 700 μm (Agostinho et al., 2011; Singh et al., 2010; Chatterjee et al., 2014). Therefore, it is not surprising that several studies have already shown that mature biofilms are orders of magnitude more resistant to several antibiotics (Nickel et al., 1985; Mah and O'Toole, 2001). Similarly to previously published studies and reviews, we can safely assume that the same principle also applies to the efficacy of bacteriophages against biofilms (Abedon, 2023). This may be due to

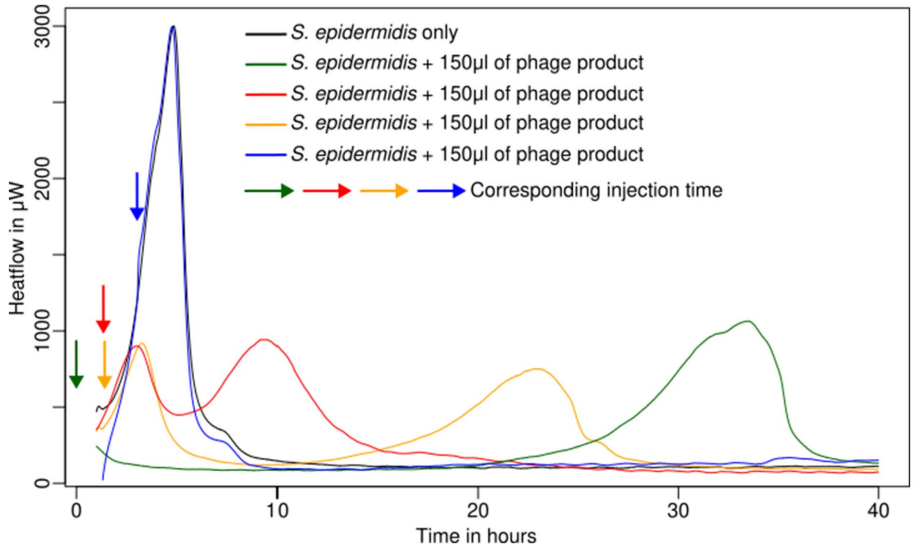

FIGURE 1
Metabolic activity of planktonic cells of *S. epidermidis* ATCC 49461 in liquid culture monitored using IMC.

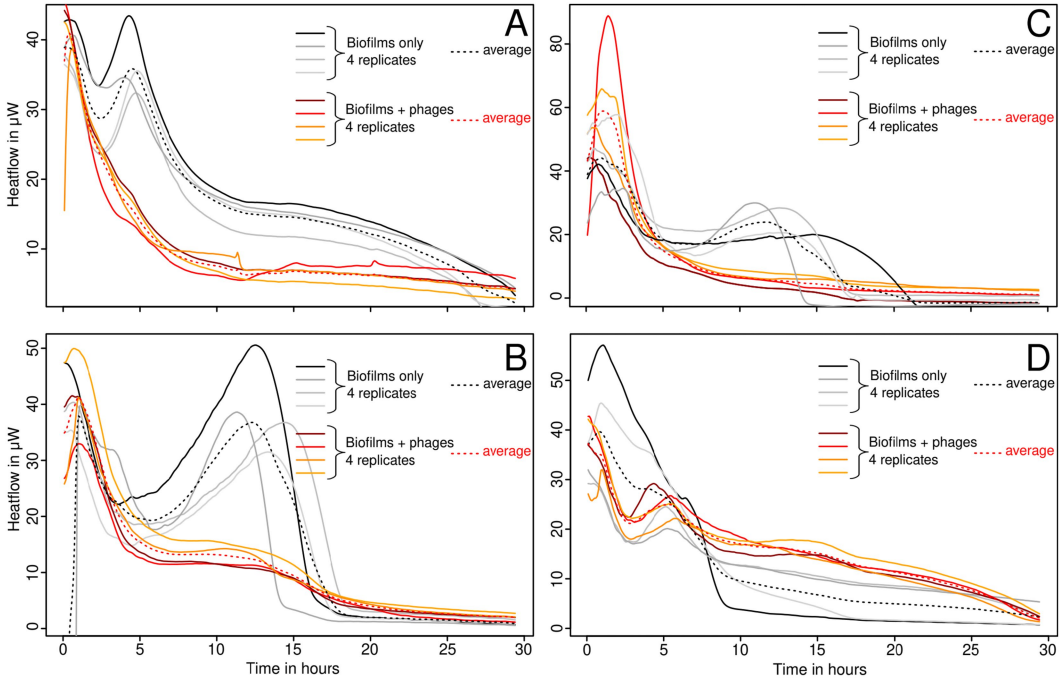

FIGURE 2
Growth of thin biofilms of *S. epidermidis* ATCC 49461 **(A)**, *S. aureus* ATCC 43300 **(B)**, ATCC 25923 **(C)**, and ATCC 29213 **(D)**, monitored using IMC with and without bacteriophages.

several factors such as the barrier against chemical and physical substances provided by to the exopolysaccharide matrix of the biofilm and thus the inability of the phages to penetrate, the binding and trapping of phage on the EPS matrix, the acquired resistance mechanisms expressed only in biofilms or a metabolism that is too slow to allow the phages to reproduce sufficiently (Abedon, 2023). From a more clinical perspective, thick biofilms are a significant factor in inhibiting the healing of chronic wounds, and optimal management to remove such biofilms requires surgical debridement as an additional step (Scalise et al., 2015). While debridement remains the most cost-effective strategy for reducing biofilm, it cannot completely eradicate it. Continued debridement is essential to maintain the biofilm in a weakened state, which allows adjunctive treatments such as phages or antibiotics to play a critical role in the healing of chronic wounds (Wolcott et al., 2009; Anghel et al., 2016). These adjunctive therapies help disrupt biofilm formation and improve the overall effectiveness

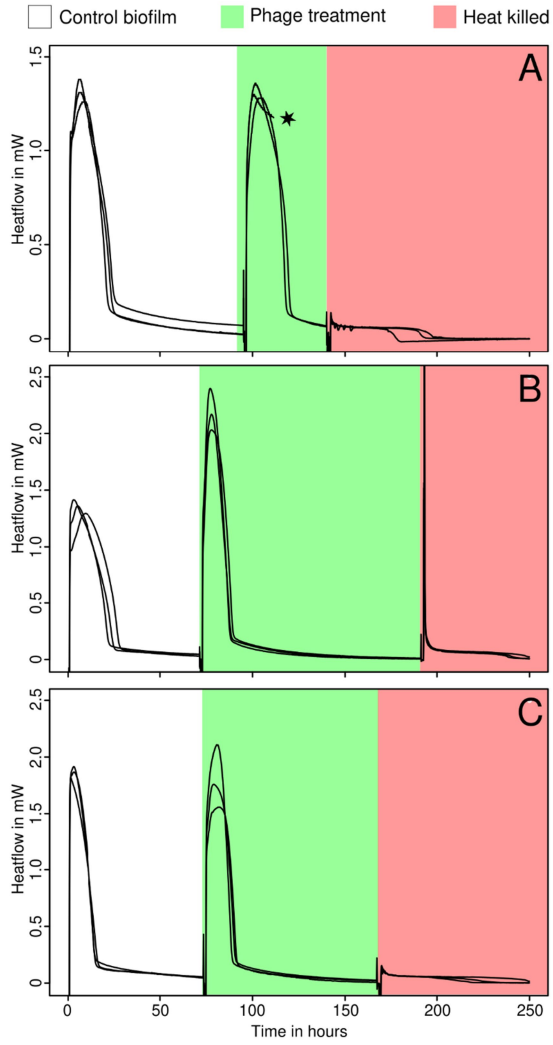

FIGURE 3
Growth of thick biofilms of *S. epidermidis* ATCC 49461 **(A)**, *S. aureus* ATCC 25923 **(B)**, and ATCC 43300 **(C)** monitored using IMC before (white) and during the addition of bacteriophages (green) and after heat killing (red). The star indicates that some data were omitted due to technical difficulties or methodological issues.

of wound care (Chan and Abedon, 2012). Although more data are required to support this statement, it appears that the combination of debridement and phages should be further investigated as a therapeutic option (Chan and Abedon, 2012; Parracho et al., 2012).

In the context of phage therapy, the present data and previous studies show that the use of IMC has proven to be an effective method for analyzing bacteriophage-bacteria interactions and their kinetics, as it proved to be faster method than traditional cultures (i.e., agar overlay requiring up to 24 h) without requiring additional work. Compared to optical density-based methods, IMC is also suitable for analyzing opaque liquid and solid media, which has proven effective for testing thin and thick biofilms without the need for destructive methods (Stewart and Franklin, 2008). In addition, the growth and inhibition kinetics can be studied using heat curve analysis as described before (Braissant et al., 2013). Still, a thorough comparison of all current methods to assess phages with IMC should be conducted in order to assess the potential of this technique.

It must also be noted that IMC has some limitations. In particular, it uses sealed airtight vials that limit the amount of oxygen in the system. In addition, as oxygen diffuses poorly in aqueous solution, this may lead to severe limitations when using strictly aerobic microbes (Maskow et al., 2014). This was not the case for the Staphylococci and Streptococci used here, which are capable of fermenting a wide range of substrates present in the medium used. Another important limitation of isothermal microcalorimetry is that most of the heat generated during growth comes from catabolic reactions. The synthesis of phages, like other anabolic processes, does not release heat (or a negligible amount – see the study by Battley, 1998; Battley, 1992; Kell and Battley, 1987) and remains invisible despite its cost to the cell. Therefore, combining IMC with ATP measurements, flow cytometry, protein assays, or PFU count might be valuable (Braissant et al., 2020; Braissant et al., 2015; Morais et al., 2014). Similarly, the calorespirometric approach may also be of interest, as well as the heat per O_2 and the heat per CO_2, which may provide additional information. To the best of our knowledge, calorespirometry has not been investigated with bacteriophages yet. In addition to the limitations imposed by IMC itself, the following limitations of the study should also be taken into account. Firstly, only one strain of *Streptococcus* was investigated in detail and found to be resistant (preliminary studies have also shown that other dental strains were not sensitive to phage cocktails – data not shown). However, the limited number of strains tested does not allow for any conclusions on the efficacy of Streptococci. Similarly, with respect to chronic wounds, Gram-negative pathogens such as *Pseudomonas aeruginosa* should also be included in future studies as they can represent an important proportion of causative pathogens in diabetic foot infections and various ulcer-related infections (Rahim et al., 2017; Ramakant et al., 2011; Kirketerp-Møller et al., 2008). This is certainly a limitation of the current study, especially as phages against *Pseudomonas aeruginosa* are indeed available in online pharmacies. Finally, it should be noted that infection by both pathogens is also common, emphasizing the need to test several phage products simultaneously (Ibberson et al., 2017; Lichtenberg et al., 2023). From a more technical standpoint, during experiments with planktonic cells, the injection system may have altered the metabolism by mixing the medium and resuspending cells that otherwise would have sedimented; thus, creating a potentially more favorable environment for bacterial growth, we believe that the effect is extremely limited and did not influence the results. Similarly, for a thick biofilm, the handling with sterile tweezers might have altered the surface of the biofilm. We estimate that <1% of the surface of the biofilm might have been altered during the transfer of the filters to fresh medium. This may have been due to the presence of an entry window for phages in the Fersici cocktail. Still, all biofilms proved to be resistant, which supports that the idea that handling did not affect the results.

Conclusion

Bacteriophages appear to be a valid solution to the growing resistance to antibiotics as they are an effective agent for killing bacteria in planktonic cells and thin biofilms, such as those found in many skin infections. With increasing biofilm thickness and maturation, it is likely that more aggressive measures (cleaning and debridement) need to be taken prior to the application of

phages, as our study demonstrated that thick biofilms of sensitive microbes are not affected by phages. However, it should be noted that antibiotics face similar, if not greater, challenges in treating thick biofilms. Thus, emphasizing the need for further studies, especially *in vivo* studies combining debridement and phage therapy. In addition, a better understanding of bacterial metabolism when infected with phages would be desirable, as IMC is rather insensitive to phage production. The use of incorporation assays, such as stable isotope labeling or substrate analogue labeling, may provide some significant insights into phage production and energetic costs (Braissant et al., 2020; Hatzenpichler et al., 2014). In addition, the use of substrate analogues would allow tracking the phages using fluorescent markers through click chemistry.

Data availability statement

The raw data supporting the conclusions of this article will be made available by the authors, without undue reservation.

Author contributions

TL: Data curation, Formal analysis, Investigation, Methodology, Visualization, Writing – original draft, Writing – review & editing. GB: Conceptualization, Supervision, Writing – original draft, Writing – review & editing. MR: Conceptualization, Supervision, Writing – original draft, Writing – review & editing. OB: Conceptualization, Data curation, Formal analysis, Investigation, Methodology, Supervision, Validation, Visualization, Writing – original draft, Writing – review & editing.

Funding

The author(s) declare that no financial support was received for the research and/or publication of this article.

Conflict of interest

Authors GB and MR are employed by company alta uro AG.

The remaining authors declare that the research was conducted in the absence of any commercial or financial relationships that could be construed as a potential conflict of interest.

Generative AI statement

The authors declare that no Gen AI was used in the creation of this manuscript.

Publisher's note

References

Abedon, S. T. (2023). Ecology and evolutionary biology of hindering phage therapy: the phage tolerance vs. phage resistance of bacterial biofilms. *Antibiotics* 12:245. doi: 10.3390/antibiotics12020245

Agostinho, A. M., Hartman, A., Lipp, C., Parker, A. E., Stewart, P. S., and James, G. A. (2011). An in vitro model for the growth and analysis of chronic wound MRSA biofilms. *J. Appl. Microbiol.* 111, 1275–1282. doi: 10.1111/j.1365-2672.2011.05138.x

Alves, D. R., Gaudion, A., Bean, J. E., Perez Esteban, P., Arnot, T. C., Harper, D. R., et al. (2014). Combined use of bacteriophage K and a novel bacteriophage to reduce *Staphylococcus aureus* biofilm formation. *Appl. Environ. Microbiol.* 80, 6694–6703. doi: 10.1128/AEM.01789-14

Anghel, E. L., DeFazio, M. V., Barker, J. C., Janis, J. E., and Attinger, C. E. (2016). Current concepts in debridement: science and strategies. *Plast. Reconstr. Surg.* 138, 82S–93S. doi: 10.1097/PRS.0000000000002651

Battley, E. H. (1992). On the enthalpy of formation of *Escherichia coli* K-12 cells. *Biotechnol. Bioeng.* 39, 5–12. doi: 10.1002/bit.260390103

Battley, E. H. (1998). The development of direct and indirect methods for the study of the thermodynamics of microbial growth. *Thermochim. Acta* 309:357. doi: 10.1016/s0040-6031(97)00357-2

Bonkat, G., Braissant, O., Widmer, A. F., Frei, R., Rieken, M., Wyler, S., et al. (2012). Rapid detection of urinary tract pathogens using microcalorimetry: principle, technique and first results. *BJU Int.* 110, 892–897. doi: 10.1111/j.1464-410X.2011.10902.x

Braissant, O., Astasov-Frauenhoffer, M., Waltimo, T., and Bonkat, G. (2020). A review of methods to determine viability, vitality, and metabolic rates in microbiology. *Front. Microbiol.* 11:547458. doi: 10.3389/fmicb.2020.547458

Braissant, O., Bachmann, A., and Bonkat, G. (2015). Microcalorimetric assays for measuring cell growth and metabolic activity: methodology and applications. *Methods* 76, 27–34. doi: 10.1016/j.ymeth.2014.10.009

Braissant, O., Bonkat, G., Wirz, D., and Bachmann, A. (2013). Microbial growth and isothermal microcalorimetry: growth models and their application to microcalorimetric data. *Thermochim. Acta* 555, 64–71. doi: 10.1016/j.tca.2012.12.005

Butini, M. E., Abbandonato, G., Di Rienzo, C., Trampuz, A., and Di Luca, M. (2019). Isothermal microcalorimetry detects the presence of Persister cells in a *Staphylococcus aureus* biofilm after vancomycin treatment. *Front. Microbiol.* 10:332. doi: 10.3389/fmicb.2019.00332

Chan, B. K., and Abedon, S. T. (2012). Phage therapy pharmacology. Phage cocktails. *Adv Appl Microbiol* 78, 1–23. doi: 10.1016/B978-0-12-394805-2.00001-4

Chatterjee, S., Biswas, N., Datta, A., Dey, R., and Maiti, P. (2014). Atomic force microscopy in biofilm study. *Microscopy* 63, 269–278. doi: 10.1093/jmicro/dfu013

Clokie, M. R. J., Millard, A. D., Letarov, A. V., and Heaphy, S. (2011). Phages in nature. *Bacteriophage* 1:14942. doi: 10.4161/bact.1.1.14942

Di Stefano, A., D'Aurizio, E., Trubiani, O., Grande, R., Di Campli, E., Di Giulio, M., et al. (2009). Viscoelastic properties of Staphylococcus aureus and *Staphylococcus epidermidis* mono-microbial biofilms. *Microb. Biotechnol.* 2:120. doi: 10.1111/j.1751-7915.2009.00120.x

Fanaei Pirlar, R., Wagemans, J., Ponce Benavente, L., Lavigne, R., Trampuz, A., and Gonzalez Moreno, M. (2022). Novel bacteriophage specific against Staphylococcus epidermidis and with Antibiofilm activity. *Viruses* 14:340. doi: 10.3390/v14061340

Fernández-García, L., Kirigo, J., Huelgas-Méndez, D., Benedik, M. J., Tomás, M., García-Contreras, R., et al. (2024). Phages produce Persisters. *Microb. Biotechnol.* 17:e14543. doi: 10.1111/1751-7915.14543

Gordillo Altamirano, F. L., and Barr, J. J. (2019). Phage therapy in the Postantibiotic era. *Clin. Microbiol. Rev.* 32:32. doi: 10.1128/CMR.00066-18

Gündoğdu, A., Kiliç, H., Ulu Kiliç, A., and Kutateladze, M. (2016). Komplike Deri ve Yumuşak Doku Enfeksiyonu Etkeni Çoklu Dirençli Patojenlerin Standart Bakteriyofaj Kokteyllerine Karşi Duyarliliklannin Araştinlmasi. *Mikrobiyol. Bul.* 50, 215–223. doi: 10.5578/mb.24165

Hatlen, T. J., and Miller, L. G. (2021). Staphylococcal skin and soft tissue infections. *Infect. Dis. Clin. N. Am.* 35, 81–105. doi: 10.1016/j.idc.2020.10.003

Hatzenpichler, R., Scheller, S., Tavormina, P. L., Babin, B. M., Tirrell, D. A., and Orphan, V. J. (2014). In situ visualization of newly synthesized proteins in environmental

microbes using amino acid tagging and click chemistry. *Environ. Microbiol.* 16, 2568–2590. doi: 10.1111/1462-2920.12436

Ibberson, C. B., Stacy, A., Fleming, D., Dees, J. L., Rumbaugh, K., Gilmore, M. S., et al. (2017). Co-infecting microorganisms dramatically Alter pathogen gene essentiality during Polymicrobial infection. *Nat. Microbiol.* 2:17079. doi: 10.1038/nmicrobiol.2017.79

Jiang, Y., Xu, Q., Jiang, L., and Zheng, R. (2021). Isolation and characterization of a lytic *Staphylococcus aureus* phage WV against *Staphylococcus aureus* biofilm. *Intervirology* 64, 169–177. doi: 10.1159/000515282

Kahm, M., Hasenbrink, G., Lichtenberg-Fraté, H., Ludwig, J., and Kschischo, M. (2010). Grofit: fitting biological growth curves with R. *J. Stat. Softw.* 33, 1–21. doi: 10.18637/jss.v033.i07

Kell, D. B., and Battley, E. H. (1987). Energetics of microbial growth. *Q. Rev. Biol.* 62:654. doi: 10.1086/415654

Kelly, D., Mcauliffe, O., Ross, R. P., and Coffey, A. (2012). Prevention of *Staphylococcus aureus* biofilm formation and reduction in established biofilm density using a combination of phage K and modified derivatives. *Lett. Appl. Microbiol.* 54, 286–291. doi: 10.1111/j.1472-765X.2012.03205.x

Kiani, A. K., Anpilogov, K., Dhuli, K., Paolacci, S., Benedetti, S., Manara, E., et al. (2021). Naturally-occurring and cultured bacteriophages in human therapy. *Eur. Rev. Med. Pharmacol. Sci.* 25, 101–107. doi: 10.26355/eurrev_202112_27339

Kim, S. G., Kwon, J., Giri, S. S., Yun, S., Kim, H. J., Kim, S. W., et al. (2021). Strategy for mass production of lytic *Staphylococcus aureus* bacteriophage PSa-3: contribution of multiplicity of infection and response surface methodology. *Microb. Cell Factories* 20:5498. doi: 10.1186/s12934-021-01549-8

Kirketerp-Møller, K., Jensen, P., Fazli, M., Madsen, K. G., Pedersen, J., Moser, C., et al. (2008). Distribution, organization, and ecology of bacteria in chronic wounds. *J. Clin. Microbiol.* 46:8. doi: 10.1128/JCM.00501-08

Kumar, S., Chandra, N., Singh, L., Hashmi, M. Z., and Varma, A. (2019). Biofilms in human diseases: Treatment and control. Cham: Springer.

León, M., and Bastías, R. (2015). Virulence reduction in bacteriophage resistant Bacteria. *Front. Microbiol.* 6:343. doi: 10.3389/fmicb.2015.00343

Lichtenberg, M., Kirketerp-Møller, K., Kvich, L. A., Christensen, M. H., Fritz, B., Jakobsen, T. H., et al. (2023). Single cells and bacterial biofilm populations in chronic wound infections. *APMIS* 132:13344. doi: 10.1111/apm.13344

Liu, H., Zhao, Y., Zhao, D., Gong, T., Wu, Y., Han, H., et al. (2015). Antibacterial and anti-biofilm activities of Thiazolidione derivatives against clinical Staphylococcus strains. *Emerg. Microbes Infect.* 4:e17. doi: 10.1038/emi.2015.1

Lowy, F. D. (1998). *Staphylococcus aureus* infections. *N. Engl. J. Med.* 339, 520–532. doi: 10.1056/nejm199808203390806

Łusiak-Szelachowska, M., Weber-Dąbrowska, B., and Górski, A. (2020). Bacteriophages and Lysins in biofilm control. *Virol. Sin.* 35, 125–133. doi: 10.1007/s12250-019-00192-3

Mah, T. F. C., and O'Toole, G. A. (2001). Mechanisms of biofilm resistance to antimicrobial agents. *Trends Microbiol.* 9, 34–39. doi: 10.1016/s0966-842x(00)01913-2

Maskow, T., Morais, F. M., Rosa, L. F. M., Qian, Y. G., and Harnisch, F. (2014). Insufficient oxygen diffusion leads to distortions of microbial growth parameters assessed by isothermal microcalorimetry. *RSC Adv.* 4, 32730–32737. doi: 10.1039/c4ra03921a

McCallin, S., Sarker, S. A., Sultana, S., Oechslin, F., and Brüssow, H. (2018). Metagenome analysis of Russian and Georgian Pyophage cocktails and a placebo-controlled safety trial of single phage versus phage cocktail in healthy *Staphylococcus aureus* carriers. *Environ. Microbiol.* 20, 3278–3293. doi: 10.1111/1462-2920.14310

Merritt, J. H., Kadouri, D. E., and O'Toole, G. A. (2011). Growing and analyzing static biofilms. *Curr. Protoc. Microbiol.* 22:1B-01. doi: 10.1002/9780471729259.mc01b01s22

Moffarah, A. S., Al Mohajer, M., Hurwitz, B. L., and Armstrong, D. G. (2016). "Skin and soft tissue infections" in Diagnostic microbiology of the immunocompromised host. eds. R. T. Hayden, K. C. Carroll, Y. W. Tang and D. M. Wolk (Hoboken, NJ: John Wiley & Sons), 691–708.

Molendijk, M. M., Phan, M. V. T., Bode, L. G. M., Strepis, N., Prasad, D. K., Worp, N., et al. (2023). Microcalorimetry: a novel application to measure in vitro phage susceptibility of *Staphylococcus aureus* in human serum. *Viruses* 15:14. doi: 10.3390/v15010014

Morais, F. M., Buchholz, F., Hartmann, T., Lerchner, J., Neu, T. R., Kiesel, B., et al. (2014). Chip-calorimetric monitoring of biofilm eradication with bacteriophages reveals an unexpected infection-related heat profile. *J. Therm. Anal. Calorim.* 115:3494. doi: 10.1007/s10973-013-3494-4

Morozova, V. V., Vlassov, V. V., and Tikunova, N. V. (2018). Applications of bacteriophages in the treatment of localized infections in humans. *Front. Microbiol.* 9:1696. doi: 10.3389/fmicb.2018.01696

Nickel, J. C., Ruseska, I., Wright, J. B., and Costerton, J. W. (1985). Tobramycin resistance of *Pseudomonas aeruginosa* cells growing as a biofilm on urinary catheter material. *Antimicrob. Agents Chemother.* 27, 619–624. doi: 10.1128/AAC.27.4.619

Nykyri, J., Herrmann, A. M., and Håkansson, S. (2019). Isothermal microcalorimetry for thermal viable count of microorganisms in pure cultures and stabilized formulations. *BMC Microbiol.* 19:65. doi: 10.1186/s12866-019-1432-8

Paharik, A. E., and Horswill, A. R. (2016). The staphylococcal biofilm: Adhesins, regulation, and host response. *Microbiol. Spectr.* 4:2015. doi: 10.1128/microbiolspec.vmbf-0022-2015

Parracho, H. M., Burrowes, B. H., and Enright, M. C. (2012). The role of regulated clinical trials in the development of bacteriophage therapeutics. *J. Mol. Genet. Med.* 6:1000050. doi: 10.4172/1747-0862.1000050

Presterl, E., Hajdu, S., Lassnigg, A. M., Hirschl, A. M., Holinka, J., and Graninger, W. (2009). Effects of azithromycin in combination with vancomycin, Daptomycin, Fosfomycin, Tigecycline, and ceftriaxone on *Staphylococcus epidermidis* biofilms. *Antimicrob. Agents Chemother.* 53, 3205–3210. doi: 10.1128/AAC.01628-08

R Core Team (2019). R: A language and environment for statistical computing. Vienna: R Core Team.

Rahim, K., Saleha, S., Zhu, X., Huo, L., Basit, A., and Franco, O. L. (2017). Bacterial contribution in chronicity of wounds. *Microb. Ecol.* 73, 710–721. doi: 10.1007/s00248-016-0867-9

Ramakant, P., Verma, A. K., Misra, R., Prasad, K. N., Chand, G., Mishra, A., et al. (2011). Changing microbiological profile of pathogenic Bacteria in diabetic foot infections: time for a rethink on which empirical therapy to choose? *Diabetologia* 54, 58–64. doi: 10.1007/s00125-010-1893-7

Scalise, A., Bianchi, A., Tartaglione, C., Bolletta, E., Pierangeli, M., Torresetti, M., et al. (2015). Microenvironment and microbiology of skin wounds: the role of bacterial biofilms and related factors. *Semin. Vasc. Surg.* 28:3. doi: 10.1053/j.semvascsurg.2016.01.003

Schierle, C. F., De La Garza, M., Mustoe, T. A., and Galiano, R. D. (2009). Staphylococcal biofilms impair wound healing by delaying Reepithelialization in a murine cutaneous wound model. *Wound Repair Regen.* 17, 354–359. doi: 10.1111/j.1524-475X.2009.00489.x

Severn, M. M., and Horswill, A. R. (2023). Staphylococcus epidermidis and its dual lifestyle in skin health and infection. *Nat. Rev. Microbiol.* 21, 97–111. doi: 10.1038/s41579-022-00780-3

Shi, S. F., Jia, J. F., Guo, X. K., Zhao, Y. P., Chen, D. S., Guo, Y. Y., et al. (2016). Reduced *Staphylococcus aureus* biofilm formation in the presence of chitosan-coated iron oxide nanoparticles. *Int. J. Nanomedicine* 11:1371. doi: 10.2147/IJN.S41371

Shittu, A. O., and Lin, J. (2006). Antimicrobial susceptibility patterns and characterization of clinical isolates of *Staphylococcus aureus* in KwaZulu-Natal Province, South Africa. *BMC Infect. Dis.* 6:125. doi: 10.1186/1471-2334-6-125

Shukla, S. K., and Rao, T. S. (2013). Effect of calcium on *Staphylococcus aureus* biofilm architecture: a confocal laser scanning microscopic study. *Colloids Surfaces B Biointerfaces* 103, 448–454. doi: 10.1016/j.colsurfb.2012.11.003

Singh, R., Ray, P., Das, A., and Sharma, M. (2010). Penetration of antibiotics through Staphylococcus aureus and *Staphylococcus epidermidis* biofilms. *J. Antimicrob. Chemother.* 65, 1955–1958. doi: 10.1093/jac/dkq257

Solokhina, A., Bonkat, G., and Braissant, O. (2019). Measuring the metabolic activity of mature mycobacterial biofilms using isothermal microcalorimetry. *Methods Mol Biol* 1964, 141–149. doi: 10.1007/978-1-4939-9179-2_11

Solokhina, A., Bonkat, G., Kulchavenya, E., and Braissant, O. (2018). Drug susceptibility testing of mature *Mycobacterium tuberculosis* H37Ra and *Mycobacterium smegmatis* biofilms with calorimetry and laser spectroscopy. *Tuberculosis* 113, 91–98. doi: 10.1016/j.tube.2018.09.010

Stewart, P. S., and Franklin, M. J. (2008). Physiological heterogeneity in biofilms. *Nat. Rev. Microbiol.* 6, 199–210. doi: 10.1038/nrmicro1838

Sultan, A. R., Tavakol, M., Lemmens-Den Toom, N. A., Croughs, P. D., Verkaik, N. J., Verbon, A., et al. (2022). Real time monitoring of *Staphylococcus aureus* biofilm sensitivity towards antibiotics with isothermal microcalorimetry. *PLoS One* 17:e0260272. doi: 10.1371/journal.pone.0260272

Tan, C. S., Aqiludeen, N. A., Tan, R., Gowbei, A., Mijen, A. B., Louis, S. R., et al. (2020). Could bacteriophages isolated from the sewage be the solution to methicillin-resistant *Staphylococcus aureus*? *Med J Malaysia* 75, 110–116. Available at: https://pubmed.ncbi.nlm.nih.gov

Tong, S. Y. C., Davis, J. S., Eichenberger, E., Holland, T. L., and Fowler, V. G. (2015). Staphylococcus aureus infections: epidemiology, pathophysiology, clinical manifestations, and management. *Clin. Microbiol. Rev.* 28, 603–661. doi: 10.1128/CMR.00134-14

Tsiodras, S., Gold, H. S., Sakoulas, G., Eliopoulos, G. M., Wennersten, C., Venkataraman, L., et al. (2001). Linezolid resistance in a clinical isolate of *Staphylococcus aureus*. *Lancet* 358, 207–208. doi: 10.1016/S0140-6736(01)05410-1

Whittard, E., Redfern, J., Xia, G., Millard, A., Ragupathy, R., Malic, S., et al. (2021). Phenotypic and genotypic characterization of novel polyvalent bacteriophages with potent in vitro activity against an international collection of genetically diverse *Staphylococcus aureus*. *Front. Cell. Infect. Microbiol.* 11:698909. doi: 10.3389/fcimb.2021.698909

Wojdyr, M., Gierlotka, S., and Palosz, B. (2004). FITYK – peak-fitting software with support for powder patterns analysis. *Acta Crystallogr. Sect. A Found. Crystallogr.* 60:s246. doi: 10.1107/s010876730409511x

Wolcott, R. D., Kennedy, J. P., and Dowd, S. E. (2009). Regular debridement is the Main tool for maintaining a healthy wound bed in Most chronic wounds. *J. Wound Care* 18, 54–56. doi: 10.12968/jowc.2009.18.2.38743

Frontiers in Microbiology

Explores the habitable world and the potential of microbial life

The largest and most cited microbiology journal which advances our understanding of the role microbes play in addressing global challenges such as healthcare, food security, and climate change.

Discover the latest Research Topics

See more →

Frontiers

Avenue du Tribunal-Fédéral 34
1005 Lausanne, Switzerland
frontiersin.org

Contact us

+41 (0)21 510 17 00
frontiersin.org/about/contact